U.S. Department of Energy Office of Environmental Management

Fire Forensic Analysis of the Radiological Release Event at the Waste Isolation Pilot Plant on February 14, 2014

April 6, 2015

Prepared in Support of the U.S. DOE Accident Investigation Board for the Radiological Release Event at the Waste Isolation Pilot Plant on February 14, 2014

Disclaimer

On February 14, 2014, an airborne radiological release occurred at the Department of Energy Waste Isolation Pilot Plant (WIPP) near Carlsbad, New Mexico. On March 4, 2014, an Accident Investigation Board (the Board) was appointed by Matthew Moury, Deputy Assistant Secretary, Safety, Security, and Quality Programs to determine the cause of the release. Because access to the underground was restricted following the event, the investigation was broken into two phases. The first phase, Phase 1, focused on how the radiological material was released into the atmosphere and the results were issued on April 22, 2014, in a Phase 1 investigation report.

On May 19, 2014, James Hutton, Deputy Assistant Secretary, Safety, Security, and Quality Programs, U.S. Department of Energy, Office of Environmental Management, appointed an Accident Investigation Board to complete the investigation (Phase 2). Phase 2 was performed once limited access to the underground was re-established and focused on how the radiological material was released. For both Phases, the Board was appointed to perform an accident investigation and to prepare an investigation report in accordance with Department of Energy Order 225.1B, *Accident Investigations*.

During the Phase 2 investigation, the Board established a Fire Forensic Team to evaluate the fire behaviors that occurred during the February 14, 2014 radiological release. This team was responsible for the preparation of this report.

The discussion of the facts as determined by the Board and the views expressed in the report do not assume and are not intended to establish the existence of any duty at law on the part of the U.S. Government, its employees or agents, contractors, their employees or agents, or subcontractors at any tier, or any other party.

This fire forensic report neither determines nor implies liability.

Approvals

D. Allan Coutts, Lead Author
URS Professional Solutions, LLC
AECOM
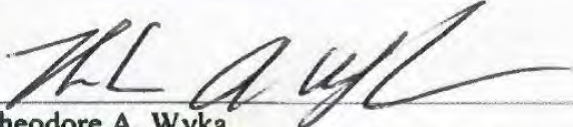
Theodore A. Wyka,
DOE Accident Investigation Board Chairman
U.S. Department of Energy
Office of Environmental Management

Report Authors

D. Allan Coutts, PE (SC), PhD, FSFPE
AECOM, Aiken, SC

Stephanie J Harrington, PhD
AECOM, Richland, WA

Daniel R, Geary
AECOM, Richland, WA

Fire Forensic Team Members (Chapter 4 Material)

D. Allan Coutts, Lead Author, AECOM

Roger Claycomb, Accident Investigation Board Vice Chairman, DOE - Idaho Field Office

Heidi Lowe, Administrative Assistant, ATA Services, Inc.

John Vandekraats, Array Inspection Analyst, NWP

Craig Suggs, Array Inspection Analyst, NWP

Curtis Chester, Array Inspection Analyst, NWP

Tim Burns, Array Inspection Analyst, Los Alamos National Laboratory - Carlsbad Operations

Roger Allan Nelson, Array Inspection Analyst, DOE Carlsbad Field Office

Kerry Watson, Array Inspection Analyst, DOE Carlsbad Field Office

James Landmesser, Array Inspection Analyst, DOE-Headquarters

John Young, Array Inspection Analyst, Savannah River National Laboratory

Neil Robert Sorensen, Array Inspection Analyst, Sandia National Laboratories

David Funk, Array Inspection Analyst, Los Alamos National Laboratory

Kirk Viers, Array Inspection Analyst, Los Alamos National Laboratory

EXECUTIVE SUMMARY

On February 14, 2014, a radiological release event occurred in Panel 7 Room 7 waste array in the Waste Isolation Pilot Plant (WIPP) near Carlsbad, New Mexico. Elevated airborne radiological contamination was detected by a continuous air monitor in the Panel 7 exhaust drift. This instrument initiated a switch to the Filtered Ventilation Mode at 2314. Inspections on April 30, 2014 established that fire behaviors might have been associated with the radiological release event. Because of this, the Accident Investigation Board established a Fire Forensic Analysis Team. The results of the fire forensic analysis are documented in this report.

To support preparation of this report the investigation team conducted a systematic and comprehensive visual inspection of the Panel 7 Room 7 array. This inspection was conducted with video cameras suspended over and in the array. The results of this inspection are documented in this report. The inspection results form the basis for the fire forensic analysis.

The fire forensic analysis established an ongoing exothermic reaction in waste drum 68660 created a release of radiological material and initiated a fire in the Panel 7 Room 7 disposal array. The intensity of the fire was low to moderate and direct fire effects were primarily in rows 8 through 18 of the array. Damage within the array was not uniform and there were multiple small fires that caused direct flame impingement on several waste packages. In some locations the fire intensity was significant. The fire self-extinguished without consuming all combustibles present.

TABLE OF CONTENTS

TABLE OF FIGURES

TABLE OF TABLES

ACRONYM LIST

55GD	55 Gallon capacity waste container (Drum)
100GD	100 Gallon capacity waste container (Drum)
AIS	Air Intake Shaft
BH	Bulkhead
CAM	Continuous Air Monitor
CH	Contact Handled
CPR	Cellulose, Plastic, and Rubber
DAC	Derived Air Concentration
DOE	U.S. Department of Energy
DOT	Department of Transportation
dP	Differential Pressure
ES	Exhaust Shaft
HDPE	High Density Polyethylene
HEPA	High-Efficiency Particulate Air
HRR	Heat Release Rate
MgO	Magnesium Oxide
NWP	Nuclear Waste Partnership LLC
POP	Pipe Overpack Waste Container
RH	Remote Handled
SHS	Salt Handling Shaft
SLB2	Standard Large Box 2

SWB	Standard Waste Box
SWB OP	Standard Waste Box Overpack
TDOP	10-Drum Overpack
TRU	Transuranic
WIPP	Waste Isolation Pilot Plant
WS	Waste Shaft

LIST OF UNITS

°C	degrees centigrade
%	percent
°F	degrees Fahrenheit
cfm	cubic-feet-per-minute
fpm	feet per minute
ft	foot/feet
ft^2	square feet
ft^3	cubic feet
gal	gallon
in. w.g.	inches of water, gage
J	Joule
K	degrees Kelvin
kcfm	thousand cubic-feet-per-minute
kg	kilogram
kJ	kilojoule
kW	kilowatt
lbs	pounds
m	meter
m^2	square meter
m^3	cubic meters
min	minute

MJ   Megajoule, 10^6 Joules

mm   millimeter

MW   Megawatt, 10^6 Watts

Pa   Pascal

psig   pounds per square inch, gage

s   second

1.0   INTRODUCTION

On February 14, 2014, at approximately 2300, a fire occurred in the Panel 7 Room 7 waste array at the underground Waste Isolation Pilot Plant (WIPP). The cause of the fire was an exothermic reaction within a waste container which resulted in a thermal runaway, overpressurization of the container, loss of container integrity, and the expulsion of container contents. The expelled materials ignited exposed combustibles materials in the array. The fire was small to moderate in severity. Direct fire damage was limited to the array. No equipment was damaged by this event. The fire was associated with the release of radiological contamination. Contamination spread was measured in upstream portions of Panel 7; the exhaust drifts between Panel 7 and the Exhaust Shaft (ES); and the aboveground ventilation system. Onsite and offsite monitoring stations provided evidence of the radiological material release.

At the time of the event, the underground was not occupied. The location where the fire occurred was last occupied prior to 1600 on the day of the event. Reentry to the underground did not occur until April 2, 2014, and Panel 7 was first reentered on April 16, 2014. No physical damage was observable at the waste array face from the room floor (photograph AIB-FST-02082[*]) but damage was observable from above the array (photographs AIB-FST-02090 and AIB-FST-02091).

Forensic investigation of the event included the collection of visual inspection, photographic evidence, ventilation data, radiological contamination monitoring, and physical samples. The hazards associated with the disassembly of the array were significant, and deemed inappropriate for the expected benefits. As such the analysis presented in this report is based on the evaluation of the collected evidence, fire modeling and a combination of qualitative and quantitative analyses.

This fire forensic analysis report was prepared at the request of the Accident Investigation Board for the Phase 2 Radiological Release Event at the Waste Isolation Pilot Plant on February 14, 2014. Phase 1 of this investigation was published in April 2014. [1] The scope of this fire forensic report was to evaluate the available fire evidence and establish a physical description of the fire behaviors that occurred on February 14, 2014. Radiological forensic analysis was outside the scope of this effort. Detailed chemical forensic within the initiating waste container was also not in the scope of the fire forensic analysis. Rather, this latter activity was the responsibility of the Technical Assessment Team. [2]

The report presentation is grouped into chapters that present logical grouping of information. These are:

- Facility Description (Chapter 2) – Presents an overall description of the WIPP underground with sufficient detail to facilitate an understanding of the other report chapters.
- Waste Descriptions (Chapter 3) – Presents a physical description of the waste containers as an input to the evaluation and analysis chapters.

---

[*] Photographs use the designator AIB-FST-xxxxx and are located in Appendix B.

- Post-Release Waste Array Evaluation (Chapter 4) – Presents the physical description and evaluation of observed array damage in Room 7.
- Ventilation Evaluation (Chapter 5) – Presents a summary of the ventilation conditions that existed both before and after the radiological release.
- Haul Truck Fire Evaluation (Chapter 6) – Presents an analysis of the fire that occurred on February 5, 2014, and demonstrates that this fire had no direct effect on the February 14, 2014, fire and release.
- Fire Analysis (Chapter 7) – Presents the analysis of the waste array condition described in Chapter 4 using the ventilation information described in Chapter 5.

The fire analysis segments the event by physical process. These segments are:

- Establishment of fire cause,
- Evaluation of the event timing,
- Explanation for initial fire expansion within the array, and
- Explanation for continued fire spread within the array.

All illustrations referenced in this document are provided in Appendix A. All photographs referenced using a designator or AIB-FST-xxxxx can be found in Appendix B.

2.0   FACILITY DESCRIPTION

This chapter provides a facility description of the WIPP facility.

The WIPP facility is a deep geologic repository located in southeastern New Mexico near Carlsbad. It was constructed to determine the efficacy of an underground repository for disposal of transuranic (TRU) waste (Figure 2-1) and was mined within a 2,000 foot-thick bedded-salt formation. The underground is 2,150 feet beneath the ground surface. TRU mixed waste management activities underground are confined to the southern portion of the 120 acre mined area.

Figure 2-1: Waste Isolation Pilot Plant near Carlsbad, New Mexico

Four shafts connect the underground area with the surface. The Waste Shaft (WS) headframe and hoist are located within the Waste Handling Building and are used to transport TRU mixed waste, equipment, and materials to the repository. The Waste Hoist can also be used to transport personnel and materials. The Air Intake Shaft (AIS) and the Salt Handling Shaft (SHS) provide ventilation to all areas of the underground except for the Waste Shaft station. This area is ventilated by the Waste Shaft itself. The SHS is also used to hoist mined salt to the surface and serves as the principal personnel transport shaft. The ES serves as a common exhaust air duct for all areas of the underground (Figure 2-2). The underground physical dimensions for the drifts and shafts provided by Nuclear Waste Partnership LLC (NWP) based on their ventilation system modeling inputs. Key values are reproduced in Table 2-1.

Table 2-1: Panel 7 Ventilation Flow Model Inputs [3]

Branch ID	Length, ft	Height, ft	Width, ft	Area, ft^2	Perimeter, ft
130	223.5	19.2	18.1	347.52	74.6
131	133	13 [a]	33	429	92
132	133	13 [a]	33	429	92
133	133	13 [a]	33	429	92
134	133	13 [a]	33	429	92
135	133	13 [a]	33	429	92
136	133	13 [a]	33	429	92
137	332.5	13 [a]	33	429	92
138	87.1	13 [a]	33	429	92
138	87.1	3.75	33	123.75	73.5
139	133	13 [a]	33	429	92
140	133	13 [a]	33	429	92
141	133	13 [a]	33	429	92
142	133	13 [a]	33	429	92
143	133	13 [a]	33	429	92
144	223.5	9.2	20	184	58.4
148	280.3	13 [a]	33	429	92
149	283.3	13 [a]	33	429	92
150	281.3	13 [a]	33	429	92
151	276.3	13 [a]	33	429	92
152	274.3	13 [a]	33	429	92
153	283.3	13 [a]	33	429	92
315	45.9	13 [a]	33	429	92
316	49.2	13 [a]	33	429	92
317	58.2	13 [a]	33	429	92
318	56.2	13 [a]	33	429	92
319	51.2	13 [a]	33	429	92
320	49.2	13 [a]	33	429	92
321	52.2	13 [a]	33	429	92

Note: [a] The height of all waste branches in Panel 7 were set to 13 feet, as described in the WIPP Documented Safety Analysis. [4 p. 2.20]
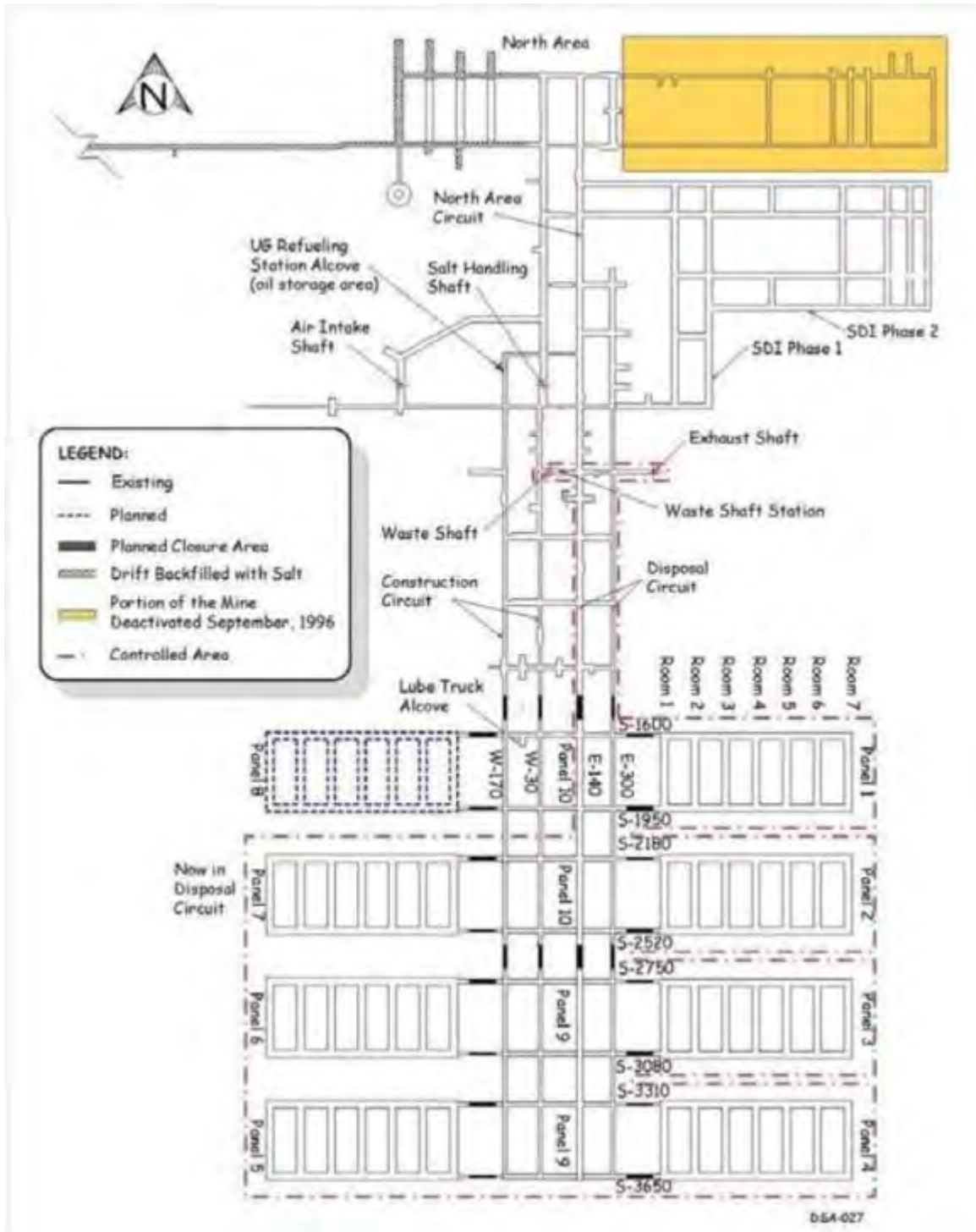
Figure 2-2: WIPP Underground Layout

The WIPP underground consists of the waste disposal circuit, construction circuit; north circuit intake, waste station circuit intake, and exhaust air intake. (See Illustration 1 in Appendix A). The location of the suspected waste container breach at Panel 7 and Continuous Air Monitor (CAM)-151 are shown in Figure 2-3.

The principle contact-handled (CH) waste operations at the WIPP involve the receipt and disposal of TRU waste, and the mining of underground rooms in which the waste is disposed. In the underground, the waste containers are removed from the waste hoist conveyance, placed on the underground transporter, and moved to a disposal room. In the disposal rooms, the CH waste containers are removed from the transporter and placed in the waste stack. Remote-handled (RH) waste is placed in boreholes in the walls (ribs) of the disposal rooms.
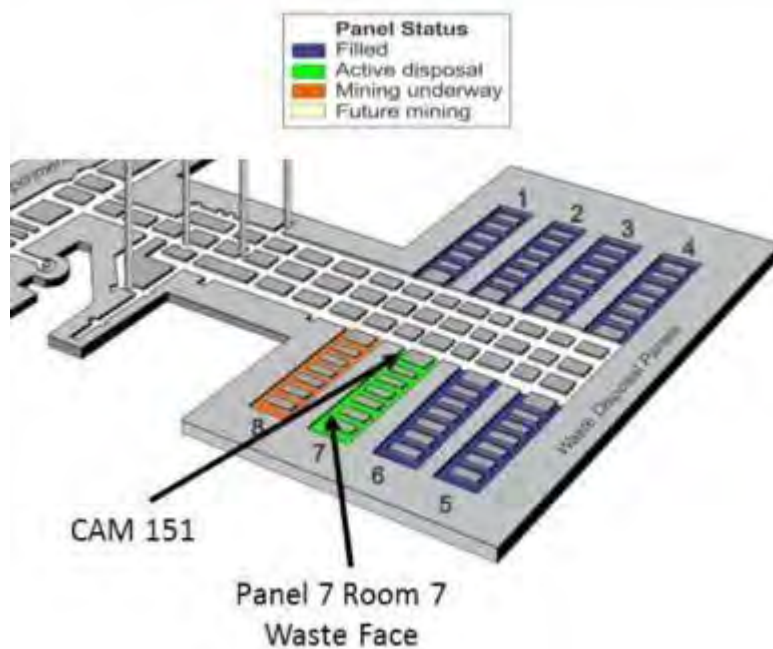
Figure 2-3: Location of Room 7 Panel 7 and CAM-151 in the WIPP Underground

Much of the TRU waste received at WIPP also contains hazardous constituents that are regulated under Resource Conservation and Recovery Act. WIPP has been issued a hazardous waste facility permit by the New Mexico Environment Department for Resource Conservation and Recovery Act authorization as a treatment, storage and disposal facility. TRU waste that has hazardous constituents is known as TRU mixed waste.

The WIPP site has 55 permanent buildings and four temporary buildings (trailers) in operation, one temporary building (lab trailer) in excess status, and various connexes (used for storage). The site buildings provide a total of 358,647 square feet of office and industrial space. Additional leased office space, the Skeen-Whitlock Building, is located in Carlsbad. Approximately 800 workers are assigned to the WIPP, representing the Carlsbad Field Office, the Maintenance and Operations contractor, the warehouse, the document services subcontractor, the information technologies subcontractor, the Carlsbad Field Office Technical Assistance Contractor, Los Alamos National Laboratory - Carlsbad, Sandia National Laboratories - Carlsbad, and the New Mexico Environment Department - Carlsbad. Prominent features of the WIPP site include:

- **AIS**. The primary source of intake air for the underground ventilation and also used for emergency egress. (See Figure 2-2.)

- **Waste Handling Building**. This structure provides a confinement barrier. Ventilation is operated to maintain a negative pressure with high-efficiency particulate air (HEPA) filtration.
- **Waste Hoist**. The Waste Hoist transports waste, material and personnel from the surface to the underground and is designed to prevent an uncontrolled fall or descent of the waste conveyance into the Waste Shaft. (See Figure 2-2.)
- **SHS Hoist**. This hoist transports mined salt to the surface, material, and personnel between the surface and the underground. (See Figure 2-2.)
- **Radiation Monitoring**. Consists of CAMs, fixed air samplers, and other external radiation monitors.
- **Central Monitoring Room**. Provides a monitoring function and must be staffed and operational, with the ability to shift underground ventilation to filtration.
- **Underground Ventilation System**. Provides acceptable working conditions and a life-sustaining environment during normal operations and off-normal events, including waste handling events.
- **Exhaust Filter Building**. Contains the underground ventilation exhaust HEPA filtration equipment and is located north of the Exhaust Shaft.
- **Waste Handling Equipment**. Selected items are designated safety class or safety significant.
- **Emergency Services Bay**. Houses the ambulance, rescue truck, and fire engine.
- **Guard and Security Building**. Houses the security monitoring and alarm systems.
- **Parking Lot**. The east portion of the front parking lot is used for employee parking, and the two west rows of the lot are designated for trailer storage and staging of empty TRU package transporters for U.S. Department of Energy (DOE) carrier transport to the generator sites and trailer maintenance facility.

3.0   WASTE DESCRIPTIONS

This chapter describes the configuration of waste in Panel 7 prior to the release event. The topics covered in the section include:

- Panel 7 Room Arrangement;
- Room 7 Individual Package Descriptions;
- Room 7 Package Components;
- Room 7 Package Assemblies;
- Room 7 Contact Handled Waste Array; and
- Room 6 and 7 Remote Handled Waste.

3.1.   Panel 7 Room Arrangement

Panel 7 consisted of seven disposal rooms with an intake and an exhaust drift. Each room within the panel was approximately 33 feet wide by 13 feet high by 280 feet long. Room 7 was larger than the other six rooms, having a length of approximately 332.5 feet. The width and height measurements are the same. Each disposal room was separated from the adjacent room(s) by pillars of salt approximately 100 feet wide and 280 feet long. The panel intake drift was approximately 18 feet wide by 19 feet high, while the exhaust drift was approximately 20 feet wide by 9 feet high. The dimensions for the rooms and drifts were provided by NWP. Illustration 2, in Appendix A, provides a layout of Panel 7.

Each room was designed for disposal of both CH waste and RH waste. The CH waste array is described in Section 3.4. At the time of the release fire event, only Room 7 contained CH waste material in Panel 7. The RH waste present in Panel 7 is described in Section 3.5.

A bulkhead was installed between each room and the exhaust drift. A typical bulkhead is shown in Illustration 3. The exhaust-side of the Room 7 bulkhead is shown in AIB-FST-11136.

3.2.   Room 7 Individual Package Descriptions

This section provides generic descriptions of the individual waste packages that constitute the waste array in Panel 7 Room 7.

3.2.1.   55-Gallon Drum

The 55 gallon drum (55GD) containers are a Department of Transportation (DOT) Type 7A steel drum that comes in a 17C model or a 17H model, both with a lap-welded bottom and numerous lid configurations. (See Illustration 4.) They have a maximum gross weight of 1,000 lbs. The 17C drum is approximately 0.06 inches thick and the 17H drum is approximately 0.05 inches thick. A typical 55GD has a gross internal volume of approximately 7 ft^3. A HEPA vent filter is

installed on each 55GD, which contains waste,[*] to prevent the buildup of internal pressure and limit particulate leakage during shipment, staging, and emplacement.

3.2.2.   100-Gallon Drum

The 100 gallon drum (100GD) containers are a DOT Type 7A steel drum that can either be direct loaded or loaded with compacted 55GD (see Illustration 5). They have a maximum gross weight of 1,000 lbs. A typical 100GD has a height of 35 inches, a diameter of 32 inches, and a gross internal volume of approximately 13 ft^3. A HEPA vent filter is installed on each 100GD, which contains waste, to prevent the buildup of internal pressure and limit particulate leakage during shipment, staging, and emplacement.

3.2.3.   Standard Waste Box

The Standard Waste Box (SWB) is a DOT Type 7A steel-fabricated box with a lap-welded bottom and an internally flanged, bolted closure lid. (See Illustration 6.) The weight of an empty SWB is approximately 680 lbs and the maximum gross weight of a loaded SWB is 4,000 lbs. One to four HEPA vent filters are installed on each SWB to prevent the buildup of internal pressure and limit particulate leakage during shipment, staging, and emplacement. The quantity of filters varies and would have been established by the waste generator based on the contents of the box. A typical SWB has an internal volume of approximately 66 ft^3.

3.2.4.   10-Drum Overpack

The 10-Drum Overpack (TDOP) is a DOT Type 7A welded-steel cylinder that may contain up to 10 standard 55GD or one SWB. (See Illustration 7.) An empty TDOP weighs approximately 1,600 lbs and has a maximum loaded weight of 6,700 lbs. A typical TDOP is approximately 74 inches tall and 71 inches in diameter. Multiple HEPA vent filters are installed on each TDOP to prevent the buildup of internal pressure and limit particulate leakage during shipment, staging, and emplacement. Filter ports are located near the top of the TDOP. A typical TDOP has an internal volume of approximately 155 ft^3.

3.2.5.   Standard Pipe Overpack

The Standard Pipe Overpack (POP) consists of a stainless-steel pipe component surrounded by fiberboard and plywood dunnage in a DOT Type 7A 55GD with a rigid polyethylene liner and lid. (See Illustration 8.) The pipe components are a stainless-steel pipe with a closed-bottom cap and a bolted stainless-steel lid sealed with a butyl rubber O-ring. (See Illustration 9.) This configuration comes in a six inches diameter and a 12 inches diameter. Both are 2 feet long. The maximum weight of the six inch diameter POPs are 328 lbs, while the 12 inches diameter POP is 547 lbs. [4 p. 2.100]

---

[*] A dunnage drum, which is an empty drum used when the waste drum count in a 55GD assembly is less than seven, does not contain waste so does not typically have a filter.

3.2.6. Standard Large Box 2

The Standard Large Box 2 (SLB2) containers are a DOT Type 7A steel-fabricated box with a lap-welded bottom and an internally flanged, bolted closure lid. (See Illustration 10.) SLB2s weigh approximately 2,700 lbs and have a loaded maximum gross weight of 10,500 lbs. Each SLB2 is approximately 108 inches long, 69 inches wide and 73 inches high. Threaded couplings are installed on each side of the SLB2 provide for the insertion of HEPA vent filters to prevent the buildup of internal pressure and limit particulate leakage during shipment, staging, and emplacement. Each SLB2 has an internal volume of approximately 246 ft^3.

3.3. Room 7 Package Components

This section provides generic descriptions of the waste package and waste assembly components that were part of the waste array in Panel 7 Room 7 on February 14, 2014.

3.3.1. Vent Filters

Each waste container was furnished with at least one HEPA vent filter. A typical filter has a carbon-carbon composite filter media. There was no standard vent filter for use on the waste containers. The quantity and type were determined by the waste generator.

3.3.2. Reinforcement Plate

A typical reinforcement plate is shown in Illustration 11. They were placed on the top of a drum assembly to add rigidity to the assembly and to protect the drums from material handling impacts. The plates are made of a high density polyethylene (HDPE). [5] A typical plate for 55GD plate has a thickness of 0.15 inches [6] and weighs approximately 22.6 lbs. [5] A typical 100GD reinforcement plate weighs 20.7 lbs.

3.3.3. Drum Assembly Slip Sheet

A typical 55GD slip sheet is shown in Illustration 12. They are used to correctly arrange seven 55GDs so they can be shipped and stored as one assembly. The sheets were made of a high-density polyethylene. [5] A typical sheet has a thickness of 0.15 inches and weighs approximately 20.8 lbs. [5] Slip sheets for 100GDs typically weigh 19.4 lbs. They are used to correctly arrange three 100GDs.

3.3.4. Super Sack Slip Sheet

A typical super sack slip sheet is shown in Illustration 13. They were placed under each MgO super sack to permit handling with a push-pull lift assembly. The sheets were made of high-density polyethylene. [5] A typical sheet has a thickness of 0.15 inches [7] and weighs approximately 18.8 lbs. [5]

3.3.5. SWB &TDOP Slip Sheet

A typical SWB &TDOP Slip Sheet is shown in Illustration 14. They were placed under SWB and TDOP containers to permit handling with a push-pull lift assembly. They are fiberboard cut

into an octagon shape. They are 61.5 inches wide and 77 inches long with a minimum thickness of 0.09 inches. [8] A typical sheet weighs approximately 7 lbs.

3.3.6. MgO Super Sack

A typical super sack is shown in Illustration 15. They are constructed from woven polypropylene fabric and cardboard, filled with MgO, and tied off at the top with a fastener. [9] The sacks are hexagonal shape, nominally 61 inches across the flats, and nominally 25.5 inches high. They have a volume of 47.6 ft^3. The length of the cardboard insert that goes into each side is 2 feet, 7.375 inches and the height is 1 foot, 7.5 inches. [10] The sacks are constructed such that they retains its shape well enough to not deform beyond a 65 inch hexagon with 12 inches radius corners after filling and shipping. Each sack contained either 3,000 lbs or 4,200 lbs of MgO.

3.3.7. Room 7 Package Assemblies

This section provides descriptions of the waste packages that constituted the waste array in Panel 7 Room 7 on February 14, 2014.

3.3.8. 55-Gallon Drum Assembly

A typical 55GD assembly is shown in Illustration 16. Each assembly consisted of seven containers assembled on a slip sheet with a reinforcement plate placed on top. The top half was then wrapped with stretch wrap to keep the containers in a tight packet. The containers in a 55GD assembly may be direct loaded drums or POPs. In some cases one or more dunnage drums, which are empty drums, are placed in an assembly to ensure assembly stability. Dunnage drums are used when the total waste container count does not equal seven because of waste acceptance criteria limitations.

3.3.9. 100-Gallon Drum Assembly

A typical 100GD assembly is shown in Illustration 17. The assembly consisted of three 100GDs assembled on a slip sheet with a reinforcement plate placed on top. The top half was then wrapped with stretch wrap to keep all of the containers in a tight packet. In some cases one or two dunnage drums are placed in an assembly to ensure assembly stability.

3.3.10. Standard Waste Box Assembly

A typical SWB assembly consisted of a SWB placed on top of a cardboard slip sheet.

3.3.11. 10-Drum Overpack Waste Assembly

A typical TDOP assembly consisted of a TDOP placed on top of a cardboard slip sheet.

3.4. Room 7 Contact Handled Waste Array

Waste container assemblies were initially placed near the bulkhead in the back of a room. This was designated as Row 2. As additional containers were introduced to the room, they were

placed adjacent to the previous row. As the room was filled, the working face moved away from the bulkhead.

Illustration 18 and Illustration 19 present the arrangement of the waste array on February 14, prior to the release event. The face of the array as it existed on the afternoon of February 14 is shown in photograph AIB-FST-01002. No change in the arrangement occurred between February 5 and February 14, 2014. Table 3-1 summarizes the container assembly type that is in each location within the array.

The content of each waste container was inspected using real-time radiography and captured in the WIPP Waste Data System. The contents of the containers are categorized based on the groupings in Table 3-2. Categories 1 through 12 are waste container contents. Typically, the materials fitting categories 1 through 8 are explicitly categorized and the mass is estimated. The mass split for categories 9 through 12 is usually established based on the waste stream information. The mass associated with categories 13 through 22, which involve packaging or emplacement material, are based on standard default values for each waste container type.

Table 3-3 summarizes the mass of material present by location within the array. The information in these tables was developed from information in the WIPP Waste Data System. Illustration 20 indicates the quantity of combustibles outside of the waste containers by location (row:column). The color thresholds are set at 10 kg and 15 kg. Illustration 20 presents the same information, but includes the elevation. The combustible loading analysis, as shown in Illustration 20, is subject to round-off error.

3.4.1.   MgO Stack Density

The density of MgO stack placement has evolved with time. Photograph AIB-FST-01003 provides an image from *Appendix MgO: Magnesium Oxide as an Engineering Barrier.*[11] The commitment was to emplace "the MgO super sacks on every other row of waste stacks, and adjusted this frequency if necessary to accommodate high cellulose, plastic, and rubber (CPR) waste streams." Photograph AIB-FST-01002 has substantially fewer MgO super sacks.

3.4.2.   Combustibles in Array

Table 3-4 presents the waste array contents for R2:C6 as it was extracted from the WIPP Waste Data System. (R2:C6 is presented since it is the first stack listed in Table 3-1 with a 55GD unit. It is provided as an example.) The exposed emplacement combustibles in this location based on the waste container descriptive material (see Sections 3.2, 3.3 and 3.4) are presented in Table 3-5. The quantity of plastics at this location is 40 percent higher than are indicated in the Waste Data System (WDS).

Table 3-1: Room 7 Waste Array Pre-release Configuration

Location[*]	MgO bag weight, lbs	Assembly[**]		
		Top	Middle	Bottom
R02:C2	4,200	SWB OP (2)	NA	SLB2
R02:C4	4,200	SWB	NA	SLB2
R02:C6	4,200	55GD (5)	NA	SLB2
R03:C1	4,200	55GD (5)	NA	TDOP (10)
R03:C3	4,200	55GD (5)	NA	TDOP (10)
R03:C5	4,200	100GD (3)	NA	TDOP (10)
R04:C2	4,200	100GD (3)	NA	TDOP (10)
R04:C4	3,000	SWB OP (2)	NA	TDOP (10)
R04:C6	3,000	SWB	NA	TDOP (10)
R05:C1	None	55GD (5)	NA	TDOP (10)
R05:C3	None	SWB	NA	TDOP (10)
R05:C5	None	SWB	NA	TDOP (9)
R07:C1	None	SWB OP (4)	NA	SLB2
R07:C3	None	SWB	NA	SLB2
R07:C5	None	SWB OP (4)	NA	SLB2
R08:C2	3,000	SWB	NA	TDOP (10)
R08:C4	3,000	SWB	NA	TDOP (10)
R08:C6	4,200	SWB	NA	TDOP (10)
R09:C1	None	SWB OP (2)	NA	TDOP (10)
R09:C3	None	POP (6)	NA	TDOP (10)
R09:C5	None	POP (7)	NA	TDOP (9)
R10:C2	4,200	55GP (5)	NA	TDOP (10)
R10:C4	4,200	55GP (5)	NA	TDOP (10)
R10:C6	4,200	100GD (3)	POP (7)	POP (7)
R11:C1	None	100GD (3)	SWB	SWB
R11:C3	None	SWB	NA	TDOP (10)
R11:C5	None	SWB	SWB	SWB
R12:C2	4,200	SWB OP (4)	NA	TDOP (6)
R12:C4	4,200	SWB	SWB	SWB
R12:C6	4,200	SWB OP (4)	NA	TDOP (6)
R13:C1	None	SWB OP (4)	SWB OP (4)	SWB
R13:C3	None	SWB	55GD (5)	55GD (5)
R13:C5	None	SWB	SWB	SWB
R14:C2	4,200	100GD (3)	100GD (3)	100GD (3)
R14:C4	4,200	SWB	SWB	SWB OP (4)
R14:C6	4,200	SWB	NA	TDOP (6)
R15:C1	None	SWB OP (4)	NA	TDOP (6)
R15:C3	None	55GD (7)	NA	TDOP (10)
R15:C5	None	SWB OP (4)	55GD (5)	55GD (5)
R16:C2	4,200	SWB	NA	TDOP (10)
R16:C4	4,200	55GD (5)	NA	TDOP (10)

Location[*]	MgO bag weight, lbs	Assembly[**]		
		Top	Middle	Bottom
R16:C6	4,200	SWB OP[***] (4)	NA	TDOP (10)
R17:C1	None	SWB	NA	TDOP (10)
R17:C3	None	SWB OP (4)	NA	TDOP (10)
R17:C5	None	SWB OP (4)	NA	TDOP (10)
R18:C2	3,000	SWB	SWB	SWB
R18:C4	3,000	SWB OP (4)	NA	TDOP (10)
R18:C6	3,000	SWB	POP (6)	POP (7)
R19:C3	None	SWB	NA	TDOP (6)
R20:C2	3,000	SWB OP (4)	NA	SLB2
R20:C4	3,000	SWB	NA	TDOP (10)
R20:C6	3,000	SWB OP (4)	NA	SLB2
R21:C1	None	SWB OP (2)	NA	TDOP (10)
R21:C3	None	SWB OP (2)	NA	TDOP (10)
R21:C5	None	SWB OP (4)	NA	TDOP (10)
R22:C2	3,000	SWB OP (4)	NA	TDOP (10)
R22:C4	4,200	SWB	NA	TDOP (10)
R22:C6	3,000	SWB	SWB	SWB
R23:C1	None	SWB	NA	TDOP (10)
R23:C3	None	POP (7)	NA	TDOP (10)
R23:C5	None	POP (5)	POP (6)	POP (7)
R24:C2	3,000	SWB	SWB	SWB

* Row:Column

** Number in brackets represents the number of waste filled drums per specified assembly.

*** Standard Waste Box Overpack.

Table 3-2: Waste Code Matrix

Material Parameter	Description	Category	Group
1	Iron base metal alloys	Waste material	FE
2	Aluminum base metal/alloys	Waste material	Non-FE
3	Other metal/alloys	Waste material	Non-FE
4	Other inorganic materials	Waste material	Other
6	Cellulosics	Waste material	CPR
7	Rubber	Waste material	CPR
8	Plastics	Waste material	CPR
9	Solidified inorganic material	Waste material	Other
10	Solidified organic material	Waste material	Other
12	Soils	Waste material	Other
13	Steel container materials	Steel packaging material	FE
14	Plastic/liners container materials	Plastic packaging material	CPR
15	Cellulosics packaging materials	Cellulosic packaging material	CPR
16	Magnesium oxide	Emplacement material	MgO
17	Steel emplacement material	Emplacement material	FE
18	Cellulosic emplacement material	Emplacement material	CPR
19	Rubber emplacement material	Emplacement material	CPR
20	Plastic emplacement material	Emplacement material	CPR
21	Steel liner materials	Steel liner material	FE
22	Lead packaging material	Non-ferrous metal packaging material	Non-FE

Table 3-3: Room 7 Waste Array Content Summary

| Location* | Waste Contents & Packaging, kg | | | | Emplacement Material, kg | | Total, kg |
	Non-Combustible (except Solidified Inorganic)	Combustible (except Solidified Organic)	Solidified Inorganic	Solidified Organic	MgO	Combustibles	
R02:C2	1742	135	21	0	1905	11	3813
R02:C4	1967	363	0	0	1905	11	4246
R02:C6	2998	549	802	0	1905	24	6277
R03:C1	1303	132	216	922	1905	27	4505
R03:C3	1315	132	424	904	1905	27	4707
R03:C5	1555	436	0	1006	1905	25	4927
R04:C2	1404	610	0	919	1905	25	4863
R04:C4	1557	93	1	1158	1361	14	4184
R04:C6	1562	107	1	999	1361	14	4045
R05:C1	1289	140	599	993	0	21	3041
R05:C3	1745	280	0	831	0	7	2863
R05:C5	1957	275	0	914	0	7	3154
R07:C1	1815	210	1124	0	0	4	3153
R07:C3	2157	456	15	0	0	4	2632
R07:C5	1855	363	1159	0	0	4	3381
R08:C2	1504	107	0	1003	1361	14	3989
R08:C4	1461	84	886	926	1361	14	4733
R08:C6	1454	82	836	821	1905	14	5113
R09:C1	1489	133	7	1012	0	7	2648
R09:C3	1705	328	0	1024	0	21	3078
R09:C5	1794	366	0	780	0	21	2960
R10:C2	1276	126	340	959	1905	27	4634
R10:C4	1290	174	481	1065	1905	27	4943
R10:C6	2098	828	313	0	1905	55	5200
R11:C1	1268	389	1709	0	0	22	3387
R11:C3	1458	80	871	895	0	7	3311
R11:C5	1203	9	2519	0	0	11	3743
R12:C2	1576	29	2180	0	1905	14	5704
R12:C4	1102	89	1826	0	1905	18	4939
R12:C6	1634	48	2323	0	1905	14	5924
R13:C1	1809	159	1739	0	0	11	3718
R13:C3	845	97	1712	0	0	37	2692

| Location* | Waste Contents & Packaging, kg | | | | Emplacement Material, kg | | Total, kg |
	Non-Combustible (except Solidified Inorganic)	Combustible (except Solidified Organic)	Solidified Inorganic	Solidified Organic	MgO	Combustibles	
R13:C5	1210	24	2485	0	0	11	3730
R14:C2	2371	673	0	0	1905	51	4999
R14:C4	1118	223	1177	0	1905	18	4441
R14:C6	1550	10	2306	0	1905	14	5785
R15:C1	1655	57	2459	0	0	7	4179
R15:C3	1247	132	1620	969	0	21	3989
R15:C5	992	146	1950	0	0	37	3126
R16:C2	1402	301	5	1120	1905	14	4748
R16:C4	1287	135	436	1027	1905	27	4817
R16:C6	1550	124	1172	1029	1905	14	5795
R17:C1	1410	92	1	1083	0	7	2593
R17:C3	1551	119	1235	947	0	7	3859
R17:C5	1550	127	1160	1096	0	7	3940
R18:C2	1214	18	2612	0	1361	18	5222
R18:C4	1550	119	1204	1027	1361	14	5275
R18:C6	1792	555	830	0	1361	44	4582
R19:C3	1473	27	1270	0	0	7	2777
R20:C2	2810	918	1120	0	1361	11	6219
R20:C4	1466	20	1230	0	1361	14	4090
R20:C6	1689	499	1156	0	1361	11	4715
R21:C1	1488	130	23	848	0	7	2497
R21:C3	1572	120	26	1187	0	7	2913
R21:C5	1551	120	1130	1112	0	7	3920
R22:C2	1565	115	1074	997	1361	14	5125
R22:C4	1455	92	923	919	1905	14	5308
R22:C6	1202	28	2581	0	1361	18	5189
R23:C1	1457	92	886	900	0	7	3343
R23:C3	1778	369	0	1021	0	21	3189
R23:C5	1940	748	0	0	0	50	2738
R24:C2	1202	19	2553	0	1361	18	5153
Total	97286	13559	56726	32414	57692	1087	258763

* Row:Column

Table 3-4: Waste Emplacement Records for Row 2:Column 6 (R02:C6)

Row	Column	Tier	Container type	Waste Material							Packaging				Emplacement materials		
				Iron MP01	Other metal MP03	Inorganics MP04	Cellulosic MP06	Rubber MP07	Plastic MP08	Solidified inorganic MP09	Steel packaging MP13	Plastic liners MP14	Cellulosic packaging MP15	Steel dunnage Other – MP13	MgO MP16	Cellulosic MP18	Plastic MP20
2	6	S1	MgO												1,905.00	3.45	3.45
2	6	T	55GD		8.00		1.50		4.00	151.10	27.70	2.00	3.70				16.80
2	6	T	55GD		31.60				6.00	115.00	27.70	2.00	3.70				
2	6	T	55GD	10.00	23.00				1.00	195.60	27.70	2.00	3.70				
2	6	T	55GD	5.00	23.00					201.60	27.70	2.00	3.70				
2	6	T	55GD	10.00	8.00				6.00	138.60	27.70	2.00	3.70				
2	6	T	55GD											28.6			
2	6	B	SLB2	1454.80		3.80	277.50	3.10						28.6			
2	6			1479.80	93.60	3.80	279.00	3.10						57.20	1,905.00	3.45	20.25

Table 3-5: Row 2:Column 6 (R2:C6) Emplacement Combustibles

Component	Cellulosic material (MP18) kg	Plastic material (MP20) kg
Polyethylene reinforcement plate	0.0	9.4
Polyethylene slip sheet drum	0.0	9.4
Polyethylene stretch wrap	0.0	0.2*
Bump pads (sorbtex)	0.0	0.2*
MgO polyethylene slip sheet	0.0	8.5
MgO polypropylene bag	3.45*	0.5*
Total	3.45	28.2

*Assumed

3.5. Panel 7 Remote Handled Waste

The RH waste was emplaced in Panel 7 as shown in Illustration 21. Each horizontal borehole was 30 inches in diameter, approximately 17 feet deep, and 64 inches off the floor (see photograph AIB-FST-01004). The content of each location is summarized in Table 3-6. Only 16 of the 50 boreholes in Room 7 were filled. In Room 6, only two locations were filled.

The boreholes were nominally spaced 8 feet on center. Illustration 22 shows a typical layout for boreholes. In disposal rooms, the boreholes are kept 26 feet from a corner. The panel specific layout is provided in Illustration 23. For the Room 7 exhaust drift, where the CH waste involved in the release event is located, there were no boreholes.

After each RH waste canister was slipped into a borehole, a shield plug was then slipped into position (see photograph AIB-FST-01005). The plug's function was to reduce radiation exposure to workers in the disposal panel. Shield plugs are concrete-filled steel shells that weigh approximately 3,900 lbs. They are 29 inches in diameter and 61 inches long. While a steel shield ring could have been installed after the plug, no such rings were used in Panel 7.

On February 5, the day of the haul truck fire, a waste canister was inserted at borehole 075. This was followed by a shield plug. This process was completed before the emergency evacuation alarm (yelp) sounded at about 1051. No additional RH waste has been emplaced in Panel 7 since February 5.

Table 3-6: Remote Handled Waste in Panel 7

Room	Borehole	Plastic waste material kg	Steel packaging material kg	Plastic packaging material kg	Steel liner material kg
6	073	14.8	90.6	0	0
	075	4.2	43.18	0	0
7	027	104.4	49.08	14.28	55.4
	029	12.8	132.3	0	0
	031	74.7	49.08	21.42	0
	032	5.4	88.2	0	0
	033	1.2	44.1	0	0
	034	78.9	49.08	21.42	0
	035	76.9	49.08	21.42	0
	036	97.2	49.08	0	166.2
	037	50.2	32.72	0	110.8
	038	72.5	49.08	0	170.7
	039	87.8	49.08	0	170.7
	040	88.7	49.08	0	170.7
	041	93.2	49.08	0	166.2
	042	80.4	49.08	11.1	155.1
	043	73.5	49.08	21.42	0
	044	52.8	32.72	0	110.8
Total		1050.6	869.92	111.06	1276.6

4.0   POST-RELEASE WASTE ARRAY EVALUATION

This chapter provides a description of the array damage that was identified through visual inspections of the Panel 7 Room 7 waste array.[*] The visual inspections were conducted in two phases. Phase 1 occurred between April 23 and May 30, 2014. Phase 2 occurred in January 2015 using equipment capable of reaching all the locations in the array. These visual inspections provided a means to identify material discoloration, deformation, melting, and char. The inspections also allowed observation of container damage (e.g., with deformation, ejected material, and lid loss) but not container seal leakage or internal container damage. Cumulatively, these inspections resulted in a systematic and comprehensive evaluation of the array damage.

This chapter arrangement contains a short generalized damage assessment that presents the overall damage in context (Section 4.1), a description of the rib and back (roof) inspection evidence (Section 4.2), and a description of the bulkhead inspection evidence (Section 4.3). These sections are then followed by sections that describe the visually acquired damage evidence grouped by row and column (Sections 4.4 through 4.25). Key observations described in this chapter are:

- The intensity of the overall fire was low to moderate.
- Direct fire effects were primarily in Rows 8 through 18 of the array.
- Damage within the array was not uniform and there were multiple small fires that caused direct flame impingement on several waste packages.
- The fire self-extinguished without consuming all combustibles present.
- Los Alamos National Laboratory waste drum 68660, which was at R16:C4, was the only waste container in the array with evidence of bulging, buckling or other permanent deformation associated with the release event.

4.1.   Array Damage Summary

The array inspections and visual evaluation demonstrated that the primary fire damage was intermittently dispersed in the array between Rows 8 through 18. Figure 4-1 provides an overview of the array damage, which is more fully described in Sections 4.4 through 4.25. No physical damage was evident for waste containers in Rows 2 through 7 (yellow box in Figure 4-1), or Rows 19 through 24 (red box in Figure 4-1). The most significant damage occurred in the regions marked in blue on Figure 4-1.

There was wide variation in local temperatures during the event that would have been dependent on local flaming behaviors. Areas within the array had undamaged, but exposed, polyethylene stretch wrap and MgO super sack polypropylene fabric, both materials with low temperature melting thresholds. As such, local temperatures ranged from ambient to about 1,000°C (flame

---

[*] Photographs collected throughout this process are contained in Appendix B and cited in the text using the applicable photograph identification number (e.g. AIB-FST-#####) noted parenthetically.

temperature). The lack of uniformity in temperatures and the nonuniform damage supports the conclusion that flashover[*] did not occur in Panel 7 Room 7.
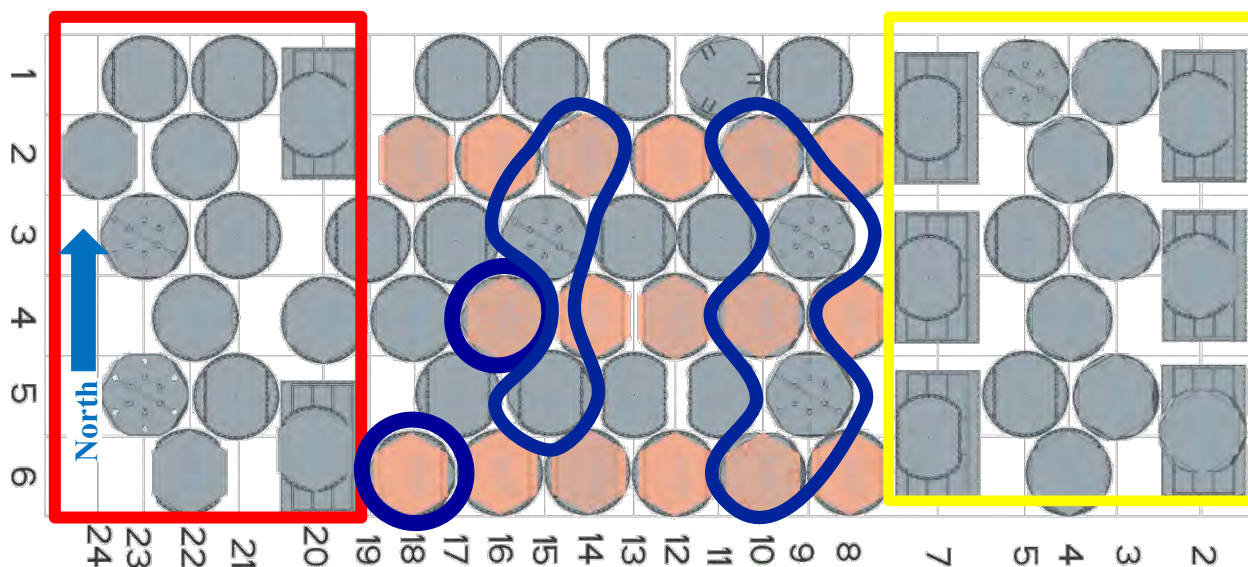
Figure 4-1: Array Damage Summary

The inspections did not identify any evidence of container relocation or significant horizontal displacement of the MgO after original emplacement. Movement of the MgO during the release event was dominated by gravity. Additionally, there was no indication of bulged, buckled, dented, or torn waste containers that could not attributed to material handling activities or a fire. These observations support the conclusion that the fire was not initiated by or accompanied by a detonation.

The visual inspections identified slight localized discoloration of the Panel 7 Room 7 south rib (wall) that was the result of fire exposure. There were no such discolorations of the north rib, back (overhead), or bulkhead and no significant accumulations of soot on these three surfaces.

Rows 2 through 7 contained a mix of TDOPs, SWBs, 55GD assemblies, 100GD assemblies, and SLB2s. These rows were closest to the bulkhead. There was one fiberboard slip sheet that had localized char damage; it was at R7:C5. This was the only fire-related damage in Rows 2 through 7. The inspections identified no fire-related damage to the polyethylene stretch wrap or the polypropylene super sacks in these rows. The lack of damage to the stretch wrap in these rows establishes that the bulk air temperature passing over the array was low, nominally below 135°C, which is the upper value of the melting temperature range of the polyethylene stretch wrap[†] (AIB-FST-10093, AIB-FST-10164, and AIB-FST-11145).

---

[*] A flashover is "a transition phase in a ….compartment fire which surfaces exposed to thermal radiation reach ignition temperature more or less simultaneously and fire spreads rapidly throughout the space." [NFPA 921, pg 16]

[†] The upper value melting temperature range for the polypropylene fabric used for the MgO super sacks is higher, 176°C.

Rows 19 through 24 contained a mix of TDOPs, SWBs, 55GD assemblies, and Standard Large Box Type 2s. These rows were closest to the array face. With the exception of some char material from a cardboard stiffener that had fallen onto R:19:C3 from R18:C2, the inspections identified no fire-related damage in these rows.

Rows 8 through 18 contained a mix of TDOPs, SWBs, 55GD assemblies, and 100GD assemblies. Damage in these rows was not uniform and there were multiple small fires that caused direct flame impingement on several waste packages. Some locations exhibit evidence of significant flame impingement on waste containers (i.e., clean burn, where all paint and surface carbon has been burned away). In other locations the stretch wrap was undamaged, but surrounded by fire damage. With the exception of the MgO super sack at R18:C4, which had minor fire damage, the fabric on the other 17 sacks in rows 8 through 18 was badly damaged or missing. Throughout this region MgO had accumulated on the exposed horizontal surfaces and the floor. The depth in some locations was sufficient to obscure most of the bottom tier assembly (AIB-FST-10044, AIB-FST-10226, AIB-FST-10319, and AIB-FST-10959).

Visual damage within the waste array was most severe at, or near, locations with 55GD and 100GD assemblies. These were locations with higher quantities of combustibles external to the waste containers such as fiberboard and polyethylene slip sheets, reinforcement plates, stretch wrap, cardboard stiffeners and polypropylene super sack fabric. Evidence of both melting and ignition were identified at these locations.

The array inspections and evidence evaluation identified just one location with a partially separated waste container lid, and no locations indicating other fire-related container deformation. The partially separated lid occurred at R16:C4 where the lid to waste drum 68660 was deflected upward from its original position (AIB-FST-02085 and AIB-FST-02107).

As has already been indicated in this section, the observed physical damage resulting from fire exposure can be used to judge the range of temperature and heat flux exposure to specific components present in or near flames. These thresholds are introduced where they first occur within this chapter. Common heat flux damage thresholds include:

- Maximum heat flux as currently measured in a post-flashover fire compartment; [12] 170 kW/m^2
- Flux at floor that exists just prior to flashover; [12] 20 kW/m^2
- Wood volatiles ignite with extended exposure and piloted ignition; [12] 12.5 kW/m^2
- Human skin experiences pain with a 13-sec. exposure and blisters in 29 sec. with second-degree burn injury; [12] and 5 kW/m^2
- Nominal solar constant on a clear summer day. [12] 1 kW/m^2

4.1.1. Back, Ribs and Bulkhead

The array inspections and evidence evaluation identified localized discoloration of the Panel 7 Room 7 south rib (wall) that was the result of fire exposure. There were no such discolorations of the north rib, back (overhead), or bulkhead and no significant accumulations of soot on the back, ribs or bulkhead. Aside from the bulkhead fabric seals, the material most susceptible to thermal damage for these features is the galvanized steel on the back. The melting point of the

zinc, which was the material coating the steel ground control fabric, is 375°C. [12] There was no evidence of melting or the whitish coating from zinc oxidation that is often observed on fire-exposed galvanized steel. (12)

4.1.2. Stretch Wrap

Polyethylene stretch wrap was used to stabilize the 55GD and 100GD assemblies. The array inspections and evidence evaluation identified multiple locations in rows 8 through 18 where the stretch wrap was damaged (AIB-FST-10661). It also identified locations where there was no damage.

Polyethylene is a thermoplastic, so has no explicit melting point; rather it will soften, melt, and flow over the temperature range of 122 to 135°C. [12] This wrap was thin (120 gage, 0.0012 inches, 0.030 mm), as such, the thermal mass was negligible and any thermal exposure that could heat the material to about 130°C would result in deformation. When exposed to a flame, the stretch wrap could melt and fall away from the fire exposure or ignite. [13 p. 816] Both behaviors might be observed depending on the geometry and local conditions. Evidence of melting was observed in the array. Visual evidence of ignition is unlikely because the vertical configuration facilitates complete combustion should ignition occur.

There was wide variation in local temperatures during the event that would have been dependent on local flaming behaviors. As such, local temperatures ranged from ambient to about 1,000°C (flame temperature). Temperatures near the Panel 7 Room 7 bulkhead were nominally below 135°C based on the undamaged polyethylene stretch wrap and super sack polypropylene fabric.

4.1.3. MgO Super Sacks

The array inspections and evidence evaluation demonstrated that all of the MgO super sacks in Rows 8 through 18 were damaged. With the exception of the MgO super sack at R18:C4, the polypropylene fabric that formed the sacks was severely damaged or missing from most of these locations. In some locations remnants of fabric were present on top of the residual MgO, horizontal materials within the array, and on the floor of Room 7 (AIB-FST-10479, AIB-FST-10522, and AIB-FST-10624). When the fabric was damaged, the cardboard stiffeners collapsed, the MgO flowed and formed piles of loose material at the damaged MgO super sack locations. At most of these locations the angle of repose (e.g., slope) was very steep, almost 60°, indicating gravity was the dominant force acting on the MgO after the super sacks were damaged by or consumed by the fire.

The fabric damage was caused by melting or ignition (AIB-FST-02104); evidence of both mechanisms was identified during the array inspections.

Melting. Polypropylene is a thermoplastic with a melting temperature in the range of 160°-176°C. [12] As the temperature of the fabric approaches this range the tensile strength will decrease, the material will tear, and the sack will release the MgO. Vertical sections of fabric will fall away as the MgO shifts. Horizontal sections may solidify and adhere to the MgO (AIB-FST-10036, AIB-FST-10303, and AIB-FST-10416). This accounts for the crust behavior observed at R14:C4.

Ignition. Polypropylene is categorized as an easy-to-ignite material. [14] The ignition time for thin, non-fire-retardant polypropylene (3 mm, 0.13 inches) is 27 seconds for an exposure of 50 kW/m^2 and 117 seconds for an exposure of 20 kW/m^2. [15 p. 45] Extrapolation of this data demonstrates that a heat flux of 80 kW/m^2 will produce an ignition time of 15 seconds in a 3 mm thick material. Thinner samples, such as the super sack fabric, will have lower times to ignition for a given heat flux. As such, flame exposure can readily ignite the super sack fabric. Where the side of the sack is ignited, the flames and slumping MgO will destroy the ignition evidence.

There was limited damage to the MgO super sack at R18:C4 (AIB-FST-10080). The fabric damage on the bulkhead (east) side, the side facing to the majority of the other MgO super sack damage, was indicative of heat flux damage, rather than overheat created by global elevated room temperature.

In some locations the super sack fabric draped over the side of an upper-tier SWB and burned in this orientation. The most pronounced evidence was the south side of R13:C5 (AIB-FST-10121).

4.1.4.   Polyethylene Slip Sheets and Reinforcement Plates

The array inspections and evidence evaluation identified multiple locations in rows 8 through 18 where polyethylene slip sheets and reinforcement plates were damaged. Damage to these sheets and plates was nonuniform. The two primary mechanisms for damage were melting and burning. Evidence of both were observed. For example:

- The super sack slip sheet array face (west) side at R12:C4 was undamaged, while the bulkhead (east) side was missing (AIB-FST-10743 and AIB-FST-10771).
- The reinforcement plate for the middle-tier assembly at R18:C6 was damaged on the array face (west) side. The missing material followed the outline of the middle-tier drums. There was evidence of drips on the sides of the drums. There was no damage to the plate on the other three sides.
- The reinforcement plate on the top-tier 55GD assemblies at R9:C3, R9:C5 and R15:C3 had melted and puddled on the 55GD lids. After the fire exposure the material froze. During or after the freezing process the material cracked into pieces as it cooled and solidified. These were the only locations that had both severe fire damage and reinforcements plates that were not under an MgO super sack or a waste assembly.
- The reinforcement plates and slip sheets at R14:C2, which contained three stacked 100 GD assemblies, were missing up to the outline of the drums. The quantity of plastic below the damage was insufficient to justify a judgment that the damage was caused by melting.

Melting. The polyethylene slip sheets and the reinforcing plates will soften as the temperature approaches the melting temperature range of 122 – 135°C. [12] Evidence of heat distortion and melting was observed in the array.

Ignition. Polyethylene is categorized as an easy-to-ignite material. [14] Ignition of high-density polyethylene (6 mm, 0.23 inches) occurs in 59 seconds at an exposure of 50 kW/m^2, and 422 seconds at an exposure of 20 kW/m^2. [15 p. 38] Data for thinner samples (2 mm, 0.079 inches), is 54 and 257 seconds. [15 p. 62] The polyethylene slip sheets and reinforcement plates were 3.8 mm

(0.15 inches) thick. Based on extrapolation of this information, an exposure of 80 kW/m^2 for 22 seconds is necessary to ignite the polyethylene sheets within the array. Once ignited, polyethylene objects will burn and melt simultaneously; this behavior creates flaming drips that can cause ignition of combustible materials below the burning polyethylene.

4.1.5. Cardboard and Fiberboard

The array inspections and evidence evaluation identified char damage to many of the SWB fiberboard slip sheets and super sack corrugated cardboard stiffeners. The fiberboard slip sheets are a minimum 0.09-inches thick. [16] Illustration 14 provides the other dimensions. The cardboard super sack inserts were $^7/_{16}$-inches thick, 19 ½-inches high, and 31 ⅜-inch long. [10]

The stiffeners had collapsed into multiple final orientations: hanging from a stack edge, cantilevered over the edge of a waste package, bridging between two stacks, or resting on the floor. Some of the locations where the stiffeners were cantilevered or bridging exhibited irregular edge surfaces (AIB-FST-02099). At R15:C5 there was a concave burn pattern in the portion of the cardboard that was cantilevered over the edge of the lid of a SWB (AIB-FST-02075). The burn-pattern is typical of horizontal material exposed to a flame from below. Similar materials may burn as long as exposed to an external flame, but will likely self-extinguish once the flame is removed. There were also smaller cardboard remnants lying on the lid. These remnants display striations of the corrugated layer within the original cardboard matrix.

Fiberboard is a generic term for many paper or wood-based materials. Corrugated cardboard is a subset of fiberboard. In this report the super sack stiffeners are referred to a cardboard since they were part of this subset, while the slip sheets are referred to as fiberboard since they were formed from pressed wood fibers. Where empirical test data is presented, the use of terms cardboard and fiberboard is maintained to be consistent with the cited reference.

Corrugated cardboard ignites at a heat flux of 15 kW/m^2. [13 p. 899] Fiberboard ignites spontaneously after five seconds when exposed to 52 kW/m^2. [12] Higher fluxes require less exposure time to initiate ignition. Corrugated fiberboard (2.8 mm, 0.11 inches) requires four seconds for ignition at an exposure of 80 kW/m^2, eight seconds at an exposure of 50 kW/m^2, and 68 seconds at an exposure of 20 kW/m^2. [17] The ignition flux is not dependent on the thickness. Ignition is most likely to occur at the exposed edge of the material. Complete ignition would not be instantaneous and combustion may cease when the exposing flame is removed if the fiberboard orientation is horizontal or vertical with downward burning. Such conditions were observed in the array (AIB-FST-02008, AIB-FST-02022, AIB-FST-02030, AIB-FST-10404, AIB-FST-10408). Thus, the flame damage to the stiffeners indicates that some fell into their current position before or while flames extended from below and impinged on the cardboard edges.

Ignition of a fiberboard slip sheet did occur at R7:C5. The fiberboard charred over a short region and self-extinguished (AIB-FST-10541). This region is adjacent to R8:C4, which had a fire-damaged MgO super sack, so ignition could have occurred by direct thermal heat transfer from the fire at R8:C4, from impact by burning material (cardboard or fabric) falling from R8:C4, or

by embers generated elsewhere in the array. Damage to this fiberboard was identified as fire damage closest to the bulkhead.

4.1.6.   Container Labels and Paint

The array inspections and evidence evaluation identified damaged waste container labels and paint. The damage was not uniform, with many in rows 8 through 18 undamaged. Many labels in the array were covered with spray paint that was applied by the generating waste generator site. Such discolorations were not related to the fire event; rather, this is a common practice to conceal obsolete labels.

The ignition temperature of paper ranges from 229°C to over 400°C. The lower value is attributed to newspaper. [13 p. 1067]. Glossy labels, which usually have high clay content, will have ignition temperatures in the upper portion of this range.

Paint on steel surfaces will often darken with heat exposure, but may lighten on longer or more intense exposure. The paint may also decompose to a gray or white powder. This process can result in lighter surface colors that are actually indicative of greater thermal exposure. The nature of the current inspection process, which was limited to a macroscopic visual inspection, could not readily differentiate these damage states.

4.2.   Back and Ribs

The condition of ribs and back (roof) of Room 7 in the vicinity of the array was inspected during January 2015.

Some of the roof bolts slipped from their installed positions and were suspended by their lanyards (AIB-FST-10315). In other locations lanyards were attached to the back (roof) but the expected bolt was not present. Roof bolts are used to transfer loads near the exposed salt surface to the undisturbed salt matrix. A typical roof bolt used at WIPP is typically 13 feet long (See Figure 4-2). The roof bolt consists of a 13 or 14 foot 7/8" diameter threaded bar, bolt plate, and nut. The rod is anchored into the hole using composite resin.

Roof bolt hardware was scattered among the containers and, in some cases was atop containers (AIB-FST-10813). Two roof bolt plates were present, one on the floor near R7:C3 and other on the floor near R7:C5 (AIB-FST-10811 and AIB-FST-10813). In addition, at many locations salt pieces were laying on waste packages, horizontal emplacement materials, and residual MgO piles (AIB-FST-10028, AIB-FST-10414, AIB-FST-10415, AIB-FST-10812, and AIB-FST-10828). These materials most likely came from the back (roof) or rib.

The back (roof) exhibited evidence of geological formation colorations. There were no discolorations that could be attributed to heat or flame exposure (AIB-FST-10809, AIB-FST-10810).

Threaded bar (Dywidag)
bolt and resin tube

36" resin tube fills about
42" around bolt after spinning

Plate — — Nut

Bolt (6" pigtail)
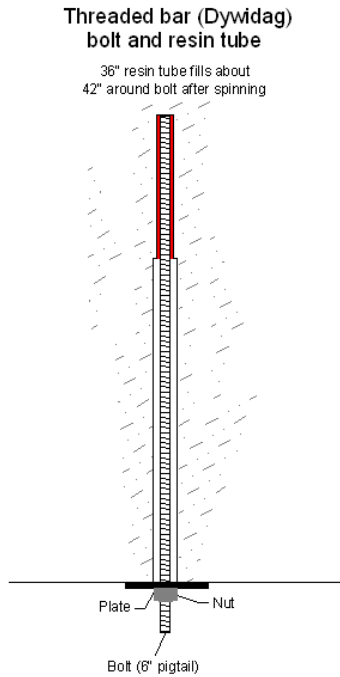
Figure 4-2: Typical Roof Bolt Assembly

Along both ribs evidence of the mining process were observable. These marks were left by the cutting head used to mine the room (AIB-FST-10817 and AIB-FST-10550). The north rib exhibited evidence of discoloration indicative of geological formation colorations, but no evidence that could be attributed to heat or flame exposure. The VOC sample tubing on the north rib had no evidence of damage (AIB-FST-11134). All visible rib bolts appear to be tight to the rib. Multiple images were captured during the north-rib inspection:

Location	Photo Number
North Rib toward Bulkhead	AIB-FST-10814
Near Row 21Column 1	AIB-FST-10815
Near Row 20 Column 1	AIB-FST-10816
Near Row 19 Column 1	AIB-FST-10817
Near Row 3 Column 1	AIB-FST-10818
Near Row 2 Column 1	AIB-FST-10819
Near Row 9 Column 1	AIB-FST-10820

Two types of discoloration were observed on the south rib. As with the north rib, some of these were geological formation colorations. There were also darkened areas (charred/blackened) that were not typical in the geological formation. Typical formation colors are shown in photos listed below:

Location/Description	Photo Number
South rib at miter (chamfered corner near row 24)	AIB-FST-10537
Near Rows 20 and 22	AIB-FST-10559
Near Rows 8 and 6	AIB-FST-10539
Near Rows 7 and 5	AIB-FST-10554
Near Row 4	AIB-FST-10555
Near R2:C6	AIB-FST-10546
Near Row 2	AIB-FST-10556
View of South Rib looking back from near the bulkhead	AIB-FST-10550

Four locations with evidence of discoloration due to the flames close to or in contact with the south rib were identified:

Location	Photo Number
Near Row 10	AIB-FST-10538
Near Row 12	AIB-FST-10557
Near Row 16	AIB-FST-10558
Near Row 18	AIB-FST-10449

The discoloration at Row 16 was directly above a damaged MgO super sack. Combustion of the super sack fabric and the cardboard stiffener would have caused discoloration of the rib. The discolorations at Row 10, 12 and 18 were near damaged MgO super sacks and were likely caused by cardboard stiffeners from the damaged super sack that fell against the rib, burned to create the rib discoloration, and then fell to the floor.

4.3.   Bulkhead

A visual inspection of the east (downstream) side of the Room 7 bulkhead was conducted on April 26, 2014 as viewed from the Room 6 bulkhead (AIB-FST-11136). This inspection was documented with a video camera. There was no evidence indicating that fire occurred in Room 7 and no visual evidence of material spread into the exhaust drift (AIB-FST-11137).

Visual inspections of the west (array) side of the Room 7 bulkhead was conducted as part of the January 2015 inspections. Multiple images were captured during this inspection:

- Along north rib   AIB-FST-11131, -11132
- Nearest column 2   AIB-FST-10683, -11130, -11135
- Nearest column 4   AIB-FST-10662, -10644, -10932
- Nearest column 6   AIB-FST-10435, -10438, -10439, -11210, -11211, -11212
- Along south rib   AIB-FST-10437, -10440, -10441, -10442

No fire-related evidence (damage or combustion products) at the bulkhead was observed.

4.4.   Row 2

Row 2 contained three stacks. (There was no row 1 in the array.) Each stack included a 4,200 lbs MgO super sack. R2:C2 consisted of a SWB set on a SLB2. R2:C4 consisted of a SWB set

on a SLB2. R2:C6 consisted of five 55GD and two dunnage drums in an assembly resting on an SLB2.

4.4.1.   Column 2

There was no observed fire damage at R2:C2. The MgO super sack, polyethylene slip sheet, SWB, fiberboard slip sheet beneath the SWB, TDOP, and fiberboard slip sheet beneath the TDOP were intact and there was no evidence of exposure to heat or flame. White dust-like material was present on some of the exposed top horizontal surfaces of the waste containers and slip sheets (AIB-FST-02009, AIB-FST-10683, AIB-FST-10684, AIB-FST-10686, AIB-FST-10688, AIB-FST-10691, AIB-FST-10692, AIB-FST-10694). There was a spider web-like accumulation on the south face at the super sack's slip sheet (AIB-FST-10684). This was not caused by exposure to heat or flames, and was consistent with other stacks such as R2:C4.

4.4.2.   Column 4

There was no observed fire damage at R2:C4. The MgO super sack and polyethylene slip sheet (AIB-FST-10642, AIB-FST-10643, AIB-FST-10644, AIB-FST-10646, AIB-FST-10647, AIB-FST-10662, AIB-FST-10663, AIB-FST-10937), SWB and fiberboard slip sheet, and SLB2 (AIB-FST-10091, AIB-FST-932) were undisturbed and had no evidence of exposure to heat or flame (AIB-FST-10501, AIB-FST-10502, AIB-FST-10639, AIB-FST-10640, AIB-FST-10641, AIB-FST-10645, AIB-FST-10931, AIB-FST-10933, AIB-FST-10934, AIB-FST-10935, AIB-FST-10936).

There were spider web-like accumulations on the MgO super sack (AIB-FST-10642, AIB-FST-10643, AIB-FST-10645, AIB-FST-10937). The filaments resemble spider webs but were thicker, possibly due to MgO dust adhering to their surface. A survey of MgO super sacks in the aboveground storage area demonstrated 3 out of 50 super sacks had visible spider webs.

There was a rock bolt retaining plate present on the south top of the SLB2 near the bulkhead (AIB-FST-10641).

4.4.3.   Column 6

There was no observed fire damage at R2:C6. The MgO super sack and the waste containers were undamaged. Materials such as the stretch wrap around the 55GD assembly and polyethylene slip sheets were undisturbed and had no evidence of exposure to heat or flame. Text written in black marker on the stretch wrap was completely legible and provided no indication of disturbance (AIB-FST-10090, AIB-FST-10163, AIB-FST-10164, AIB-FST-10165, AIB-FST-10179, AIB-FST-11210, AIB-FST-11211, AIB-FST-11212).

4.5.   Row 3

Row 3 contained three stacks. Each stack included a 4,200 lbs MgO super sack. R3:C1 and R3:C3 consisted of a 55GD assembly set on a TDOP. R3:C5 consisted of 100GD assembly set on TDOP. Row 3 was the only odd numbered row with MgO super sacks.

4.5.1.   Column 1

There was no observed fire damage at R3:C1. The MgO super sack (AIB-FST-11140), polyethylene slip sheet, 55GD assembly, and TDOP were intact and there was no evidence of exposure to heat or flame (AIB-FST-11139, AIB-FST-10688, AIB-FST-10689, AIB-FST-11143, AIB-FST-11141, AIB-FST-11142). There was no evidence that the stretch wrap was overheated.

4.5.2.   Column 3

There was no observed fire damage at R3:C3. The MgO super sack (AIB-FST-10780, AIB-FST-10092, AIB-FST-10093, AIB-FST-10094, AIB-FST-10792), 55GD assembly was undamaged (AIB-FST-10092, AIB-FST-10093), and TDOP (AIB-FST-10776, AIB-FST-11147) were intact and there was no evidence of exposure to heat or flame. There was no evidence that the stretch wrap was overheated (AIB-FST-10783, AIB-FST-10784, AIB-FST-11146). There were some spider web-like accumulations on the top of the MgO super sack (AIB-FST-10775).

4.5.3.   Column 5

There was no observed fire damage at R3:C5. The MgO super sack and slip sheet was undisturbed and had no evidence of exposure to heat or flame (AIB-FST-10164, AIB-FST-10177, AIB-FST-10334, AIB-FST-10335, AIB-FST-10336, AIB-FST-10337, AIB-FST-10338, AIB-FST-10339, AIB-FST-10340, AIB-FST-10737, AIB-FST-10740, AIB-FST-10877, AIB-FST-10878). The sack was closed and the closure loop was intact.

The 100GD assembly was intact and there was no evidence of exposure to heat or flame (AIB-FST-10335, AIB-FST-10337, AIB-FST-10338, AIB-FST-10340, AIB-FST-10738, AIB-FST-10877, AIB-FST-10878). The stretch wrap was present and had no evidence of melting or burning. Labels on the side of the drums were legible.

The TDOP was intact and there was no evidence of exposure to heat or flame (AIB-FST-10177, AIB-FST-10333, AIB-FST-10335, AIB-FST-10337, AIB-FST-10341, AIB-FST-10738, AIB-FST-10739, AIB-FST-10877, AIB-FST-10878). The paint remained white, with no evidence of discoloration. Writing on the side of the overpack was legible.

4.6.   Row 4

Row 4 contained three stacks. R4:C2 consisted of a 4,200 lbs MgO super sack and a 100GD assembly set on the TDOP. R4:C4 and R4:C6 consisted of a 3,000 lbs MgO super sack and SWB set on a TDOP.

4.6.1.   Column 2

There was no observed fire damage at R4:C2. The MgO super sack was intact (AIB-FST-10106). The stretch wrap around the top 100GD assembly was intact and undamaged (AIB-FST-10107, AIB-FST-10115), and the labels were legible and undamaged (AIB-FST-10108).

The TDOP was intact and there was no evidence of exposure to heat or flame (AIB-FST-10109 and AIB-FST-10110).

4.6.2.   Column 4

There was no observed fire damage at R4:C4. The MgO super sack was intact with no evidence of exposure to heat or flame. There was no indication of any damage to the waste containers. Materials such as slip sheets were undisturbed and there was no evidence of exposure to heat or flame (AIB-FST-10510, AIB-FST-10517, AIB-FST-10518, AIB-FST-10519).

4.6.3.   Column 6

There was no observed fire damage at R4:C6. The MgO super sack and polyethylene slip sheet located at the top of this waste column were intact and there was no evidence of exposure to damaging heat or flame (AIB-FST-10306, AIB-FST-10310, AIB-FST-10311).

The SWB and fiberboard slip sheet were intact and there was no evidence of exposure to heat or flame (AIB-FST-10305, AIB-FST-10313). The TDOP was intact and there was no evidence of exposure to heat or flame (AIB-FST-10308, AIB-FST-10309, AIB-FST-10312, AIB-FST-10314).

4.7.   Row 5

Row 5 contained three stacks. R5:C1 consisted of five 55GD and two dunnage drums in an assembly on top of a TDOP. R5:C3 and R5:C5 consisted of an SWB on top of a TDOP. Row 5 contained no MgO super sacks.

4.7.1.   Column 1

There was no observed fire damage at R5:C1. The 55GD assembly and the TDOP were intact and there was no evidence of exposure to heat or flame (AIB-FST-11116, AIB-FST-11117, AIB-FST-11118, AIB-FST-11144, and AIB-FST-11145).

4.7.2.   Column 3

There was no observed fire damage at R5:C3. The SWB, fiberboard slip sheet, and TDOP were intact and there was no evidence of exposure to heat or flame (AIB-FST-10237, AIB-FST-10238, and AIB-FST-10239). There was a rock bolt retaining plate and plastic retaining ring from a bolt on the SWB lid (AIB-FST-10237). Additionally, two more plastic retaining rings were on the SWB fiberboard slip sheet on the array face (west) side (AIB-FST- 10238). Labels and markings on both containers were legible.

4.7.3.   Column 5

There was no observed fire damage at R5:C5. The SWB and TDOP were intact and there was no evidence of exposure to heat or flame (AIB-FST-10018, AIB-FST-10019, AIB-FST-10492, AIB-FST-10493, AIB-FST-10494, AIB-FST-10495, AIB-FST-10496, AIB-FST-10497, and

AIB-FST-10498,). The SWB fiberboard slip sheet had straight edges and corners on the side toward the heated zone (AIB-FST-10492).

4.8.   Row 7

Row 7 contained three stacks. (There was no row 6 in the array.) The bottom of each stack was an SLB2. R7:C1 and R7:C5 had an SWB placed on the SLB2. R7:C3 had an SWB placed on the SLB2. There were no MgO super sacks on these stacks.

4.8.1.   Column 1

There was no observed fire damage at R7:C1 (AIB-FST-10849, AIB-FST-10850, AIB-FST-10851 and AIB-FST-10963). There was a torn slip sheet that straddles the LSB2s at R7:C1 and R7:C3. This sheet likely was used to emplace a waste container, but was inadvertently pulled from under that container during placement. The sheet was then left on the SLB2s to allow emplacement of the next waste row. There was no evidence of exposure to heat or flame to this sheet and the tear damaged is attributed to handling. Burned debris from the MgO super sack on R8:C2 fell on the SLB2 and superfluous slip sheet (AIB-FST-10849 and AIB-FST-10964). There was evidence where the north rib sloughed material, which landed on adjacent horizontal surfaces (AIB-FST-10967).

4.8.2.   Column 3

There was no observed fire damage at R7:C3. There was no discoloration or char present on either the SWB or the SLB2. The slip sheet between the SWB and SLB2 had no evidence of fire damage (AIB-FST-10410, AIB-FST-10434, AIB-FST-10707, AIB-FST-10708, AIB-FST-10710, AIB-FST-10712 and AIB-FST-11115). The slip sheet was torn on the bulkhead (east) side (AIB-FST-10707, AIB-FST-10708). There were minor debris on top of the SLB2 including what appears to be a metal ring on the south side (AIB-FST-10230, AIB-FST-10410, AIB-FST-10433 and AIB-FST-10434). A rock bolt plate and a Titan load indicator, which had been installed on a rock bolt, were on the floor between R7:C3 and R7:C5 (AIB-FST-10433, AIB-FST-10434). Another rock bolt retaining plate was on the floor between R7:C3 and R5:C3 (AIB-FST-10707). A fiberboard slip sheet with some debris including MgO bridged between the tops of the SLB2 containers of R7:C1 and R7:C3, as described in subsection 4.8.1 (AIB-FST-10709, AIB-FST-10710, AIB-FST-10711).

4.8.3.   Column 5

There was minor fire damage observed at R7:C5; there was localized charring of the SWB fiberboard slip sheet on the array face (west) side of the stack (AIB-FSB-10490, AIB-FST-10541, and AIB-FST-10542). The damaged area was about 2 feet long. The remaining edges of the slip sheet were undamaged (AIB-FST-10540, AIB-FST-10543, AIB-FST-20544, AIB-FST-10545, and AIB-FST-10566). The SWB and SLB2 were intact and there was no evidence of exposure to heat or flame, with the exception of the damaged slip sheet. There were debris on top of the SLB2. The debris at the charred area of the slip sheet were charred slip sheet (AIB-FST-10542). The debris on the top of the SLB2 near the rib are attributed to salt sloughed from the rib (AIB-FST-10545). In either case, there was no damage to the SLB2 or the SWB.

4.9.   Row 8

Row 8 contained 3 stacks. R8:C2 and R8:C4 consisted of a 3,000 lbs MgO super sack and SWB set on a TDOP. R8:C6 consisted of a 4,200 lbs MgO super sack and SWB set on a TDOP.

4.9.1.   Column 2

There was severe fire damage observed at R8:C2. Most of the MgO super sack is missing. There are remnants and debris from the burned and melted super sack fabric present (AIB-FST-10143 and AIB-FST-10144, and AIB-FST-10145).

The array face (west) side had evidence of dripping from the edge of the lid and along the sides of the SWB. In addition deposits from the melted or burned super sack and its polyethylene slip sheet were present on the lifting clips and filters. These deposits appear white due to MgO deposited when the super sack failed and the MgO slumped (AIB-FST-10147, and AIB-FST-10148). The SWB fiberboard slip sheet was also burnt on the south end of the array face edge (AIB-FST-10148). There was also some evidence of dripping from the top edge of the TDOP in this area. MgO was deposited on the remaining SWB slip sheet and on the exposed top of the underlying TDOP.

The north side had some evidence of dripping from the top and MgO was deposited on the SWB bumpers, the SWB slip sheet and on the top edge of the TDOP below. However, much of the super sack remains unmelted, suggesting that this side was partially shielded from the heat source (AIB-FST-10149). Several dark spots thought to be melted polyethylene slip sheet or ash were noted on top of the SWB slip sheet toward the array face (west) side. Darkened rectangular areas were present on the east and north sides of the SWB; they were painted over obsolete labels. There was no evidence of TDOP damage. MgO was deposited on the floor to the depth of the bottom TDOP offset tube (ring).

On the bulkhead (east) side drips were present at the top and on the side of the SWB as well as on the top and side of the TDOP (AIB-FST-10146). MgO and debris from the super sack were deposited on the exposed top of the TDOP. The SWB fiberboard slip sheet appears to be torn or folded under the SWB on the south end and there was a westward displacement on the north side, but this was the result of emplacement activities and there was no evidence of fire damage where not covered by the MgO deposit (AIB-FST-10146 and AIB-FST-10149). MgO was deposited on the floor to the depth of the bottom TDOP offset tube (ring).

The south side of the stack likewise had drips from the top and top bumper of the SWB. (AIB-FST-10150). The SWB slip sheet was undamaged in this area. There was no damage to the TDOP. A piece of a cardboard super sack stiffener was present on the floor partially buried in MgO and leaning against the TDOP. MgO was deposited on the floor to the bottom offset tube (ring).

4.9.2.   Column 4

There was severe fire damage observed at R8:C4. The MgO super sack was substantially gone and the residual MgO had slumped to its angle of repose on all sides (AIB-FST-10044, AIB-

FST-10045, AIB-FST-10046, AIB-FST-10047, AIB-FST-10048, and AIB-FST-10049). Small pieces of fabric remain on at the edge between R8:C4 and R9:C5 (AIB-FST-10044). MgO was accumulated on the SWB slip sheet, the horizontal surfaces of the SWB and TDOP, and the floor.

The array face (west) side of the SWB had dark streaks extending down from the top of SWB lid and the MgO slip sheet was melted or burned such that it does not extend beyond the SWB edge (AIB-FST-10047 and AIB-FSB-10048). The streaks appear to be the result of melting of the polyethylene slip sheet above the SWB. MgO was deposited on the top of the TDOP that extends beyond the SWB footprint (AIB-FST-10047 and AIB-FST-10048) and on the fiberboard slip sheet. The fiberboard slip sheet between the SWB and TDOP extends over the edge of the TDOP. There was damage on the center edge that appears to be from material movement and not fire damage. The TDOP was intact, but minor discoloration was present (AIB-FST-10048).

The north side had some black material extending down from the lid of the SWB on to the side of the SWB and on the upper bumper. The black residue was present in the form of drips extending from the edge of the SWB and generally covering the sides of the lifting clips (AIB-FST-10049). The super sack slip sheet does not extend beyond the SWB lid (AIB-FST-10049). The black material appears to be the result of dripping of melted slip sheet material from above. MgO was deposited on the top of the slip sheet that the SWB sits on. There was no evidence of damage or discoloration to the TDOP (AIB-FST-10049).

The bulkhead (east) side of the SWB had some shading or darkening along its side (AIB-FST-10044). The MgO slip sheet was melted or burned away such that it does not extend beyond the SWB edge (AIB-FST-10044). Black residue was present in the form of drips extending from the top edge of the SWB and generally covering the lifting clips (AIB-FST-10044) and the side of the SWB. The array face (west) side of R8:C4 had very legible labels with grey streaks down this side. There was MgO deposited on the top of the fiberboard slip sheet and the top of the TDOP (AIB-FST-10044 and AIB-FST-10049). The black drips present in this pile of MgO appear to be from the slip sheet above. There was no evidence of damage or discoloration to the TDOP or the SWB fiberboard slip sheet (AIB-FST-10044 and AIB-FST-10049). The fiberboard slip sheet does not extend beyond the edge of the TDOP on this side of TDOP (AIB-FST-10044).

The south side of the stack was adjacent to R9:C5 (AIB-FST-10047) the slip sheet of the MgO super sack does not extend beyond the lid of the SWB. The Slip sheet between the SWB and TDOP was intact and had MgO piled on top of it and the TDOP. Although there were some black marks present, the SWP and TDOP appear to be undamaged (AIB-FST-10695).

4.9.3.   Column 6

There was severe fire damage observed at R8:C6; the MgO super sack fabric was substantially gone. There was a small amount of polypropylene fabric and a portion of the MgO super sack cardboard stiffener, both located on the bulkhead (east) side of the SWB, near the south rib. (AIB-FST-10475, AIB-FST-10476, AIB-FST-10477, AIB-FST-10479, AIB-FSB-10491). An MgO super sack cardboard stiffener had fallen against the south rib and partially burned (AIB-FST-10477). The cardboard stiffener from the array face (west) side had fallen and bridged

between R8:C6 and R10:C6 (AIB-FST-10489). The stiffener from the bulkhead (east) side could not be located (AIB-FSB-10490). The stiffener from the north side of the MgO super sack fell onto the top of the assembly at R9:C5 and to was covered with MgO (AIB-FSB-10491).

The MgO slip sheet was missing beyond the outline of the SWB (AIB-FST-10475, AIB-FST-10476, AIB-FST-10478, AIB-FST-10481, AIB-FST-10482, AIB-FST-10484). There was evidence of dripping of the polyethylene that flowed over the lid of the SWB and down the side of the SWB (AIB-FST-10476, AIB-FST-10481, AIB-FST-10484). The flow originated above the lid providing an indication that the dark marks were from the polyethylene slip sheet rather than the neoprene gasket of the SWB. Some melted polyethylene froze as it flowed over the lid of the SWB but before it dripped onto the SWB bumper. A smoke pattern was also present above the same bumper that was likely caused by burning of the polypropylene fabric, the polyethylene slip sheet, or both (AIB-FST-10481).

The SWB was undamaged on the south side, toward the salt rib (AIB-FST-10475, AIB-FST-10476, AIB-FST-10488). The array face (west) side of the SWB had dark areas from melted polyethylene drips, but no apparent flame patterns (AIB-FST-10484), The bulkhead (east) side of the SWB had dark areas from polyethylene dripping down from above the SWB lid, but no smoke patterns associated with flames (AIB-FST-10476, AIB-FST-10490).

The north face side of the SWB had some dark areas; these were either from melted polyethylene that dripped down from above the SWB lid (AIB-FST-10481, AIB-FST-10484) or flame impingement (AIB-FST-10481, AIB-FST-10605, AIB-FST-10482). The flame pattern above the top bumper was above an area where polyethylene dripped down, however, it does not spread to the left, where other melted polyethylene was present. (AIB-FST-10481) The burn pattern on the lower portion of the SWB appears to have initiated at the level of the TDOP below the SWB and spread upward onto the SWB. (AIB-FST-10605, AIB-FST-10482).

The fiberboard slip sheet between the SWB and TDOP was present and undamaged on the south rib side of the assembly. The pointed corners can be seen (AIB-FST-10475, AIB-FST-10489) as well as a straight side (AIB-FST-10488, AIB-FST-10489). On the array face (west) side, there was damage apparently caused by burning but much of the slip sheet remains, although covered with MgO (AIB-FST-10478, AIB-FST-10484). The slip sheet on the bulkhead (east) side was concealed by a layer of MgO (AIB-FST-10475, AIB-FST-10476, AIB-FST-10490) but likely was undamaged since there were no smoke patterns on the bulkhead side of the SWB. The slip sheet on the north side was stained with a smoke pattern (AIB-FST-10482). However, there was an uncharred edge visible in the middle of the smoke damage. This may indicate that the straight edge of the slip sheet did not extend past the curvature of the TDOP below it and did not actually burn at this location.

The TDOP on the bottom of the stack had no damage on the south side. (AIB-FST-10475, AIB-FST-10486, AIB-FST-10487). The array face (west) side of the TDOP had no damage (AIB-FST-10484, AIB-FST-10485, AIB-FST-10486). The bulkhead (east) side of the TDOP also appears undamaged. (AIB-FST-10490, AIB-FST-10500). The north face side of the TDOP had two areas of damage. At the very bottom, there was some mild light brown fire pattern, mostly covered by MgO, and not extending past the second spacer ring (24.5 inches from the bottom of

the TDOP). The lower portion of the fire pattern discoloration was covered by MgO so it would have occurred before the MgO deposited (AIB-FST-10483).

A darker smoke pattern was present near the top of the TDOP on the north side (AIB-FST-10480). The "V" pattern originated above the top spacer ring of the TDOP and extends onto the SWB above. There was dark smoke deposition as well as lighter brown smoke (AIB-FST-10482). The top lip of the SWB had freckling over the short vertical section of the TDOP lip not extending past the weld.

4.10. Row 9

Row 9 contained three stacks. The bottom of each stack was a TDOP. R9:C1 had an SWB placed on the TDOP. R9:C3 and R9:C5 each had a 55GD assembly placed on the TDOP. Six of the 55GD in R9:C3 contain POPs, and seven of the 55GD in R9:C5 contain POPs. There were no MgO super sacks on these stacks.

4.10.1. Column 1

There was no observable fire damage at R9:C1. There was only a light dusting of material on top of the SWB lid that most likely originated from adjacent stacks (R10:C2 and R8:C2), which experienced MgO super sack damage during the radiological release event (AIB-FST-10585, AIB-FST-10593). The photographic evidence of the circumference indicated no discoloration or combustion of slip sheets occurred. Although there was no complete image of the north side, the absence of damage on both the bulkhead (east) side images and the array face (west) side images provides confidence that there was no damage on the north side of the stack (AIB-FST-10585 through AIB-FST-10597).

On the south side, there was material accumulation on the fiberboard slip sheet below the top tier (AIB-FST-10140). In the upper left corner of the SWB, there was black discoloration down to the upper bumper, probably originating from combustion products on the adjacent R10:C2 stack (AIB-FST-10292, AIB-FST-10142). Additionally, a small piece of debris was found protruding from the middle of the south edge of the SWB lid seam (AIB-FST-10139, AIB-FST-10141).

4.10.2. Column 3

There was severe fire damage observed at R9:C3; the 55GD assembly reinforcement plate and stretch wrap were essentially gone. Figure 4-3 provides the nomenclature for discussion of individual drums in R9:C3.
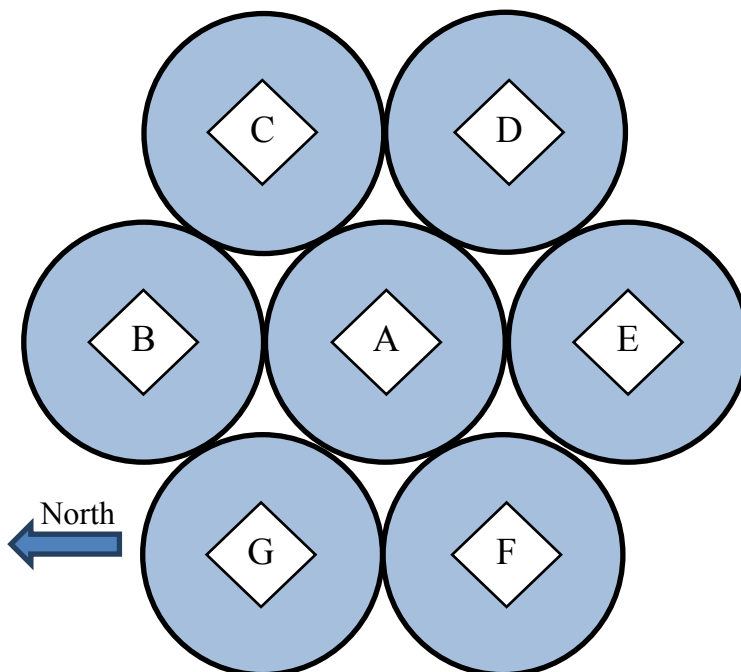
Figure 4-3: Nomenclature for 55GD Assembly Discussion

The reinforcement plate on the 55GD assembly had melted or burned with debris left in place on top of the drums, but with no part of the reinforcement plate left between the drums (AIB-FST-10049, AIB-FST-10050, AIB-FST-10051 and AIB-FST-10052). Each drum lid had areas of a smooth matrix of solidified material that had cracked into pieces with irregular edges (AIB-FST-10681). Crusty powder was present on all of the drums and MgO had slumped onto drums B, G, E and F (refer to Figure 4-3) from the R10:C4 and R10:C2 stacks (AIB-FST-10050, AIB-FST-10673, AIB-FST-10675,).

Dark marks were present on the drum sides and on the lid retention rings. This material likely came from the melted polyethylene reinforcement plate. On the array face (west) side there were black marks present, but no evidence physical damage to the vertical drum surfaces (AIB-FST-10052). Drum G overhung the TDOP. The slip sheet below the 55GD assembly had melted and dripped onto the TDOP (AIB-FST-10677). With the exception of the damaged reinforcement plate, missing stretch wrap, and damaged polyethylene slip sheet, the south side had no evidence of fire damage (AIB-FST-10829, AIB-FST-10830). The reinforcement plate on the bulkhead (east) side between drums E and D of the assembly between drums E and D however, was partially melted (AIB-FST-10049). The north side had discoloration, which was caused by melting of the reinforcement plate, but no evidence of drum damage due to heat or flame exposure.

Drum labels were legible, with only minor damage due to burning plastic melting down from overhead (AIB-FST-10049, AIB-FST-10052, AIB-FST-10060, and AIB-FST-10682).

Drum D was a dunnage drum (empty with no radiological material) with an open hole where a filter vent would nominally be installed. This was a common configuration for a dunnage drum (AIB-FST-10680, AIB-FST-10681and AIB-FST-10682).

Spilled MgO had accumulated around the TDOP base, with minor debris from combustibles and pieces of super sack stiffeners. The TDOP was undamaged although some polyethylene adhered to the sides of the container (AIB-FST-10051, AIB-FST-10059, AIB-FST-10060, and AIB-FST-10678).

4.10.3. Column 5

There was severe fire damage observed at R9:C5; the 55GD assembly reinforcement plate and stretch wrap were essentially gone. Figure 4-3 provides the nomenclature for discussion of individual drums in R9:C5.

The reinforcement plate on the 55GD assembly had melted or burned with debris left in place on top of the drums, but with no part of the reinforcement plate left between the drums. Each drum lid had areas of a smooth matrix of solidified material that had cracked into pieces with irregular edges (AIB-FST-10025). Crusty powder was present on all of the drums in the 55GD assembly and cracks in the material and irregular edges were present. MgO had slumped on top of drums D and E (refer to Figure 4-3) from the R8:C6 stack. (AIB-FST-10061, AIB-FST-10062 and AIB-FST-10212). A cardboard stiffener bridged between R8:C6 and R9:C5. The top of this stiffener was obscured with MgO (AIB-FST-10084).

Dark marks were present on the drums on their lid retention rings and sides (AIB-FST-10069), which likely came from the melted polyethylene reinforcement plate. Black marks were present on the array face (west) side (AIB-FST-10063) of the drum, but there was no physical damage other than on the drum lids. The stretch wrap was missing, and the top of the slip sheet was covered with a white substance (AIB-FST-10067 and AIB-FST-10069), which prevented visual inspection of the 55GD slip sheet. Black marks were present on drums C and D (AIB-FST-10212) and F and G near their base (AIB-FST-10067). The discoloration at the base of the drums appears to be the result of burning, melting, dripping onto the top of the slip sheet or TDOP and continuing to burn at that location.

There were several locations on the TDOP where melted plastic dripped down the side a few inches. Other than these deposits, there was no evidence of fire damage to the TDOP (AIB-FST-10022, AIB-FST-10023, AIB-FST-10025, AIB-FST-10605).

4.11.   Row 10

Row 10 contained three stacks. Each stack included a 4,200 lbs MgO super sack. R10:C2 and R10:C4 consisted of a 55GD assembly set on a TDOP. R10:C6 consisted of 100GD assembly set on two tiers of 55GD assemblies containing POP.

4.11.1. Column 2

There was severe fire damage observed at R10:C2. The MgO super sack fabric is completely missing from all sides (AIB-FST-10102 and AIB-FST-10103). Figure 4-3 provides the nomenclature for discussion of individual drums in R10:C2.

The MgO piles formed a 6-sided star pattern that conformed to the outer drum profiles. The piles had a steep angle of repose on the outer edges. Over drum A (refer to Figure 4-3) the piles converged with a small, flat area at the center. The MgO super sack slip sheet and the 55GD reinforcement plate were missing right up to the drum locking rings, and the stretch wrap was melted or burned away (AIB-FST-10977, AIB-FST-10290, AIB-FST-10291, and AIB-FST-10292).

There were black drips down the drums on the west and north side (AIB-FST-10291 and AIB-FST-10292). A ghost outline was formed by a painted-over label on drum B (refer to Figure 4-3) when it was exposed to fire conditions (AIB-FST-10111). The exposure left a combination of black paint, dripping plastic and MgO powder. The 55GD assembly slip sheet was obscured by an extensive MgO buildup spilled from above (AIB-FST-10290 and AIB-FST-10291). Drum G was labeled as dunnage (AIB-FST-10113).

The TDOP was intact and there was no evidence of exposure to heat or flame (AIB-FST-10977, AIB-FST-10112 and AIB-FST-10114). The spaces between the TDOP and the adjacent bottom tiers substantially filled with MgO spilled from above mixed with cardboard stiffener and plastic debris on the floor (AIB-FST10114).

4.11.2. Column 4

There was severe fire damage observed at R10:C4. The MgO super sack fabric was missing from all sides (AIB-FST-10352, AIB-FST-10342, and AIB-FST-10962). Figure 4-3 provides the nomenclature for discussion of individual drums in R10:C4.

The MgO that remained in place, and had not fallen to lower tiers, was slumped relatively evenly around the outer perimeter of the drums (AIB-FST-10962).

The MgO super sack slip sheet and 55GD reinforcement plate were missing right up to the drum locking rings, and the stretch wrap was melted or burned away (AIB-FST-10342, AIB-FST-10345, AIB-FST-10352, AIB-FST-10957, and AIB-FST-10961). There was no evidence of stretch wrap around the 55GD assembly (AIB-FST-10352 and AIB-FST-10961).

Drum E (refer to Figure 4-3) had a discolored yellow label just below the upper rolling hoop. A part of this label was blackened; other parts were obscured by a white powder (AIB-FST-10345). However, labels at the bottom of the drums in the top-tier assembly appear undamaged (AIB-FST-10344 and AIB-FST-10347). The 55GD assembly slip sheet was obscured by an extensive MgO buildup spilled from above (AIB-FST-10342, AIB-FST-10344, AIB-FST-10961). Visual observations from below provided no evidence of damage (AIB-FST-10960). Drum G was a dunnage drum and had no evidence of damage (AIB-FST-10958).

The TDOP was intact and there was no evidence of exposure to heat or flame (AIB-FST-10022, AIB-FST-10344, and AIB-FST-10959). The paint was white. Writing on the side of the TDOP was legible and all of the labels were intact.

4.11.3. Column 6

There was severe fire damage observed at R10:C6. The MgO super sack fabric was missing from all sides (AIB-FST-10503 and AIB-FST-10504). Figure 4-3 and Figure 4-4 provide the nomenclature for discussion of individual drums in R10:C6.
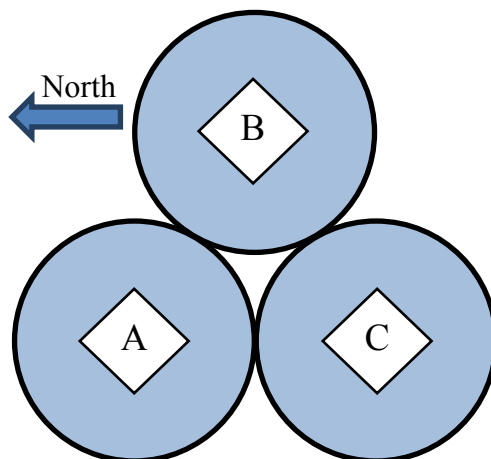
Figure 4-4: Nomenclature for 100GD Assembly Discussion

The slip sheet under the MgO super sack and 100 GD assembly reinforcement plate were missing up to the edge of the100GD containers. There were extensive remnants of melted plastic that dripped from the lips of the 100GD containers (AIB-FST-10024, AIB-FST-10504, AIB-FST-10505). The top-tier drum (black paint) sides were lightly coated with white powder. While the upper-tier stretch wrap was gone, the drum labels were legible beneath the powdery coating (AIB-FST-10504, AIB-FST-10506, and AIB-FST-10509).

The south (rib) side and southwest side of the 100GD slip sheet and middle tier reinforcement plate were intact and there was no evidence of exposure to heat or flame (AIB-FST-10504, AIB-FST-10506, AIB-FST-10511). The middle-tier stretch wrap was present in this region (AIB-FST-10512). On the northwest side of the stack, where upper-tier drum A sits above middle-tier drums B and C, the 100GD slip sheet and middle-tier reinforcement plate are missing (AIB-FST-10506). Most of the stretch wrap is gone in this region (AIB-FST-10506). Above the middle-tier drum C, the reinforcement plate tab was shifted from its emplacement position and has no evidence of fire damage (AIB-FST-10508); while the adjoining long tab of the 12-tab reinforcement sheet between drums B and C was missing (AIB-FST-10507).

Drums B and C of the middle-tier had labels on the upper half of the drums that were painted black. The underlying linear edges of the labels were apparent. There was smoke discoloration on the very bottom of drums B, C and D along the edges immediately above where the slip sheet between the bottom tier and middle-tier burned (AIB-FST-10508).

The bottom-tier was almost completely concealed by fallen MgO (AIB-FST-10507, AIB-FST-10508). Although MgO powder obscured the bottom-tier, given the available evidence the stretch wrap on the north side is judged to be missing.

4.12.   Row 11

Row 11 contained three stacks. R11:C1 contained a 100GD assembly set on two tiers of SWBs. R11:C3 contained an SWB set on a TDOP. R11:C5 contained three tiers of SWBs. There was no MgO emplaced on top of the stacks in Row 11.

4.12.1.   Column 1

There was no observed fire damage of significance at R11:C1. The stretch wrap, 100GD assembly, and TDOP were intact (AIB-FST-10102, AIB-FST-10594, AIB-FST-10595, AIB-FST-10596, and AIB-FST-10823). Except for debris on the bulkhead (east) side of the top-tier slip sheet, there was no evidence of exposure to heat or flame (AIB-FST-10597). There was also a light dusting of MgO on this plate.

4.12.2.   Column 3

There was minor fire damage observed at R11:C3. There were multiple MgO super sack stiffeners on the SWB lid, which exhibited charring (AIB-FST-10213).

There was a stiffener and debris on each corner of the SWB lid. They came from adjacent stacks (R10:C2, R10:C4, R12:C2 and R12:C4). The debris consisted of MgO, super sack stiffeners, ash, and surface char (AIB-FST-10214, AIB-FST-10215, AIB-FST-10218, and AIB-FST-10217).

There was minor darkening of the SWB on array face (west) side, but no indication of damage to the SWB, SWB slip sheet, or TDOP (AIB-FST-10217, AIB-FST-10219, and AIB-FST-10220). There were char deposits on the north-most SWB filter and slip sheet (AIB-FST-10217, AIB-FST-10218, and AIB-FST-10219).

On the south side of the stack, the underside of a cardboard stiffener from R12:C4 had fire exposure evidence, both char and pealing, which was the result of fire exposure; however, the SWB gasket was undamaged (AIB-FST-10221 and AIB-FST-10222). There were some MgO and dark spots present on the SWB slip sheet adjacent to R12:C4 (AIB-FST-10223). There was also evidence of char on the SWB slip sheet adjacent to R10:C4 (AIB-FST-10224). The TDOP had no evidence of exposure to heat or flame. MgO was deposited on the floor with the depth rising to mid-height of the TDOP (AIB-FST-10225). Black specks were present on the MgO (AIB-FST-10226).

The north edge of the bulkhead (east) side of the SWB had a dark stain near the R10:C2 stack (AIB-FST-10213). The stain is judged to be the result of super sack fabric draping on the side of the SWB and then burning. Although there was ash deposited on the SWB slip sheet and the TDOP lid, there was no evidence of damage to the bulkhead side of the SWB, SWB slip sheet, or TDOP (AIB-FST-10059 and AIB-FST-10227).

The north side of the SWB slip sheet had minor charring near the R10:C2 stack, but no evidence of damage to the SWB or TDOP (AIB-FST-10228 and AIB-FST-10229). Most of the TDOP was obscured by an extensive buildup of spilled from above (AIB-FST-10229).

4.12.3.   Column 5

There was no observed fire damage at R11:C5. The MgO super sack, slip sheets, and three SWBs were intact and there was no evidence of exposure to damaging heat or flame (AIB-FST-10231, AIB-FST-10232, AIB-FST-10233, AIB-FST-10234, AIB-FST-10235, and AIB-FST-10236). Spilled MgO had accumulated at the base of the stack, both on the array face (west) and bulkhead (east) sides, and on the slip sheet under the top-tier SWB. The labels and writing on the SWBs were clear and legible.

4.13.   Row 12

Row 12 contained three stacks. R12:C2 and R12:C6 consisted of an SWB set on top of a TDOP. R12:C4 consisted of three tiers of SWBs. Each stack was covered with a 4,200 lbs MgO super sack.

4.13.1.   Column 2

There was severe fire damage observed at R12:C2. The MgO super sack fabric was substantially gone. There was a small amount of polypropylene fabric present on the MgO pile (AIB-FST-02001, AIB-FST-10656, AIB-FST-10852 and AIB-FST-11119). Super sack cardboard stiffeners were present on the SWB on its north end (AIB-FST-11119, AIB-FST-11120, AIB-FST-11121, and AIB-FST-11122). Drips along the sides of the SWB were the result of melting of the super sack and its polyethylene slip sheet (AIB-FST-10218, AIB-FST-11123, AIB-FST-11127, and AIB-FST-11128). The side slope of the MgO on the north side was not as step as most of the MgO piles (AIB-FST-02001 and AIB-FST-11119).

The array face (west) side had evidence of plastics dripping from the top and along the sides of the SWB (AIB-FST-11122, AIB-FST-11123 and AIB-FST-11125). There were multiple darkened rectangular areas on the side of the SWB (AIB-FST-11125). There was also a darkened region near the SWB base on the north end. The SLB slip sheet appeared both torn and charred, in this darkened region; there was little ash present (AIB-FST-02002, AIB-FST-11124, AIB-FST-11126). There was a similar inversed-cone darkened area near the SWB base on the south end; however the slip sheet was covered with MgO (AIB-FST-11125). MgO and other debris were present on the SWB slip sheet and the TDOP lid (AIB-FST-11124 and AIB-FST-11125).

There was evidence of dripping plastics MgO deposited on the north-side SWB bumpers (AIB-FST-11121 and AIB-FST-11127). The north-end of the SWB overhung the TDOP. There was no evidence of damage to the TDOP (AIB-FST-11121 and AIB-FST-11124). The lower half of the TDOP was obscured by an extensive MgO spilled from above (AIB-FST-11126).

The bulkhead (east) side of the SWB was similar to the array face (west) side. Drips were present at the top and on the side of the SWB (AIB-FST-11128). MgO and char were deposited on the exposed TDOP lid (AIB-FST-11129). The MgO was several feet deep on the floor with greater depth toward the south (AIB-FST-11129).

There was evidence of black deposits on the south side of the SWB bumper. Material had dripped from the SWB lid and bumper (AIB-FST-10218, AIB-FST-10852, AIB-FST-10853, AIB-FST-10854, and AIB-FST-11129). MgO was deposited on the exposed TDOP lid of the SWB (AIB-FST-11129) and obscured the lower half of the TDOP (AIB-FST-10218).

4.13.2. Column 4

There was severe fire damage observed at R12:C4. The MgO super sack fabric was missing (AIB-FST-02012, AIB-FST-10741, AIB-FST-10742, and AIB-FST-10751, AIB-FST-10752).

The array face (west) side and bulkhead (east) side slopes of the MgO pile were asymmetric, due to the off-center emplacement of the top slip sheet (AIB-FST-10745). There were fragments of the super sack fabric located on the MgO and there was a cardboard stiffener that bridged between R12:C4 and R11:C3 (AIB-FST-10741, AIB-FST-10742, AIB-FST-10743, and AIB-FST-10744). There was a section of horizontal material near this bridge that was unique and not seen in other locations (AIB-FST-10766). There was another stiffener bridged between R12:C4 and R11:C5 (AIB-FST-10848). On the array face (west) side cardboard stiffeners extended from under the MgO pile supporting a shallow-slope region of MgO (AIB-FST-10745, AIB-FST-10754). There was localized damage to a cantilevered stiffener (AIB-FST-02004) and some undamaged fabric (AIB-FST-10763). Residual super sack fabric was present on the MgO piles (AIB-FST-10743 and AIB-FST-10744).

The south side had evidence of plastics dripping from the top and along the sides of the upper-tier SWB (AIB-FST-10392, AIB-FST-10393, and AIB-FST-10394). The three SWBs and their slip sheets were intact. MgO obscured each SWB slip sheet. There was no evidence of exposure to heat or flame to the middle or bottom-tier SWB (AIB-FST-10392 and AIB-FST-10394, AIB-FST-10395). The lower half of the bottom-tier SWB was obscured by an extensive MgO buildup spilled from above (AIB-FST-10395).

The array face (west) side of the SWB slip sheets and three SWBs were intact, and with the exception of some minor drips the SWB lid (AIB-FST-10764), there was no evidence of exposure to heat or flame (AIB-FST-02004, AIB-FST-10743, AIB-FST-10745, AIB-FST-10753, AIB-FST-10754, AIB-FST-10755, AIB-FST-10756, AIB-FST-10757, AIB-FST-10758, AIB-FST-10759). MgO obscured the top of each SWB slip sheet. Most of the bottom-tier SWB was obscured by an extensive MgO buildup spilled from above (AIB-FST-10761 and AIB-FST-10762).

The north side of the SWB slip sheets and three SWBs were intact, and with the exception of some debris hung over the SWB lid (AIB-FST-10764), there was no evidence of exposure to heat or flame (AIB-FST-10765, AIB-FST-10767, and AIB-FST-10768). The bottom-tier SWB was partly obscured by an extensive MgO buildup spilled from above (AIB-FST-10846).

The bulkhead (east) side had evidence of plastics dripping from the top and along the sides of the upper-tier SWB (AIB-FST-10742, AIB-FST-10770, AIB-FST-10771, AIB-FST-10772, AIB-FST-10773, AIB-FST-10848). The top-tier SWB slip sheet, middle-tier SWB, middle-tier SWB slip sheet, and bottom-tier SWB are intact, and with the exception of some frozen plastic drips (AIB-FST-10774), there was no evidence of exposure to heat or flame (AIB-FST-10843, AIB-

FST-10844, AIB-FST-10845, and AIB-FST-10847). The bottom-tier SWB was almost completely obscured by an extensive MgO buildup spilled from above (AIB-FST-10845, and AIB-FST-10847).

4.13.3. Column 6

There was severe fire damage observed at R12:C6. Most of the MgO super sack fabric was gone (AIB-FST-10417, AIB-FST-10432).

The residual MgO pile base conforms to the shape of the top of the SWB and the sides had steep angles of repose. The height of the pile was truncated where the top of the super sack would have been present prior to the fire. This horizontal truncated area was close to rectangular. On this horizontal surface were pebble-like debris, which were translucent with smooth edges, and a remnant of the super sack fabric with jagged edges (AIB-FST-10414, AIB-FST-10415, and AIB-FST-10416). Material remnants of the super sack fabric were present near the slip sheet interface with the SWB on the array face (west) side (AIB-FST-10406, AIB-FST-10407), the north side (AIB-FST-10406, AIB-FST-10407, AIB-FST-10412), and the south side (AIB-FST-10401, AIB-FST-10413). The remnants on the array face side and north side hung down below the top of the SWB and the fabric weave was clearly visible (AIB-FST-10423, AIB-FST-10426). Remnants with jagged edges were also present. The cardboard stiffeners were missing or relocated. A cardboard stiffener from R12:C6 under a pile of MgO was present on the top of R11:C5 (AIB-FST-10404); the edges of this stiffener were charred (AIB-FST-10408).

The north side of the SWB, SWB slip sheet, and TDOP were intact, and with the exception of black streaks originating from the interface of the MgO super sack with the SWB lid (AIB-FST-10411, AIB-FST-10418), there was no evidence of exposure to heat or flame (AIB-FST-10405, AIB-FST-10409).

The array face (west) side of the MgO slip sheet, SWB, SWB slip sheet and TDOP were intact, and with the exception of the damaged super sack fabric, there was no evidence of exposure to heat or flame (AIB-FST-10402, AIB-FST-10406, AIB-FST-10407, AIB-FST-10412, AIB-FST-10424, AIB-FST-10425). MgO covered the fiberboard slip sheet and the MgO surface had black staining towards the SWB (AIB-FST-10430).

The south side of the SWB, SWB slip sheet, and TDOP were intact and there was no evidence of exposure to heat or flame (AIB-FST-10401, AIB-FST-10402, AIB-FST-10407).

On the bulkhead (east) side of the SWB, SWB slip sheet, and TDOP were intact (AIB-FST-10404). Black streaks were present on the upper half of the SWB side (AIB-FST-10401, AIB-FST-10403, AIB-FST-10413, AIB-FST-10427). The fiberboard slip sheet between the SWB and TDOP was not exposed because the fiberboard slip sheet was skewed toward the array face (west) side (AIB-FST-10402). The top of the TDOP was obscured by MgO that had spilled from above (AIB-FST-10419). White stalactite-like formations were present hanging from the TDOP lid (AIB-FST-10403, AIB-FST-10429, AIB-FST-10431) and the top bumper below the top of the TDOP (AIB-FST-10428, AIB-FST-10429). They are judged to have originated from the black polyethylene slip sheet under the MgO super sack and then covered with white MgO prior to freezing.

There was a crease in the bulkhead (east) sidewall of the TDOP that starts below the first bumper (AIB-FST-10420), extends past the second bumper (AIB-FST-10421) to at least the third bumper beyond which MgO covers the sidewall (AIB-FST-10422). The crease appears to be unrelated to the fire event.

4.14. Row 13

Row 13 contained three stacks. R13:C1 and R13:C5 consisted of three tiers of SWBs. R13:C3 had an SWB placed on two tiers of 55GD assemblies. None of the columns in Row 13 had an MgO super sack emplaced.

4.14.1. Column 1

There was no observed fire damage at R13:C1. The SWB slip sheets and three SWBs were intact and there was no evidence of exposure to heat or flame (AIB-FST-10824, AIB-FST-10825, AIB-FST-10826 AIB-FST-10827). There were negligible debris present on the top-tier SWB lid (AIB-FST-10822, AIB-FST-10823). Sampling efforts in May 2014 left trails in the dust layer which was on the SWB lid (AIB-FST-02009).

4.14.2. Column 3

There was severe fire damage observed at R13:C3. The stretch wrap and reinforcement plate for the middle-tier 55GD assembly had evidence of exposure to heat and flame (AIB-FST-02014, AIB-FST-10254). Figure 4-3 provides the nomenclature for discussion of individual drums in R13:C3.

MgO was present on the lid of the SWB on top of R13:C3 (AIB-FST-02003, AIB-FST-02011, AIB-FST-02045, AIB-FST-10648, AIB-FST-10743). A cardboard stiffener bridged between R14:C4 and R13:C3. Suspended between R11:C3 and R13:C3 was some super sack fabric under a layer of MgO. There was a pile of MgO on both R13:C3 and R11:C3. The material forming this bridge came from R12:C2 (AIB-FST-10654, AIB-FST-10852, AIB-FST-10853, AIB-FST-10854).

On the array face (west) side the SWB slip sheet and the middle-tier reinforcement plate were damaged. The stretch wrap from the middle-tier was gone (AIB-FST-10252, AIB-FST-10254).

On the south side the stretch wrap for the middle tier was melted and clumped on the side of Drum E (AIB-FST-02014, AIB-FST-10760). In addition, the reinforcement plate was distorted (AIB-FST-02013). Drum E (refer to Figure 4-3) on the middle-tier localized blackened regions, and a charred label between the middle and top rolling hoop (AIB-FST-02014). The SWB on the top-tier was intact and with the exception some blackened streaks there was no evidence of exposure to heat or flame (AIB-FST-02012, AIB-FST-10854, AIB-FST-10855, AIB-FST-10856, AIB-FST-10768). The stretch wrap on the bottom-tier was intact (AIB-FST-10760, AIB-FST-10761).

On the north side and bulkhead (east) side the SWB on the top-tier was intact, and with the exception some blackened streaks, there was no evidence of exposure to heat or flame (AIB-

FST-10654, AIB-FST-10856). MgO was deposited on the reinforcement plate of the middle 55GD assembly (AIB-FST-10219). The stretch wrap on the bulkhead (east) side, bottom-tier was intact (AIB-FST-10220, AIB-FST-10846). The lower half of the bottom-tier 55GD assembly was obscured by an extensive MgO buildup spilled from above (AIB-FST-10928).

4.14.3.   Column 5

There was minor fire damage observed at R13:C5. There was a charred cardboard stiffener SWB lid (AIB-FST-10118) and fire exposure evidence on the top SWB.

There were debris on the lid of the top-tier SWB (AIB-FST-10117). This included a cardboard stiffener that bridged between R13:C5 from R14:C4 (AIB-FST-10118, AIB-FST-10128).

On the south side, both the top-tier and middle-tier SWB slip sheets were damaged and there was evidence of flame exposure to the corresponding SWBs (AIB-FST-10120, AIB-FST-10121, AIB-FST-10122, AIB-FST-10123). The bottom tier had no evidence of damage and was mostly obscured by MgO spilled from above.

The array face (west) side of the SWB slip sheets and three SWBs were intact, and there was no evidence of exposure to heat or flame. Labels on the top tier were undamaged and legible on both the east and west sides of the SWB (AIB-FST-10119).

The bulkhead (east) side of the SWB slip sheets and three SWBs were intact, and there was no evidence of exposure to heat or flame (AIB-FST-11198, AIB-FST-11199, AIB-FST-11200, AIB-FST-11201, AIB-FST-11202, AIB-FST-11203, AIB-FST-11204, AIB-FST-11205, AIB-FST-11206, AIB-FST-11207, AIB-FST-11209). Much of the bottom tier was obscured by an extensive MgO buildup spilled from above (AIB-FST-11208).

The north side of the SWB slip sheets and three SWBs were intact (AIB-FST-10124, AIB-FST-10125, AIB-FST-10126). Much of the bottom tier was obscured by by an extensive MgO buildup spilled from above (AIB-FST-10127).

4.15.   Row 14

Row 14 contained three stacks. While each stack included a 4,200 lb, MgO super sack, each had a different configuration. R14:C2 consisted of three tiers of 100GD assemblies. R14:C4 contained three tiers of SWBs . R14:C6 consisted of a SWB placed on TDOP.

4.15.1.   Column 2

There was severe fire damage observed at R14:C2. There was severe damage to the exposed combustible emplacement materials. Figure 4-4 provides the nomenclature for discussion of individual drums in R14:C2.

The MgO super sack was damaged and the sack fabric was missing. The MgO formed three distinct piles with a high angle of repose (AIB-FST-02101, AIB-FST-2102, AIB-FST-10649, AIB-FST-10657, and AIB-FST-10659). The cardboard stiffener from the super sack formed a bridge between drums A and B (refer to Figure 4-4; AIB-FST-11089 and AIB-FST-11091).

Some residue from a burned stiffener was present on the north side of drum A (AIB-FST-11087 and AIB-FST-11095).

The three 100GD assemblies were severely damaged. Most of the exposed combustible emplacement materials were missing or melted (AIB-FST-10648, AIB-FST-10649, AIB-FST-10652, AIB-FST-10657, AIB-FST-10658, AIB-FST-11081, AIB-FST-11082, AIB-FST-11083, AIB-FST-11084, AIB-FST-11085, AIB-FST-11086, and AIB-FST-11092). There were black streaks on many of the drums (AIB-FST-11093 and AIB-FST-11094). There was no evidence of structural damage to the 100GDs (AIB-FST-02002, AIB-FST-10923, and AIB-FST-11098).

Small pieces of damaged stretch wrap were present on the top-tier drum C (AIB-FST-10918, AIB-FST-10919, and AIB-FST-10921) and there was a larger piece on the middle-tier, bulkhead (east) side of drum B (AIB-FST-11106). The melted plastic drips on the north side of top-tier drum A were standing out from the side of the drum (AIB-FST-11084, AIB-FST-11087, AIB-FST-11089, AIB-FST-11096, AIB-FST-11097, and AIB-FST-11100). A danger label on the top-tier drum B was damaged, but other labels near this location were intact and had no evidence of exposure to heat or flame (AIB-FST-10924 and AIB-FST-10925). Labels on top-tier drum A and C were intact (AIB-FST-11081, AIB-FST-10922 and AIB-FST-11101)

The 100GDs that comprise all of the assemblies were originally glossy black. They were coated by a fine white powder (AIB-FST-10930, AIB-FST-11102, AIB-FST-11103, AIB-FST-11104, and AIB-FST-11082) and the south side of drums B at the top and middle levels (, AIB-FST-10927, and AIB-FST-10929).

Much of the bottom tier assembly was obscured by an extensive buildup of MgO spilled from above. Drum A was covered nearly to the top rolling hoop on the array face (west) side (AIB-FST-11083 and AIB-FST-11104). Drum B was nearly covered on the bulkhead (east) side, while the upper rolling hoop was exposed near the assembly center (AIB-FST-10928, AIB-FST-11091, AIB-FST-11092, and AIB-FST-11094). Drum C was mostly covered (AIB-FST-10920 and AIB-FST-10926).

4.15.2.   Column 4

There was severe fire damage observed at R14:C4. The MgO super sack on the top of the SWB was damaged and the upper portion of the super sack fabric was gone.

The south, bulkhead (east) and north sides of MgO pile had a steep angle of repose. The height of the pile was truncated where the top of the super sack would have been present prior to the fire. This horizontal truncated area was close to rectangular (AIB-FST-10271 and AIB-FST-10277). The array face and south sides of the pile base conform to the underlying hexagonal slip sheet (AIB-FST-02003 and AIB-FST-02026). The MgO slip sheet was cantilevered over the SWB to create this outline. On the south side the MgO super sack inner pocket fabric was present and supported the MgO pile (AIB-FST-10174 and AIB-FST-10278). A cardboard stiffener bridged between R14:C4 and R13:C5 (AIB-FST-10273 and AIB-FST-10186). The edges of this stiffener were charred (AIB-FST-10284). The north edge conforms to the underlying SWB (AIB-FST-10138).

The MgO spillage on array face (west) side of the array interacted with the spillage from R16:C4 (AIB-FST-10272, AIB-FST-10282, AIB-FST-10285, and AIB-FST-10584). Remnants of the MgO super stack are present below this bridge (AIB-FST-10276). The array face side had a shallower slope than other three sides of the MgO pile. A cardboard stiffener was trapped in a vertical orientation by the spill (AIB-FST-10275 and AIB-FST-10280). The exposed parts of this stiffener charred.

During sampling on May 30, 2014 it was determined that a crust-like surface had formed on parts on the horizontal surface of the MgO pile (AIB-FST-10279). Once the crust was broken the MgO flowed freely.

The three SWBs were intact and there was no evidence of exposure to flame. The writing and paint on the sides of the SWBs shows no evidence of fire exposure (AIB-FST-02013, AIB-FST-02014, AIB-FST-02024, AIB-FST -02017, AIB-FST-02028, AIB-FST-10119, AIB-FST-10174, AIB-FST-10185, AIB-FST-10056, AIB-FST-10532, AIB-FST-10534, and AIB-FST-11244). String-like material hung from the bulkhead (east) side of the top-tier SWB slip sheet. The material did not hang straight; rather it curved from the cantilevered slip sheet and adhered to the side of the SWB (AIB-FST-02005 and AIB-FST-02006). The top-tier SWB slip sheet had char on the array face (west) side (AIB-FST-10945). There was a notch in the top-tier SWB slip sheet on the south side (AIB-FST-02017). This notch is judged to be isolated damage from emplacement operations.

The bottom-tier on the bulkhead (east) and array face (west) sides of the bottom-tier SWB were obscured by an extensive buildup of MgO spilled from above (AIB-FST-11245 and AIB-FST-10952).

4.15.3.   Column 6

There was severe fire damage observed at R14:C6. The super sack fabric was substantially gone (AIB-FST-02036, AIB-FST-10034). The remaining MgO formed a pile with steep sides and a base that conformed to the underlying SWB outline (AIB-FST-10029, AIB-FST-10035). Small pieces of material remain on top of the MgO and at the rib (AIB-FST-10028, AIB-FST-10036, AIB-FST-10042, AIB-FST-10210).

The array face (west) side of the SWB had dark streaks extending down from the top of SWB lid and the MgO slip sheet was melted or burned such that it does not extend beyond the SWB edge (AIB-FST-10029 and AIB-FSB-10030). MgO obscured the top of the SWB slip sheet and TDOP that extended beyond the SWB footprint (AIB-FST-10029). Parts of the SWB slip sheet that extended over the edge of the TDOP where charred (AIB-FST-10031, and AIB-FST-10038). There was MgO and a piece of super sack fabric on the floor against the rib between R14:C6 and R16:C6 (AIB-FST-10033). The TDOP was intact, but there was minor discoloration present (AIB-FST-10031).

The north side of the SWB had black streaks extending down from the SWB lid (AIB-FST-10034, AIB-FST-10035, AIB-FST-10038). MgO was deposited on the top of the slip sheet that the SWB sits on. MgO obscured the top of the SWB slip sheet and TDOP lid. The TDOP was intact and there was no evidence of exposure to heat or flame. The MgO super sack closure cord

hung near the north end of the SWB lid; some super sack material was inside the knot (AIB-FST-10035).

The bulkhead (east) side of the SWB was discolored and had debris clinging to the surface (AIB-FST-10034,). Black streaks and drips were present (AIB-FST-10043). MgO obscured the top of the SWB slip sheet and TDOP lid (AIB-FST-10040). The TDOP was intact and there was no evidence of exposure to flames. String-like objects hung from the top TDOP offset tube (AIB-FST-10041).

The south side of the stack was very near the rib, which prevented direct inspection. Although some black marks are present, there was no evidence of damage to the south side of the SWB or TDOP (AIB-FST-10029, AIB-FST-10031, AIB-FST-10033, AIB-FST-10034, AIB-FST-10043).

4.16.   Row 15

Row 15 contained three stacks. R15:C1 and R15:C3 contained a TDOP. R15:C1 contained a SWB placed on a TDOP. R15:C3 contained a 55GD assembly placed on a TDOP. R15:C5 contained a SWB placed on two tiers of 55GD assemblies. No MgO super sacks were emplaced on these stacks.

4.16.1.   Column 1

There was no observed fire damage at R15:C1. R15:C1 was adjacent to significant damage on R14:C2 and R16:C2, but there was no evidence of exposure to heat or flame (AIB-FST-10247, AIB-FST-10249, AIB-FST-10264). No combustible material was present on the top portion of R15:C1 to sustain combustion. The labels and markings on the SWB were legible. (AIB-FST-10241, AIB-FST-10246, AIB-FST-10248) There was a significant amount of MgO on the floor between R15:C1 and R14:C2. The lower half of the TDOP was obscured by the extensive buildup of MgO spilled from above. The SWB slip sheet was torn (AIB-FST-10247). The tear appears to be from handling operations during emplacement.

4.16.2.   Column 3

There was severe fire damage observed at R15:C3. The 55GD assembly emplacement materials were damaged. Figure 4-3 provides the nomenclature for discussion of individual drums in R15:C3.

The reinforcement plate on the top of the 55GD assembly had melted or burned with debris left in place on top of the drums, but with no part of the reinforcement plate left between the drums (AIB-FST-10254, AIB-FST-10255, AIB-FST-10256, AIB-FST-10257, and AIB-FST-10653). Each drum lid had areas of a smooth matrix of solidified material that had cracked into pieces with irregular edges (AIB-FST-10255). While no MgO would have been present on the stack prior to the release event, each drum has an accumulation of MgO on its lid (AIB-FST-10255). The MgO on drums B, F and E (refer to Figure 4-3) had sufficient MgO to form piles (AIB-FST-10255).

The stretch wrap that was around the 55GD assembly was gone. There were remnants of the stretch wrap remaining on the side of some of the drums (AIB-FST-10661). The labels were legible on the drums (AIB-FST-10258). Some of the drums had remains of the stretch wrap on the side (AIB-FST-10251, AIB-FST-10260, AIB-FST-10263).

The MgO super sack stiffener bridged across from R16:C4 (AIB-FST-10256) and R14:C2 (AIB-FST-10253) and formed piles on top of the drums in R15:C3 (AIB-FST-10257). MgO accumulated on the floor on the array face (west) side between R15:C3, R16:C2 and R17:C3 (AIB-FST-10257, AIB-FST-10259).

The TDOP was intact and there was no evidence of exposure to flame (AIB-FST-10252, AIB-FST-10261, and AIB-FST-10531).

4.16.3. Column 5

There was severe fire damage observed at R15:C5. The middle-tier 55GD assembly was damaged by fire exposure.

There was a moderate quantity of clumped material and MgO spillover on the SWB lid (AIB-FST-10166, AIB-FST-10167, AIB-FST-10580, and AIB-FST-10953). The depth of this material was greatest on the northwest corner where the stack was in close proximity to R16:C4 (AIB-FST-10172). Cardboard stiffener material was present on the north end of the lid. This most likely came from the MgO super sack at R16:C4. There was a concave burn pattern in a portion of the cardboard that was cantilevered over the edge of the lid (AIB-FST-02075). Such a burn-pattern is typical of horizontal material exposed to a flame from below. There were also smaller cardboard stiffener remains on the lid. These remains displayed striations of the corrugated layers within the original cardboard matrix (AIB-FST-02047 and AIB-FST-02048).

There were two locations on the SWB lid where small white MgO piles were present; one on the southeast corner and the second on the southwest corner (AIB-FST-10187). They cover the discolored material spread across the remainder of the lid. This suggests that the MgO was deposited after the clumped material dispersed across the lid surface. Two theories exist for this: (1) The super sacks on R16:C6 and R14:C6 spilled their contents sometime after the clumped material dispersal, and (2) The piles occurred during sampling efforts in May 2014. Although not definitive, available evidence supports that the latter theory is correct for the southwest corner (AIB-FST-10187 and AIB-FST-11350).

There were several trails in the debris running in the north-south direction (AIB-FST-10173 and AIB-FST-10584), which most likely occurred during sampling operations conducted in May 2014, since no trails were evident in videos taken on May 15, 2014 (AIB-FST-10598). The sampling operations demonstrated by disturbing the debris layer that below the light gray surface, which coats much of the array, there was darker deposits (AIB-FST-02065).

On the bulkhead (east) side the SWB, SWB slip sheet and two 55GD assemblies are intact and there was no evidence of exposure to heat or flame (AIB-FST-10137, AIB-FST-10183, AIB-FST-10184, AIB-FST-10185). There was significant MgO buildup on the floor area of this flue (AIB-FST-10576).

On the south side of the stack, the exposed SWB surface had no appreciable damage. The middle tier stretch wrap was intact across the south side from the frayed end where separation occurred on the west side to the wrap on the east side. The stretch wrap for the bottom tier was undamaged on the south side between R15:C5 and R16:C4 and on the west side. There was significant MgO buildup on the floor from the adjacent stacks that concealed all but the very top of the reinforcement plate and stretch wrap on the bottom tier (AIB-FST-10599, AIB-FST-10600, AIB-FST-10601, AIB-FST-10602, AIB-FST-10603, AIB-FST-10604).

On the array face (west) side, there was evidence of flame damage on the west side of the SWB (AIB-FST-10169). The fiberboard slip sheet under the SWB was charred, especially near the interface where the two west drums (G and F) meet. Above this damage was a 12-inch high inverted cone burn pattern on the side of the SWB (AIB-FST-10168). Additionally, the fiberboard slip sheet had a U-shaped damage region (AIB-FST-10130, AIB-FST-10170). The middle tier 55GD assembly had significant flame damage that consumed the west side of the stretch wrap as well as melted the polyethylene reinforcement plate (AIB-FST-10136). Drum G on the middle tier exhibited localized overheat damage. Between the middle and upper rolling hoops there were two labels. One label was discolored; it was painted to conceal an old label. The second (yellow) label had no damage (AIB-FST-02063 and AIB-FST-10129). The size of the holes in the middle tier slip sheet, and the adjacent reinforcement plate, appeared larger than normal and were no longer fully round. There was clumped MgO resting on the middle-tier slip sheet (AIB-FST-10135, AIB-FST-10171). The stretch wrap on the bottom-tier was intact and there is no evidence of exposure to heat or flame to this tier.

On the north side of the SWB, there was burned cardboard stiffener material on the SWB lip and hanging on the SWB upper bumper (AIB-FST-10581 and AIB-FST-10583). The SWB slip sheet and middle-tier reinforcement plate between waste drums B and G (refer to Figure 4-3) were consumed on the north side, as was the stretch wrap material on the middle tier (AIB-FST-10578, AIB-FST-10582, and AIB-FST-10626). Much of the lower-tier is obscured by an extensive buildup of MgO spilled from above; where exposed for inspection, the stretch wrap was intact (AIB-FST-10572, AIB-FST-10573, AIB-FST-10574, AIB-FST-10575, AIB-FST-10576).

4.17.   Row 16

Row 16 contained three stacks. Each stack included a 4,200 lbs MgO super sack. R16:C2 and R16:C6 consisted of a SWB set on a TDOP. R16:C4 consisted of a 55GD assembly set on a TDOP.

4.17.1.   Column 2

There was severe fire damage observed at R16:C2. The super sack fabric was substantially gone. The MgO pile had a steep angle of repose on all sides, with the top essentially flat and level (AIB-FST-02099, AIB-FST-10514 and AIB-FST-10971). The base of the pile and the super sack slip sheet conform to the underlying SWB lid (AIB-FST-10513, AIB-FST-10972. A cardboard stiffener bridged between R16:C2 and R17:C3 (AIB-FST-10971 and AIB-FST-10972). A stiffener at the northeast corner of the SWB lid cantilevered toward R15:C1 (AIB-

FST-02099), and another stiffener hung at a 1:1 slope from the northwest corner of the SWB lid (AIB-FST-10973). The exposed edges of these stiffeners were charred and irregular.

The top tier SWB was intact with minor char patterns and label damage on the upper portion of the array face (west) and bulkhead (east) sides (AIB-FST-10973 and AIB-FST-10513). Labels on the south side were intact and legible (AIB-FST-10972). The TDOP was intact and there was no evidence of exposure to heat or flame (AIB-FST-10974, AIB-FST-10975 and AIB-FST10976).

4.17.2. Column 4

There was severe fire damage observed at R16:C4. There was significant damage to the MgO super sack and upper-tier reinforcement plate (AIB-FST-02049). A drum in this location breached, expelling some of its contents. Figure 4-3 provides the nomenclature for discussion of individual drums in R16:C4.

The residual MgO form five distinct cones over drums (A, B, C, F and G) that were similar to other locations where the MgO super sacks were damaged (AIB-FST-02072, AIB-FST-10521, and AIB-FST-10533). The MgO angle of repose for the two southeastern most drums (E and D) was smaller (i.e., less steep) than most of the other locations where MgO fabric was missing or damaged (AIB-FST-10523 and AIB-FST-10520). Movement of the drum E lid during the breach may have contributed to this configuration. A remnant from the super sack fabric was present on the top of the MgO pile (AIB-FST-10522).

The MgO slip sheet and the 55GD assembly reinforcement plate for the top tier was missing beyond the outline of the drums all around the assembly (AIB-FST-02072, AIB-FST-10521, AIB-FST-10536, and AIB-FST-10946). The stretch wrap was also gone.

Drum E (refer to Figure 4-3), experienced significant overheating, substantive damage, and a lid breach (AIB-FST-02051). There was an orange-yellow tinged material built up around the mouth of the breach along the south side (AIB-FST-02085 and AIB-FST-02107). A "clean" burn region, where all paint and fire deposits have been burned away, occurred on the south side of this drum between the lower and middle rolling hoop (AIB-FST-02086 and AIB-FST-10529). While much of the exposed drum surface experienced a color change, there was a portion below the lower rolling hoop that had not changed color (AIB-FST-10530). There was a damaged label between the middle and upper rolling hoop (AIB-FST-02083 and AIB-FST-02087). The label was partially charred, indicating that the heat exposure in this region was less severe than that near the clean burn.

A portion of the drum E lid breach was covered by a cardboard stiffener that bridged between R15:C5 and R16:C4 (AIB-FST-02085 and AIB-FST-10954). The drum breach was observable from the bulkhead (east) side of this bridge (AIB-FST-10955 and AIB-FST-10956). There was evidence of charred and melted materials in this region.

There was no evidence indicating that the other drums in the 55GD breached:

- Drum A, at the center of the assembly, could be viewed in the gap between drums F and G. There was no evidence of damage (AIB-FST-10524).
- Drum B had no evidence of damage (AIB-FST-10533).
- Drum C had no evidence of damage (AIB-FST-10532 and AIB-FST-10536). Because the top tier assembly was not centered on the TDOP, the assembly overhung the bulkhead (east) side of the TDOP and drum C was substantially unsupported (AIB-FST-10945 and AIB-FST-10951).
- Drum D, which was a dunnage drum, had no evidence of damage (AIB-FST-10534 and AIB-FST-10536)
- Drum F was damaged (AIB-FST-02049 and AIB-FST-10524). Black streaks and frozen drips were present on the side of drum F (AIB-FST-02083, AIB-FST-10525, AIB-FST-10526, AIB-FST-10749, and AIB-FST-10750). There were two labels between the middle and top rolling hoops (AIB-FST-10525). The south-most label had minor damage, but the west-most was undamaged (AIB-FST-10527 and AIB-FST-10750). The south side of the drum had significant surface discoloration (AIB-FST-02083).
- Drum G had no evidence of damage (AIB-FST-02049, AIB-FST-10524, and AIB-FST-10531).

Much of the 55GD assembly slip sheet was obscured by MgO spilled from above. A small undamaged region was partially uncovered near drum G (AIB-FST-10948 and AIB-FST-10947). The slip sheet was missing below portion drum D that overhung the TDOP (AIB-FST-10535).

There was a gap above the southeast lip drum D and below the overlying reinforcement plate (AIB-FST-10949). Along the eastern most mouth of the gap, an orange-yellow tinted granular material appears to ooze out (AIB-FST-10950). The reinforcement plate plastic had melted and drooped (AIB-FST-10950). Immediately to the east of the ooze, an apparent gap had opened between the top of the drum and the material above (AIB-FST-10892). The reinforcement sheet and MgO super sack slip sheet were missing. There was material deep within the gap that appeared to be vertically striated. Above the gap was undamaged polypropylene fabric. Comparing the periodicity of the striations to the fabric weave characteristics, the striated material could be a single ply of cardboard stiffener.

The TDOP was intact and there was no evidence of exposure to heat or flame on the west and south sides (AIB-FST-02051, AIB-FST-02066, AIB-FST-10951, and AIB-FST-10535). Polyethylene drips and some discoloration were present on the east side of the TDOP (AIB-FST-10952).

4.17.3.   Column 6

There was severe fire damage observed at R16:C6. The MgO super sack was substantially gone. The residual MgO pile base conforms to the shape of the top of the SWB and the sides had steep angles of repose. A cardboard stiffener, under a coating of MgO, bridged between R16:C6 and R17:C5 (AIB-FST-10199 and AIB-FST-10200). MgO was slumped onto the south rib and was judged to be supported by cardboard stiffener (AIB-FST-10204). Some sack fabric was trapped between this MgO and the rib (AIB-FST-10201). A burn mark was present on the rib where the super sack contacted the rib (AIB-FST-10204).

The array face (west) side of the SWB had dark streaks extending down from the lid and the MgO slip sheet was melted or burned away such that it did not extend beyond the SWB lid (AIB-FST-10199). MgO obscured the top of the SWB slip sheet and the TDOP. The TDOP was intact and there was no evidence of exposure to heat or flame (AIB-FST-10202).

The north side of the SWB had black discoloration extending down from the lid of the SWB, on the upper bumper and below the lower bumper adjacent to R17:C5 (AIB-FST-10203). There was some black material present on the top of the SWB slip sheet immediately below the discoloration located below the lower bumper (AIB-FST-10386). The super sack slip sheet did not extend beyond the lid except in the location where the cardboard bridged between R16:C6 and R17:C5 and covered the slip sheet (AIB-FST-10203). The SWB slip sheet was intact and top obscured by MgO spilled from above (AIB-FST-10205). The TDOP was intact and there was no evidence of exposure to heat or flame (AIB-FST-10206). MgO was deposited on the floor adjacent to the TDOP (AIB-FST-10207).

The bulkhead (east) side of the SWB had some shading or darkening (AIB-FST-10210). The MgO slip sheet was melted or burned away such that it did not extend beyond the SWB lid (AIB-FST-10208). Black residue was present in the form of drips extending from the edge of the SWB and generally covering the sides of the lifting clips (AIB-FST-10210). The top of the SWB slip sheet and the TDOP lid were obscured by MgO spilled from above. The TDOP and the SWB fiberboard slip sheet were intact and there was no evidence of exposure to flame (AIB-FST-10208 and AIB-FST-10209). Several (i.e., 3 to 5) string-like features appear to hang from the top of the TDOP (AIB-FST-10208).

The south side of the stack was close to the rib, which prevented direct visual inspection. The SWB slip sheet between R16:C6 and the south rib was intact and had negligible material debris accumulation (AIB-FST-10211). There was also no damage to the adjacent array face (west) and bulkhead (east) sides. Given the available evidence the south side of R16:C6 is judged intact with no evidence of heat or fire exposure.

4.18.   Row 17

Row 17 contained three stacks. Each stack consisted of an SWB set on a TDOP. There were no MgO super sacks on these stacks.

4.18.1.   Column 1

There was no observable fire damage at R17:C1. The SWB and TDOP were intact and there was no evidence of exposure to heat or flame (AIB-FST-10240, AIB-FST-10241). The markings and labels were legible on both the TDOP and SWB. There was negligible residual material present on the SWB lid (AIB-FST-02099). The material was from the damage to the MgO super sacks on top of R16 C2 and R18 C2 (AIB-FST-10240, AIB-FST-10241). The fiberboard slip sheet under the SWB in R17:C1 was torn; this would have occurred during waste emplacement activities. There was no evidence of it being charred or exposed to flames (AIB-FST-10879).

4.18.2.   Column 3

There was minor fire damage observed at R17:C3. The south side of the TDOP had evidence of flame impingement (AIB-FST-10885).

SWB slip sheet was charred (Damage to the waste containers was very minor, primarily from melted and burning material falling onto R17:C3 from adjoining assemblies. A cardboard stiffener formed a bridge between R16:C2 and R17:C3 (AIB-FST-10881). A second stiffener formed a bridge between R16:C4 and R17:C3 (AIB-FST-10883). MgO sits on both bridges. Aside from this, there was little residual material present on the SWB lid (AIB-FST-10887).

There was very minor discoloration at the base of the TDOP on the south side. This was caused by burning plastics falling from R16:C4 (AIB-FST-10885). There was some very minor physical damage to the SWB slip sheet on the southwest corner next to R18:C2; this would have occurred during emplacement operations. There is a piece of cardboard stiffener with burned edges at the base of the TDOP (AIB-FST-10889 and AIB-FST-10890). Except as noted, the SWB, fiberboard slip sheets, and TDOP were intact and there was no evidence of exposure to heat or flame (AIB-FST-10884, AIB-FST-10886, AIB-FST-10882, AIB-FST-10888, AIB-FST-10891, AIB-FST-10880, AIB-FST-10889). While fire and heat damage to the stack immediately east (R15:C3) was severe, the R17:C3 stack was unaffected.

4.18.3.   Column 5

There was minor fire damage observed at R17:C5; SWB sides were discolored and SWB slip sheet was damaged.

There were debris on the SWB lid and a cardboard stiffener bridged between R16:C6 and R17:C5. The edges of the stiffener were charred and the top was obscured by a by the MgO released from R16:C6 (AIB-FST-10373, AIB-FST-10378, AIB-FST-10389, AIB-FST-10390, AIB-FST-10398, and AIB-FST-10788).

The array face (west) side of the SWB and TDOP were intact, and with the exception of minor discoloration on the bottom south corner of the SWB (AIB-FST-10381), there was no evidence of exposure to heat or flame (AIB-FST-10373, AIB-FST-10374, AIB-FST-10375, AIB-FST-10376, AIB-FST-10377, AIB-FST-10378, AIB-FST-10379, and AIB-FST-10389). There was minor damage to the southwest corner of the SWB slip sheet (AIB-FST-10375 and AIB-FST-10377). This may have been damaged during material handling or char; available evidence supports both theories.

The south side of the SWB, SWB slip sheet, and TDOP were intact and there was no evidence of exposure to heat or flame (AIB-FST-10746, AIB-FST-10375, AIB-FST-10380, AIB-FST-10381, and AIB-FST-10391).

The bulkhead (east) side of the SWB and TDOP were intact. The SWB was discolored (AIB-FST-10383, AIB-FST-10385, and AIB-FST-10386, AIB-FST-10747, and AIB-FST-10748), but the TDOP had no evidence of exposure to heat or flame. The SWB slip sheet, TDOP lid and the

upper surface of the TDOP offset tubes were obscured by MgO spilled from above and other debris (AIB-FST-10384, AIB-FST-10387, and AIB-FST-10388).

The north side of the SWB and TDOP were intact. The SWB was discolored, but the TDOP had no evidence of exposure to heat or flame (AIB-FST-02073, AIB-FST-10396, AIB-FST-10397, AIB-FST-10398, AIB-FST-10399, AIB-FST-10400, AIB-FST-10749, and AIB-FST-10786). The northeast corner of the SWB slip sheet (adjacent to R16:C4) was damaged and debris obscured the top of the sheet (AIB-FST-10387, AIB-FST-10388, and AIB-FST-10750).

4.19.   Row 18

Row 18 contained three stacks. R18:C2 consisted of three stacked SWBs and a 3,000 lbs MgO super sack. R18:C4 consisted of a 3,000 lbs MgO super sack and a SWB placed on a TDOP. R18:C6 consisted of a 3,000 lbs MgO super sack placed and a SWB placed on two stacked 55GD assemblies. These two assemblies contained 13 POP assemblies.

4.19.1.   Column 2

There was severe fire damage observed at R18:C2. Much of the super sack fabric was missing and other exposed emplacement materials were damaged.

The residual MgO pile is present on the upper-tier SWB lid. The sides of this pile were steep and the pile top was truncated where the top of the super sack would have been present prior to the release event. Residue super sack fabric was present on this horizontal surface (AIB-FST-11163). Two cardboard stiffeners bridged to neighboring stacks; one to R19:C3 and another to R17:C3 (AIB-FST-11164, AIB-FST-11177). A third stiffener was cantilevered on the array face (west) side; this stiffener was supported by the super sack slip sheet (AIB-FST-11184 and AIB-FST-11185). A stiffener was also cantilevered from the north side (AIB-FST-11183, AIB-FST-11165, AIB-FST-11175, and AIB-FST-11187). The top of each stiffener was obscured by MgO and the edges were charred. No cardboard stiffener was present on the bulkhead (east) side and the base of the MgO pile conformed with the edge of the SWB lid (AIB-FST-11170 and AIB-FST-11171).

The bulkhead (east) side of the super sack slip sheet was obscured by the residual MgO pile (AIB-FST-11170, AIB-FST-11171, AIB-FST-11172, and AIB-FST-11173). The top-tier SWB has black streaks and drips near the lid. They are judged to be slip sheet material that was exposed to heat or fire. Damage was present on the northeast corner of the sheet (AIB-FST-11187).

The top-tier SWB was intact, but was discolored on the bulkhead (east) side (AIB-FST-11170, AIB-FST-11171, AIB-FST-11172, and AIB-FST-11173). The array face (west) side of this SWB was discolored near the base and the top-tier slip sheet was charred (AIB-FST-11166, AIB-FST-11174, and AIB-FST-11184). Super sack fabric hung across this face (AIB-FST-11162). The south side had dark colored staining from the SWB base, up to the bottom bumper, on the vertical face of the bottom bumper, and above the bottom bumper. This discoloration was directly above the charred middle-tier SWB slip sheet (AIB-FST-11178 and AIB-FST-11179).

There was no evidence that the north side of the SWB or slip sheet was exposed to heat or flame (AIB-FST-11187 and AIB-FST-11186).

The middle-tier SWB was intact, but the south side was discolored. Dark vertical lines were present below the slip sheet on the south face of the middle position SWB. Dark and light colored debris and what appeared to be dark colored drips were present on the top horizontal surface of the middle position SWB top bumper (AIB-FST-11178 and AIB-FST-11179). The north east section of the middle-tier slip sheet had charred material and possible damage (AIB-FST-11184). Except as noted, there was no evidence of heat or fire exposure to the middle-tier SWB and SWB slip sheet (AIB-FST-11172, AIB-FST-11173, AIB-FST-11186, and AIB-FST-11187).

The bottom-tier SWB was partially obscured by MgO buildup spilled from above. The exposed portions of the SWB were intact and there was no evidence of exposure to heat or flame (AIB-FST-11169, AIB-FST-11184, AIB-FST-11186, AIB-FST-11182). Debris were present at the south side of R18:C2 (AIB-FST-11182).

4.19.2.   Column 4

There was minor fire damage observed at R18:C4. The MgO super sack was partially damaged on the bulkhead (east) side (AIB-FST-10080 and AIB-FST-10087). The other sides were undamaged (AIB-FST-02104, AIB-FST-10075, AIB-FST-10389, and AIB-FST-10390). The damage was likely the result of exposure to a heat flux source that melted the polypropylene fabric but did not damage the underlying cardboard stiffener. The slip sheet below the MgO super sack has no evidence of damage (AIB-FSB-02073, AIB-FST-10075, AIB-FST-10080, AIB-FST-10786, AIB-FST-10789). There was no damage to the top of the MgO super sack (AIB-FST-02049, AIB-FST-02092); but a small quantity of salt particles were present towards the array face (west) side of the sack (AIB-FST-10828).

The SWB and TDOP were intact and there was no evidence of exposure to heat or flame (AIB-FST-10075, AIB-FST-10080, AIB-FST-10099, AIB-FST-10100, AIB-FST-10376, AIB-FST-10377, AIB-FST-10400, AIB-FST-10714, AIB-FST-10786, AIB-FST-10788, and AIB-FST-10789).

4.19.3.   Column 6

There was severe fire damage observed at R18:C6. Most of the super sack fabric was gone and the middle-tier assembly is damaged. Figure 4-3 provides the nomenclature for discussion of individual drums in R18:C6.

Most of the super sack fabric was gone. There are fabric remnants remaining on the top of the pile (AIB-FST-02104, AIB-FTS-10303). The residual MgO pile base conforms to the SWB lid shape on the bulkhead (east) and array face (west) sides. On the north and bulkhead sides the pile sides are step (AIB-FTS-10303 and AIB-FST-10444). The super sack slip sheet on these bulkhead and array face sides was damaged. The south side of the pile was in contact with the rib; it had a steep slope near the top and flattened near the rib. There was a dark spot on the rib near R18:C6 (AIB-FST-10449). The slope of the bulkhead (east) side was irregular (AIB-FTS-

10445). A very short section of metal square tubing (AIB-FST-10443) rests atop the MgO mound in the bulkhead-rib quadrant. This tubing was from the MgO storage rack system. The bar was inadvertently left atop the MgO super sack when the sack was emplaced.

The MgO pile overhung the north side of the SWB; there was a stiffener supporting this portion of the pile (AIB-FST-10445 and AIB-FST-10611). The top of the stiffener was obscured by the MgO. There was a fraying pattern along the leading edge of the MgO that was indicative of the fabric weave (AIB-FST-10445 and AIB-FST-10446).

The SWB is intact, and there was no evidence of heat or flame exposure to the north or south sides. There were black deposits and drips on the array face (west) and bulkhead (east) sides of the SWB; the lifting clips and filter ports also had black deposits and a light dusting of MgO powder (AIB-FST-10302, AIB-FST-10303, AIB-FST-10448, AIB-FST-10455, and AIB-FST-10456). At the center-bottom of the array face (west) side, directly above drum E and F (refer to Figure 4-3) of the middle-tier 55GD assembly, there was a darkened section that resembles a flame exposure pattern. The darkened section was more pronounced on in the area closest to the rib (AIB-FST-10455).

The middle-tier 55GD assembly was damaged on the array face (west) side. There was no evidence of exposure to heat or flame on the other three sides (AIB-FST-10302, AIB-FST-10450, AIB-FST-10452, AIB-FST-10453). Above drums F and G the SWB slip sheet and adjacent middle-tier reinforcement plate were gone (AIB-FST-10457). The missing portions followed the contour of the underlying 55GDs (AIB-FST-10001, AIB-FST-10002, AIB-FST-10300, AIB-FST-10301, and AIB-FST-10457). The stretch wrap along the entire array face (west) side was absent (AIB-FST-10457). The corresponding ends of the stretch wrap on both the north side (AIB-FST-10459) and rib side (AIB-FST-10460) are clumped along the sides of their respective drums. Both drum F and G had black stains that likely came from the melted reinforcement plate (AIB-FST-10458, AIB-FST-10461, AIB-FST-10462, and AIB-FST-10609). Melted polyethylene adhered to its side of drum F near the top rolling hoop with a small amount of residual drip directly below on the next rolling hoop (AIB-FST-10463). The top of drum F contains a cracked residual substance with a white coating (AIB-FST-10610).

The middle-tier slip sheet was obscured by a variety of debris (AIB-FST-10614, AIB-FST-10613, AIB-FST-10612, AIB-FST-10622, and AIB-FST-10625). All of the debris were coated with a white material, which was likely MgO. There were localized areas where melted materials, most likely polyethylene, landed on the horizontal surface. There was a small region at the base of Drum F that displayed a shiny surface surrounded by dark discoloration. This was likely caused by flame impingement on the drum that involved burning material which landed on the slip sheet.

Most of the stretch wrap for the bottom tier was undamaged with labeling and features of the reinforcement plate clearly discernible (AIB-FST-10554). On the bulkhead (east) side, the bottom 55GD assembly was concealed since the small space between it and the stack in position R16:C6 was nearly filled by spilled MgO (AIB-FST-10458 and AIB-FST-10302). There was damage to the stretch wrap at the northwest corner of the stack (AIB-FST-10615). It was very likely that damaged super sack fabric fell onto this corner, draped over the edge of the lower tier of the 55GD assembly and burned. This burning damaged the stretch wrap.

Along the floor area of the bottom 55GD assembly on the array face (west) side of the stack there was an MgO super sack cardboard stiffener leaning against the drums (AIB-FST-10458 and AIB-FST-10618). There was char on the vertical edges of the stiffener (AIB-FST-10616 and AIB-FST-10620). About half of the stiffener was buried in MgO (AIB-FST-10621). There was a hole in the right center of the stiffener. This damage was adjacent to fallen debris (AIB-FST-10617, AIB-FST-10619, and AIB-FST-10623), which might be fallen super sack fabric. The hole was likely created by the combustion of the fallen debris. There were other debris on the floor adjacent to stacks R17:C5, R18:C6 and R20:C6. These appear to be fallen MgO super sack (AIB-FST-10624).

4.20.   Row 19

Row 19 contained a single stack in position R19:C3. The stack comprised of an SWB on a TDOP.

There was minor fire damage observed at R19:C3. There was an MgO super sack cardboard stiffener, which had fallen onto the SWB lid, was charred.

There was light dusting of MgO powder over the SWB lid. There was also ash and char material on the lid. A cardboard stiffener bridged between R18:C2 and R19:C3; the top of the stiffener was obscured by MgO spilled from R18:C2 (AIB-FST-11340, AIB-FST-11342, AIB-FST-11343, AIB-FST-11344, and AIB-FST-11347).

The SWB, SWB slip sheet and TDOP were intact and there was no evidence of exposure to heat or flame (AIB-FST-11315, AIB-FST-11316, AIB-FST-11317, AIB-FST-11322, AIB-FST-11336, AIB-FST-11337, AIB-FST-11338, AIB-FST-11339, AIB-FST-11341, AIB-FST-11345, AIB-FST-11346, AIB-FST-11347, and AIB-FST-11348).

4.21.   Row 20

Row 20 contained three stacks. R20:C2 and R20:C6 contained a 3,000 lbs MgO super sack and an SWB placed on an SLB2. R20:C4 contained a 3,000 lbs MgO super sack and an SWB placed on a TDOP.

4.21.1.   Column 2

There was no observed fire damage at R20:C2. The MgO super sack, polyethylene slip sheet, SWB, SWB slip sheet, and SLB2 were intact and there no evidence of exposure to heat or flame (AIB-FST-10664, AIB-FST-10665, AIB-FST-10666, AIB-FST-10667, AIB-FST-10668, AIB-FST-10669, AIB-FST-10670, AIB-FST-10671, AIB-FST-10672, AIB-FST-10911, AIB-FST-10912, AIB-FST-10913, AIB-FST-10914, AIB-FST-10938, AIB-FST-10939, AIB-FST-10940, AIB-FST-10941, AIB-FST-10942, AIB-FST-10943). There was a small amount of MgO deposited on the south bulkhead top corner of the SLB2 which came from damage to R18:C2 (AIB-FSB-10914). The cardboard stiffener on the southeast side of the MgO super sack was exposed about 9-inches above the pocket. The adjacent stiffeners were slightly exposed (AIB-FST-02097, AIB-FST-10665, AIB-FST-10670). This condition was a result of material handling activities, not the release event.

4.21.2.   Column 4

There was no observed fire damage at R20:C4. The MgO super sack, polyethylene slip sheet SWB, SWB slip sheet, TDOP were intact and there was no evidence of exposure to heat or flame (AIB-FST-10098, AIB-FST-10099, AIB-FST-10100, AIB-FST-10101, AIB-FST-10104, and AIB-FST-10116). The labels and markings on the side of the SWB were legible.

4.21.3.   Column 6

There was no observed fire damage at R20:C6. The MgO super sack, polyethylene slip sheet SWB, SWB slip sheet, SLB2 were intact and there was no evidence of exposure to heat or flame (AIB-FST-10353, AIB-FST-10354, AIB-FST-10355, AIB-FST-10356, AIB-FST-10357). The labels and markings on the side of the SWB were legible. The SWB slip sheet was not centered under the SWB (AIB-FST-10353, AIB-FST-10356); this would have occurred during waste emplacement activities. There were debris on the SLB2 lid adjacent to the lid (AIB-FST-10357).

4.22.   Row 21

Row 21 contains three stacks. All three stacks consisted of an SWB set on a TDOP. There were no MgO super sacks on these stacks.

4.22.1.   Column 1

There was no observed fire damage at R21:C1. The SWB, SWB slip sheet, TDOP were intact and there was no evidence of exposure to heat or flame (AIB-FST-10793, AIB-FST-10794, AIB-FST-10795, AIB-FST-10796, AIB-FST-10797, and AIB-FST-10798).

4.22.2.   Column 3

There was no observed fire damage at R21:C3. The SWB, SWB slip sheet, TDOP were intact and there was no evidence of exposure to heat or flame (AIB-FST-11233, AIB-FST-11234, AIB-FST-11235, AIB-FST-11236, AIB-FST-11237, AIB-FST-11238, AIB-FST-11239, AIB-FST-11240, AIB-FST-11241, and AIB-FST-11242).

4.22.3.   Column 5

There was no observed fire damage at R21:C5. The SWB, SWB slip sheet, TDOP were intact and there was no evidence of exposure to heat or flame (AIB-FST-10095, AIB-FST-10096, and AIB-FST-10097).

4.23.   Row 22

Row 22 contained three stacks. R22:C2 had a 3,000 lbs MgO super sack and a SWB placed on a TDOP. R22:C4 had a 4,200 lbs MgO super sack and a SWB placed on a TDOP. R22:C6 consisted of three SWBs and a 3,000 lbs MgO super sack.

4.23.1. Column 2

There was no observed fire damage at R22:C2. The MgO super sack, polyethylene slip sheet, SWB, SWB slip sheet, TDOP, and TDOP slip sheet were intact and there was no evidence of exposure to heat or flame. White dust-like material was present on the exposed top horizontal surfaces of the waste containers and slip sheets (AIB-FST-10968, AIB-FST-11152, AIB-FST-11153, AIB-FST-11155, AIB-FST-11156, AIB-FST-11157, AIB-FST-11158, AIB-FST-11159, AIB-FST-11160, and AIB-FST-11161).

4.23.2. Column 4

There was no observed fire damage at R22:C4. The MgO super sack, polyethylene slip sheet, SWB, SWB slip sheet, TDOP, and TDOP slip sheet were intact and there was no evidence of exposure to heat or flame (AIB-FST-10316, AIB-FST-10317, AIB-FST-10318, AIB-FST-10319, AIB-FST-10322, AIB-FST-10323, AIB-FST-10324, AIB-FST-10327). White dust-like material was present on the exposed top horizontal surfaces of the waste containers and slip sheets.

4.23.3. Column 6

There was no observable fire damage at R22:C6. The MgO super sack, three SWBs, and three SWB slip sheets intact and there was no evidence of exposure to heat or flame (AIB-FST-10197, AIB-FST-10198).

4.24. Row 23

Row 23 contained three stacks. R23:C1 consisted of an SWB placed on a TDOP. R23:C3 consisted of a 55GD assembly placed on a TDOP. All of these 55GDs contain POPs. R23:C5 consisted of three stacked 55GD assemblies. There were eighteen POPs in these 55GDs. There were no MgO super sacks on these stacks.

4.24.1. Column 1

There was no observed fire damage at R23:C1. The SWB, SWB slip sheet, TDOP were intact and there was no evidence of exposure to heat or flame (AIB-FST-10243, AIB-FST-10244, AIB-FST-10245, AIB-FST-10795, and AIB-FST-10814). The labels and markings were legible on the SWB. This stack was located at the face of the disposal array.

4.24.2. Column 3

There was no observed fire damage at R23:C3. The 55GD assembly, and the TDOOP were intact and there was no evidence of exposure to heat or flame (AIB-FST-10331, AIB-FST-10515, AIB-FST-10516, AIB-FST-10965, and AIB-FST-10966). The labels and markings on the waste containers were legible. This stack was located at the face of the disposal array.

4.24.3. Column 5

There was no observed fire damage at R23:C5. The three 55GD assemblies were intact and there was no evidence of exposure to heat or flame (AIB-FST-10367, AIB-FST-10368, AIB-

FST-10369, AIB-FST-10370, AIB-FST-10371, AIB-FST-10372, AIB-FST-10197). This stack was located at the face of the disposal array.

4.25.   Row 24

Row 24 contained a single stack in position R24:C2. The stack comprised a 3,000 lbs MgO super sack on three SWBs.

There was no observed fire damage at R24:C2. The MgO super sack, three SWBs, and the slip sheets were intact and there was no evidence of exposure to heat or flame (AIB-FST-10328, AIB-FST-10329, AIB-FST-10330, AIB-FST-10331, AIB-FST-10332, AIB-FST-11149, AIB-FST-11150, AIB-FST-11151). White dust-like material was present on the exposed top horizontal surfaces of the waste containers and slip sheets . This stack was located at the face of the disposal array.

5.0   VENTILATION EVALUATION

This chapter documents the underground ventilation conditions that existed at WIPP before, during and after the radiological release event, which occurred on the evening of February 14, 2014. The topics covered in this chapter include:

• Underground ventilation and event description (Section 5.1)
• Description of ventilation-related sensors and available data (Section 5.2)
• Analysis of ventilation data averaged over 1 minute periods (Section 5.3)
• Analysis of ventilation data averaged over ⅛ second periods (Section 5.4)
• Summary (Section 5.5)

5.1.   Release Event Ventilation Description

On February 14, 2014, the WIPP underground was running in the Alternate Ventilation Mode. In this ventilation mode, one 700 series fan is used to ventilate the facility, pulling air out the ES with an approximate flow of 260 thousand cubic-feet-per-minute (kcfm). [18] Workers had been in the underground February 14 collecting additional information for the fire investigation and inspecting Panel 7 Room 7 due to previous findings of protruding roof bolts and cracks in the rib near the active waste face. [1] By 1652 on February 14, 2014, bulkhead (BH)-707 had been manually shut and all individuals had left the underground and been accounted for. [1]

At 2313 February 14, 2014, a "HI RAD" alarm from CAM-151 in the underground, monitoring the Panel 7 exhaust drift, was received on the central monitoring system. This was followed by a "HI-HI RAD" alarm from the same instrument at 2314. The "HI RAD" alarm setpoint was 30 Derived Air Concentration (DAC) for alpha and beta contamination and the "HI-HI RAD" setpoint was 50 DAC. [1] The central monitoring system indicated that the CAM reading got as high as 210,000 DAC. The "HI-HI RAD" alarm initiated a change to Filtered Ventilation Mode for the mine ventilation system.

During this switch to Filtered Ventilation Mode, the active 700 series fan, with a rating of 260 kcfm, is shutdown, one 860A fan rated at 59 kcfm flow is started, and two of the bulkheads in the underground close. Prior to leaving the underground that day, BH-707 had been manually shut in W-170 just north of Panel 7. (See Figure 5-1 for bulkhead locations and Illustration 1, in Appendix A, for drift nomenclature.) The switch to Filtered Ventilation Mode closed BH-313, located in S1000 between W-30 and E-140, and BH-336, located in E-300 just north of S-400. Bulkhead-521, located in E-300 just north of S-90, had been shut during the switch to alternate flow conditions. Bulkhead-503, located in W-30 just south of S-90, was propped open, but was manually shut several days following this event according to NWP engineers. Figure 5-1 indicates where the bulkhead doors are located that were shut during the alternate flow mode, and where the bulkhead doors are that were shut during the switch to Filtered Ventilation Mode. This figure also shows the locations of the five different circuits of the underground, identified by differing colors.
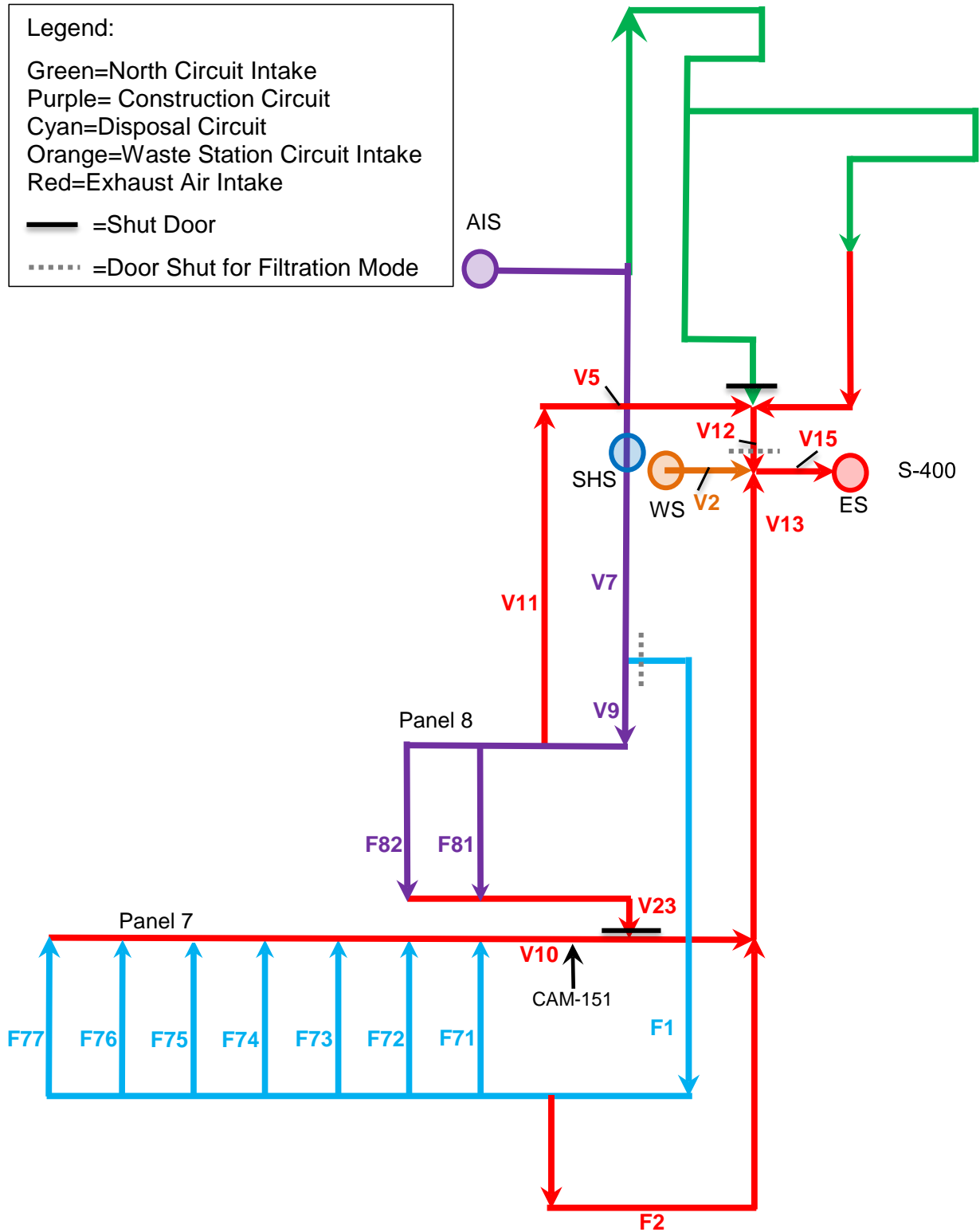
Figure 5-1: Ventilation Model Nomenclature

In the switch to Filtered Ventilation Mode, the closure of the bulkhead doors eliminated direct flow paths between the primary underground air inlets (the AIS and SHS) and the ES. This resulted in the WS as the only air inlet flow path directly connected to an exhaust air drift. There also was no path for the air from the WS to the disposal circuit except through closed airlocks. Therefore flows from the exhaust air drift (E-300) and disposal circuit (S-2180) to the ES are the result of air leakage through the bulkheads and airlocks in the underground.

5.2.   Sensors and Available Data

A variety of sensors are located both on the surface and in the underground to keep track of the environmental conditions during operations. These include pressure, temperature, relative humidity, flow, and pressure differentials. Table 5-1 presents their location and functional status. Calibration data provided by the engineers at the facility for the flow sensors is also included in Table 5-1, along with all calibration data from the 2013 Mine Ventilation Services, Inc. report (DN-3590-03). [18]

There were twelve flow sensors located in the underground. Two flow sensors were not functional during the February 14 release event; V1, near the AIS, and V8, in W-30 just north of V9. There were open repair requests for them to be fixed. The available flow data is analyzed in subsections 5.3.1 and 5.4.1. There were ten available differential pressure (dP) sensors; all of them were functional except dP1, which measures across BH-521 in the North circuit. The pressure differential data are analyzed in subsection 5.3.2 and 5.4.2. An error of 10 percent was established as acceptable for flow and pressure sensors. [18]

The functional temperature, pressure, and relative humidity meters were those at the top of the SHS, top of the WS, the ES duct, and the Meteorological Tower. Since there was little variability in these measurements the values are introduced as they are used. None of the temperature, pressure, or relative humidity sensors were functional in the underground during the release on February 14. Data from the non-functional instruments is not presented in this report.

5.3.   Analysis of 1 Minute Data

This section presents the analysis of the 1 minute averaged flow and differential pressure data. This provides an understanding of the basic flow behaviors in the underground on February 14 and 15 and illustrates the changes that took place in the transition from Alternate Ventilation Mode to Filtered Ventilation Mode. Subsection 5.3.1 presents the analysis of the flow measurements from the underground from noon on February 14, 2014, through noon on February 16, 2014. Subsection 5.3.2 presents the analysis of the available 1 minute averaged dP measurements from the same time period; it provides an indication of flow directions that changed during the transition from Alternate Ventilation Mode to Filtered Ventilation Mode.

Table 5-1: Sensors Present on February 14, 2014

Sensor ID	Location (North/South/East/West = N-/S-/E-/W-)	Functional	Sensor Calibration Error; Date (from NWP)	Calibration Data [18]
V1 Flow [a]	N-215/W-500	No	No value	No data
V2 Flow [a]	S-400/E-220	Yes	0.0%; 6/12/13	2%
V5 Flow [a]	N-150/E-0	Yes	2.1%; 5/14/12	4%
V7 Flow [a]	S-345/W-30	Yes	-1.4%; 5/14/12	8%
V8 Flow [a]	S-900/W-90	No	No data	No data
V9 Flow [a]	S-1085/W-30	Yes	6.4%; 6/12/13	7 to 10%
V10 Flow [a]	S-2180/W-270	Yes	3.8%; 1/08/14	No data
V11 Flow [a]	S-620/W-170	Yes	-1.5%; 7/09/08	Sensor BO
V12 Flow [a]	S-300/E-300	Yes	1.7%; unknown	10%
V13 Flow [a]	S-475/E-300	Yes	0.8%; 1/25/10	8%
V15 Flow [a]	S-400/E-420	Yes	No data	6%
V23 Flow [a]	S-2000/W-170	Yes	No data	Not installed
DP1	S-80/E-300	No	—	No data
DP2	N-140/E-0	Yes	—	2.4%
DP3	S-170/E-140	Yes	—	Needs calibration
DP4	S-400/E-300	Yes	—	9.1% (>0.25 in. w.g.)
DP5	S-600/E-140	Yes	—	Needs calibration
DP6	S-1000/E-0	Yes	—	Needs calibration
DP8	N-0/W-620	Yes	—	No data
DP12	S-1300/E-140	Yes	—	No data
DP13	S-2000/W-170	Yes	—	No data
DP-Waste Hoist Tower (WHT)	Outside of WHT to inside of WHT at waste shaft collar	Yes	—	No data
Pressure (P) / Temperature (T) / Relative Humidity (φ)	Bottom of AIS	No	—	0.0%
P / T / φ	Bottom of the SHS	No	—	0.1%
P / T / φ	Bottom of the WS	No	—	28.6%
P / T / φ	Bottom of the ES	No	—	8.6%
P / T / φ	Top SHS	Yes	—	0.7%
P / T / φ	Top WS	Yes	—	0.0%
P / T / φ	ES Duct	Yes	—	22.8%
P / T / φ	Station A (Roof)	No	—	No data
P / T / φ	Met Tower (6.6 ft)	Yes	—	No data

[a] Only 4 flow sensors are part of a formal calibration program. The remaining units are checked during every Test & Balance of the ventilation system (e.g. every 12-18 months). They are either calibrated at that time, or later by engineering.

5.3.1.   Flow

From the functional flow sensor data, Figure 5-2 and Figure 5-3 present their measurements over a 24 hour period that brackets the release event. Figure 5-1 indicates where the flow measurement locations. The flow perturbation began at 2314 on February 14, 2014, when the switch to Filtered Ventilation Mode began, and ended at approximately 2320. Ventilation data indicates that the flow to the ES decreased from an average of 287 kcfm prior to the CAM alarm to an average of 53 kcfm following the switch to Filtered Ventilation Mode. This correlates well to the fan range ratings of 260 kcfm and 59 kcfm stated in the DN-3590-03 report. [18] Figure 5-4 and Figure 5-5 present a closer view of the same flow measurements during the period of time around the transition from Alternate Ventilation Mode to Filtered Ventilation Mode (2300 February 14, 2014, to 0000 February 15, 2014).

Average "steady-state" flow conditions during both the alternate and filtered flow regimes were calculated from the average 1 minute measurements provided by NWP personnel. These averages are presented in Table 5-2, with a visualization provided in Figure 5-6 and Figure 5-7. The proportional flow changes resulting from the switch in ventilation was not the same at all locations. The most significant changes (Figure 5-1) were observed at the overcast return from Panel 8 (V5), the return from Panel 7 (V10) and return from the North Ventilation Circuit (V12). Flow from Waste Shaft Station Circuit (V2) had the lowest percentage reduction, whereas the flow in the closed branch linking Panel 8 to Panel 7 (V23) increased after the transition to Filtered Ventilation Mode.

Table 5-2: Flow Conditions Surrounding the February 14, 2014 Event

Measurement Location	Flow, kcfm		Percent Change
	from 2024 to 2312 on 2/14/2014	from 2320 2/14/2014 to 0000 2/16/2014	
V2	32.4	21.5	34%
V5	22.6	1.7	92%
V7	150.7	23.5	84%
V9	27.9	12.0	57%
V10	90.2	4.4	95%
V11	23.2	6.5	72%
V12	106.8	4.7	96%
V13	159.2	34.4	78%
V15	286.9	53.2	81%
V23	3.2	4.7	-46%

The calculations in this section evaluate if the physical changes in the underground match the available flow data by performing continuity checks at three different locations. This is followed by a more in-depth analysis of the flow through Panel 7, providing flow and velocity data for this area of interest. Section 5.3.2 analyzes the available dP data and correlates the results to the flow data.
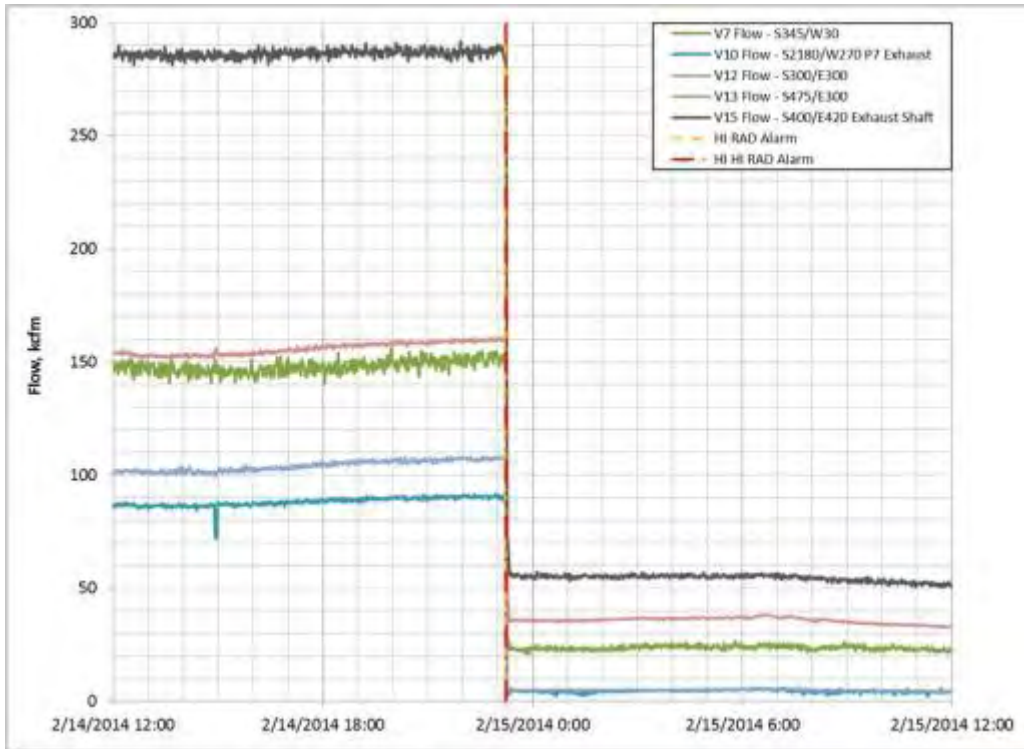
Figure 5-2: Select Flow Data from February 14 and 15 (noon to noon)
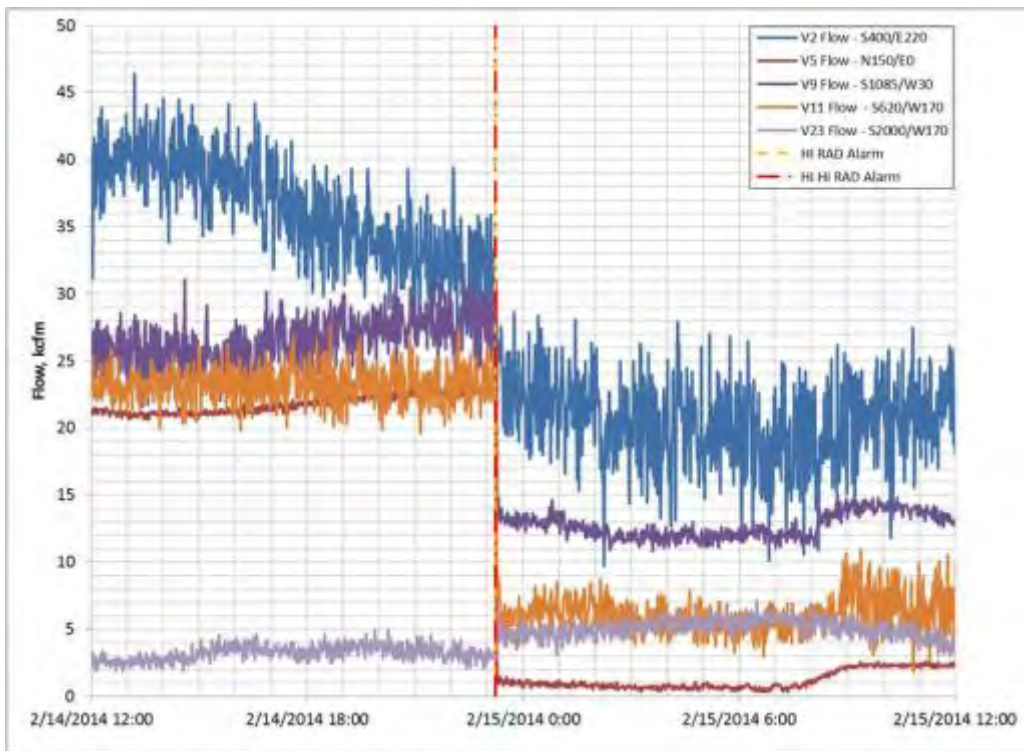
Figure 5-3: Select Flow Data from February 14 and 15 (noon to noon)
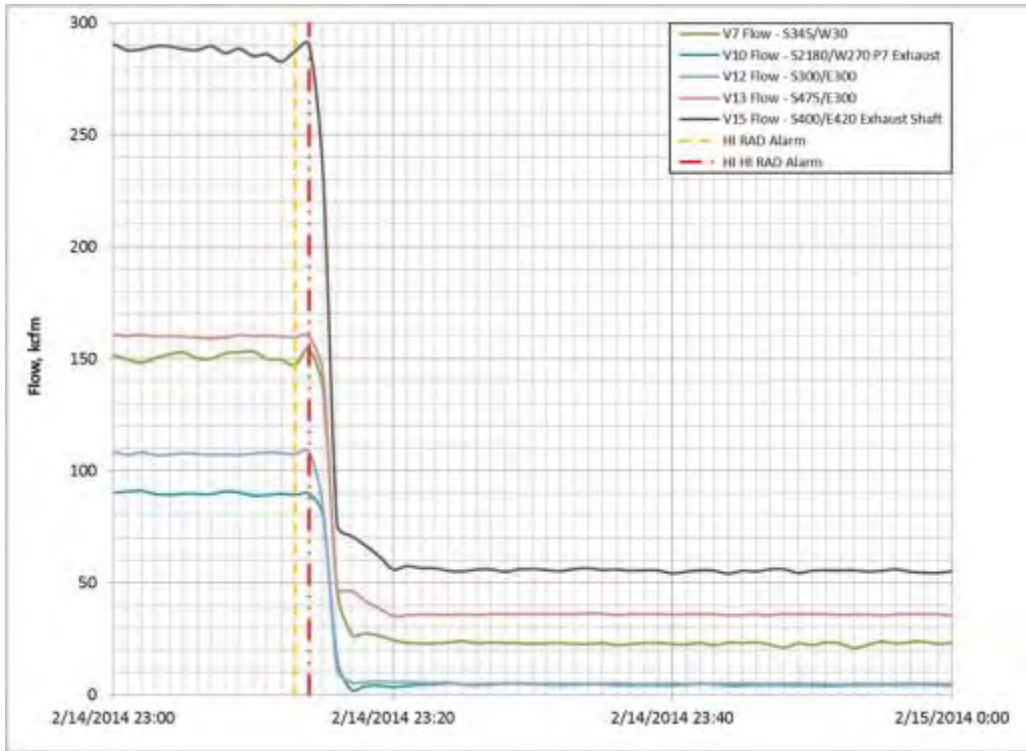
Figure 5-4: Select Flow Data from February 14
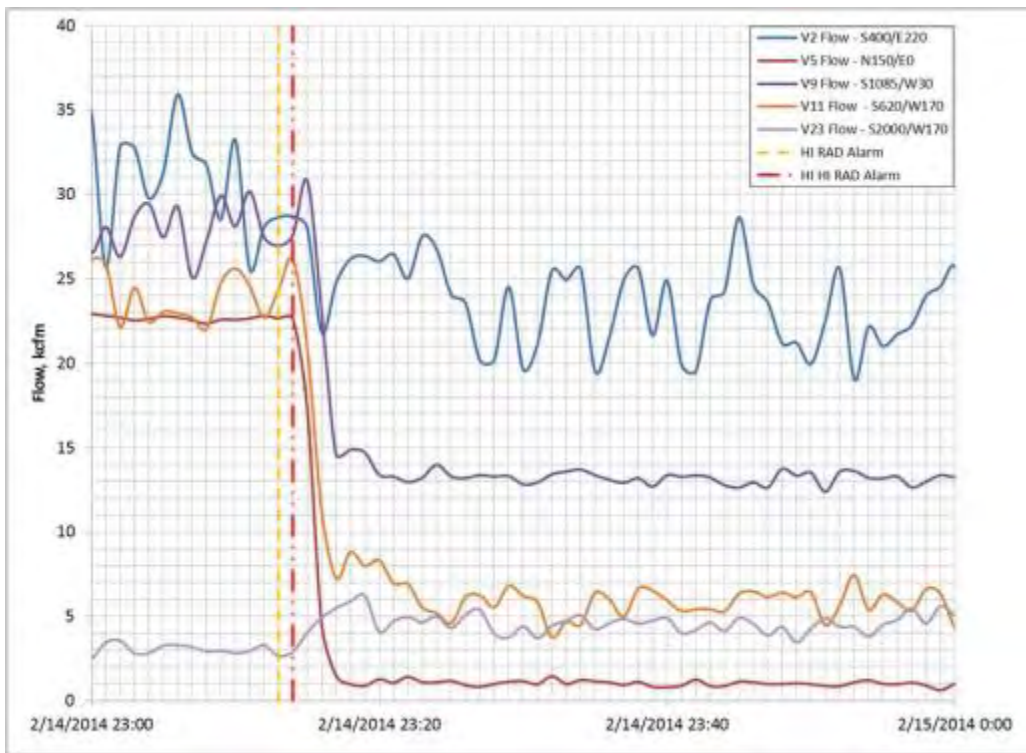
Figure 5-5: Select Flow Data from February 14
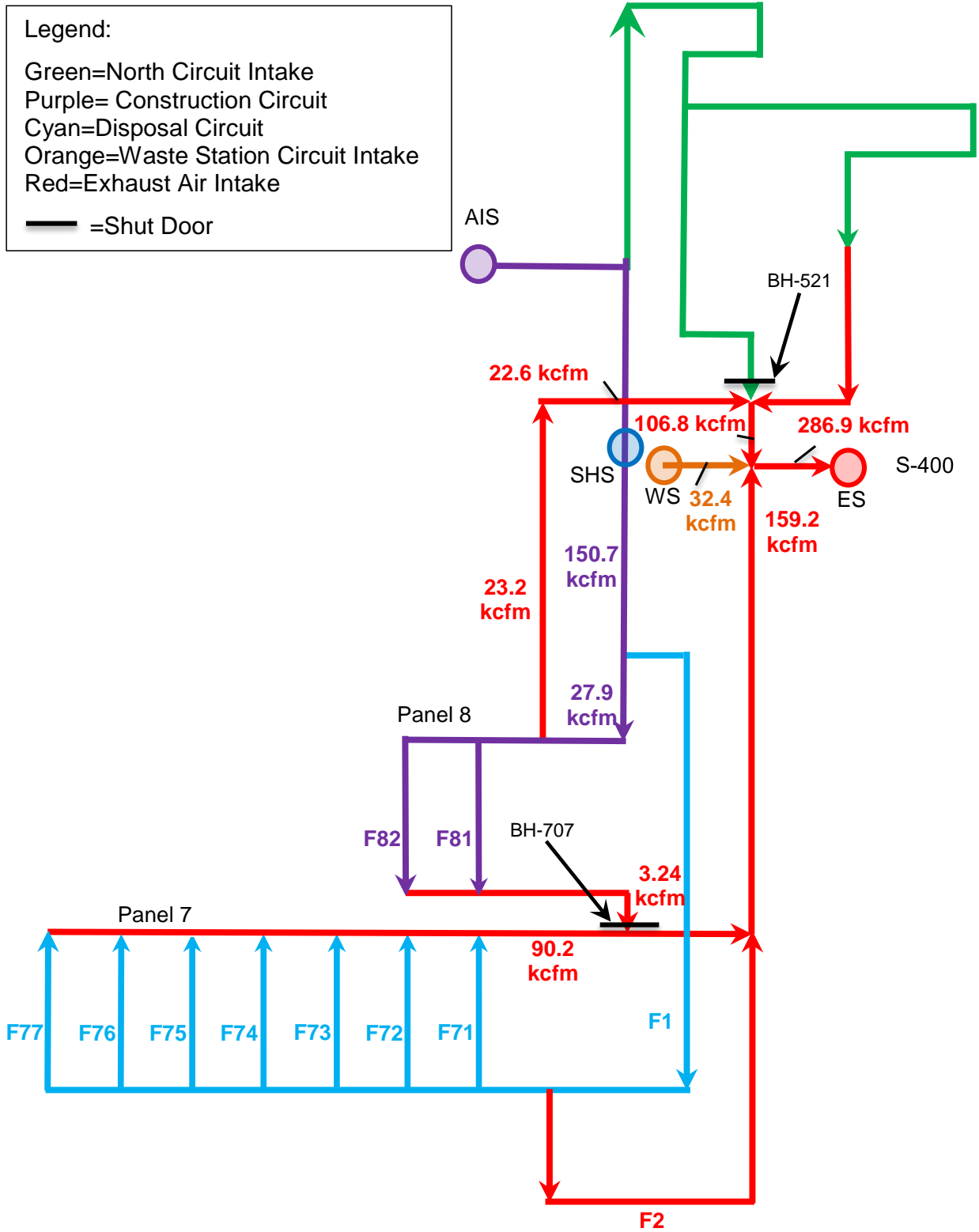
Figure 5-6: Average Flow Data from February 14 Prior to CAM Alarm
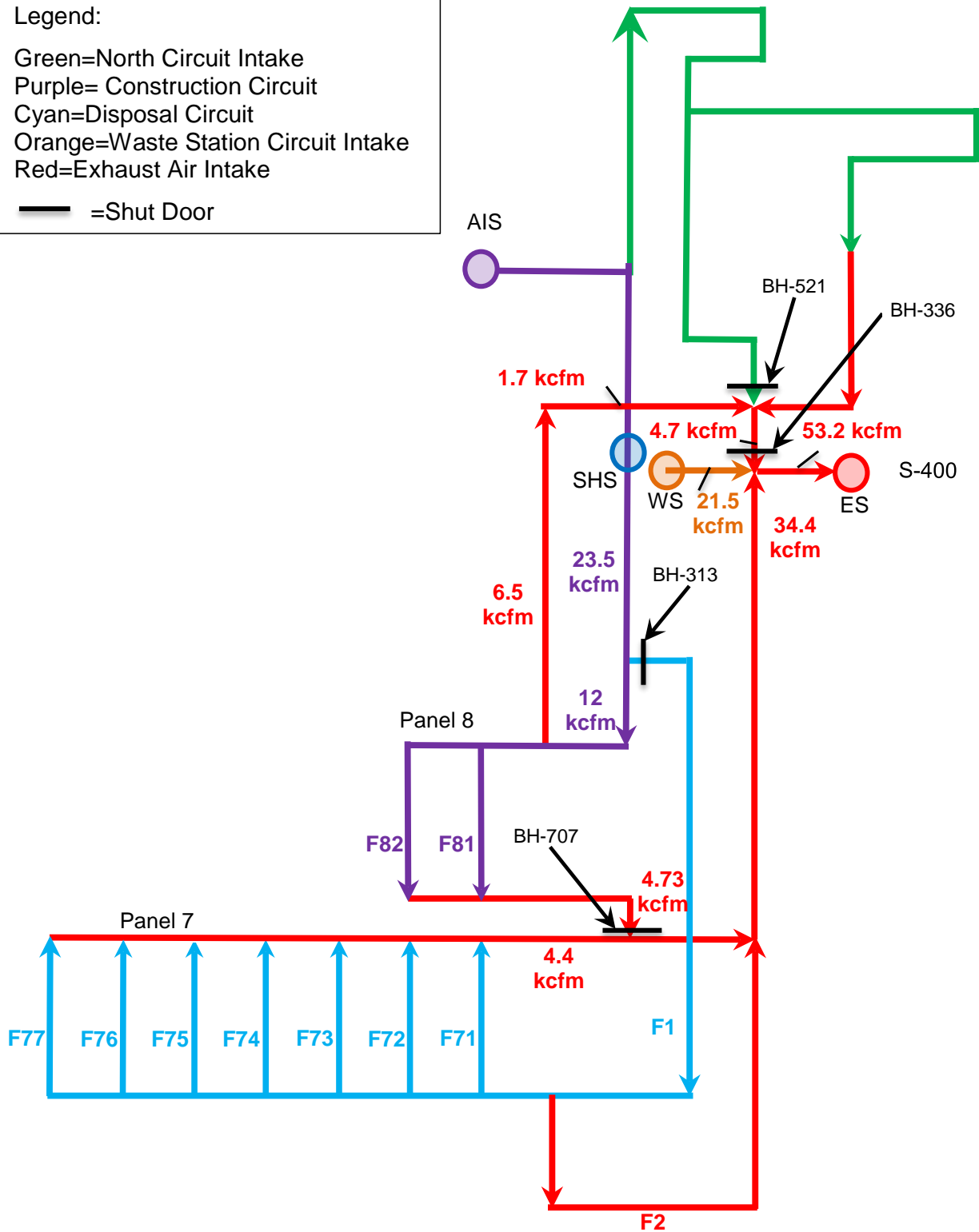
Figure 5-7: Average Flow Data after Switch to Filtered Ventilation Mode

Continuity Check

Continuity checks were performed on the available flow sensor data in order to:

- evaluate the integrity of the data from the sensors;
- understand the measurement uncertainties; and
- verify system understanding.

Figure 5-1 was used to determine where continuity checks could be made with the available flow data for the underground prior to and following the change to Filtered Ventilation Mode. These are provided below.

Check 1: The flow measured at V9 should be equal to the sum of V11 and V23.

$$\dot{V}_9 = \dot{V}_{11} + \dot{V}_{23}$$

Prior to event:

$$\mathbf{27.9\ kcfm} \approx 23.2\ \text{kcfm} + 3.24\ \text{kcfm} = \mathbf{26.4\ kcfm}$$

During Filtered Ventilation Mode:

$$\mathbf{12\ kcfm} \approx 6.5\ \text{kcfm} + 4.7\ \text{kcfm} = \mathbf{11.2\ kcfm}$$

Approximate error is acceptable at 5-7 percent.

Check 2: The flow measured at V15 should be equal to the sum of V12, V2 and V13 prior to the event.

$$\dot{V}_{15} = \dot{V}_{12} + \dot{V}_2 + \dot{V}_{13}$$

Prior to event:

$$\mathbf{286.9\ kcfm} \approx 106.8\ \text{kcfm} + 32.35\ \text{kcfm} + 159.2\ \text{kcfm} = \mathbf{298.4\ kcfm}$$

During Filtered Ventilation Mode, V12 is closed off:

$$\mathbf{53.2\ kcfm} \approx (\text{closed}) + 21.5\ \text{kcfm} + 34.4\ \text{kcfm} = \mathbf{55.9\ kcfm}$$

Approximate error is acceptable at 4-5 percent.

Check 3: The flow measured at V15 should be equal to the sum of V2 and V13 after the switch to Filtered Ventilation Mode following the event.

$$\dot{V}_{15} = \dot{V}_2 + \dot{V}_{13}$$

$$\mathbf{53.2\ kcfm} \approx 21.5\ \text{kcfm} + 34.4\ \text{kcfm} = \mathbf{55.9\ kcfm}$$

Approximate error is acceptable at 5 percent.

Checks 2 and 3 indicate that BH-336 near V12 did shut during the switch to Filtered Ventilation Mode. The error in these checks is approximately 5 percent, which is comparable to errors accepted in the flow sensor calibration data shown in Table 5-1. Also, as noted in the 2013 underground ventilation survey [18] an error of 10 percent was acceptable for the functioning flow and pressure differential sensors.

The average flow conditions in Table 5-2 are provided in an overlay of the underground prior to (Figure 5-6) and after (Figure 5-7) the change to Filtered Ventilation Mode for ease of visualization. On closer inspection of Figure 5-7, flow is shown as coming from Panel 7 and down the E-300 drift toward the ES, but all flow into this area has been shut off due to the closure of BH-313 and BH-707. The only places air could be entering Panel 7 after the switch to Filtered Ventilation Mode would be from leakage across bulkhead doors and/or air from the WS. This is also shown in in the 2013 underground ventilation survey, Figure 15 [18], although BH-336 is closed in this instance so no flow would be coming from the North Underground. Evidence of leakage can be observed in the difference between the V7 and V9 flows in W-30 and the difference between the V10 (Panel 7 exhaust) and V13 (E-300 exhaust air) flows in Figure 5-7. The leakage flow through the bulkheads that separate the E-140 and E-300 drifts is not fully quantified and therefore not included in this evaluation.

Panel 7 Flow

The Underground Ventilation System Design Description [19] indicates that "a minimum velocity of 60 fpm shall be maintained in the active disposal room where rooms are being prepared for disposal." Table 5-3 summarizes flow predictions in Panel 6 in June 2013. This prediction was performed before Panel 7 was available for waste placement and prior to starting construction on Panel 8. Table 5-4 presents the NWP derived flow splits for the 7 rooms in Panel 7 that will be used for further evaluation. The flows are based on the Panel 6 flows in Table 5-3, with detailed branch flows for Panel 7 provided in Figure 5-8 and Figure 5-9.

Table 5-3: Predicted Flow Conditions for Panel 6 during June 2013

Room	Predicted Flows, kcfm			Fraction of Total Flow		
	Normal Ventilation Mode	**Alternate Ventilation Mode**	**Filtered Ventilation Mode**	**Normal Ventilation Mode**	**Alternate Ventilation Mode**	**Filtered Ventilation Mode**
63	69.02	60.53	13.06	0.73	0.73	0.73
62	22.96	20.16	4.36	0.24	0.24	0.24
61	2.94	2.58	0.56	0.03	0.03	0.03
Sum	94.92	83.27	17.98	—	—	—

Table 5-4: Estimated Flow Conditions for Panel 7 on February 14, 2014

Room	Alternate Ventilation Mode		Filtered Ventilation Mode	
	Flow, kcfm	Fraction of total	Flow, kcfm	Fraction of Total
77	42.0	0.467	2.04	0.466
76	42.0	0.467	2.04	0.466
75	1.23	0.014	0.06	0.014
74	1.23	0.014	0.06	0.014
73	1.23	0.014	0.06	0.014
72	1.23	0.014	0.06	0.014
71	1.23	0.014	0.06	0.014
Sum	90.16	1.00	4.38	1.00
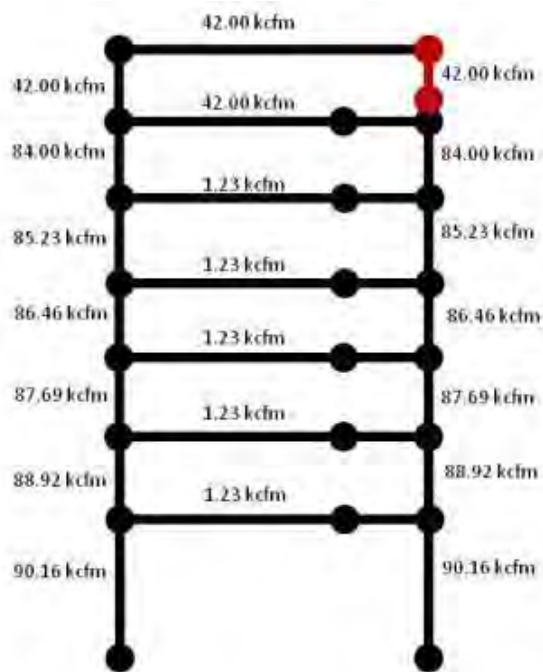
**Figure 5-8: Flow Rates in Panel 7
Prior to Filtered Ventilation
Mode- Red branch is waste array**
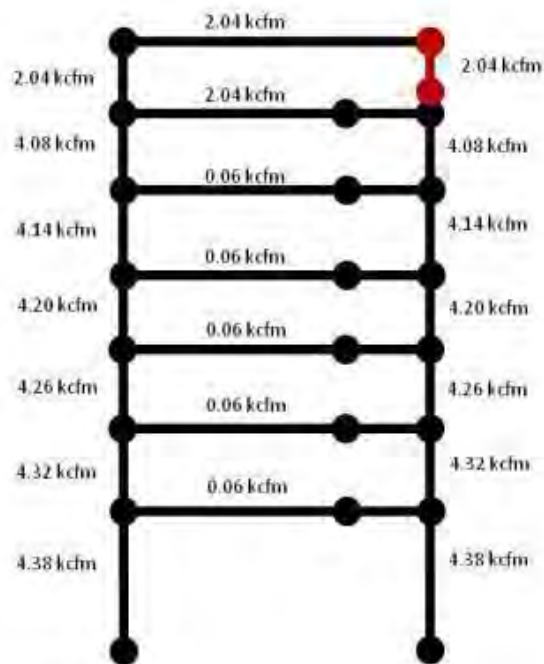
**Figure 5-9: Flow Rates in Panel 7
Following Switch to Filtered
Ventilation Mode- Red branch is
waste array**

The flow split in Table 5-4 was used to determine the velocities within Panel 7 as well as the air volume changes in the area of Room 7 Panel 7 where the waste was emplaced. This influences whether the waste was adequately ventilated during both Alternate and Filtered Ventilation Mode flow conditions.

The exhaust flow (V10) from Panel 7 on February 14 prior to the switch to filtration mode was an average of 90.16 kcfm from 2024 to 2312 hours. The flow through Room 7, based on the weighting factor in Table 5-4, was:

$$\dot{V}_{77} = (0.466)(90,160 \text{ cfm}) = 42,000 \text{ cfm} = \mathbf{19.82} \; \frac{\mathbf{m^3}}{\mathbf{s}}$$

using the conversion factors of 1 cfm = 4.72×10^{-4} m³/s.

The flow velocity in Room 7, branches 137 and 138 (see Figure 5-10) were:

$$v_{77-137} = \frac{(42,000 \text{ cfm})}{(346.5 \text{ ft}^2)} = 121.2 \text{ fpm} = \mathbf{0.62} \; \frac{\mathbf{m}}{\mathbf{s}}$$

$$v_{77-138} = \frac{(42,000 \text{ cfm})}{(504.9 \text{ ft}^2)} = 83.2 \text{ fpm} = \mathbf{0.42} \; \frac{\mathbf{m}}{\mathbf{s}}$$

using the conversion factor of 1 foot = 0.3048 meter and 1 min = 60 s.

Further flow analyses were performed incorporating the waste stacked in Branch 138 of Room 7. Most waste stacks are two to three bundles high, with standard waste boxes having a height, width, and length of 37-, 54-, and 71 inches respectively. This type of waste bundle is stacked three high. An average height of 9.25 feet $\left[\left(37 \, in * \frac{1 \, ft}{12 \, in} \right) * 3 \right]$ for the waste is used for this analysis. The waste is modeled as a solid volume with a footprint of 33 feet wide, 87.1 feet long, and 9.25 feet tall in Branch 138.

The dimensions of Panel 7 were initially provided by NWP in table form correlating to the various branches within the underground. When comparing the waste branch height remaining after subtracting the height of the waste containers to photographs of the underground, the photographs did not indicate that the calculated value of slightly more than 6 feet was logical. The WIPP documented safety analysis [4] states that the height of the waste branches is approximately 13 feet. This height would leave a clearance of 3.75 feet of empty space above the waste containers, which is a better fit to the visual comparison to the photographs taken within the underground. The 13 foot height was used for all branches within Panel 7 except the entrance and exit branches 130 and 144, respectively. All other dimensions are based on the values in Table 2-1.
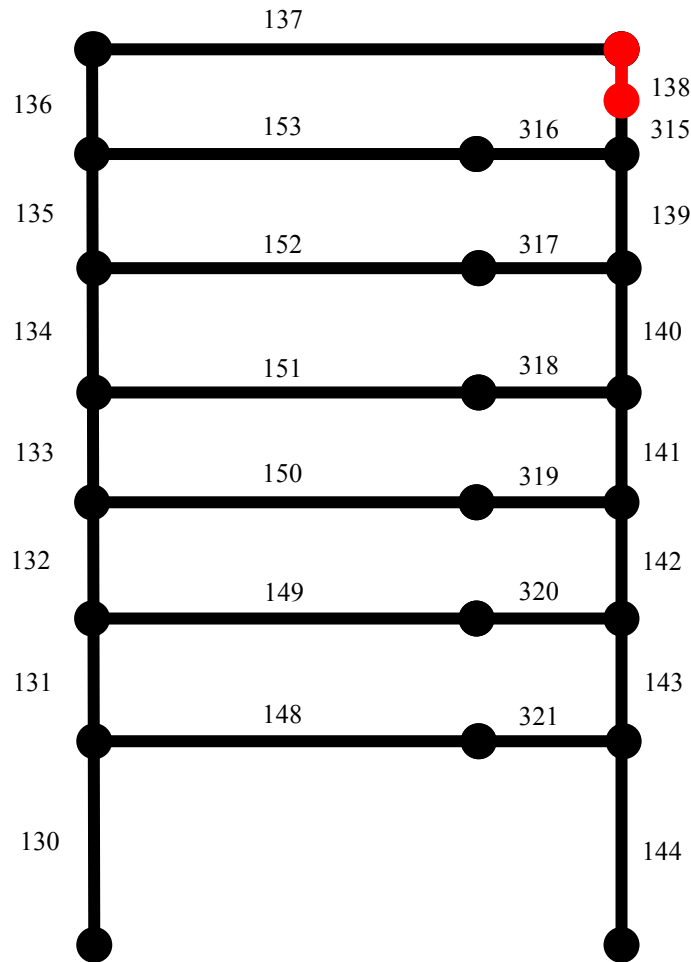
Figure 5-10: Panel 7 flow model geometry - Red branch is waste array

With a room width of 33 foot and height above waste of 3.75 feet, the air flow velocity over the waste containers prior to the release event would have been:

$$v_{77-138} = \frac{(42,000 \text{ cfm})}{(123.8 \text{ ft}^2)} = 339 \text{ fpm} = \textbf{1.7} \; \frac{\textbf{m}}{\textbf{s}}$$

The total volume of empty space for air in the filled section of Branch 138 Room 7 is 10,780 ft³ (product of 33 feet, 87.1 feet and 3.75 feet). This could be used to calculate the air turnover rate in Room 7 Panel 7:

$$T_{77} = \frac{(42,000 \text{ cfm})}{(10,780 \text{ ft}^3)} = 3.9 \; \frac{\text{changes}}{\text{minute}} = \textbf{234} \; \frac{\textbf{changes}}{\textbf{hour}}$$

Such a turnover rate is considered well ventilated. [20]

The exhaust flow from Panel 7 (V10) during Filtered Ventilation Mode was 4.38- kcfm. The flow through Room 7, based on the weighting factor in Table 5-4, was:

$$\dot{V}_{77} = (0.466)(4{,}380 \text{ cfm}) = 2{,}040 \text{ cfm} = \mathbf{0.96} \ \frac{\mathbf{m^3}}{\mathbf{s}}$$

The flow velocity in Room 7, empty branches 137 and 138 were:

$$v_{77-137} = \frac{(2{,}040 \text{ cfm})}{(346.5 \text{ ft}^2)} = 5.89 \text{ fpm} = \mathbf{0.03} \ \frac{\mathbf{m}}{\mathbf{s}}$$

$$v_{77-138} = \frac{(2{,}040 \text{ cfm})}{(504.9 \text{ ft}^2)} = 4.04 \text{ fpm} = \mathbf{0.02} \ \frac{\mathbf{m}}{\mathbf{s}}$$

and for Room 7 Branch 138 with waste:

$$v_{77-138} = \frac{(2{,}040 \text{ cfm})}{(123.8 \text{ ft}^2)} = 16.5 \text{ fpm} = \mathbf{0.08} \ \frac{\mathbf{m}}{\mathbf{s}}$$

During Filtered Ventilation Mode, the air turnover rate for Room 7 Branch 138 with waste was:

$$T_{77} = \frac{(2{,}040 \text{ cfm})}{(10{,}780 \text{ ft}^3)} = 0.19 \ \frac{\text{changes}}{\text{minute}} = \mathbf{11.4} \ \frac{\mathbf{changes}}{\mathbf{hour}}$$

Such a turnover rate is considered adequately ventilated, with a turnover rate of six changes per hour documented as "adequately ventilated" in NFPA 497. [20]

Velocities within Panel 7 during both alternate flow and filtration flow conditions with waste in Branch 138 are provided in Figure 5-11 and Figure 5-12.

5.3.2.   Differential Pressure

A majority of the dP sensors were functional at the time of this incident, with the functioning sensors' measurements for the 24 hour period of time around this incident provided in Figure 5-13. All of the functional dP data indicated a response to the switch to Filtered Ventilation Mode. It is uncertain whether this dP data can be used to calculate leakage across their respective bulkheads and airlocks, or whether it is just measuring the pressure difference between two different drifts blocked off from one another. This information is therefore only used to provide a qualitative picture of any major changes that occurred in the underground due to the switch in ventilation from alternate to Filtered Ventilation Mode.

Only two of the dP sensors indicated a change in sign due to the change to Filtered Ventilation Mode. The first was dP3, which was the sensor for the air lock just north of the WS in E-140. (See Figure 5-14.) The pressure in the north circuit was lower than the pressure near the WS prior to the CAM alarm. This changed during the switch to Filtered Ventilation Mode, where the pressure in the north circuit became higher than that near the WS. This may have been due to a greater negative pressure being pulled by the ES in this closed off section of the underground (Figure 5-7). Due to the closure of all bulkhead doors connecting the ES to the North and Construction Circuit Intakes, there would not have been any pull of air from these circuits from the ES except for any air leakage through closed bulkheads and airlocks.
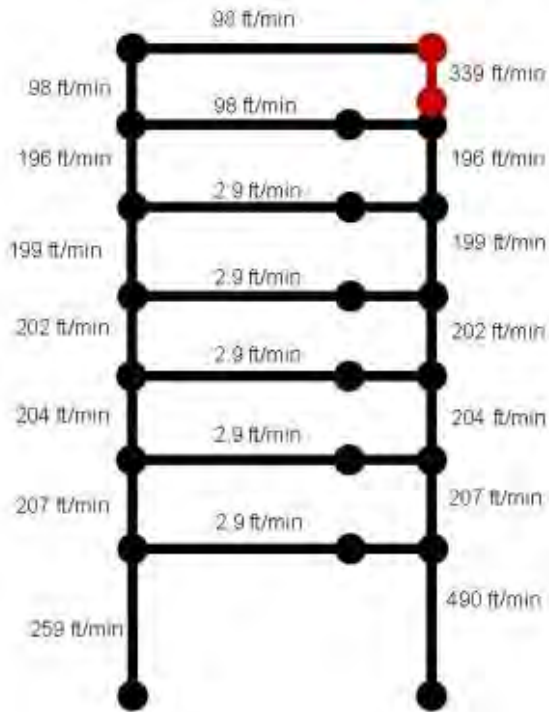
Figure 5-11: Velocities in Panel 7 prior to filtered ventilation mode with waste in branch 138
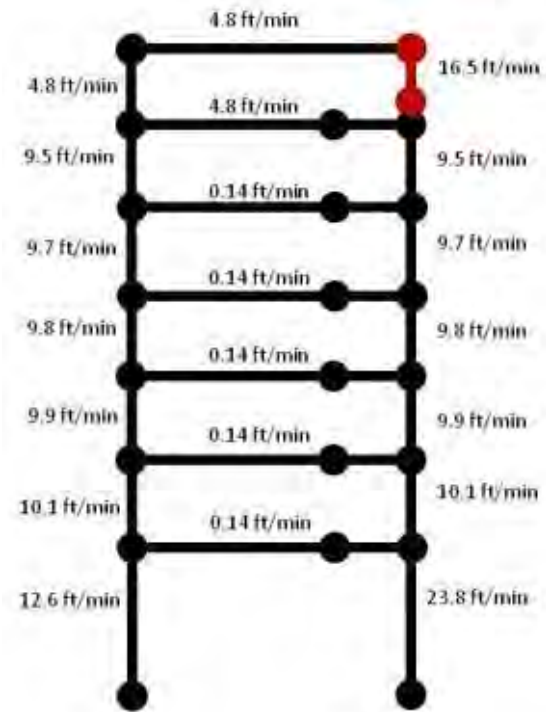
Figure 5-12: Velocities in Panel 7 following switch to filtered ventilation mode with waste in branch 138
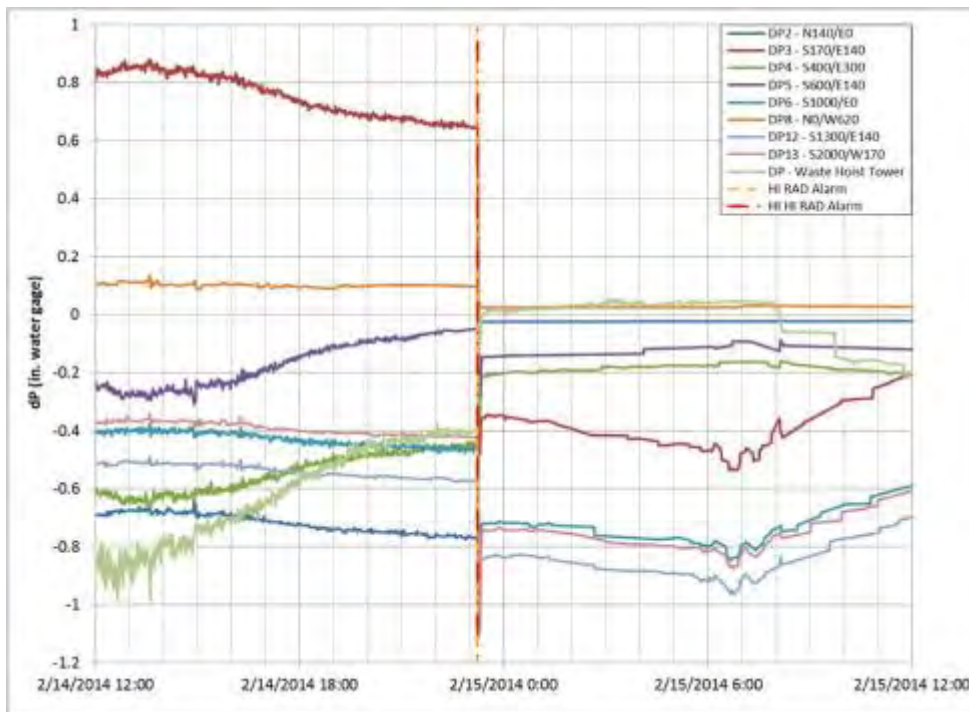
Figure 5-13: Available Pressure Drop Data from February 14 and 15 (noon to noon)
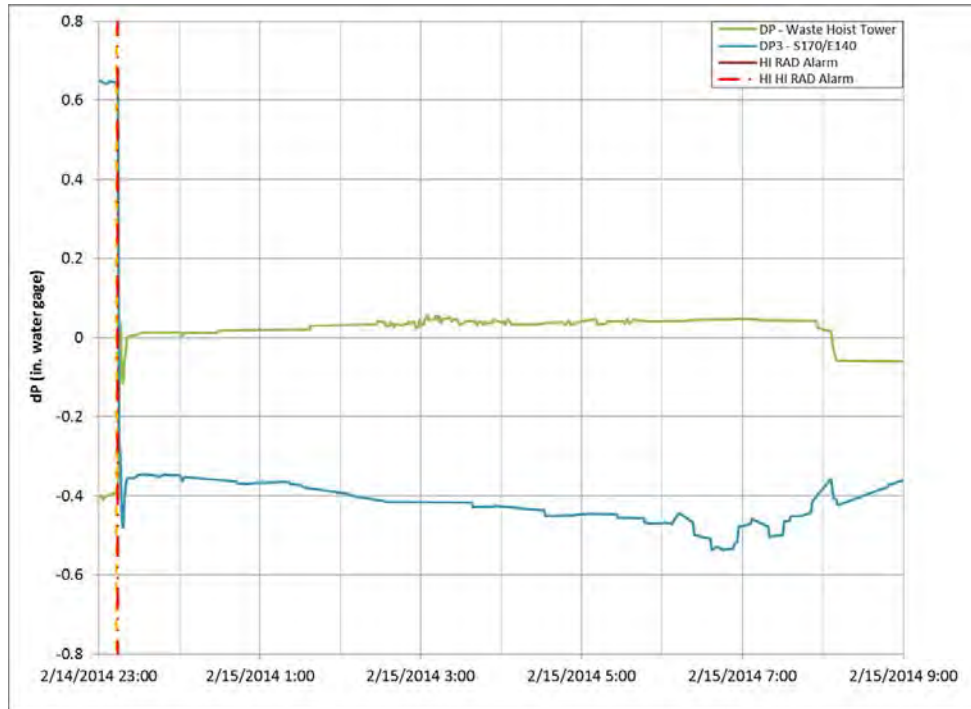
**Figure 5-14: Available Pressure Drop Data from February 14 and 15
(noon to noon)**

The second sensor that indicated a change in air pressure was dP-Waste Hoist Tower. This
sensor measures from the outside of the Waste Hoist Tower (atmosphere) to the inside of the
Waste Hoist Tower at the waste shaft collar. Prior to the CAM alarm the pressure drop was
negative. This changed shortly after the ventilation switched to Filtered Ventilation Mode
(2321) until approximately 0806 on February 15, 2014, transitioning from negative to slightly
positive. The measurements then went negative again after 0806 on February 15, 2014. This
timing correlates to when the central monitoring room operator closed the auxiliary air intake
tunnel louvers to ensure negative differential pressure in the underground. [1 p. 14] It is assumed
that these were opened at the time of the "HI-HI RAD" CAM alarm, causing this change in dP at
the Waste Hoist Tower.

All other dP sensors indicated a change in dP value, but did not indicate a change in sign. These
are shown in Figure 5-13.

- The dP2 change indicates that the flow across BH-302 is significantly reduced. This is
  observed in the comparison of Figure 5-6 to Figure 5-7, where the flow is reduced from
  22.6 kcfm to 1.7 kcfm for V5. This section is blocked from the ES during Filtered
  Ventilation Mode, so there would be less pull of air from this section of the underground.
- Sensor dP4 becomes less negative in Filtered Ventilation Mode, indicating a reduction in
  flow from the WS to the ES across BH-308. This is also observed in the reduction of flow
  from 32.4 kcfm to 21.5 kcfm between Figure 5-6 and Figure 5-7.
- An increase in negative pressure is indicated for dP6, dP12 and dP13. These sensors all
  measure across bulkheads between the construction and disposal circuit. This is a result of

shutting off air flow to these sections by closing BH-313. The intake air is being pulled without an open flow path, increasing the differential pressure across the bulkheads.

- Sensor dP5 indicates an increase in negative pressure due to the switch to Filtered Ventilation Mode. This sensor measures across the airlock in E-140, south of the WS. This indicates that there is a higher pressure near the WS than in the disposal circuit south of the airlock. The WS is open to the surface, indicating that the disposal circuit is under a vacuum.
- Sensor dP8 is located near the AIS and indicates that the pressure near this shaft is reduced due to the change to Filtered Ventilation Mode. This area is shut off from the disposal and exhaust circuits of the underground, leading to a near zero pull of air into the underground through this shaft during Filtered Ventilation Mode.

5.4. ⅛th-Second Data Analysis

This section provides an in-depth analysis of the available eight-samples per second flow and differential pressure sensor data in the underground for the two hours surrounding the "HI-RAD" and "HI-HI RAD" CAM alarms on February 14. The sensor data measurements were averages at ⅛th-second intervals from 2215 on February 14 to 0015 on February 15. The goal of this analysis was to determine if the more detailed sensor data provided insight into the events that occurred prior to the "HI-RAD" CAM alarm that sounded at 2313 on February 14. Subsequently, analysis of the data after the switch to Filtered Ventilation Mode in the underground at 2314 was performed to determine if additional information could be observed in the data. This analysis specifically looked at the flow sensor data (Figure 5-15) and differential pressure data (Figure 5-16) in the underground.

5.4.1. Flow

Two statistical calculations were performed on the flow data to improve its analysis. The first calculation was to determine the arithmetic average value from each sensor during the time leading up to and following the switch from alternate flow to filtered flow. This was performed using the AVERAGEA function in Excel® which performs the following calculation:

$$\text{AVERAGEA} = \frac{\sum_{t=1}^{n} X(t)}{n}$$

Where $X(t)$ is the value of the flow sensor or differential pressure sensor X at time t and n is the sample size.
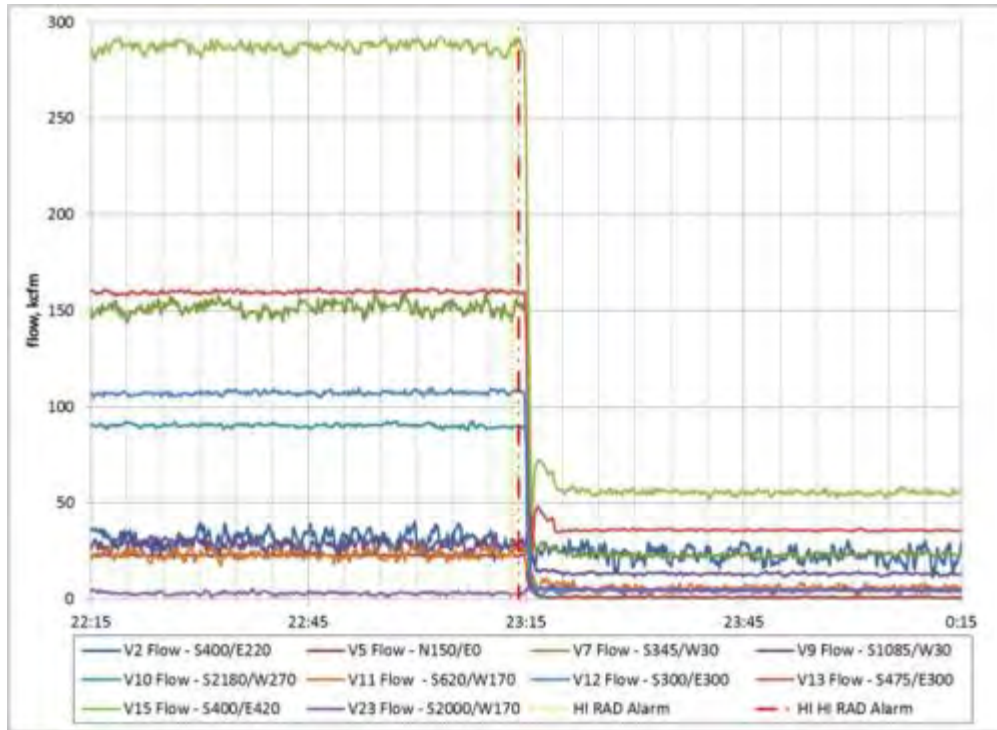
Figure 5-15: All ⅛th-Second Flow Data One Hour Before to One Hour After HI RAD CAM Alarms
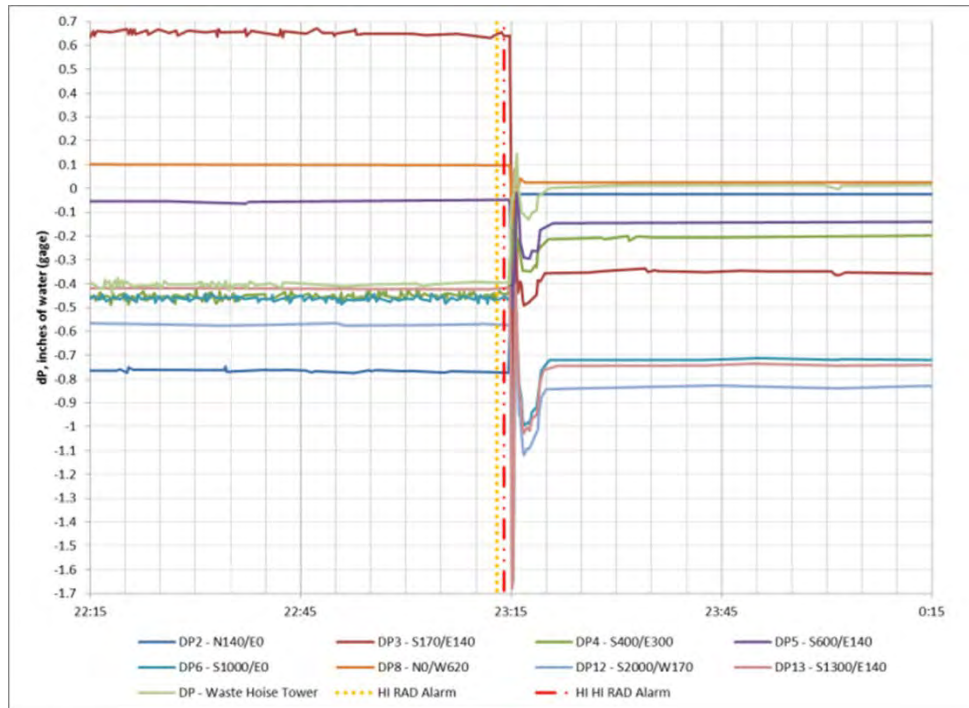
Figure 5-16: All ⅛th-second pressure drop data one hour before to one hour after HI RAD CAM alarms.

The second calculation was to determine the standard deviation of the data. For a normal bell-curve type distribution of data, ± 1 standard deviation would include approximately 68 percent of the data and ± 2 standard deviations would include approximately 95 percent. Although the error in the sensor data may not be normally distributed, this method is an appropriate first check to determine if a majority of the flow measurements fall within these bounds. The standard deviation of the data was calculated for the same timeframes using the STDEV.P function in Excel®. This is calculated using the following equation:

$$\mathrm{STDEV.P} = \sqrt{\frac{\sum_{t=1}^{n}(X(t) - \overline{X})^2}{n}}$$

Where $X(t)$ is the value of the sensor X at time t, $\overline{X}$ is the sample arithmetic average (equivalent to AVERAGEA above) and n is the sample size.

The results of these calculations are provided in Table 5-2.

5.4.1.1. Analysis Prior to CAM alarm

Figure 5-17 presents one-hour of the flow data just prior the CAM alarm and switch to Filtered Ventilation Mode. The data are noisy, but there are no trends over the time presented. To better characterize the individual flow sensor measurements leading up to the CAM alarm data for each sensor is presented separately in Figure 5-18 through Figure 5-27. These plots include lines indicating the average, the average ± 1 standard deviation, and the average ± 2 standard deviations. In analyzing the flow data, it is difficult to definitively state that anything out of the ordinary is observable in this time frame. A majority of the data is very noisy and within the ± 2 standard deviation bounds marked in the figures.

Flow sensor V2, shown in Figure 5-18, contains noise in the time leading up to the CAM alarm. There is a slight decrease in flow near 2310 up to the time of the alarm, but nothing substantial. Data from V5, shown in Figure 5-19, also has a large amount of noise, with possibly a few peaks in flow near 2235, 2245, and 2254. Sensor V7, see Figure 5-20, has a slight dip in flow from 2236 to 2244, but nothing considerably outside the bounds of ±2 standard deviations. Sensor V9, see Figure 5-21, is very noisy with no distinct observations.

A more thorough inspection of Figure 5-22, which provides the V10 flow sensor data located in the Panel 7 exhaust drift (at the exit of the panel), also presents no substantial observations. There was a slight decrease in flow between 2240 and 2245, a peak from 2255 to 2257, and a somewhat large delta in flow at 2307 that had a very short duration. Flow after 2307 was below average. All of the data provided for V10 stayed relatively within the ± two standard deviation bounds.

No observations could be made through the noise observed for sensors V11 (Figure 5-23), V12 (Figure 5-24) or V13 (Figure 5-25). The flow from V15 (Figure 5-26) shows a slight decrease in trend for the flow from 2302 to 2312, but all of the data stayed relatively within the ±2 standard

deviations and had a good amount of noise. Sensor V23 (Figure 5-27) also did not have anything statistically significant, just much noise within the ±2 standard deviation bounds.
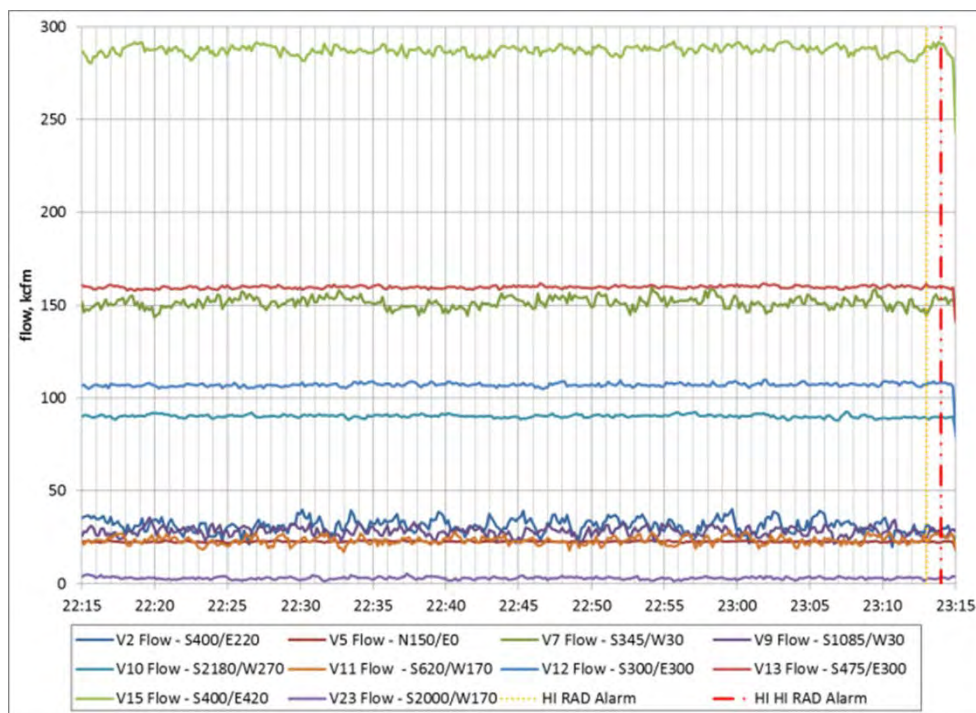
Figure 5-17: All ⅛th-Second Flow Data Leading up to Switch to Filtered Ventilation Mode
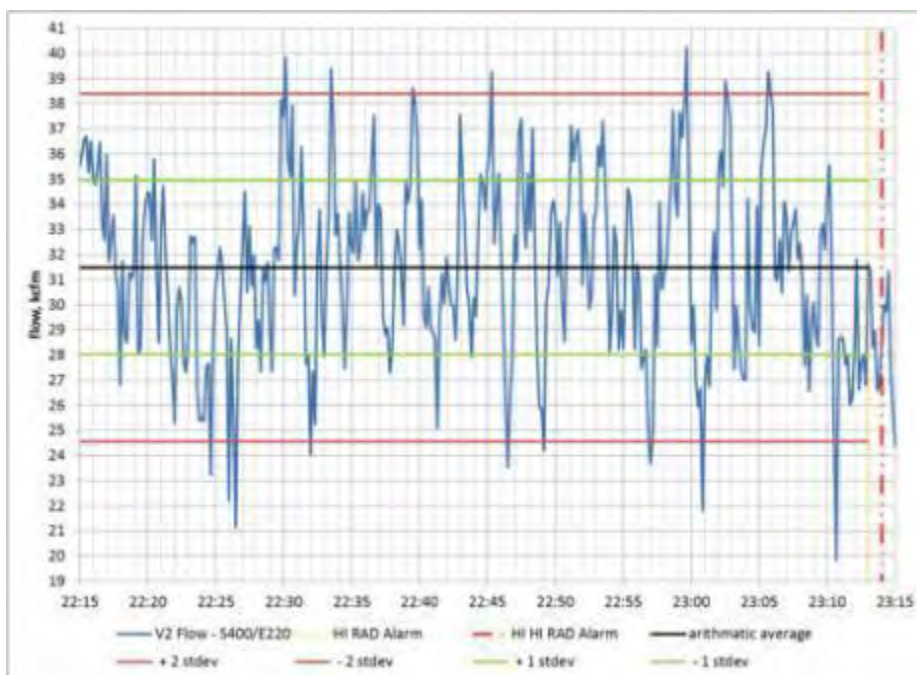
Figure 5-18: V2 Sensor Data Prior to Filtered Ventilation Mode, Located Near Waste Shaft in S-400 Just East of E-140
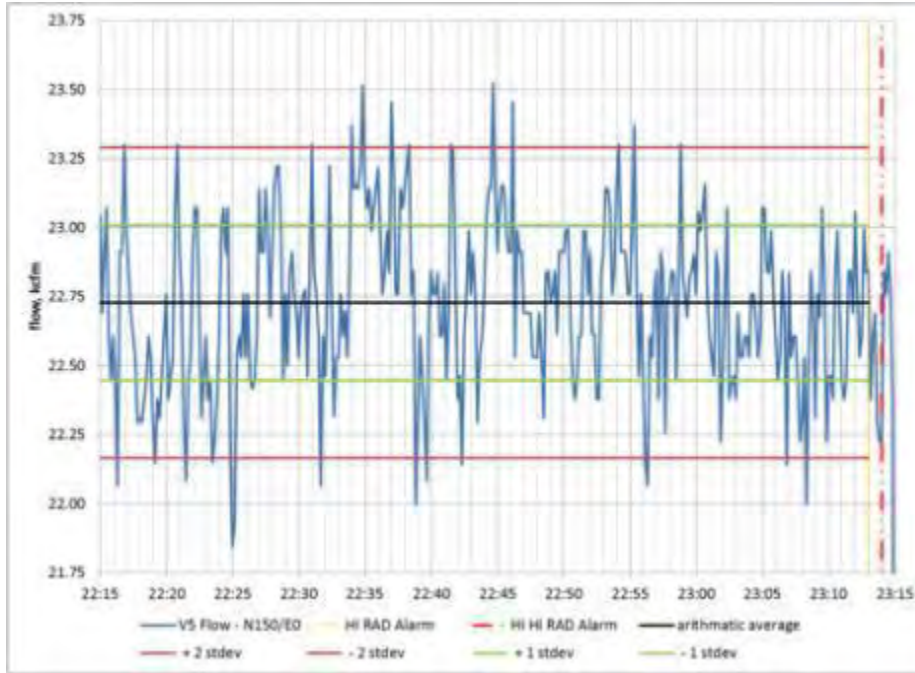
**Figure 5-19: V5 Sensor Data Prior to Filtered Ventilation Mode,
Located in Ventilation Overcast above W-30 in N-150**
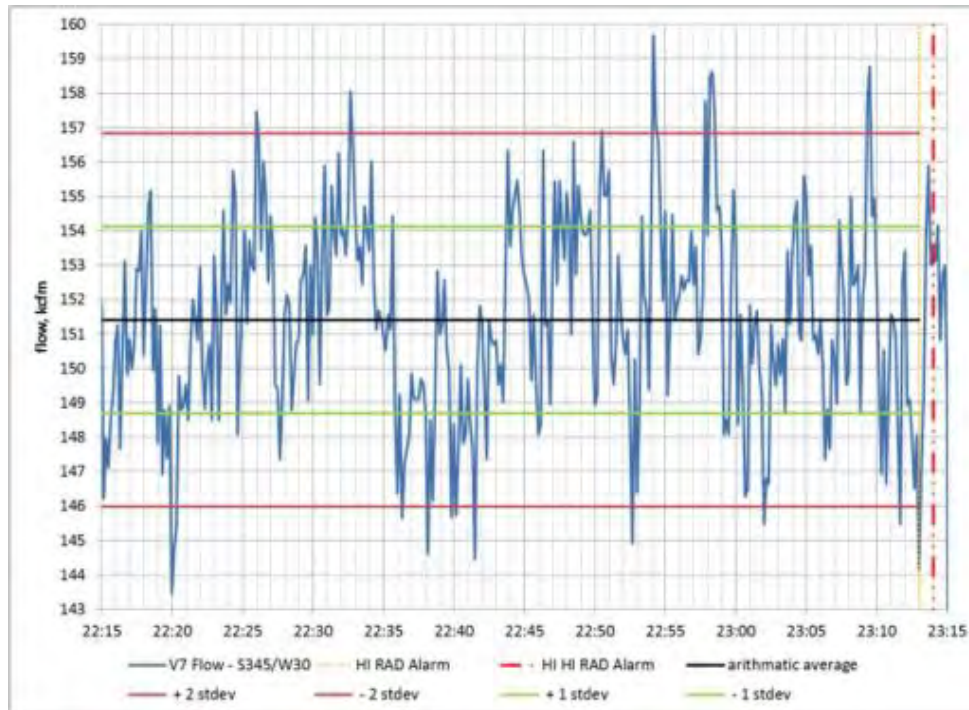
**Figure 5-20: V7 sensor Data Prior to Filtered Ventilation Mode,
Located in W-30 South of the Salt Handling Shaft**
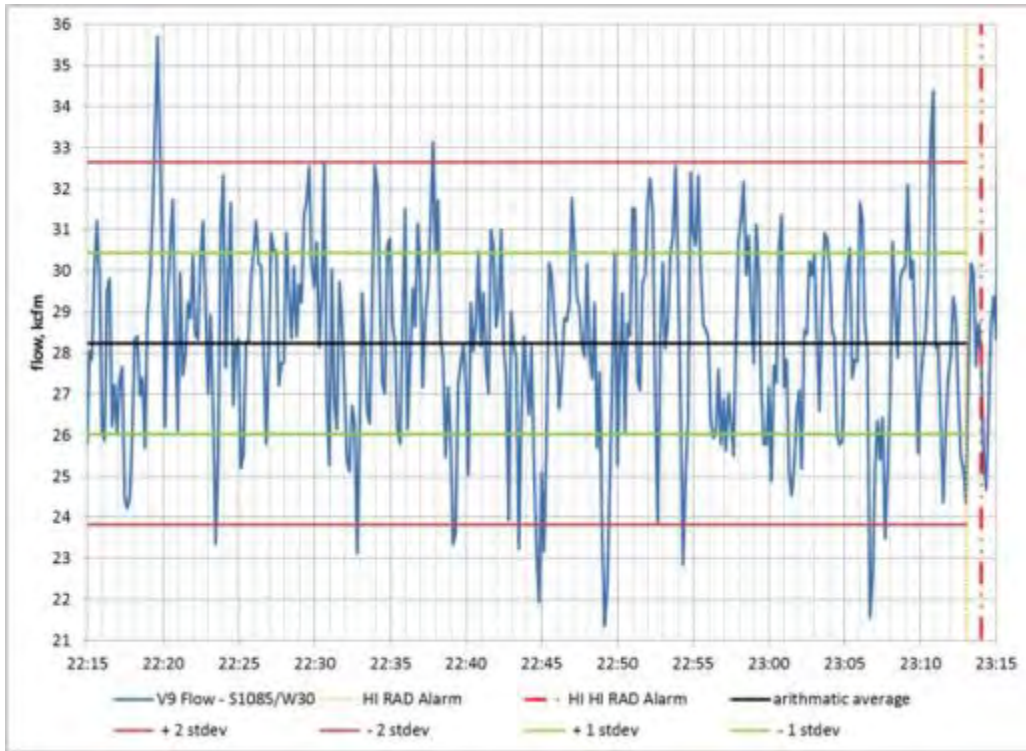
**Figure 5-21: V9 Sensor Data Prior to Filtered Ventilation Mode,
Located in W-30 South of S-1000**
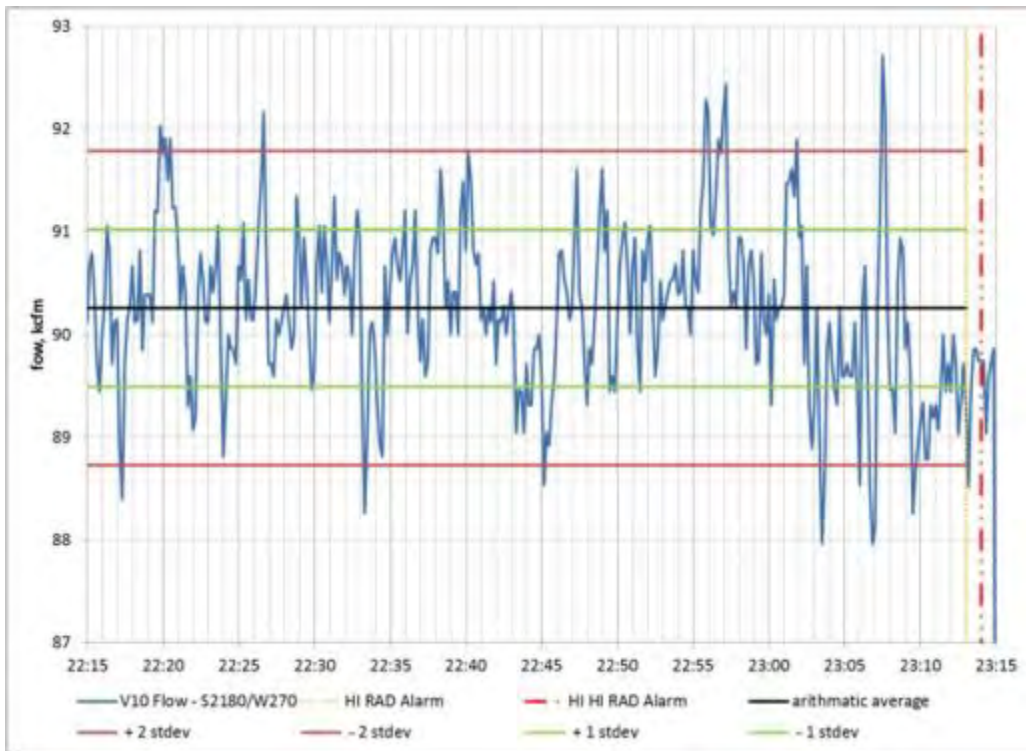
**Figure 5-22: V10 Sensor Data Prior to Filtered Ventilation Mode,
Located in Panel 7 Exit Exhaust S-2180 East of Room 1**
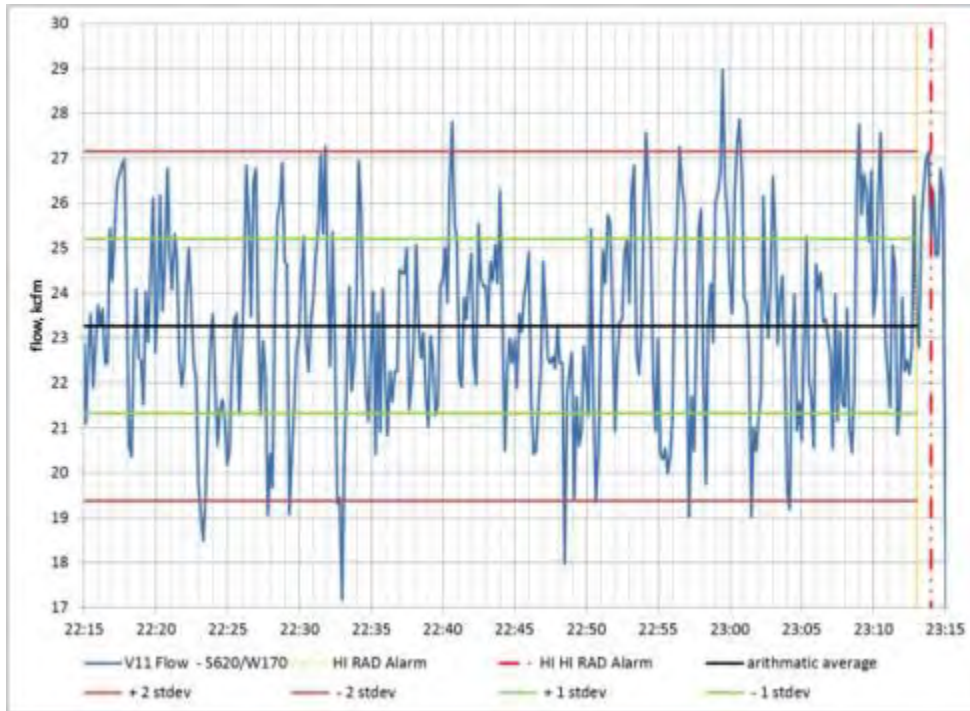
**Figure 5-23: V11 Sensor Data Prior to Filtered Ventilation Mode,
Located in W-170 to the West of the Waste Shaft**
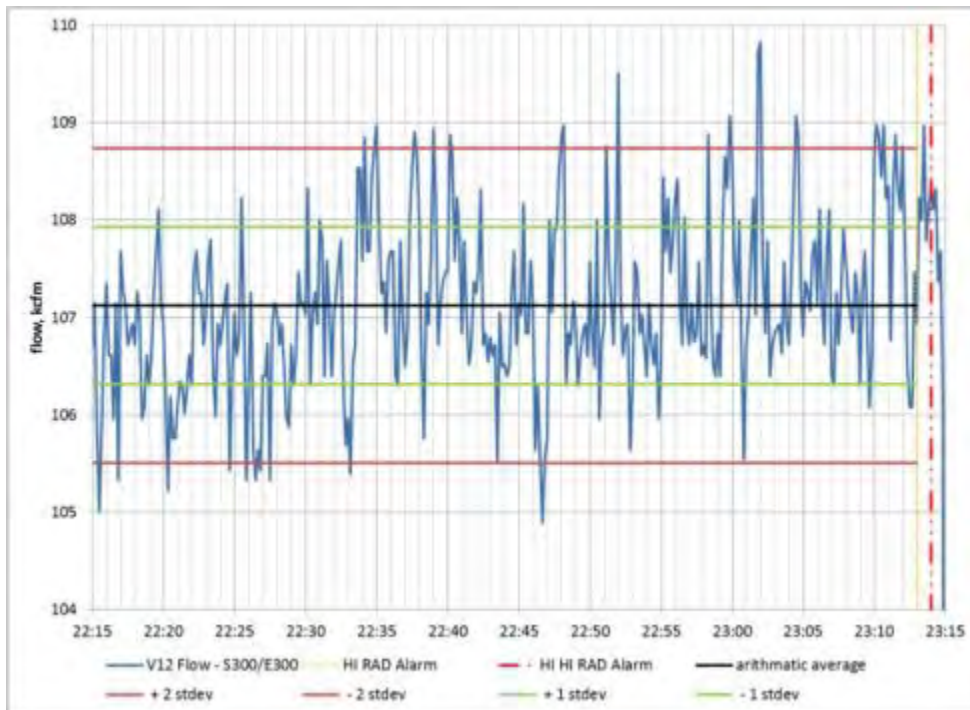
**Figure 5-24: V12 Sensor Data Prior to Filtered Ventilation Mode,
Located in E-300 North of the Exhaust Shaft**
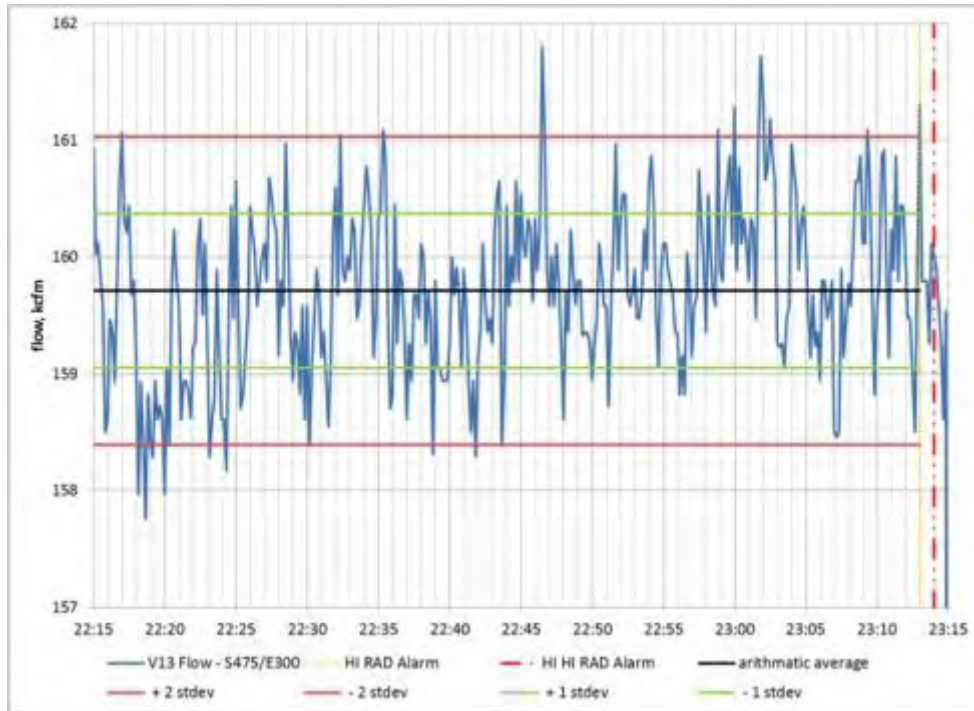
Figure 5-25: V13 Sensor Data Prior to Filtered Ventilation Mode, Located in E-300 South of the Exhaust Shaft
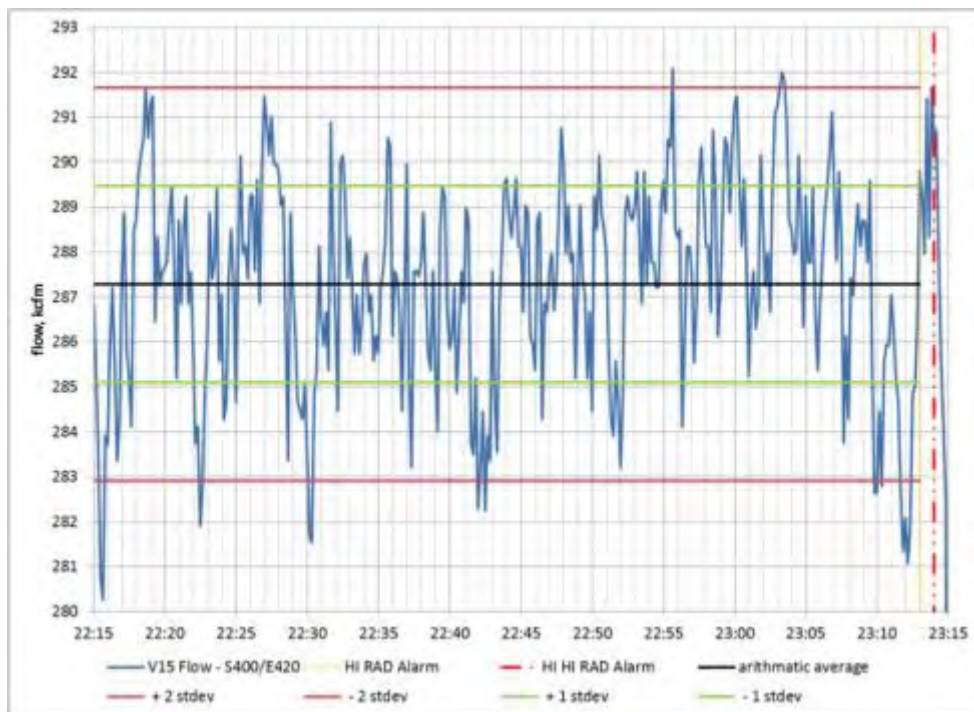
Figure 5-26: V15 Sensor Data Prior to Filtered Ventilation Mode, Located in S-400 Next to the Exhaust Shaft
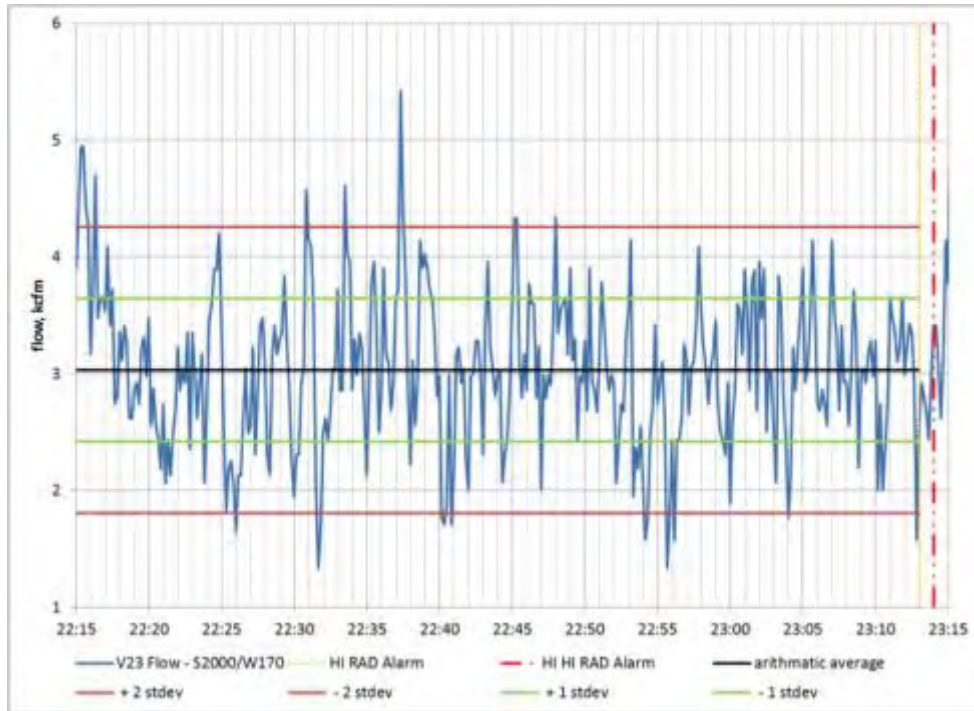
**Figure 5-27: V23 sensor Data Prior to Filtered Ventilation Mode,
Located in W-170 North of BH-707 Between Panel 7 and Panel 8**

5.4.1.2. Analysis Following Switch to Filtration

Flow data after the switch to Filtered Ventilation Mode are provided for all of the flow sensors in Figure 5-28, with each individual sensor measurements provided in Figure 5-29 through Figure 5-38. The flow took until up to 9 minutes to reach a stable flow regime following the switch at 2315 from alternate flow to filtered flow (Table 5-5).

As with the flow data prior to the CAM alarm, the data following the switch to filtration flow also showed a large amount of noise and no distinguishing observations. Sensor V2, shown in Figure 5-29, and sensor V23, shown in Figure 5-38, did not take any time to reach a steady-state flow regime following the switch to Filtered Ventilation Mode. They both had much noise, with a slight decrease in flow observed for V2 from 0000 to 0007. Nothing was largely outside the ±2 standard deviations of the data.

It took until approximately 2317 to reach a steady-state flow for sensor V5 (Figure 5-30), which had two slightly high peaks in flow at 2321 and 2332. These were not considerably outside the noise of the data. Sensor V7 (Figure 5-31) and sensor V9 (Figure 5-32) reached a steady-state flow by 2320, with no definitive observations from the data other than noise.
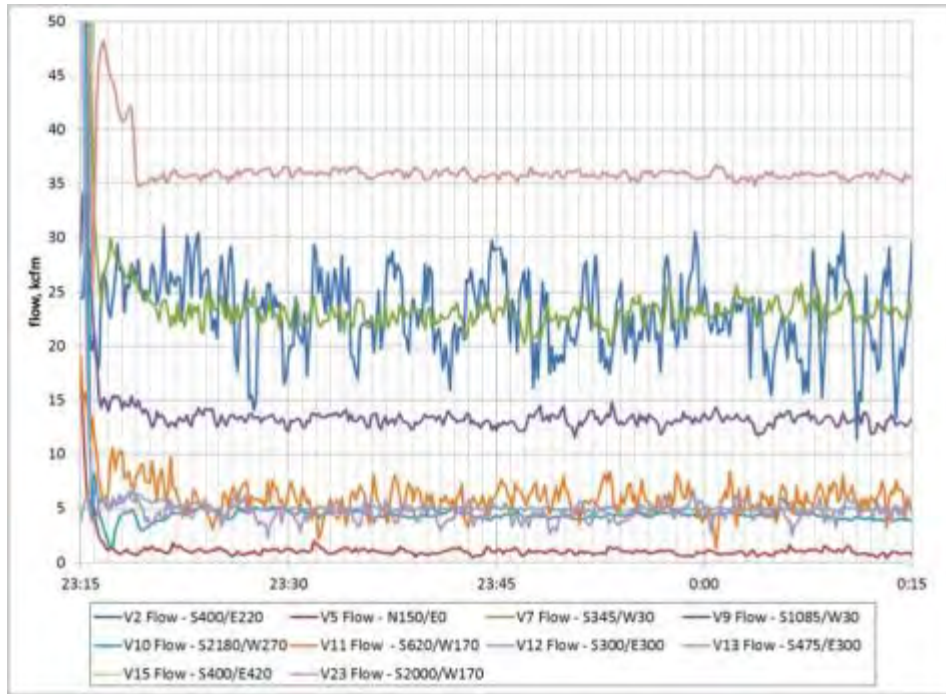
Figure 5-28: All ⅛th-Second Flow Data Following Switch to Filtered Ventilation Mode
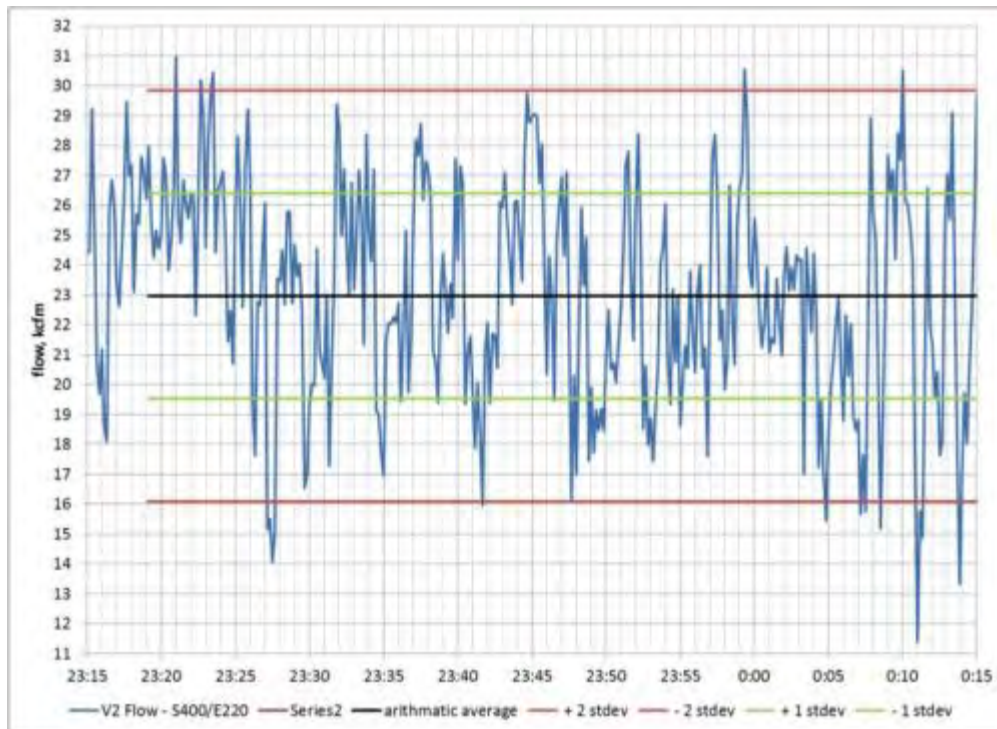
Figure 5-29: V2 sensor Data after Switch to Filtered Ventilation Mode, Located near the Waste Shaft in S-400 Just East of E-140
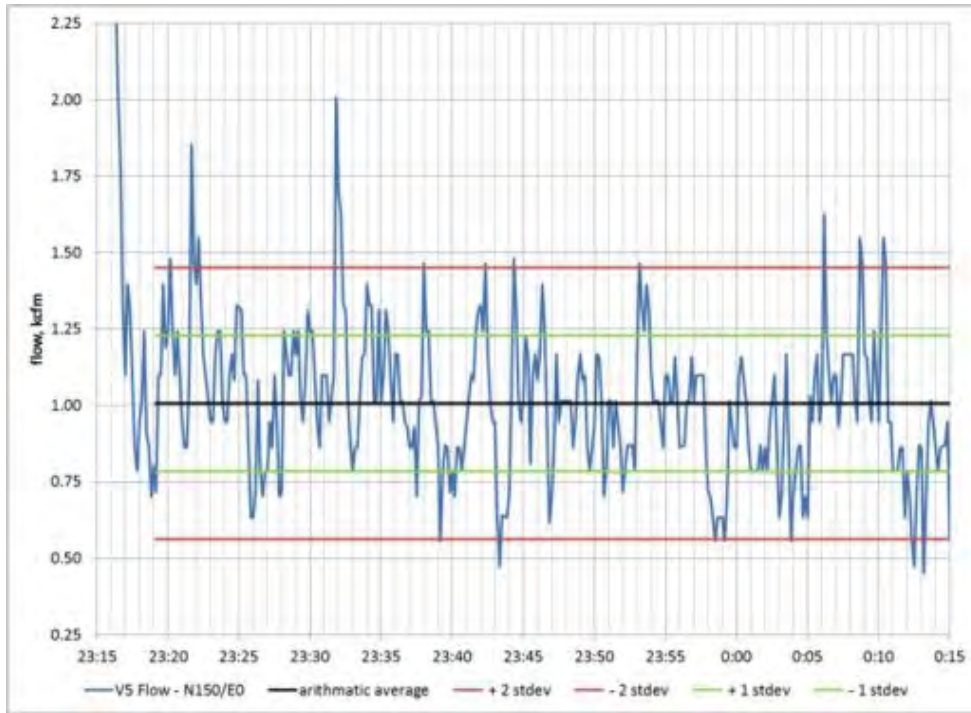
**Figure 5-30: V5 Sensor Data after Switch to Filtered Ventilation
Mode, Located in Ventilation Overcast above W-30 in N-150**
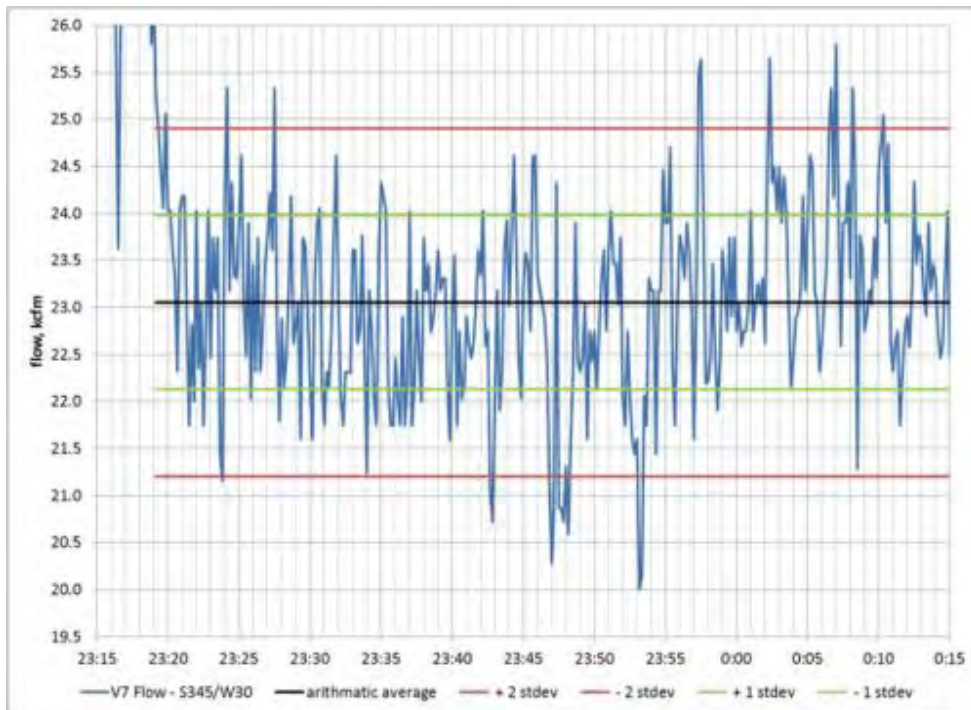
**Figure 5-31: V7 sensor Data after Switch to Filtered Ventilation
Mode, Located in W-30 South of the Salt Handling Shaft**
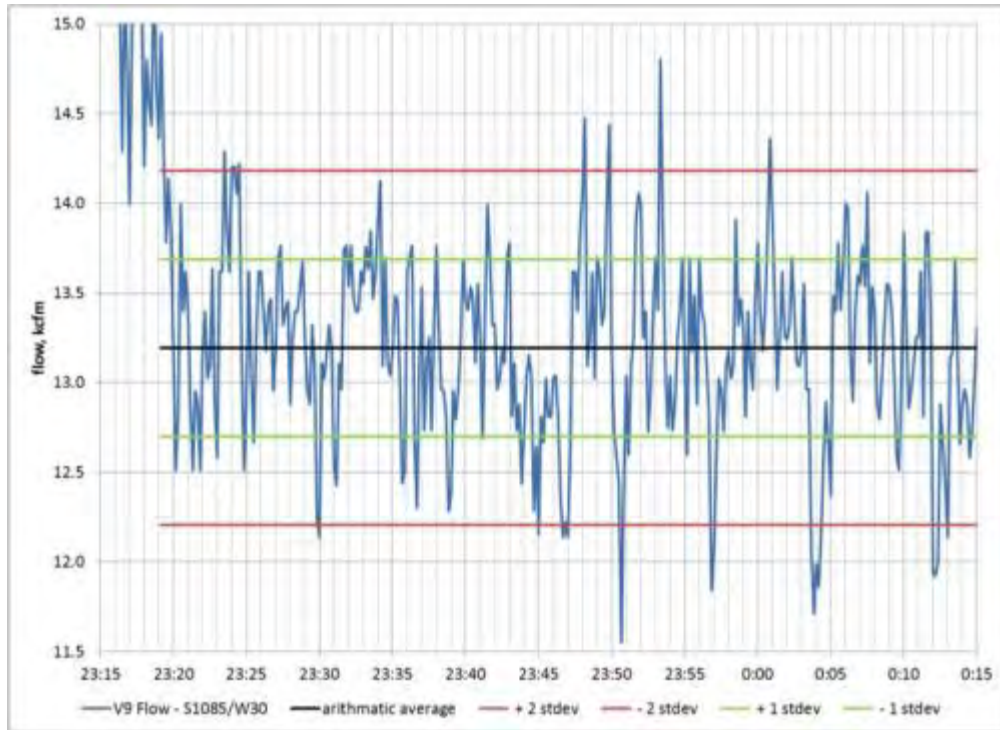
**Figure 5-32: V9 Sensor Data after Switch to Filtered Ventilation
Mode, Located in W-30 South of S-1000**
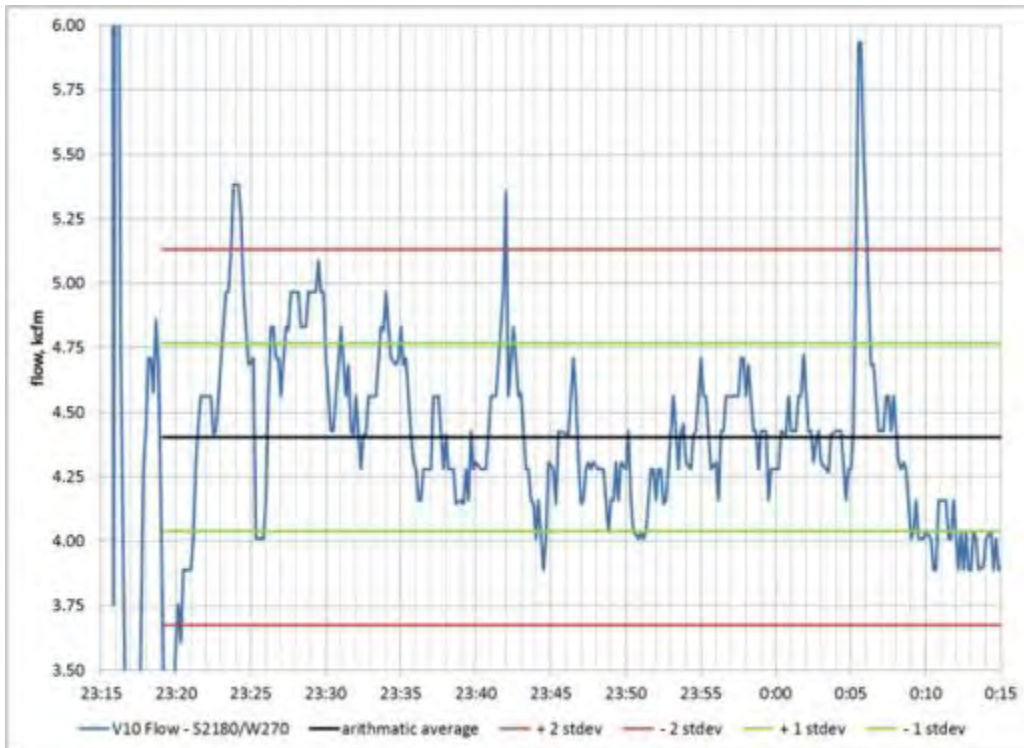
**Figure 5-33: V10 Sensor Data after Switch to Filtered Ventilation
Mode, Located in Panel 7 Exit Exhaust S-2180 East of Room 1**
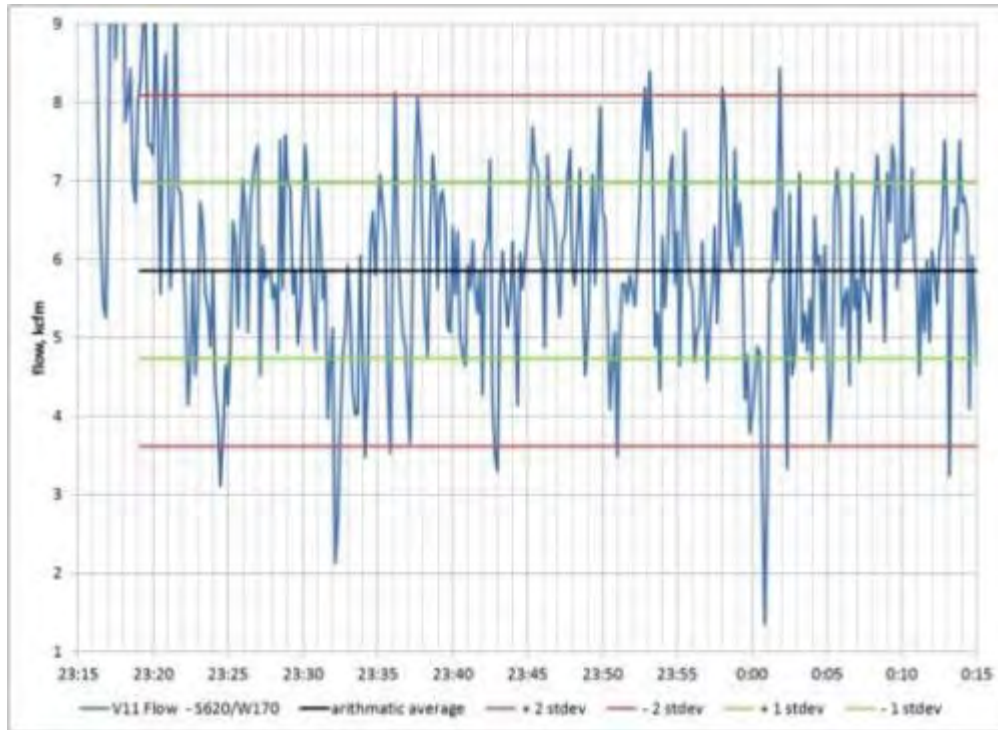
**Figure 5-34: V11 Sensor Data after Switch to Filtered Ventilation
Mode, Located in W-170 to the West of the Waste Shaft**
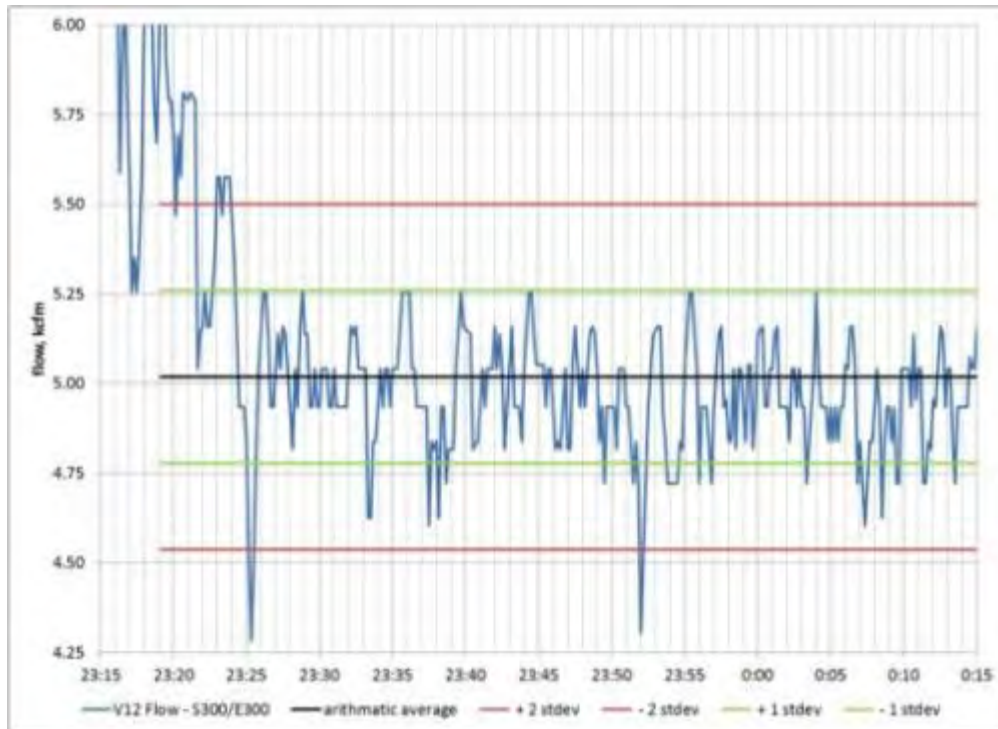
**Figure 5-35: V12 Sensor Data after Switch to Filtered Ventilation
Mode, Located in E-300 North of the Exhaust Shaft**
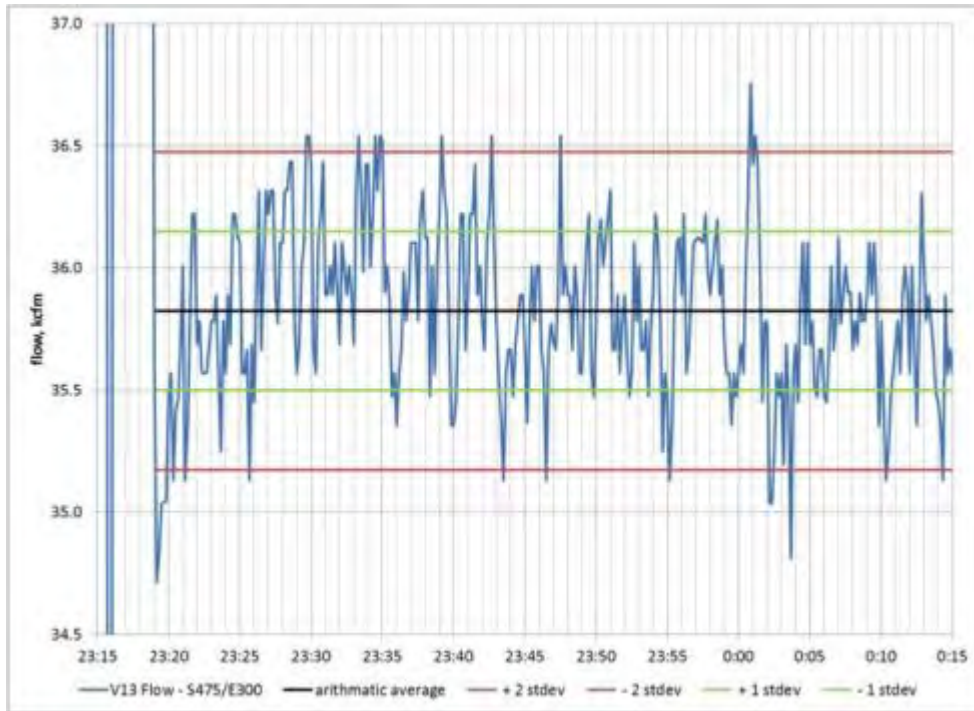
**Figure 5-36: V13 Sensor Data after Switch to Filtered Ventilation
Mode, Located in E-300 South of the Exhaust Shaft**
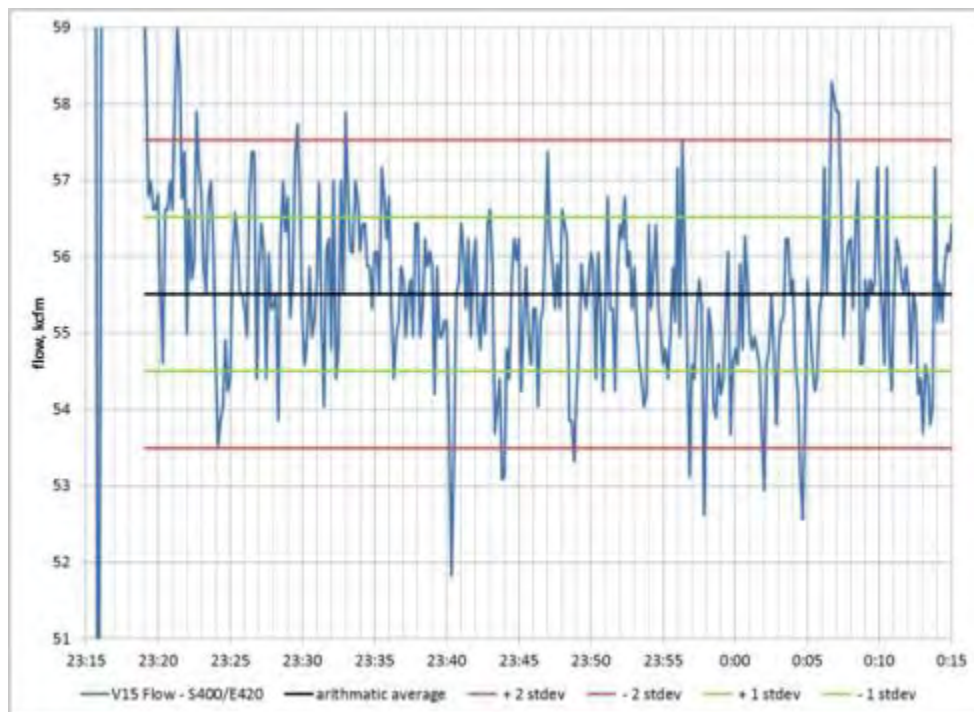
**Figure 5-37: V15 Sensor Data after Switch to Filtered Ventilation
Mode, Located in S-400 Next to the Exhaust Shaft**
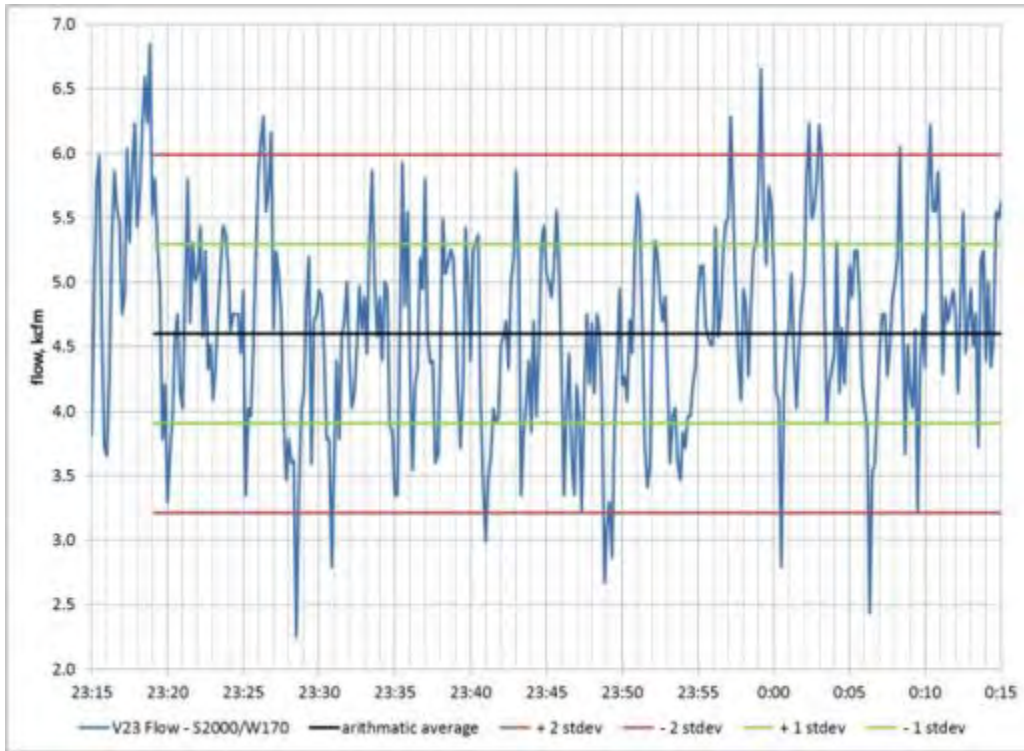
**Figure 5-38: V23 Sensor Data after Switch to Filtered Ventilation Mode,
Located in W-170 North of BH-707 between Panel 7 and Panel 8**

Table 5-5: Approximate time taken to re-equilibrate following flow switch

Sensor ID	Time to approximate steady state (minutes)
V2	0
V5	2
V7	5
V9	5
V10	6
V11	7
V12	9
V13	6
V15	8
V23	0
dP2	1
dP3	5
dP4	5
dP5	6
dP6	6
dP8	2
dP12	5
dP13	7
dP-WHT	6

Flow sensor V10 indicated the most systematic flow pattern following the switch to Filtered Ventilation Mode of all of the flow sensors. The sensor data (Figure 5-33) took until approximately 2321 to begin to show a steady-state flow pattern, after which it had distinct dips and peaks. One peak, at approximately 0005 on February 15, 2014, may indicate that something occurred, but the CAM-151 unit was disabled at 2342 on February 14 due to a malfunction indication. (1) Therefore there is no data to compare to in order to determine if there is any significance to this reading.

Steady-state flow was achieved for sensor V11 (Figure 5-34) at approximately 2322, with two dips below the ±2 standard deviations observed at 2332 and 0001. It is not certain whether these indicate anything or are due to the very low flow rate. The systematic steady-state noise for sensor V12 (Figure 5-35) was reached at approximately 2324 and did not show any substantial deviations. Sensor V13 (Figure 5-36) took until approximately 2321 to reach steady-state and sensor V15 (Figure 5-37) took until approximately 2323.

No substantive trends were observed with the flow data both prior to and following the switch to filtered flow. The measured values had much noise and no direct link could be made to the events that occurred in the underground prior to the "HI-RAD" CAM alarm at 2313.

5.4.2.   Differential Pressure

The ⅛th-second differential pressure data are summarized in Figure 5-16.

5.4.2.1. Analysis Prior to CAM alarm

The individual pressure drop sensor data leading up to the switch to Filtered Ventilation Mode is provided in Figure 5-39 through Figure 5-47. Of all of the sensors, only dP2, dP3 and dP-WHT show any interesting changes in trends prior to the CAM alarm and switch to Filtered Ventilation Mode. These sensors are all located in the north end of the underground; dP2 is just north of the SHS (Figure 5-39), dP3 is across the north airlock near the WS (Figure 5-40), and dP-WHT measures the pressure drop from the outside (atmosphere) of the waste hoist tower to the inside of the waste hoist tower at the waste shaft collar (Figure 5-47) at the surface.

- The pressure drop at dP2 shows two peaks; one near 2220 and the second near 2234 on February 14. The pressure drop then has three oscillations between -0.76 inch and 0.775 inch of water, gage (in. w.g.) until the CAM alarm results in the change to Filtered Ventilation Mode at 2315.
- The pressure drop at dP3 fluctuates between approximately 0.64 inch w.g. and 0.67 inch w.g. through 2253, after which it stops fluctuating and then drops near 0.63 inch w.g. at 2312, spikes up just before the CAM alarms at 2313 and then drops following the "HI-RAD" CAM alarm and switch to Filtered Ventilation Mode.
- The pressure drop at dP-WHT has one spike in pressure differential at 2218, fluctuates between approximately -0.39 inch w.g. and -0.42inch w.g. up until 2243 and then flattens out comparatively until the switch to Filtered Ventilation Mode at 2315.
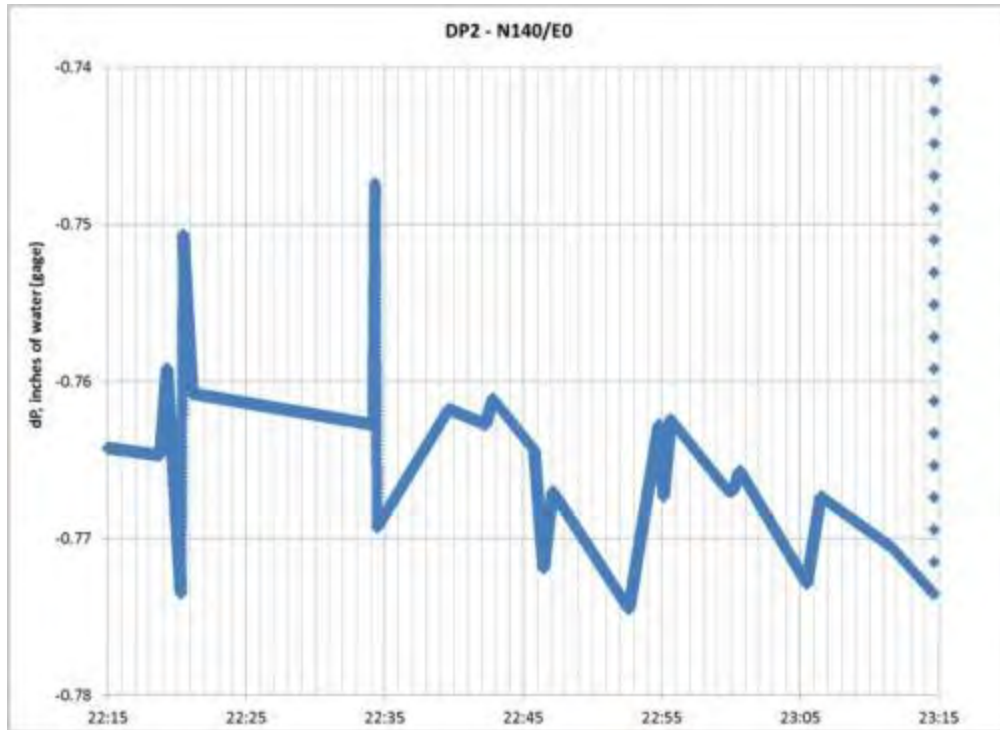
**Figure 5-39: dP2 Sensor Data Prior to Switch to Filtered Ventilation
Mode, Located in E-0 across BH-302**
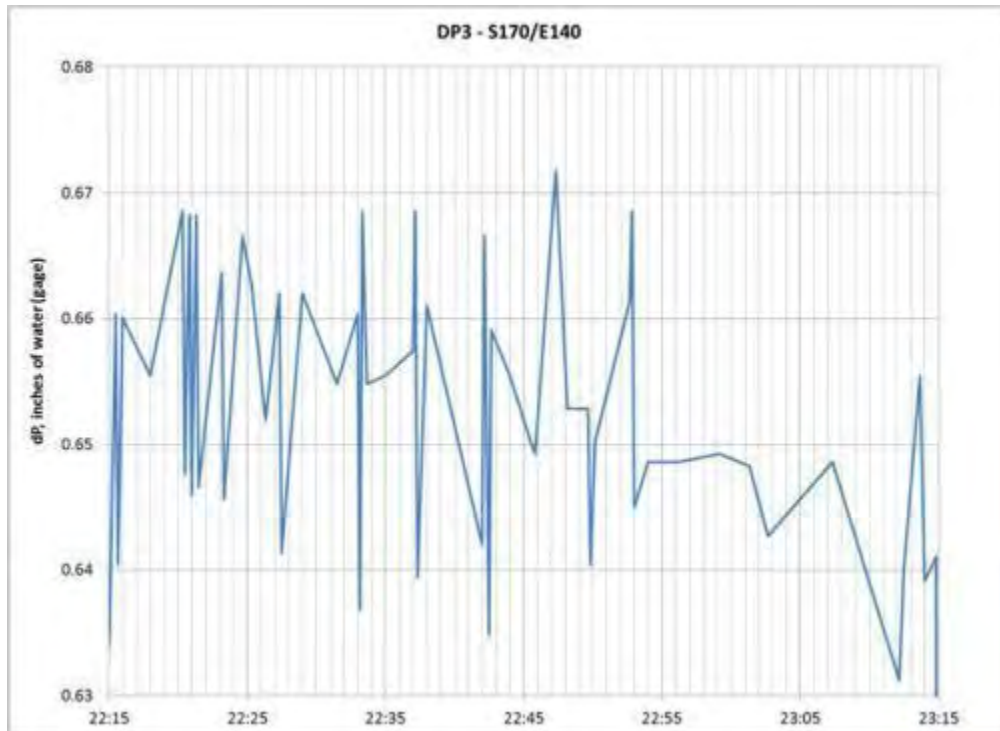
**Figure 5-40: dP3 Sensor Data Prior to Switch to Filtered Ventilation
Mode, Located in E-140 North Airlock (303, 310) near Waste Shaft**
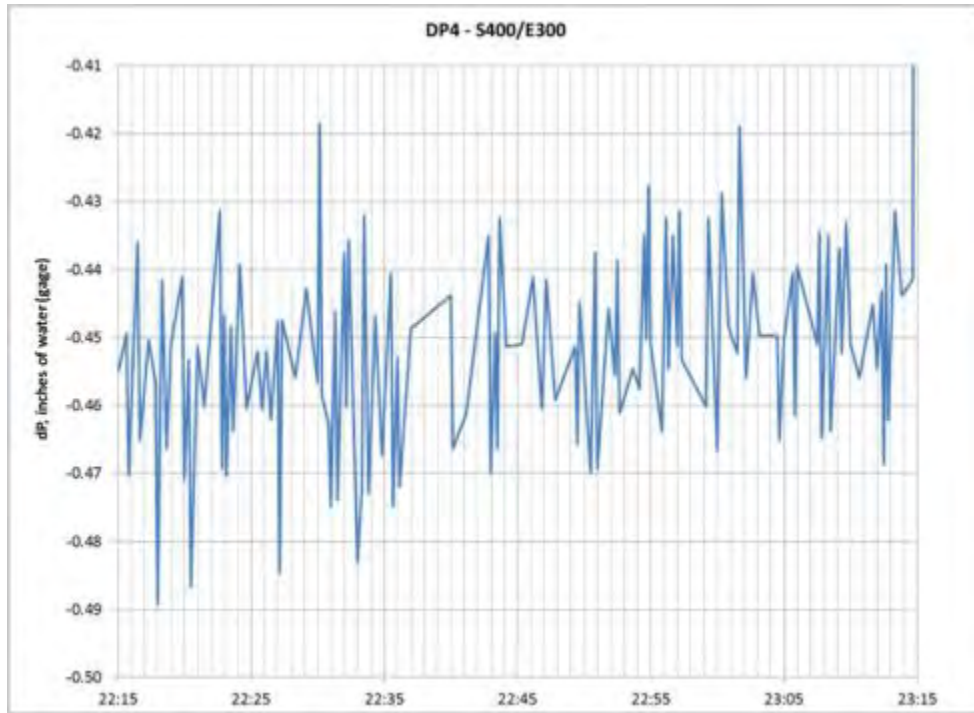
**Figure 5-41: dP4 Sensor Data Prior to Switch to Filtered Ventilation
Mode, Located in S-400 across BH-308**

**Figure 5-42: dP5 Sensor Data Prior to Switch to Filtered Ventilation
Mode, Located in E-140 South Airlock (415, 416) near Waste Shaft**
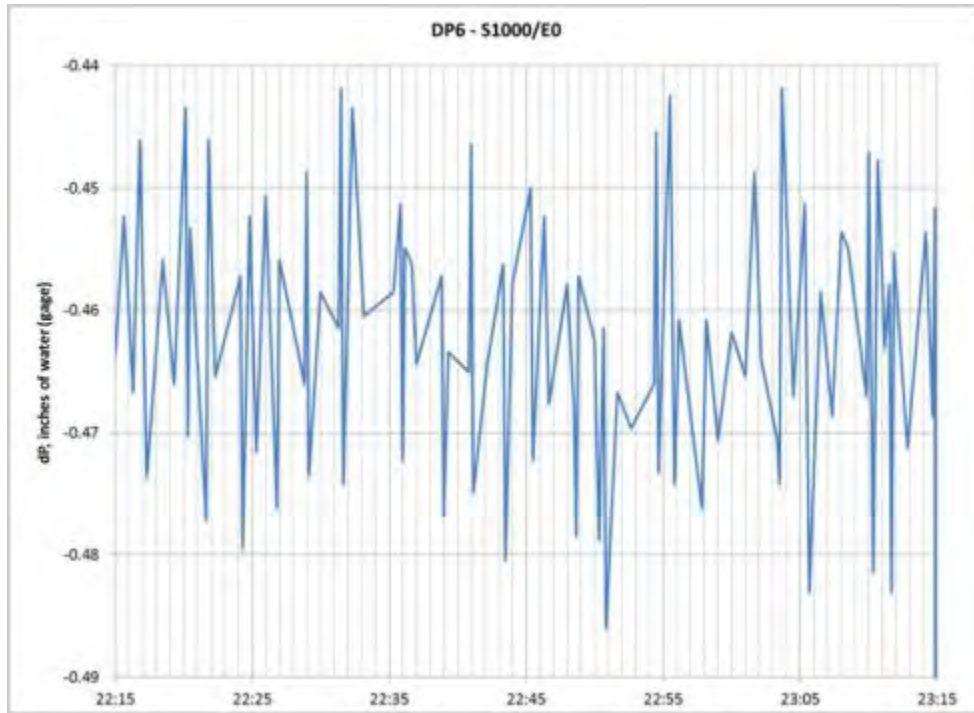
**Figure 5-43: dP6 Sensor Data Prior to Switch to Filtered Ventilation
Mode, located in S-1000 across BH-313**
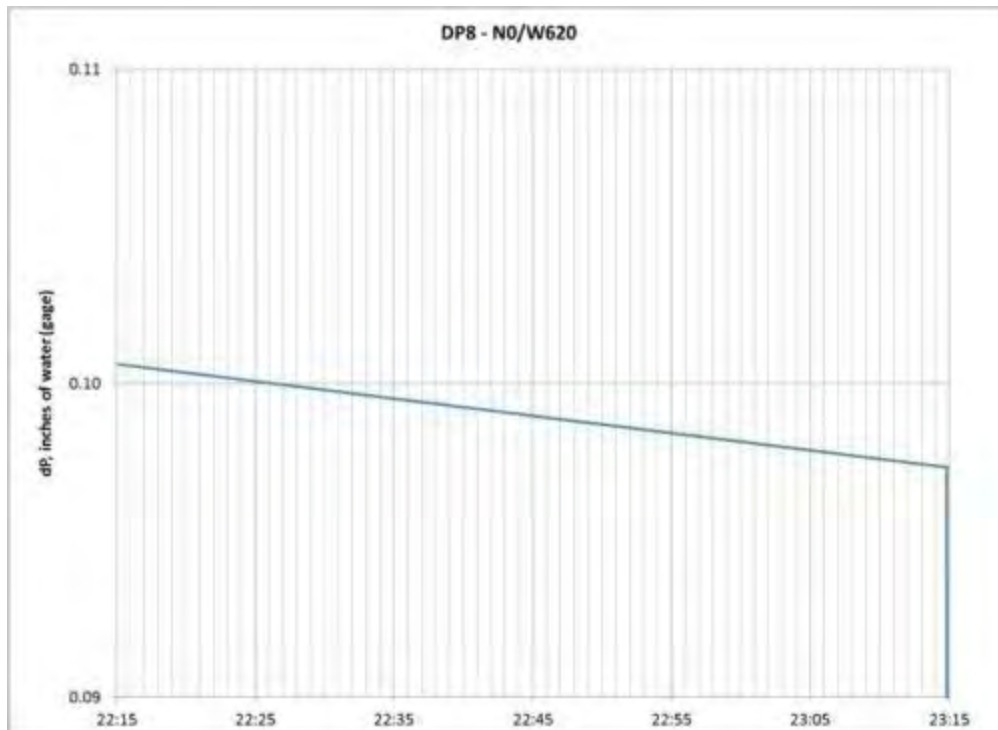
**Figure 5-44: dP8 Sensor Data Prior to Switch To Filtered Ventilation
Mode, Located near Air Intake Shaft**
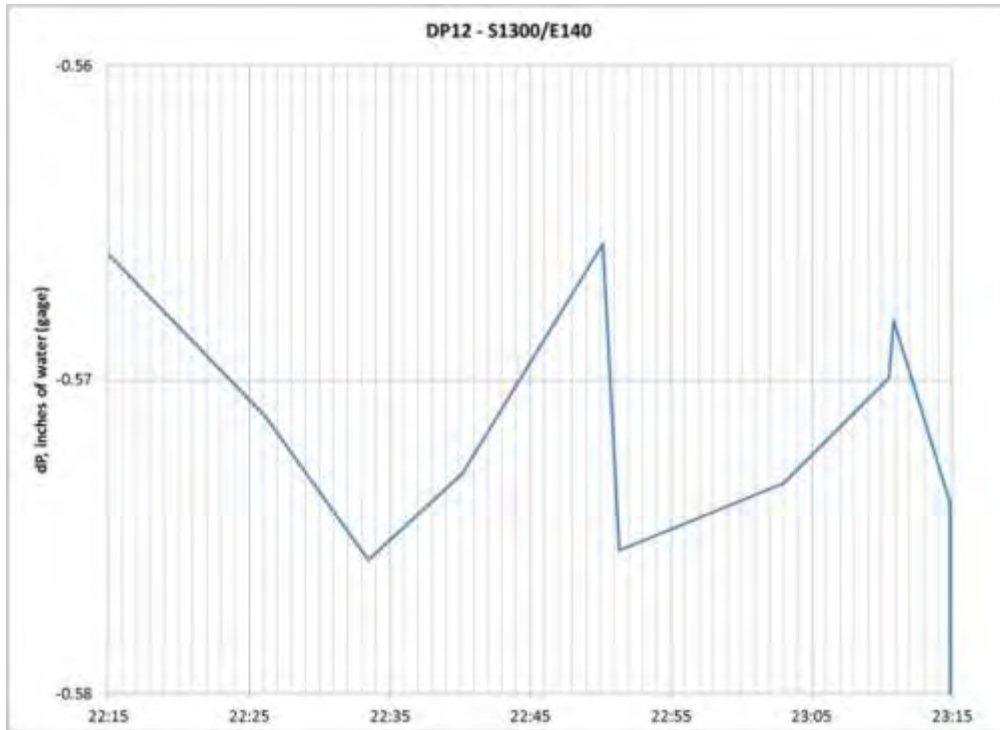
**Figure 5-45: dP12 Sensor Data Prior to Switch to Filtered Ventilation
Mode, Located in S-1300 across BH-324**
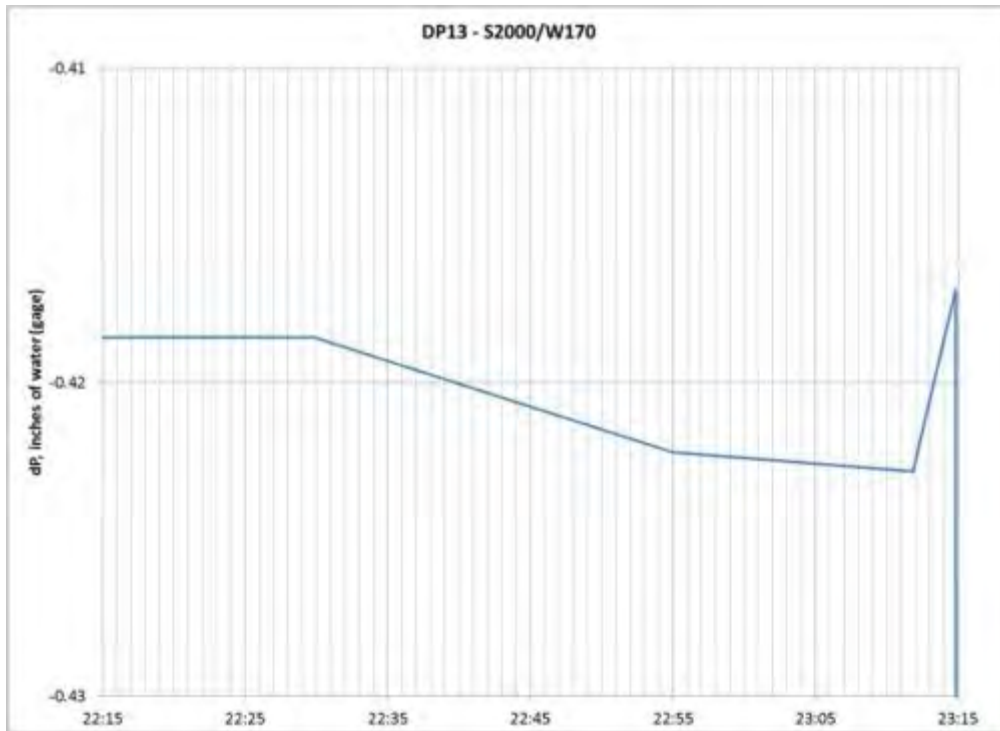
**Figure 5-46: dP13 Sensor Data Prior to Switch to Filtered Ventilation
Mode, Located in W-170 across BH-707 between Panel 7 and Panel 8**
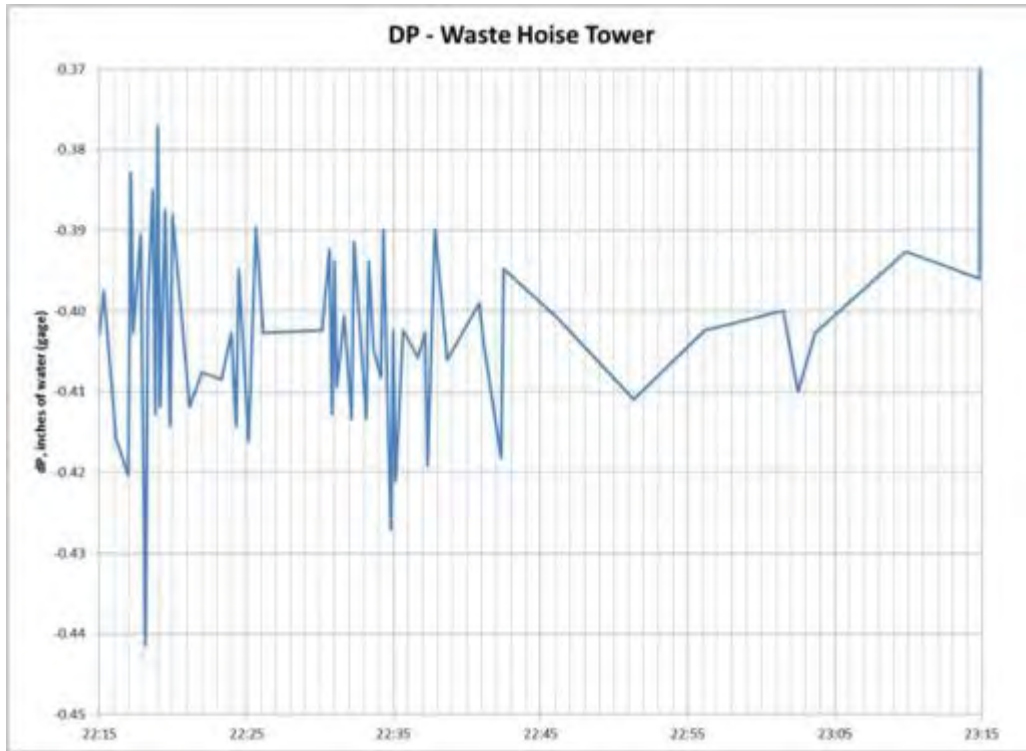
**Figure 5-47: dP-WHT sensor Data Prior to Switch to Filtered
Ventilation Mode, Located in the Waste Hoist Tower on the Surface**

It is uncertain what the change in dP for these three sensors means, if anything. All of the data is still within an acceptable amount of error for the sensors (±10 percent). No conclusions could be made from the available data.

Two sensors, dP4 near the exhaust shaft, (Figure 5-41), and dP6 in S-1000 between the construction and disposal circuits (Figure 5-43), show fluctuations in the dP measurements throughout the pre-CAM timeframe with no noteworthy observations. The remaining four sensors: dP5 (Figure 5-42), dP8 (Figure 5-44), dP12 (Figure 5-45), and dP13 (Figure 5-46) do not show much variation in measurement throughout the pre-CAM timeframe.

5.4.2.2.   Analysis Following Switch to Filtration

Following the switch to Filtered Ventilation Mode, none of the dP sensors showed any of the noise that was observed previously. Most of the sensors showed very straight and direct ups and downs over the course of the measurement timeframe. The only real observation that could be made from the sensor data (Figure 5-48 through Figure 5-56) were the time it took to reach a somewhat steady-state measurement regime (Table 5-5).
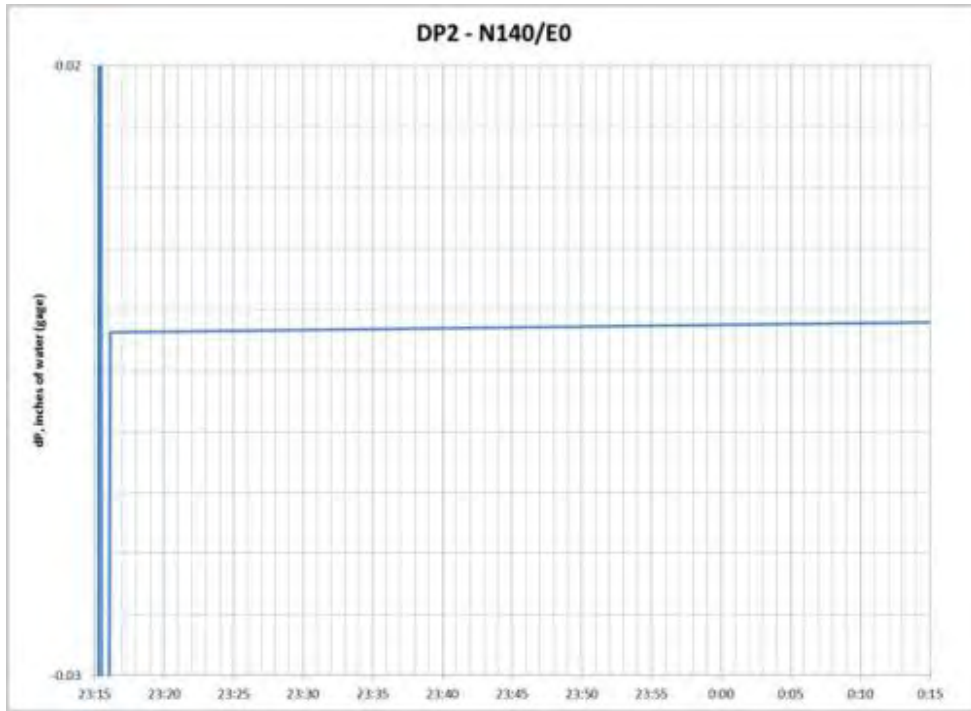
**Figure 5-48: dP2 Sensor Data after Switch to Filtered Ventilation
Mode, Located in E-0 across BH-302**

**Figure 5-49: dP3 Sensor Data after Switch to Filtered Ventilation
Mode, Located in E-140 North Airlock (303, 310) near Waste Shaft**

**Figure 5-50: dP4 Sensor Data after Switch to Filtered Ventilation
Mode, Located in S-400 across BH-308**
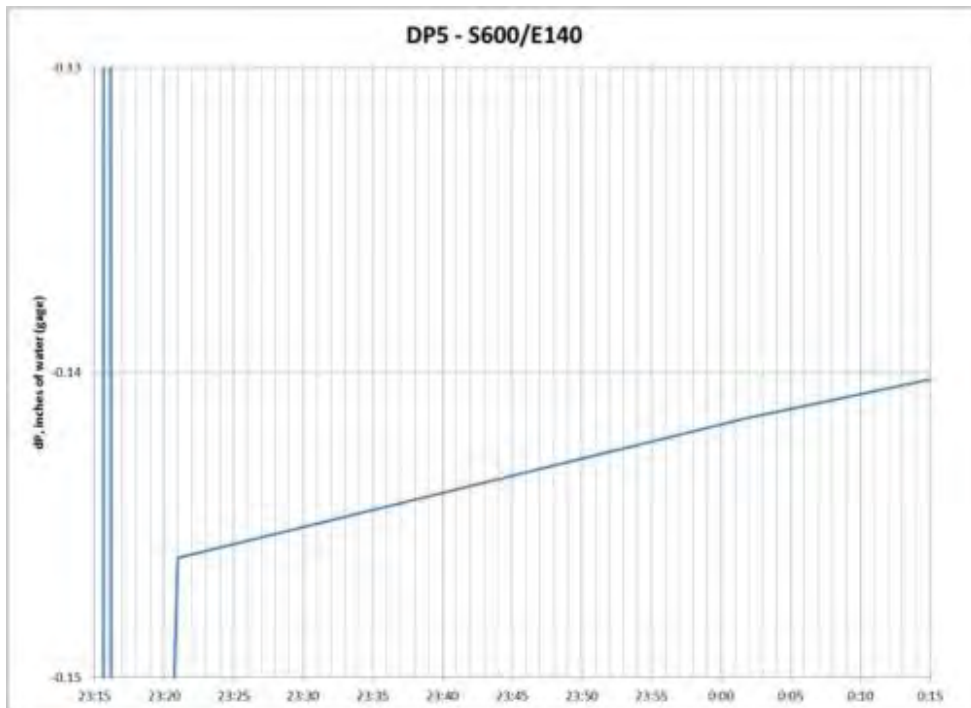
**Figure 5-51: dP5 sensor Data after Switch to Filtered Ventilation
Mode, Located in E-140 South Airlock (415, 416) near Waste Shaft**

**Figure 5-52: dP6 Sensor Data after Switch to Filtered Ventilation
Mode, Located in S-1000 across BH-313**
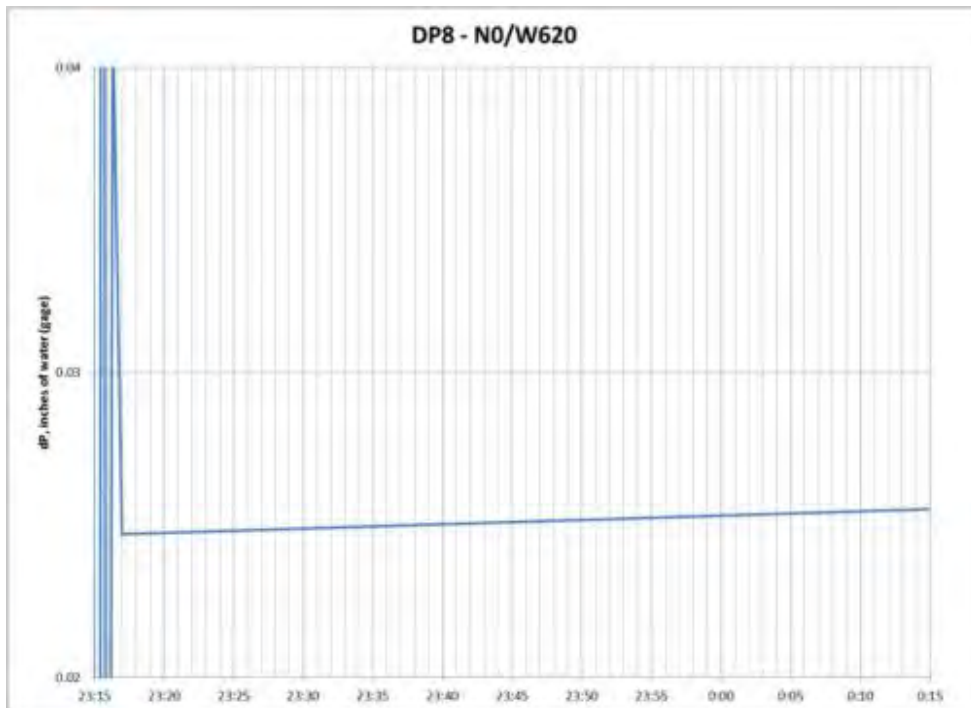
**Figure 5-53: dP8 Sensor Data after Switch to Filtered Ventilation
Mode, Located near Air Intake Shaft**

**Figure 5-54: dP12 Sensor Data after Switch to Filtered Ventilation
Mode, Located in S-1300 across BH-324**

**Figure 5-55: dP13 Sensor Data after Switch to Filtered Ventilation
Mode, Located in W-170 across BH-707 between Panel 7 and Panel 8**
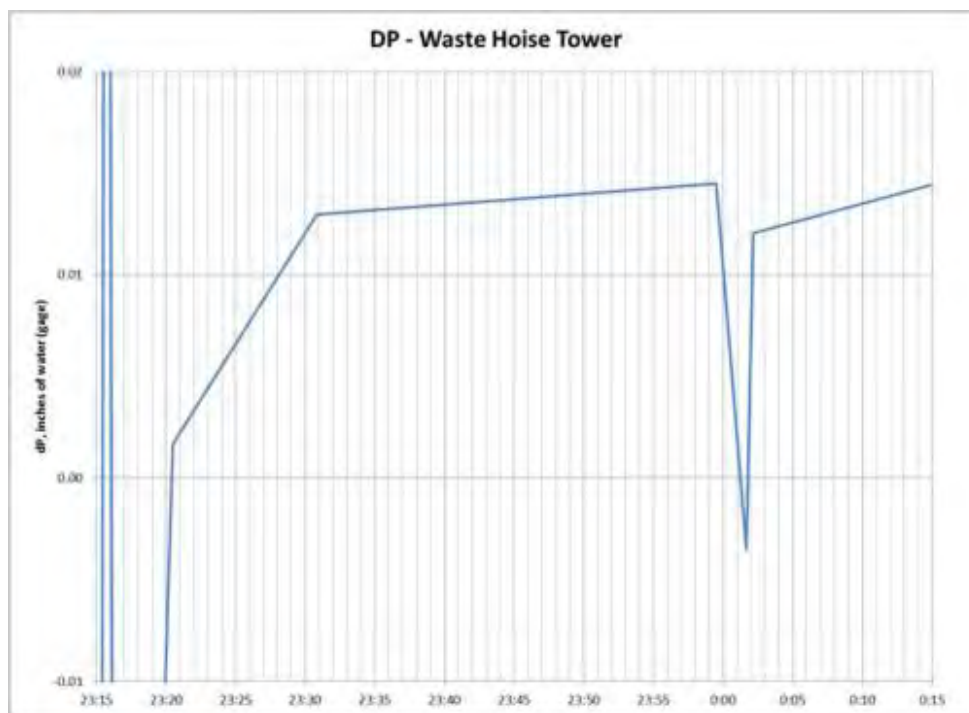
**Figure 5-56: dP-WHT Sensor Data after Switch to Filtered
Ventilation Mode, Located in the Waste Hoist Tower on the Surface**

Differential pressure sensor dP2 reached a quasi-steady-state by about 2316 on February 14, 2014, (Figure 5-48) and did not change in value considerably after. Sensor dP3 reached an approximate steady-state by 2320 and showed some slight fluctuation (Figure 5-49), but nothing that stood out. An approximate steady-state was achieved by 2320 for sensor dP4, with the dP increasing slowly over the time observed in Figure 5-50. Figure 5-51 indicates that dP5 reached a quasi-steady-state by about 2321, with a slowly increasing trend in dP during the remaining timeframe analyzed.

Two small peaks in dP data were observed in Figure 5-52 for dP6 during its steady-state regime after 2321. Figure 5-53 indicates that dP8 reached a steady-state by 2317 and had a slight increasing trend in dP for the remainder of the hour following the release event. Sensor dP12 began to settle down to a steady-state reading by 2320 (Figure 5-54), with steady ups and downs in its readings. Sensor dP13 (Figure 5-55) began to settle at 2322 and dP-WHT (Figure 5-56) stopped its large oscillations due to the change in flow regimes at 2321.

5.5.   Summary

Sensor data was analyzed from 0000 on February 14, 2014, to 0000 on February 16, 2014. Included in this analysis was a check of whether the bulkhead door closures during both alternate flow and the change to filtered flow correlated with the changes in the measured data, which they did. A detailed analysis of the flow and velocities within Panel 7 was performed in Section 5.3.1. Panel 7 flow utilized the flow at V10 coming out of Panel 7, along with branch dimensions and derived flow splits for Panel 7. Results indicated adequate ventilation during both alternate and filtered flow conditions over the waste in Branch 138.

During Filtered Ventilation Mode, all of the air that enters the AIS or the SHS must pass through closed bulkhead doors to reach the ES. The path from the WS to the ES crosses two drifts, one is closed off by airlocks to the north and south (E-140) and the other is the exhaust circuit where air from the south end of the underground intersects with the ES. There is no clear source of air flow into the exhaust and disposal circuits following the change to Filtered Ventilation Mode. Leakage across bulkhead doors is known to occur, but the extent of this leakage at individual locations is not known. Therefore, it is assumed that leakage is uniform across all bulkheads along the flow path to the ES.

The ES looks to draw a vacuum from the waste shaft station, disposal circuit and exhaust sections of the underground during Filtered Ventilation Mode, leading to higher vacuum pressures across bulkheads and airlocks along with slower flow rates. Differential pressure data also indicated that there was a change in the air pressures; some of which is associated with the lower fan pressure due to the switch to Filtered Ventilation Mode. Two of the sensors indicated a change in sign, with only one sensor (dP3 in E-140 across the airlock north of the WS) indicating a stable change. The dP data measures a difference in the pressure on either side of the doors but, with no information on whether there is leakage across the doorways, quantification of airflow leakage across individual airlocks or bulkheads could not be determined.

It was uncertain if a more refined analysis using ⅛ second average data would provide any substantial observations of out of the ordinary peaks or dips in the sensor readings. The ⅛th-second average data was obtained for the two hours surrounding the CAM alarm event, from 2215 February 14, 2014, to 0015 February 15, 2014, and analyzed in Section 5.4. All of the individual flow and differential pressure sensors were analyzed in depth for the one hour time periods before and after the switch in flow regimes in the underground.

The flow data showed considerable noise in all sensor measurements. Further refinement of analysis was performed by calculating the average and standard deviation of the flow prior to and following the switch to Filtered Ventilation Mode. These are provided in Table 5-2. Included are lines indicating the average, ± 1 standard deviation, and ± 2 standard deviations for the individual sensor to get a better indication of any outliers within the data. With this, no noteworthy abnormalities were observed. The dP data similarly did not indicate any major abnormalities. One key piece of information that was obtained from this analysis was the time it took for the various sensors to re-equilibrate after the switch in flow in the underground from the alternate flow to filtered flow. These times have been summarized in Table 5-5.

6.0   SALT HAUL TRUCK FIRE EVALUATION

This chapter analyzes the potential impact of the February 5, 2014, salt haul truck fire incident upon the initiation of the radiological release that occurred on February 14. The areas of interest are:

• Conditions at the SHS during the fire event;
• Conditions at the Waste Disposal Circuit during the fire event;
• Conditions at Panel 7, specifically Room 7, during the fire event; and
• Potential changes in MgO super sack chemistry due to the fire event.

6.1.   Ventilation

On February 5, 2014, at approximately 1048, a salt haul truck caught fire in the E-0 drift at the intersection with N-300, which connects to the AIS. [21] A majority of the flow through the AIS reaches this intersection, where it splits between the North Circuit Intake and the Construction Circuits. At the start of the fire the ventilation system was operating in Maintenance Ventilation Mode.

At 1058, the Facility Shift Manager directed the Central Monitoring Room Operator to change ventilation from Maintenance Ventilation Mode to Filtered Ventilation Mode, believing this would reduce both the fire and smoke. [21] At 1147, the Central Monitoring Room Operator secured the ventilation in the underground [21], turning off all operating fans in order to reduce the air flow (oxygen supply) to the fire. Virtually all flow was through the southern portion of the underground, with no substantive flow through the North Circuit Intake.

Illustration 1 displays the locations of the flow sensors throughout the underground. This illustration also serves as a basis for the flow maps that will be used to show the direction and magnitude of airflow during Normal Ventilation Mode, Filtered Ventilation Mode, and Secured Ventilation Mode. It is important to note that the flow sensors only record the magnitude of the flow in a particular location, not the direction of the airflow. To determine the direction of airflow, dP sensor data must be analyzed. The flow directions shown in Illustration 1 occur in Normal Ventilation Mode. It is important to note that Illustration 1 does not highlight all possible flow paths in the underground, only those for which sensors can be used to determine the airflow. Leakage into grey non-colored paths does exist, but is assumed not to occur at a magnitude comparable to those paths measured by sensors.

Figure 6-1 shows the average flow in the underground from 0800-1040, prior to the salt haul truck fire. The ventilation system, operating in Maintenance Ventilation Mode, allowed for flow through the Construction Circuit (purple), Northern Circuit Intake (green), Disposal Circuit (cyan), and Exhaust Air Intake (red). The volumetric flow balance presented in Figure 6-1, does not explicitly balance. This was in part due to the extremely cold temperatures at the surface on February 5, which created large temperature gradients throughout the underground. As such, the air densities were not equivalent and the continuity checks were developed on an air mass balance basis.
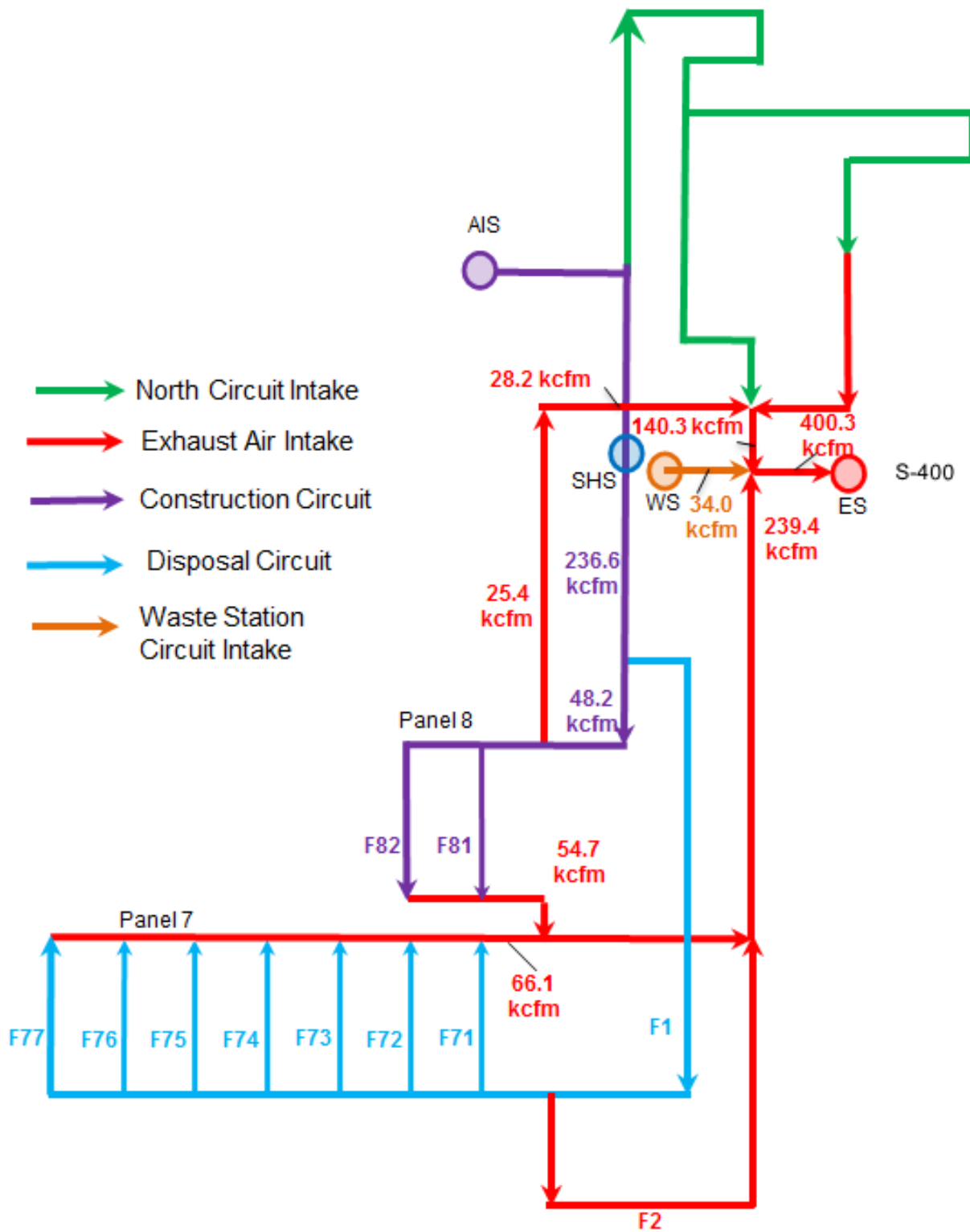
Figure 6-1: Maintenance Ventilation Mode Flow Map for February 5, 2014, 0800-1040

At the time of the fire, BH-308 (S-400/E-300), BH-401 (N-215/W-500), and BH-504 (north of SHS) were chained open. Bulkhead-707 (S-2000/W-170), which can only be operated manually, was also open. [21] Upon the switch from Maintenance Ventilation Mode to Filtered Ventilation Mode, BH-313 (S-300/E-300) and BH-336 (S-1000/E-0) were shut automatically. [18] This change effectively limited airflow to the Disposal Circuit by cutting off the Northern Circuit Intake exhaust flow. The two 700 series fans that were operating in Maintenance Ventilation Mode were shut off, and one 860A fan was turned on, reducing the flow rate through the underground exhaust shaft. [18] The combination of the reduction in airflow and fewer potential flow paths resulted to the significant buildup of smoke in the underground. When ventilation was secured, the one operating 860A fan was turned off, leaving only passive means, such as temperature and pressure differentials, to create airflow.

Figure 6-2 shows ventilation flow data on the day of the incident for the ES (V15), WS (V2), and the exit drift of Panel 7 (V10). Immediately prior to the initiation of the fire (1048), these sensors measured approximately 401 kcfm, 34 kcfm, and 64 kcfm respectively. The red vertical line in this figure represents the start of the fire (1048) and the green vertical line represents the beginning of the shift to Filtered Ventilation Mode (1058). The flow rates remained relatively unchanged between the fire's initiation and the switch to Filtered Ventilation Mode (1048-1057). When the shift to Filtered Ventilation Mode was initiated, the ES and Panel 7 drift flows dropped to 64 kcfm and 59 kcfm, respectively, with the WS flow averaging approximately 32 kcfm. The Filtered Ventilation Mode timeframe is located between the green and purple vertical lines on Figure 6-2. After ventilation was secured (1147), the ES flow rate (V15) went down to 4 kcfm, Panel 7 exit drift flow rate (V10) fell to 40 kcfm, and the WS flow rate (V2) averaged approximately 35 kcfm. The flow rates for V2, V10, and V15 are displayed in Table 6-1. Figure 6-3 shows these flows from 1030-1230.

Table 6-1: Flow Rates during Ventilation Modes

Ventilation Mode	Timeframe	V2 – WS kcfm	V10 – Panel 7 Exhaust kcfm	V15 – ES kcfm
Maintenace	1048-1057	33	67	400
Filtered	1058-1146	32*	59	64
Secured	1147-0000	35*	40	4

Note: * These flows are in the opposite direction from Normal or Maintenance Ventilation Mode

Figure 6-4 presents the temperatures at the top of the SHS, WS and in the ES duct. The WS air is taken from or rejected to a temperature controlled environment, which is reflected in its relatively stable temperature of approximately 61°F (16°C).
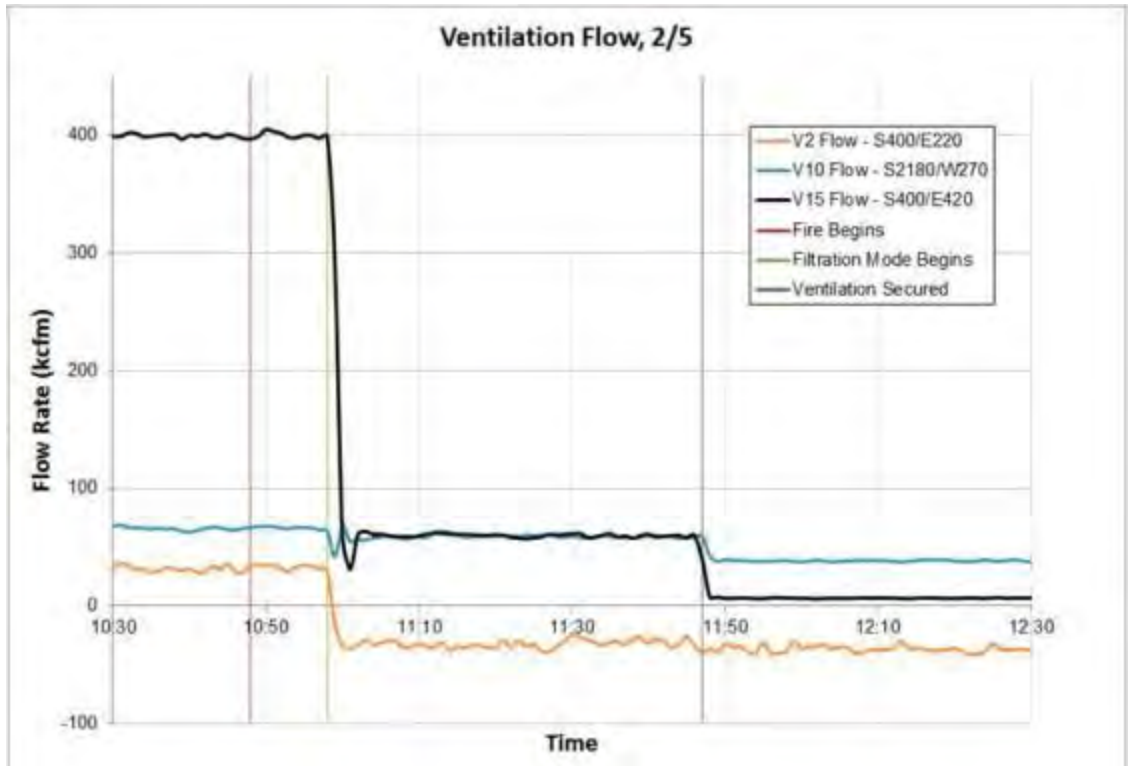
Figure 6-2: Flow Data from February 5, 2014, 0000 to February 6, 2014, 0000
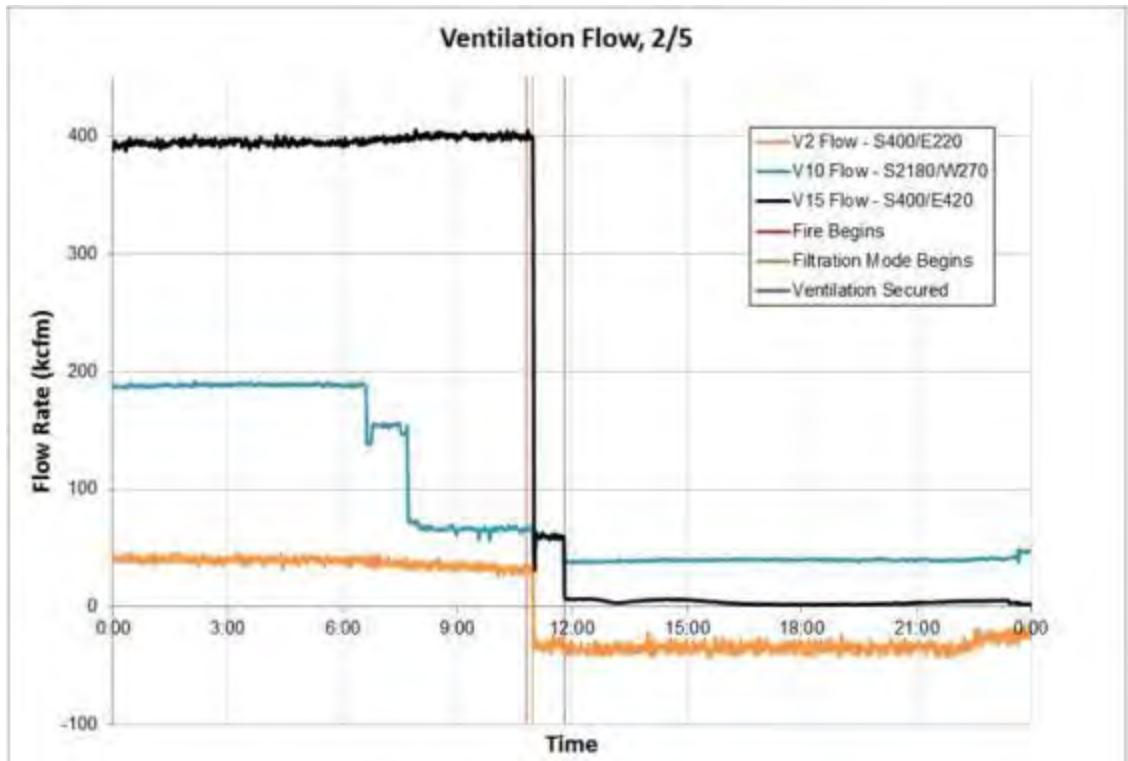
Figure 6-3: Flow Data from 1030-1230 on February 5, 2014
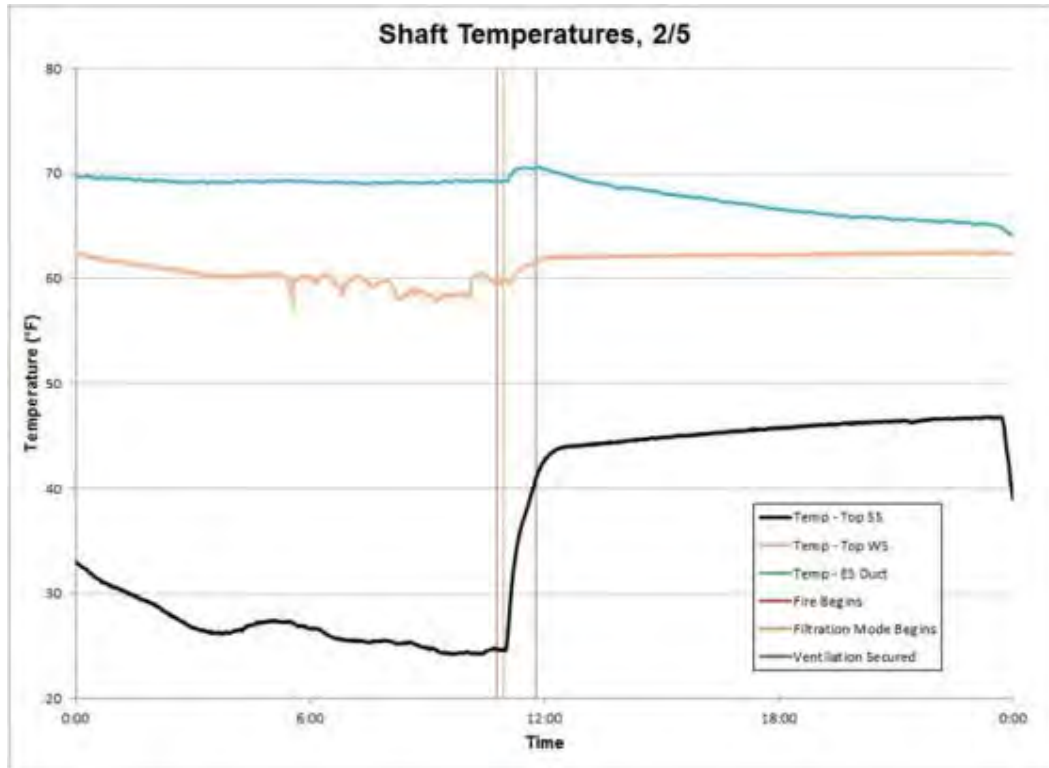
**Figure 6-4: Shaft Temperatures from February 5, 2014, 0000 to
February 6, 2014, 0000**

The temperature in the ES duct, which indicates the bulk temperature of air exiting through the
ES to the natural environment, averaged at about 69°F (21°C) until it began to decrease upon the
securing of ventilation at 1147. The temperature decreased linearly for the rest of the day. This
temperature decrease was a result of the minimal flow through the ES during secured mode.
Without the warm exhaust air passing through the duct, the temperature began to equilibrate with
the surface temperature.

The SHS temperature shows the temperature of air at the surface where it enters/exits the mine.
This sensor can thus be used to approximate the surface air temperature prior to the initiation of
the fire. Immediately before the fire began, the temperature at the top of the SHS was about
25°F (-4°C). During filtered flow, the temperature rose from the baseline 25°F to approximately
41°F (5°C). After ventilation was secured, the temperature continued to rise sharply until about
45°F (7°C) was reached. For the rest of the day, the SHS top temperature slowly increased to
47°F (8°C).

The switch of the ventilation system impacted the dPs throughout the underground due to the
significant reductions in flow through the ES (Figure 6-5). The dP measurements only indicate a
relative difference in pressure across a bulkhead or an airlock, and thus can only be used for
determining the direction of flow if the path is open.
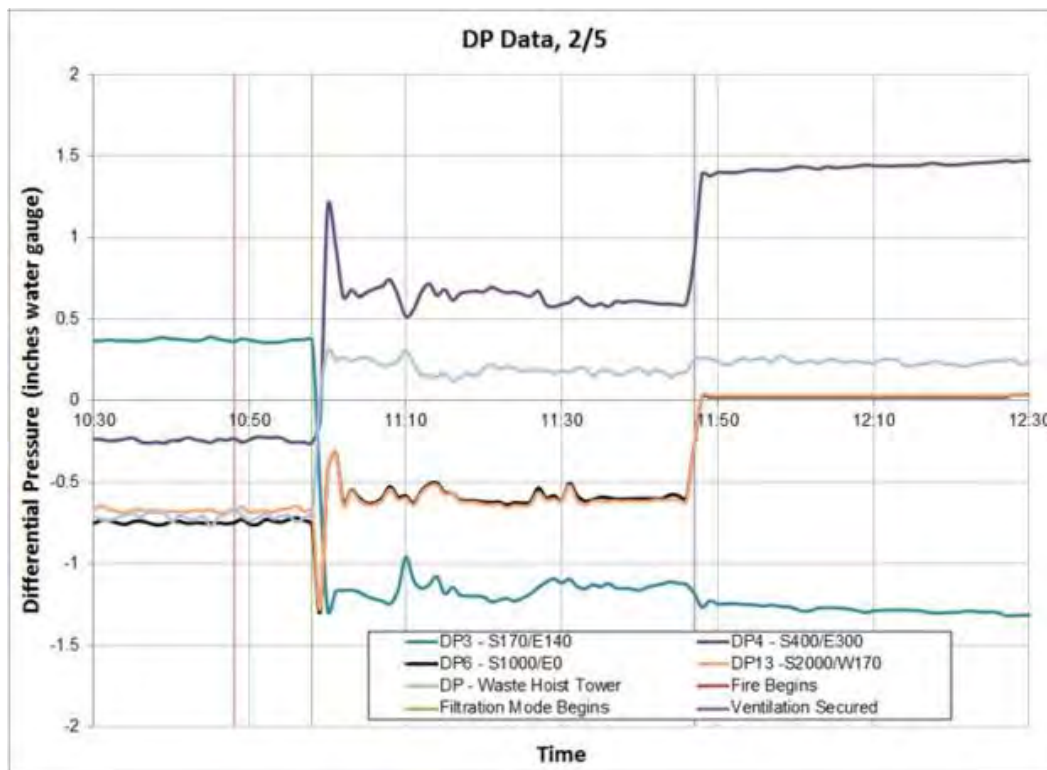
Figure 6-5: Differential Pressure Data from 1030-1230 on February 5, 2014

Upon the initiation of Filtered Ventilation Mode (1058), the dP-Waste Hoist Tower sensor measurement changed from a negative reading to a positive reading. This indicates that flow reversed direction from entering the underground through the WS to exiting the underground. To illustrate this change, the reversed direction V2 flows are shown as negative values in Figure 6-2 and Figure 6-3. The flow reversal in the WS was also visually confirmed by the presence of soot deposits inside the shaft. Sensors dP3 and dP4 also recorded measurements with changes in sign.

Sensor dP4, located at the BH-308, west of the ES, changed from a negative reading to a positive reading. The negative measurements indicate some of the air pulled by the exhaust fans was moving toward the WS. This air was not pulled out of the ES as expected due to the cold temperatures at the time of the incident (~25°F or -4°C - SHS temperature in). The large temperature gradient between the exhaust air and surface air creates a significant density difference. The flow path exiting through the WS presented a less resistant path. Therefore, the air flow exiting the underground after the switch to Filtered Ventilation Mode was the sum of the WS and the ES flows.

Sensor dP3 also showed a sign change from positive to negative. This sensor is located at the 303/310 Airlock, slightly north of the path connecting the WS and ES. The sign change indicates that air was now flowing south, where it would merge with the air flowing toward the WS. This flow reversal is in a branch not explicitly shown on the flow maps. These flow reversals, with average flow rate measurements from 1059-1146, are shown in Figure 6-6.
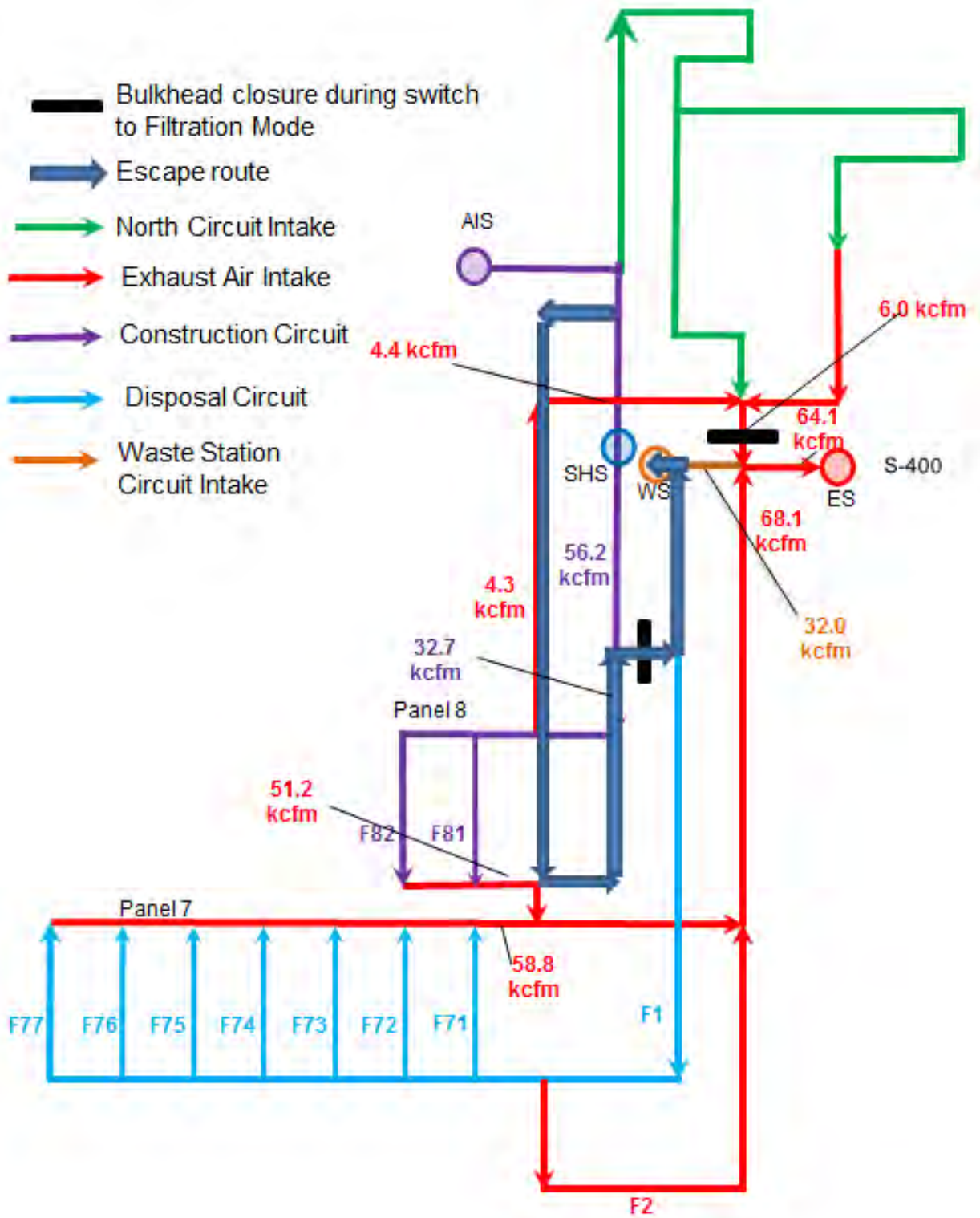
Figure 6-6: Filtered Ventilation Mode Flow Map on February 5, 2014, 1059-1146

It is important to note that the workers in the underground crossed several bulkheads and doors along their evacuation, (Figure 6-6) including BH-313, which was closed during the switch to Filtered Ventilation Mode. According to NWP personnel, all doors and bulkheads crossed during the evacuation were closed after the workers passed through. Therefore, the flow in these branches would not be significantly impacted and do not require special consideration during numerical analysis.

Once the ventilation was secured at 1147, dP6 and dP13 changed from negative to positive measurements. These sensors correspond to BH-313 (E0/S1000, south of SHS) and BH-707 (W170/S2000, near Panel 7) respectively. The measurement changes imply air was traveling north from Panel 7 toward the SHS. This leaves no principle path for air to flow into Panel 7. Figure 6-7 shows a flow map during secured ventilation mode from 1147-1300.

Flow balance checks as developed for the Maintenance Ventilation Mode (Figure 6-1), could not be reconciled for the Filtered Ventilation Mode (Figure 6-6) or Secured Ventilation Mode (Figure 6-7). Resolution of these flow balances is not necessary to fully analyze the February 5 fire effects in Panel 7. It is recognized that approximately 58.8 kcfm and 38.5 kcfm of air was passing through Panel 7 in Filtered Ventilation Mode and Secured Ventilation Mode, respectively. Coupling this with the significant updrafting in the WS previously described is sufficient.

6.2.   Fire Intensity

The salt haul truck damage was limited to the forward half of the vehicle (two tires and most of the combustible fluids). Typical peak heat release rate (HRR) values for most vehicles range from 5 MW to 200 MW, where the smaller values are for passenger cars and the larger are transport trucks with combustible loads. [22] A burning pool of diesel fuel with a 1 m^2 (10.7 ft^2) surface area would produce a peak HRR of 1.7 MW (based on kerosene; heat of combustion = 43 MW/kg, specific burn rate = 0.039 kg/m^2 s). The peak HRR for a pair of tires in a tandem wheel arrangement has been shown to be almost 1 MW. [23]

Based on the observed damaged and the peak HRR information in the previous paragraph, the peak HRR during the haul truck fire would have been between 2 MW and 20 MW.

Fire ignition occurred at about 1048, minutes prior to the switch to Filtered Ventilation Mode at 1058. During this period, the fire transitioned from an incipient fire to involving the entire forward half of the salt haul truck. It is uncertain if the fire became fully developed before or after the transition to Filtered Ventilation Mode. However, the fire severity was significantly reduced when the ventilation was secured at 1147 due to the greatly reduced airflow in the underground. For this reason, the effects of the fire after ventilation was secured will not be analyzed.

Since it is not known if the fire became fully developed before or after the switch to Filtered Ventilation Mode, the fire HRR for Maintenance Ventilation Mode will be bracketed between 5 MW and 10 MW for subsequent analysis. It is assumed here that the fire would have become fully developed during the filtered flow timeframe, so higher bracketing values of 10 MW and 15 MW will be used in the filtered flow analysis.

Figure 6-7: Secured Mode Flow Map on February 5, 2014, 1148-1300

6.3. Temperature Analysis – Salt Handling Shaft

This subsection presents an estimate of the air temperature at the base of the SHS for the normal and filtered ventilation conditions.

6.3.1. Maintenance Ventilation Mode

Figure 6-8 shows a simplified flow diagram for the February 5 salt haul truck fire during Maintenance Ventilation Mode (1048-1057). Air flows downward through the AIS and SHS. The high air intake flow rate does not allow for buoyancy driven flow to occur in the SHS. For simplification, Figure 6-8 does not show the alternate flow routes between the two shafts or the 2 meter elevation drop in the underground hallways between them. Both of these simplifications are incorporated into the analysis as implicit assumptions with no significant effect.
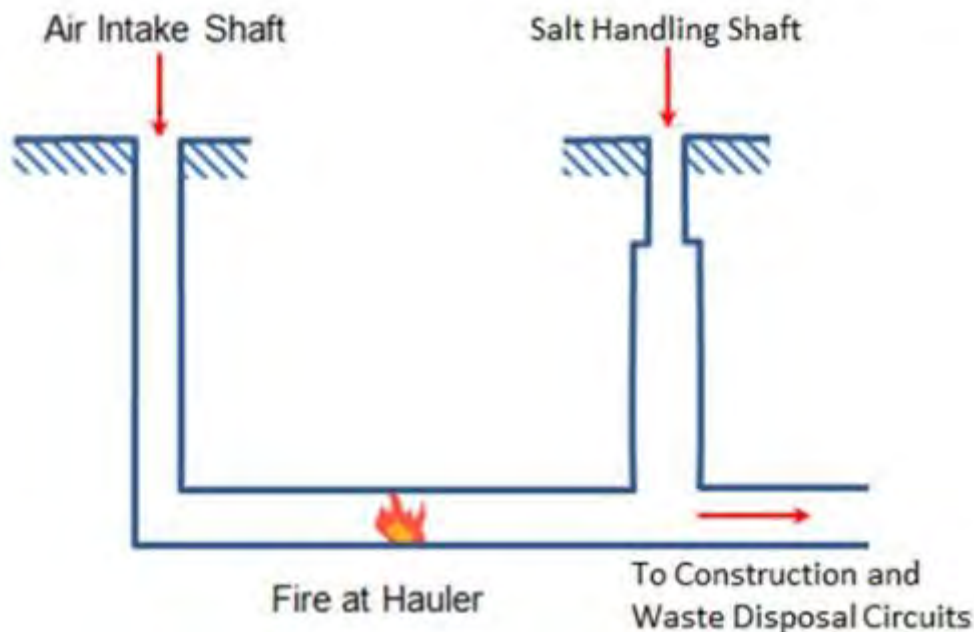
Figure 6-8: Flow Schematic for Maintenance Ventilation Mode

Assumptions

- The HRR of the salt haul truck is bracketed between 5 MW and 10 MW for the normal ventilation timeframe.
- The nominal ventilation flow at V7 (air passing SHS) is 235.5 kcfm (111 m^3/s, 142 kg/s).
- Flows through the North Ventilation Circuit and the Waste Handling Shaft are neglected.
- The system is at steady state – There is no gas expansion term at the fire, nor are there transient flow effects.
- Air entering the AIS is taken as 0°C. This is based upon data from Figure 6-4. The value is intended to account for heat transfer from the AIS walls.

Analysis

The temperature at the SHS, downstream of the fire, can be estimated using the conservation of energy:

$$T_2 = \frac{\dot{Q}}{\dot{m}c_p} + T_1 \tag{1}$$

Where:

T_2 Bulk air temperature downstream of the fire (at the SHS) [°C]
T_1 Air temperature upstream of the fire (at the AIS) [0°C]
$\dot{Q}$ Heat release rate of the fire [5,000 kW; 10,000 kW]
$\dot{m}_g$ Ventilation mass flow [142 kg/s]
c_p Specific heat of air [1.014 kJ/kg·K]

The calculation will be presented for the 5 MW bracketing condition.

Equation (1) after incorporating the stated assumptions and published air property data [24] yields:

$$T_2 = \frac{5,000 \text{ kW}}{\left(142 \frac{\text{kg}}{\text{s}}\right)\left(1.014 \frac{\text{kJ}}{\text{kg}\cdot\text{°C}}\right)} + 0\text{°C} = 34.8\text{°C}$$

For the 10 MW bracketing condition, the result of the equation above is 69.6°C. At the beginning phase of the fire, while the underground was operating in normal ventilation mode, the temperature at the base of the SHS is between 34.8°C and 69.6°C. Temperatures in this range are not high enough to cause damage to equipment.

6.3.2. Filtered Ventilation Mode

Figure 6-9 presents a simplified ventilation flow diagram for the February 5 salt haul truck fire for Filtered Ventilation Mode. Ventilation in the SHS is buoyancy driven due to the elevated temperature at the base of the SHS. Airflow through the AIS is downward. For simplification, Figure 6-9 does not show the alternate flow routes between the base of the AIS and the base of the SHS or the 2 meter elevation drop between the AIS and the SHS. Both of these simplifications are incorporated into the analysis as implicit assumptions with no significant effect.

Assumptions

- The HRR of the haul truck is bracketed between 10 MW and 15 MW for the filtered ventilation timeframe.
- The nominal ventilation flow is 96 kcfm, the sum of air exiting through the ES and WS (45 m³/s, 54 kg/s).
- The air exiting the underground through the ES and WS is at 20°C (approximate flow weighted average temperature of ES air and WS air).
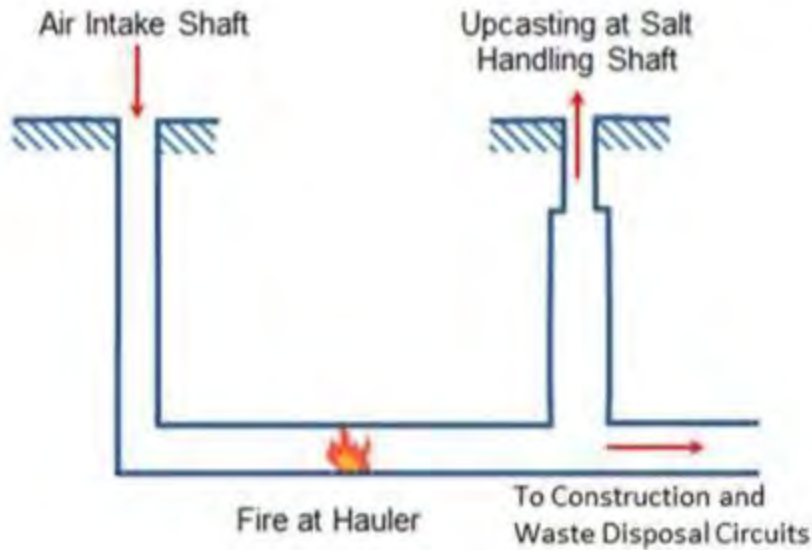
Figure 6-9: Flow Schematic for Filtered Ventilation Mode

- Flow through the North Ventilation Circuit is neglected.
- The average air temperature in the SHS is taken as a constant and is estimated as:

$$T_{SHS-bulk} = 0.5(T_{SHS-bot} - T_{SHS-wall}) + T_{AIS} \qquad (2)$$

The 0.5 coefficient recognizes that the bulk temperature will vary through the SHS. As air rises in the shaft, the temperature will asymptotically approach the shaft wall temperature. In addition, the wall temperature at the base of the shaft will not be constant, but will increase with time. The coefficient importance will be addressed parametrically.
- Energy losses to the walls and to upcasting in the SHS are neglected.
- SHS wall temperature is 9.4°C. This is based upon salt thermal gradient data for February 5 provided by NWP personnel.
- There are no pressure losses between the base of the AIS and SHS
- The system is at steady-state – there is no gas expansion term at the fire, nor are there transient flow effects.
- Air entering the AIS (upstream of fire) is at 0°C. This is based upon data from Figure 6-4.
- The shaft geometry is summarized in Table 6-2.

Table 6-2: Shaft Geometry

Location	Diameter		Length		Roughness	Area
	ft	m	ft	m	m	m²
Air Intake Shaft	20.5	6.25	2129	649	0.003	30.68
Salt Handling Shaft	10	3.05	2151.4	656	0.003	7.31

Solution Method

Air movement throughout the underground can be represented by Bernoulli's equation. The simplified form, accounting for flow loses and assuming constant fluid density is: [25]

$$\frac{\rho V_1^2}{2} + P_1 + g\rho z_1 = \frac{\rho V_2^2}{2} + P_2 + g\rho z_2 + \Delta P_{1\to 2} \tag{3}$$

Where:

ρ density [kg/m^3]
V   average velocity [m/s]
P   local pressure [Pa]
g   local gravity constant [9.81 m/s^2]
z   elevation [m]
$\Delta P_{1\to 2}$ pressure losses between location 1 and location 2 [Pa]

The friction pressure losses are estimated using the Darcy and Colebrook Equations: [25]

$$\Delta P_f = \frac{f\,L}{D_H} \cdot \frac{\rho V_1^2}{2} \tag{4}$$

Where:

ΔP_f friction losses in terms of total pressure [Pa]
f friction factor [unitless]
L   duct length [m]
D_H hydraulic diameter [m]
ρ density [kg/m3]
V   velocity [m/s]

$$\frac{1}{\sqrt{f}} = -2\log\left(\frac{\varepsilon}{3.7\,D_H} + \frac{2.51}{Re\sqrt{f}}\right) \tag{5}$$

Where:

ε roughness factor [m]
f friction factor [unitless]
D_H hydraulic diameter [m]
Re   Reynolds number [unitless]

The Reynolds number is:

$$Re = \frac{D_H V}{\nu} \tag{6}$$

Where:

  D_H hydraulic diameter [m]
  ν kinematic viscosity [m2/s]
  V velocity [m/s]

The Hydraulic Diameter is:

$$D_H = \frac{4\,A}{P} \tag{7}$$

Where:

  A cross-sectional area [m2]
  P wetted perimeter [m]

For a circular duct:

$$D_H = \frac{4\,\pi\,r^2}{2\,\pi\,r} = 2\,r = D$$

Where:

  r radius [m]
  D diameter [m]

The dynamic pressure losses are estimated as: [25]

$$\Delta P_d = C \cdot \frac{\rho V^2}{2} \tag{8}$$

Where:

  ΔP_d dynamic pressure loss [Pa]
  C local loss coefficient [unitless]
  ρ density [kg/m3]
  V velocity [m/s]

The required flow past the fire can be estimated based on conservation of energy:

$$\dot{m}_g = \frac{\dot{Q}}{c_p(T_2 - T_1)} \tag{9}$$

Where:

  T_2 Bulk air temperature downstream of the fire [°C]
  T_1 Air temperature upstream of the fire [°C]

$\dot{Q}$ Heat release rate of the fire [kW]

$\dot{m}_g$ Ventilation mass flow [kg/s]

c_p Specific heat of air [kJ/kg·K]

The solution is iterative. As presented, the air temperature at the base of the SHS must be assumed. From this the mass/energy balance, equation (9) is used to estimate mass flows; the pressure loss terms are estimated using equation (4) and equation (8); equation (3) is used to predict the local pressure at the base of the AIS; and then equation (3) must be demonstrated valid for the SHS.

Analysis

During filtered flow, the air temperature at the base of the SHS will be elevated. The elevated temperature will cause an updraft in the SHS, increasing the airflow past the fire. This subsection presents a sample calculation for this condition. The following calculations were carried out in Microsoft Excel® using a greater number of significant figures than displayed in the tables and equations. For this reason, the displayed calculation results here may not perfectly align with direct calculations using the numbers provided. Calculations will be shown for the 10 MW bracketing condition.

The air temperature at the base of the SHS is taken as 60.9°C, the solution of the iterative process determined using Excel®. The solution will be validated in the following calculations. Substituting this value into equation (2), the corresponding average air temperature in the SHS is:

$$T_{SHS-bulk} = 0.5(60.9°C - 9.4°C) + 0°C = 25.7°C$$

Thermal properties of air at the various temperatures in the underground are presented in Table 6-3.

Table 6-3: Thermal Properties of Air [24]

Location	Temperature		Air density (ρ) kg/m³	Viscosity (ν) m²/s	specific heat (c_p) kJ/kg-K
	°C	K			
Air Intake Shaft	0.0	273.0	1.2769	1.32E-05	1.014
Salt Handling Shaft (base near fire)	25.7	298.7	1.1669	1.55E-05	1.017
Exhaust at ES and WS	20.0	293.0	1.1897	1.50E-05	1.016

Inserting the data from Table 6-3 into equation (9), the mass flow past the fire to maintain a temperature of 60.9°C would be:

$$\dot{m}_{AIS} = \frac{10,000 \text{ kW}}{\left(1.014 \frac{kJ}{kg \cdot °C}\right)(60.9°C - 0°C)} = 161.6 \frac{kg}{s}$$

Balancing this result with the assumed flow rate exiting through the ES and WS, the mass flow up the SHS would be:

$$\dot{m}_{SHS} = 161.6\ \frac{kg}{s} - 54.0\ \frac{kg}{s} = 107.6\ \frac{kg}{s}$$

The volumetric flows are the mass flow rate divided by the density. The flow velocities are then calculated from the volumetric flows divided by the flow area. Sample calculations for the AIS are shown below using data from Table 6-2 and Table 6-3.

$$\dot{V}_{AIS} = \frac{\dot{m}}{\rho} = \frac{161.6\ kg/s}{1.2769\ kg/m^3} = 126.6\ \frac{m^3}{s}$$

$$V_{AIS} = \frac{\dot{V}}{A} = \frac{126.6\ m^3/s}{30.68\ m^2} = 4.13\ \frac{m}{s}$$

The flow and velocity values are presented in Table 6-4.

Table 6-4: Flow and Velocity Information

Location	$\dot{m}$ kg/s	Flow m³/s	V m/s	Re	ε/D$_H$	f
Air Intake Shaft	161.6	126.6	4.13	2.0E+06	0.00048	0.017
Salt Handling Shaft	107.6	92.2	12.62	2.5E+06	0.00098	0.020

With the data from Table 6-2, Table 6-3, and Table 6-4, the friction pressure loss can be calculated using equation (4):

$$\Delta P_f = \frac{(0.017)\ (649\ m)}{(6.25\ m)} \cdot \frac{\left(1.2769\ \frac{kg}{m^3}\right)\left(4.13\ \frac{m}{s}\right)^2}{2} = 19.0\ Pa$$

Solving equation (8) for the dynamic pressure loss, using data from Table 6-2, Table 6-3, and Table 6-4:

$$\Delta P_d = (2.0) \cdot \frac{\left(1.2769\ \frac{kg}{m^3}\right)\left(4.13\ \frac{m}{s}\right)^2}{2} = 21.7\ Pa$$

The loss coefficient, C, value of 2.0 is a sum of the 1.0 entrance loss coefficient and a 1.0 exit loss coefficient for piping. This assumes the shaft cross-sectional area is negligible in size compared to the cross-sectional area of the environments it connects, [26] in this case the underground and the surface environment. Since the properties in the shafts are taken to be

uniform, using a loss coefficient of 2.0 is equivalent to adding the individual pressure losses with the 1.0 coefficient.

The pressure loss results for the AIS and SHS are summarized in Table 6-5.

Table 6-5: Pressure Loss Results

Location	C	ΔP_f Pa	ΔP_d Pa	ΔP_t Pa
Air Intake Shaft	2.0	19.0	21.7	40.7
Salt Handling Shaft	2.0	393.7	185.8	579.5

Equation (3) is used to predict the pressure at the base of the AIS using data from Table 6-2, Table 6-3, Table 6-4, and Table 6-5:

$$P_{bot} = P_{top} + \frac{\rho}{2}\left(V_{top}^{2} - V_{bot}^{2}\right) + g\rho\left(z_{top} - z_{bot}\right) - \Delta P_{top \to bot}$$

$$P_{bot} = (0 \text{ Pa}) + \frac{\left(1.2769 \frac{kg}{m^3}\right)}{2}\left[\left(4.13 \frac{m}{s}\right)^{2} - \left(4.13 \frac{m}{s}\right)^{2}\right]$$
$$+ \left(9.81 \frac{m}{s^2}\right)\left(1.2769 \frac{kg}{m^3}\right)\left[(0 \text{ m}) - (-649 \text{ m})\right] - 40.7 \text{ Pa}$$

$$P_{bot} = (0 \text{ Pa}) + (0 \text{ Pa}) + (8130 \text{ Pa}) - 40.7 \text{ Pa} = 8089 \text{ Pa}$$

(**Note**: P_{top} is a gage pressure measurement and is taken as 0, assuming the surface pressure is 1 atmosphere.)

For the SHS, equation (3) must balance using the result for P_{bot} above and data from Table 6-2, Table 6-3, Table 6-4, and Table 6-5:

$$P_{top} + \frac{\rho}{2}V_{top}^{2} + g\rho z_{top} = P_{bot} + \frac{\rho}{2}V_{bot}^{2} + g\rho z_{bot} + \Delta P_{bot \to top}$$

$$(0 \text{ Pa}) + \frac{\left(1.1669 \frac{kg}{m^3}\right)}{2}\left(12.62 \frac{m}{s}\right)^{2} + \left(9.81 \frac{m}{s^2}\right)\left(1.1669 \frac{kg}{m^3}\right)(0 \text{ m})$$
$$= (8089 \text{ Pa}) + \frac{\left(1.1669 \frac{kg}{m^3}\right)}{2}\left(12.62 \frac{m}{s}\right)^{2} + \left(9.81 \frac{m}{s^2}\right)\left(1.1669 \frac{kg}{m^3}\right)(-656 \text{ m})$$
$$+ (-579 \text{ Pa})$$

$$(0 \text{ Pa}) + (93 \text{ Pa}) + (0 \text{ Pa}) = (8089 \text{ Pa}) + (93 \text{ Pa}) + (-7509 \text{ Pa}) + (-579 \text{ Pa})$$
$$93 \text{ Pa} = 93 \text{ Pa}$$

Since the equation for the SHS balances, the initial temperature assumption of 60.9°C is valid. A comparison of the bracketed HRRs can be found in Table 6-6.

Table 6-6: Bracketing Conditions Analysis Summary

HRR MW	$T_{SHS-base}$ °C	Ventilation Flow, SHS m^3/s	V_{SHS} m/s	Pressure Balance Pa
10	60.9	92.2	12.62	93
15	81.8	111.9	15.31	132

The analysis places the temperature at the base of the SHS in the range of 60.9°C to 81.8°C using 10 MW or 15 MW HRRs, respectively.

Filtered Ventilation Mode Plume Height Check

A check is made between the observed plume at the SHS and the flow velocity calculated in the SHS, assuming a neutrally buoyant condition at the shaft collar, using equation (3) coupled with data from Table 6-3, and Table 6-4. Here we assume the plume height reaches equilibrium with the outside atmospheric conditions, so the thermal properties for the plume are for air at 0°C.

$$P_{SHS} + \frac{\rho}{2}V_{SHS}^2 + g\rho z_{SHS} = P_{plume} + \frac{\rho}{2}V_{plume}^2 + g\rho z_{plume}$$

$$(0\text{ Pa}) + \frac{\left(1.1669\frac{kg}{m^3}\right)}{2}\left(12.62\frac{m}{s}\right)^2 + \left(9.81\frac{m}{s^2}\right)\left(1.1669\frac{kg}{m^3}\right)(0\text{ m})$$

$$= (0\text{ Pa}) + \frac{\left(1.2769\frac{kg}{m^3}\right)}{2}\left(0\frac{m}{s}\right)^2 + \left(9.81\frac{m}{s^2}\right)\left(1.2769\frac{kg}{m^3}\right)\left(z_{plume}\right)$$

$$z_{plume} = \frac{(0\text{ Pa}) + (93\text{ Pa}) + (0\text{ Pa}) - (0\text{ Pa}) - (0\text{ Pa})}{\left(9.81\frac{m}{s^2}\right)\left(1.2769\frac{kg}{m^3}\right)} = 7.4\text{ m}$$

The plume height check for the 10 MW and 15 MW HRRs are provided in Table 6-7.

Table 6-7: Bracketing Conditions Check Summary

HRR MW	$T_{SHS-base}$ °C	V_{SHS} m/s	Plume Height	
			m	ft
10	60.9	12.62	7.4	24
15	81.8	15.31	10.5	35

The result places the height of the plume exiting the SHS in the range of 24 feet to 35 feet. In Figure 6-10, the observed plume height is estimated at about 40 feet, which is greater than the predicted range. The difference is within the accuracy of the analysis.

**Figure 6-10: Upcasting Observed at the Salt Shaft
on February 5, 2014**

6.4.   Temperature Analysis - Panel 7 Room 7

This subsection presents an air temperature estimate in Panel 7 Room 7 during the February 5 salt haul truck fire.

Observations

Based on the flow direction, the most significantly damaged locations at the disposal array in Panel 7 Room 7 following the February 5 fire would have been on the working face. Such damage was not observed prior to the February 14 release event (photograph AIB-FST-01002). The lack of damage to the polyethylene stretch wrap and the polypropylene MgO stacks observed on the morning of February 14, 2014, supports the conclusion that the salt haul truck fire did not cause elevated temperatures above 120°C, the melting temperature of the stretch wrap, at the waste array in Panel 7 Room 7.

Assumptions

- Salt temperature is 20°C. This implies that the heat transfer between the air at the base of the SHS and the salt at the base of the SHS is insufficient to significantly increase the local bulk salt temperature. This assumption mirrors assumption 6 from subsection 6.3.2, which neglected energy loss to salt in the SHS.
- Temperature at base of SHS corresponds to previous calculation (i.e. 60.9°C for Filtered Ventilation Mode, 10 MW HRR)
- Heat transfer coefficient is 0.01 kW/m^2/°C – for forced convection the typical range is 0.01- to 0.5 kW/m^2/°C
- The mass flow through the array corresponds to V10 flow (Panel 7 exit drift) for appropriate timeframe – (i.e. 59 kcfm, 33 kg/s for Filtered Ventilation Mode).
- The heat transfer area consists of the back and ribs of the drift (e.g., no heat transfer to the floor). The area is 23,000 m^2 (248,000 ft^2) as calculated in Table 6-8.
- 46.6 percent of the flow exiting Panel 7 goes through Room 7 (Chapter 5.0, Table 5-4)

Analysis

The following calculations apply to the Filtered Ventilation Mode, 10 MW HRR scenario.

The temperature in Panel 7 Room 7 may be estimated based on a mass-energy balance:

$$\dot{m}c_p(T_{SHS} - T_{Rm7}) = hA\Delta T_m \tag{10}$$

Where:

    m mass flow rate [kg/s]
    c_p Specific heat of air [kJ/kg·K]
    T_{SHS} air temperature at the base of the SHS [°C]
    T_{Rm7} air temperature in room 7 [°C]
    h heat transfer coefficient [kW/m^2/°C]
    A drift surface area [m^2]
    ΔT_m log mean temperature difference [°C]

The log mean temperature difference is calculated by:

$$\Delta T_m = \frac{(T_{Rm7} - T_{c2}) - (T_{SHS} - T_{c1})}{\ln \dfrac{T_{Rm7} - T_{c2}}{T_{SHS} - T_{c1}}} \tag{11}$$

Where:

    T_{SHS} air temperature at the base of the SHS [°C]
    T_{Rm7} air temperature in room 7 [°C]
    T_{c1} salt temperature at the base of the SHS [°C]
    T_{c2} salt temperature in room 7 [°C]

Table 6-8: Geometry Data for Branches

Branch	Length feet	Width feet	Height feet	Area ft²	L x (W + 2H) ft²
From Fire to SHS					
186	139.9	25.1	18	451.8	
193	80.1	12	10.3	123.6	
54	167	25	18	450	
From SHS to Panel 7 Entrance					
53	92.9	32	18	576	6317
184	271.2	20	13.2	264	12584
52	34	20	12.8	256	1550
51	300.8	20	12.8	256	13716
50	300	21.8	14	305.2	14940
170	169.1	25	14	350	8962
34	300.1	25	18	450	18306
35	310	25	18	450	18910
36	310	25	18	450	20710
37	339.5	25	18	450	15659
194	309.3	25	18	450	18867
128	175	20	18	360	9800
129	149.5	20	18	360	8372
From Panel 7 Entrance to Room 7 Waste Face					
130	223.5	18.1	19.2	347.52	12628
131	133	33	13*	429	7847
132	133	33	13*	429	7847
133	133	33	13*	429	7847
134	133	33	13*	429	7847
135	133	33	13*	429	7847
136	133	33	13*	429	7847
137	332.5	33	13*	429	19618
Total	4749.1				248021

Note: * These values taken from WIPP Documented Safety Analysis. [4]

The solution is obtained iteratively. The calculations below will verify the iterative solution of 20.0°C obtained using Excel® is valid. As in subsection 6.3.2, calculations were done with more significant figures than displayed.

Substituting the Room 7 temperature of 20.0°C and assumptions provided above into equation (13), the log mean temperature difference would be:

$$\Delta T_m = \frac{(20.0°C - 20°C) - (60.9°C - 20°C)}{\ln[(20.0°C - 20°C)/(60.9°C - 20°C)]} = 2.78°C$$

Substituting this result into equation (12), including the 46.6 percent flow spilt for Room 7, yields:

$$\left(33\,\frac{kg}{s}\right)(0.466)\left(1.016\frac{kJ}{kg\cdot°C}\right)(60.9°C-20.0°C)=\left(0.01\frac{kW}{m^2\cdot°C}\right)(23{,}000\ m^2)(2.78°C)$$

$$640\ kJ = 640\ kJ$$

This supports the assumption of 20.0°C as the Room 7 temperature. The temperature analysis for each of the ventilation modes and their associated HRR values is provided in Table 6-9.

Table 6-9: Summary of Room 7 Temperature Analysis

Ventilation Mode	HRR MW	Mass Flow Rate kg/s	SHS Temp °C	Room 7 Temp °C	Log Mean Temp Difference °C	Balanced Energy kJ
Normal	5	37	34.8	20.0	1.14	262
	10		69.6	20.0	3.81	878
Filtration	10	33	60.9	20.0	2.78	640
	15		81.8	20.0	4.20	968

Based upon the above calculations, there was no significant temperature increase in Room 7, indicating that no damage would have occurred from this event. The lack of damage was visually confirmed during the inspection of the array after the incident (photograph AIB-FST-01002). Additionally, the temperature increases predicted during normal ventilation mode were unlikely to occur prior to the switch to Filtered Ventilation Mode due to airflow conditions in the underground. Air travelling past the fire at its onset would not reach Room 7 prior to the shift to Filtered Ventilation Mode. This concept will be explored in greater detail in Section 6.5.1.

6.5. Combustion Products

The haul truck combustibles involved in the February 5 fire are summarized in Table 6-10. During the fire, all of these materials were either consumed or released. Combustion products that would have been formed during the salt haul truck fire would primarily include carbon dioxide, carbon monoxide, water vapor and soot. For liquid hydrocarbons, the typical CO_2 generation fractions range from 2.3 to 2.8 kg produced per kg burned, and the CO generation fractions range from 0.01 to 0.06. The tires are a mixture of materials. The CO_2 and CO ranges for solid materials that are similar to tires are 0.06 to 2.3 kg/kg and 0.01 to 0.1 kg/kg. [27] The net heat of combustion for the liquid hydrocarbons is approximately 40 MJ/kg and 30 MJ/kg for the tires.

Table 6-10: Combustibles Consumed or Released During the Salt Haul Truck Fire

Material	Quantity	Density kg/m³	Mass kg	Net Heat of Combustion MJ/kg	Chemical Combustion Energy MJ
Tires	2 @ 500 lbs		500.0	30.6	15,300
Crankcase	4.6 gal	760	13.2	46.4	612
Transmission	10.5 gal	760	30.2	46.4	1,401
Hydraulics	35 gal	760	100.7	46.4	4,672
Differential	6.25 gal	760	18.0	46.4	835
Wheel ends	2 @ 2 gal	760	11.5	46.4	534
Diesel fuel	24.8 gal	820	57.7*	43.2	2,493
Total					25,847

* Value reduced by 25 percent to reflect fuel usage prior to fire.

Table 6-11 provides an estimate of the CO_2, CO and soot generation during the fire event. Following the shift to filtered ventilation mode, between approximately 30 percent (54/180.2 = 0.30, 15 MW HRR) and 33 percent (54/161.6 = 0.33, 10 MW HRR) of this material would travel past the SHS and move towards Panel 7. The actual portion that reached Room 7 would be less because of the multiple flow splits between the SHS and Room 7.

Table 6-11: Combustibles Consumed or Released During the Salt Haul Truck Fire

Material	Mass, kg	CO_2 kg/kg	CO_2 kg	CO kg/kg	CO kg	Soot kg/kg	Soot kg
Tires	500.0	1.5	750	0.05	25.0	0.1	50.0
Crankcase	13.2	2.5	33	0.04	0.5	0.05	0.7
Transmission	30.2	2.5	76	0.04	1.2	0.05	1.5
Hydraulics	100.7	2.5	252	0.04	4.0	0.05	5.0
Differential	18.0	2.5	45	0.04	0.7	0.05	0.9
Wheel ends	11.5	2.5	29	0.04	0.5	0.05	0.6
Diesel fuel	57.7*	2.5	144	0.04	2.3	0.05	2.9
Totals	731.3		1329		34.2		61.6

6.5.1. Effect of Soot

The salt haul truck fire began at approximately 1048 and the transfer to Filtered Ventilation Mode occurred at 1058. The dynamic effects of this flow change took about six minutes to reach steady-state. During this period, the flow moving across the salt haul truck fire was split between the North Circuit Intake and the Construction Circuit Intake. During the 10 minutes between the start of the fire and transition to Filtered Ventilation Mode, the North Circuit Intake was fully inundated with combustion products. Following the flow path in Figure 6-1, in order for the combustion products to reach Panel 7 Room 7 from the site of the fire, 24 mine branches would have to be traversed. Geometry information for the pertinent braches is displayed in Table 6-8.

Based upon corresponding flow measurement data, the flow velocity in each branch can be calculated. The flow rate data used was the average from 1048 to 1058, the time after the fire began but before Filtered Ventilation Mode was initiated. Flow rates were taken from sensors V7, V9, and V10. These sensors were assumed as operating with 1.4 percent, 6.4 percent, and 3.8 percent error respectively (Chapter 5.0, Table 5-1).

$$t = \frac{(L \cdot A)}{\dot{V}} \qquad (12)$$

Where:

t time required to pass through branch [min]
$\dot{V}$ flow rate through branch [cfm]
A cross-sectional area of branch [feet^2]
L length of branch [feet]

Assumptions

- Fire occurs exactly at intersection of branch 186 and branch 105;
- Branches are unobstructed;
- Flow travels linearly (no time required for directional changes);
- No flow escapes into other branches;
- Any elevation changes in underground are negligible;
- Significant soot creation starts immediately as fire begins; and
- Flow divisions in Panel 7 are as described in Chapter 5.0, Table 5-4.

Analysis

Substituting in data from Table 6-8 and Table 6-12 for Branch 186 into equation (12) yields:

$$t = \frac{(451.8 \text{ ft}^2 \cdot 139.9 \text{ ft})}{236,000 \text{ cfm}}$$

$$t = 0.3 \text{ min}$$

Table 6-12: Time Required to Reach Panel 7 Room 7

Branch	Corresponding Flow Measurement	Average flow kcfm	Panel 7 flow fraction	Time in branch min	Cumulative time min
186	V7	236		0.3	0.3
193	V7	236		0.0	0.3
54	V7	236		0.3	0.6
53	V7	236		0.2	0.8
184	V7	236		0.3	1.1
52	V7	236		0.0	1.1
51	V7	236		0.3	1.4
50	V7	236		0.4	1.8
170	F1 = V7 – V9	185		0.3	2.1
34	F1	185		0.7	2.8
35	F1	185		0.8	3.6
36	F1	185		0.8	4.4
37	F1	185		0.6	5.0
194	F1	185		0.8	5.8
128	F1	185		0.3	6.1
129	F1	185		0.3	6.4
130	V10	67	1.000	1.2	7.6
131	V10	67	0.986	0.9	8.5
132	V10	67	0.972	0.9	9.4
133	V10	67	0.958	0.9	10.3
134	V10	67	0.944	0.9	11.2
135	V10	67	0.930	0.9	12.1
136	V10	67	0.466	1.8	13.9
137	V10	67	0.466	4.6	18.5

By keeping a cumulative log of time required to transverse each branch, flow originating at the fire would be in Branch 133, the branch between Panel 7 Room 3 and Panel 7 Room 4, at the time Filtered Ventilation Mode began, having travelled approximately 84.6 percent of the distance to the waste in Panel 7 Room 7. An additional 8.5 minutes (for a total of 18.5 minutes) would have been required for combustion products to reach the waste in Panel 7 Room 7. A summary of the calculations is presented in Table 6-12.

No substantive amount of soot and combustion products would have been produced in the first few minutes of the fire. If it was assumed that it took two minutes for a significant amount of combustion products to be created by the fire rather than immediately, only eight minutes of travel time would be available before the switch to Filtered Ventilation Mode. In this case, the combustion products would have only reached Branch 131, located between Panel 7 Room 1 and Panel 7 Room 2, before Filtered Ventilation Mode began.

Upon the switch to Filtered Ventilation Mode, the flow rates dropped significantly in the northern part of the mine, but less drastically in the southern portion of the underground (Figure 6-1, and Figure 6-6). The decrease in flow velocity in the northern part of the mine would not have allowed for prolonged soot suspension and resulted in the significant soot depositions found in the North Circuit Intake (Figure 6-11). The flow in Panel 7 dropped 11 percent from the transition between normal ventilation to Filtered Ventilation Mode. This comparatively small difference would have kept soot airborne, so any soot entering Panel 7 and Room 7 would have simply flowed through the panel without leaving any depositions. This lack of deposition is shown in photograph AIB-FST-01002. The soot would have remained suspended until it reached the WS, where the flow rate was approximately 32 kcfm. At this point soot depositions would have occurred, which was visually confirmed upon reentrance to the underground.

6.5.2.   Fire Product Reaction with MgO

MgO is a hygroscopic solid material that will react with water vapor to form magnesium hydroxide or carbon dioxide to form magnesium carbonate:

$$MgO + H_2O \rightarrow Mg(OH)_2 \tag{13}$$
$$MgO + CO_2 \rightarrow MgCO_3 \tag{14}$$

Water vapor and carbon dioxide are significant combustion products during hydrocarbon and cellulosic fires. This subsection demonstrates that the combustion products formed during the February 5 salt haul truck fire did not cause damage to the MgO super sacks in Room 7. It recognizes that the MgO reactions with water vapor and carbon dioxide are exothermic, but that these reactions are very slow:

- The formation of magnesium hydroxide [$Mg(OH)_2$] in a mixture of MgO and deionized water requires 33 days to be detected. [28] To support a quantitative evaluation, the concentration at 33 days is taken as 1 percent $Mg(OH)_2$. This is conservative since the data is for liquid water, and the reaction rate for exposure to the 75 percent – 78 percent relative humidity of the air in the underground will be lower.
- The formation of magnesite ($MgCO_3$) will occur well after the formation of $Mg(OH)_2$, and there are intermediate materials formed between these two materials.

Figure 6-11: North Circuit

The energy released by the reaction of water vapor with MgO is calculated using equation (15) below, with the reactants and products of equation (13) above and property data calculated on www.wolframalpha.com. [29]

$$E = \sum (\Delta H_i * M_i)_{products} - \sum (\Delta H_j * M_j)_{reactants} \qquad (15)$$

Where:

ΔH specific heat of formation [kJ/g]
M_i molar mass [g/mole]

$$E = \left[\left(-15.85 \frac{kJ}{g}\right)\left(58.32 \frac{g}{mole}\right)\right] - \left[\left(-14.93 \frac{kJ}{g}\right)\left(40.30 \frac{g}{mole}\right) + \left(-13.42 \frac{kJ}{g}\right)\left(18.02 \frac{g}{mole}\right)\right]$$

$$E = -80.9 \frac{kJ}{mole}$$

This results in a total energy release of 1,390 J/g (80.9 kJ/mole ÷ 58.32 g/moles). The specific heat of MgO is 0.923 J/g/°C. [29] The theoretical heat-up of the MgO when exposed to water vapor can be estimated from the following energy balance:

$$\Delta T = \frac{\text{Energy generated}}{m_{MgO}\, c_p} = \frac{m_{Mg(OH)_2}\, E}{m_{MgO}\, c_p} = \frac{(0.01)m_{MgO}\left(1390\,\frac{J}{g}\right)}{m_{MgO}\left(0.923\,\frac{J}{g \cdot °C}\right)} = 15°C$$

This theoretical temperature increase occurs over 33 days producing only 1 percent (or 0.01) $Mg(OH)_2$, as stated in the first bullet above. As such, the presence of water vapor and carbon dioxide did not create conditions that would have resulted in the melting of the polypropylene MgO super sacks. Any excess water vapor or carbon dioxide would have left Room 7 prior to the 33 days.

7.0   FIRE ANALYSIS

This chapter presents the fire analysis. The chapter is segmented into multiple parts that focus on different stages of the fire event.

7.1.   Ignition Cause

This section documents possible ignition causes, their credibility and proposes the most likely ignition causes. Ignition sources both inside and outside of the waste disposal array were evaluated. This portion of the analysis was performed prior to the systematic and comprehensive array inspection described in Chapter 4.0.

7.1.1.   Option 1: Ignition from Outside of Room 7

Ignition hazards outside of Room 7 require propagation of flames, embers or pyrolysis gases to the waste array in Room 7. Ventilation velocities and directions in the North Ventilation Circuit, the Waste Shaft Intake Circuit and the Construction Intake Circuit south of the Disposal Circuit Intake are sufficiently high that no credible ignition mechanisms exist in these locations. The same is true of drifts associated with the underground exhaust.

Table 7-1 summarizes the potential ignition sources in the northern portion of the Construction Intake Circuit and the Waste Disposal Intake Circuit. No credible ignition sources were identified for these locations.

Table 7-1: Ignition Source External to Panel 7 Room 7

Ignition Source	Discussion
Lightning	The evening of February 14 was clear with no such storms.
Diesel vehicle	Diesel vehicles were last operated prior to February 6.
Electric vehicle	Electric vehicles were operated on February 13 and 14. Any that had operated were parked outside of the Disposal Circuit Intake prior to 1649 on February 14. Electric vehicles that were not operated on February 13 or 14, which were in the Disposal Circuit Intake, were last operated prior to February 6.
Fixed electrical systems	On February 14th operating electrical systems within the Disposal Circuit Intake were limited to lighting and instrumentation circuits (110 VAC or less).
Hot work	No hot work had been performed after February 6.
Portable electrical equipment	No portable electrical equipment was left operating in the Disposal Circuit Intake on February 14.

7.1.2.   Option 2: Ignition in Room 7, but Outside of the Waste Array

Table 7-2 summarizes the analysis results for fire ignition hazards occurring in Room 7, but external to the waste disposal array. No credible ignition sources were identified for this location.

Table 7-2: Ignition Sources in Panel Room 7, but External to the Waste Disposal Array

Ignition Source	Discussion
Diesel vehicle	Diesel vehicles in Room 7 were last operated prior to February 6. Visual inspection of these vehicles did not identify a credible source to ignite the February 14 fire.
Electric vehicle	Electric vehicles in Room 7 were last operated prior to February 6. Visual inspection of these vehicles did not identify a credible source to ignite the February 14 fire.
Fixed electrical systems	Fixed lighting systems were turned off prior to exiting Panel 7 on February 14. Visual inspection of these vehicles did not identify a credible source to ignite the February 14 fire.
Portable electrical equipment	No portable electrical equipment was left operating in Room 7 on February 14.
Postulated liquid pool fire	Flammable and combustible liquids are readily absorbed into the salt floor. Visual inspection of the locations where combustible liquid spills were possible (e.g., mining vehicles) did not identify evidence of a combustible liquid fire in Room 7.

7.1.3.   Option 3: Ignition in the Waste Array

Eleven potential ignition hazards were identified and evaluated. Several are credible mechanisms, all of which fit into two basic categories: exothermic reaction or release of a combustible gas with ignition.

- **Ignition of hydrogen created by chemical reaction**. Hydrogen produced by a chemical reaction can collect within a waste container if the vent is impaired. In sufficient quantity, this would result in an increase in the internal container pressure and subsequent seal failure. A rapid release, if ignited, could cause secondary ignitions. This mechanism is judged credible and fits within the release of combustible gas with ignition category.
- **Ignition of hydrogen created by radiolysis**. Hydrogen produced by radiolysis can collect within a waste container if the vent is impaired. In sufficient quantity, this would result in an increase in the internal container pressure and subsequent seal failure. A rapid release, if ignited, could cause secondary ignitions. This mechanism is judged credible and fits within the release of combustible gas with ignition category.
- **Ignition of a flammable gas**. A container with flammable gas contents could inadvertently be loaded into a waste container and not be identified through the RTR or visual examination

process. If the container fails, it can release its contents as a rapid release, which if ignited, could cause secondary ignitions. While the likelihood of such a container being present is low, it will be evaluated as part of the combustible gas with ignition category.

- **Exothermic reaction involving contents of a waste container**. This cause, which includes spontaneous ignition and chemical reactions, is judged credible and fits within the exothermic reaction category.

- **Exothermic reaction involving MgO**. An exothermic reaction involving the MgO will not create elevated temperatures. Thus, this cause is judged not credible. See discussion in subsection 6.5.2.

- E**xothermic reaction involving packaging external to waste containers**. No credible exposure to incompatible materials that would cause an exothermic reaction of the exposed emplacement combustibles has been identified, thus this ignition cause is judged not credible for the February 14 release event.

- **Overheat ignition of packaging external to waste containers**. An exothermic reaction within a drum will be hottest at the container core. Surface temperature of the waste container will be close to ambient temperature. Temperatures sufficiently elevated to ignite combustibles outside a waste container without thermal runaway is not credible. An exothermic reaction within a drum will be hottest at the core of the susceptible material within the waste container. Surface temperature of the waste container will be close to ambient temperature. Ignition of the adjacent polyethylene will require surface temperatures in excess of 270°C. [12] To produce such an external surface temperature would require an internal core temperature that would not be sustainable without thermal runaway. Thus, this cause is judged not credible.

- **Electrical ignition within waste container**. The presence of a battery in the waste stream would provide sufficient energy to cause ignition within a waste container. While this mechanism is credible, the radiographic inspection process or visual examination of waste container contents makes the likelihood sufficiently low that it is has not been further evaluated.

- **An internally generated spark ignition within waste container**. Some waste containers contain metals and similar materials with the potential to produce impact-generated sparks. While credible during movement, the waste containers had been in a stable configuration since before February 6. No mechanism has been identified to produce the needed impact within a waste container, thus this ignition cause is not credible for the February 14 release event.

- I**ncompatible materials within waste container**. This cause is judged credible and fits within the exothermic reaction category.

- **Inappropriate material in waste container**. This cause is judged credible and fits within the exothermic reaction category.

Each hazard fits into one of two basic categories: exothermic reaction or release of a combustible gas with ignition.

7.1.3.1. Exothermic Reactions, Self-Heating and Spontaneous Combustion

Self-heating behaviors can occur through several mechanisms:

- Exothermic chemical reactions;
- Biological metabolic reactions; and
- Heat-producing physical processes (e.g., water absorption).

One or a combination of these behaviors can result in ignition which is typically referred to as spontaneous combustion. The remainder of this subsection reviews specific aspects associated with some of the MIN02 waste stream which included the addition of Swheat Scoop® and KOLORSAFE® Liquid Acid Neutralizer.

Organic Absorbent. Swheat Scoop® is a wheat-based cat litter that was used as an absorbent material in the MIN02 waste stream. Spontaneous combustion of grains has been studied since the 1700s, but quantitative modeling has provided limited results. [13 p. 867] Studies involving dry, clean, pure substances are of limited value since spontaneous combustion events typically do not occur where these conditions exist. Wheat with moisture content over 14.5 percent has been observed to spontaneously ignite during rail shipments. [13 p. 887] Moisture content exceeding 50 percent is recognized as preventing thermal runaway because of increased conductive cooling through some agricultural materials (e.g., hay). [13] This region is not well studied because such high moisture contents equate to poor product quality. Precautions to avoid spontaneous heating of distiller's dried grains with no oil content are to maintain the moisture contents between 7 and 10 percent and cooling below 38°C prior to storage. [30 p. 6.288] Also, extremely low or high moisture content should be avoided when bulk feed materials are handled. [30 p. 6.289]

The salt-containing liquid components in the MIN02 waste stream, prior to the addition of the absorbent material, typically were a mixture of water, nitric acid and neutralizing agents. As such, the spontaneous combustion thresholds discussed in the previous paragraph must be extrapolated. Just as with plain water, low liquid concentrations will prevent spontaneous combustion because of low reaction rates and high liquid concentrations will prevent spontaneous combustion by ensuring good heat conduction through the waste material. In September 2013, LANS changed the quantity of absorbent used during the drum repackaging procedure. The quantity increased from a minimum ratio of 1.5:1 to a "minimum ratio of 3-parts absorbent to 1-part waste or at a ratio as directed by supervision." [31; 32] To quantitatively understand the impact of this change, consider that on a weight basis if all the liquid is treated as water, this equates to a moisture content reduction from 95 percent to well within the 15 to 50 percent range:

$$M_{1.5:1} = \frac{1 \text{ part water } \left(1000\,\frac{\text{kg}}{\text{m}^3}\right)}{1.5 \text{ parts absorbent } \left(700\,\frac{\text{kg}}{\text{m}^3}\right)} = 0.95$$

$$M_{3:1} = \frac{1 \text{ part water } \left(1000\,\frac{\text{kg}}{\text{m}^3}\right)}{3 \text{ parts absorbent } \left(700\,\frac{\text{kg}}{\text{m}^3}\right)} = 0.48$$

While these estimates do not account for the moisture in the as-delivered absorbent, the value is below 10 percent. As such, explicitly accounting for this moisture is unnecessary given the

accuracy of the absorbent addition process used for treatment of waste drum 68660. In actuality, the liquid content was just part of the total waste component, thus prior to the procedure change the water content was likely already below 50 percent, thus having potential for spontaneous combustion. Following the procedure change, the moisture content was within the 15-50 percent range. While the water content approached 15 percent in portions of the waste matrix, exothermic reactions involving the other absorbed liquids likely created conditions favorable for thermal runaway. Therefore, the procedural change resulted in an increased potential for self-heating behavior resulting in thermal runaway.

Nitrates. The MIN02 waste stream included a variety of nitrates. Both sodium nitrate and magnesium nitrate mixed with cellulosic materials have been observed to ignite with limited heating.[13] Iron oxides, cobalt, copper, magnesium, lead carbonate, potassium carbonate, and lead acetate are recognized as increasing the self-heating behavior. It has been demonstrated that iron compounds can double the chemical oxidation rate of wet sawdust.[13 p. 966] Inorganic nitrates can melt under fire conditions, release oxygen, and intensify the fire severity. The "molten nitrates can react with organic materials with considerable violence."[33]

The KOLORSAFE® Liquid Acid Neutralizer, which was used during packaging of the MIN02, contains triethanolamine, alizarin and water. The MSDS for KOLORSAFE® identifies the material as have an NFPA health rating of 1, a flammability rating of 1 and a reactivity rating of 0. Thermal decomposition in a limited air supply will produce "carbon monoxide, carbon dioxide, ammonia, irritating aldehydes and ketones."

Acid Neutralizer. The DOW Triethanolamine Product Safety Assessment indicates that the product "can react exothermically (producing heat) with many other materials, including strong oxidizing agents, strong acids, strong bases, aldehydes, ketones, acrylates, organic anhydrides, organic halides, formates, lactones, oxalates, and copper and zinc metal alloys." The potential for exothermic reactions is not unique, and does not imply a significant hazard. In some of the cited cases the other material represents the dominant hazard and exothermic reaction might occur with common combustible materials. The reaction hazard risk for triethanolamine has been established as negligible based on the National Fire Protection Association (NFPA) reactivity rating of 0. A reaction rating of 1 would be applied to "materials that in themselves are normally stable but that can become unstable at elevated temperatures and pressures."[34]

7.1.3.2. Combustible Gas Release with Ignition

The timing of the radiological release discussed in Section 7.2 implies that the ignition source must be close to R16:C4 and the air velocities when ignition occurred were high. The visual inspection results did, fire modeling and other analysis efforts did not support hypotheses associated with a gases release followed by ignition. Credible ignition delays and the available specific energy density for a gas would be insufficient to cause ignition upstream of the release point (i.e., R18:C2 and R18:C6). Thus, this ignition hypothesis is judged not credible.

7.2.   Event Timing

This section presents a quantitative estimate of the release timing with a comparison to ventilation and fire conditions. The analysis evaluates the material transit timing from the

intersection of the flows coming from Room 6 and Room 7 to the exhaust drift to the Panel 7 exit.

Figure 7-1 provides the arrangement of Panel 7 with the nomenclature used in this section. The locations a, c and e are fixed and represent the start, a significant flow area change, and the exit. Locations b and d are variable, and represent the positon where a flow transient occurs. Chapter 5 provides the flow velocities in Panel 7 before (Figure 5-11) and after (Figure 5-12) the transition to Filtered Ventilation Mode. The flow through the exhaust drift to the exit can be simplified as two flow sections. The first section, the exhaust drift has an average flow velocity of 201.6 fpm (196, 199, 202, 204, and 207 fpm) prior to the transition to Filtered Ventilation Mode, and 9.8 fpm (9.5, 9.7, 9.8, 9.9 and 10.1 fpm) after the transition to Filtered Ventilation Mode. In the second section, the exit drift, the velocities are 490 fpm and 23.8 fpm, respectively. The travel distances for the two regions are:

- Exhaust drift   698 feet (798 feet – 133 feet + 33 feet)
- Exit drift   190.5 feet (223.5 feet – 33 feet)

7.2.1.   Ventilation/Contamination Migration Timing

Figure 7-2 presents the transient flow data for the ES and Panel 7. Two forms of data have been reviewed, one sample per second data and eight samples per second data. Both forms of the data are presented for the ES flow. This plot demonstrates that most of the flow transient occurred in about one minute. It also demonstrates a delay of about 0.8 minutes between the published alarm point and the time where the ES flow initially changed.

Figure 7-3 presents a comparison of the Panel 7 exhaust ventilation flow data with the contamination concentration measurements at the exit of Panel 7. The Hi-Alarm was received at 2313. The setting was 30 DAC. The Hi-Hi-Alarm, which initiated the switch to ventilation mode, was received at 2314. The setting was 50 DAC. The contamination concentration values presented in Figure 7-3 are noisy, but the early period (2310 to 2330) can be binned into four distinct levels:

- Threshold detection   2310 to 2319
- Low   2319 to 2322
- Intermediate   2322 to 2328
- High   2328 and beyond

These grouping levels, while somewhat arbitrary, facilitate a detailed evaluation of the event timing.

Figure 7-4 presents the same data as Figure 7-3, but over a very limited timeframe (2310 to 2320). This figure clearly demonstrates that during the ventilation transient that occurred after the shift to Filtered Ventilation Mode, the contamination concentration at the exit to Panel 7 was at alarm threshold levels. Low, intermediate or high concentration levels did not reach the CAM until after 2318.
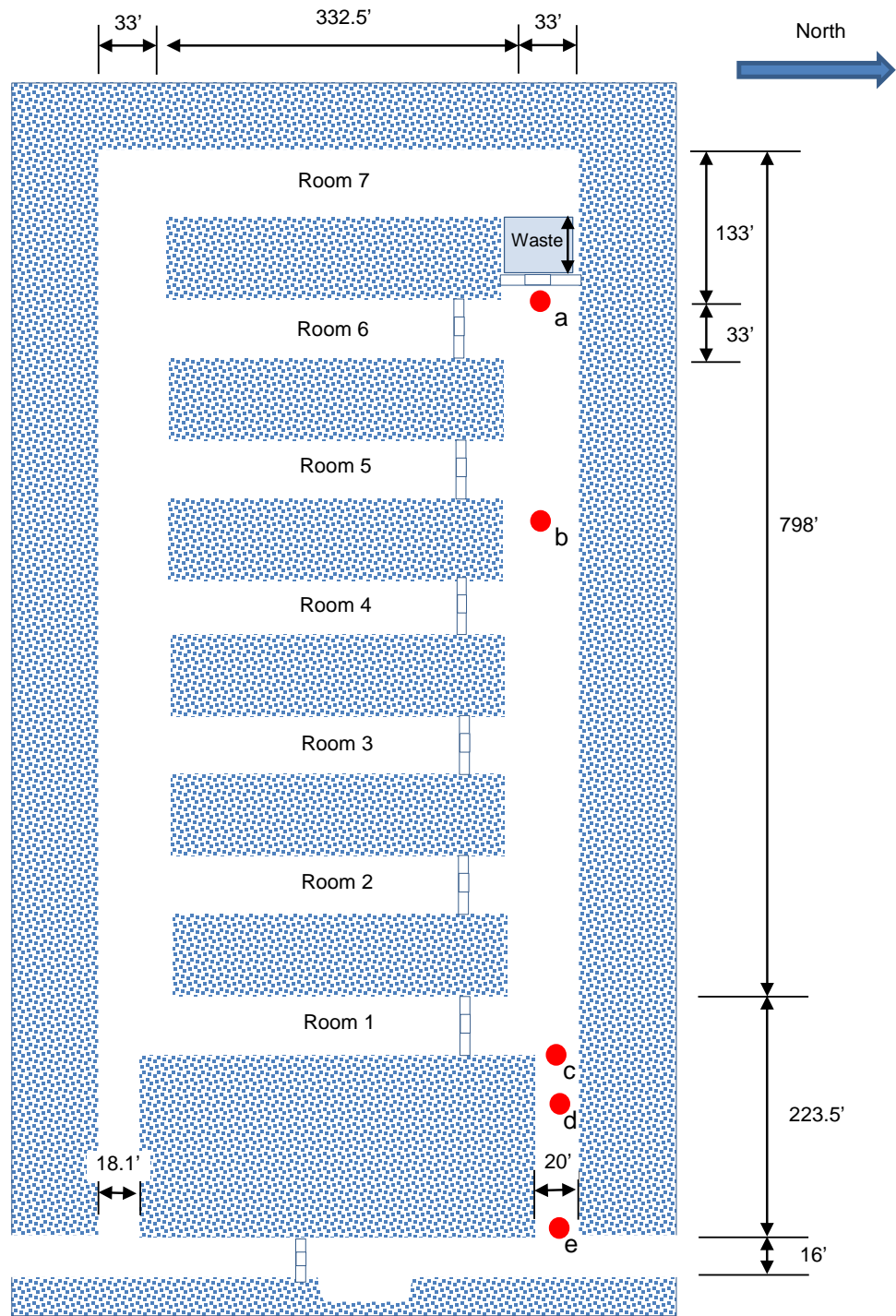
Note: Not to Scale

Figure 7-1: Panel 7 Plan View
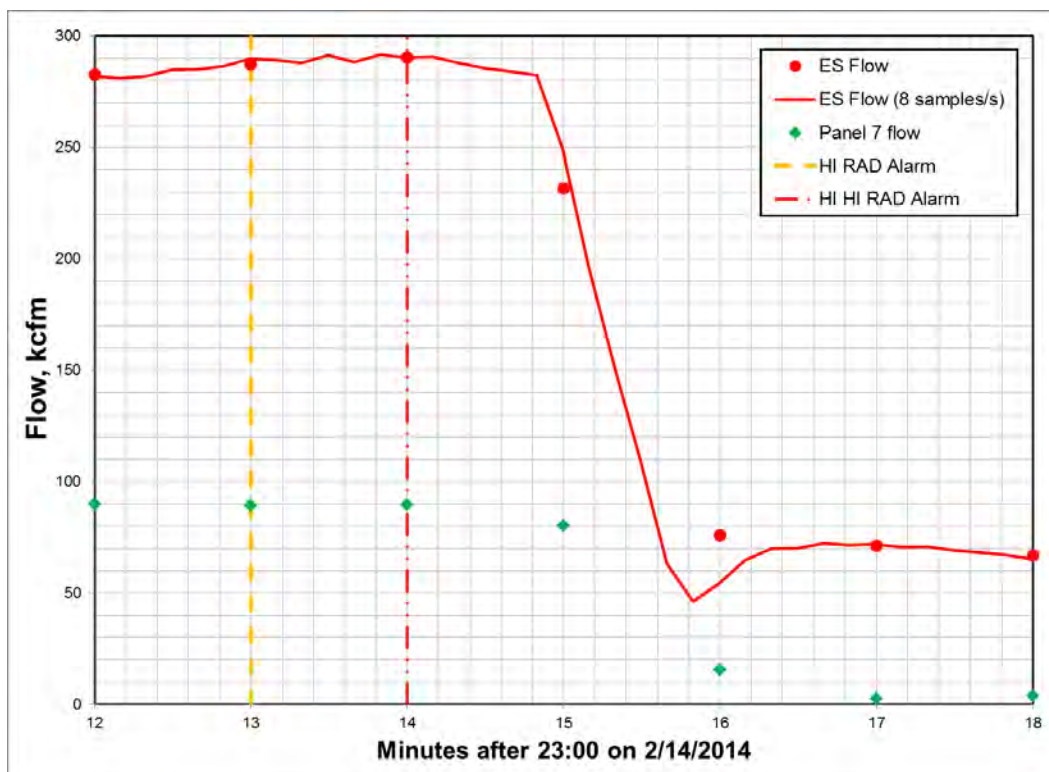
Figure 7-2: Exhaust Shaft and Panel 7 Flow during Transient
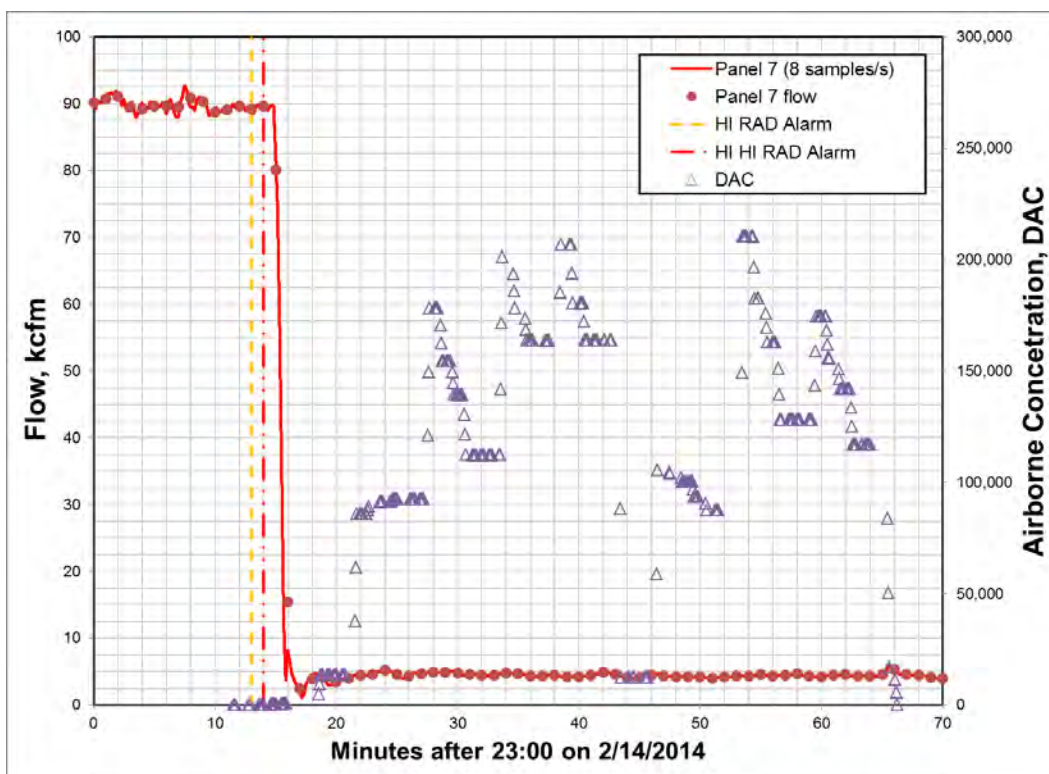
Figure 7-3: Panel 7 Flow & CAM Data
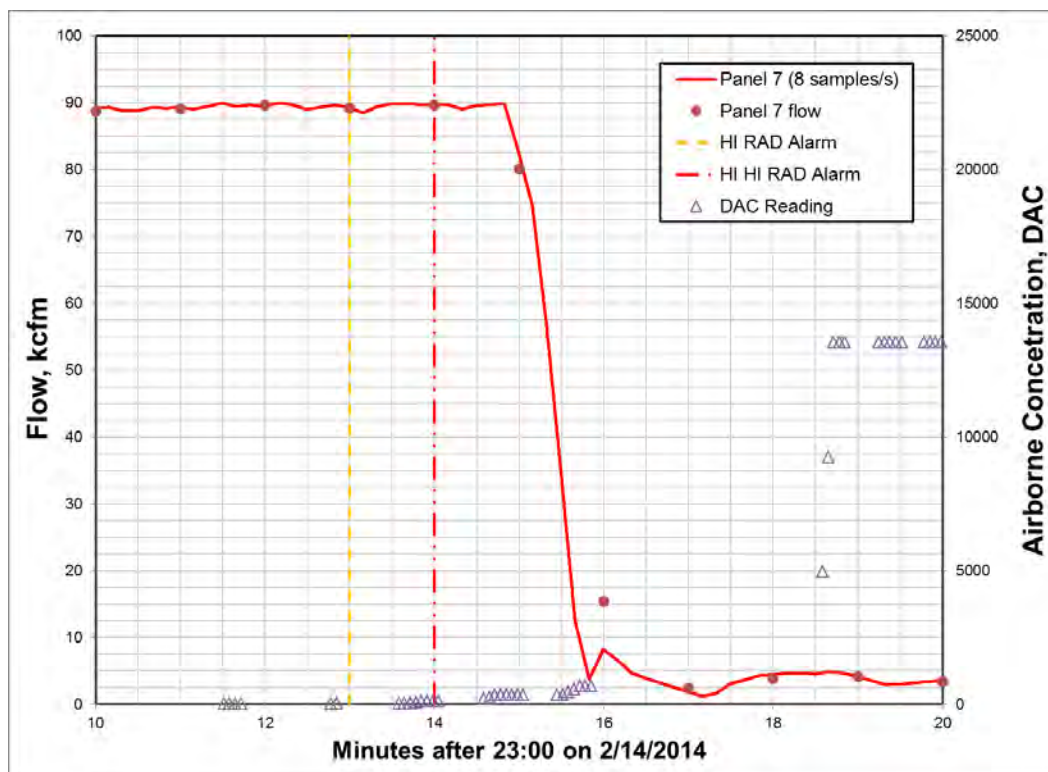
Figure 7-4: Panel 7 Flow & CAM Data (30 minute window)

Figure 7-5 presents a smaller timeframe (2312 to 2316) than either Figure 7-3 or Figure 7-4. This figure demonstrates the uncertainties in establishing alarm times, ventilation response times, and contamination levels. From this information the uncertainties of these values are judged to be less than one minute.

Figure 7-6 presents the information in Figure 7-3 with a focus on the time period prior to the first contamination alarm. It is clear that contamination first arrived at 2311:30, approximately 1.5 minutes before the first alarm.

Table 7-3 provides the filter change times for the CAM at the exit to Panel 7. Figure 7-7 presents the CAM filter change information overlaid on Figure 7-3. Figure 7-8 presents the active filter times and change filter durations as a function of time. Table 7-4 presents the laboratory-generated descriptions of the filters removed from the CAM at the exit to Panel 7.
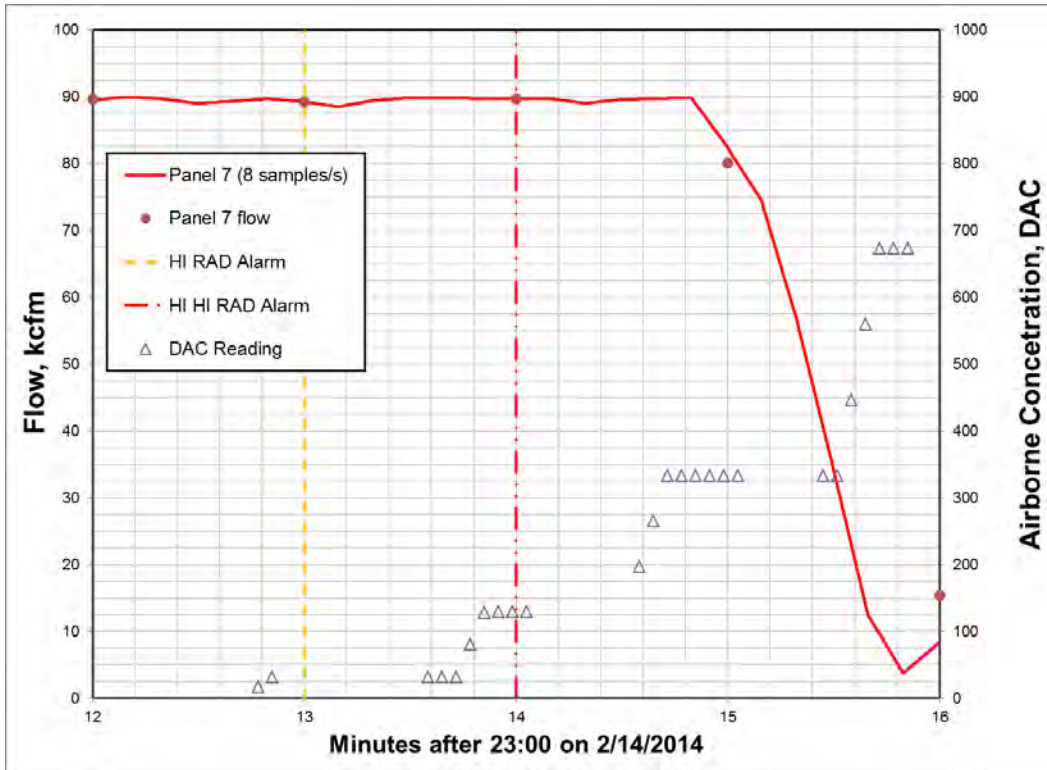
Figure 7-5: Panel 7 Flow & CAM Data (4 minute window)
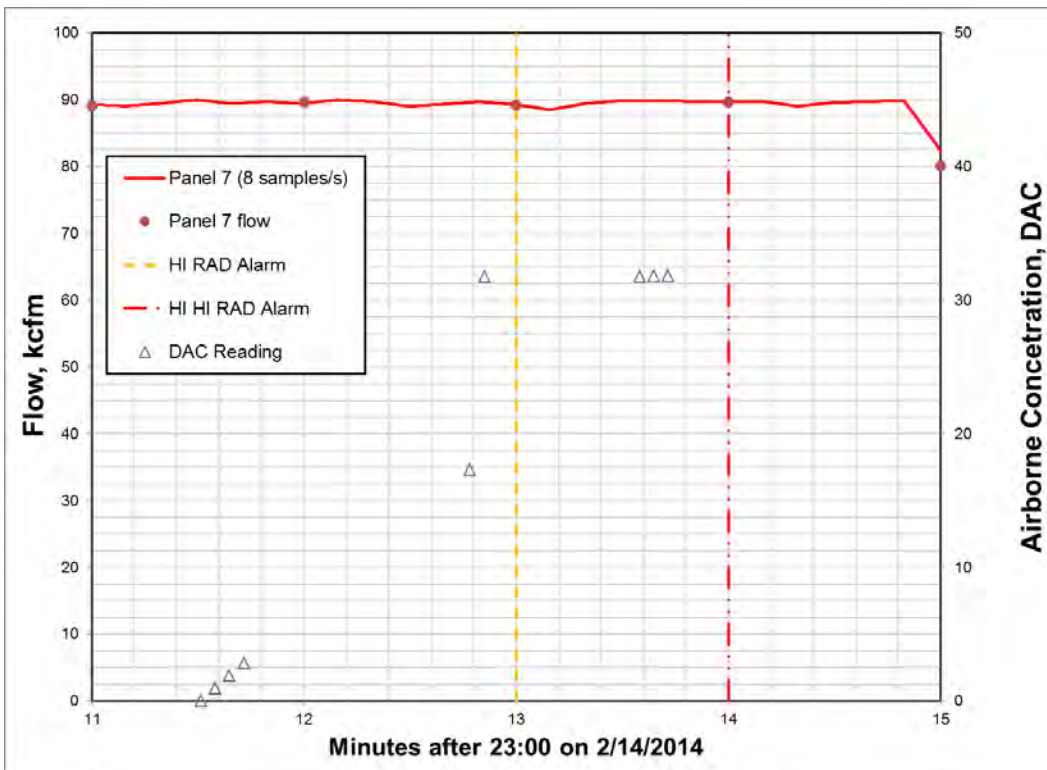
Figure 7-6: Panel 7 Flow & CAM Data (4 minute window during alarms)

Table 7-3: CAM filter Change-Out Timing

	Start Time	Stop Time	Active Time minutes	Change Duration minutes
Filter 1	2/12/2014 15:04:43	2/13/2014 15:11:48	1447	1.90
Filter 2	2/13/2014 15:13:42	2/14/2014 15:20:45	1447	1.55
Filter 3	2/14/2014 15:22:18	2/14/2014 23:15:54	473.6	1.77
Filter 4	2/14/2014 23:17:40	2/14/2014 23:18:49	1.15	1.87
Filter 5	2/14/2014 23:20:41	2/14/2014 23:24:26	3.75	2.20
Filter 6	2/14/2014 23:26:38	2/14/2014 23:30:44	4.10	1.87
Filter 7	2/14/2014 23:32:36	2/14/2014 23:35:42	3.10	1.87
Filter 8	2/14/2014 23:37:34	2/14/2014 23:40:39	3.08	1.88
Filter 9	2/14/2014 23:42:32	2/14/2014 23:43:40	1.13	1.87
Filter 10	2/14/2014 23:45:32	2/14/2014 23:50:38	5.10	1.87
Filter 11	2/14/2014 23:52:30	2/14/2014 23:56:35	4.08	1.87
Filter 12	2/14/2014 23:58:27	2/15/2014 00:02:33	4.10	1.87
Filter 13	2/15/2014 00:04:25	2/15/2014 00:05:34	1.15	...

The time required to travel from a to e as shown on Figure 7-1 is:

$$t_{a-f} = t_{a-b} + t_{b-c} + t_{c-d} + t_{d-e} \tag{16}$$

Where:

t_{a-b} is the time traveled between a and c at high velocity [minutes]
t_{b-c} is the time traveled between a and c at low velocity [minutes]
t_{c-d} is the time traveled between c and e at high velocity [minutes]
t_{d-e} is the time traveled between c and e at low velocity [minutes]

The travel times are:

$$t_{1-2} = \frac{d_{1-2}}{v_{1-2}} \tag{17}$$

Where:

t_{1-2} is the time to travel from 1 to 2 [minutes]
d_{1-2} is the distance between 1 and 2 [feet]
v_{1-2} is the average velocity when moving from 1 to 2 [fpm]
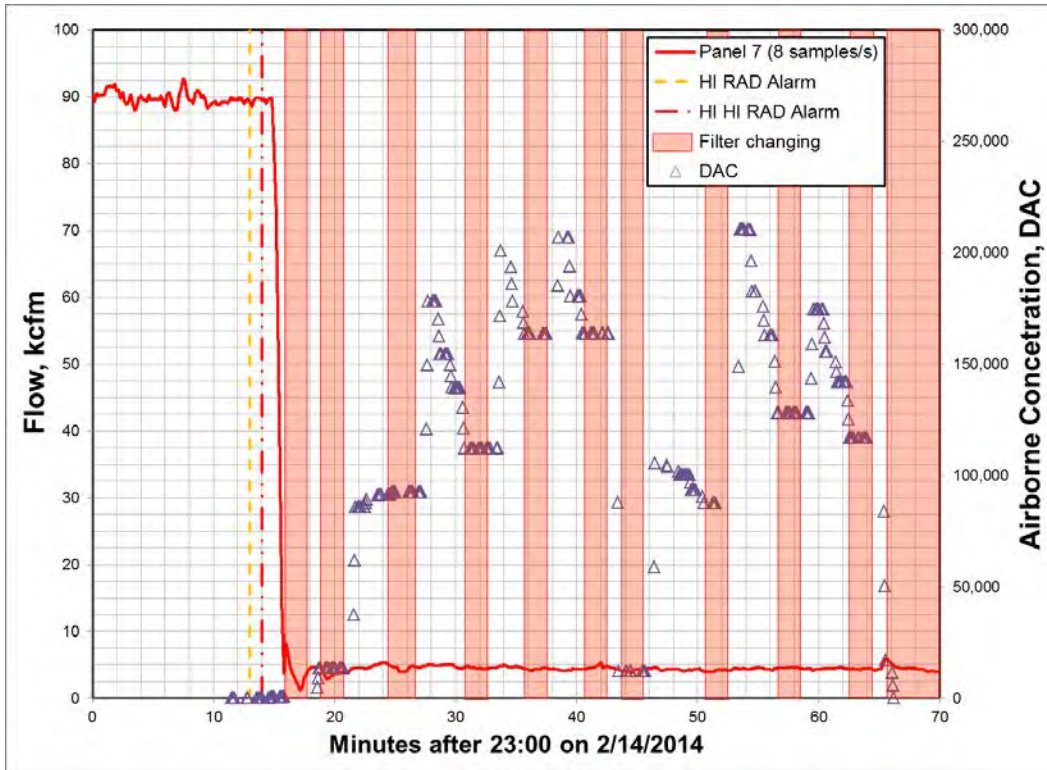
Figure 7-7: Panel 7 CAM Filter Function Timing
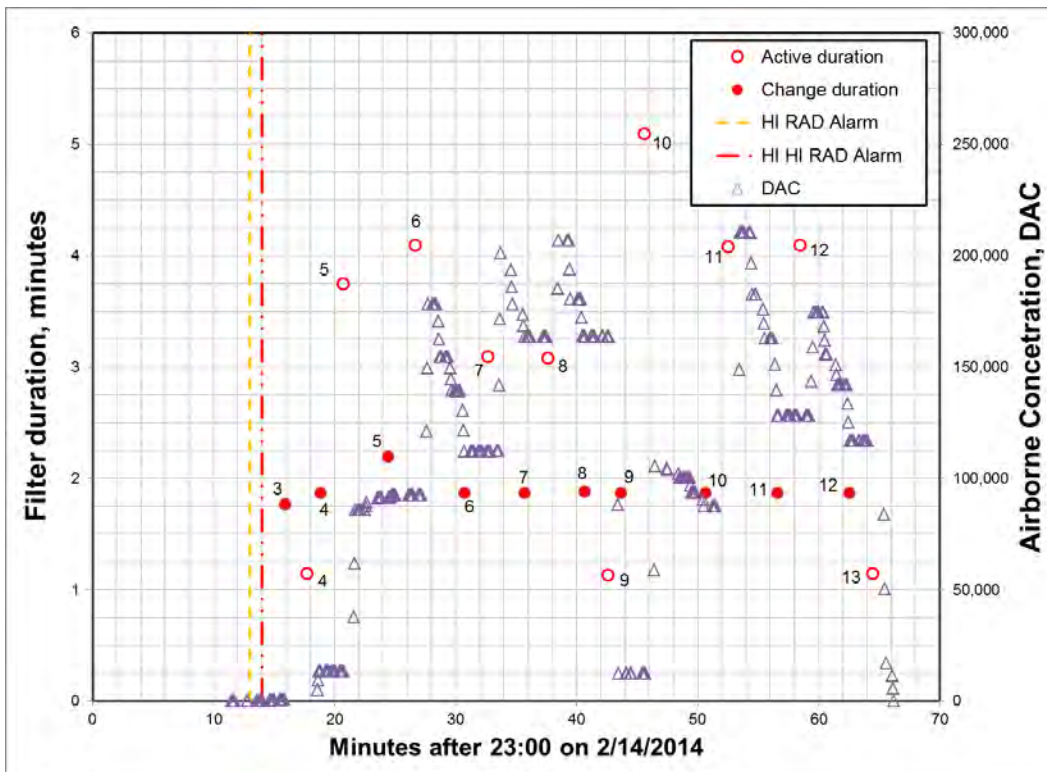
Figure 7-8: Panel 7 CAM Filter Active and Change Duration

Table 7-4: CAM Filter Descriptions

	Change duration, minutes
Filter 2	Very clear light brown color. No caking of material. Appears to have a very light material load
Filter 3	Charcoal brown in color. Similar to #5, #6, # 7, and #8. Uniform distribution of material.
Filter 4	More brown in color. Some charcoal color nonuniformly distributed with some area of filter lighter in color. There is one mark.
Filter 5	Charcoal brown in color. Similar in color to Filter #6, #7, and #8
Filter 6	Charcoal brown in color. Similar in color to Filter #7 and #8
Filter 7	Charcoal brown in color. Similar in color to Filter #8
Filter 8	Charcoal brown in color uniformly distributed.
Filter 9	Brownish-gray more uniform. May high a lighter color particulate collected with the dark material
Filter 10	Black uniform color except for areas that seem scored and expose the filter paper. There seems to be a thin layer of crust of black on the filter
Filter 11	Black in color. The filter was deformed and appears to have cracking of the back layer exposing some of the filter beleath (sic) the black layer. Deformation from the back of the filter is obvious. Filter is pushed out from back
Filter 12	Charcoal-black color. The back side of the filter was white with a small smear of black
Filter 13	Brown – back side of filter is white with black ring partially around the perimeter of the filter paper

Early in the event, prior to the transition to Filtered Ventilation Mode, the values of t_{b-c} and t_{d-e} would be zero. Late in the event, well after the transition, the values of t_{a-b} and t_{c-d} would be zero. The timing estimates for the event are presented in Table 7-5.

Sample calculation – Low level contamination concentration

Solution of equation (16) is iterative. The low level concentration arrives at the CAM about 19 minutes after 2300. Since the flow transient was complete at 2315, the low velocity flow duration was four minutes (19 minutes – 15 minutes). The travel distance d-e was thus:

$$d_{d-e} = t_{d-e}v_{d-e} = (4 \text{ min})(23.8 \text{ fpm}) = 95 \text{ ft}$$

Table 7-5: Transit time estimate

Event	Minutes after 2300 at location a	High velocity		Low velocity		Minutes after 23:00 at location c	High velocity		Low velocity		Minutes after 2300 at location e
		$d_{a\text{-}b}$ ft	$t_{a\text{-}b}$ minutes	$d_{b\text{-}c}$ ft	$t_{b\text{-}c}$ minutes		$d_{c\text{-}d}$ ft	$t_{c\text{-}d}$ minutes	$d_{d\text{-}e}$ ft	$t_{d\text{-}e}$ minutes	
	7.6	698	3.46	0	0.00	11.1	191	0.39	0	0.00	11.5
Hi alarm	9.1	698	3.46	0	0.00	12.6	191	0.39	0	0.00	13.0
Hi-HI alarm	10.1	698	3.46	0	0.00	13.6	191	0.39	0	0.00	14.0
	11.1	698	3.46	0	0.00	14.6	191	0.39	0	0.00	15.0
	11.2	698	3.46	0	0.00	14.7	165	0.34	25	1.05	16.1
Low level	11.3	698	3.46	0	0.00	14.8	95	0.19	95	4.00	19.0
Intermediate level	11.5	698	3.46	0	0.00	15.0	24	0.05	167	7.00	22.0
Hi level arrives	11.8	649	3.22	49	5.00	20.0	0	0.00	191	8.00	28.0
	12.0	609	3.02	89	9.11	24.1	0	0.00	191	8.00	32.1
	12.2	568	2.82	130	13.22	28.2	0	0.00	191	8.00	36.2
	12.4	528	2.62	170	17.34	32.3	0	0.00	191	8.00	40.3
	12.6	488	2.42	210	21.45	36.5	0	0.00	191	8.00	44.5
	12.8	447	2.22	251	25.57	40.6	0	0.00	191	8.00	48.6
Release end	13.6	277	1.37	421	43.00	58.0	0	0.00	191	8.00	66.0
	14.0	202	1.00	496	50.65	65.7	0	0.00	191	8.00	73.7
	14.5	101	0.50	597	60.94	75.9	0	0.00	191	8.00	83.9
	15.0	0	0.00	698	71.22	86.2	0	0.00	191	8.00	94.2

The travel time from c to d is thus:

$$t_{c-d} = \frac{t_{d-e}}{v_{d-e}} = \frac{(190.5 \text{ ft} - 95 \text{ ft})}{490 \text{ fpm}} = 0.19 \text{ min}$$

The time after 2300 when the low level concentration was at location c would have been:

$$T_c = 19.0 \text{ min} - 0.19 \text{ min} - 4.00 \text{ min} = 14.8 \text{ min}$$

The travel time for b to c is zero, because the low level concentration reached location c prior to the flow transient. Thus, the time after 2300 when the low level concentration was at location "a" was:

$$T_a = 14.8 \text{ min} - \frac{698 \text{ ft}}{201.6 \text{ fpm}} = 11.3 \text{ min}$$

The time when the high concentration contamination was leaving location "a" will never experience a high velocity flow is 2315. There is a three minute window between these two times, that then smears the arrival time at location "e" to about 66 minutes (94.2 minutes – 28.0 minutes).

The high flow velocity above the array was 339 fpm. The travel distance from the center of the array to the bulkhead was about 40 feet. This travel time was negligible (0.1 minutes = 40 ft/339 fpm). The release duration associated with the breached drum at R16:C4 would also have been short (< 1 minute). As such, there is no substantive delay between the release and the arrival at location "a" and little smearing of the flow stream prior to the arrival at location "a."

7.2.2. CAM Filter Observations

The first CAM filter change associated with the radiological release occurred at 2315:54, approximately three minutes after the initial alarm. This filter, filter 3, was automatically swapped during the flow transient to filtered ventilation mode. The swap time for the change from filter 2 to filter 3 was 1.55 minutes. Subsequent swaps required about 1.9 minutes (Figure 7-8).

The CAM concentration measurements correlated with filter swap timing (Figure 7-7). During the filters swaps, the concentration indications remained consent. This is expected based on the operation of the CAM unit. The duration between filter swaps varied from 1.13 minutes to 5.10 minutes. The shorter durations occurred for filters 3, 9 and 13. The longest duration occurred for filter 10.

Visual inspection of the filters indicates that filters 3, 5, 6, 7, and 8 were similar and had a charcoal brown color. This implies that the combustion products during this period were similar. The timing of flowstream associated with these filters, as established at location "a", was from 2307:36 to 2312, which brackets the large scale release arrival at Station A. Filter 6 corresponds with the arrival of the high contamination concentration at the CAM filter. Filter 4 was in place

just after the flow transient, and was more brown in color. A change in ventilation typically causes salt dust to become airborne. The difference in color for filter 4 is likely the result of this.

Visual characterization of filters 9, 10, 11, 12 and 13 varied in uniformity. These filters captured material that was at location a between 2312:30 and 2313:36. The distance traveled at low velocity varied from about 200 feet to about 400 feet.

7.2.3.   Summary

The material developed in this section establishes:

• Something occurred in the Room 7 waste array prior to 2308 that caused a release of radioactive contamination from a waste container. This release was extremely small in comparison to the overall magnitude of the contamination that arrived at the exit to Panel 7 about 17 minutes later.
• There was a substantive delay between the initial arrival of contamination at the Panel 7 exit and the large-scale release of radiological material. This delay was approximately four minutes.
• The majority of the material from the initial large scale release had arrived in the exhaust drift prior to the switching the ventilation system to Filtered Ventilation Mode, but had not arrived at the CAM at the Panel 7 exit.
• The actual duration of radiological release from Panel 7 cannot be established based on the CAM at the Panel 7 exit, because the CAM operation ceased at 0005 on February 15, about 52 minutes after the initial contamination alarm.

7.3.   Initial Release from Waste Drum 68660

During the evening of February 14, 2014, an ongoing exothermic reaction in a waste drum 68660 initiated a fire in Room 7 of the Panel 7 waste array. This section develops an explanation for how this reaction caused ignition of other materials in the waste array.

7.3.1.   Thermal Runaway

Table 7-6 presents the contents of waste drum 68660 as recorded in the WIPP Waste Data System. The data system did not account for the addition of a combustible liquid-absorbent material (Swheat Scoop®) to the waste matrix. Rather, the mixture of TRU waste, treatment materials, and liquid-absorbent material was assigned to the category of solidified inorganic material. This mixture, as discussed in subsection 7.1.3.1, can produce an exothermic reaction that can result in thermal runaway.

Table 7-6: Contents of Waste Drum 68660 per WIPP Waste Data System

Material Parameter	Description	Mass, kg
1	Iron base metal alloys	0.00
2	Aluminum base metal/alloys	0.00
3	Other metal/alloys	5.00
4	Other inorganic materials	0.00
6	Cellulosics	0.00
7	Rubber	5.00
8	Plastics	6.00
9	Solidified inorganic material	71.60
10	Solidified organic material	0.00
12	Soils	0.00
13	Steel container materials	27.70
14	Plastic/liners container materials	2.00
15	Cellulosics packaging materials	3.70
Total		116.00

Figure 7-9 presents a common sketch that is used to explain the temperature threshold[*], T_t, necessary to initiate sustained smoldering. [35] A self-heating material will establish a stable internal temperature as long as the ambient temperature is below the temperature threshold; point I in Figure 7-9. Key variables in establishing the threshold temperature include the material; volume, geometry, and the exothermic reaction kinetics. [12] Fluctuations in the ambient temperature will establish new internal temperatures that remain stable if the ambient temperature does not exceed the temperature threshold. If a self-heating material is placed in an ambient environment that is warmer than the threshold temperature, the condition will not be stable.

Figure 7-10 illustrates how the instability might have been approached for drum 68660. It is based on the U.S. Environmental Protection Agency Method 1050. [36] The loaded drum is placed in an environment where the ambient temperature exceeds the threshold temperature. The drum contents warm until the internal temperature equals the ambient temperature. The presence of the exothermic process causes the internal temperature to continue to rise until the threshold temperature is exceeded and thermal runaway occurs. Once established, the drum contents will

---

[*] The more standard term is critical temperature, however temperature threshold is used to avoid confusion with other critical threshold terminology associated with DOE Nuclear Facilities.

continue to combust unless the contents are cooled below condition E in Figure 7-9 or the fuel is exhausted.
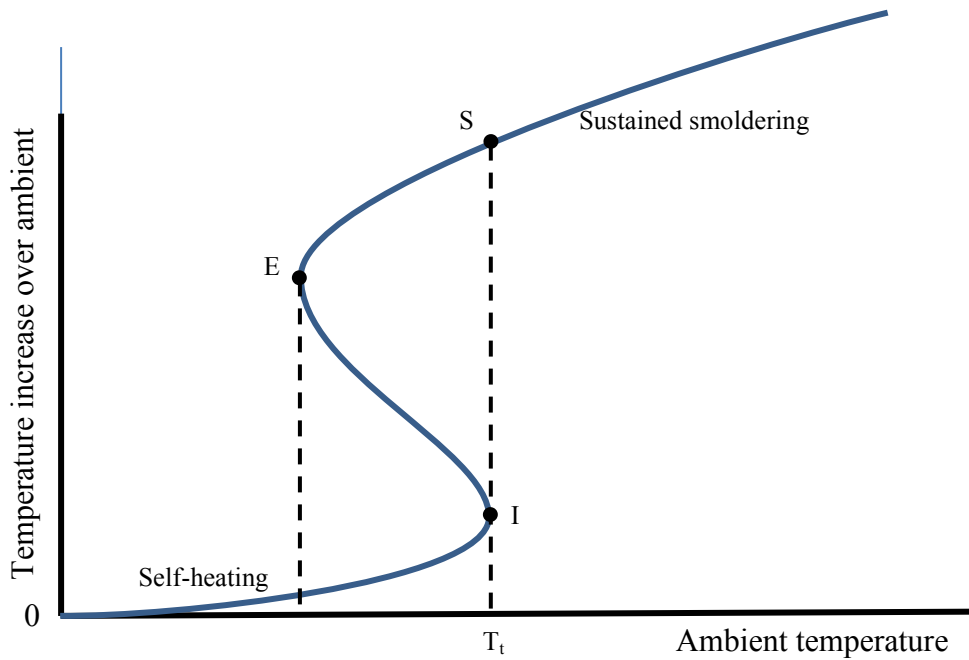
Figure 7-9: Spontaneous ignition threshold
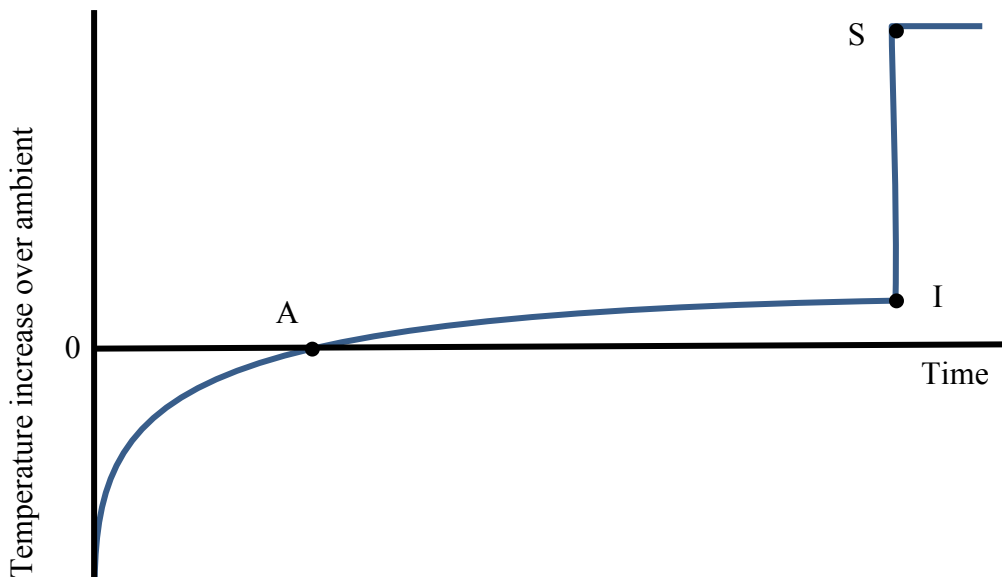
Figure 7-10: Thermal runaway threshold

Drum 68660 was a vented container; the vent opening it was equipped with a HEPA filter. This filter the vent was sized to prevent drum overpressurization resulting from radiolysis. It was not sized to vent gases generated smoldering combustion. In addition, the combustion products would have a tendency to plug the HEPA filter. The ongoing reaction caused the pressure within drum 68660 to increase. Both the conversion of solid materials to gas and a temperature increase of the drum contents would contribute to this pressure increase.

Between 2311 and 2314 the pressure within drum 68660 was sufficient to extrude the drum lid past the retention ring. This occurred because the rate of pressure rise in the drum exceeded the drum-vent capacity. The unrestrained portion of the drum lid deflected, permitting a rapid release of heated combustible gases, solid wastes, and solid organic materials (Swheat Scoop®) into the ventilation flow stream.

The lower value time estimate was derived from the arrival time for contamination concentrations exceeding 50,000 DAC (about 2321 in Figure 7-3). This contamination would have been released from the array at about 2311. (See Table 7-5.) The upper value time estimate was taken directly from Table 7-5.

7.3.2.   Material Ejection, Combustion and Dispersion

When the lid of drum 68660 deflected, the gaseous drum contents were rapidly released. Such a release tends to also cause the ejection of solid contents from the drum. This ejected material was released into a local flow velocity was more than 300 fpm (Figure 5-11). Since a portion of the drum contents were heated and ignited, conditions were conducive to further combustion of the ejected gases and solids.

The liquid-absorbent material was a significant portion of the ejected waste matrix. A 14 lbs bag of Swheat Scoop®, which was the liquid-absorbent material, was obtained in 2014 and inspected. The sample was a hard irregularly-shaped granular material. The largest pieces were typically about 5 mm in diameter, but not thicker than 2 mm. Many pieces were smaller than a 1 mm diameter sphere, and there was a perceptible quantity of fine dust. When wetted, Swheat Scoop® retained its original shape, but becomes pliable or pasty. The inspection established that Swheat Scoop® has significantly more specific surface area than typical contaminated waste (e.g., gloves, plastic sheet, paper).

Swheat Scoop®, with its high surface to mass ratio would burn quickly when ejected from the drum. In addition, it is a solid and will have a high energy density as compared with compressed gas releases. A few kilograms of this material can create a large-scale energy release (10 kg x 18.6 MJ/kg = 190 MJ) that would be released over a few seconds.

The flame front created a mixture of pyrolysis gases and high-specific surface area organic material created by the ejection of material from drum 68660 is unique. It does not fit into the classical fire behavior terms used in NFPA 921:

- It was not a dust explosion since dust explosions typically involve particulates with a diameter less than 500 microns (0.02 inches). [12 p. 228] As described in section 7.3.2 the particles the liquid-absorbent material particles were closer to 5 mm (0.2 inches).

- It was not a classical combustible gas ignition since much of the combustion energy was from the combusting solid
- It was not a flash fire since the flame front was not moving through a diffuse fuel. [12 p. 16] The high specific surface area of the waste matrix facilitated rapid combustion

A Fire Dynamic Simulator (FDS) model was prepared to evaluate the combustion behavior during the February 14, 2014 event. FDS is a computational fluid dynamics model that has been developed and maintained over the past 25 years by the National Institute of Standards and Technology (NIST) Building and Fire Research Lab. Parametric calculations [37] from this effort established that 10 kg to 16 kg of cellulosic-like material released over 2 seconds from R16:C4 can create an expanding flame front lasting about 3 seconds with the potential to cause ignition at R18:C2 and R18:C6. (See Figure 7-11.) Ignition could have been by direct flame impingement or ember transfer. The model also predicted that ignition of exposed combustibles in rows 7 through 17 might occur. For the larger release, there was also a potential for ignition in rows 4 and 5. (There is no row 6.) The effort also demonstrated that ignition in row 2, row 3, and rows 19 through 24 would not be expected.

Actual local ignition would be random since:

- The predicted flame exposure duration was near the threshold required for polypropylene fabric ignition (subsection 4.1.3) and was insufficient to ignite the thicker polyethylene sheets (section 4.1.4) and fiberboard (subsection 4.1.5).
- Ember ignition requires the embers to land on the exposed combustibles and be of sufficient size to cause ignition of the exposed combustibles.
- There were few exposed combustibles in rows 5 and 7.

These predictions are consistent with the damage pattern described in Chapter 4.0. In addition, drum 68660 contained 71.6 kg of material that was categorized as solidified inorganic material (Table 7-6). As discussed in subsection 7.3.1, this material could ignite. As such there was sufficient material present to create the predicted flame front.

The SWB at R15:C5 was adjacent to drum 68660. Ejected material from this drum would travel across, or strike this SWB. The clumped debris on the SWB lid at R15:C5, as described in subsection 4.16.3, were unique as compared with the debris at other stacks within the waste array, but consistent with the contents 68660. The depth of material was greatest at the northwest corner, the location nearest drum 68660. The material on this lid was layered. The bottom layer was dark, and covered with a lighter colored layer (AIB-FST-02065). (Note: AIB-FST-10172 shows additional disruption as compared to AIB-FST-02065 between May 2014 and January 2015.) This would be consistent with the expulsion of the drum contents followed by MgO dust from the damaged MgO super sacks. An additional layer, the two cardboard stiffeners present at the north end of the lid, were also above the dark clumped debris (AIB-FST-10584 and AIB-FST-10954). Above the stiffeners were piles of MgO. These observations reinforce the credibility of the scenario that the MgO super sack fabric was damaged after the initial release.
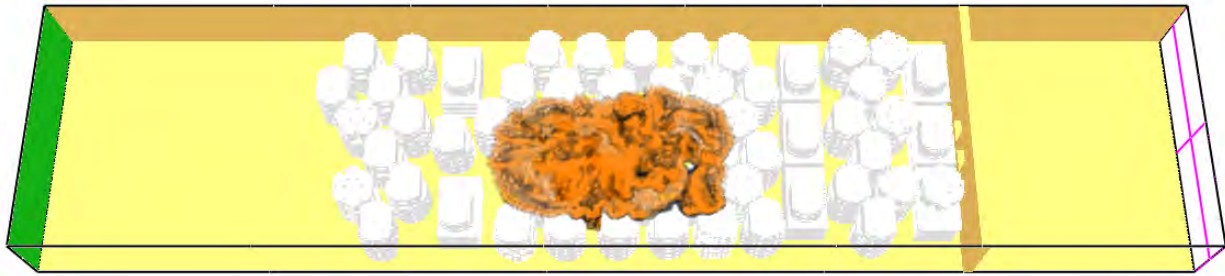
(a) 1 Second after the Start of the Release
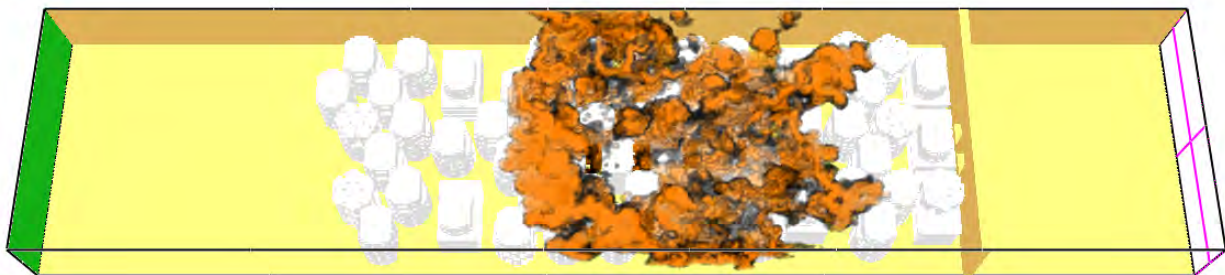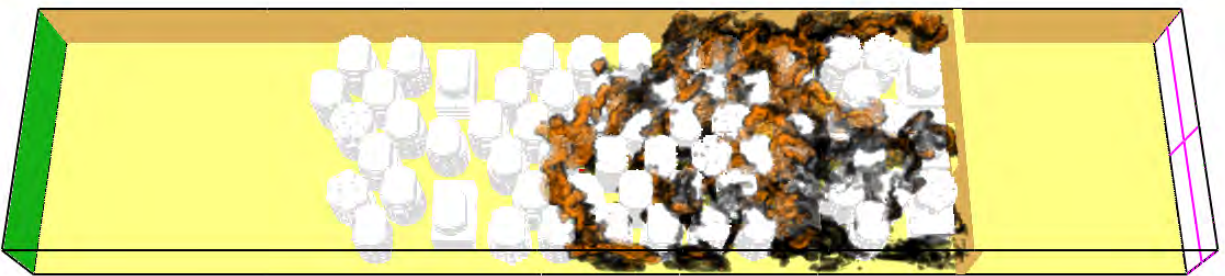
(b) 2 Seconds after the Start of the Release

(c) 3 Seconds after the Start of the Release

**Figure 7-11: HRR Isosurfaces for the 8 kg/s Fuel Release Showing the
Maximum Extent of Flame Volume**

7.3.2.1. Flame Impingement

As discussed in subsection 4.1.3 and 4.1.4 both polypropylene and polyethylene are easy-to-ignite plastics. The lower-bound peak heat flux for objects immersed in a flame is 80 kW/m^2.[38] At this exposure the polypropylene MgO super sack fabric would ignite in much less than 15 seconds (4.1.3); polyethylene slip sheets and reinforcement plates would require longer, 22 seconds (4.1.5). The FDS model demonstrated that ignition of the MgO super sacks adjacent to R16:C4 is likely (Figure 7-11). Ignition by flame impingement of super sacks on the edges of the array are less likely. Ignition of the horizontal polyethylene by flame impingement generated by the material release from 68660 is not expected since the flame duration is very short (< XX seconds).

7.3.2.2. Ember Ignition

Some of the material that was expelled from 68660 would be expected to burn after landing on horizontal materials in the array. Because the MgO super sacks would not have spilled their contents in advance of the flaming release from 68660, there would be no buildup of MgO on these surfaces. If the horizontal surface is combustible (polypropylene, polyethylene, or fiberboard) and the eject material continues to burn on contact, ignition of horizontal material is likely. Such conditions did occur in the array and are referred to as ember ignitions. The best example of this was the array face side of R18:C6 where a fiberboard SWB slip sheet burned. Ember ignition of materials "downwind" of R16:C4 is more likely.

7.3.3. Summary

The fire in the Panel 7 Room 7 waste array started in waste drum 68660. The basis for this conclusion is:

- Section 7.1 establishes that the fire in the Panel 7 Room 7 waste array originated in the waste array and concludes that an exothermic reaction is the expected ignition source.
- The visual inspection described in Chapter 4.0 demonstrates that waste drum 68660 was the only breached drum in the array.
- Section 7.2 establishes that the radiological release was initiated early in the event sequence. It also establishes that an expulsion of the radiological material from 68660 followed by the reduction in airflow associated with the Filtered Ventilation Mode would create the release profile measured at the exit to Panel 7 by CAM 151.
- This section, 7.3, explains how the initial reaction in waste drum 68660 caused ignition of neighboring exposed combustible materials.

7.4. Fire Spread

While this initial flame front created by the ejection of material from drum 68660 directly caused some of the observed damage described in Chapter 4.0, it would not account for all of the array damage. Secondary fire propagation within the array was necessary to create all of the observed damage. Multiple fire propagation mechanisms likely occurred during the event. This section describes the most likely mechanisms.

7.4.1.   Downward Propagation

Propagation by flaming droplets is a commonly observed phenomena associated with burning plastic. A heated thermoplastic, such as polyethylene, will tend to melt and flow when heated. When flaming, the material can drip and carry flames downward as burning tar-like drops. [33] When these flaming drops land on an exposed combustible material, ignition of the exposed combustible can occur.

Darchem Flare conducted fire testing on HDPE slip sheets similar to those at WIPP for the Rocky Flats Site in 2001. [39] Three tests were conducted that involved 24inch by 48 inch horizontal HDPE sheets supported on a steel frame 19 inches above a concrete surface. The ⅛ inch thick sheets were ignited by a "propane gas burner" that impinged on a short edge of the sheet. The torch was adjusted to provide "a strong blue flame." While not further described, a photo in the test report suggests that the flame length was nominally a few inches long.

For all three tests, the HDPE was ignited and moved away from the ignition point. Initial burn rates ranged from 1.1 inches/minute to 3.2 inches/minute. This variability is partially the result of test technique. Data for test 2 was initially recorded at 20 minutes, while data for test 3 was recorded at 5 minutes. The highest initial rate was for test 3. At the end of the tests, when the flame front was well away from the ignition point, the burn rate ranged from 0.4 inches/minute to 0.8 inches/minute. The time for complete sheet involvement ranged from 60 minutes to 101 minutes; however, flame extinction occurred at 90 minutes to 120 minutes. During the testing, flaming drops of material dripped to the concrete floor, pooled and continued to burn for a few seconds.

Within the Panel 7 Room 7 array, the dripping material would not be striking a cool concrete surface, but possibly a fiberboard or polyethylene surface. Such surfaces would not have the same heat absorption capability as concrete. [12 p. 26] As such, longer burn times would be expected, with the potential for ignition of the fiberboard or polyethylene surface.

7.4.2.   Ember Transport Propagation

Propagation can occur by transport of hot or burning materials landing on combustible materials and causing secondary ignition. Both convective propagation associated with burning embers transported by air currents, and the fall of burning objects onto other exposed combustibles are discussed in this subsection.

The potential for burning embers or hot materials ejected from drum 68660 is discussed in subsection 7.3.2.2. In addition, embers can be produced by combusting, polypropylene super sack fabric, cardboard stiffeners, fiberboard slip sheets, plastic slip sheets and reinforcement plates, and stretch wrap. As these items are consumed, portions may separate from the main body and be lofted into a fire plume. These lofted materials can travel with the airflow. The transport distance will vary and depend on the lofted material geometry, mass and airstream velocity. This mechanism permits fire propagation without sequential involvement of neighboring stacks in the array as occurred at R18:C6, which is the damage location furthest upstream of R16:C4. In this location an ember landed on the upstream side of the stack and

caused ignition of the SWB fiberboard slip sheet. The mechanism is also consistent with the damage observed in rows 9 and 10, without significant damage in row 11 and 12.

A variation on ember transport mechanism occurs for objects too heavy to be lofted by the fire plume. An example would be an ignited cardboard stiffener that falls one location (e.g., vertical in original orientation, or from a horizontal position bridging between two stack) to land on or adjacent to exposed combustibles. Such propagation could have occurred from R8:C4 to R7:C5.

Locations were identified where the super sack fabric fell from its original location and draped along the side of a top-tier SWB. This occurred on the north side of R15:C5 (AIB-FST-10581 and AIB-FST-10583) and the south side of R13:C5 (AIB-FST-10121). These instances demonstrate the potential for the super sack fabric to contribute to fire propagation.

The Room 7 ventilation established a flow that traveled from row 24 to the bulkhead. This basic flow patterned ensured that convective propagation did not occur. In addition, the exposed combustible material in row 20 limited the likelihood of fire propagation by falling cardboard stiffeners and super sack fabric.

With one minor exception, convective probation to rows 2 through 7 was prevented by the limited amount of exposed combustibles in rows 5 and 7. (There was no row 6.) In addition, the local air velocity began to increase and channel over rows 2, 3 and 4 as the bulkhead opening was approached. In addition to the potential for burnout, the increasing local velocity reduced the likelihood for ignition by embers in these rows.

7.4.3.   Upward Vertical Propagation

Vertical propagation within an individual stack was evaluated using an FDS model. [37] The analysis demonstrated that vertical propagation in stacks of 55GD and 100GD assemblies can readily occur. As such, ignition of a bottom or middle-tier slip sheet on one of these assemblies can cause ignition of the top-tier and the MgO super sack. The FDS model, which is based on nominal material parameters, demonstrated that it required about 5 minutes from initial ignition of the middle-tier slip sheet to ignition of the top-tier reinforcement plate. [37] The key propagation mechanism for upward vertical propagation was flame impingement.

7.4.4.   Incremental Horizontal Propagation

Horizontal propagation between stacks was evaluated using an FDS model. [37] The analysis demonstrated that horizontal fire propagation between stacks should be expected when 55GD or 100GD assemblies are separated horizontally by less than 10 cm (4 inches), and may occur for separations of 30 cm (12 inches) if the flow velocity is 0.5 meters/second (100 fpm). Where separation exists the primary propagation mechanism was target ignition by heat flux exposure. Where there is no separation, or little separation, flame impingement propagation is likely.

Horizontal fire propagation in stacked waste storage was demonstrated during the DOE-sponsored waste drum fire test conducted in the 1990s. The pallet storage test conducted by Southwest Research Institute was such a test and offers a perspective on fire propagation within waste drum arrays. [40]   Three rows of steel drums, two on wooden pallets and one on steel

pallets, were exposed to a diesel pool fire. Each pallet assembly had a single steel band. There were four drums on each pallet, the drums were retained with a single horizontal steel band, and each row consisted of 12 pallets, 3 pallets high and 4 pallets deep. The pool fire footprint was limited to half the middle row and the aisles between the two outer rows (Illustration 24). The test drums were each loaded with 25.9 kg of simulated waste consisting of rubber, plastic, paper and cotton.

The initial exposure was an intense five minute fire involving a combustible liquid. Drums exposed to the intense flaming experienced lid loss, lid rupture ("lid partially removed from the metal closure ring") or lid seal failure. Some drums adjacent to the flames, both on steel and wooden pallets, experienced the same failures. Propagation between the wooden pallets continued for about 1 hour following extinguishment of the pool fire. This propagation continued to cause lid seal failures of the drums on the wooden pallets. Flame jets were produced by these venting drums that ignited adjacent wooden pallets. The process continued until all of the wooden pallets were involved.

The FDS model, coupled with a separate drum response model, was used to judge the potential for lid seal failure in the 55GD and 100GD assemblies. [37] The efforts demonstrated that the external combustible emplacement materials can produce pyrolysis gases in the drums. These gases would have the potential to exit the filter vents and ignite. Pressures generated by credible fire exposures can generate pressures associated with seal failures observed in the DOE fire tests (~ 15 psig). This portion of the analysis was not developed further since the results are highly assumption driven and the goal of the effort was to evaluate the potential for horizontal fire propagation.

The array geometry in rows 9 and 10 consist of multiple 55GD and 100GD assemblies in close proximity. In some instances the separation is less than 4 inches. As such, if each stack was not initially ignited by embers released from drum 68660 or from secondary fires, horizontal propagation was likely.

7.4.5.   Summary

The intensity of the overall fire was low to moderate and direct fire effects were primarily in Rows 8 through 18 of the array. Damage within the array was not uniform and there were multiple small fires that caused direct flame impingement on several waste packages. In some locations, the fire damage was significant.

There was no evidence of heat or fire damage to waste containers in rows 20 through 24. Fire evidence at R19:C3 was limited to char on a MgO stiffener that had fallen from R18:C2. The ventilation flow coupled with the limited exposed combustibles in rows 19 and 20 established a fire break that prevented propagation to this region.

With the exception of minor damage at R7:C5, there was no evidence of heat or fire damage to waste containers in rows 2 through 7. (There was no row 1 or 6.) The limited exposed combustibles in rows 5 and 7 established a fire break that prevented propagation to this region.

The fire damage in rows 8 through 18 was most severe in the areas with the greatest exposed combustible loading. This was at locations with 55GD and 100GD assemblies. Fire propagation within the array occurred by multiple mechanisms. These mechanisms included:

- Downward propagation from flaming droplets of burning plastic;
- Upward propagation by flame impingement on exposed combustibles within the same stack;
- Convective propagation associated with burning embers transported by air currents and landing on exposed combustibles;
- Incremental propagation by radiation heat transfer between a flame and a combustible in a nearby stack; and
- Incremental fire propagation between waste stacks by flame impingement.

8.0　CONCLUSIONS

During the evening of February 14, 2014, an ongoing exothermic reaction in waste drum 68660 created a release of radiological material and initiated a fire in the Panel 7 Room 7 disposal array. The intensity of the fire was low to moderate and direct fire effects were primarily in rows 8 through 18 of the array. Damage within the array was not uniform and there were multiple small fires that caused direct flame impingement on several waste packages. In some locations the fire intensity was significant. The fire self-extinguished without consuming all combustibles present.

Direct physical access to the array was limited because of safety considerations. A systematic and comprehensive visual inspection of the array was completed using video cameras suspended over and in the array. This report summarizes the results of this effort.

The significant fire damage in the waste array was centered on locations with the most exposed combustible materials. These areas included Rows 9 and 10; Rows 14 and 15, R16:C4 and R18:C6. (See Figure 4-1.) The extent of damage ranged from complete loss of exposed material (fiberboard and polyethylene slip sheets, reinforcement plates, stretch wrap, cardboard stiffeners and polypropylene super sack fabric) on multiple tiers such as at R14:C2, to a loss on just one face such as at R18:C6, where much of the polyethylene stretch wrap for the assemblies was undamaged. On top of the waste containers, there were 17 damaged MgO super sacks leaving loose MgO in a high angle of repose; however, there were no substantive soot deposits on the drift back, the ribs, or visible portions of the bulkhead.

Flashover in Panel 7 Room 7 did not occur. Rather there were wide variations in local temperatures that were dependent on local flaming behaviors. As such, local temperatures ranged from ambient to flame temperature (~1,000°C). Temperatures near the Panel 7 Room 7 bulkhead did not exceed 135°C based on the undamaged polyethylene stretch wrap and MgO super sack polypropylene fabric.

8.1.　Most Likely Fire Sequence

The most likely fire sequence is:

- Self-heating created an internal temperature within drum 68660 sufficient to cause thermal runaway, which is characterized as an exponential temperature rise within the container core. This rapid reaction created a variety of gaseous reaction products and some of these products were combustible.
- The combined thermal expansion rate and production rate of reaction products exceeded the waste container venting rate.
- At approximately 2300 on February 14, 2014 the lid of drum 68660 breached and a part of the drum contents was ejected. This ejected material combusted, created burning embers, disrupted the ventilation flow stream, and caused ignition of some MgO super sacks.
- The burning embers caused secondary ignitions within the waste array. The fire propagated through multiple mechanisms to involve many stacks in rows 8 through 18. In the process all 18 of the MgO super sacks in these rows were damaged and 17 released their contents.

- Radioactive contamination and combustion products exited Room 7 and traveled to CAM 151 at the Panel 7 exit. CAM 151 initiated two separate alarms; the second initiated a change to filtered ventilation mode. These alarms (at 2313 and 2314 on February 14, 2014) were the first indication of the release event.
- The fire in Room 7 continued to burn until the combustible material geometry was no longer favorable for continued combustion.
- Recognition that the event was associated with a fire occurred in April 2014, when a visual inspection of the array was conducted.

8.2.   Ventilation

Electronic data for underground ventilation system was obtained from the WIPP Ventilation Data Records. This information included volumetric flows, pressure differentials, temperature, and humidity at instrumented locations. A comprehensive review of the records for February 14 and 15 was conducted for data published in one-sample/minute increments. In addition, selective reviews were conducted using data published in eight-samples/minutes increments just prior to and just after, the detection of airborne contamination (Section 5). This effort established that:

- Ventilation transient behavior was limited to the automatic shift to the filtration flow rate. (Note: Direction of flow to HEPA filters requires a manual action, but the flow rate change is automatic.) There was no measured transient established by fire or explosion behaviors.
- The flow rate through Room 7 prior to the release event was 42 kcfm.
- The flow rate through Room 7 after the transition to Filtered Ventilation Mode was 4 kcfm.
- The flow rate through Panel 7 prior to the release event was 90 kcfm.
- The flow rate through Panel 7 after the transition to Filtered Ventilation Mode was 4.4 kcfm.

8.3.   Salt Haul Truck Fire

The possible effects of haul truck fire, which occurred on February 5, 2014, on the waste array were evaluated. This included development of a fire model that established temperatures estimates at Panel 7 during the haul truck fire, evaluation of the combustion products that might have reach the waste array, and the reaction of MgO to these combustion products. (Section 6.) This effort established that:

- The majority of the combustion products and energy produced by the salt haul truck fire traveled up the SHS. This occurred because of the thermal gradient established by the salt haul truck fire;
- Air temperatures near the base of the SHS did not exceed 100°C. (Calculated value for 15MW fire is 81.8°C);
- Air temperature increase in Room 7 during the February 5 event was negligible (i.e., within the uncertainties of the calculations);
- The localized reaction between MgO and the primary combustion products (H_2O and CO_2) is very slow, with no discernable temperature increase and would not have caused damage to the MgO super sacks;

- The February 5 salt haul truck fire did not directly cause the widespread MgO super sack damage; and
- The February 5 salt haul truck fire did not cause a localized MgO reaction that subsequently resulted in the February 14 release event.

9.0   REFERENCES

1. *Phase 1 Radiological Release Event at the Waste Isolation Pilot Plant on February 14, 2014.* DOE Accident Investigation Board. Washington, DC : U.S. Department of Energy, April 2014.

2. *Waste Isolation Pilot Plant Technical Assessement Team Report.* Aiken, SC : Savannah River National Laboratory, 2015. SRNL-RP-2014-01198, Rev. 0.

3. Zimmerly, Ben (Ty). E-mail to Kirk Kirkes. *Information Request.* Carlsbad, NM : Nuclear Waste Partnership, LLC, June 18, 2014.

4. *Waste Isolation Pilot Plant Documented Safety Analysis.* Carlsbad, NM : Nuclear Waste Partnership LLC, 2013. DOE/WIPP 07-3372, Rev. 4.

5. *7-Pack Slip Sheet Plate Design.* Carlsbad, NM : Washington TRU Solutions. 412-F-013-W1, Rev. K.

6. *7-Pack Reinforcement Plate Design.* Carlsbad, NM : Washington TRU Solutions. 412-F-013-W2, Rev. K.

7. *Supersack Slip Sheet Design.* Carlsbad, NM : Washington TRU Solutions. 412-F-013-W3, Rev. K.

8. *SWB and TDOP Slip Sheet.* Carlsbad, NM : Washington TRU Solutions. 412-F-025-W, Rev. A.

9. *Supersack Assembly and Details.* Carlsbad, NM : Nuclear Waste Partnership LLC, 2010. 2019-S.

10. *Supersack Assembly and Details.* Carlsbad, NM : Nuclear Waste Partnership LLC, 2013. 2020-S, Rev. A.

11. *Compliance Recertification Application 2014 for the Waste Isolation Pilot Plant.* Carlsbad, NM : U.S. Department of Energy, 2014. Title 40 CFR Part 191 Subparts B and C.

12. *Guide for Fire & Explosion Investigations.* Quincy, MA : National Fire Protection Association, 2014. NFPA 921.

13. Babrauskas, Vytenis. *Ignition Handbook.* Issaquah, WA : Fire Science Publishers, 2003.

14. Bukowski, Richard W., et al. *FRAMEworks® Fire Risk Assessment Method: Description of Methodology.* Quincy, MA : National Fire Protection Research Foundation, 1990. NISTIR 90-4242.

15. *Piloted Ignition of Solid Material Under Radiant Exposure.* Bethesda, MD : Society of Fire Protection Engineers, 2002.

16. *SWB & TDOP Slip Sheet.* Carlsbad, NM : Waste Isolation Pilot Plant, 1997. 412-F-025-W, Rev. A.

17. Wraight, H. *The Ignition of Corrugated Fibreboard ('Cardboard') by Thermal Radiation.* Hertfordshire, UK : Fire Research Station, 1974. FRN 1002.

18. *2013 Testing and Balancing of the Underground Ventilation System at the WIPP Facility.* Clovis, CA : Mine Ventilation Services, Inc., 2013. DN-3590-03.

19. *Underground Ventilation System Design Description (SDD).* Carlsbad, NM : Nuclear Waste Partnership, LLC, 2014. SDD:VU00, Rev. 20.

20. *Recommended Practice for the Classification of Flammable Liquids, Gases, or Vapors and the Hazardous (Classified) Locations for Electrical Installations in Chemical Process Areas.* Quincy, MA : National Fire Protection Association, 2012. NFPA 497.

21. *Underground Salt Haul Truck Fire at the Waste Isolation Pilot Plant, February 5, 2014.* DOE Accident Investigation Board. Washington, DC : U.S. Department of Energy, March 2014.

22. *Standard for Road Tunnels, Bridges, and Other Limited Access Highways.* Quincy, MA : National Fire Protection Association, 2014. NFPA 502.

23. Babrauskas, Vytenis. *Heat Release Rates.* National Fire Protection Assiciation. Quincy, MA : The SFPE Handbook of Fire Protection Engineering, 4th Ed., 2008.

24. Figliola, Richard S., Beasley, Donald E. *Theory and Design for Mechanical Measurements.* New York, NY : John Wiley & Sons, 2011.

25. *ASHRAE Handbook - Fundamentals.* Atlanta, GA : ASHRAE, 2013.

26. Pritchard, Philip J. *Fox and McDonald's Introduction to Fluid Mechanics, 8th.* New York, NY : John Wiley & Sons, Inc., 2011.

27. Tewarson, Archibald. Generation of Heat and Gaseous, Liquid, and Solid Products in Fires. *The SFPE Handbook of Fire Protection Engineering, 4th Ed.* Quincy, MA : National Fire Protection Association, 2008.

28. Xiong, Yongliang and Lord, Anna S. Experimental Investigations of the Reaction Path in the $MgO-CO_2-H_2O$ System in Solutions with Various Ionic Strengths and their Applications to Nuclear Waste Isolation. *Applied Geochemistry.* 23, 2008.

29. http://www.wolframalpha.com/. *WolframAlpha Computational Knowledge Engine.* [Online] August 9, 2014. www.wolframalpha.com.

30. Babrauskas, Vytenis. Tables and Charts. *Fire Protection Handbook, 20th Ed.* Quincy, MA : National Fire Protection Association, 2008.

31. *WCRRF Waste Characterization Glovebox Operations.* Los Alamos, NM : Los Alamos
    National Laboratory, 2012. EP-WCRR-WO-DOP-0233, Rev. 36.

32. *WCRRF Waste Characterization Glovebox Operations.* Los Alamos, NM : Los Alamos
    National Laboratory, 2013. EP-WCRR-WO-DOP-0233, Rev. 37.

33. Davenport, J A. Storage and Handling of Chemicals. *Fire Protection Handbook, 20th Ed.*
    Quincy, MA : National Fire Protection Association, 2008.

34. *Standard System for the Identification of the Hazards of Materials for Emergency Response.*
    Quincy, MA : National Fire Protection Association, 2012. NFPA 704.

35. Quintiere, James Q., et al. *Spontaneous Ignition in fire Investigation.* Washington, DC : US
    Department of Justice, 2012. 239046.

36. *Test Methods to Determine Substances Likely to Spontaneousely Combust.* Washington, DC :
    Environmental Protection Agency, 2007. Method 1050, Rev. 0, SW-846.

37. *Waste Isolation Pilot Plant (Fire Dynamics Simulator Model).* Chicago, IL : Fire & Risk
    Alliance, 2015.

38. *Engineering Guide: Fire Exposures to Structural Elements.* Bethesda, MD : Society of Fire
    Protection Engineers, 2004.

39. *High Density Polyethylene Slip-Sheet Fire Tests.* Stillington, England : Darchem Flare, 2001.
    DFR/01/0019.

40. Haecker, Chris F., et al. *Solid Waste Drum Array Fire Performance.* Richland, WA :
    Westinghouse Hanford Company, 1995. WHC-SD-WM-TRP-246, Rev. 0.

APPENDIX A. ILLUSTRATIONS

TABLE OF ILLUSTRATIONS

This appendix presents visual material that is cited from multiple chapters in this report.

Illustration 1: Simplified Flow Diagram with Ventilation Measurement Locations

Note: Not to scale

Illustration 2: Panel 7 Plan View
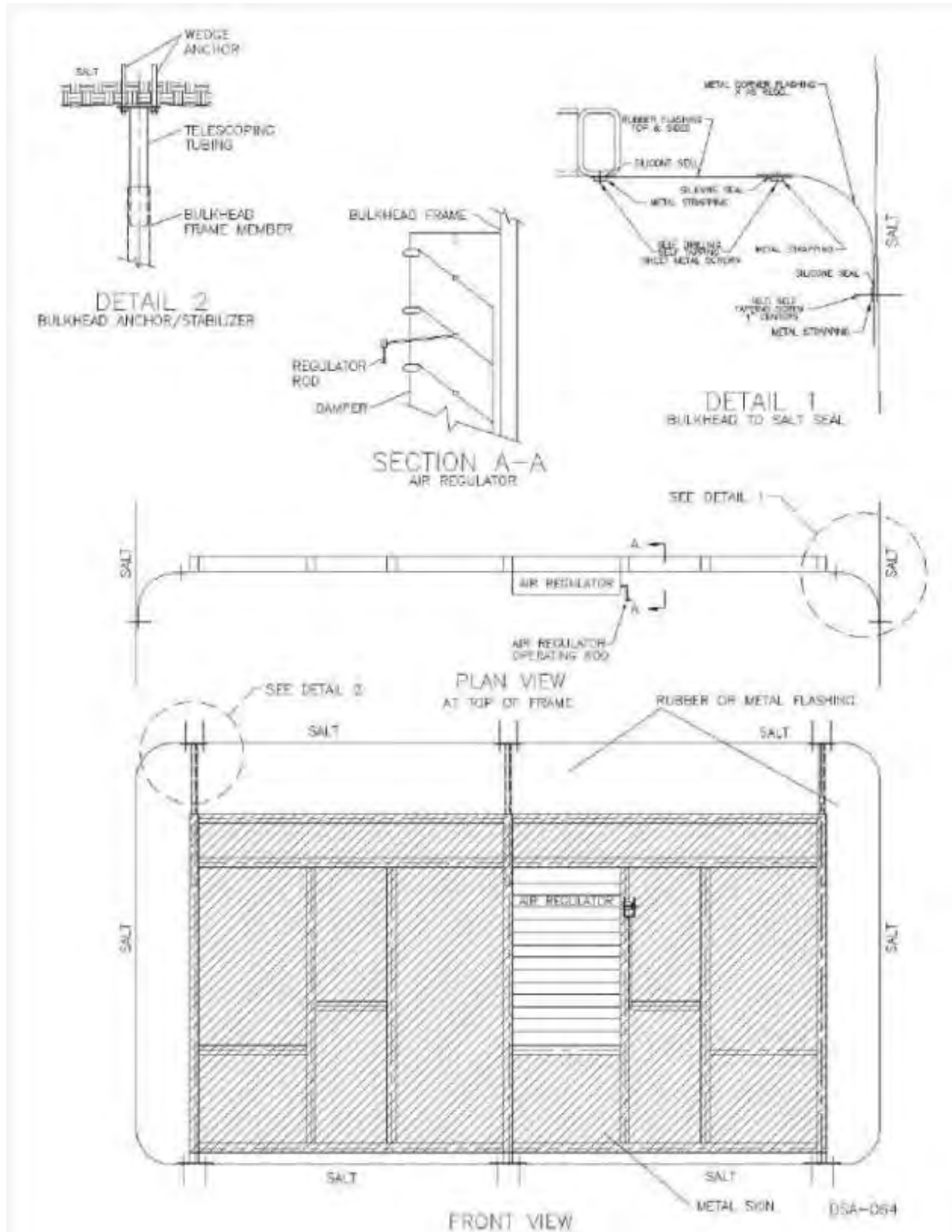
Illustration 3: Bulkhead Design

BOLT RING

FILTER
PORT

BOLT

HEAD &
GASKET

ROLLING
HOOP

BODY &
HEAD SHEET

DSA—060

OVERALL HEIGHT = 34.9 in (886 mm)
OVERALL DIAMETER = 23.9 in (608 mm)
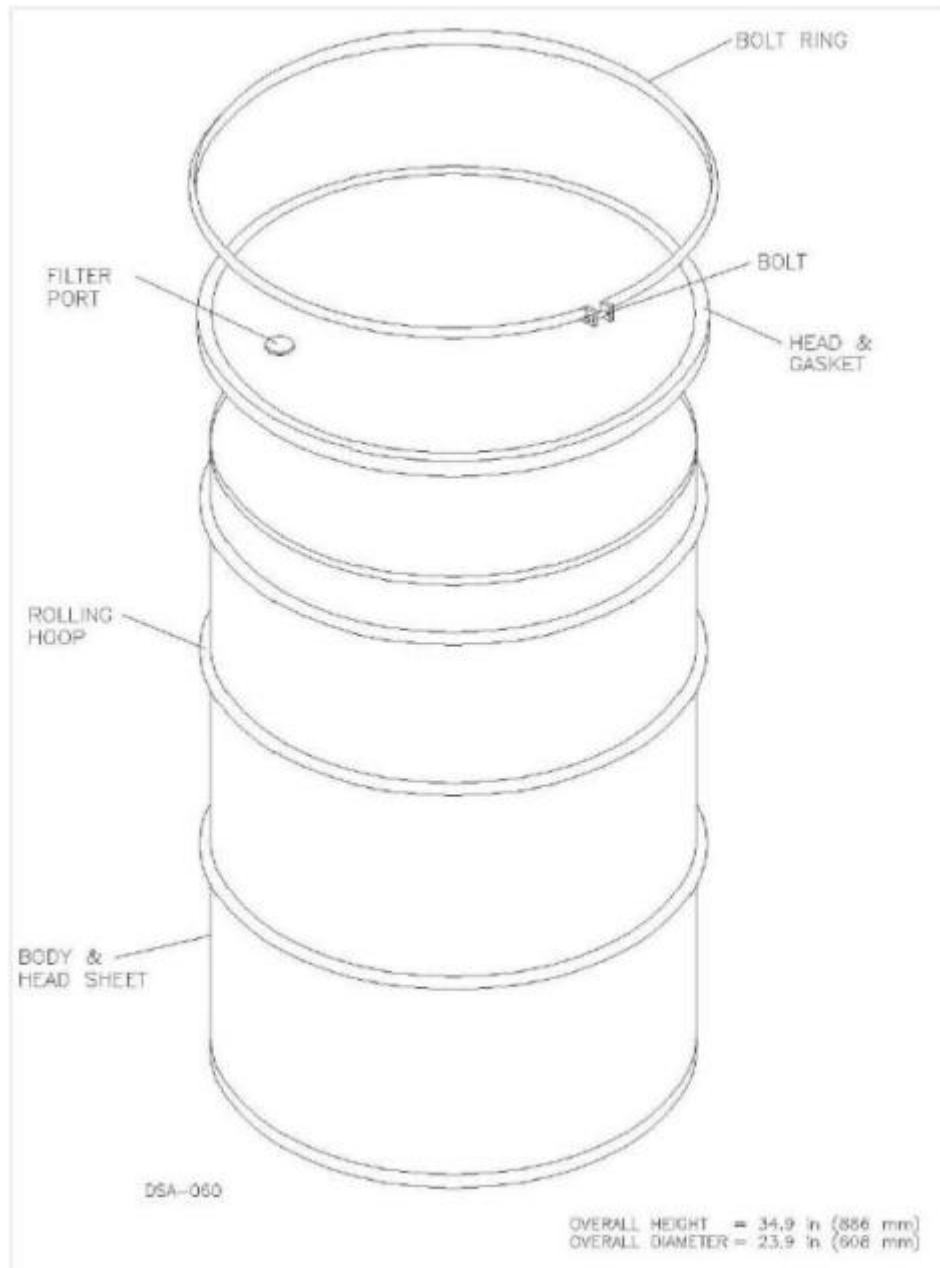
Illustration 4: Typical 55-Gallon Drum

COMPACTED
55-GALLON
DRUMS
"PUCKS"

THREE 16 GA.
CARBON STEEL
POSITIONING
STRAPS

TYPICAL DIMENSIONS
DIAMETER - 32 INCHES
HEIGHT - 35 INCHES

DSA-084
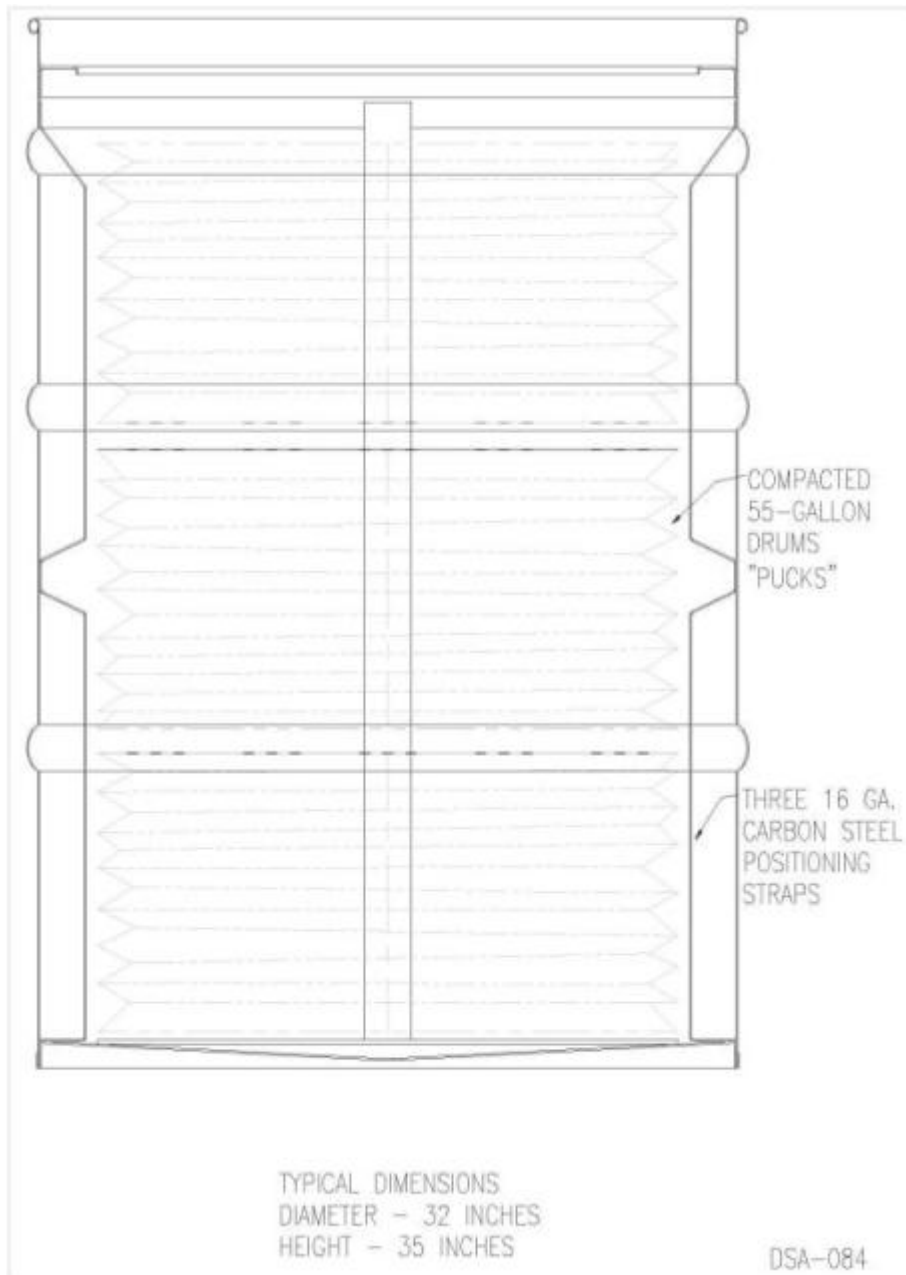
Illustration 5: Typical 100-Gallon Drum
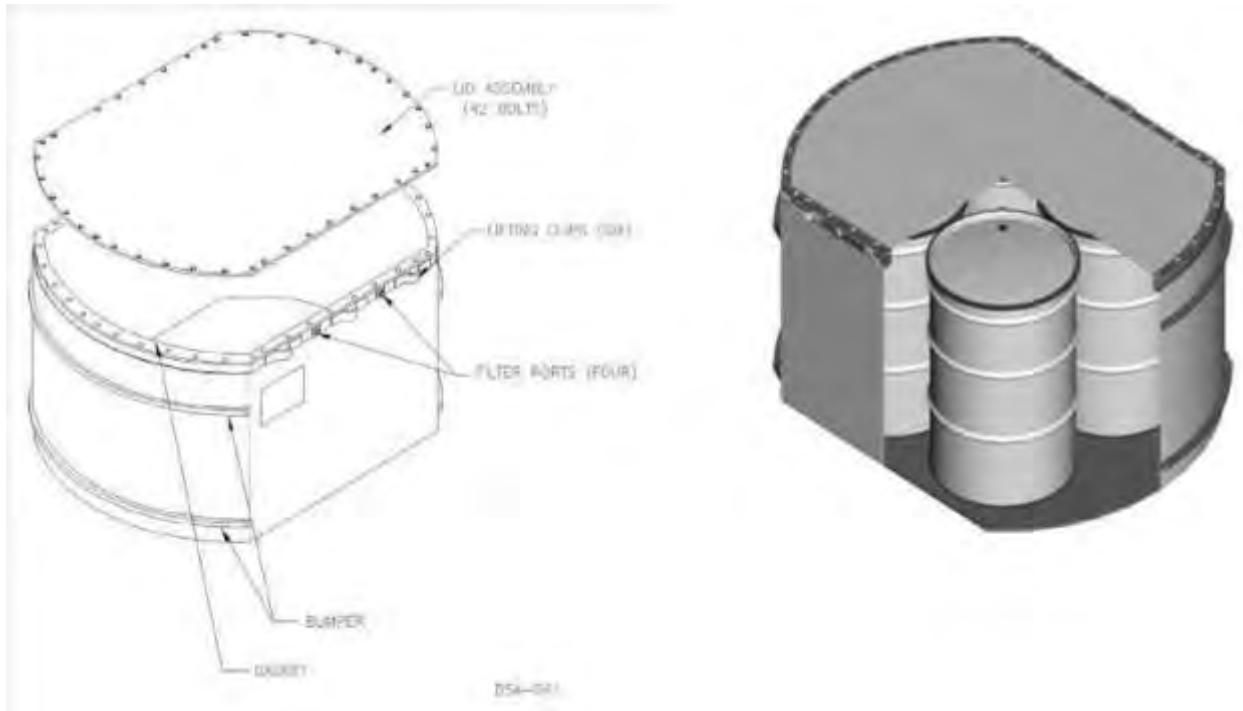
Dimension	Approximate Measurement				Approximate Volume	
	I.D. (inches)	O.D. (inches)	I.D. (mm)	O.D. (mm)		
Height	36 3/4	37	933	940	Gallons	496
Length	68 3/4	71	1,746	1,803	Liters	1,877
Width	51 7/8	54	1,318	1,372	Cubic Feet	66.3
					Cubic Meters	1.88

Illustration 6: Typical Standard Waste Box
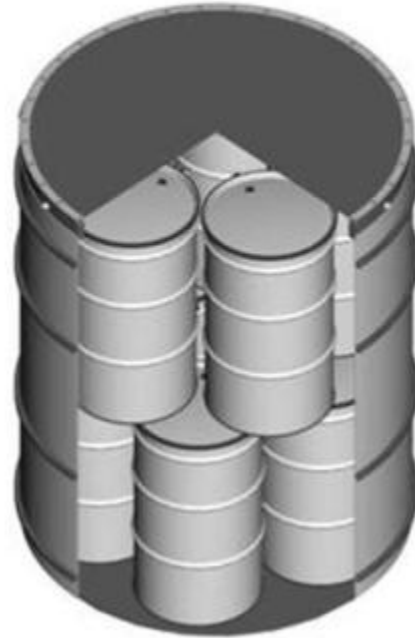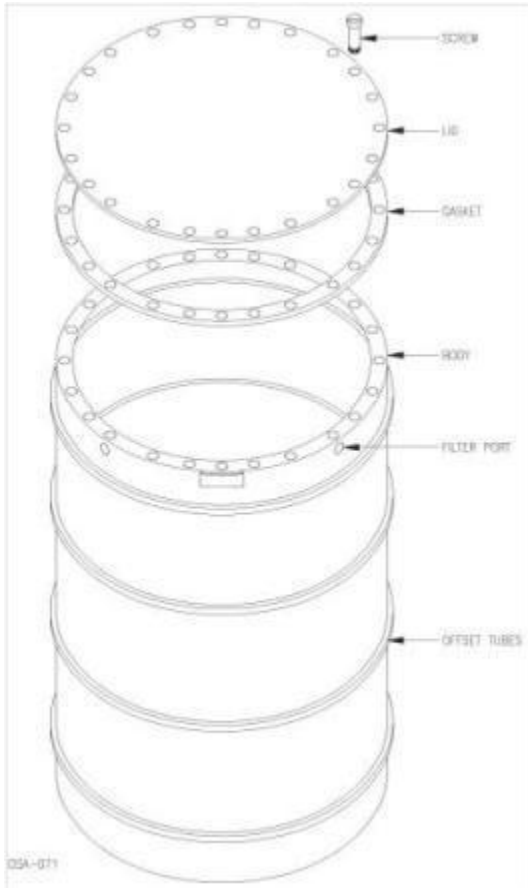
Illustration 7: Typical 10-Drum Overpack
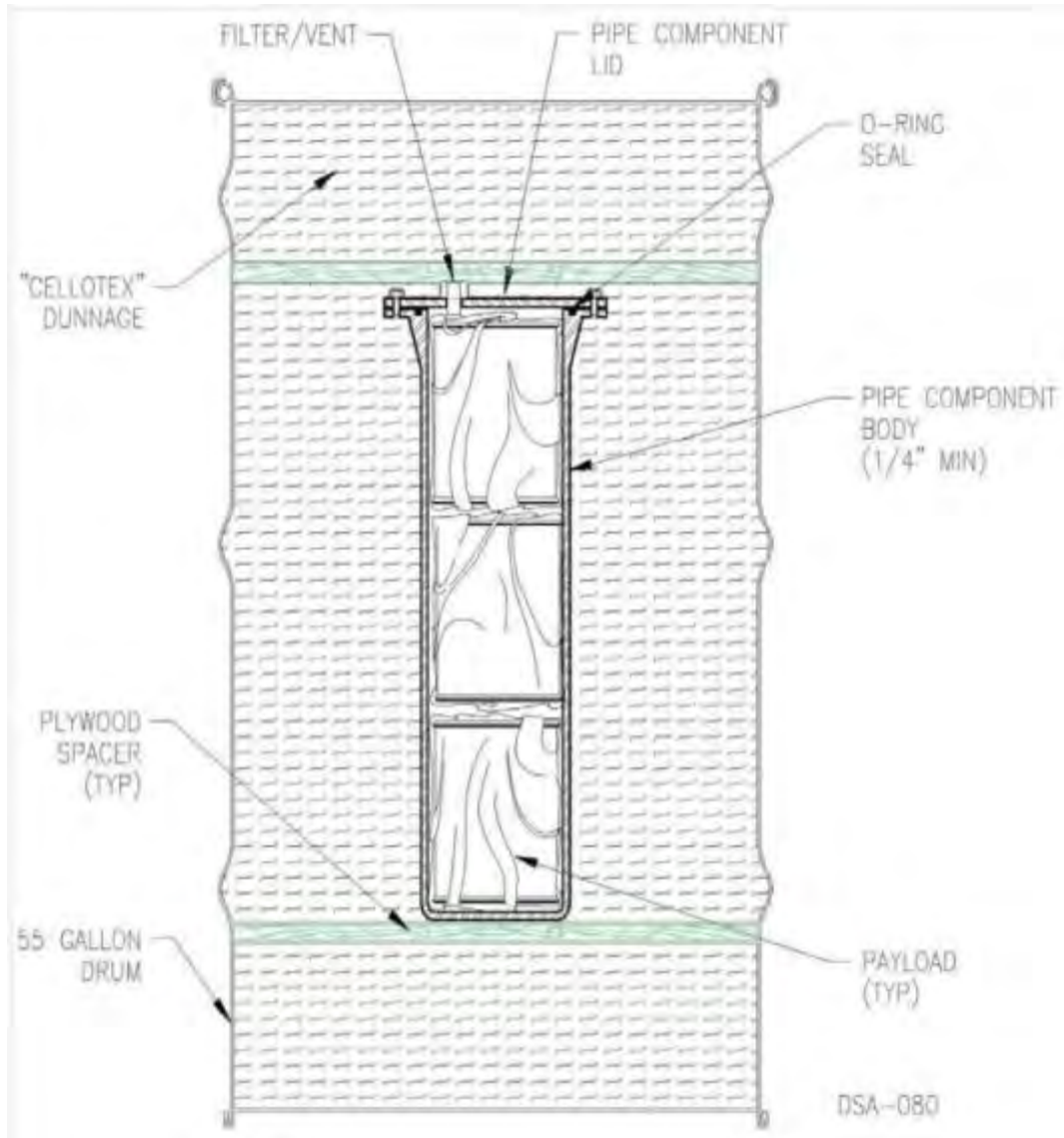
Illustration 8: Typical Standard Pipe Overpack

55–Gallon
Drum Lid
with Filter Vent
and Bolt Ring

Pipe Component
Lid with Filter Vent

Contents

Pipe Component
Body with Gasket

Shock Absorbing
Dunnage
(Fiberboard/Plywood)

Rigid Polyethylene
Liner with
Filtered/Punctured Lid

55–Gallon
Drum
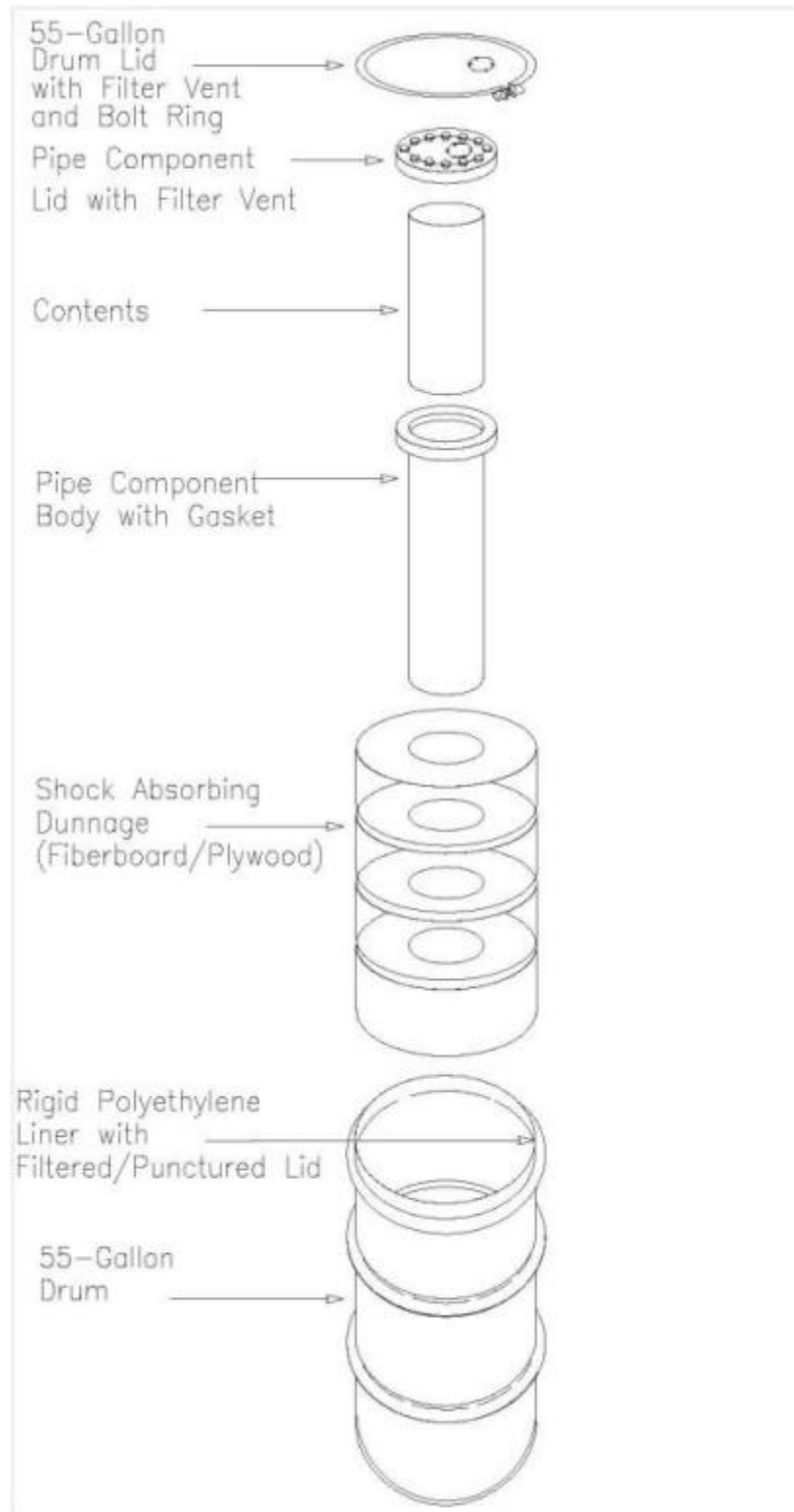
Illustration 9: Typical Standard Pipe Overpack Components
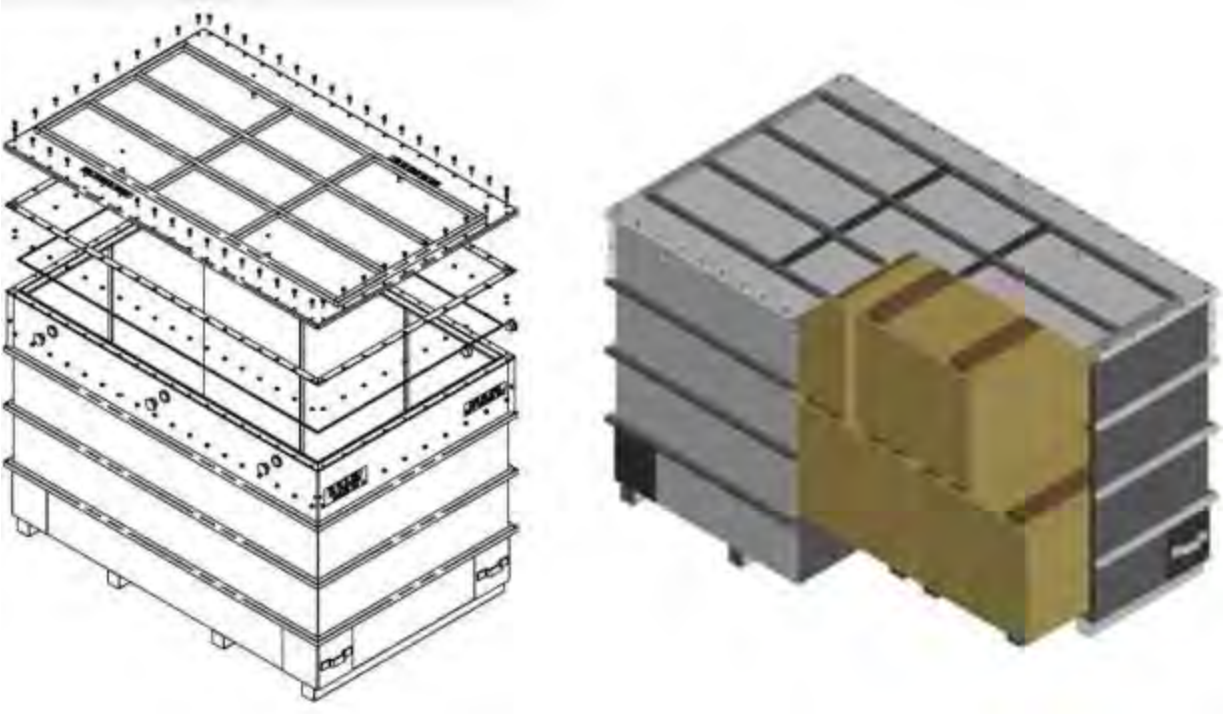
Illustration 10: Typical Standard Large Box 2
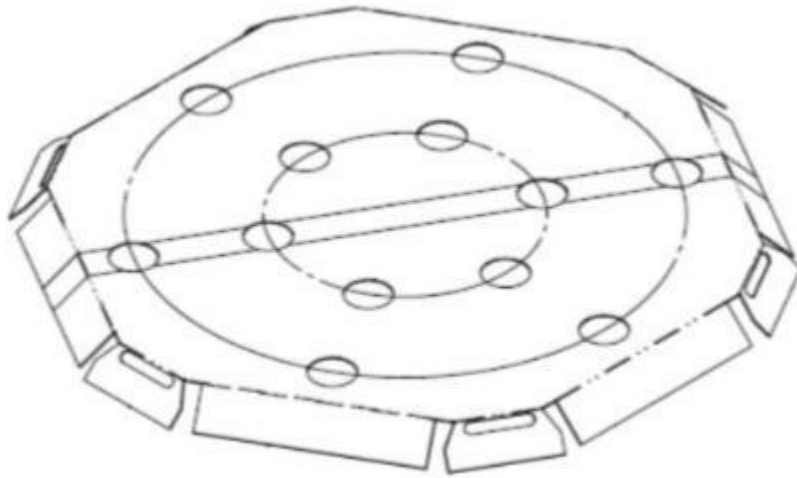
Illustration 11: Reinforcement Plate
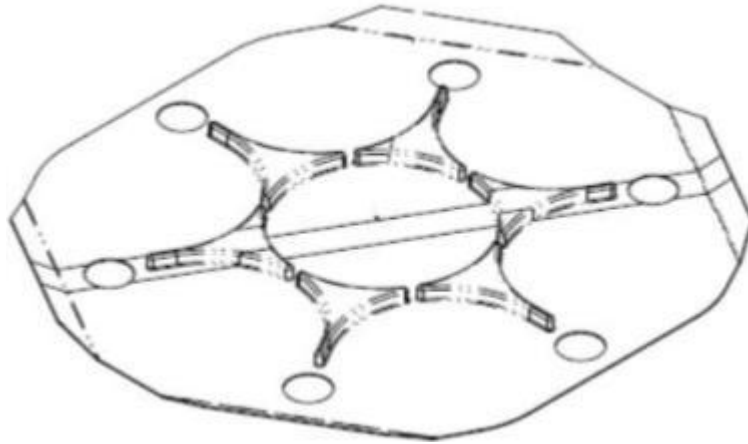
Illustration 12: Slip Sheet
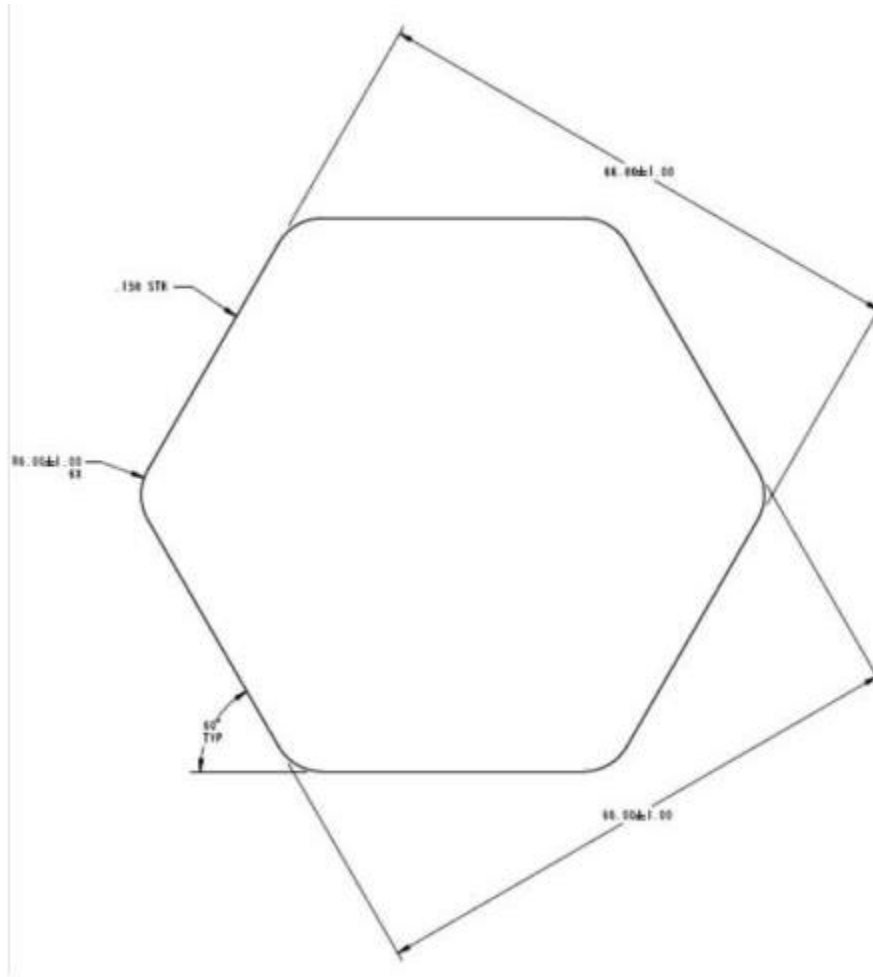
Illustration 13: Super Sack Slip Sheet
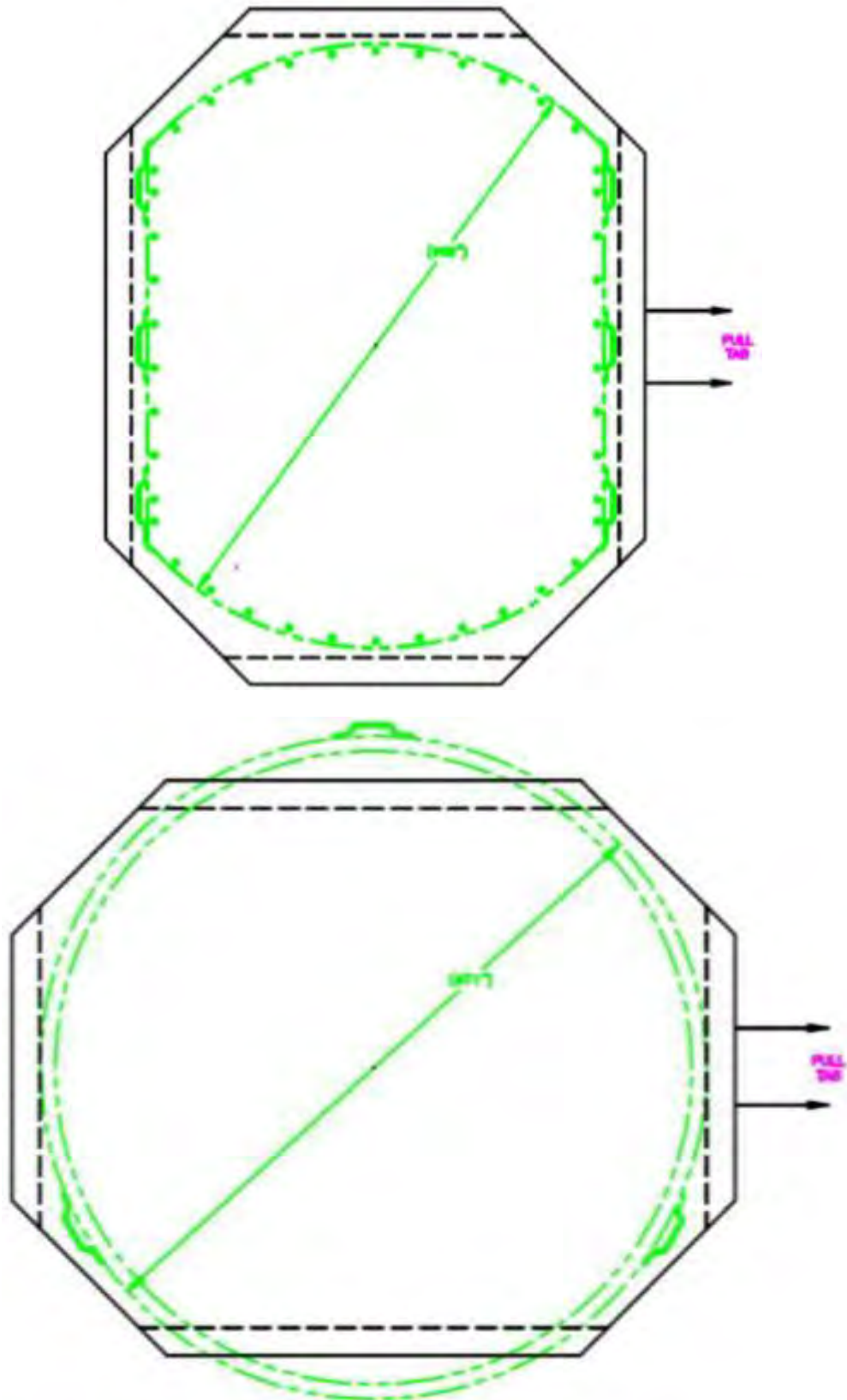
Illustration 14: SWB and TDOP Slip Sheet
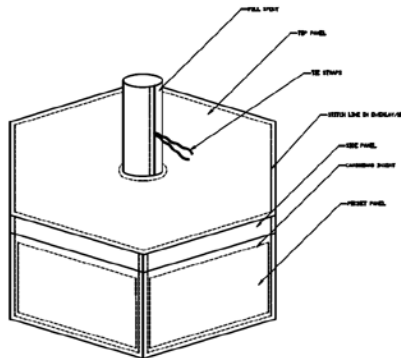
Illustration 15: MgO Super Sack
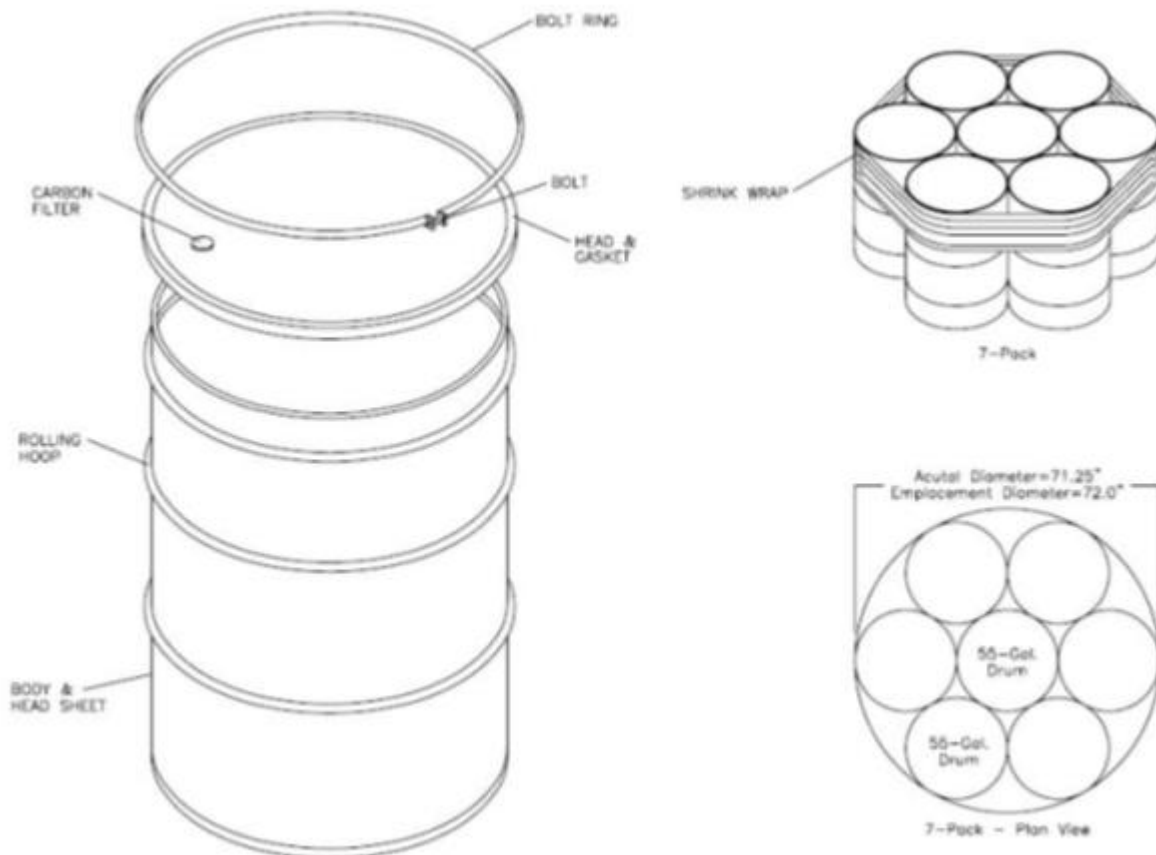
Note: Slip sheet and reinforcement plate not shown.

Illustration 16: 7-Drum Waste Assembly
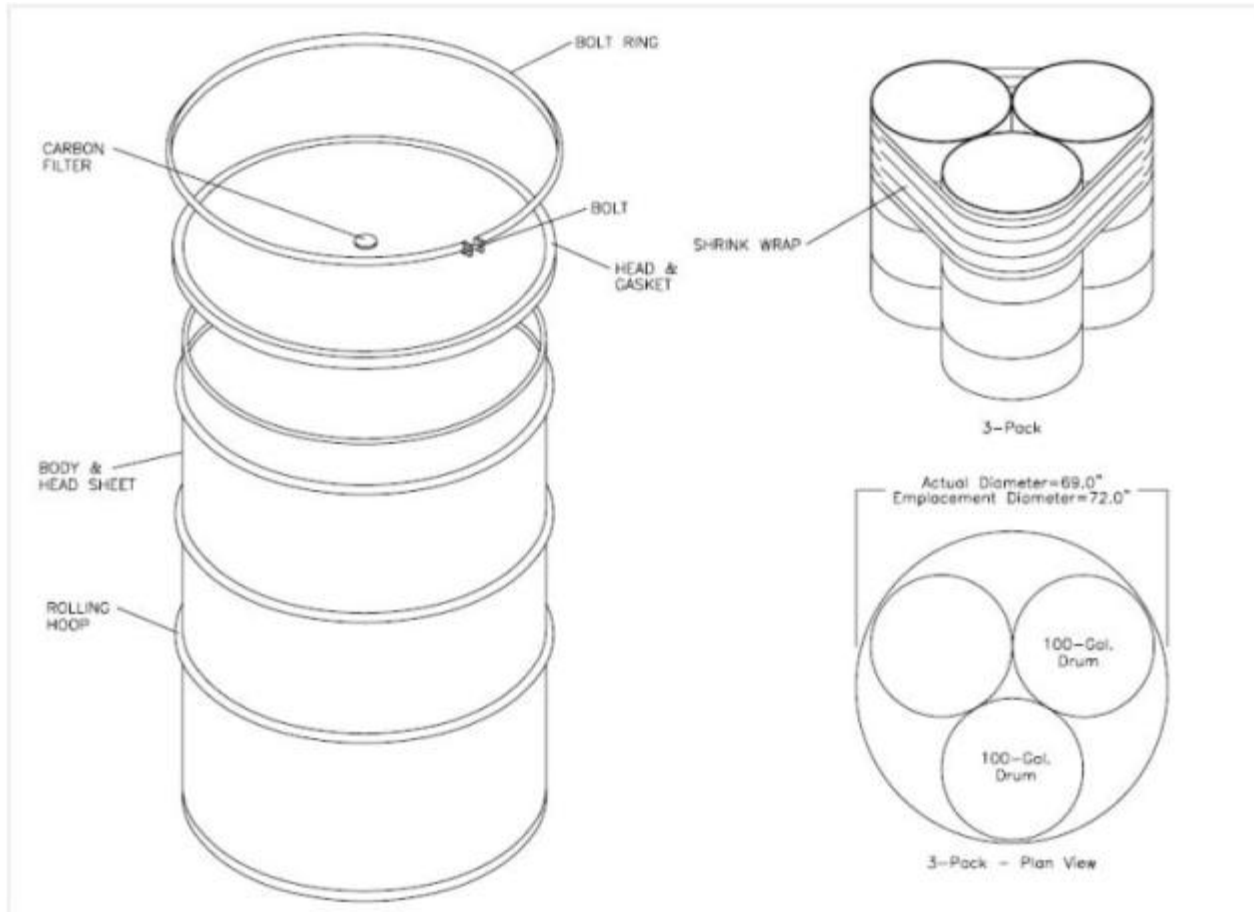
Illustration 17: Three-Drum Waste Assembly
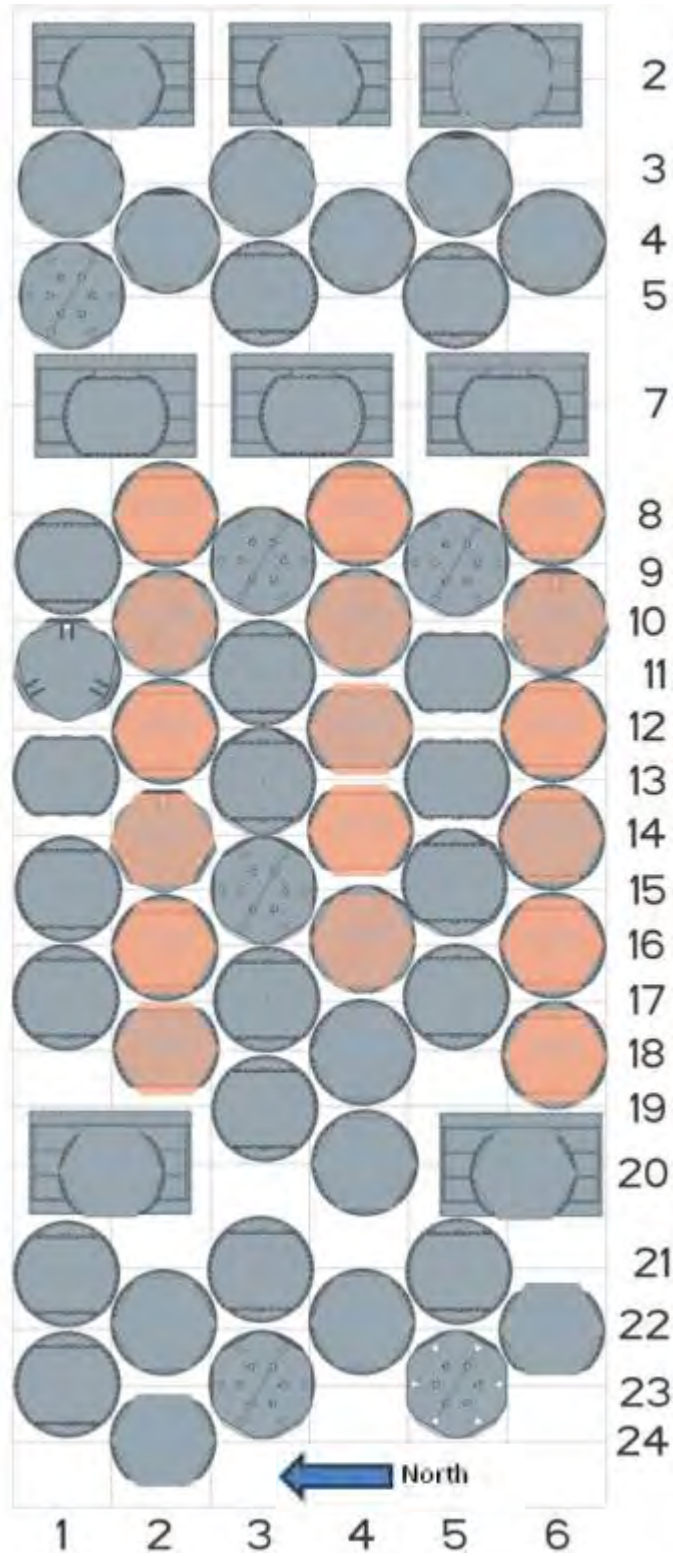
Note: Damaged MgO super sacks shown in peach.

Illustration 18: Panel 7, Room 7 Array Arrangement
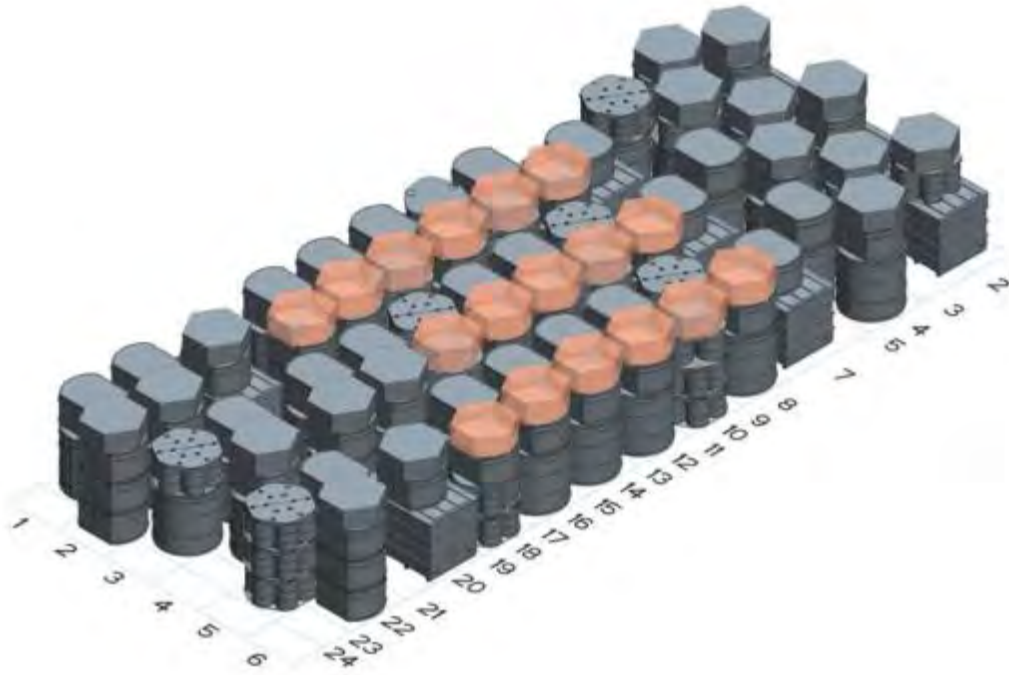
Note: Damaged MgO super sacks shown in peach.

Illustration 19: Panel 7, Room 7 Arrangement - Isometric

Row	Bottom						Middle						Top					
	1	2	3	4	5	6	1	2	3	4	5	6	1	2	3	4	5	6
2		0		0		0		0		0		0		11		11		24
3	4		4		4		0		0		0		24		24		22	
4		4		4		4		0		0		0		22		11		11
5	4		4		4		0		0		0		17		4		4	
7	0		0		0		0		0		0		4		4		4	
8		4		4		4		0		0		0		11		11		11
9	4		4		4		0		0		0		4		17		17	
10		4		4		17		0		0		17		24		24		22
11	4		4		4		4		0		4		15		4		4	
12		4		4		4		0		4		0		11		11		11
13	4		17		4		4		17		4		4		4		4	
14		15		4		4		15		4		0		22		11		11
15	4		4		17		0		0		17		4		17		4	
16		4		4		4		0		0		0		11		24		11
17	4		4		4		0		0		0		4		4		4	
18		4		4		17		4		0		17		11		11		11
19		4						0								4		
20		0		4		0		0		0		0		11		11		11
21	4		4		4		0		0		0		4		4		4	
22		4		4		4		0		0		4		11		11		11
23	4		4		17		0		0		17		4		17		17	
24		4						4						11				

White = 0-10 kg combustible emplacement material;

Light gray = 11-15 kg combustible emplacement material;

Magenta = 16+ kg combustible emplacement material

Illustration 20: Panel 7, Room 7 Combustible Matrix by Location and Elevation
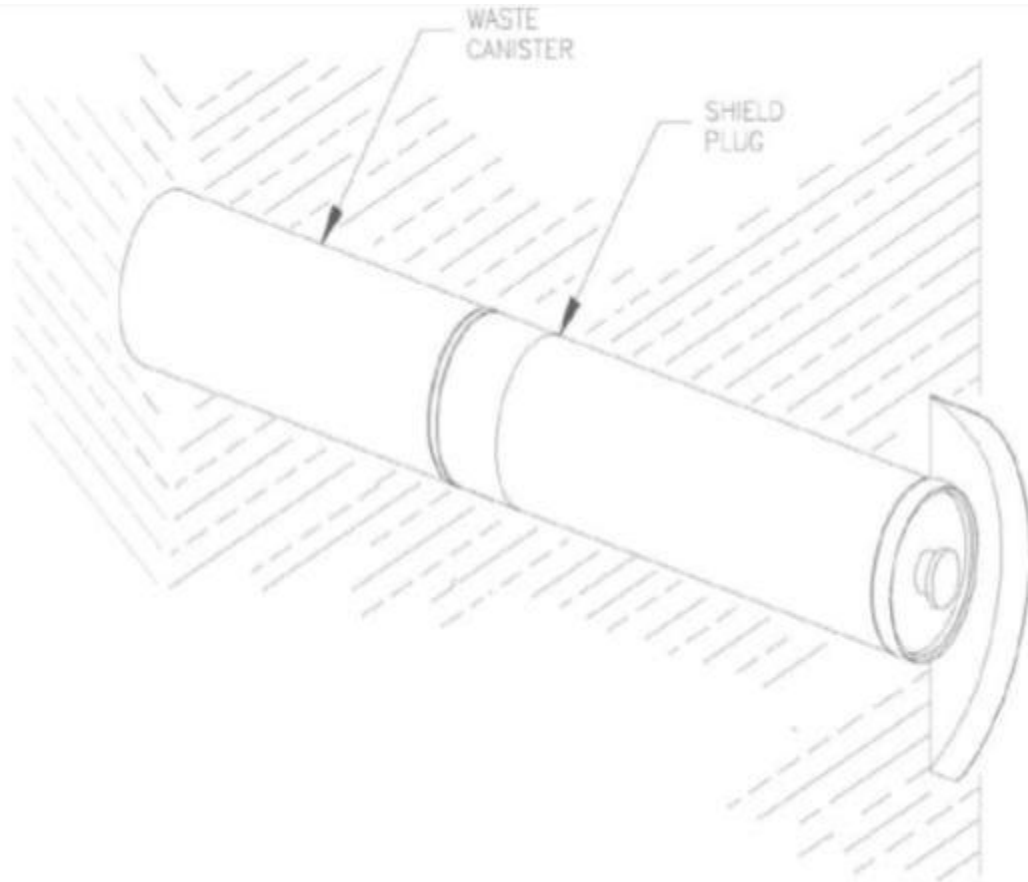
Illustration 21: Remote Handled Waste Configuration
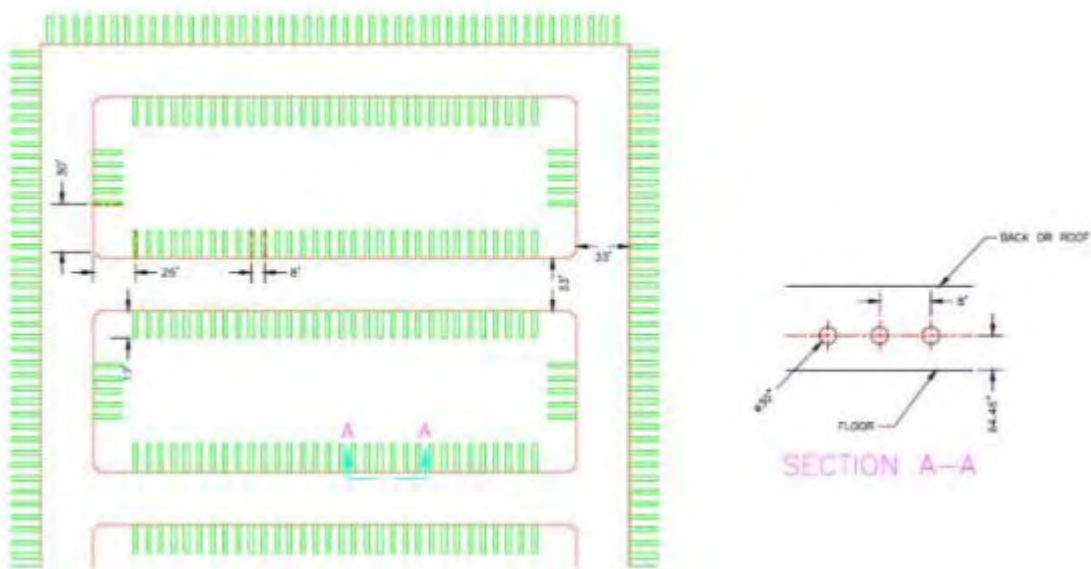
Illustration 22: Typical Locations of Boreholes
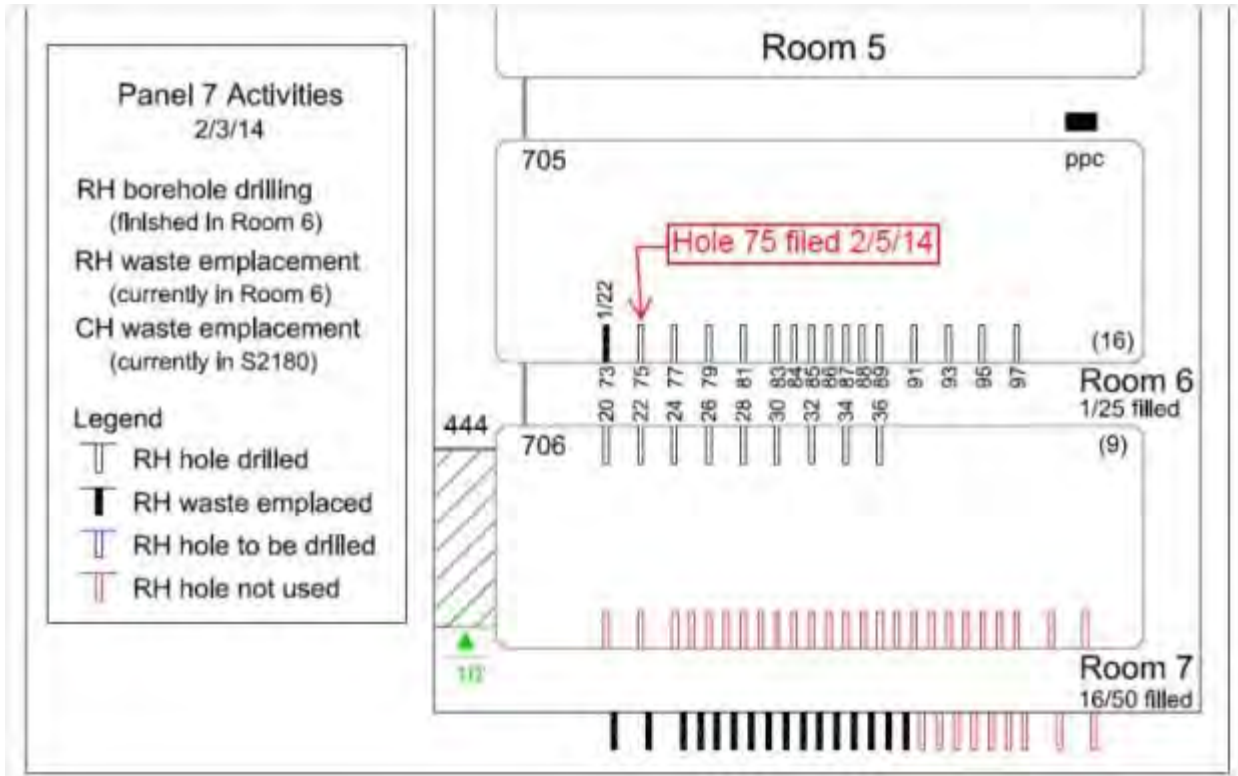
Illustration 23: Borehole Locations in Panel 7 Rooms 5, 6, and 7
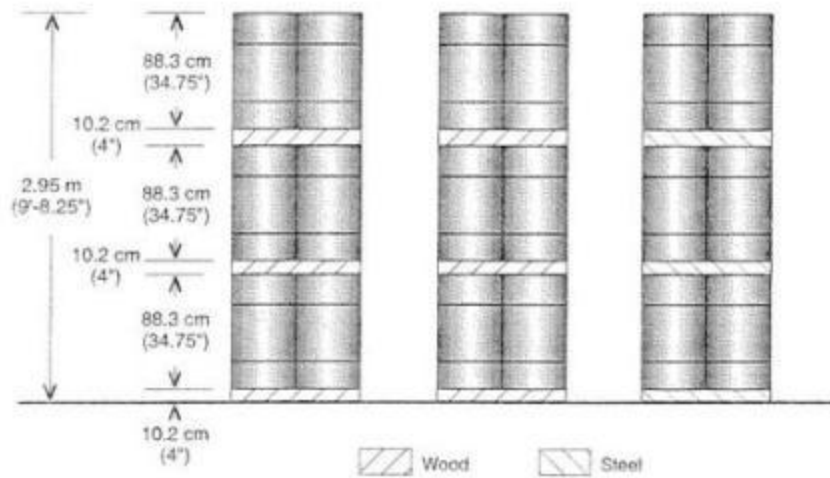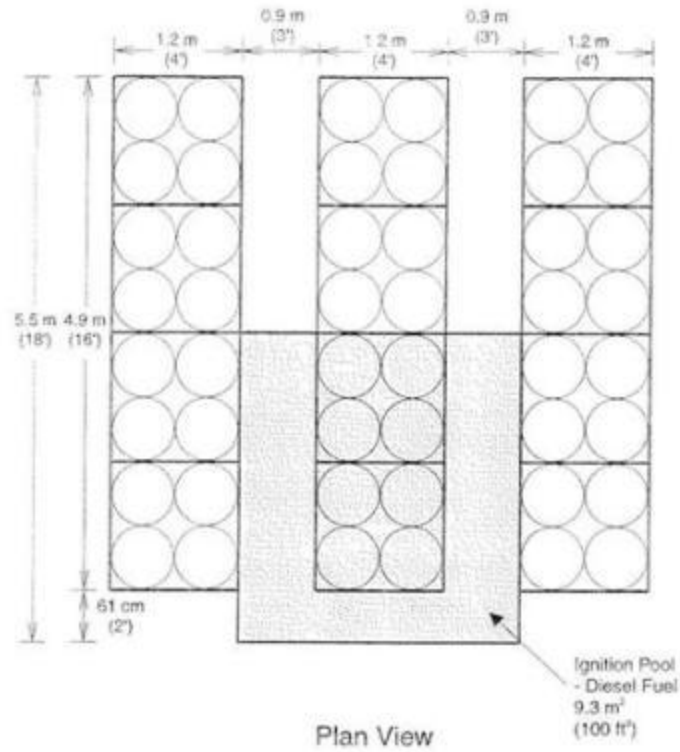
Illustration 24: Pallet Storage Test Arrangement

APPENDIX B. PHOTOGRAPHS

Table of Photographs

AIB-FST-01001: Bulkhead north of SHS, looking south

AIB-FST-01002: Panel 7, Room 7 workface prior to release event

AIB-FST-01003: Typical waste face shown in 2014 compliance recertification application

AIB-FST-01004: Remote handled waste disposal borehole

AIB-FST-01005: Remote handled waste disposal location with shield plug
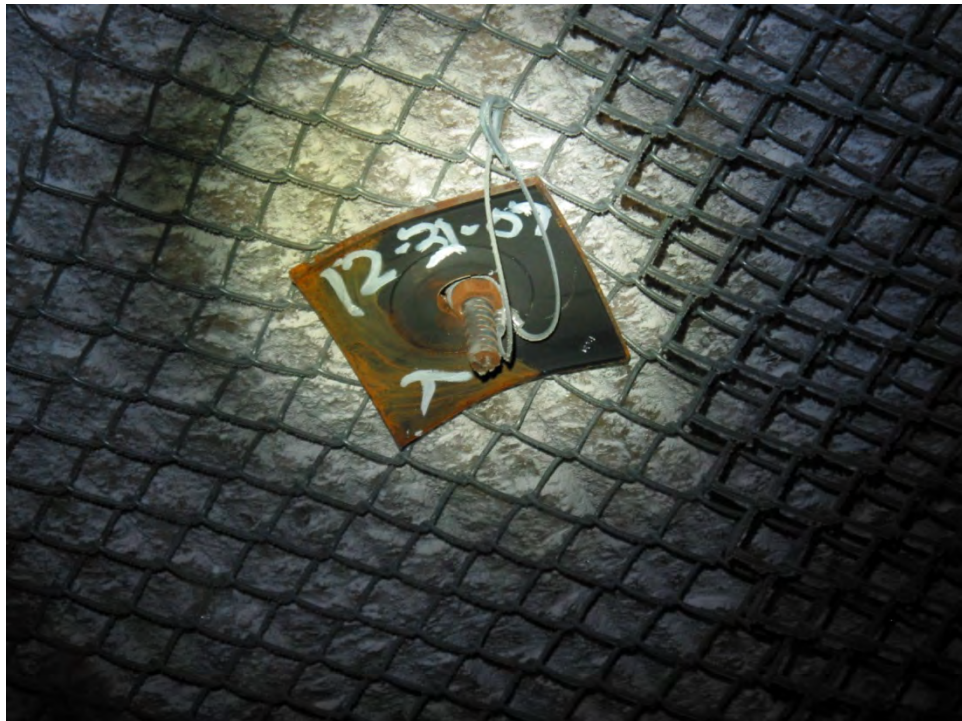
AIB-FST-01006: Typical roof bolt installation

AIB-FST-02001

AIB-FST-02002

AIB-FST-02003

AIB-FST-02004: R12:C4 – Top Tier – Array face (west) view

AIB-FST-02005

AIB-FST-02006

AIB-FST-02008

AIB-FST-02009: R13:C1 – Demonstration of dust layer

AIB-FST-02011

AIB-FST-02012

AIB-FST-02013: R13:C3 and R14:C4

AIB-FST-02014: R13:C3 and R14:C4

AIB-FST-02017

AIB-FST-02022

AIB-FST-02024: R13:C5

AIB-FST-02026: R14:C4 – Residual Mg

AIB-FST-02028: R14:C4 – Partially damaged Mg super sack

AIB-FST-02030

AIB-FST-02036: R14:C6 – Top-tier SWB - East view

AIB-FST-02045

AIB-FST-02047: R15:C5 – SWB lid debris

R15:C5

AIB-FST-02048: R15:C5 – SWB lid debris – Zoom-in view from AIB-FST-02047

AIB-FST-02049

AIB-FST-02051: Breached drum at R16:C4

AIB-FST-02063: R15:C5 – Middle tier drum G

AIB-FST-02065: R15:C5 – Top tier (after Sampling on May 30, 2014)

AIB-FST-02066: R15:C5 and R16:C4

AIB-FST-02072
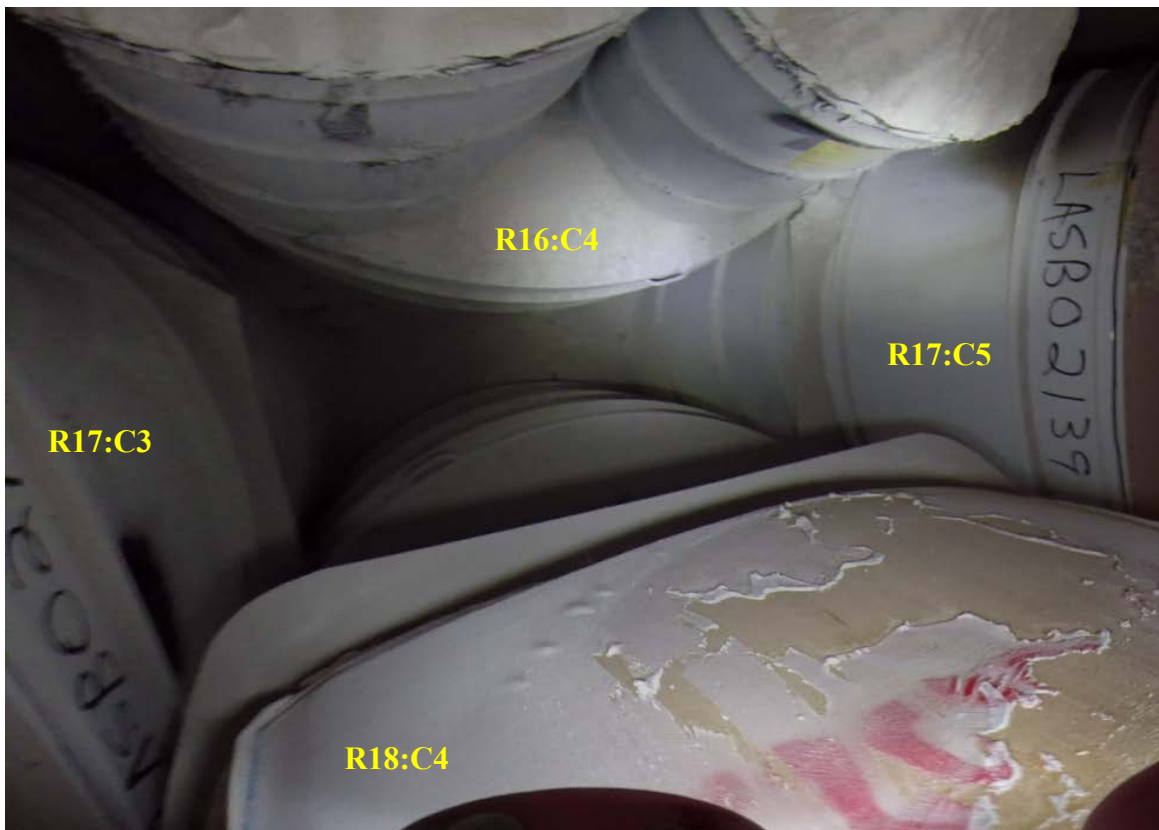
AIB-FST-02073: R18:C4 – Bulkhead (East) View

AIB-FST-02075: R16:C4 evidence of Flaming Combustion

AIB-FST-02083: R16:C4 – Drum E

AIB-FST-02085: R16:C4 – Breached lid of waste drum 68660

AIB-FST-02086: R16:C4 – Clean burn pattern on waste drum 68660

AIB-FST-02087: R16:C4 – Label damage on waste drum 68660

AIB-FST-02092

AIB-FST-02097

AIB-FST-02099

AIB-FST-02101
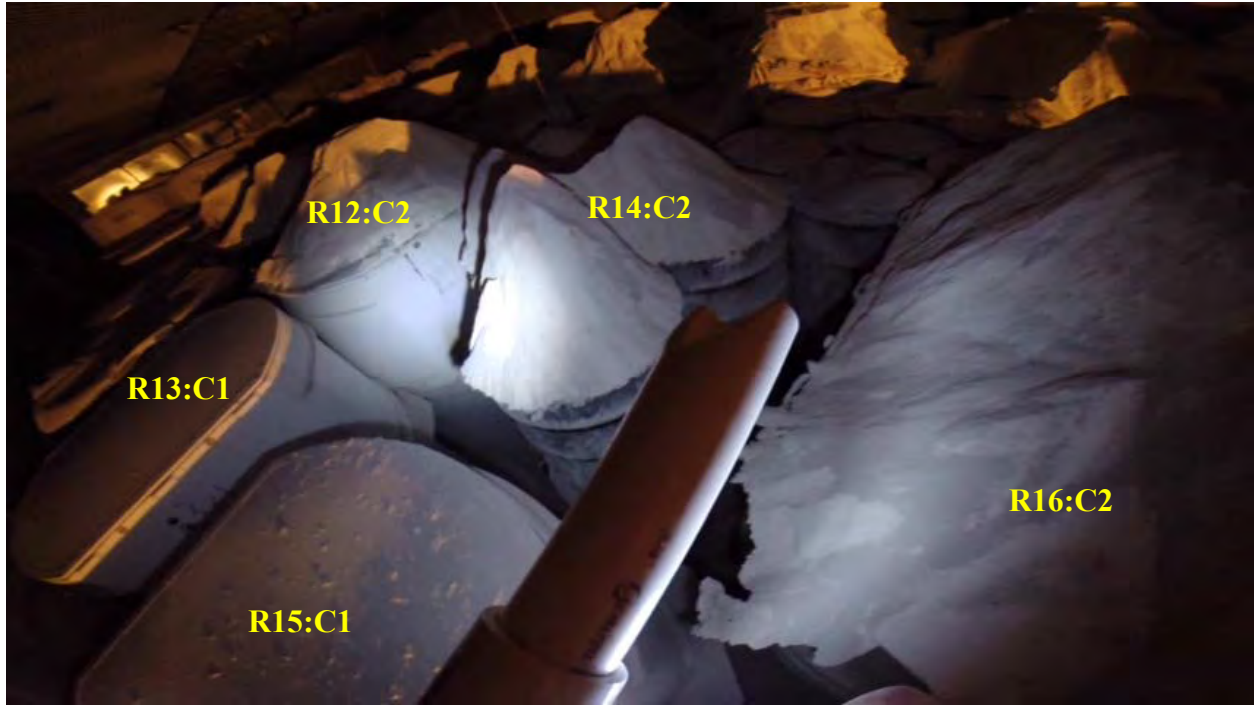
AIB-FST-02102

AIB-FST-02104

AIB-FST-02107: R16:C4 – Breached lid of waste drum 68660

AIB-FST-10001 – Face (west) view of R18:C6

AIB-FST-10002– Face (west) view of R18:C6

AIB-FST-10018

AIB-FST-10019

AIB-FST-10022

AIB-FST-10023

AIB-FST-10024: R10:C6 and R11:C5

AIB-FST-10025

AIB-FST-10028: R14:C6 – Residual Mg

AIB-FST-10029
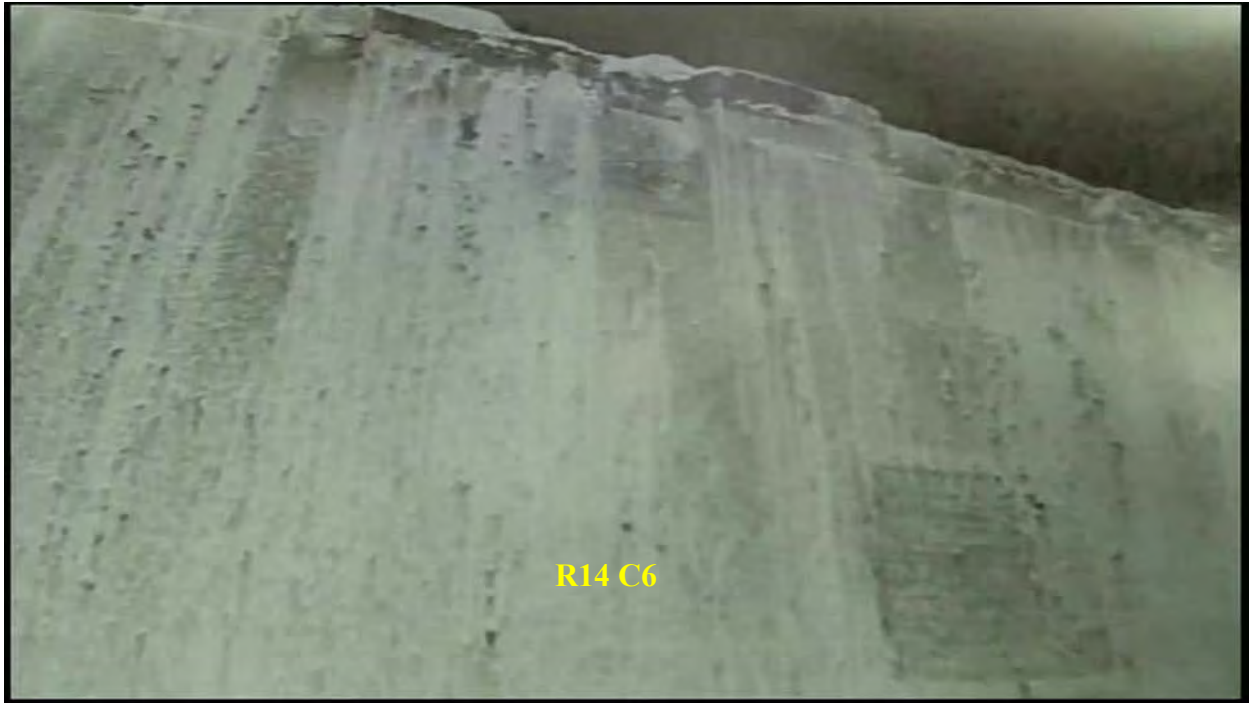
AIB-FST-10030: R14:C6 – Top tier – Array face (west) view

AIB-FST-10031: R14:C6 and R16:C6 - Charred edge of SWB slip sheet

AIB-FST-10033: R14:C6 and R16:C6

AIB-FST-10034

AIB-FST-10035

AIB-FST-10036

AIB-FST-10038 - R14:C6 show lip/slip sheet with Mg piled on slip sheet and top of TDOP

AIB-FST-10040: R14:C6 – Bulkhead (east) view
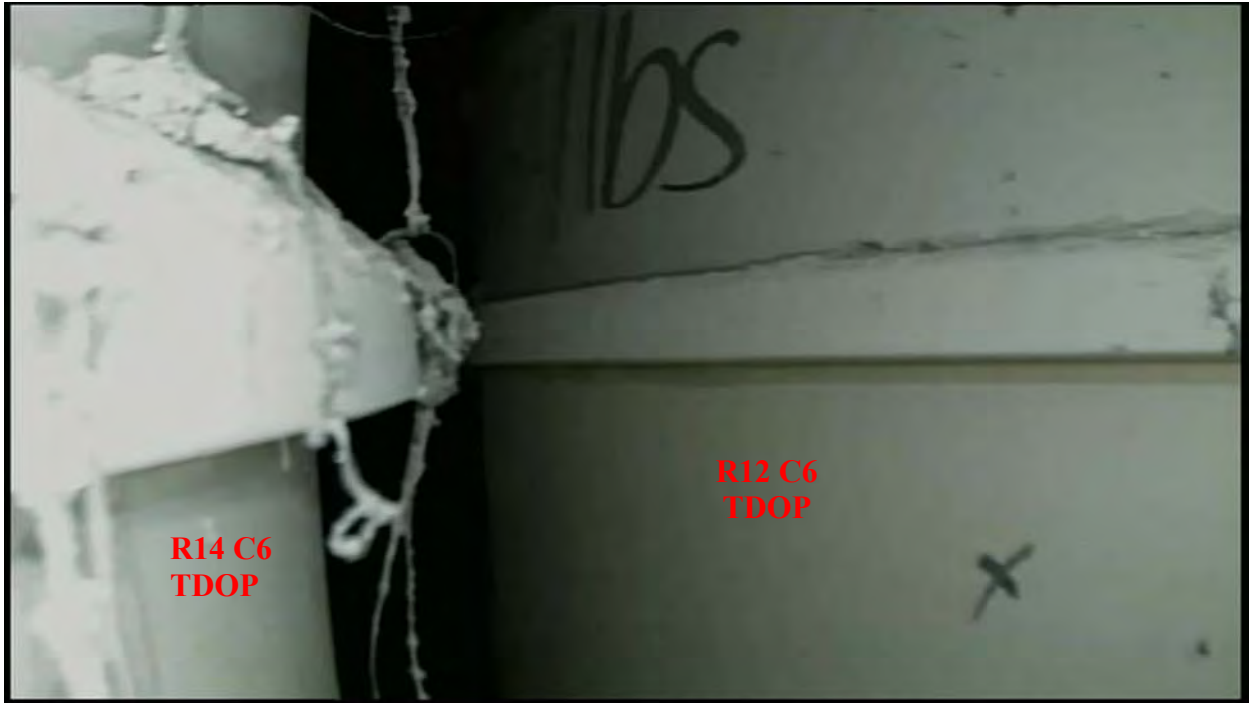
AIB-FST-10041: R14:C6 TDOP first offset tube

AIB-FST-10042

AIB-FST-10043

AIB-FST-10044: R8:C4 and R9:C5

AIB-FST-10045

AIB-FST-10046
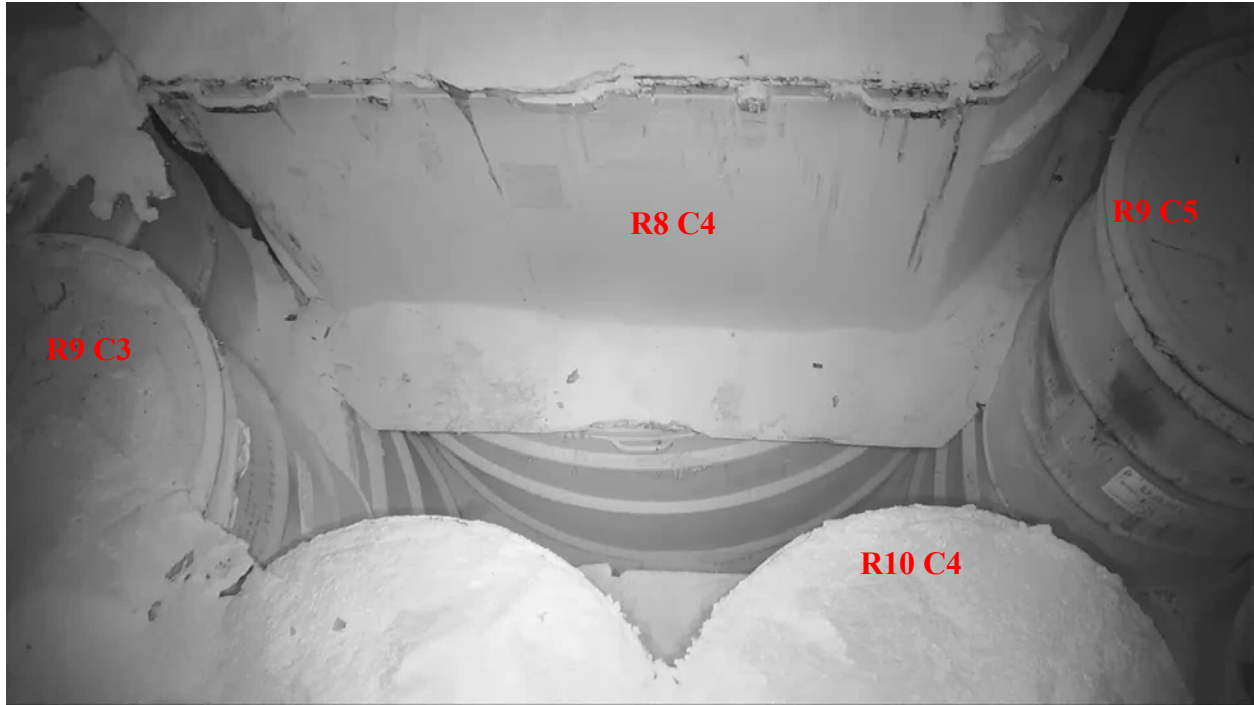
AIB-FST-10047

AIB-FST-10048

AIB-FST-10049
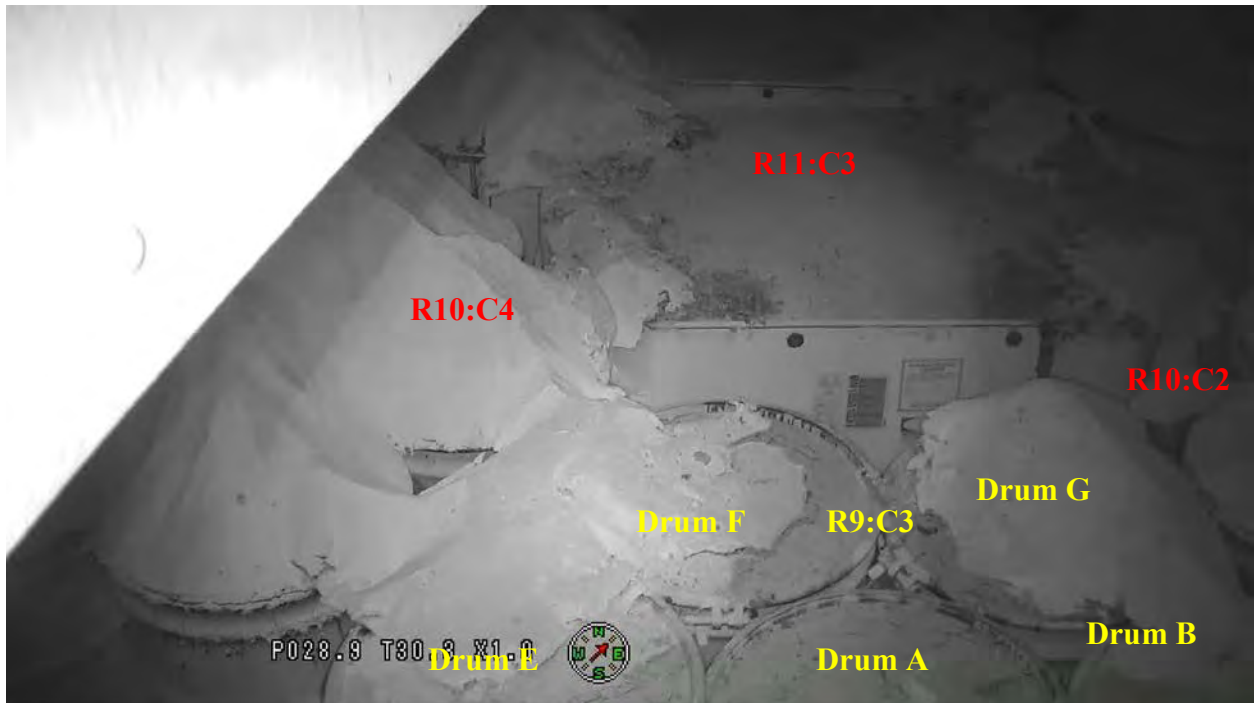
AIB-FST-10050
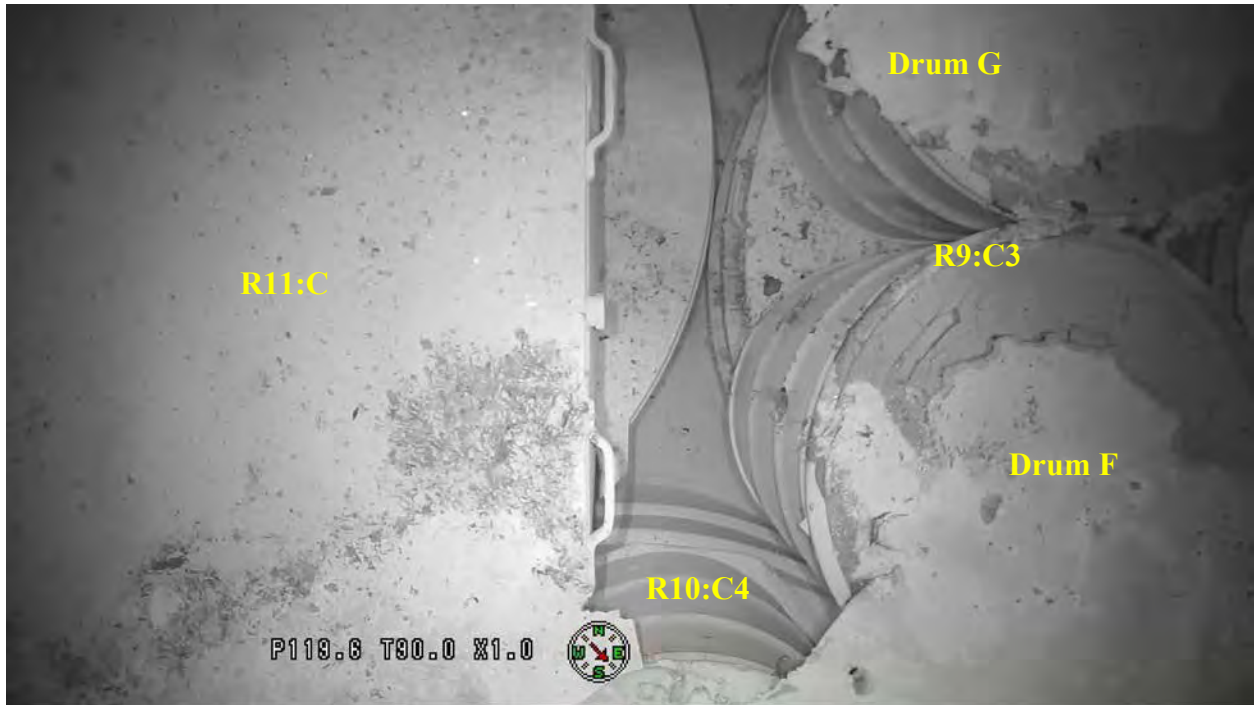
AIB-FST-10051

AIB-FST-10052

AIB-FST-10056
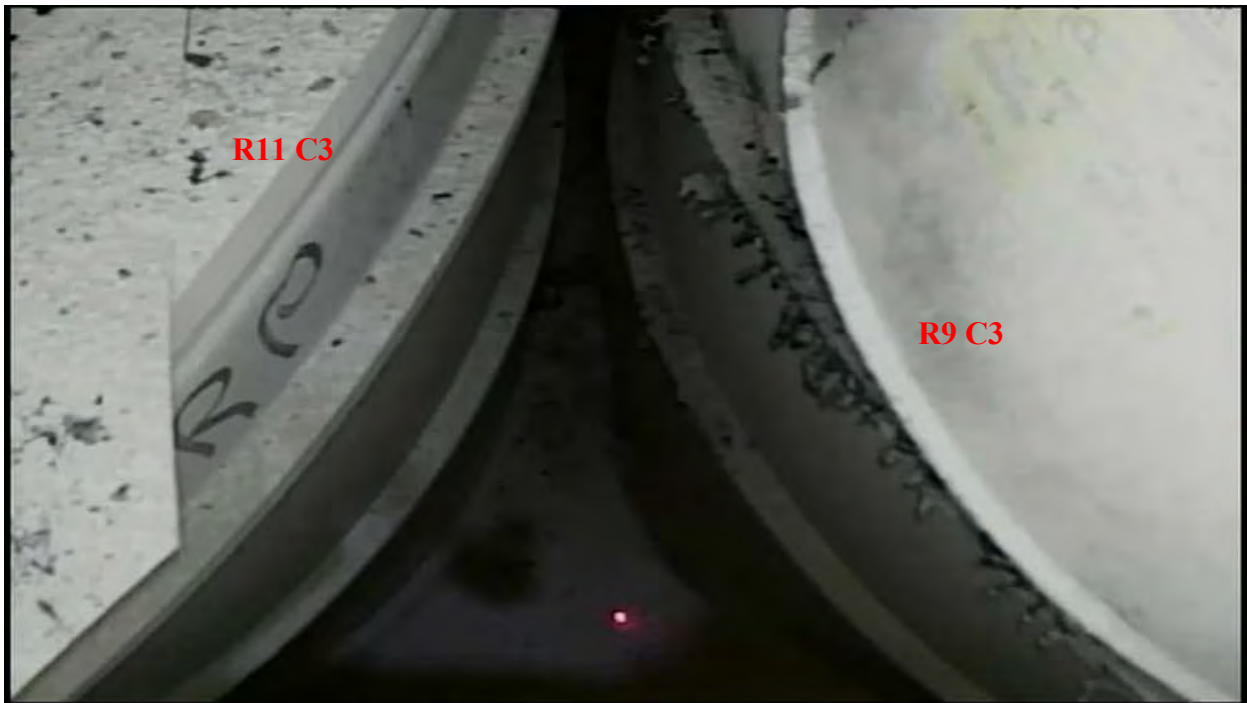
AIB-FST-10059: R9:C3 and R11:C3

AIB-FST-10060

AIB-FST-10061

AIB-FST-10062

AIB-FST-10063
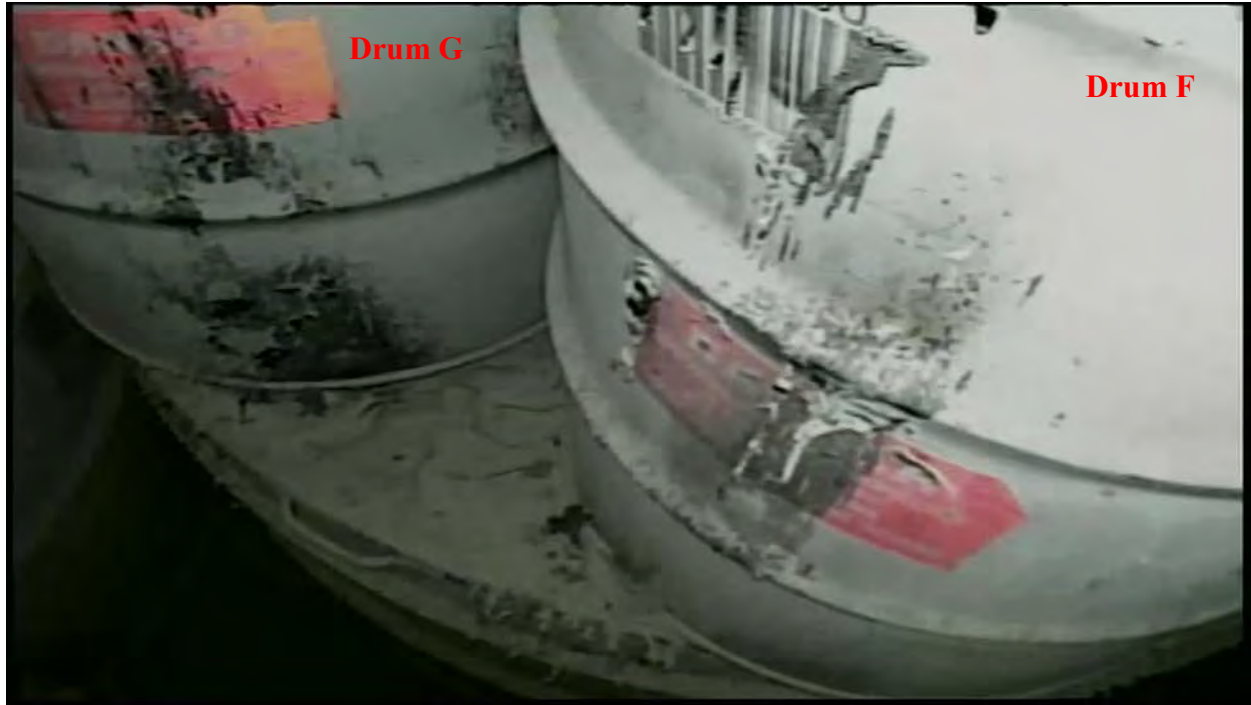
AIB-FST-10067: R9:C5 – Drum F and Drum G

AIB-FST-10069: R9:C5 – Drum F and Drum G

AIB-FST-10075

AIB-FST-10080: R18:C4 – Heat flux damage to Mg super sack fabric

AIB-FST-10084: R8:C6 and R9:C5

AIB-FST-10087: R18:C4 – Heat flux damage to Mg super sack fabric

AIB-FST-10090: R2:C6 and R3:C5

AIB-FST-10091

AIB-FST-10092: R3:C3 and R4:C4
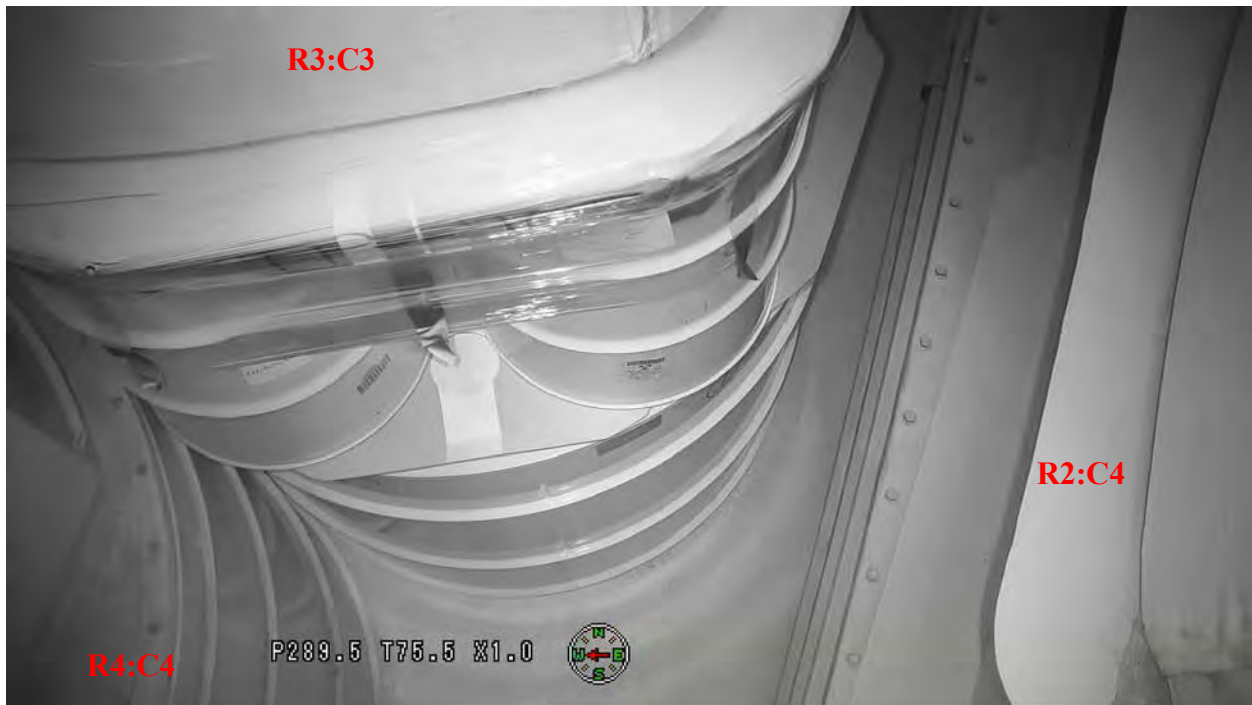
AIB-FST-10093

AIB-FST-10094: R2:C4 and R3:C3

AIB-FST-10095: R21:C5 and R23:C5

AIB-FST-10096: R21:C5
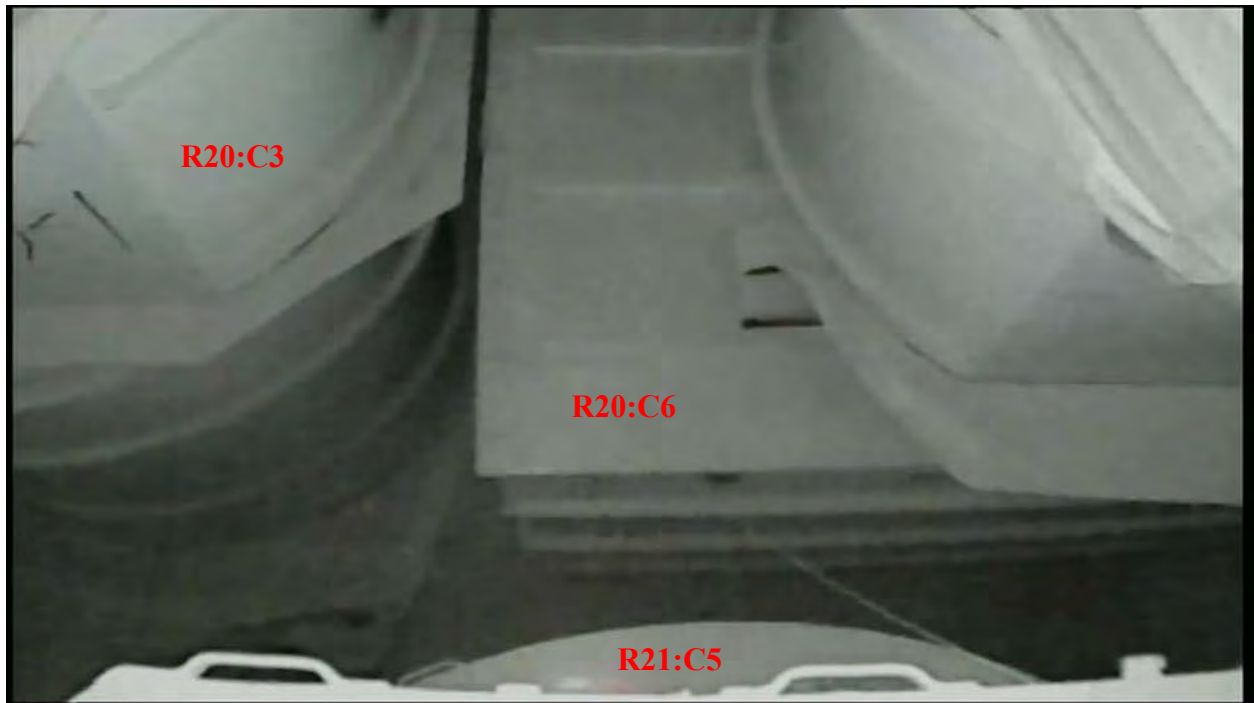
AIB-FST-10097

AIB-FST-10098
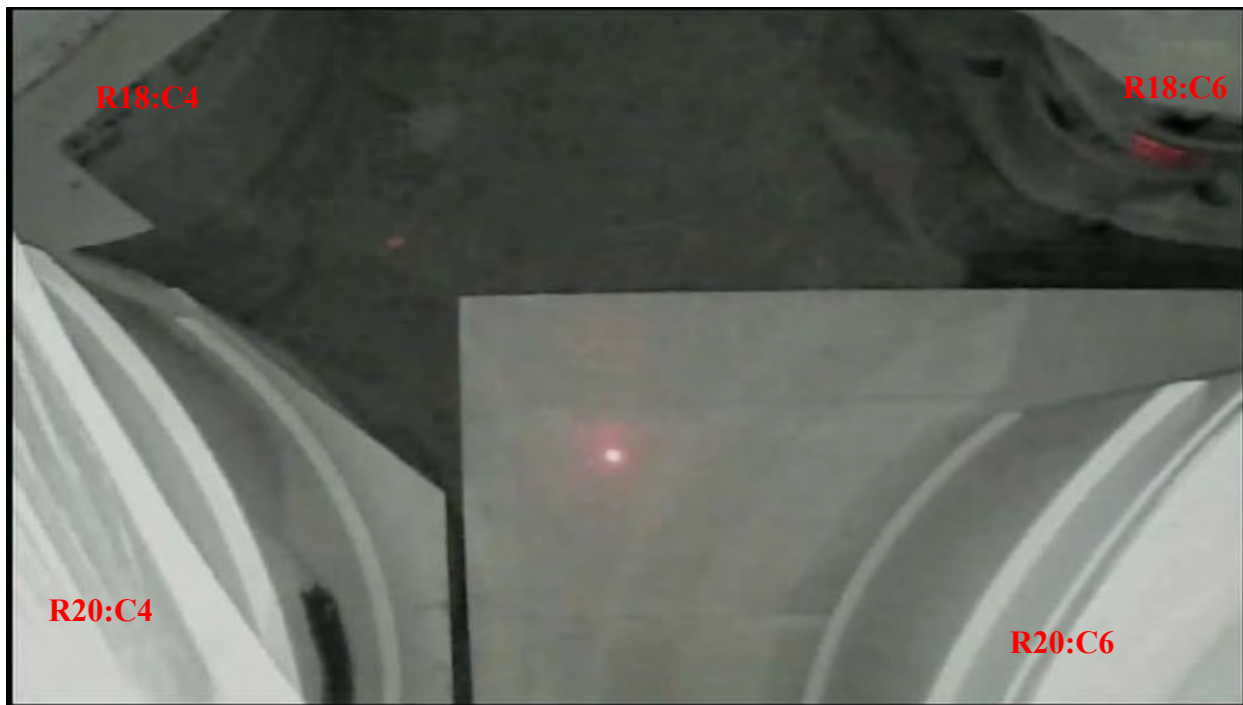
AIB-FST-10099
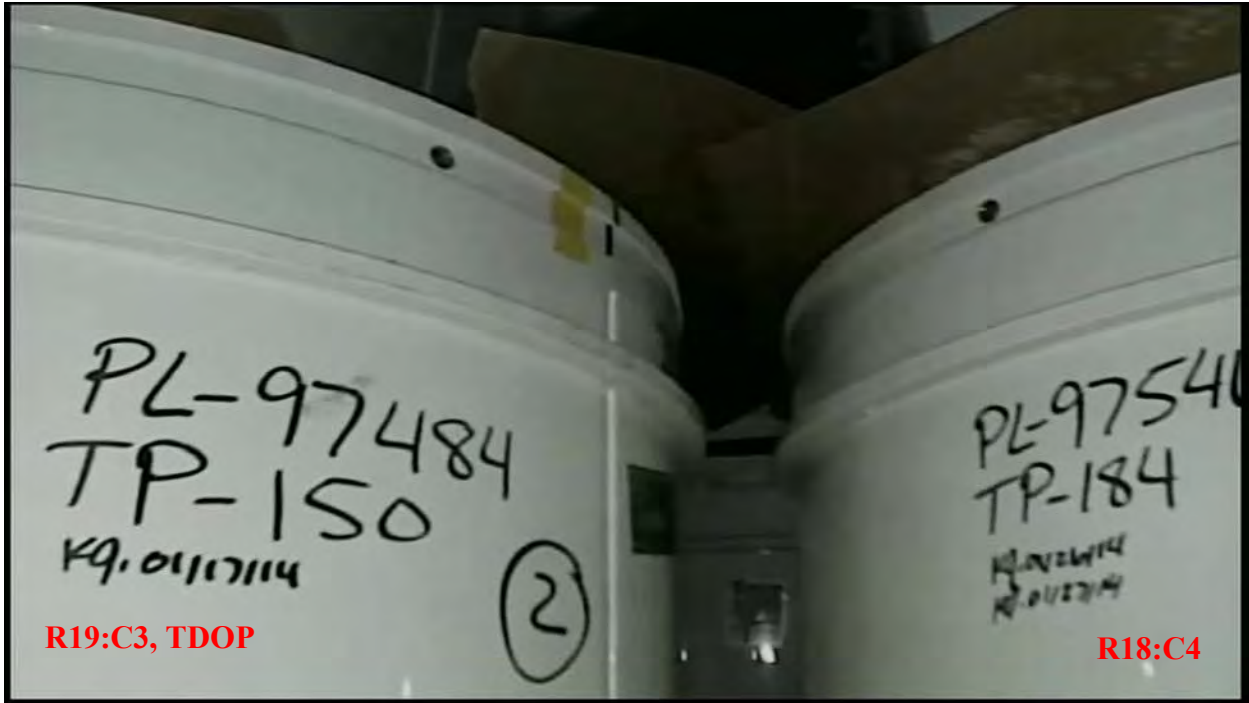
AIB-FST-10100: R18:C4 and R19:C3
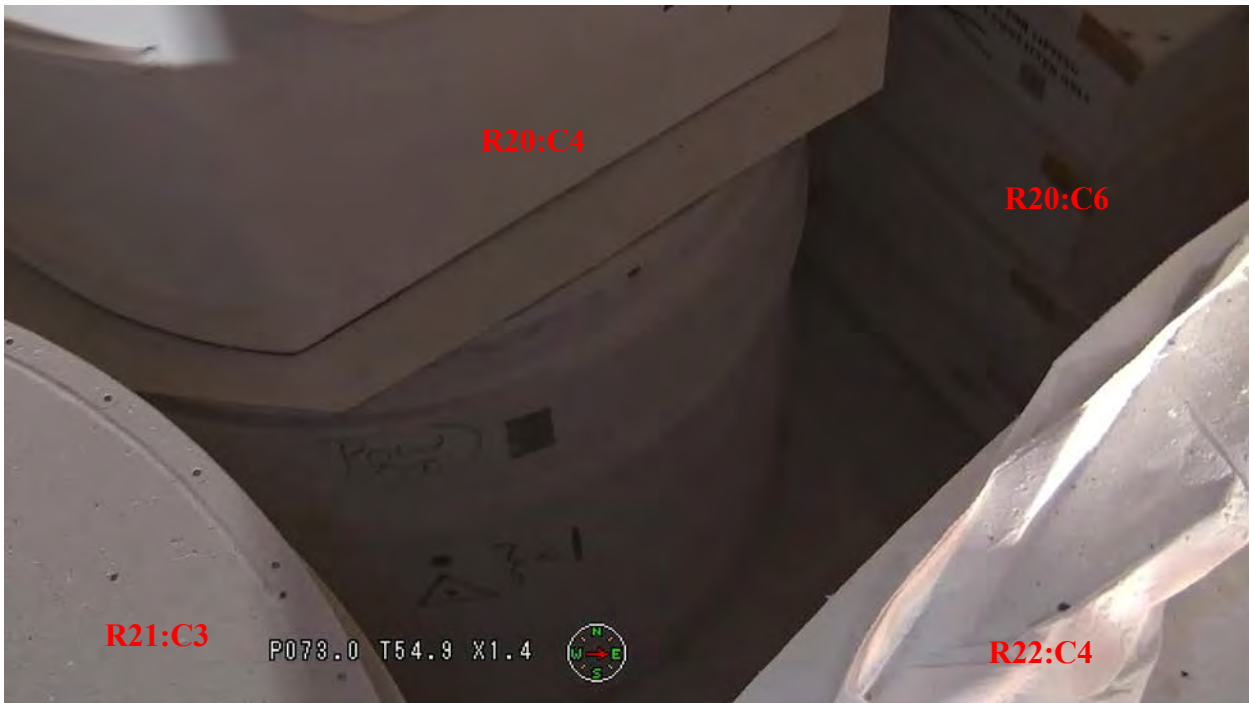
AIB-FST-10101

AIB-FST-10102

AIB-FST-10103.

AIB-FST-10104

AIB-FST-10105

AIB-FST-10106

AIB-FST-10107: R4:C2 and R5:C3

AIB-FST-10108

AIB-FST-10109

AIB-FST-10110
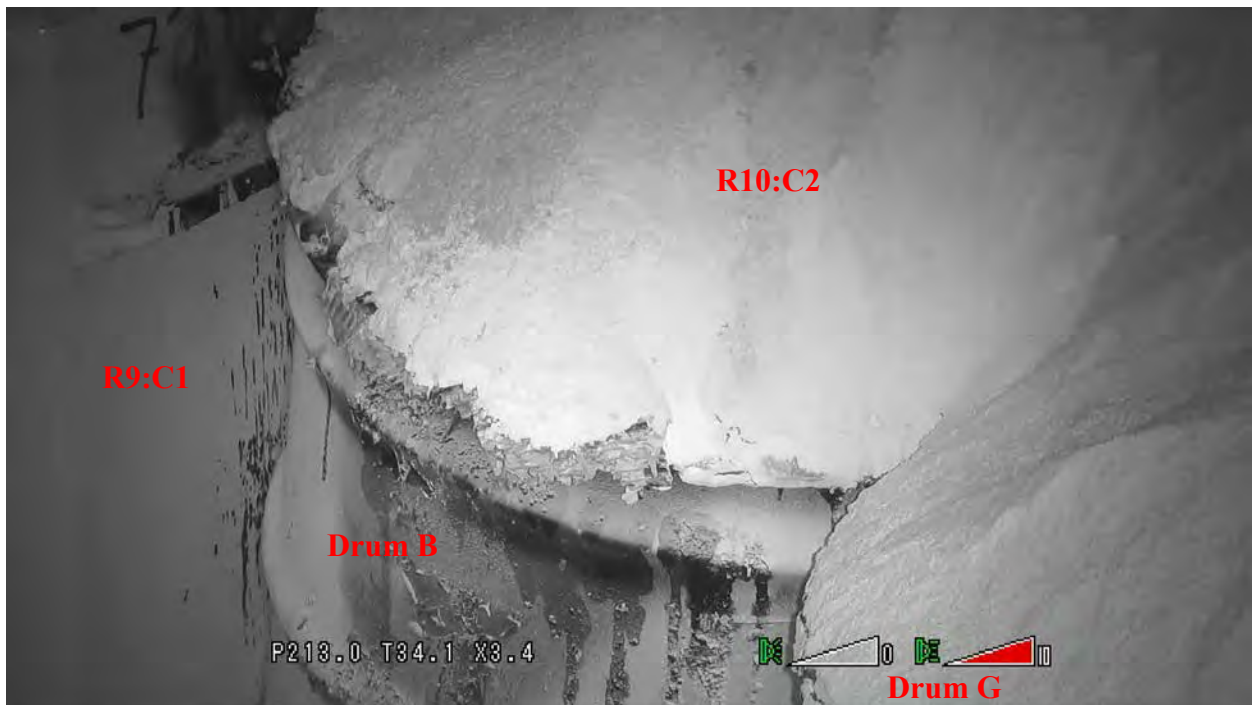
AIB-FST-10111: R10:C2 – Drum B

AIB-FST-10112
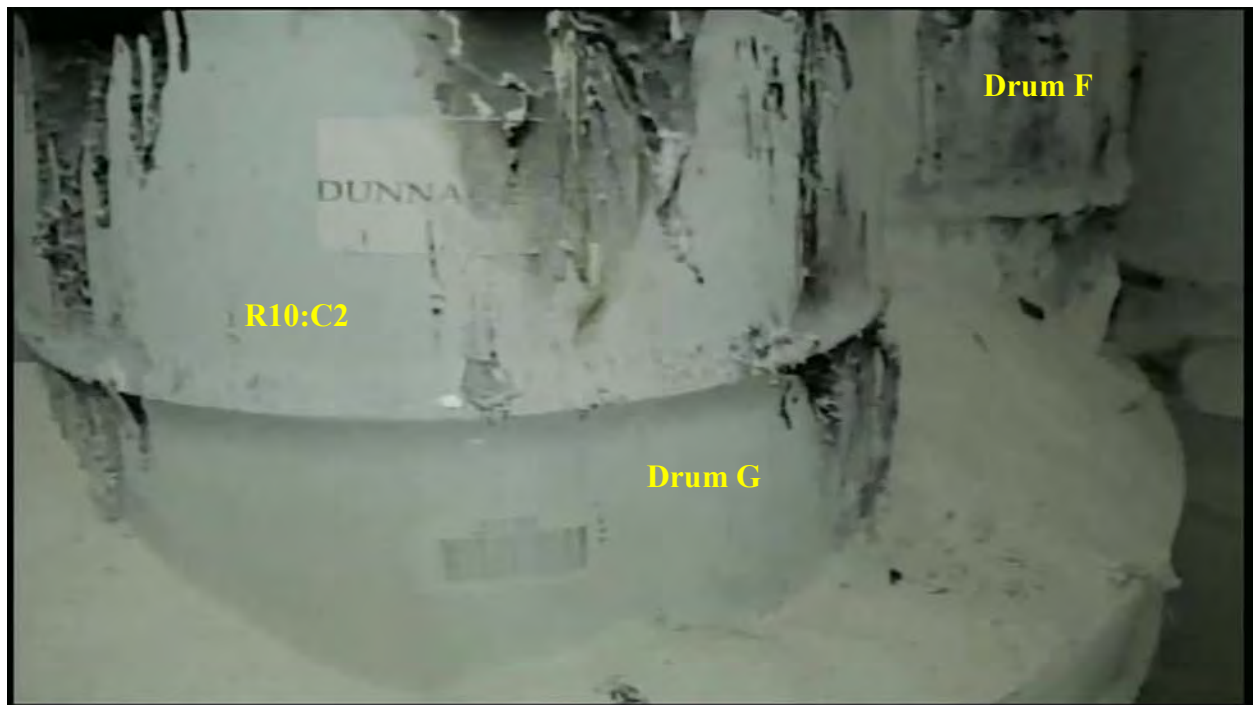
AIB-FST-10113: R10:C2 – Drum G dunnage label

AIB-FST-10114: R10:C2 and R12:C2

AIB-FST-10115

AIB-FST-10116

AIB-FST-10117

AIB-FST-10118

AIB-FST-10119
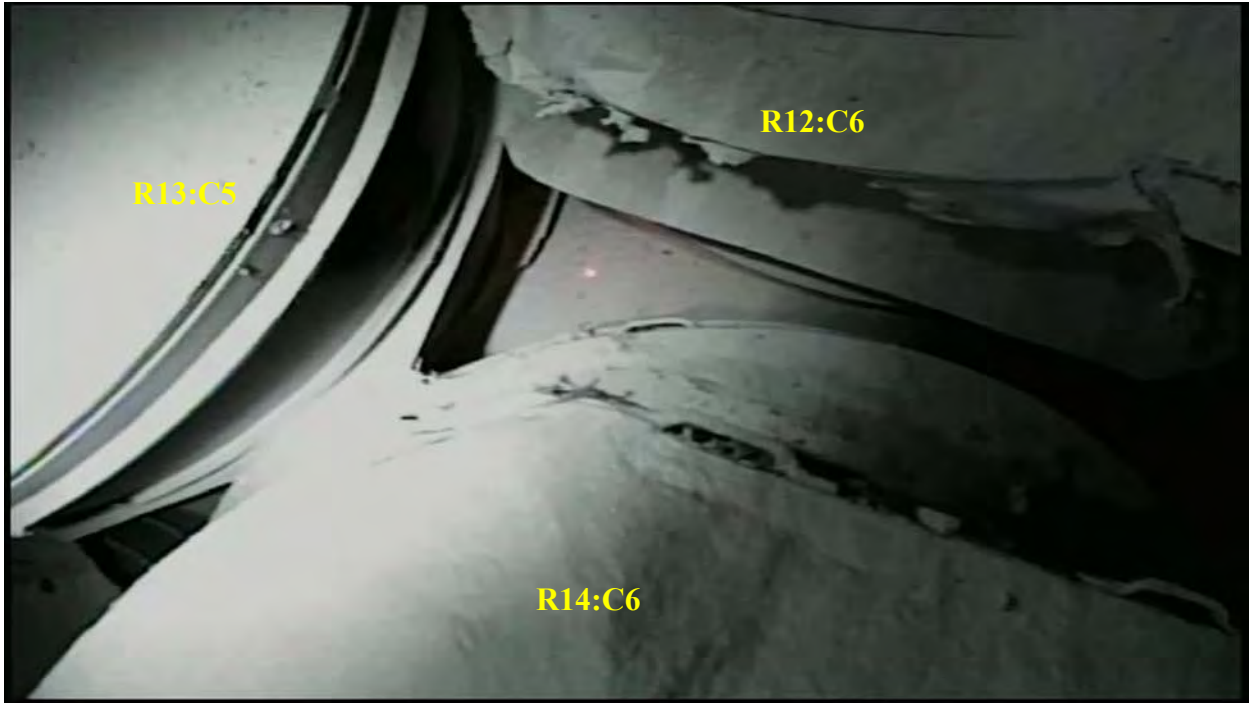
AIB-FST-10120

AIB-FST-10121: R12:C6 and R13:C5 – Damage to SWB from super sack fabric burn

AIB-FST-10122: R12:C6 and R13:C5 – Underside of slip sheets

AIB-FST-10123: R13:C5 and R14:C6 – Damage to slip sheet

R12:C4

R13:C5

R14:C4

AIB-FST-10124

R13:C5:top

R12:C4

R14:C4
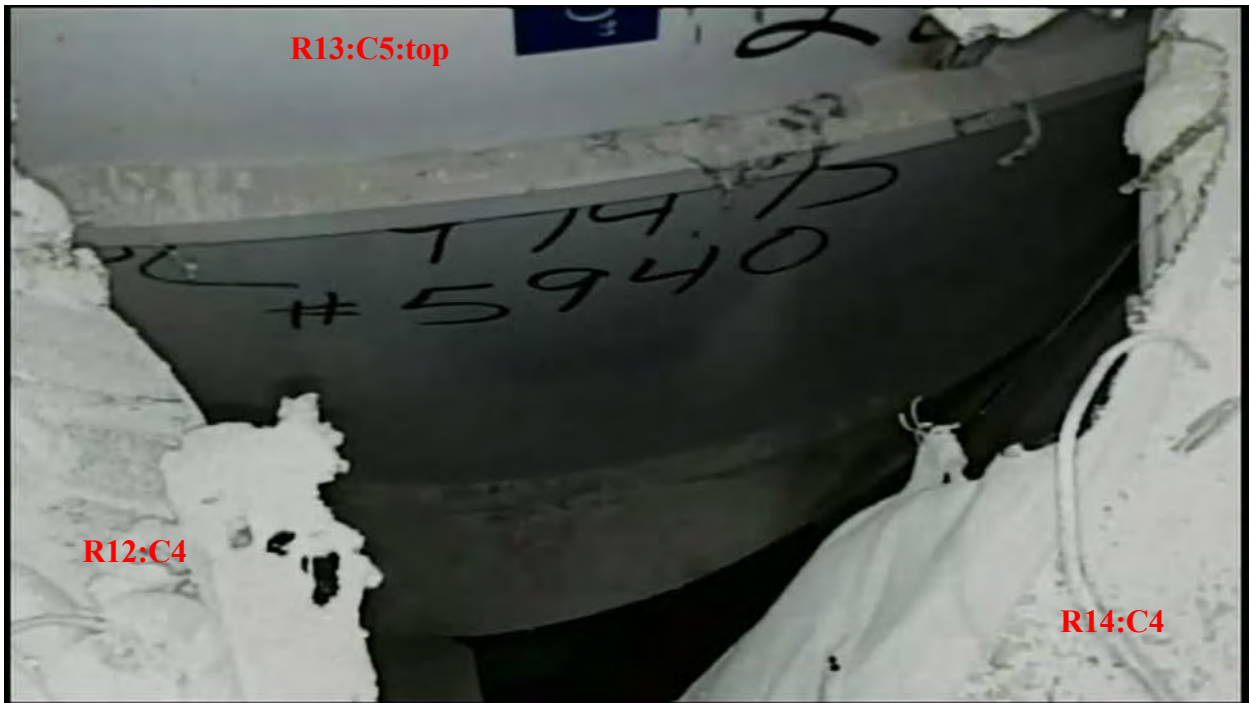
AIB-FST-10125

AIB-FST-10126: R13:C5 – Underside of top-tier slip sheet

AIB-FST-10127

AIB-FST-10128: R13:C5 – Charred stiffener on SWB lid

AIB-FST-10129: R15:C5 – Array face (west) view

AIB-FST-10130: R15:C5 – Array face (west) view

AIB-FST-10135: R15:C5:mid – Array face (west) view
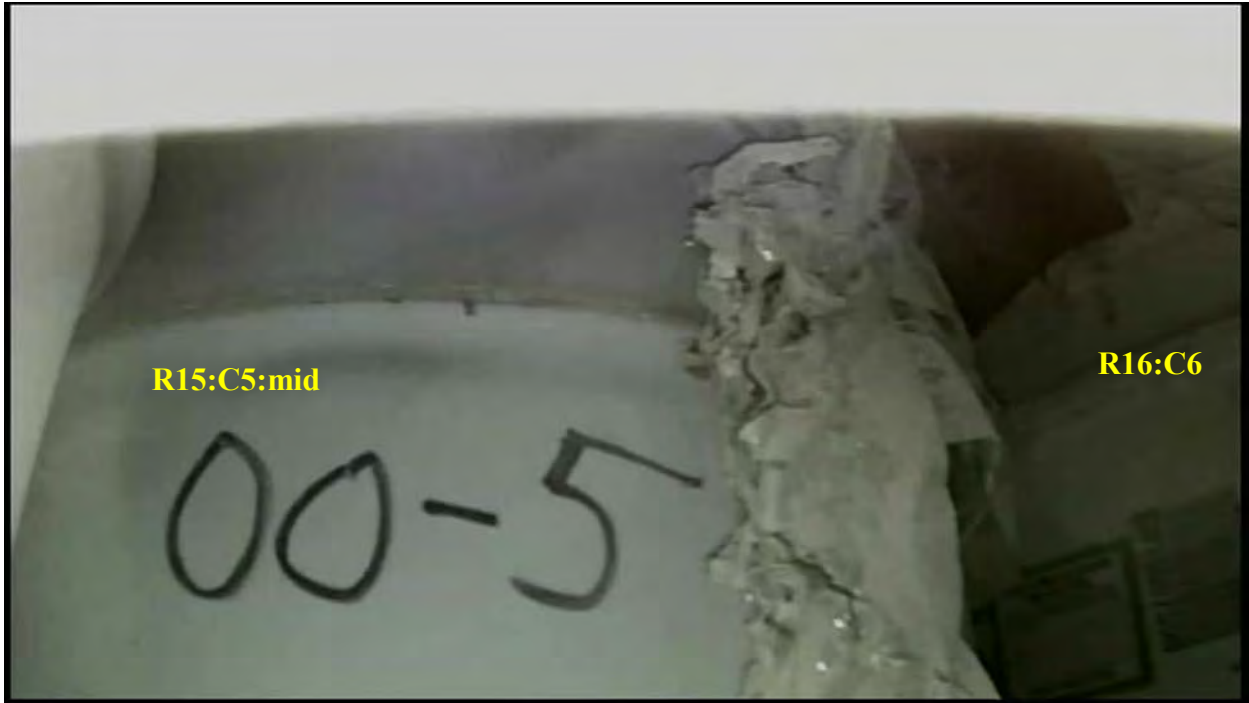
AIB-FST-10136: R15:C5 and R16:C6

AIB-FST-10137: R15:C5 – Top of middle tier reinforcement plate - bulkhead (east) view

AIB-FST-10138

AIB-FST-10139

AIB-FST-10140

AIB-FST-10141

AIB-FST-10142: R9:C1 and R10:C2
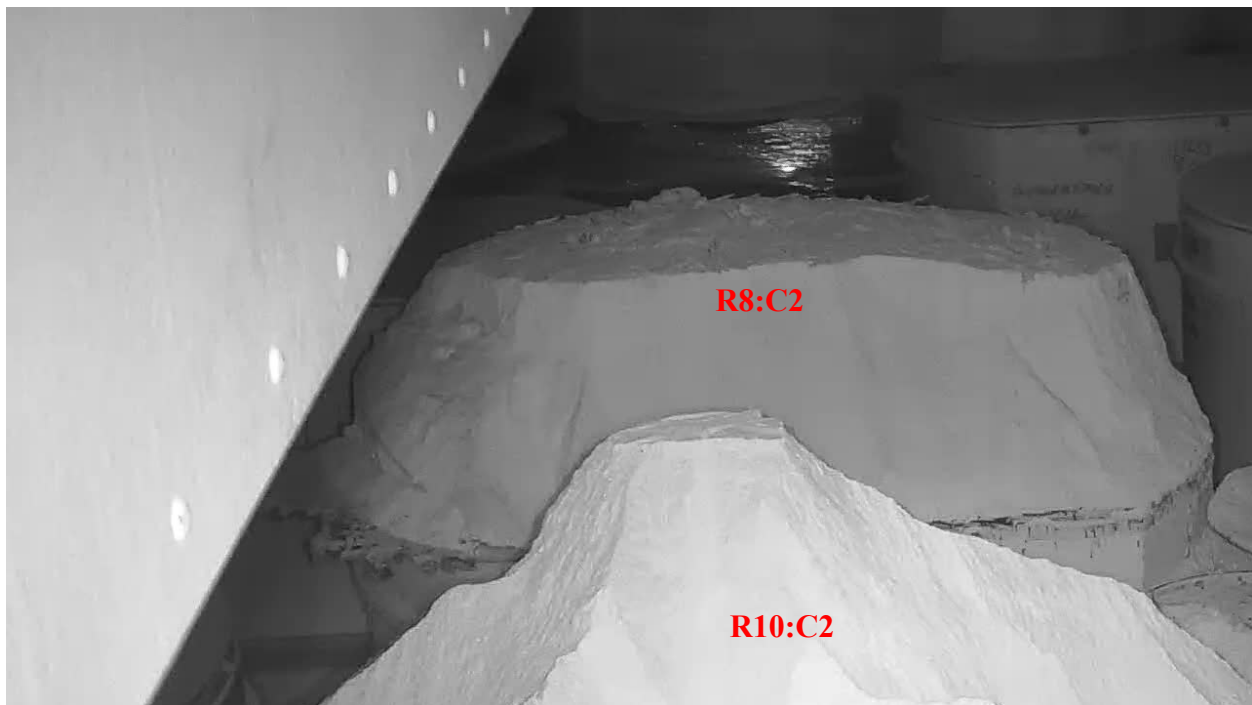
AIB-FST-10143: R8:C2 and R10:C2

AIB-FST-10144: R7:C1 and R8:C2

AIB-FST-10145

AIB-FST-10146: R8:C2 – Bulkhead (east) view

AIB-FST-10147

AIB-FST-10148

AIB-FST-10149: R8:C2 and R9:C1

AIB-FST-10150

AIB-FST-10163

AIB-FST-10164: R2:C6 and R3:C5

AIB-FST-10165: R2:C6 and R3:C5

AIB-FST-10166

AIB-FST-10167: R15:C5 and R16:C4 – Debris on SWB lid

AIB-FST-10168
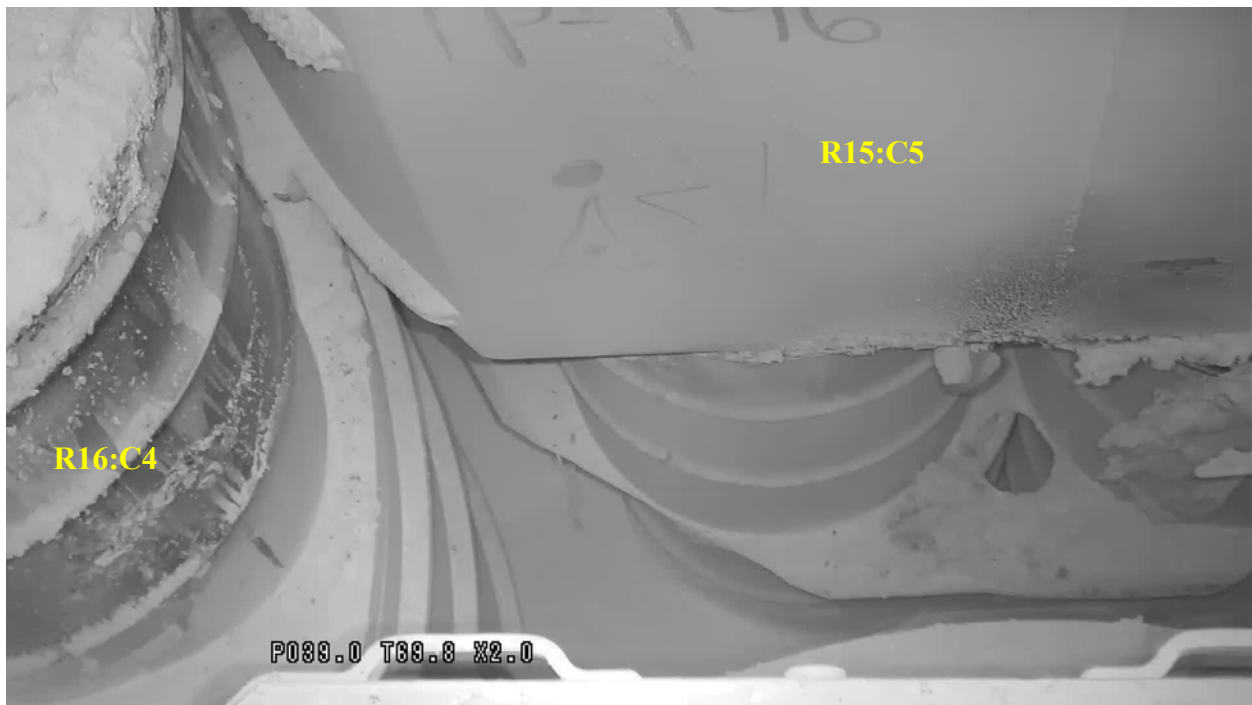
AIB-FST-10169: R15:C5 and R16:C4

AIB-FST-10170

AIB-FST-10171
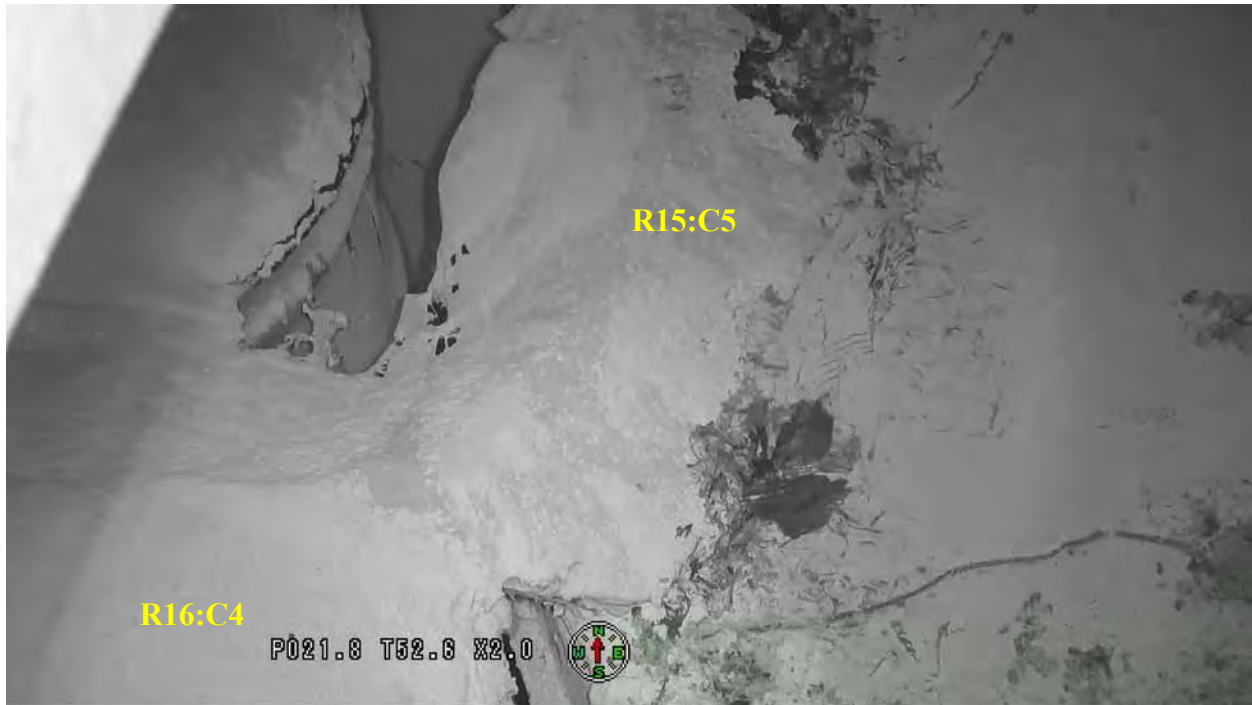
AIB-FST-10172: R15:C5 and R16:C4 – Top of SWB lid

AIB-FST-10173

AIB-FST-10174

AIB-FST-10177

AIB-FST-10179: R2:C6 and R3:C5

AIB-FST-10183: R13:C5 and R15:C5

AIB-FST-10184: R15:C5 - Bulkhead (east) view

AIB-FST-10185: R14:C4 and R15:C5

AIB-FST-10186

AIB-FST-10187

AIB-FST-10197: R22:C6 and R23:C5

AIB-FST-10198

AIB-FST-10199

AIB-FST-10200

AIB-FST-10201: R16:C6 - Mg slumped against south rib

AIB-FST-10202: R16:C6 and R17:C5
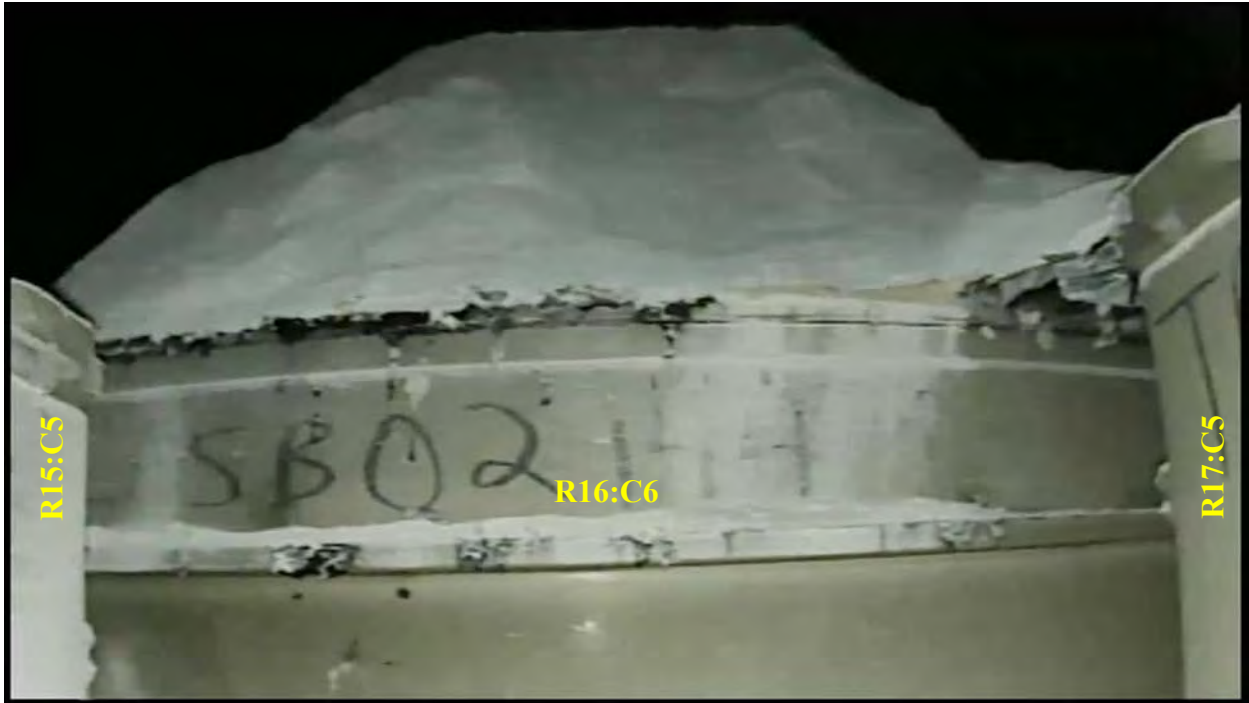
AIB-FST-10203

AIB-FST-10204

AIB-FST-10205

AIB-FST-10206

AIB-FST-10207: R15:C5, R16:C6, and R17:C5 – Mg buildup on floor

AIB-FST-10208

AIB-FST-10209: R16:C6

AIB-FST-10210: R14:C6 and R16:C6

AIB-FST-10211: R16:C6 and R18:C6
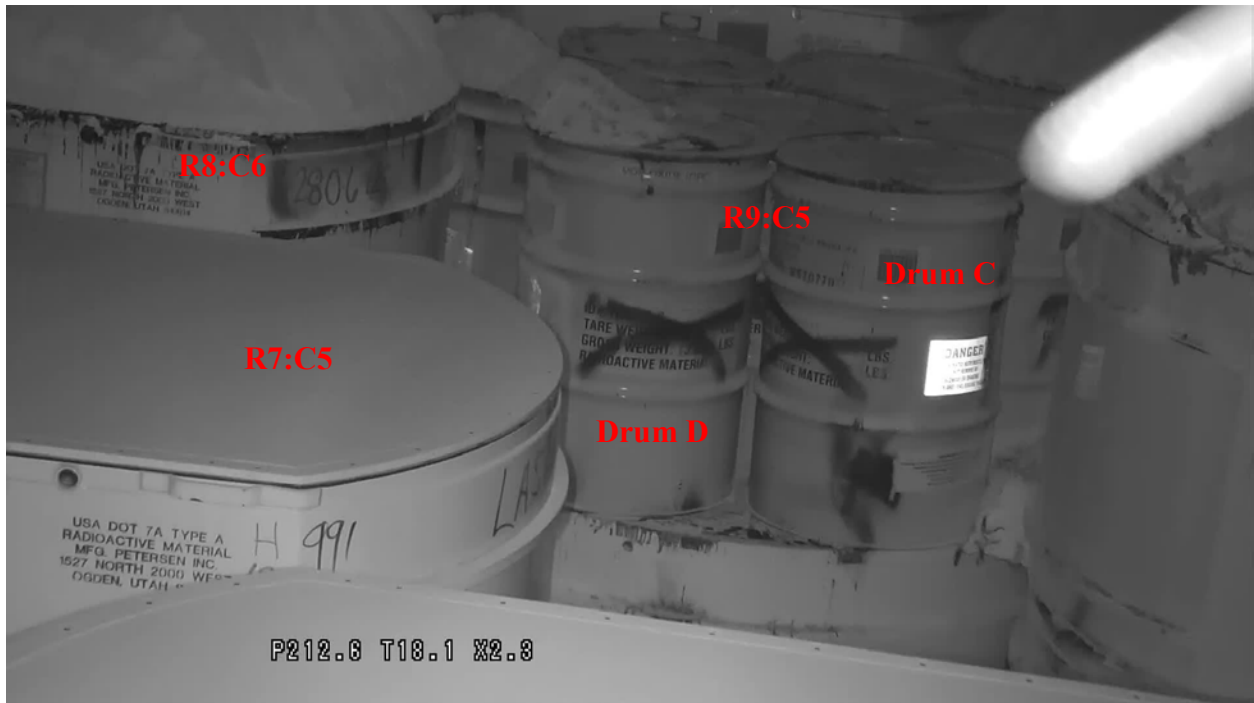
AIB-FST-10212

AIB-FST-10213

AIB-FST-10214

AIB-FST-10215

AIB-FST-10216

AIB-FST-10217: R11:C3 and R12:C2

AIB-FST-10218

AIB-FST-10219

AIB-FST-10220: R11:C3 and R13:C3

AIB-FST-10221: R11:C3 and R12:C4 – Underside of cardboard stiffener bridge

AIB-FST-10222: R11:C3 – Underside of cardboard stiffener bridge
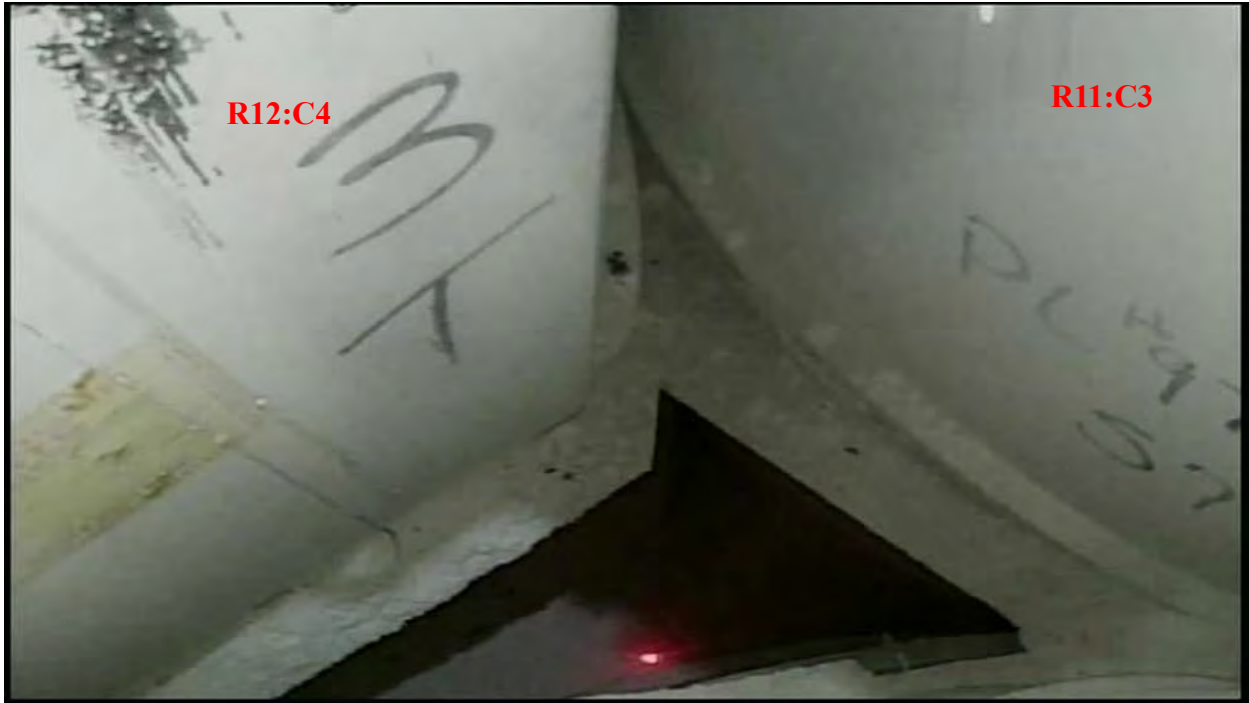
AIB-FST-10223: R11:C3 and R12:C4

AIB-FST-10224: R10:C4 and R11:C3

AIB-FST-10225: R11:C3 - South view

AIB-FST-10226: R10:C4, R11:C3 and R12:C4 – Mg buildup on floor

AIB-FST-10227

AIB-FST-10228
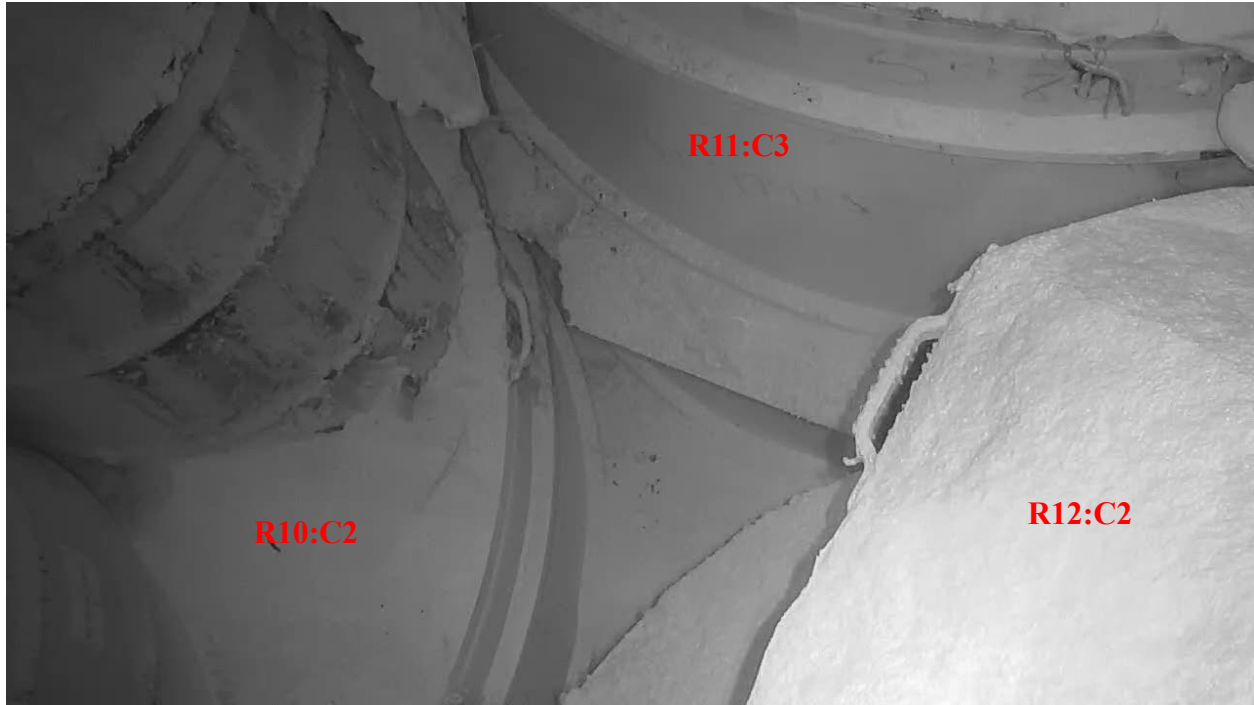
AIB-FST-10229

AIB-FST-10230: R5:C3 and R7:C3

AIB-FST-10231

AIB-FST-10232

AIB-FST-10233

AIB-FST-10234: R11:C5 – Bulkhead (east) view

AIB-FST-10235: R11:C5 and R12:C6

AIB-FST-10236: R11:C5 and R12:C6

AIB-FST-10237: R5:C3:top – Rock bolt retaining plate and plastic retaining ring

AIB-FST-10238: R5:C3 – Rock bolt retaining rings

AIB-FST-10239

AIB-FST-10240: R17:C1 and R18:C2

AIB-FST-10241
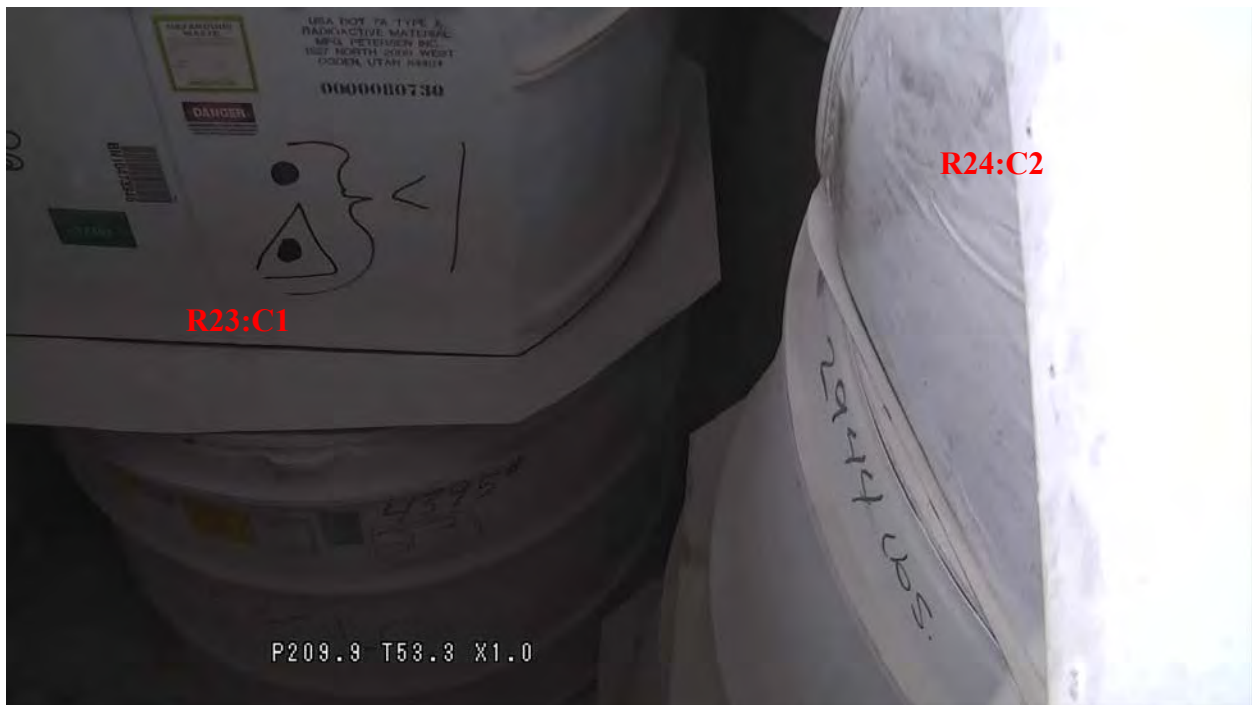
AIB-FST-10243: R23:C1 and R24:C2

AIB-FST-10244: R23:C1 and R24:C2

AIB-FST-10245: R23:C1 and north rib

AIB-FST-10246: R15:C1 and R17:C1

AIB-FST-10247: R14:C2 and R15:C1

AIB-FST-10248: R13:C1 and R15:C1

AIB-FST-10249

AIB-FST-10251: R15:C3 - Top tier

AIB-FST-10252: R13:C3 and R15:C3

AIB-FST-10253: R14:C2 and R15:C3 – Cardboard stiffener bridge

AIB-FST-10254
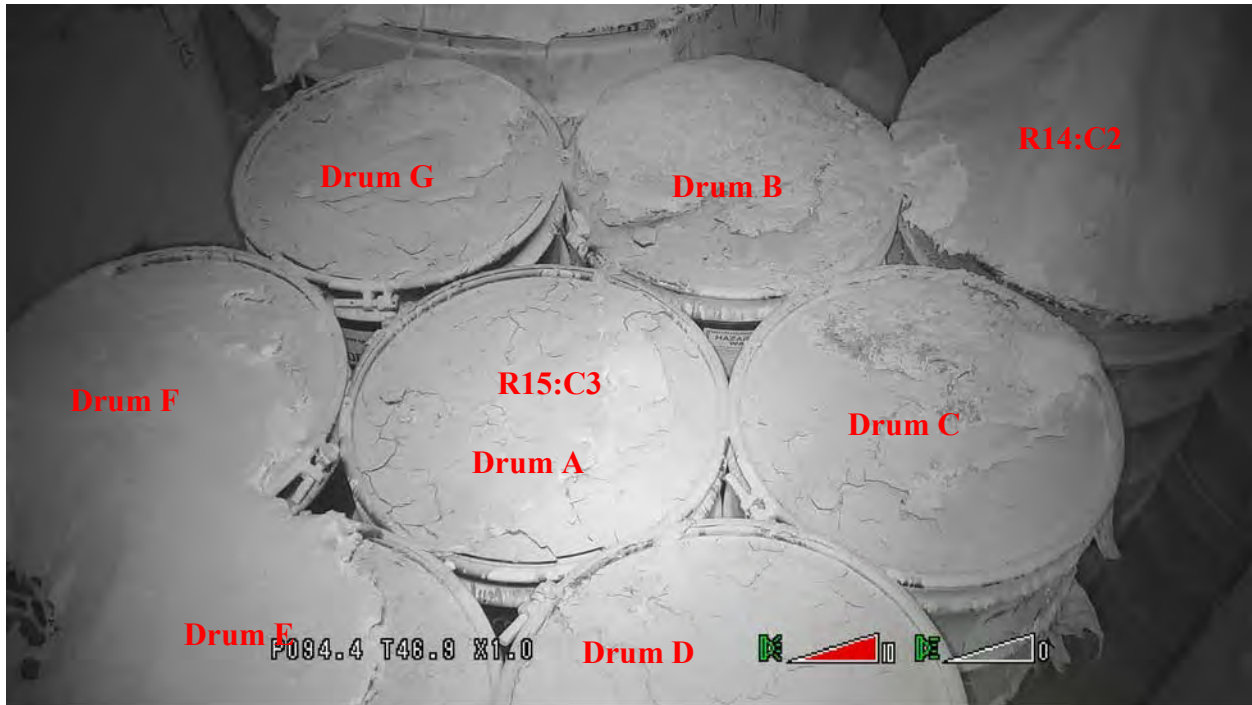
AIB-FST-10255 R14:C2 and R15:C3

AIB-FST-10256 – R15:C3 and R16:C4 – Cardboard stiffener bridge

AIB-FST-10257: R15:C3 and R16:C2 – Cardboard stiffener bridge

AIB-FST-10258
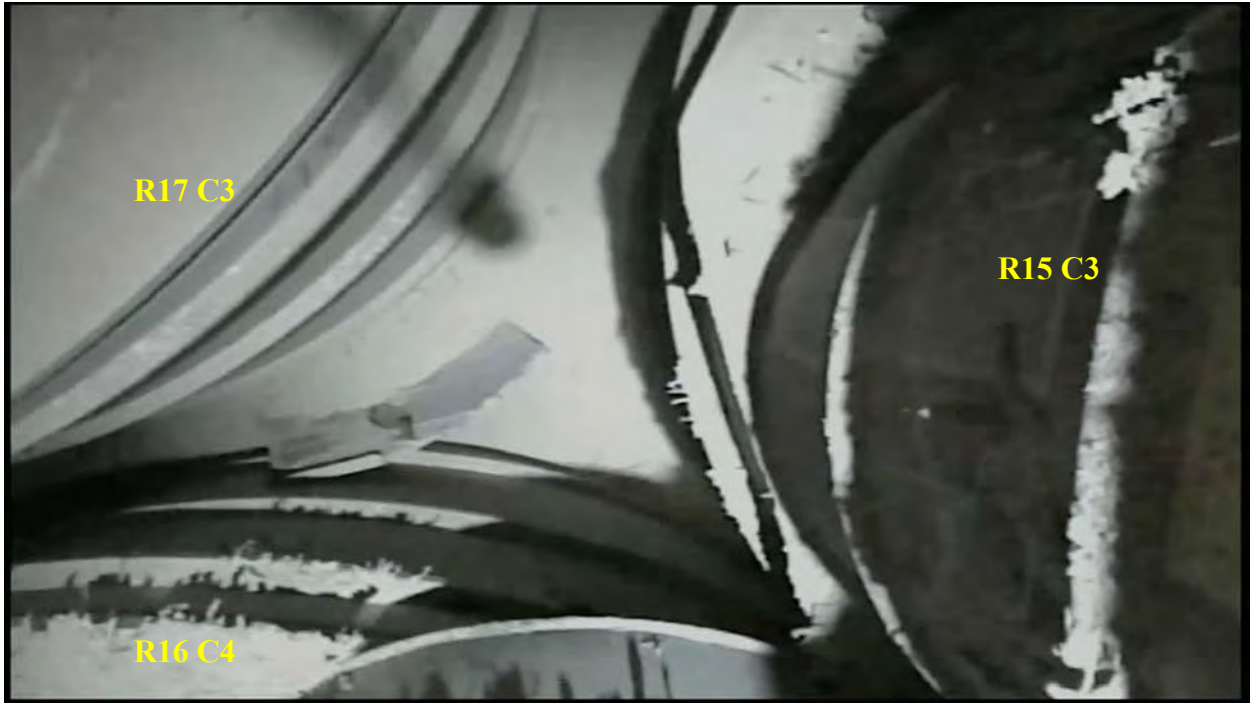
AIB-FST-10259

AIB-FST-10260: R15:C3 and R16:C2
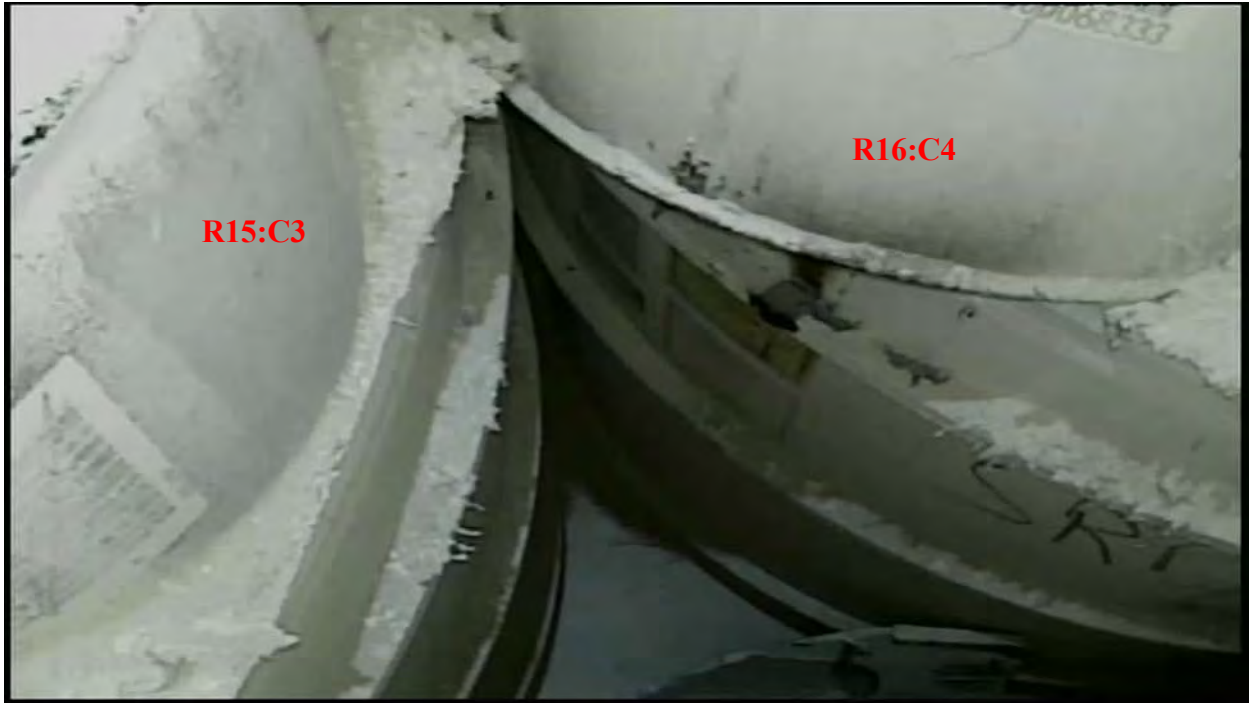
AIB-FST-10261: R15:C3 and R16:C4

AIB-FST-10263: R15:C3 and R14:C4

AIB-FST-10264

AIB-FST-10271: R14:C4 - Severe damage to MgO super sack

AIB-FST-10272: R14:C4 and R16:C4

AIB-FST-10273: R13:C5 and R14:C4 – Cardboard stiffener bridge

AIB-FST-10275: R14:C4 and R16:C4

AIB-FST-10276

AIB-FST-10277

AIB-FST-10278: R13:C5 and R14:C4 – Cardboard stiffener bridge

AIB-FST-10279: R14:C4 – Sample tool over residual MgO

AIB-FST-10280: R14:C4 and R16:C4

AIB-FST-10282: R14:C4 and R16:C4

AIB-FST-10284: R14:C4 – Charred stiffener

AIB-FST-10285: R14:C4 and R16:C4

AIB-FST-10290
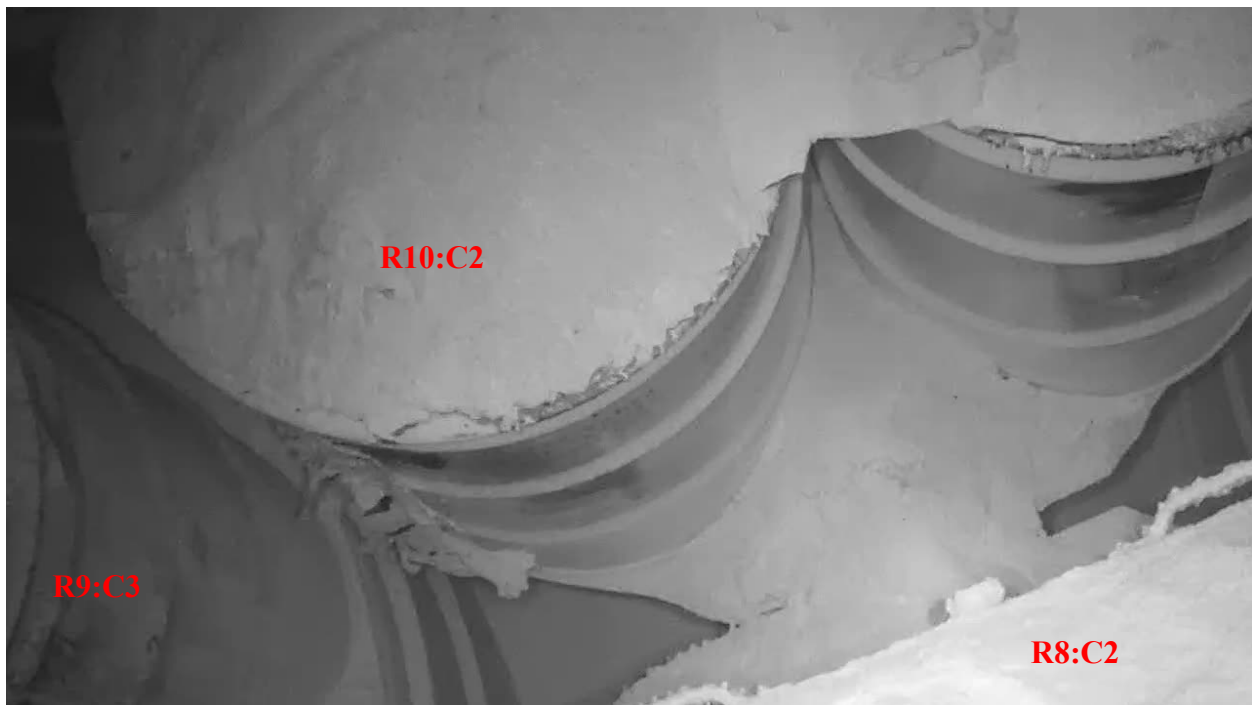
AIB-FST-10291

AIB-FST-10292

AIB-FST-10300: R17:C5 and R18:C6

AIB-FST-10301: R18:C6 – Array face (west) view

AIB-FST-10302

AIB-FST-10303: R18:C6 - Bulkhead view

AIB-FST-10305

AIB-FST-10306

AIB-FST-10308

AIB-FST-10309

AIB-FST-10310: R4:C6 - Top of MgO super sack

AIB-FST-10311

AIB-FST-10312

AIB-FST-10313

AIB-FST-10314

AIB-FST-10315: Roof bolts suspended by lanyards

AIB-FST-10316

AIB-FST-10317

AIB-FST-10318: R21:C5 and R22:C4

AIB-FST-10319: R20:C4, R21:C5 and R22:C4 – MgO buildup on floor,

AIB-FST-10322: Array face – West view

AIB-FST-10323: Array face – West view

AIB-FST-10324

AIB-FST-10327

AIB-FST-10328: Array face – Sample tool shown in foreground

AIB-FST-10329: Array face – Sample tool shown in foreground

AIB-FST-10330: R23:C1 and R24:C2

AIB-FST-10331: Array face

AIB-FST-10332: R22:C2 and R24:C2

AIB-FST-10333

AIB-FST-10334: R3:C5 and R4:C6

AIB-FST-10335: R3:C5 and R4:C6
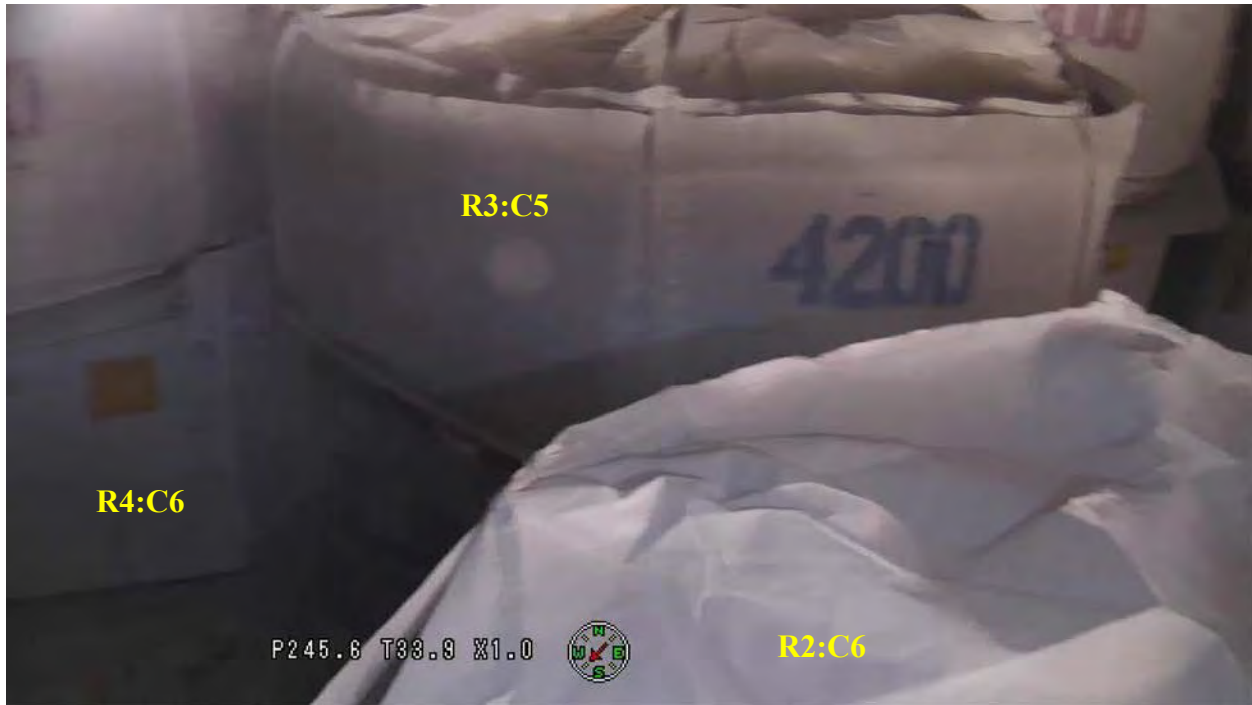
AIB-FST-10336
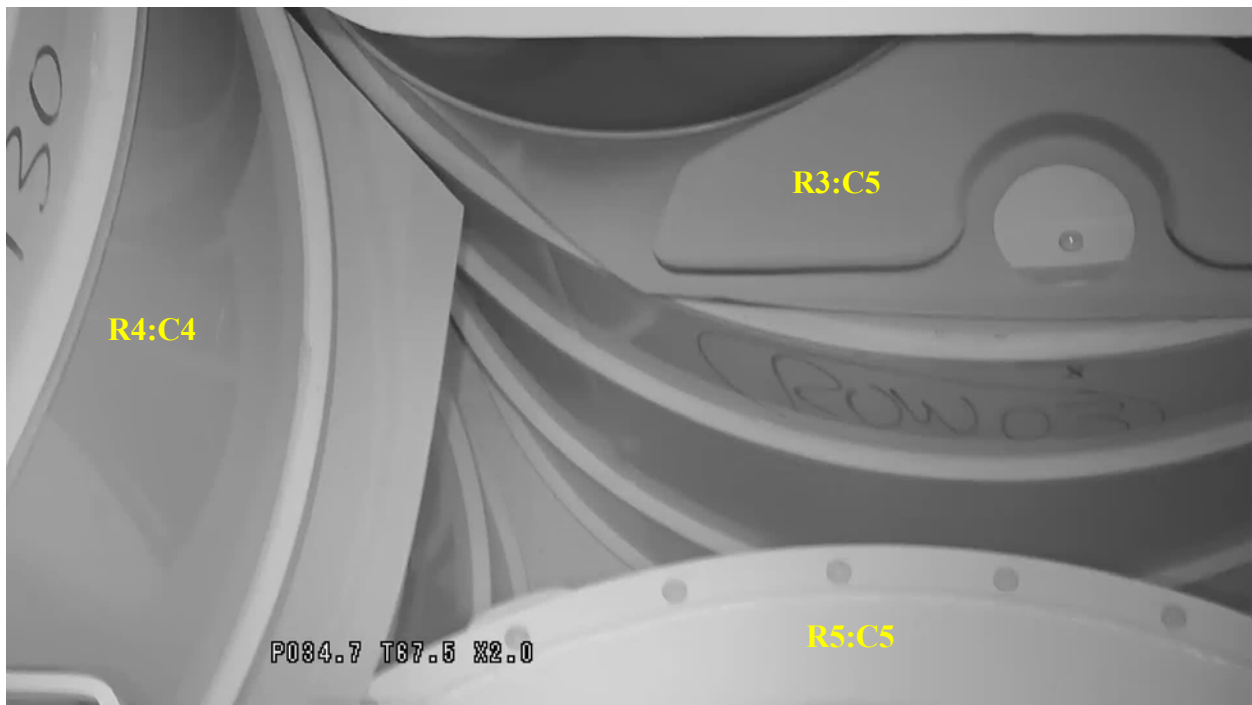
AIB-FST-10337

AIB-FST-10338: R3:C5 and R4:C4

AIB-FST-10339: Top of MgO super sack showing tied closure.

AIB-FST-10340

AIB-FST-10341: R2:C6 and R2:C5

AIB-FST-10342

AIB-FST-10344: R9:C5 and R10:C4

AIB-FST-10345: R9:C5 and R10:C4

AIB-FST-10346: R9:C5 and R10:C4

AIB-FST-10347: R10:C4 and R11:C5

AIB-FST-10350

AIB-FST-10351

AIB-FST-10352

AIB-FST-10353: R20:C6 and R21:C5

AIB-FST-10354: R18:C6 and R20:C6 – Pole was used for May 2014 inspections

AIB-FST-10355: R18:C6 and R20:C6

AIB-FST-10356: R18:C6 and R20:C6

AIB-FST-10357: R18:C6 and R20:C6
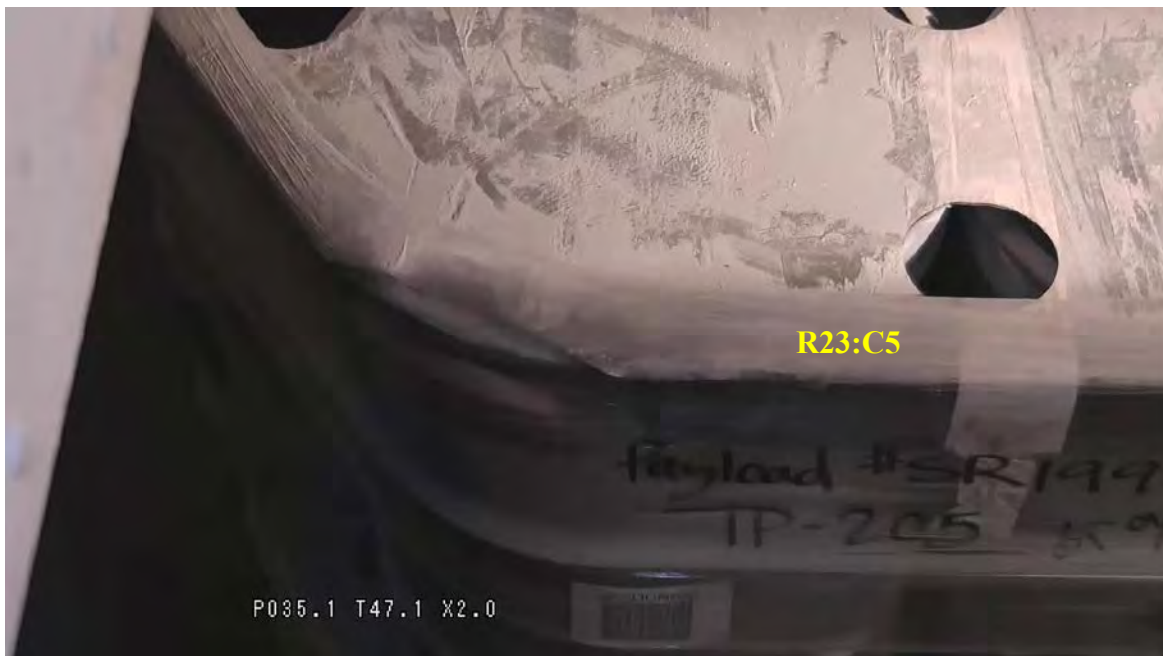
AIB-FST-10367: R23:C5 – Array face (west) view

AIB-FST-10368: R23:C5

AIB-FST-10369: R23:C5

AIB-FST-10370: R23:C5

AIB-FST-10371: R21:C5 and R23:C5

AIB-FST-10372

AIB-FST-10373: R15:c5 and R17:C5
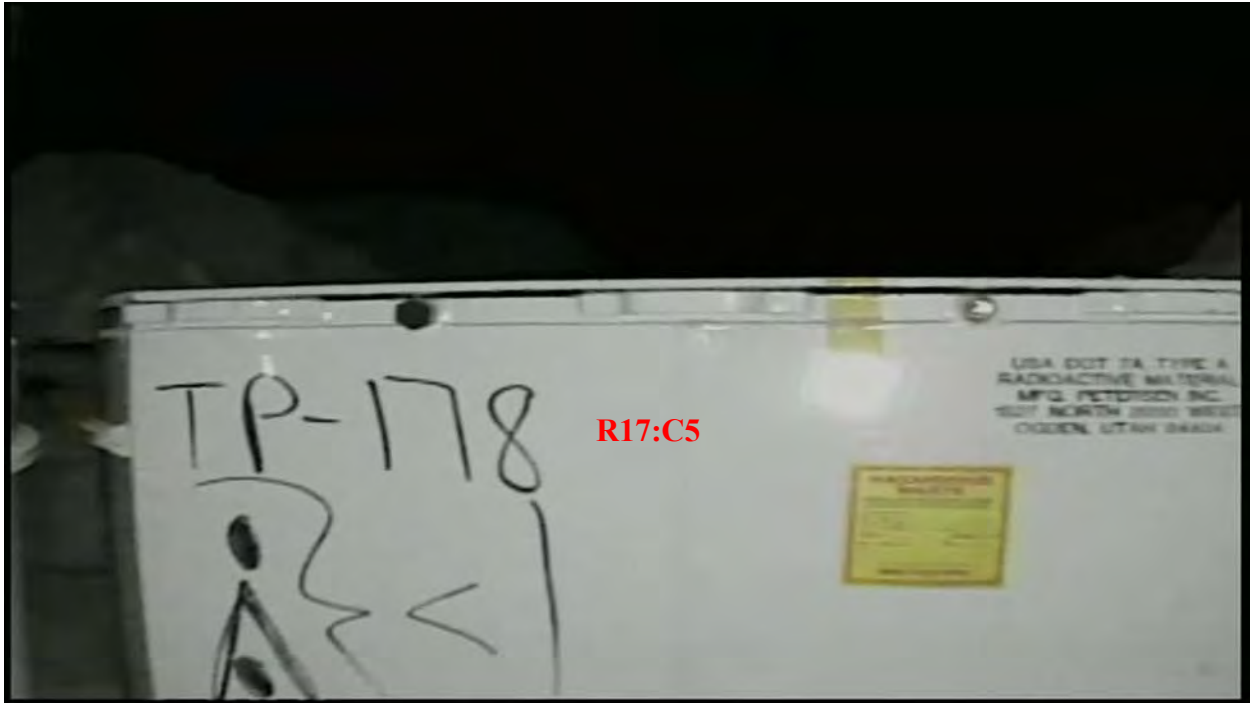
AIB-FST-10374: R17:C5 – Array face (west) view

AIB-FST-10375: R17:C5 and R18:C4
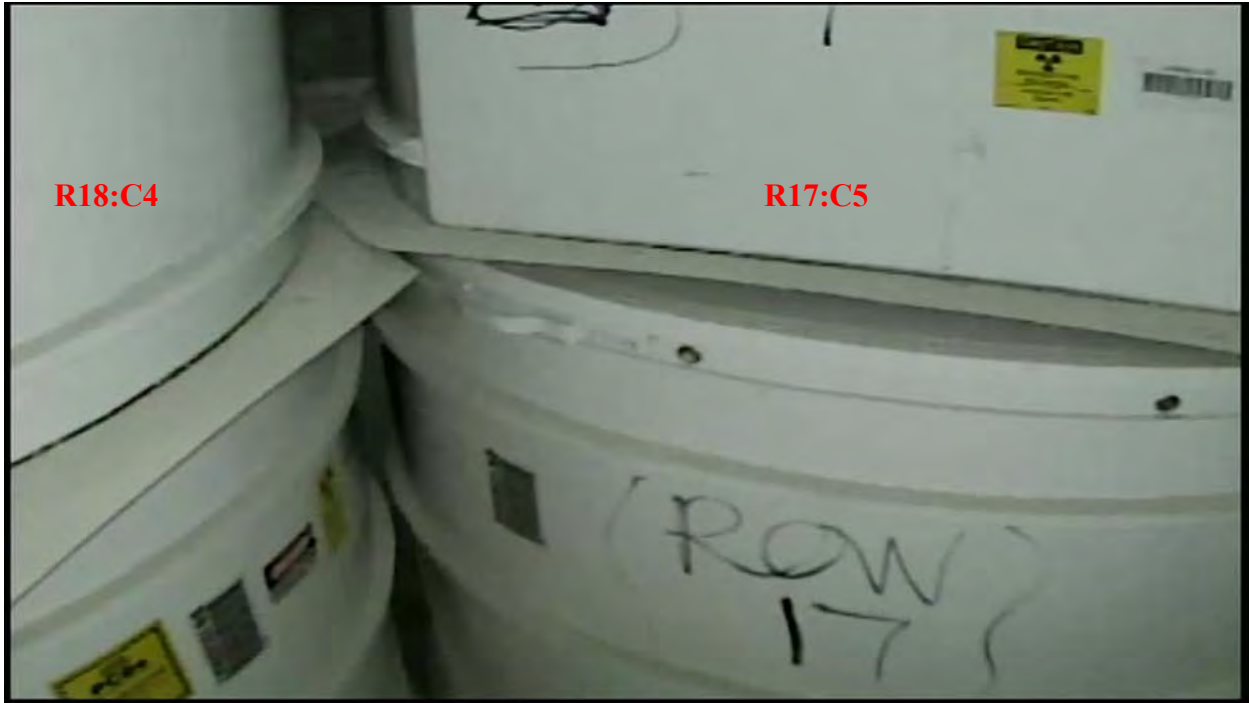
AIB-FST-10376: R17:C5 and R18:C4

AIB-FST-10377

AIB-FST-10378
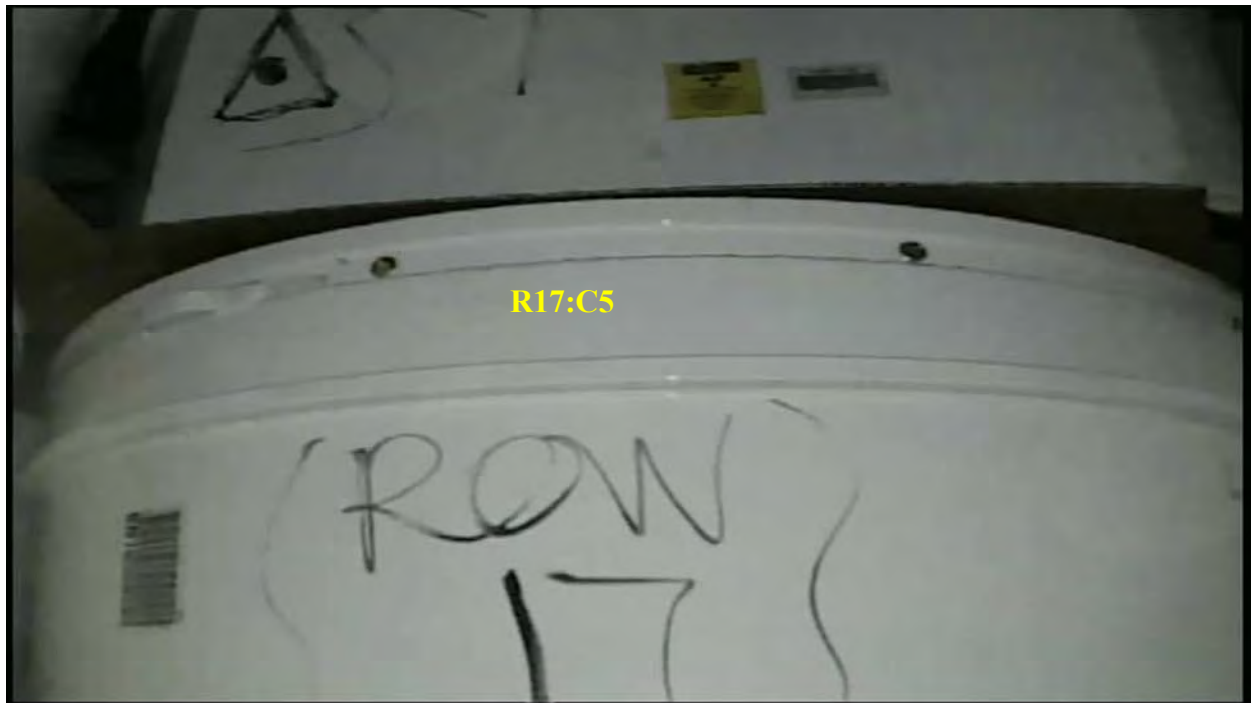
AIB-FST-10379: R17:C5 – Array face (west) view

AIB-FST-10380: R17:C5 and R18:C6

AIB-FST-10381: R17:C5 and R18:C6

AIB-FST-10382: R17:C5 – Array face (bulkhead) view
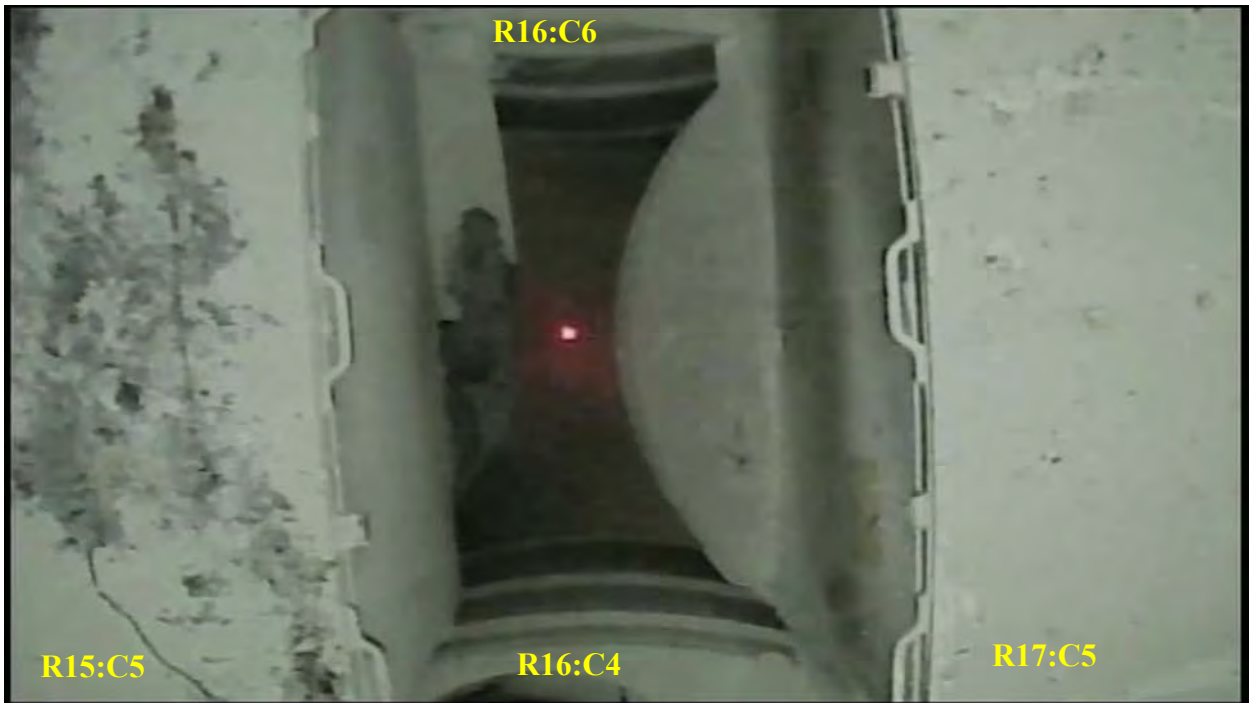
AIB-FST-10383
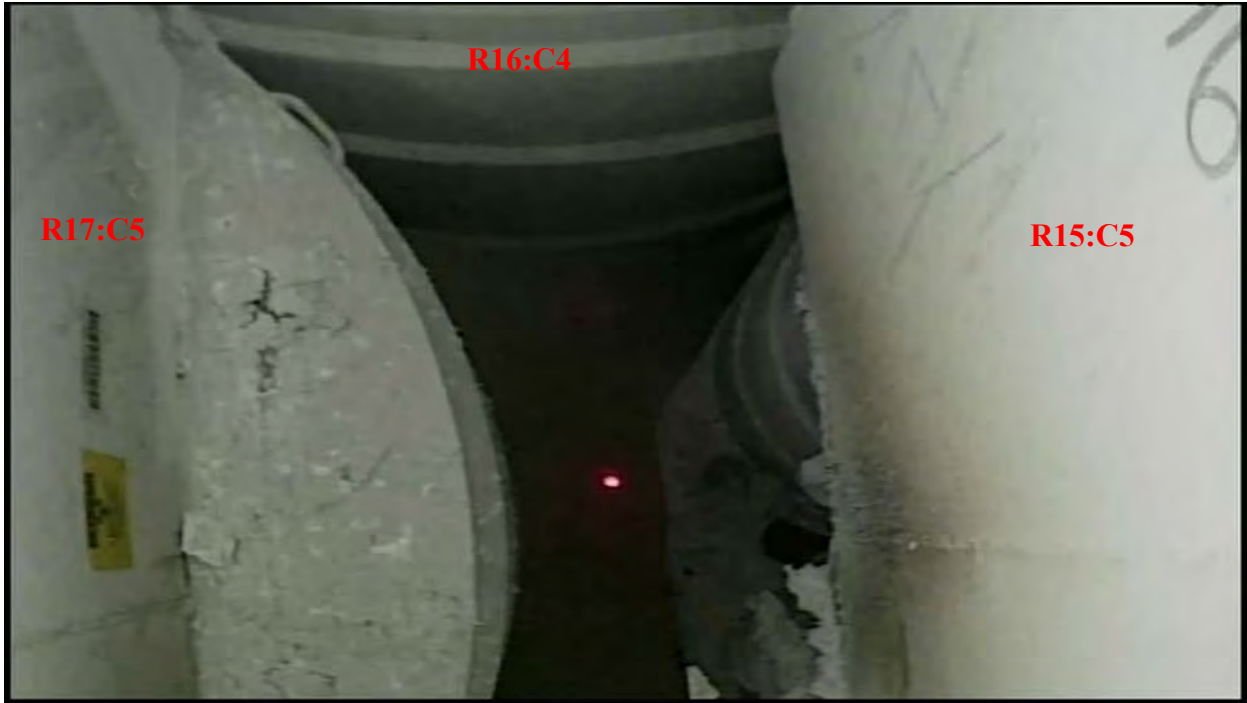
AIB-FST-10384

AIB-FST-10385: R17:C5

AIB-FST-10386: R15:C6 and R17:C5

AIB-FST-10387: R16:C4 and R17:C5

AIB-FST-10388

AIB-FST-10389
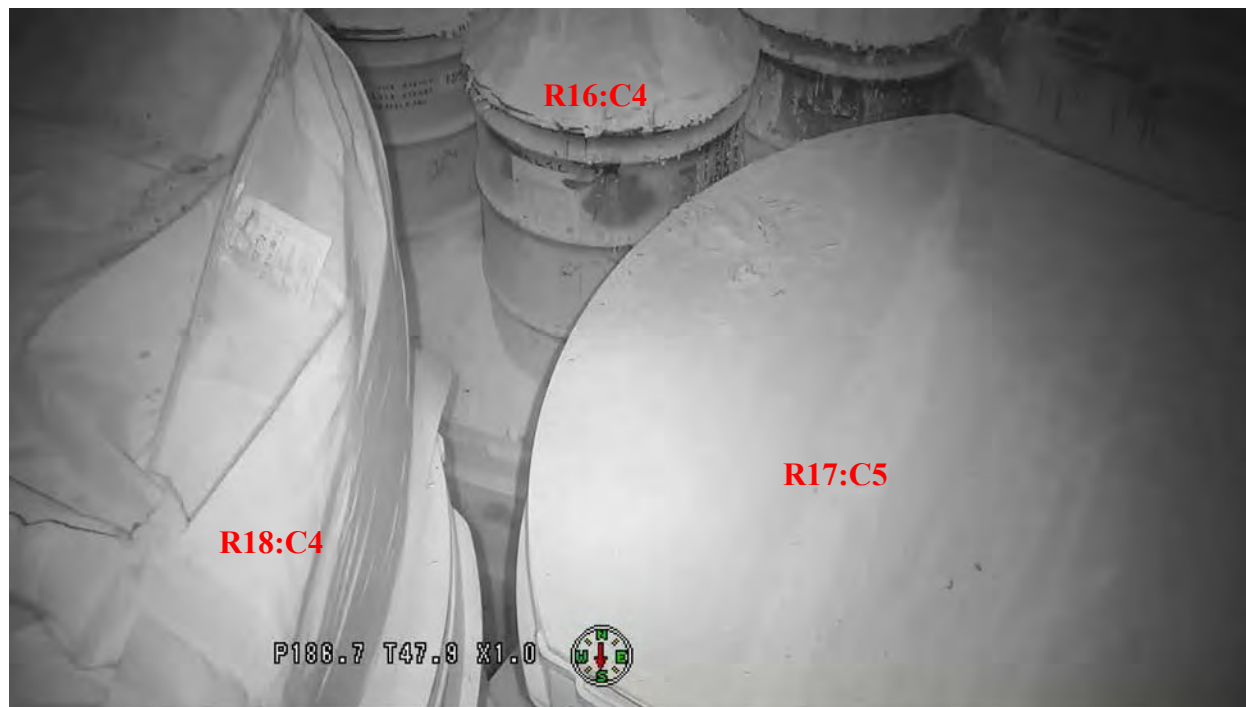
AIB-FST-10390

AIB-FST-10391: R16:C6 and R17:C5
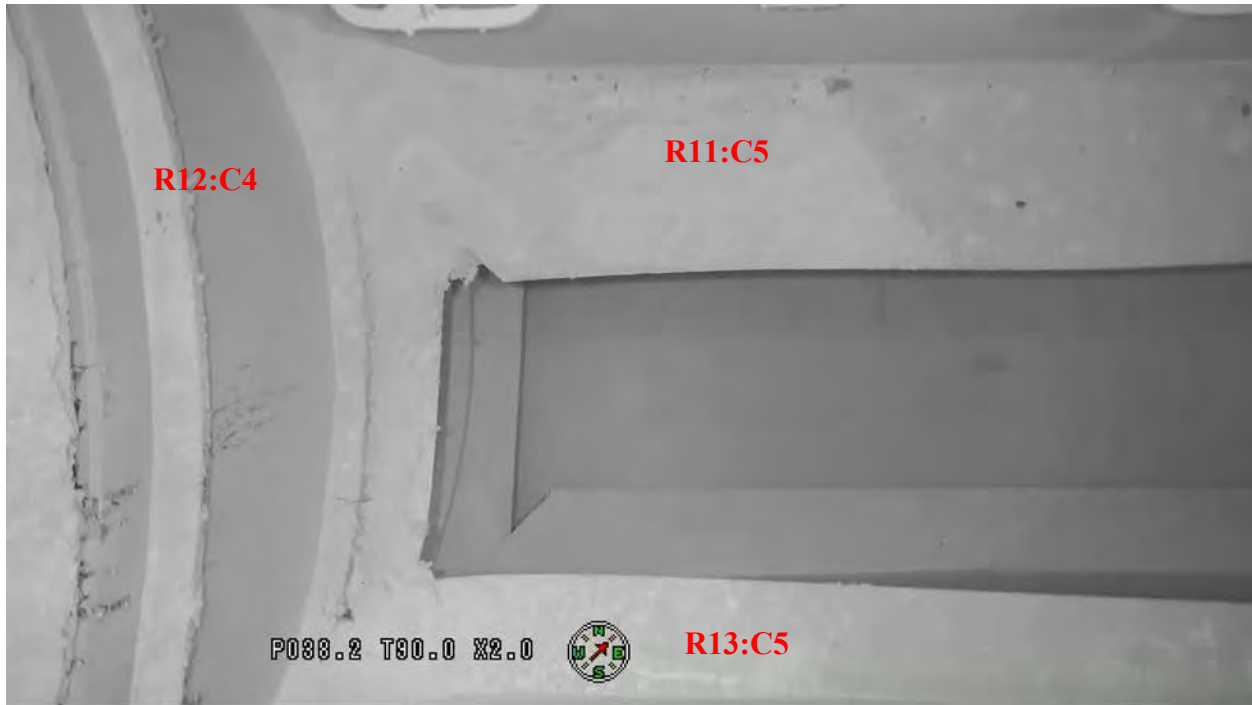
AIB-FST-10392
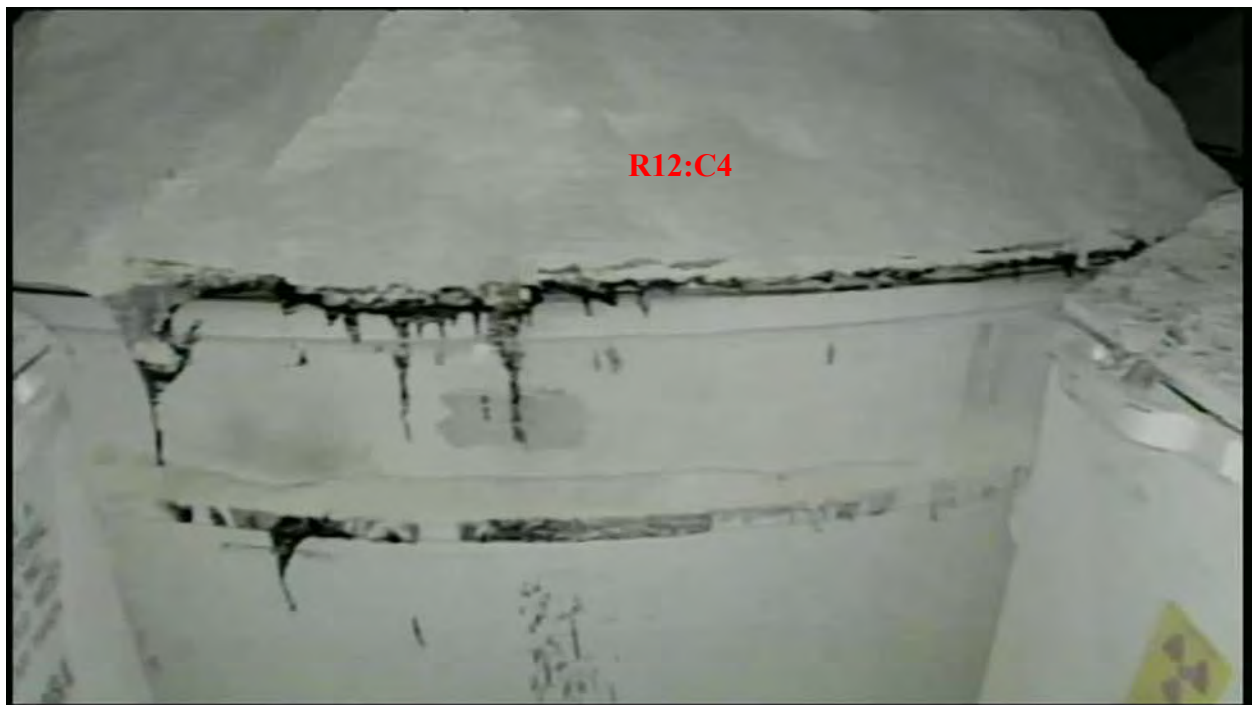
AIB-FST-10393: R12:C4 – South view
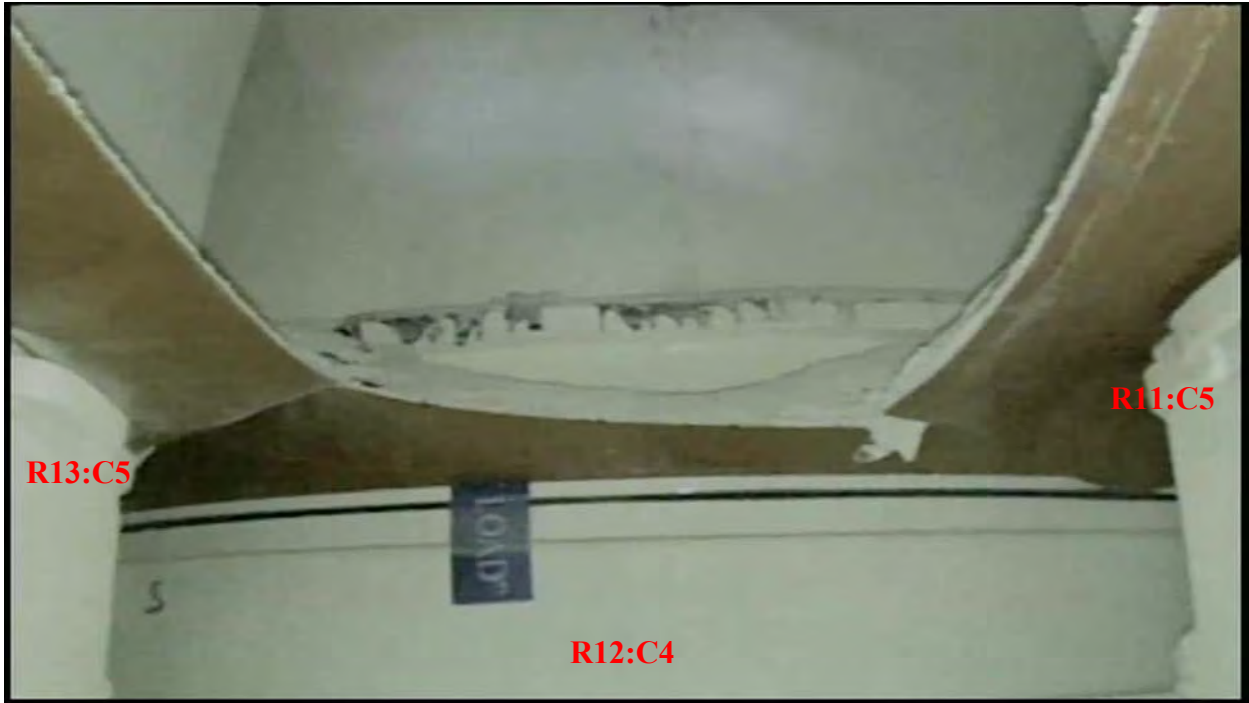
AIB-FST-10394
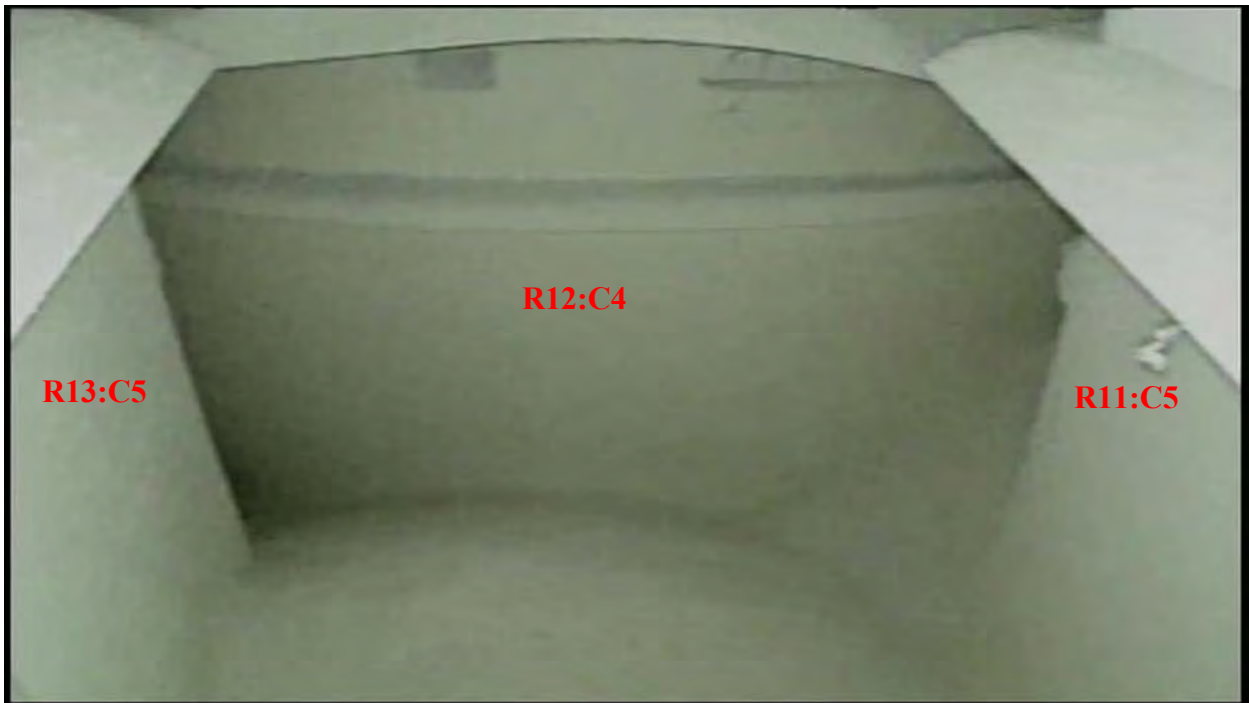
AIB-FST-10395

AIB-FST-10396

AIB-FST-10397

AIB-FST-10398

AIB-FST-10399

AIB-FST-10400

AIB-FST-10401: R12:C6

AIB-FST-10402: R12:C6 and R14:C6

AIB-FST-10403: R11:C5 and R12:C6

AIB-FST-10404

AIB-FST-10405

AIB-FST-10406
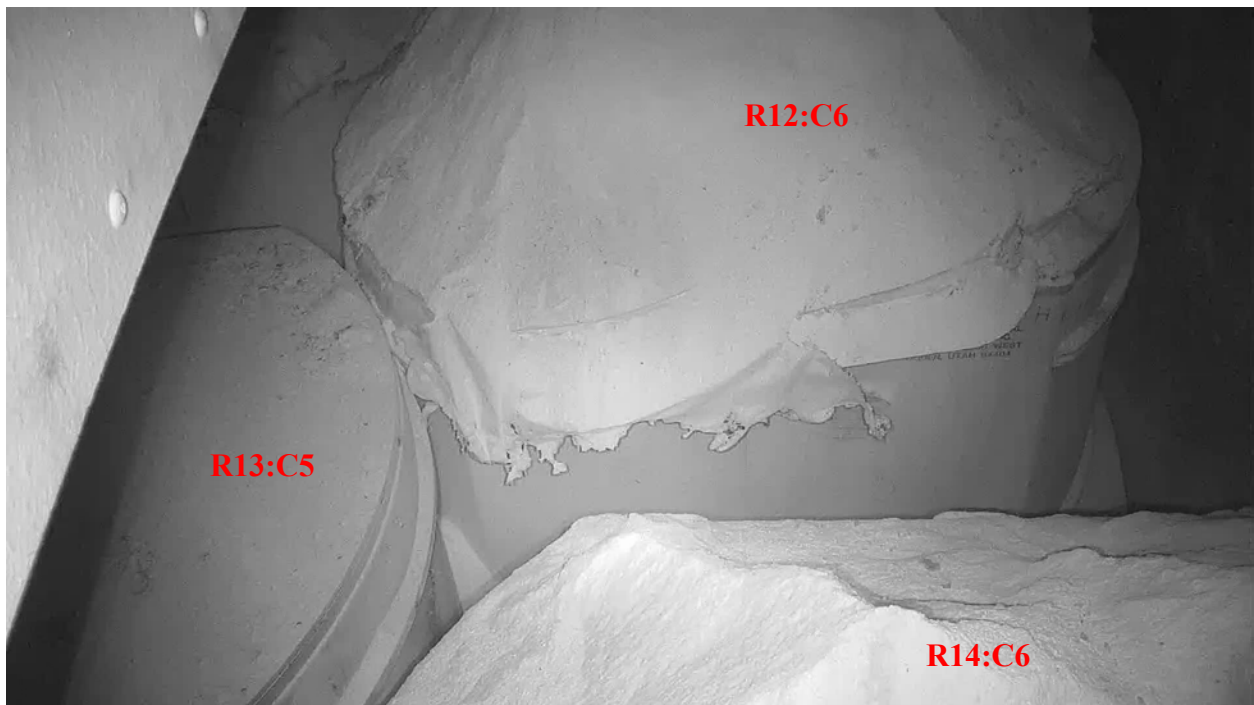
AIB-FST-10407

AIB-FST-10408: R11:C5 – Cardboard stiffener from R12:C6

AIB-FST-10409: R12:C6 – Underside of fiberboard slip sheet

AIB-FST-10410
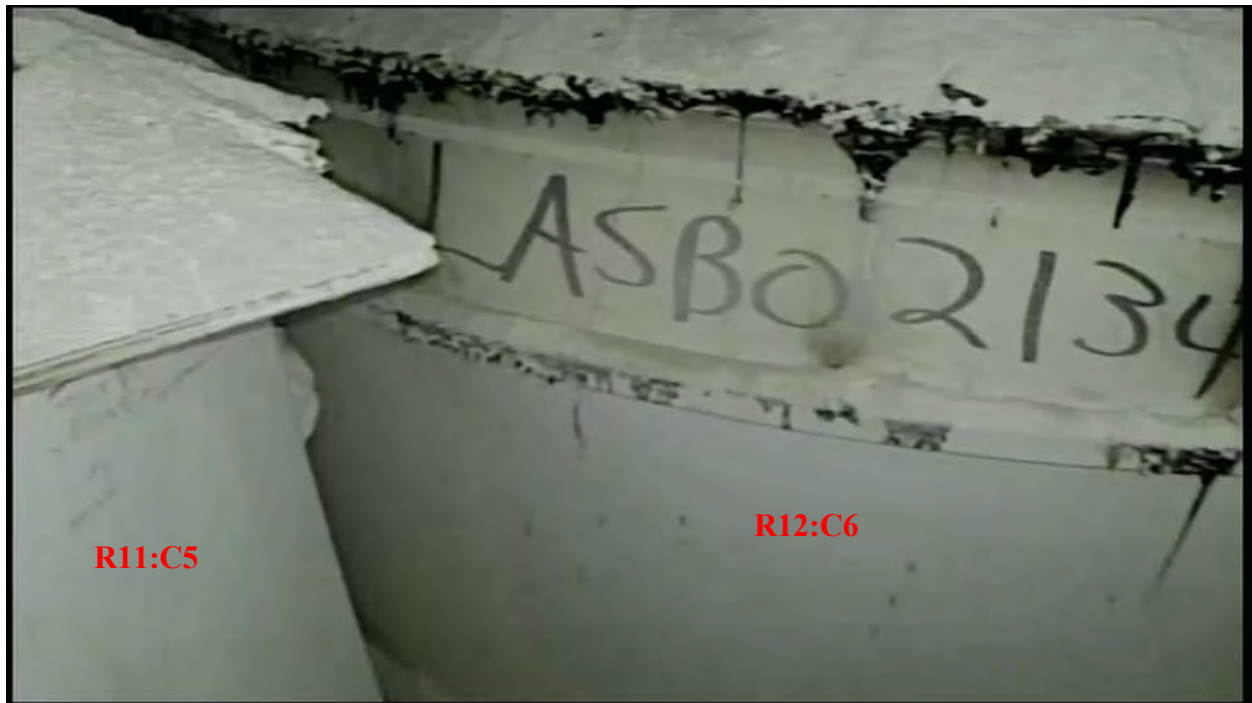
AIB-FST-10411: R11:C5 and R12:C3

AIB-FST-10412: R12:C6 and R14:C6

AIB-FST-10413: R10:C6 and R12:C6 - Remnant super sack

AIB-FST-10414: R12:C6 – Debris on residual MgO pile

AIB-FST-10415: R12:C6 – Debris on residual MgO pile

AIB-FST-10416: R12:C6 – Melted fabric remnants on residual MgO pile

AIB-FST-10417: R12:C6 and R14:C6
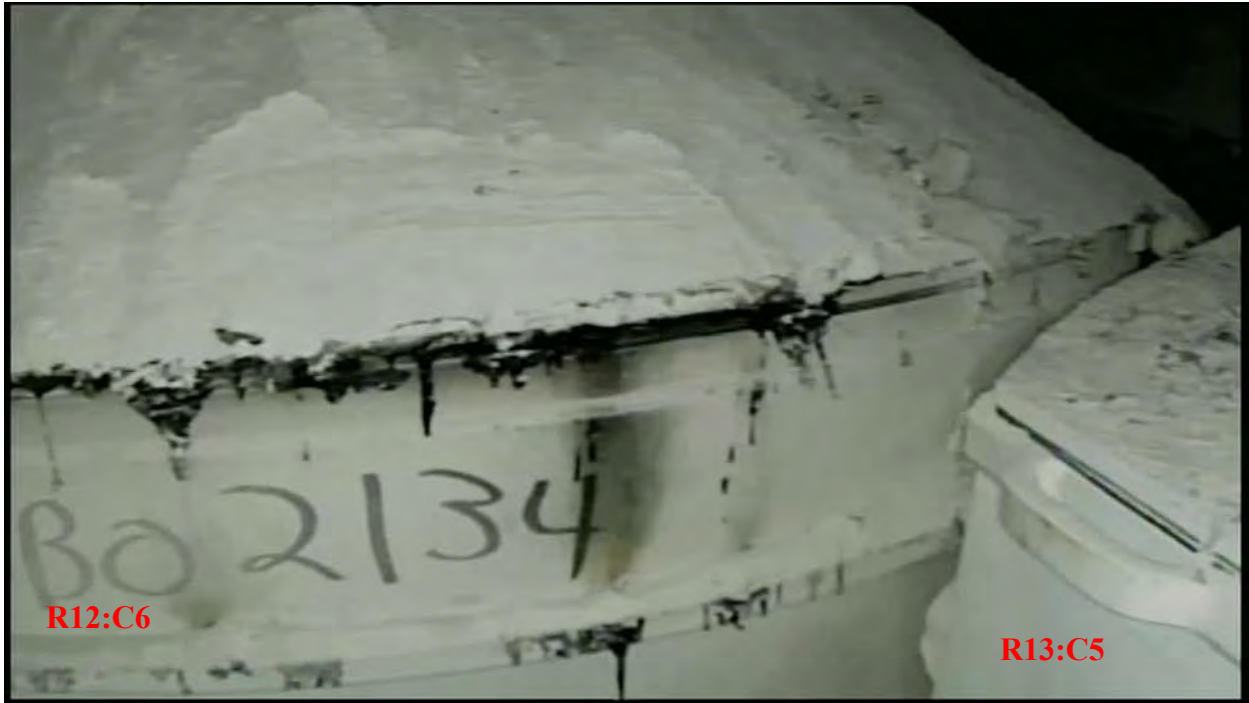
AIB-FST-10418: R12:C6 and R13:C5
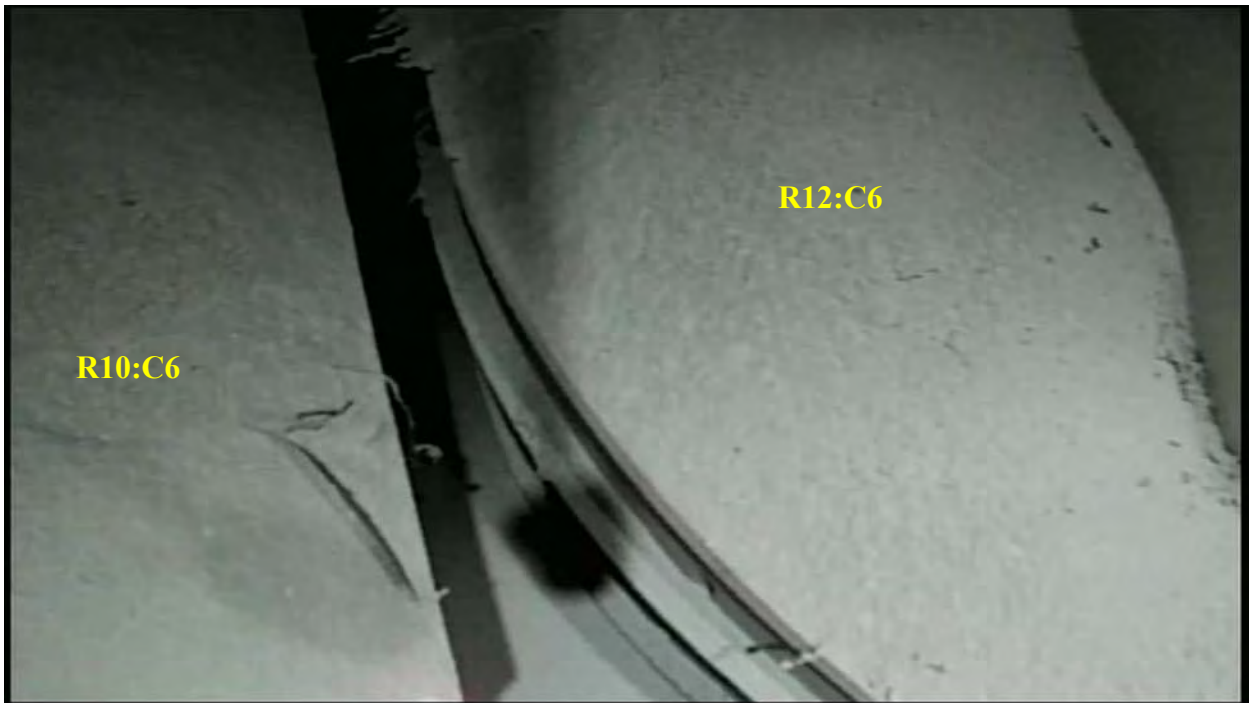
AIB-FST-10419: R10:C6 and R12:C6

R12:C6

AIB-FST-10420: R12:C6 – Bulkhead (east) view - Crease in TDOP wall below top bumper

R12:C6

AIB-FST-10421: R12:C6 – Bulkhead (east) view - Crease in TDOP wall at middle bumper

AIB-FST-10422: R12:C6 – Bulkhead (east) view - Crease in TDOP wall at bottom bumper

AIB-FST-10423: R12:C6 and R13:C5

AIB-FST-10424: R12:C6 and R13:C5 – Underside of SWB slip sheet

AIB-FST-10425: R12:C6 and R14:C6

AIB-FST-10426: R12:C6 and R13:C5

AIB-FST-10427: R11:C5 and R12:C6

AIB-FST-10428: R11:C5 and R12:C6

AIB-FST-10429: R10:C6 and R12:C6

AIB-FST-10430: R12:C6 – South view of SWB slip sheet

AIB-FST-10431: R12:C6 – Bulkhead face (east) view

AIB-FST-10432

AIB-FST-10433: R7:C3 and R7:C5 – Rock bolt debris on SLB2 and floor

AIB-FST-10434: R7:C3 and R7:C5 – Rock bolt debris on SLB2 and floor
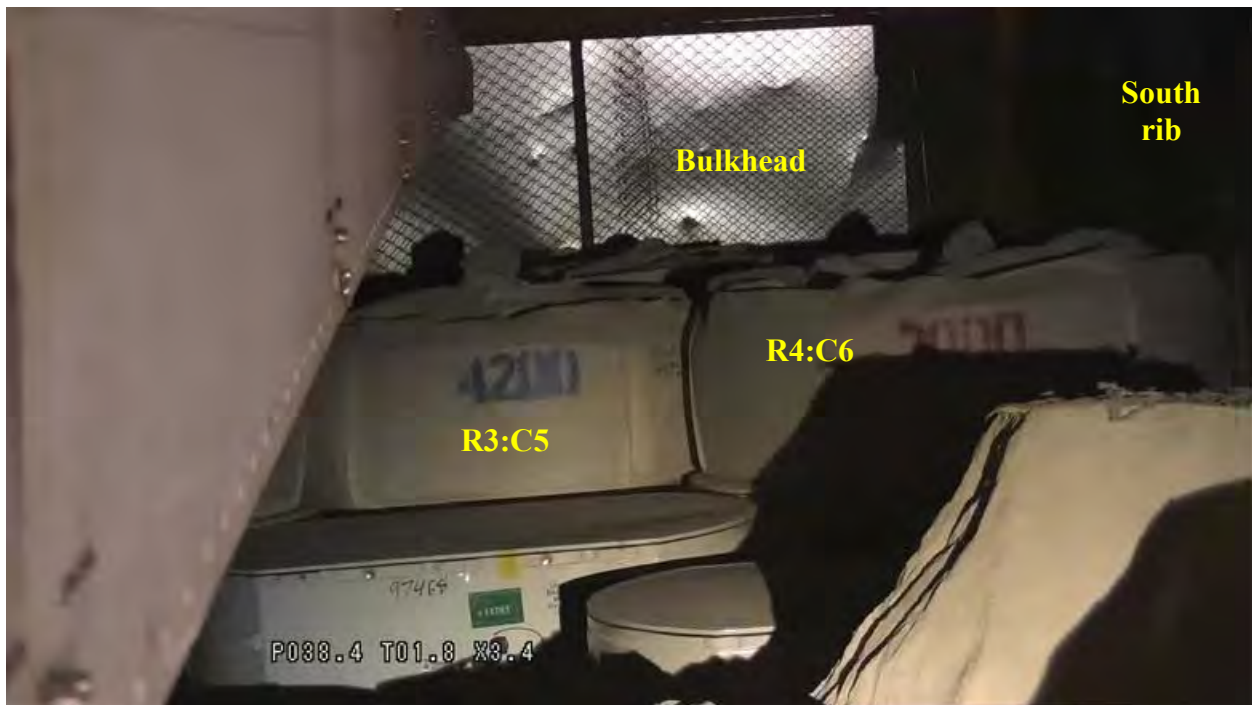
AIB-FST-10435

AIB-FST-10437

AIB-FST-10438: Panel 7, Room 7 bulkhead near column 6

AIB-FST-10439: Panel 7, Room 7 bulkhead near column 6

AIB-FST-10440: Panel 7, Room 7 bulkhead near south rib

AIB-FST-10441: Panel 7, Room 7 bulkhead near base of south rib

AIB-FST-10442: Panel 7, Room 7 bulkhead near south rib
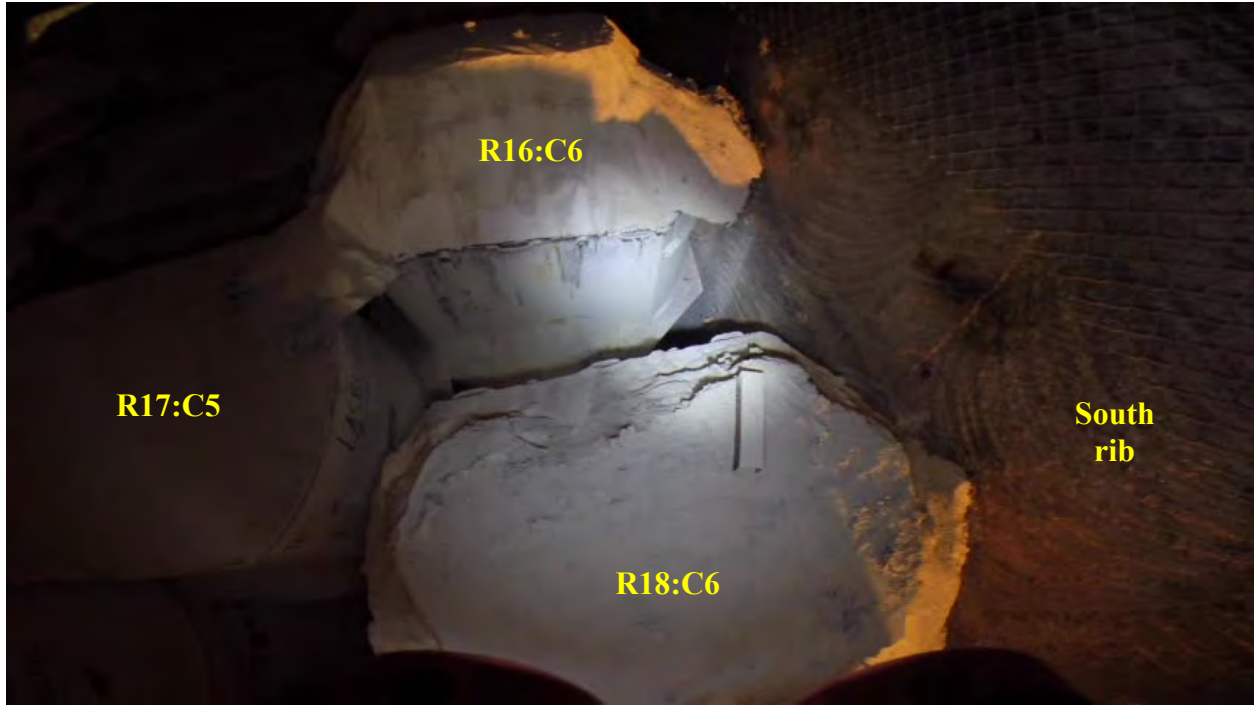
AIB-FST-10443

AIB-FST-10444

AIB-FST-10445: R18:C6 – Array face (west) view

AIB-FST-10446

AIB-FST-10448

AIB-FST-10449: R18:C6 – Dark area on south rib

AIB-FST-10450: R16:C6 and R18:C6

AIB-FST-10452: R18:C6 – North view
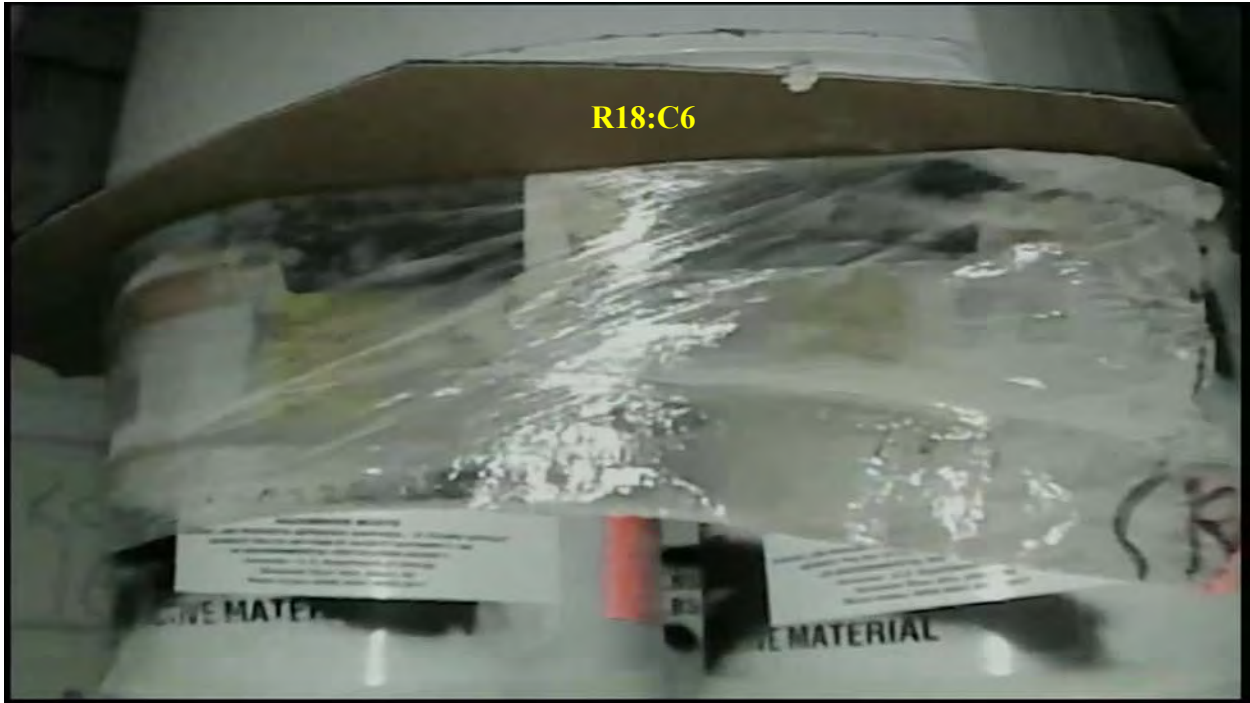
AIB-FST-10453: R18:C6 – North view

AIB-FST-10455: R18:C6 – Array face (west) view

AIB-FST-10456: R18:C6 – Array face (west) view

AIB-FST-10457: R18:C6 – Array face (west) view

AIB-FST-10458: R18:C6 – Array face (west) view

AIB-FST-10459: R18:C6 – Middle tier – Drum G

AIB-FST-10460: R18:C6 – Middle tier – Drum F

AIB-FST-10461: R18:C6 – Middle tier – Drum G

R18:C6

AIB-FST-10462: R18:C6 – Middle tier – Drum F

R18:C6

AIB-FST-10463: R18:C6 – Middle tier – Drum F

AIB-FST-10475: R6:C6 and R8:C6

AIB-FST-10476

AIB-FST-10477: R8:C6 – Adjacent to south rib

AIB-FST-10478

AIB-FST-10479: R8:C6 – Bulkhead (east) view – Damaged Mg super sack fabric

AIB-FST-10480: R8:C6 and R9:C5

AIB-FST-10481: R8:C6 and R9:C5

AIB-FST-10482: R8:C6 and R9:C5

AIB-FST-10483: R8:C6 and R9:C5

AIB-FST-10484

AIB-FST-10485: R8:C6 – Array face (west) view

AIB-FST-10486: R8:C6 and R10:C6

AIB-FST-10487: R8:C6 – Adjacent to south rib
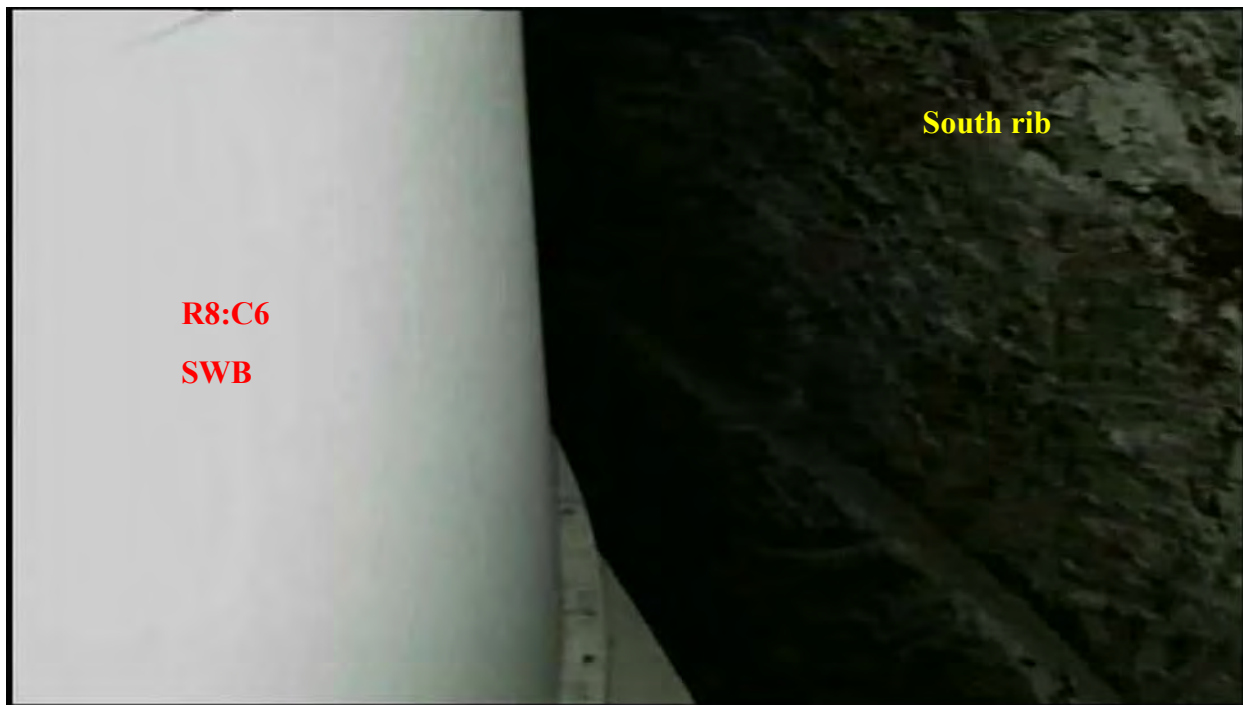
AIB-FST-10488: R8:C6 – Adjacent to south rib

AIB-FST-10489: R8:C6 and R10:C6 – Mg super sack cardboard stiffener

AIB-FST-10490

AIB-FST-10491: R8:C6 and R9:C5
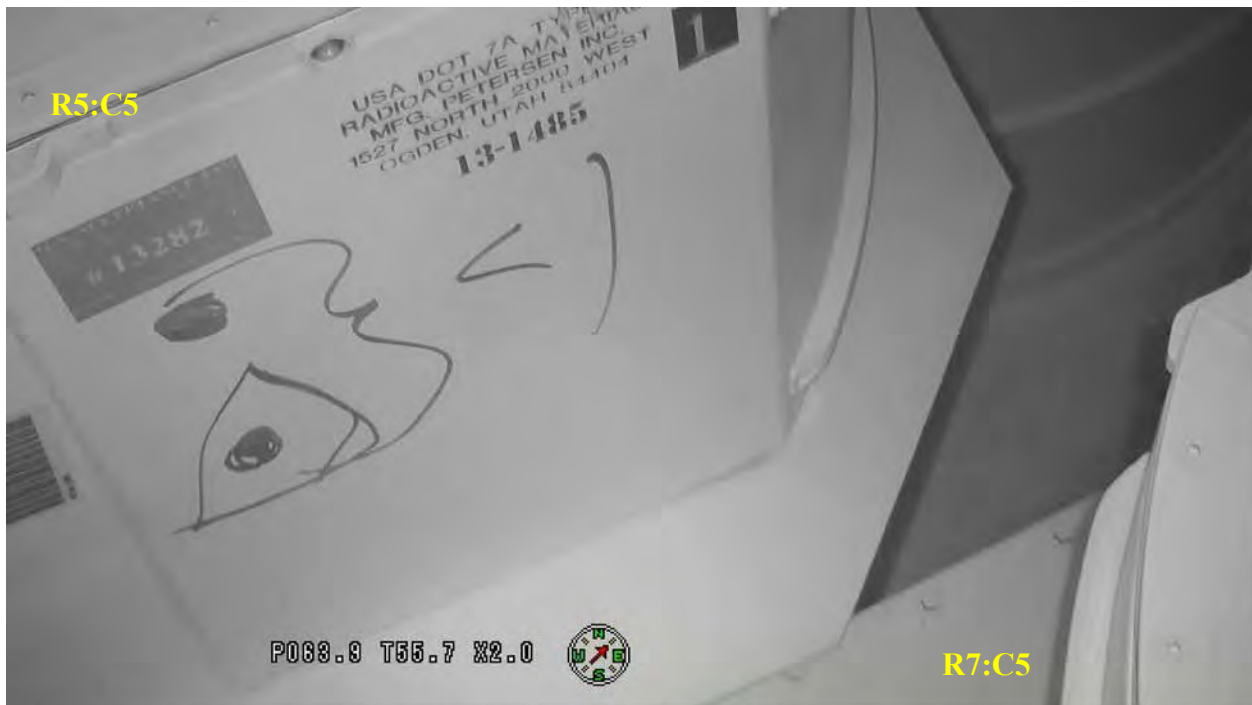
AIB-FST-10492: R5:C5 and R7:C5

AIB-FST-10493

AIB-FST-10494

AIB-FST-10495

AIB-FST-10496

AIB-FST-10497

AIB-FST-10498

AIB-FST-10500: R7:C5 and R8:C6

AIB-FST-10501

AIB-FST-10502

AIB-FST-10503

AIB-FST-10504: R10:C6 – Adjacent to south rib

AIB-FST-10505: R8:C6 and R10:C6

AIB-FST-10506: R10:C6 and R11:C5

AIB-FST-10507: R9:C5 and R10:C6 – Middle and top tiers

AIB-FST-10508: R10:C6 – Middle tier

AIB-FST-10509: R10:C6 – Top tier

AIB-FST-10510
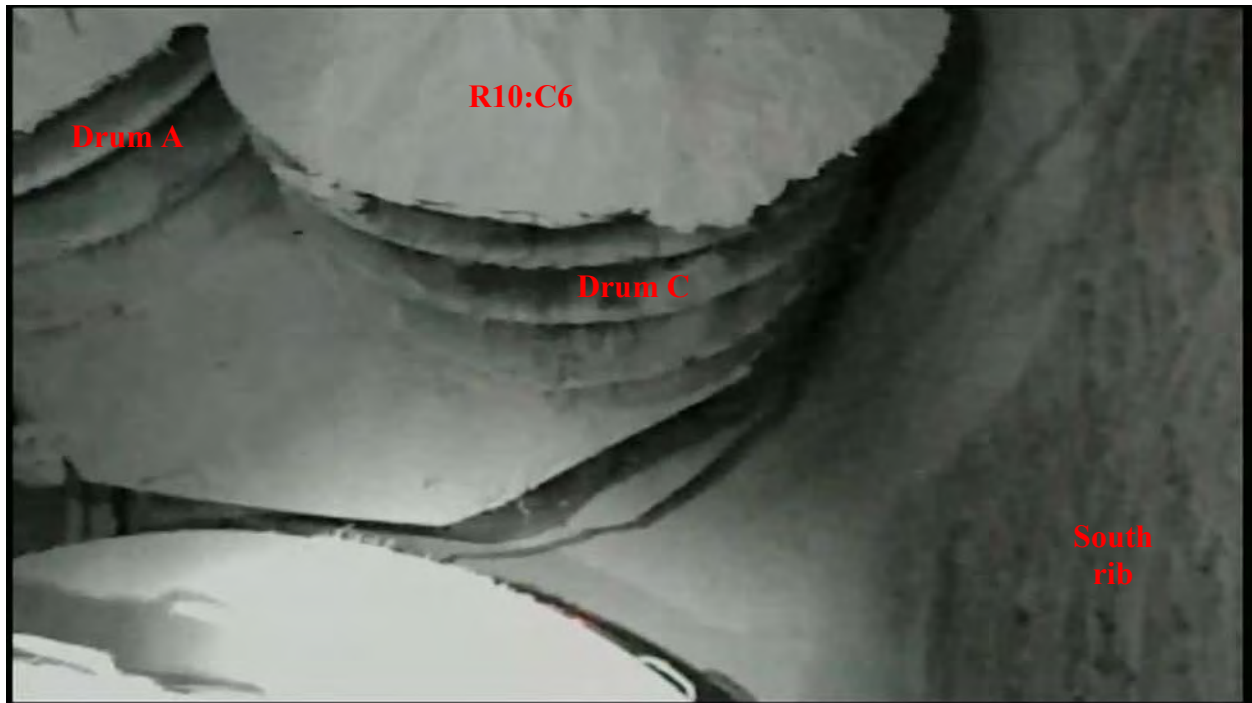
AIB-FST-10511: R10:C6 – Top tier drums

AIB-FST-10512: R10:C6 – Middle tier

AIB-FST-10513

AIB-FST-10514
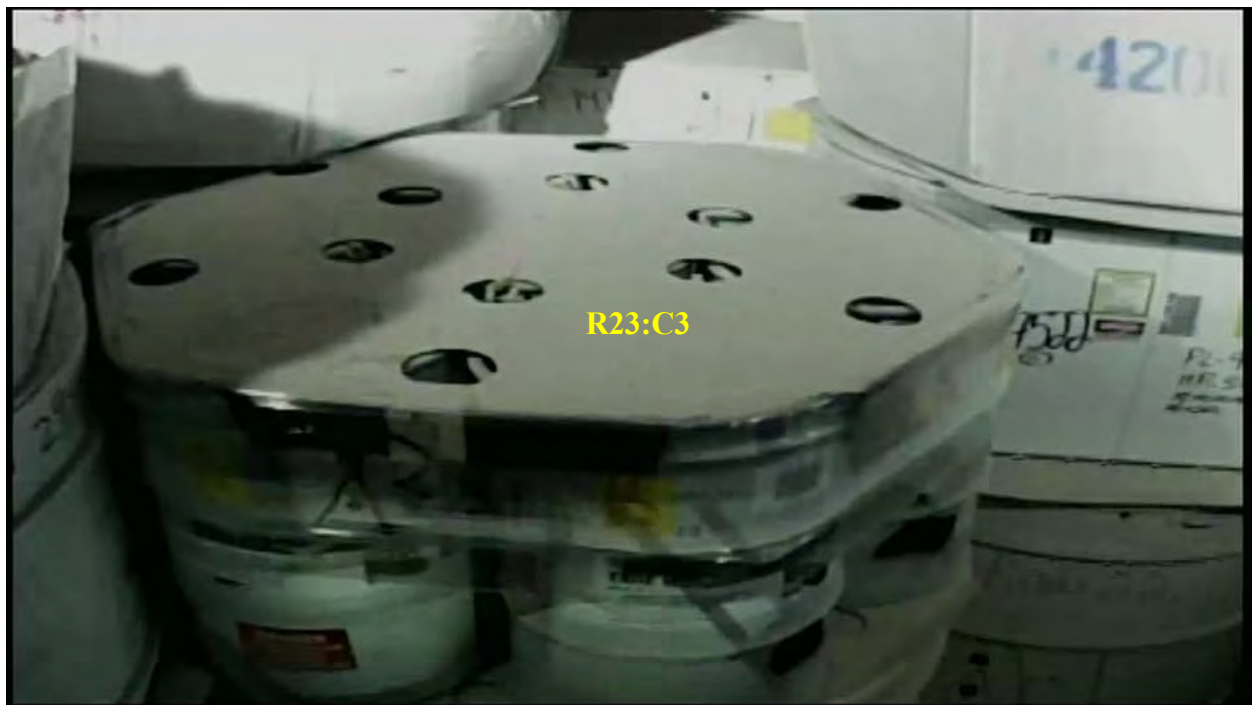
AIB-FST-10515: R23:C3 – Array face (west) view

AIB-FST-10516

AIB-FST-10517

AIB-FST-10518

AIB-FST-10519

AIB-FST-10520: R15:C5 and R16:C4

AIB-FST-10521

AIB-FST-10522: R16:C4 – Residual Mg

AIB-FST-10523
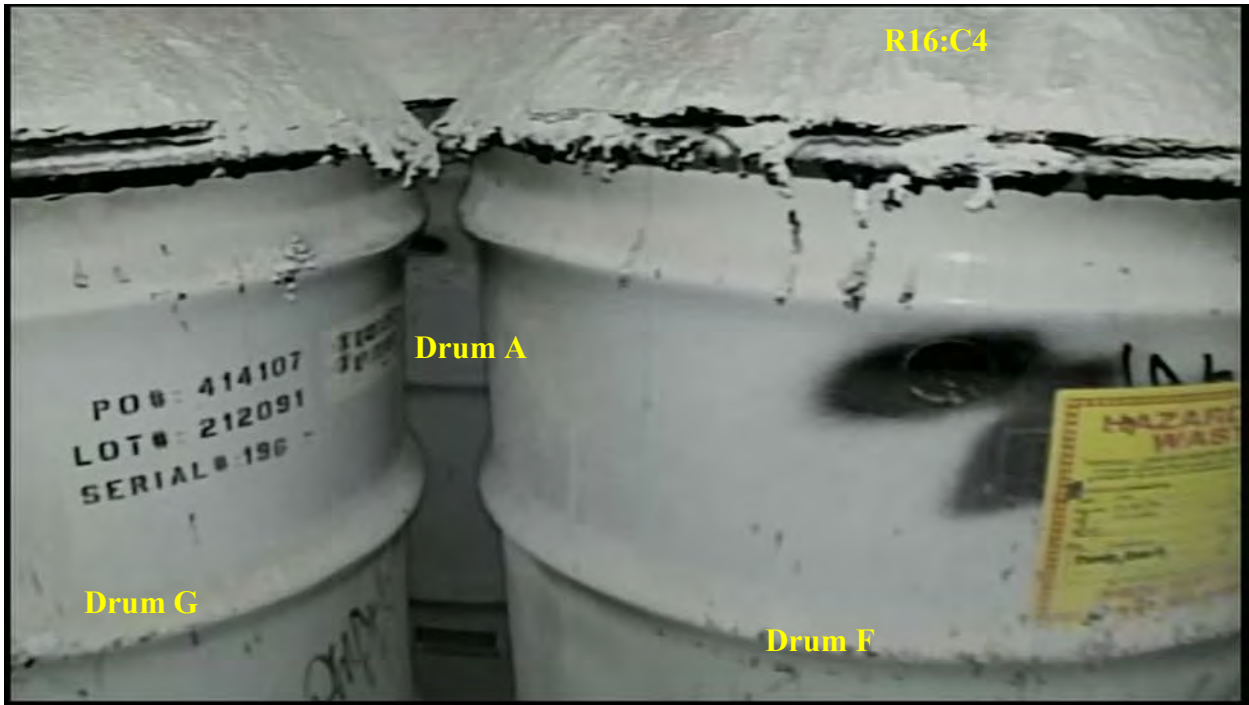
AIB-FST-10524: R16:C4 – Drums A, F and G
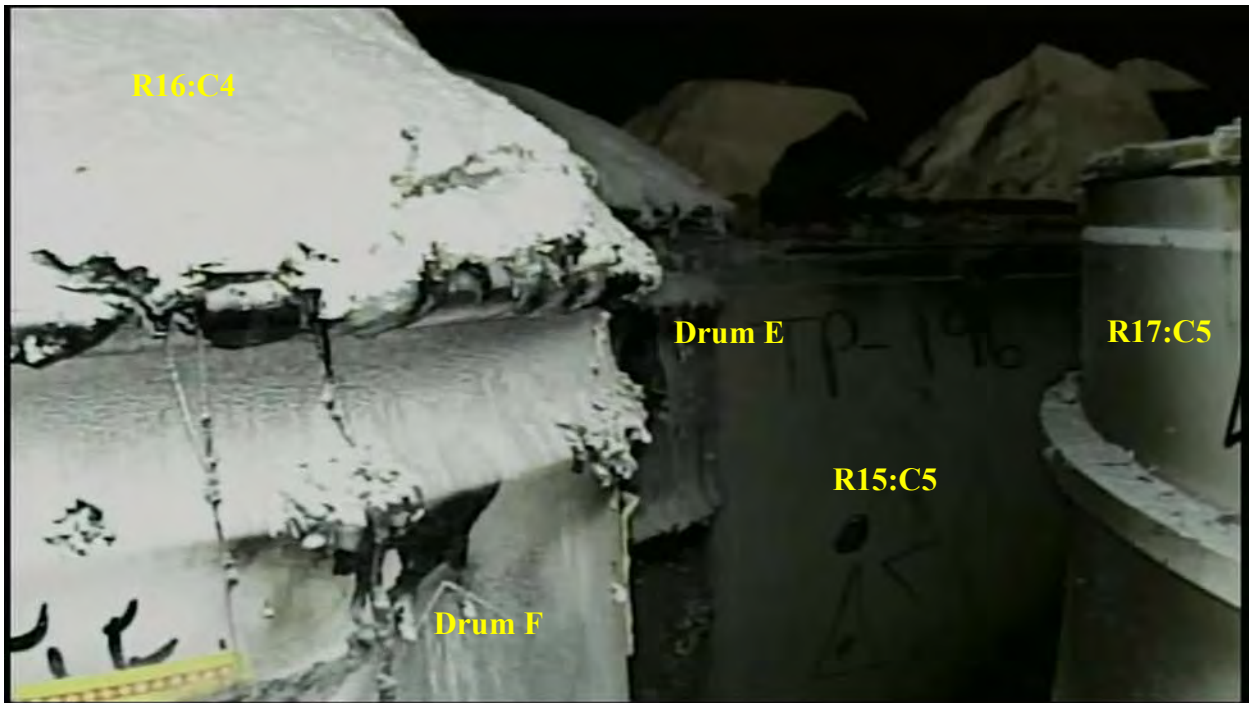
AIB-FST-10525: R16:C4 and R17:C5

AIB-FST-10526: R16:C4 and R17:C5

AIB-FST-10527: R16:C4 and R18:C4
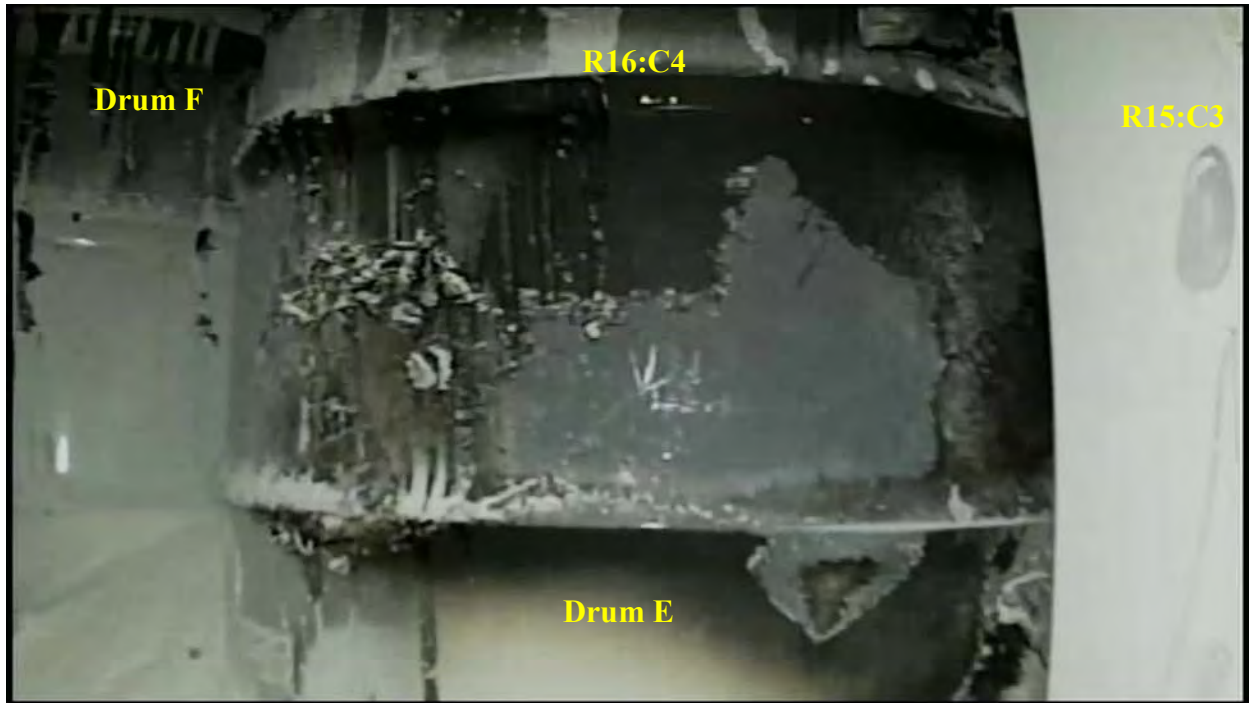
AIB-FST-10529: R16:C4 – Waste drum 68660 – Clean burn area

AIB-FST-10530: R16:C4 – Lower of waste drum 68660 (drum E)
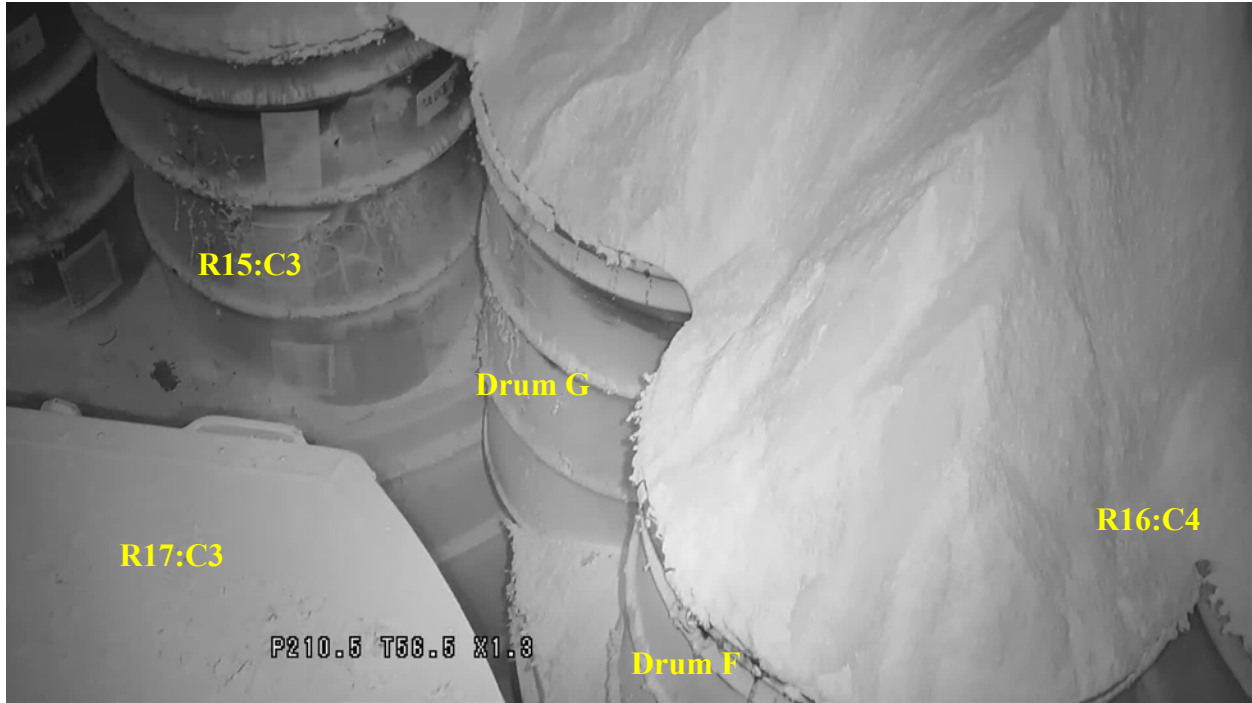
AIB-FST-10531

AIB-FST-10532

AIB-FST-10533: R16:C4
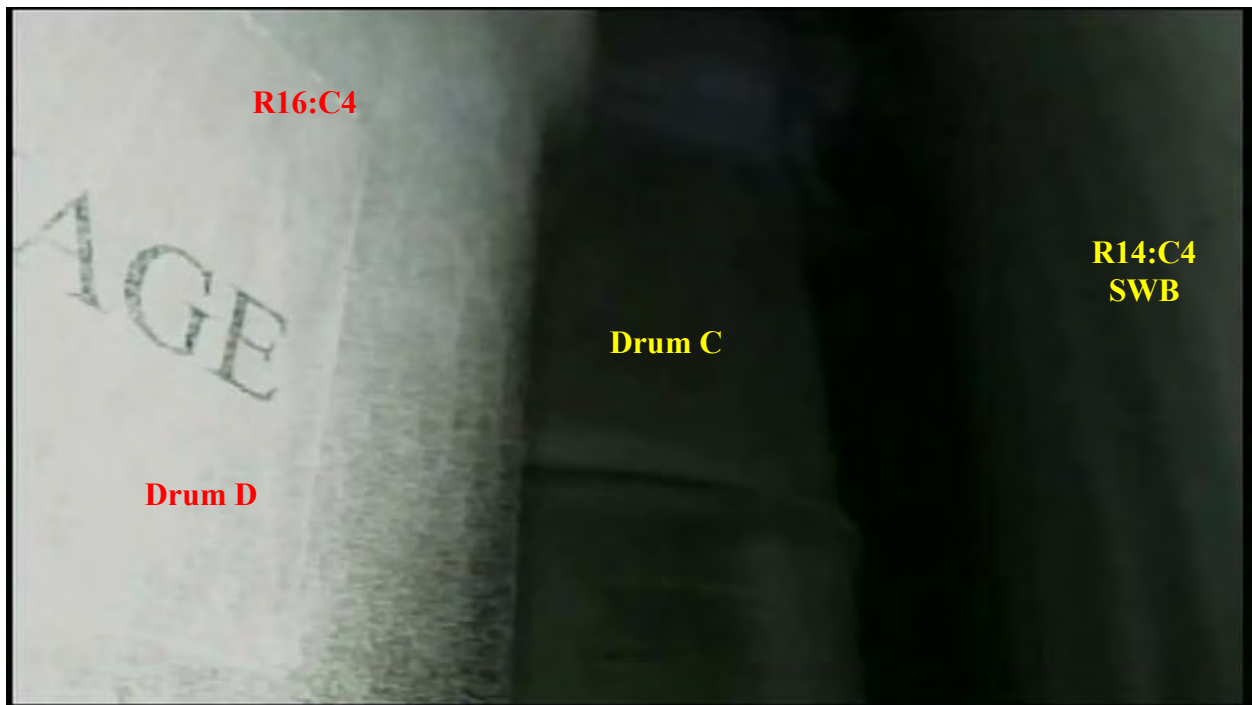
AIB-FST-10534: R16:C4 – Drums C and D
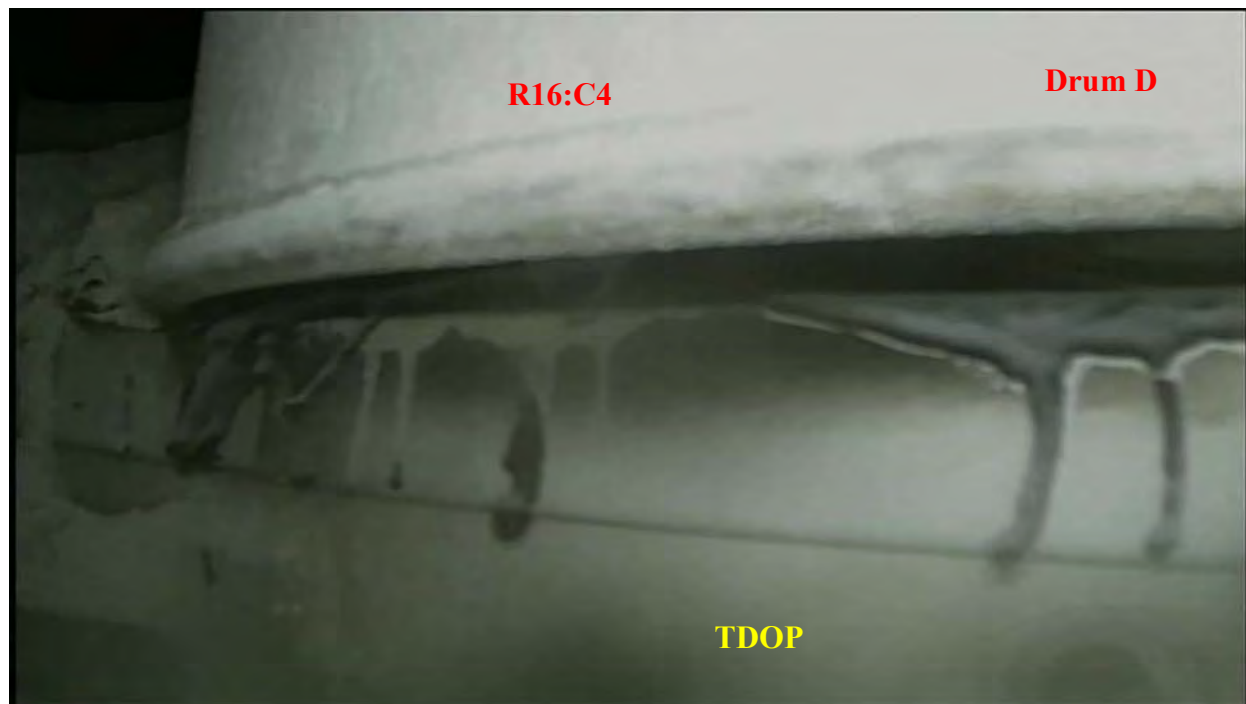
AIB-FST-10535: R16:C4 – Base of drum D

AIB-FST-10536: R15:C5 and R16:C4

AIB-FST-10537: Panel 7, Room 7 south rib at miter

AIB-FST-10538: South rib near R10

AIB-FST-10539: South rib near R8
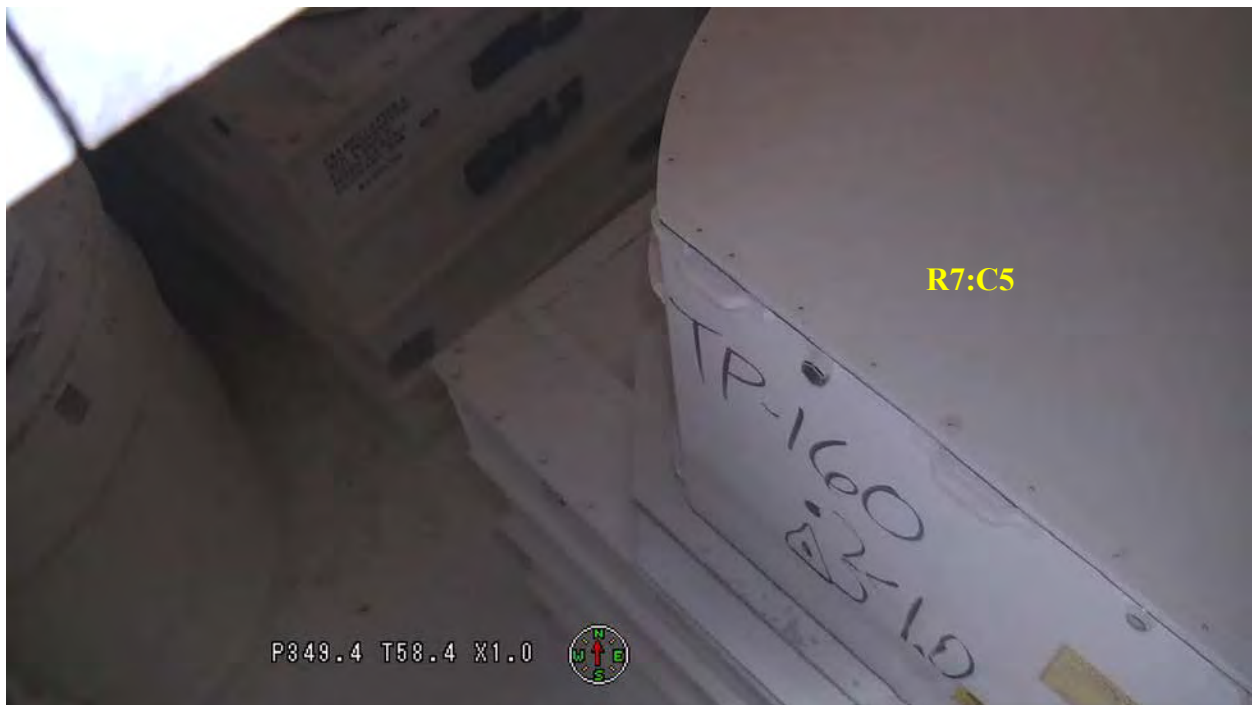
AIB-FST-10540: R7:C5 – Array face (west) view

AIB-FST-10541: R7:C5 – Array face (west) view – Slip sheet damage

AIB-FST-10542: R7:C5 – Array face (west) view – Slip sheet damage

AIB-FST-10543: R7:C5
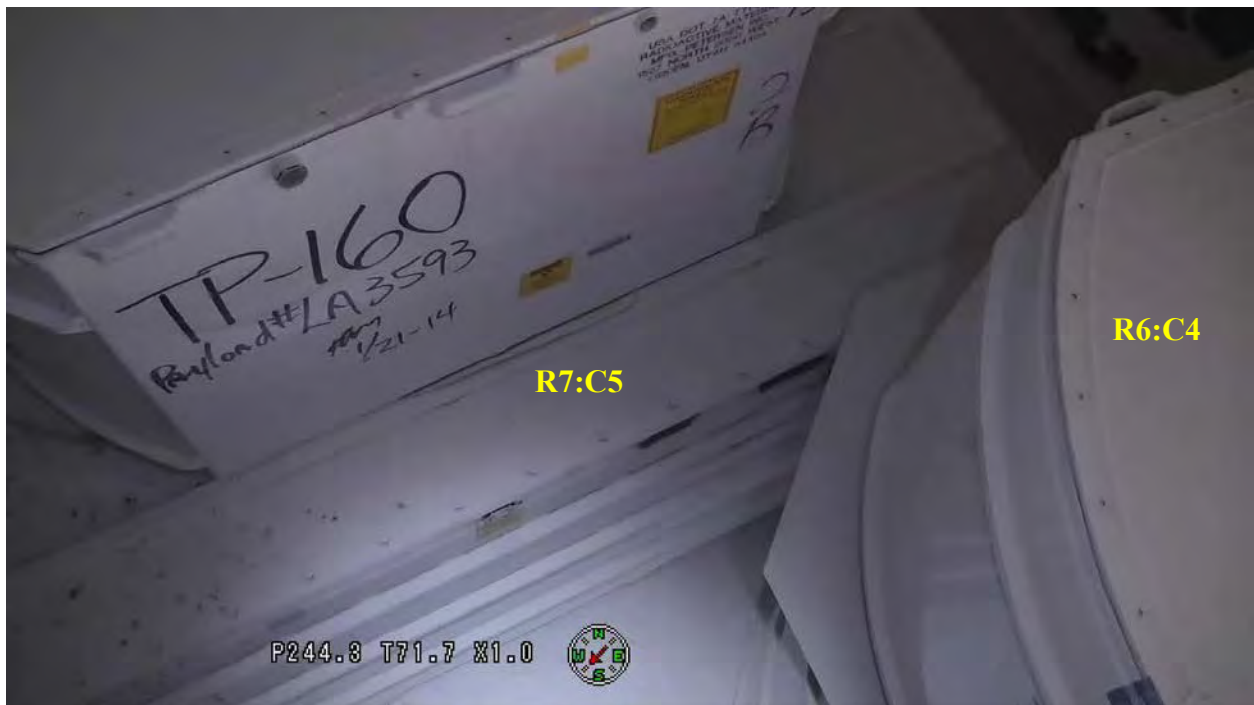
AIB-FST-10544: R6:C4 and R7:C5
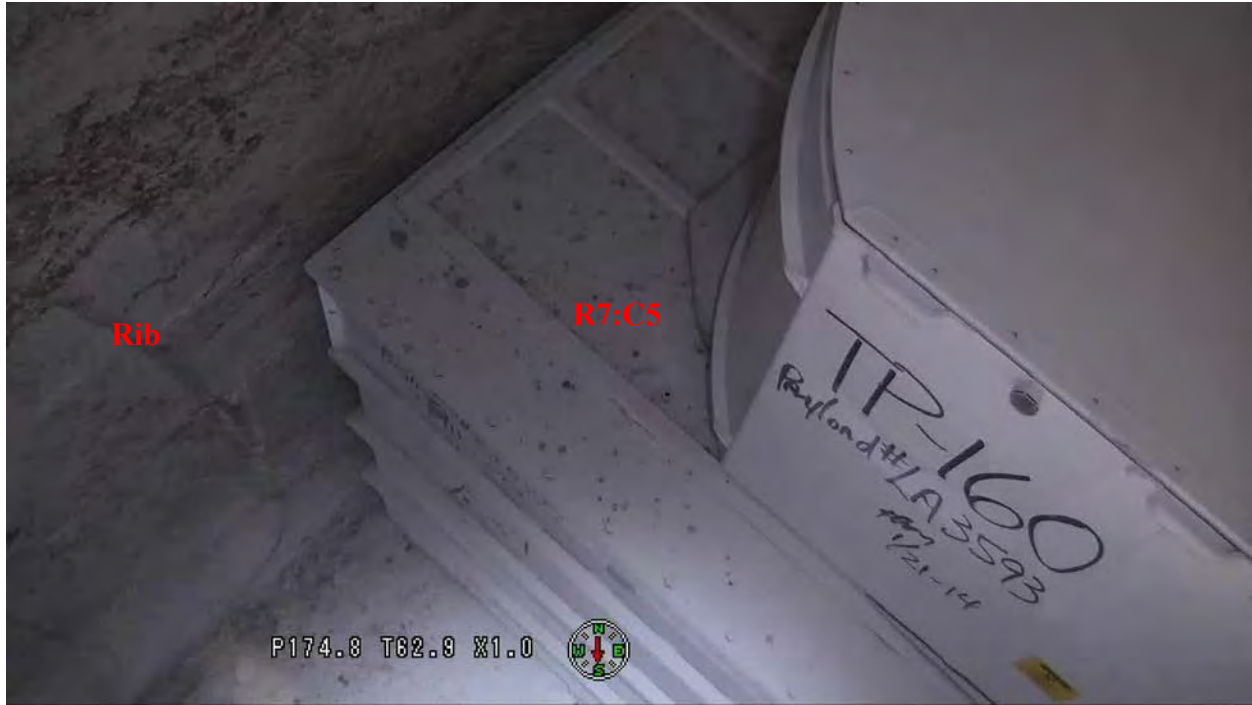
AIB-FST-10545: R7:C5

AIB-FST-10546: South rib near R2

AIB-FST-10550: South rib looking towards waste array face

AIB-FST-10554: South rib near row 7 - Formation coloration

AIB-FST-10555: South rib near row 4

AIB-FST-10556: South rib near row 2

AIB-FST-10557: South rib near row 12 and 13 – Fire evidence

AIB-FST-10558: South rib near row 16 and 18 – Fire evidence

AIB-FST-10559: South rib near row 20 and 22

AIB-FST-10566: R5:C5, R7:C3, R7:C5

AIB-FST-10572: R15:C5 - North view
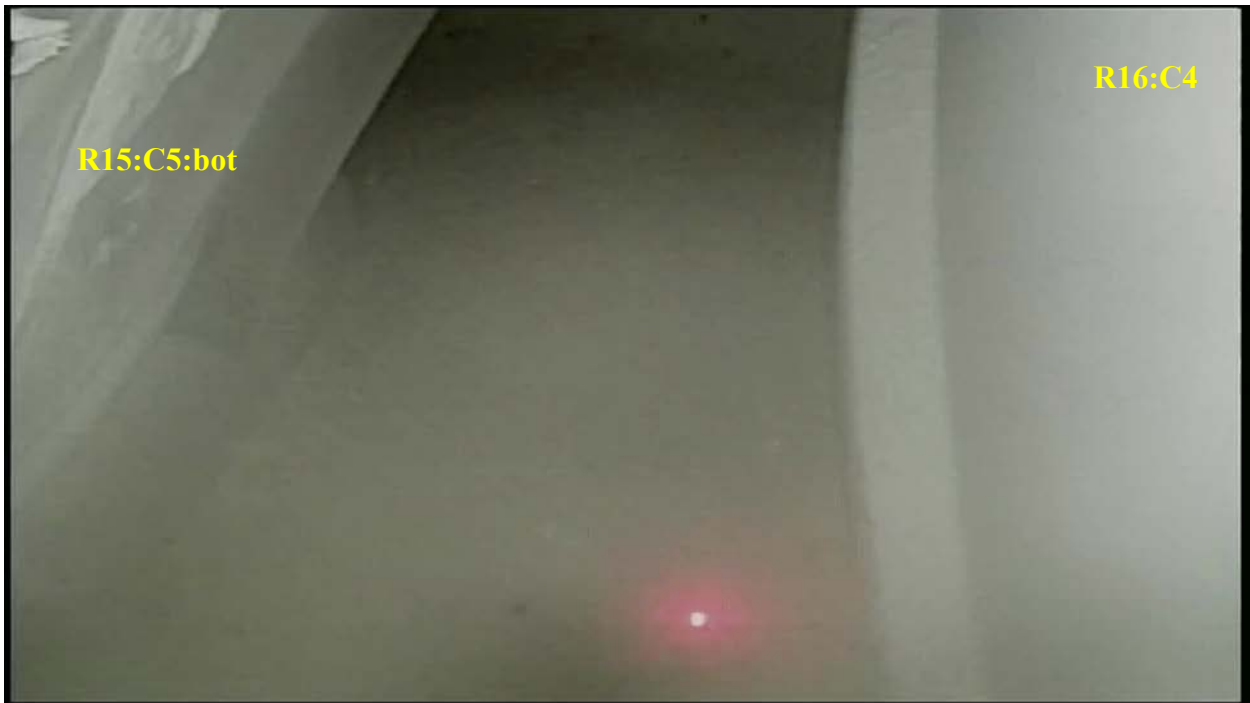
AIB-FST-10573: R15:C5 and R16:C4
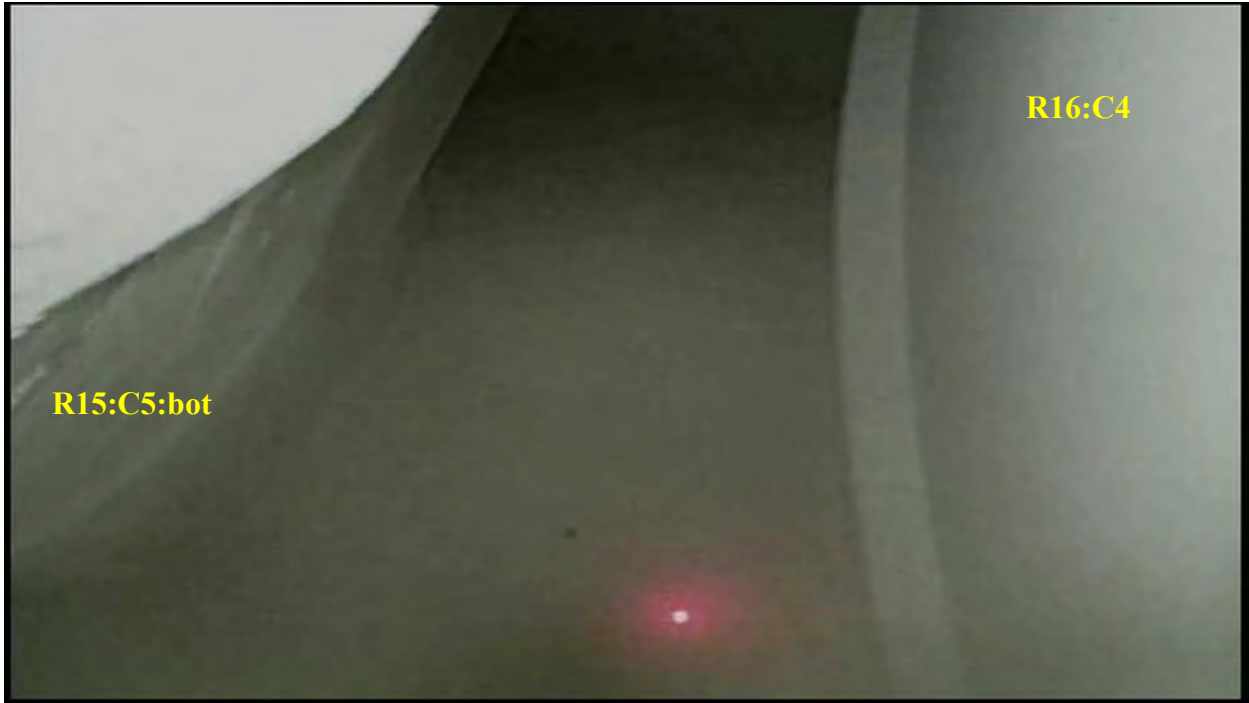
AIB-FST-10574: R15:C5 and R16:C4

AIB-FST-10575: R14:C4, R15:C5 and R16:C4

AIB-FST-10576: R14:C4 and R15:C5

AIB-FST-10578: R14:C4 and R15:C5

AIB-FST-10580: R15:C5 – SWB lid – North view

AIB-FST-10581: R15:C5 and R16:C4

AIB-FST-10582: R15:C5 and R16:C4

AIB-FST-10583: R15:C5 and R16:C4

AIB-FST-10584

AIB-FST-10585

AIB-FST-10586

AIB-FST-10587: R9:C1 – Adjacent of north rib

AIB-FST-10588

AIB-FST-10589: R8:C2 and R9:C1

AIB-FST-10590: R8:C2 and R9:C1

AIB-FST-10591

AIB-FST-10592: R8:C2 and R9:C1

AIB-FST-10593

AIB-FST-10594: R9:C1 and R11:C1

AIB-FST-10595: R9:C1 and R11:C1

AIB-FST-10596

AIB-FST-10597

AIB-FST-10598: R15:C5 - SWB lid showing no trails on May 15, 2014

AIB-FST-10599

AIB-FST-10600: R15:C5 and R16:C6

AIB-FST-10601: R15:C5 and R16:C6

AIB-FST-10602

AIB-FST-10603: R15:C5 and R16:C6

AIB-FST-10604: R15:C5 and R16:C6

AIB-FST-10605 R8:C6 and R9:C5

AIB-FST-10609: R18:C6 – Array face (west) view

AIB-FST-10610: R18:C6 – Array face (west) view

AIB-FST-10611: R18:C6 – Array face (west) view

AIB-FST-10612: R18:C6 – Array face (west) view

AIB-FST-10613: R18:C6 – Array face (west) view

AIB-FST-10614: R18:C6 – Array face (west) view

AIB-FST-10615: R18:C6 – Array face (west) view

AIB-FST-10616: R18:C6 – Array face (west)

AIB-FST-10617: R18:C6 – Array face (west) – Bottom tier

AIB-FST-10618: R18:C6 – Array face (west)

AIB-FST-10619: R18:C6 and R20:C6 – Debris at base of stacks

AIB-FST-10620: R18:C6 – Array face (west) view

AIB-FST-10621: R18:C6 and R20:C6

AIB-FST-10622: R18:C6 and R20:C6

AIB-FST-10623: R18:C6 and R20:C6 – Damaged cardboard stiffener

AIB-FST-10624: R18:C6 and R20:C6

AIB-FST-10625: R18:C6 and R20:C6

AIB-FST-10626: R15:C5 – North view

AIB-FST-10639: R2:C4 and R3:C3

AIB-FST-10640

AIB-FST-10641: R2:C4 - Web-like accumulation
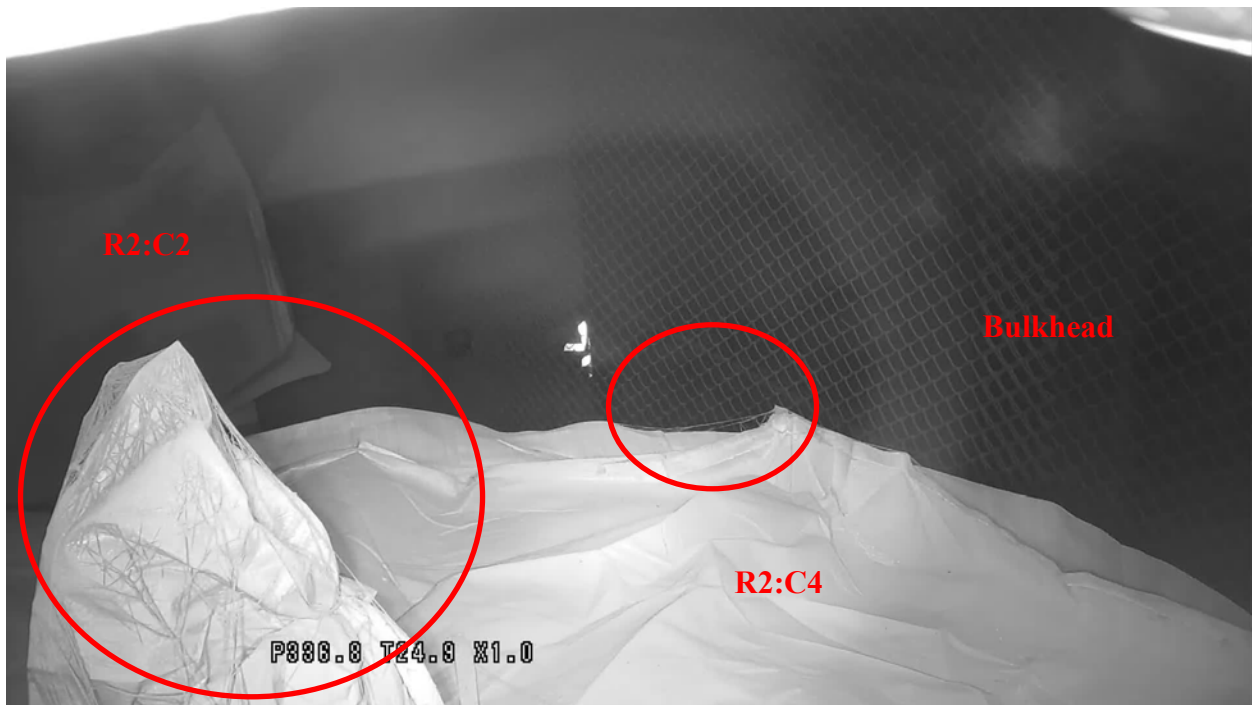
AIB-FST-10642: R2:C4 - Web-like accumulation

AIB-FST-10643: R2:C4 - Web-like accumulation

AIB-FST-10644: R2:C4

AIB-FST-10645: R2:C4 - Web-like accumulation

AIB-FST-10646: R2:C4 and R2:C6

AIB-FST-10647
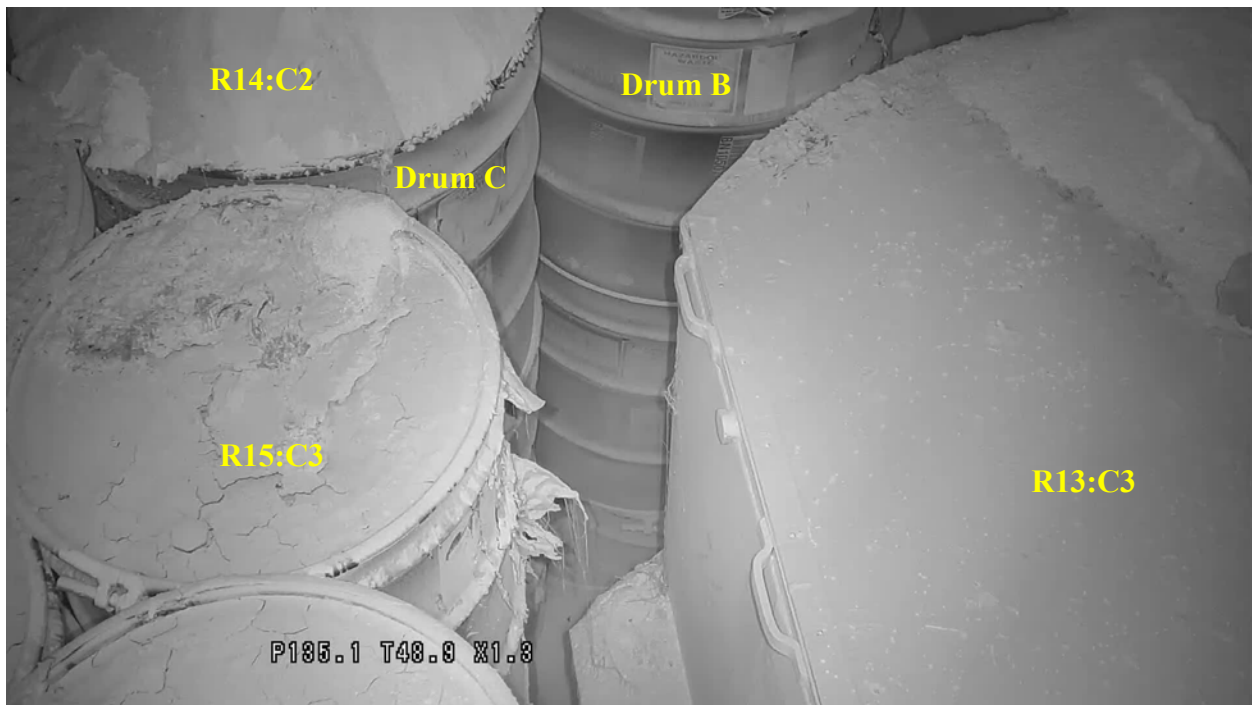
AIB-FST-10648

AIB-FST-10649

AIB-FST-10652

AIB-FST-10653

AIB-FST-10654

AIB-FST-10656
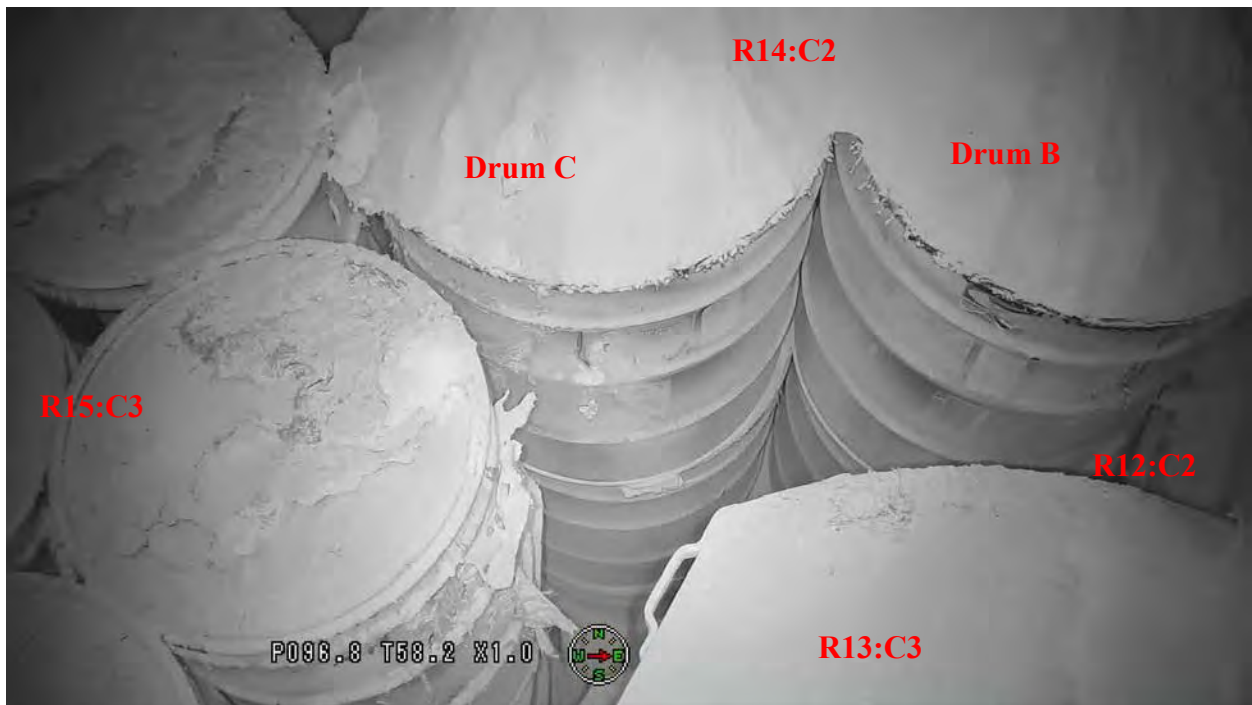
AIB-FST-10657

AIB-FST-10658

AIB-FST-10659

AIB-FST-10661

AIB-FST-10662

AIB-FST-10663: R2:C4 – Array face (west) view

AIB-FST-10664
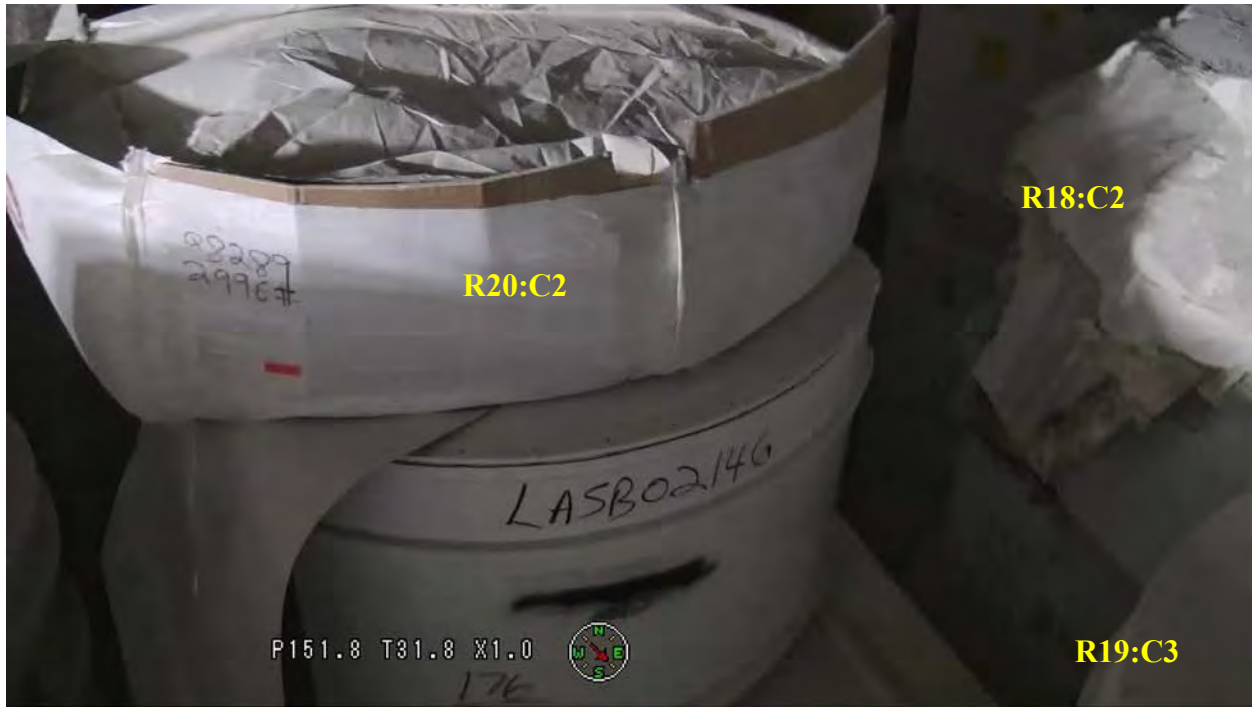
AIB-FST-10665

AIB-FST-10666

AIB-FST-10667

AIB-FST-10668
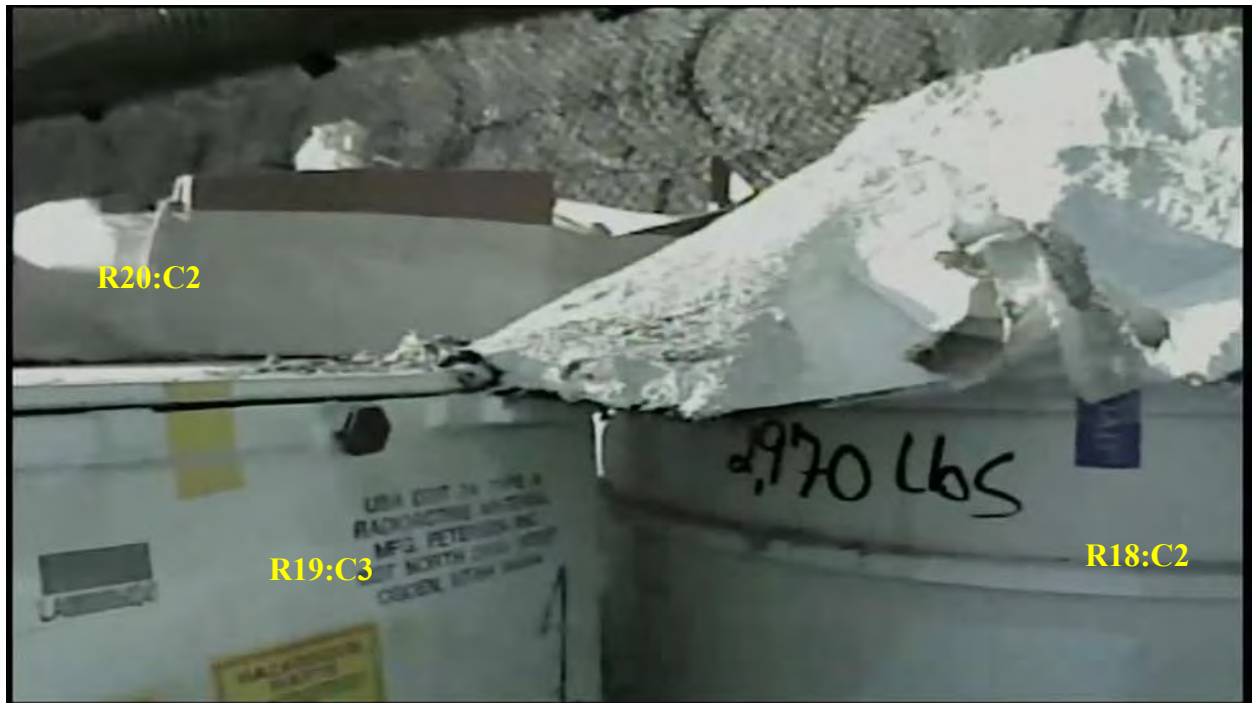
AIB-FST-10669

AIB-FST-10670

AIB-FST-10671

AIB-FST-10672

AIB-FST-10673

AIB-FST-10675
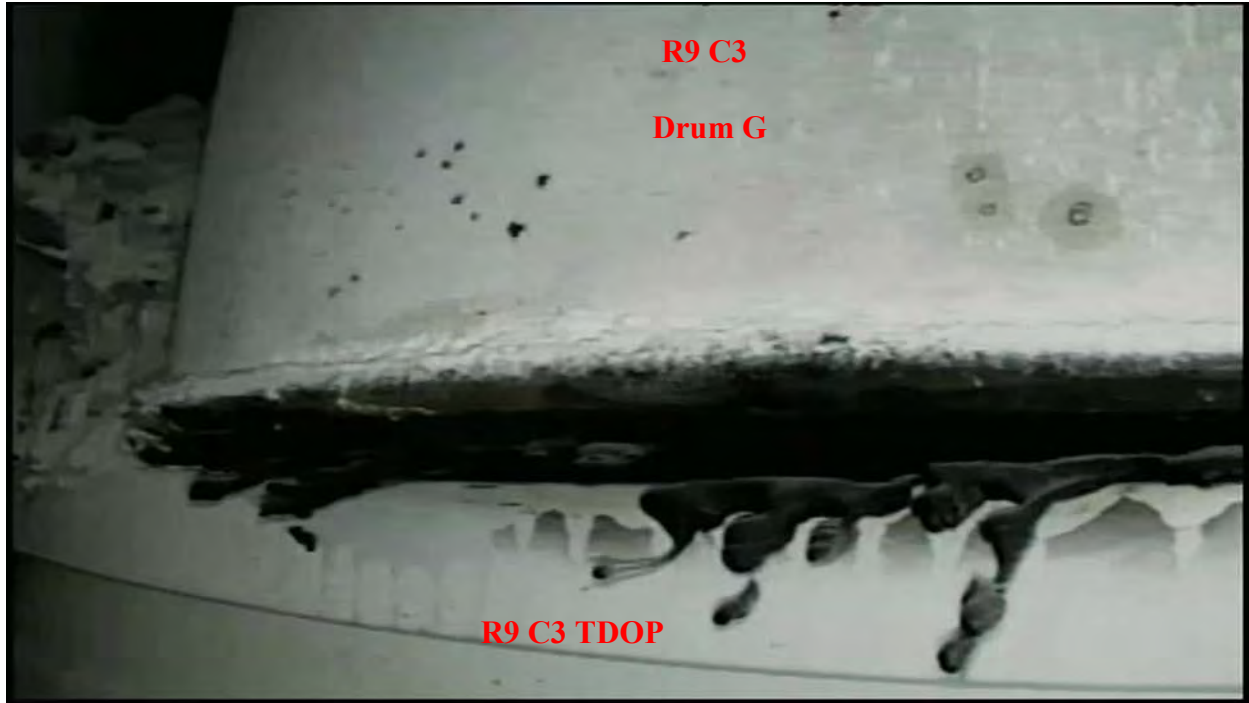
AIB-FST-10677: R9:C3 – Damaged slip sheet below drum G

AIB-FST-10678: R9:C3 and R10:C4 – Near floor
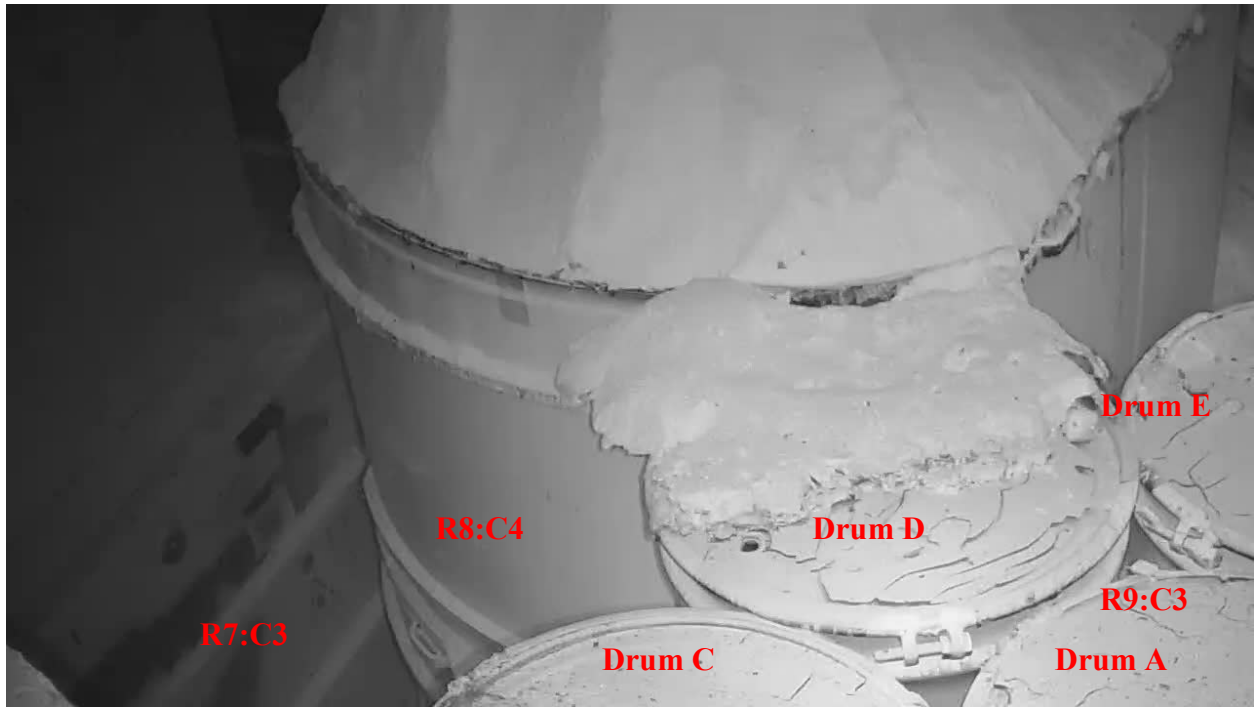
AIB-FST-10680

AIB-FST-10681: R9:C3 – Drum D lid

AIB-FST-10682: R9:C3 – Drum D identification label

AIB-FST-10683: R2:C2

AIB-FST-10684: R2:C2 and R4:C2

AIB-FST-10686

AIB-FST-10688: R2:C2 and R3:C1
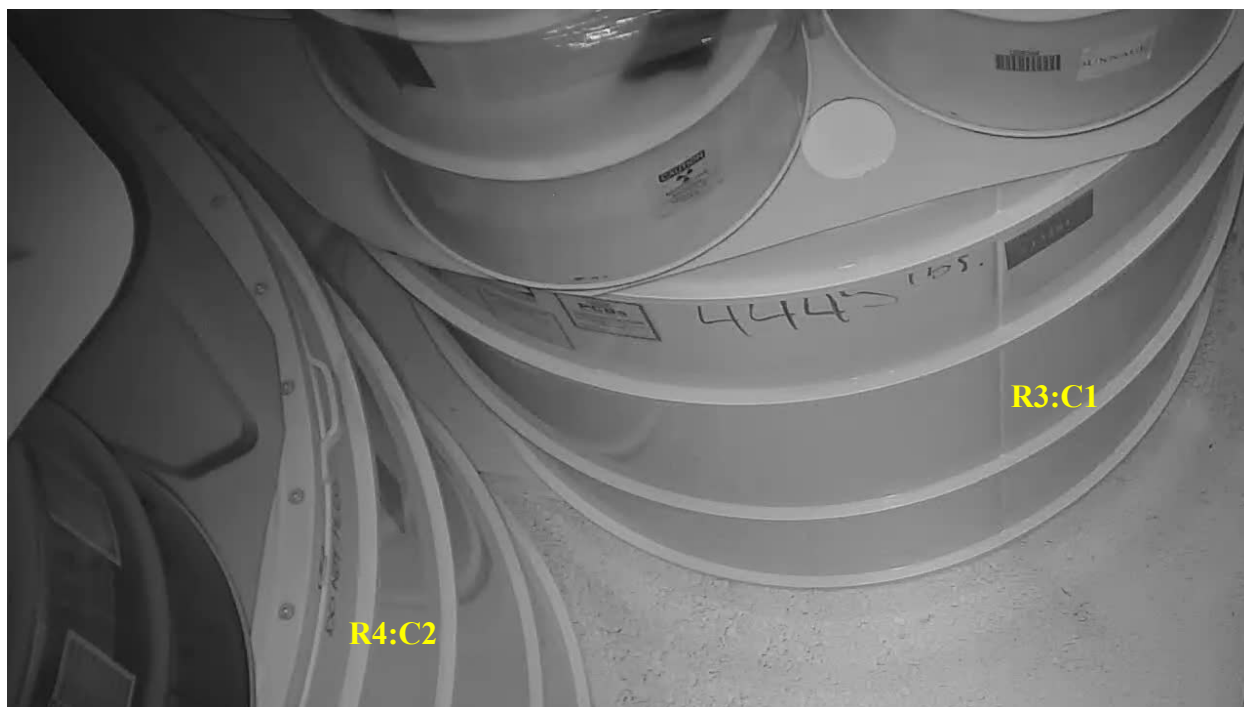
AIB-FST-10689: R3:C1 and R4:C2

AIB-FST-10691: R2:C2

AIB-FST-10692: R2:C2

AIB-FST-10694
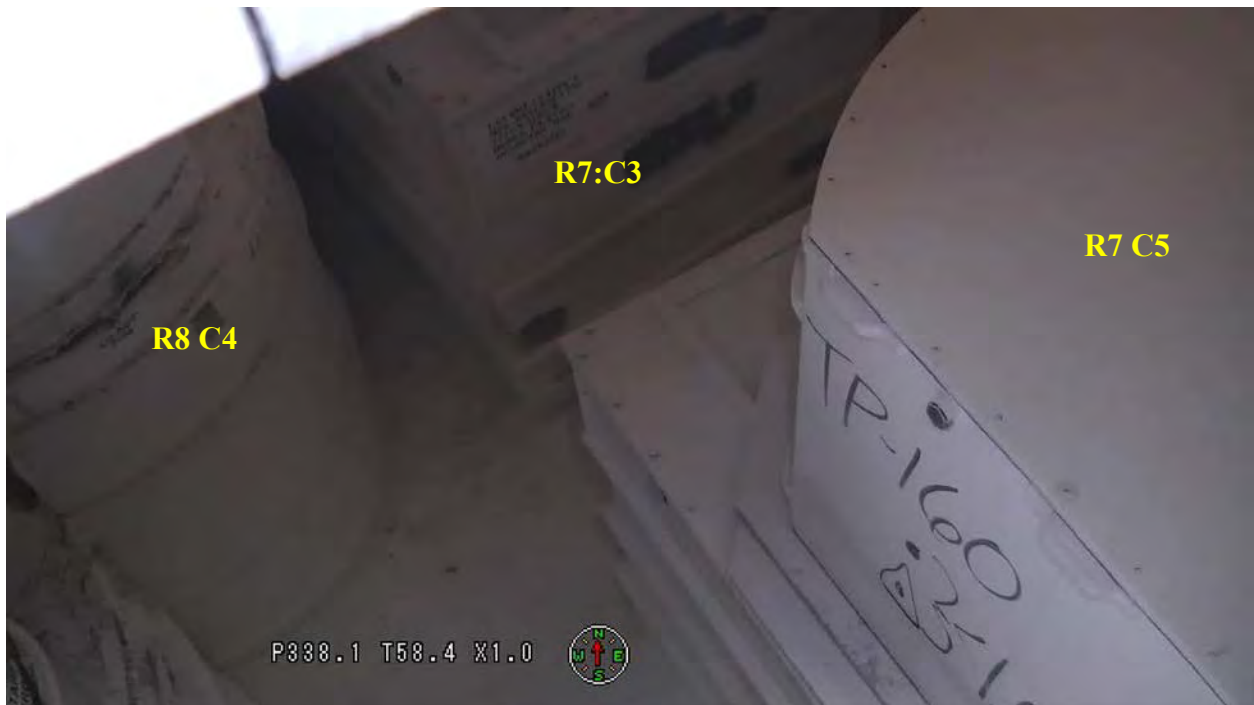
AIB-FST-10695

AIB-FST-10707: R5:C3 and R7:C3 – Rock bolt retaining plate on floor
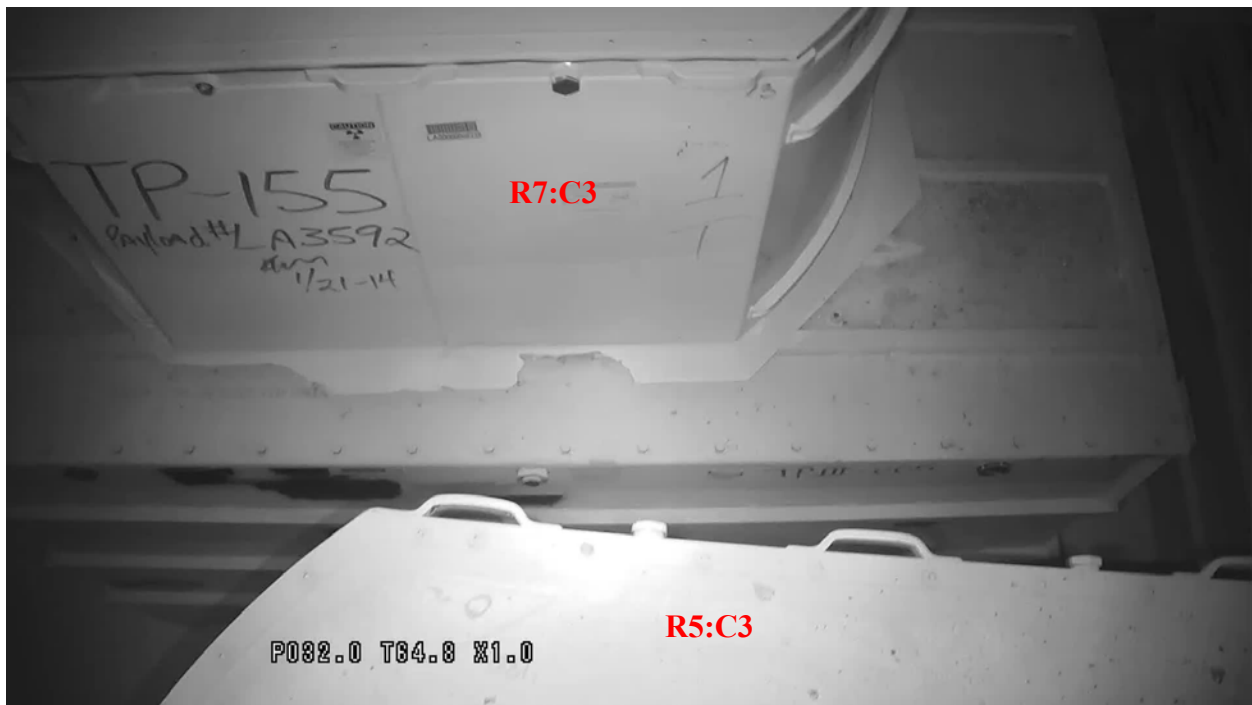
AIB-FST-10708: R5:C3 and R7:C3

AIB-FST-10709: R7:C1 and R7:C3

AIB-FST-10710

AIB-FST-10711

AIB-FST-10712: R7:C3 and R8:C4

AIB-FST-10714

AIB-FST-10737

AIB-FST-10738

AIB-FST-10739

AIB-FST-10740: R2:C6 and R3:C5

AIB-FST-10741

AIB-FST-10742

AIB-FST-10743

AIB-FST-10744

AIB-FST-10745

AIB-FST-10746
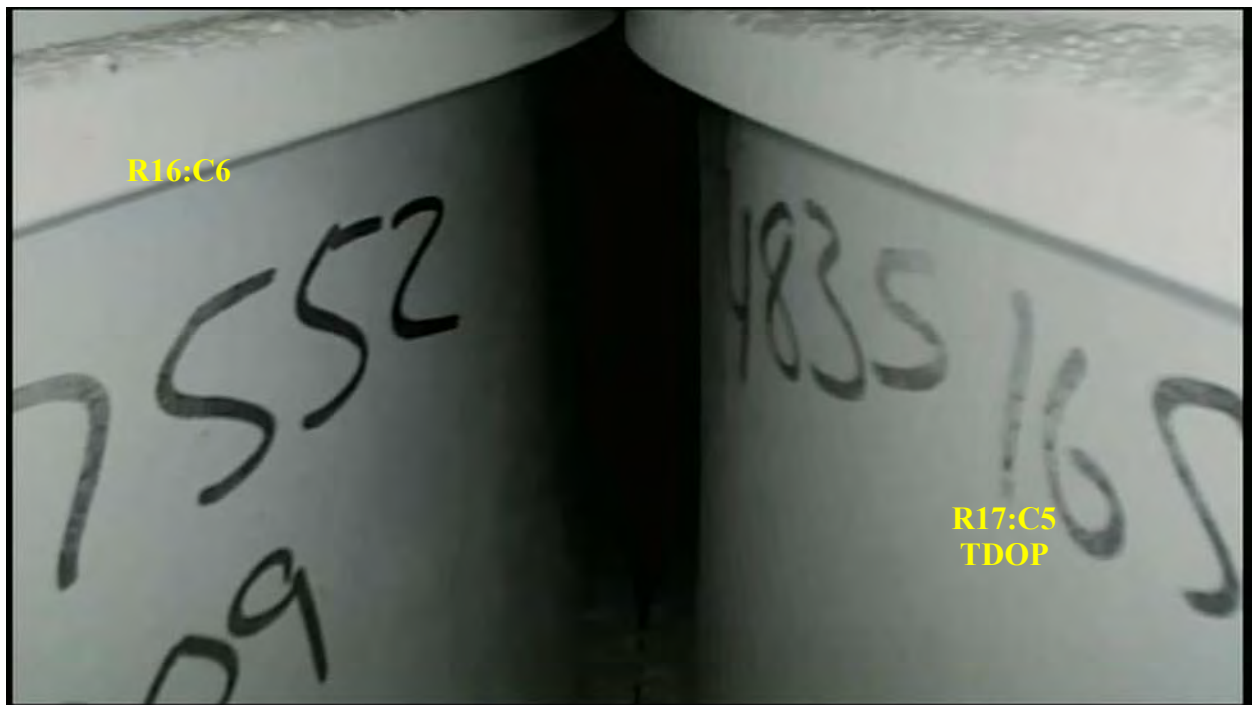
AIB-FST-10747: R16:C6 and R17:C5

AIB-FST-10748: R16:C6 and R17:C5

AIB-FST-10749: R16:C4 and R17:C5

AIB-FST-10750: R16:C4 and R17:C5

AIB-FST-10751
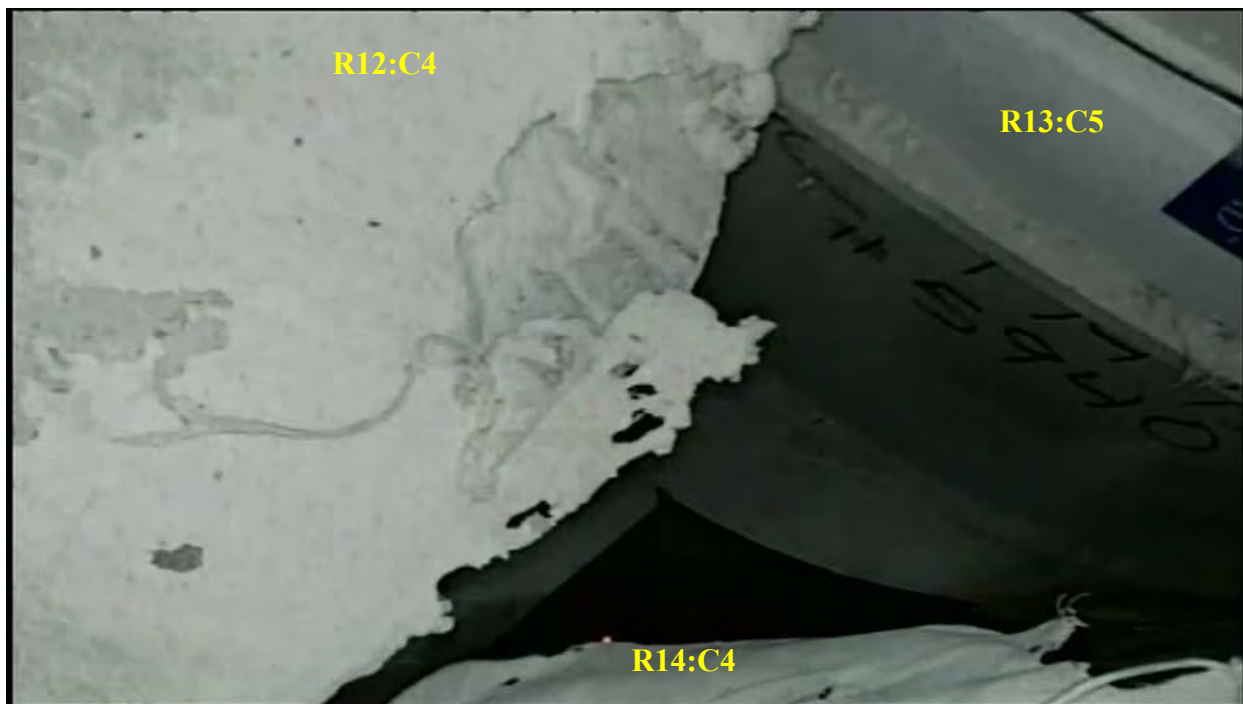
AIB-FST-10752

AIB-FST-10753: R12:C4 and R13:C5

AIB-FST-10754: R12:C4 – Array face (west) view

AIB-FST-10755: R12:C4 – Array face (west) view

AIB-FST-10756: R12:C4 and R13:C5

AIB-FST-10757: R12:C4 and R13:C5

AIB-FST-10758: R12:C4 – Array face (west) view

AIB-FST-10759: R12:C4 and R13:C5

AIB-FST-10760

AIB-FST-10761: R12:C4 and R13:C3
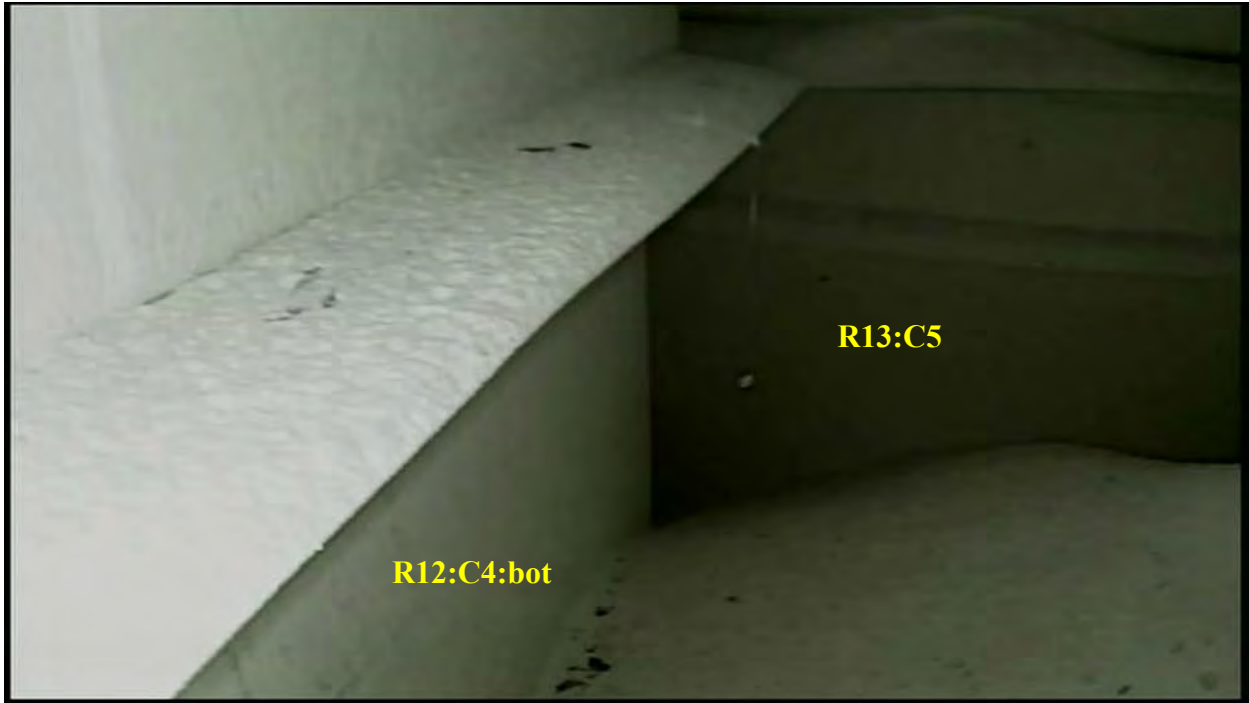
AIB-FST-10762: R12:C4 and R13:C5

AIB-FST-10763: R12:C4 - Array face (west) view - Top

AIB-FST-10764: R12:C4 and R13:C3
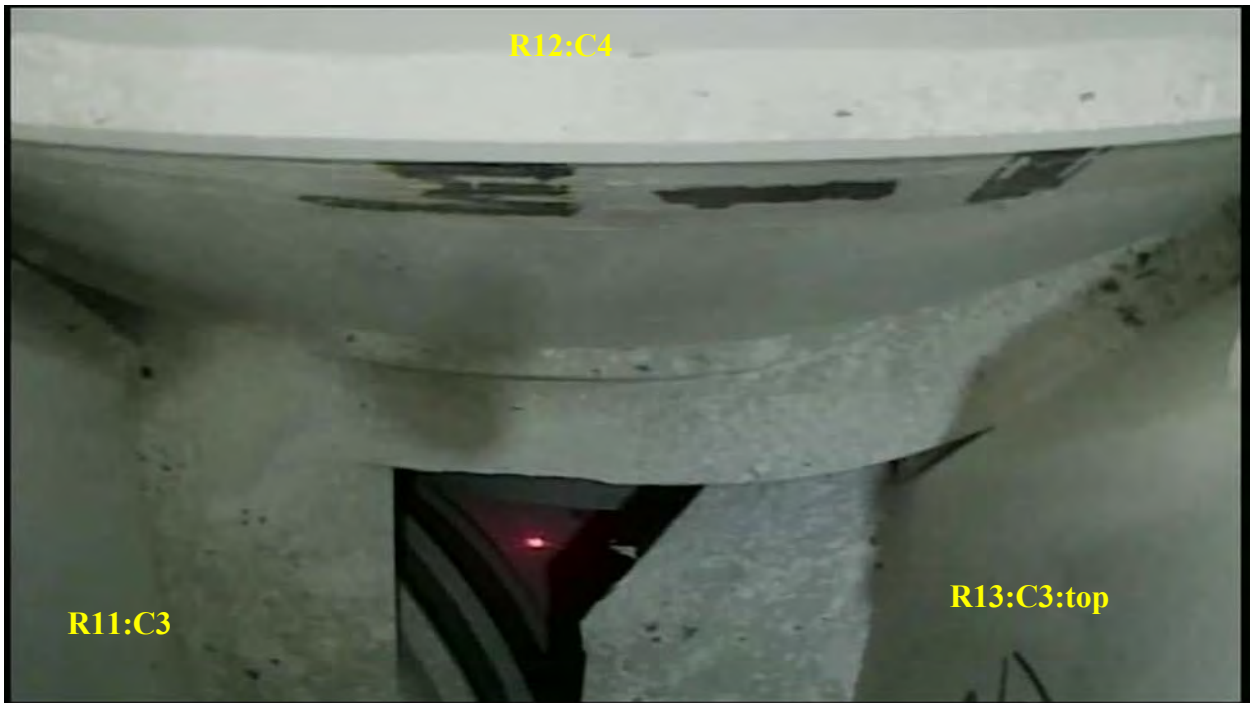
AIB-FST-10765

AIB-FST-10766: R11:C3 and R12:C4 – Cantilevered material

AIB-FST-10767: R11:C3 and R12:C4
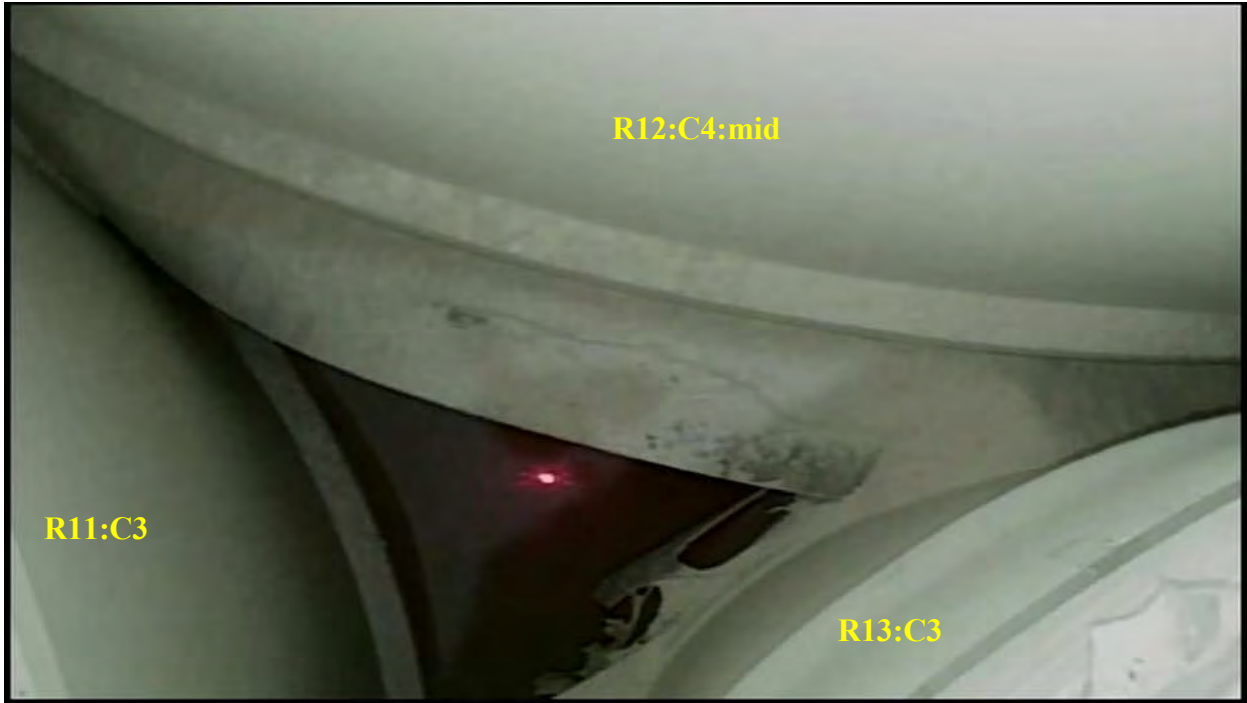
AIB-FST-10768

AIB-FST-10770: R12:C4 – Bulkhead (east) view

AIB-FST-10771: R11:C5 and R12:C4

AIB-FST-10772: R11:C3 and R12:C4

AIB-FST-10773: R11:C3 and R12:C4

AIB-FST-10774: R10:C4 and R12:C4

AIB-FST-10775: R3:C3 – Web-like accumulation

AIB-FST-10776: R3:C3 and R2:C4 – Web-like accumulation

AIB-FST-10780: R3:C1, R3:C3 and R4:C4

AIB-FST-10783: R3:C3 – South view

AIB-FST-10784: R3:C3 – South view

AIB-FST-10786
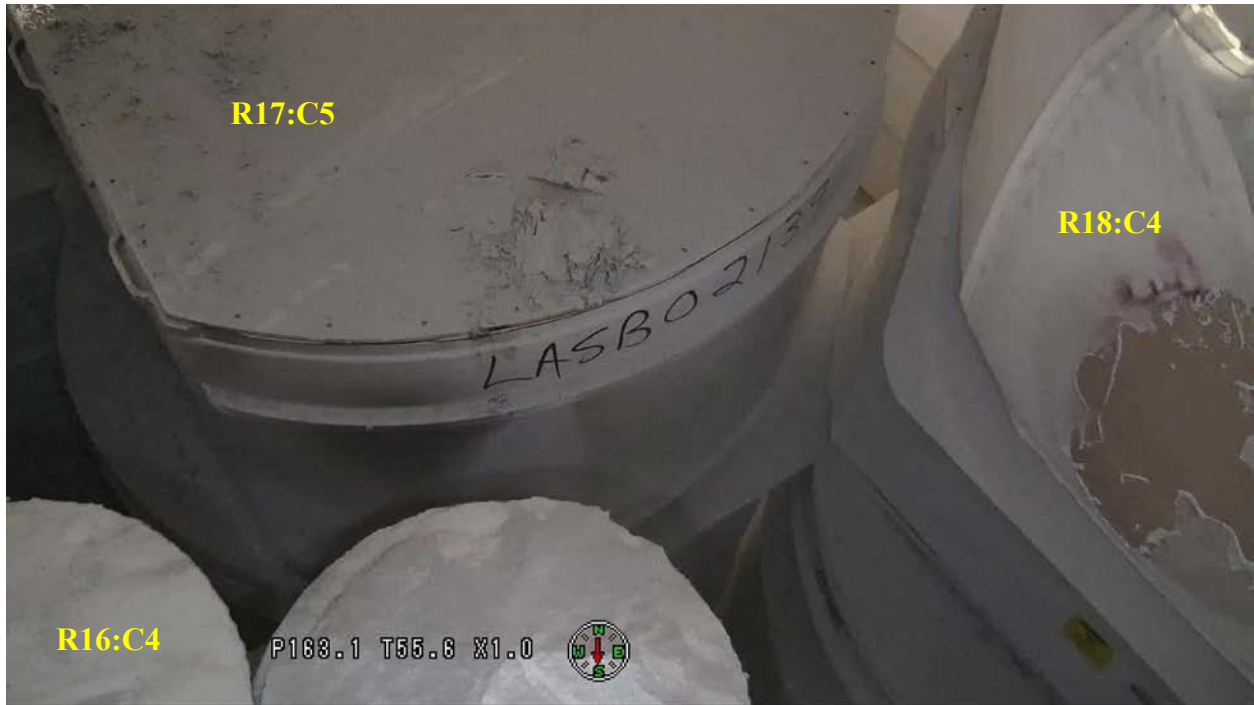
AIB-FST-10788

AIB-FST-10789

AIB-FST-10792: R3:C3 and R4:C2

AIB-FST-10793: R20:C2 and R21:C1
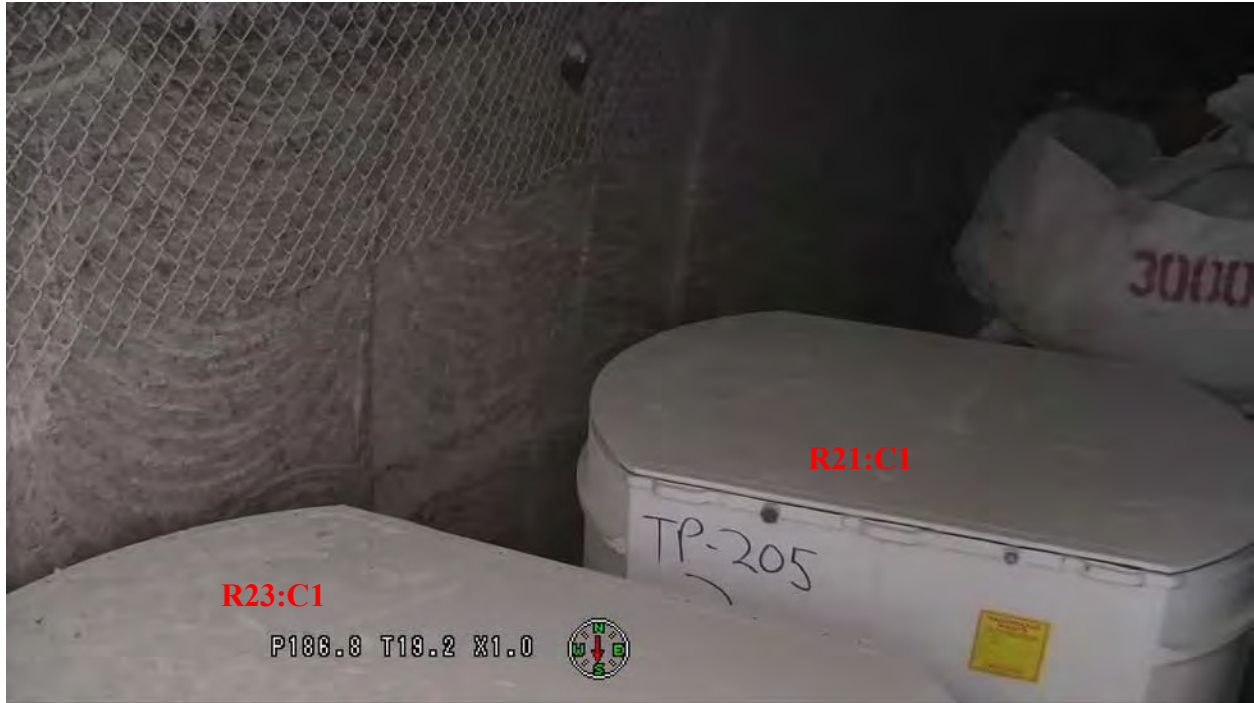
AIB-FST-10794: R21:C1 and R23:C1
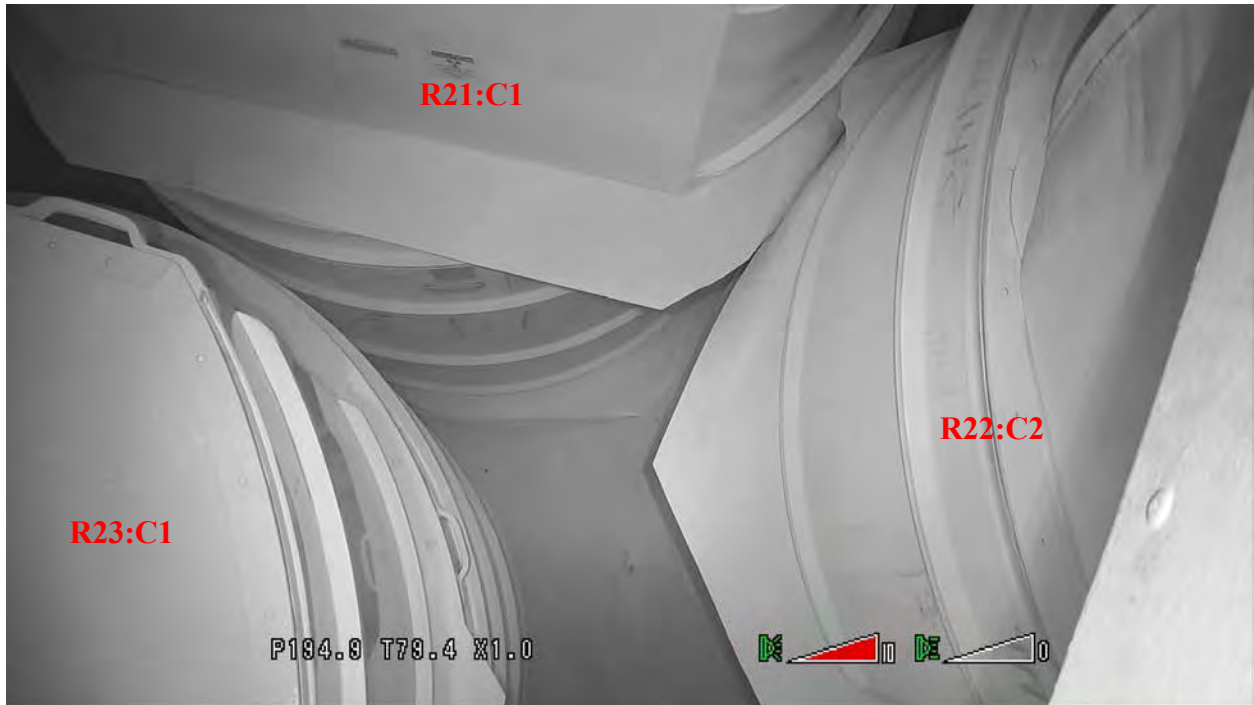
AIB-FST-10795

AIB-FST-10796: R20:C2 and R21:C1

AIB-FST-10797: R20:C2 and R21:C1

AIB-FST-10798

AIB-FST-10809: North side of beam looking east toward bulkhead

AIB-FST-10810: South side of beam looking east toward bulkhead

AIB-FST-10811: R7:C3 and R5:C3 - Bolt plate on floor

AIB-FST-10812: R12:C6 – Salt debris

AIB-FST-10813: R7:C3 and R7:C5 – Bolt plate and compression nut on floor

AIB-FST-10814: North rib looking east toward bulkhead from row 24

AIB-FST-10815: North rib near row 21

AIB-FST-10816: North rib near row 20

AIB-FST-10817: North rib near row 19

AIB-FST-10818: North rib near row 3

AIB-FST-10819: North rib near row 2

AIB-FST-10820: North rib near row 9

AIB-FST-10822

AIB-FST-10823: R11:C1 and R13:C1

AIB-FST-10824: R13:C1 and R15:C1

AIB-FST-10825

AIB-FST-10826: R13:C1 – Array face (west) view

AIB-FST-10827

AIB-FST-10828: R18:C4 - Salt on top of super sack

AIB-FST-10829

AIB-FST-10830

AIB-FST-10843: R11:C5 and R12:C4

AIB-FST-10844: R11:C5 and R12:C4

R11:C5

AIB-FST-10845: R10:C4 and R12:C4

AIB-FST-10846: R12:C4 and R13:C3

AIB-FST-10847: R10:C4 and R12:C4

AIB-FST-10848

AIB-FST-10849

AIB-FST-10850

AIB-FST-10851

AIB-FST-10852

AIB-FST-10853

AIB-FST-10854

AIB-FST-10855

AIB-FST-10856

AIB-FST-10877

AIB-FST-10878: R3:C5 and R4:C4

AIB-FST-10879

AIB-FST-10880

AIB-FST-10881: R16:C2 and R17:C3 – Cardboard stiffener bridge
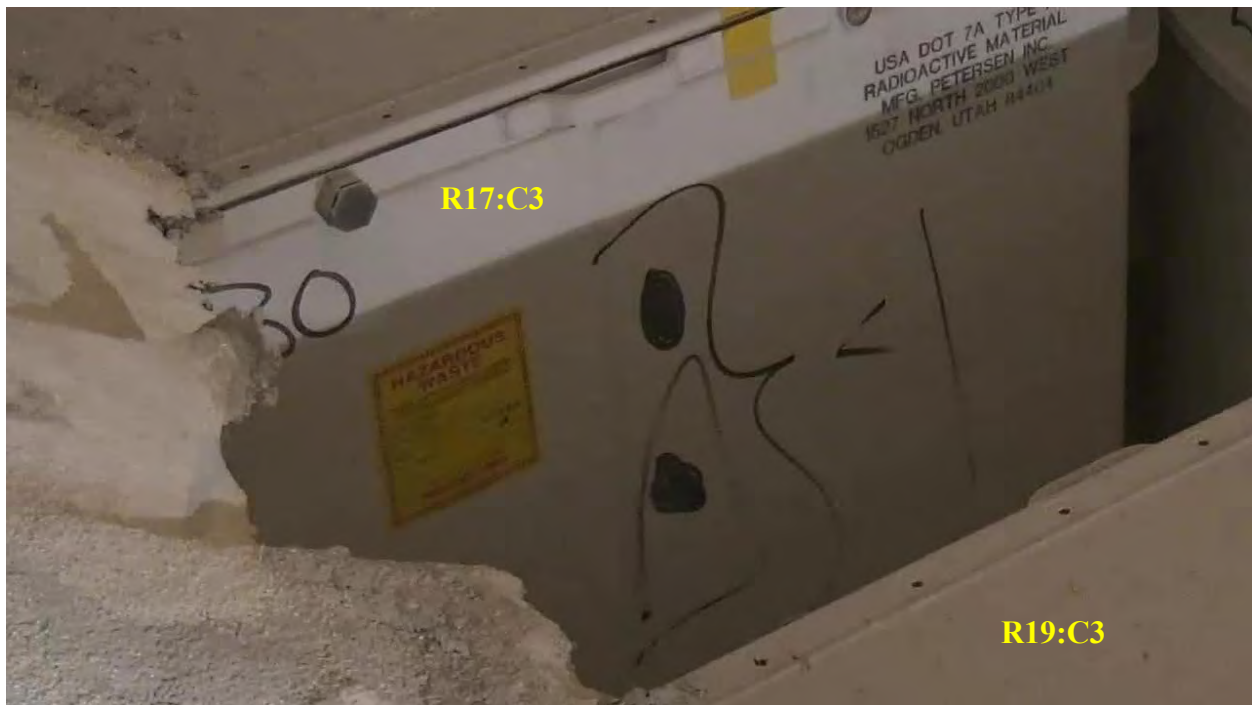
AIB-FST-10882: R17:C3 and R19:C3

AIB-FST-10883

AIB-FST-10884

AIB-FST-10885

AIB-FST-10886: R17:C3 and R17:C3
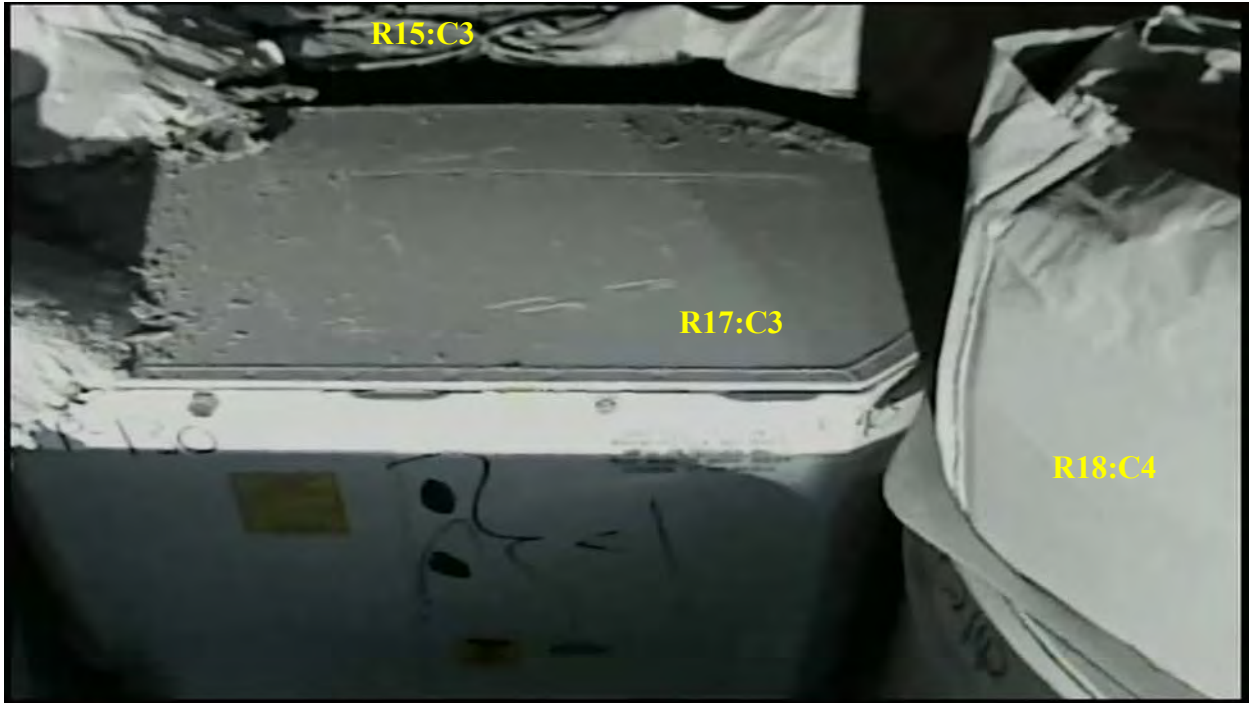
AIB-FST-10887

AIB-FST-10888

AIB-FST-10889

AIB-FST-10890: R16:C4 and R17:C3 – Cardboard stiffener on floor
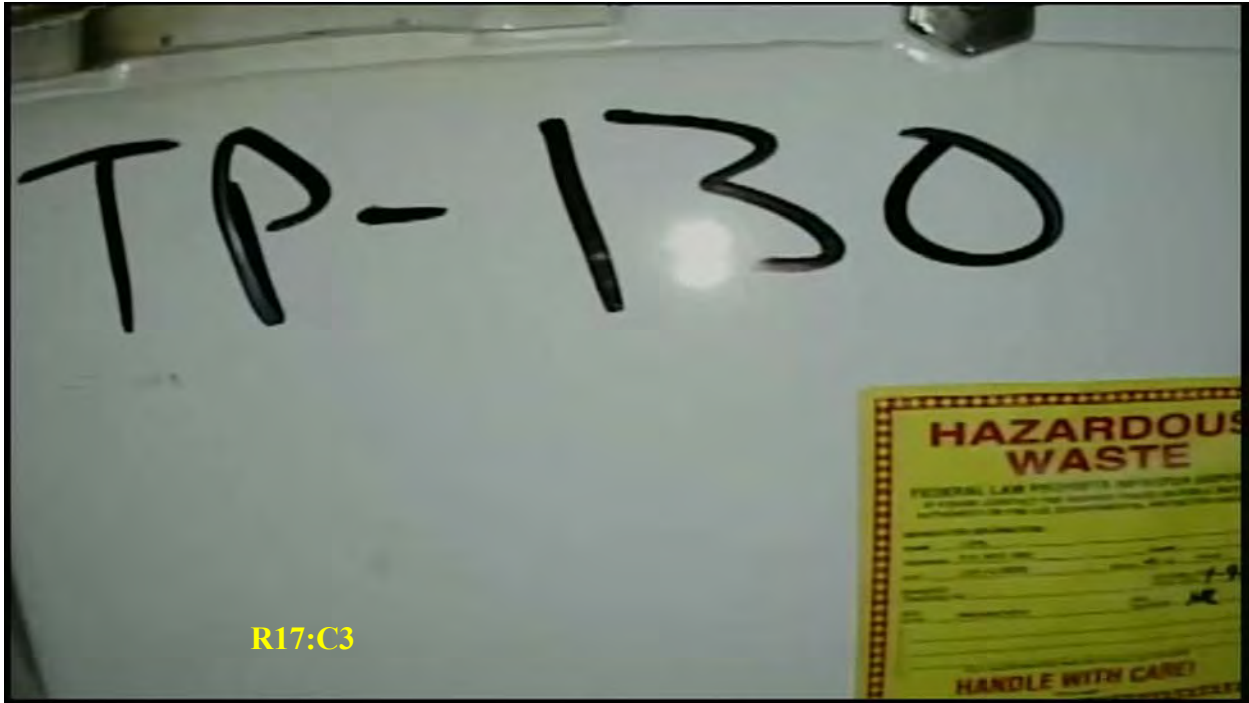
AIB-FST-10891: R17:C3 – Bulkhead (east) view

AIB-FST-10892: R16:C4 - Unidentified material above dunnage drum

AIB-FST-10911

AIB-FST-10912

AIB-FST-10913: R18:C2 and R20:C2

AIB-FST-10914

AIB-FST-10918

AIB-FST-10919

AIB-FST-10920: R13:C3 and R14:C2
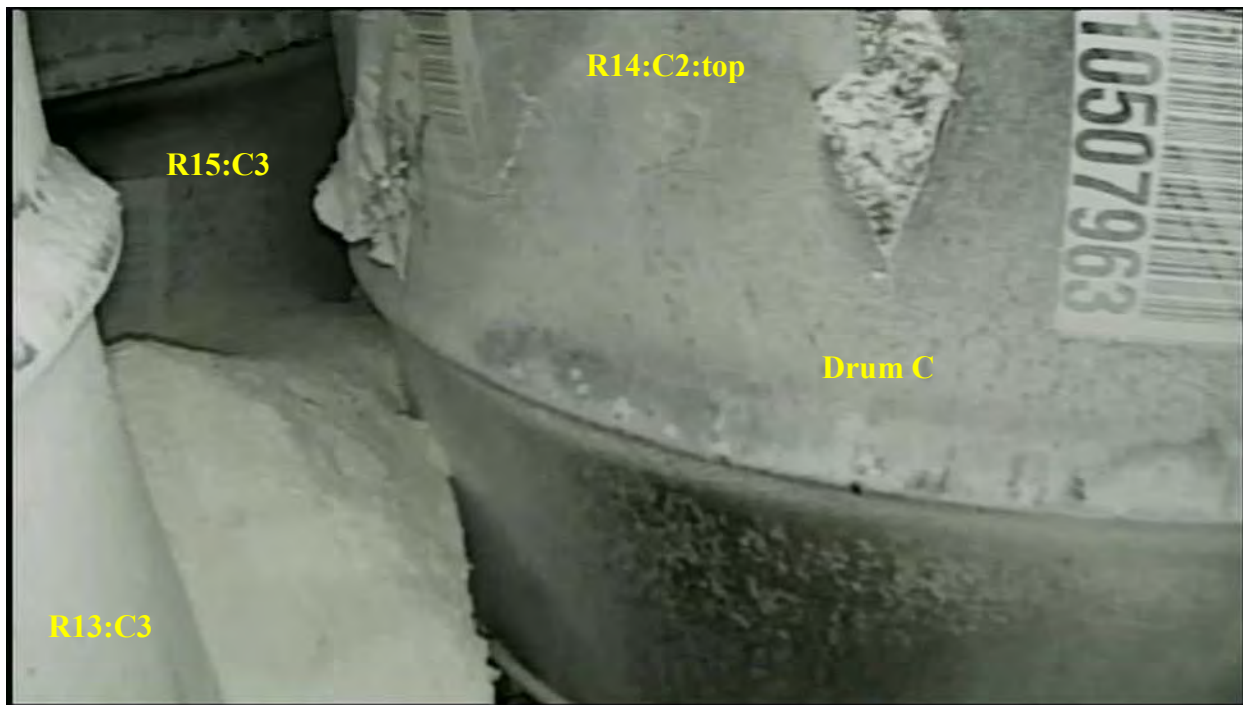
AIB-FST-10921

AIB-FST-10922: R14:C2 – Drum C
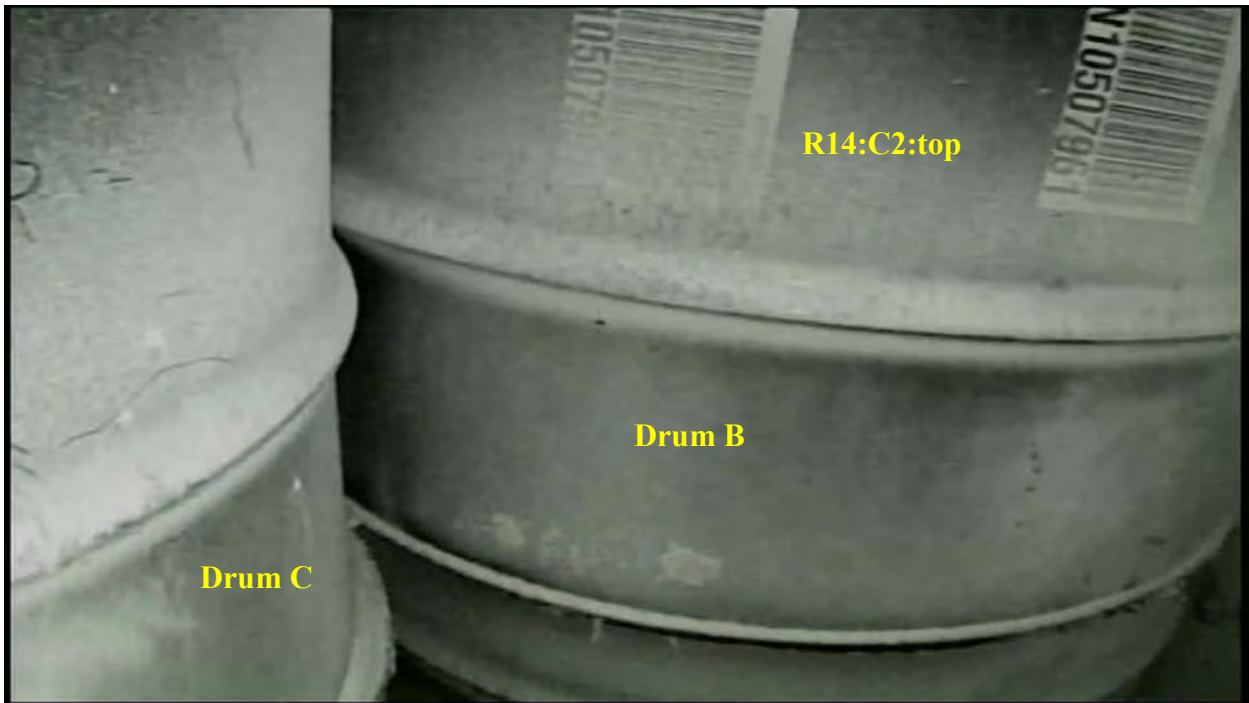
AIB-FST-10923: R14:C2 – Drum B and Drum C
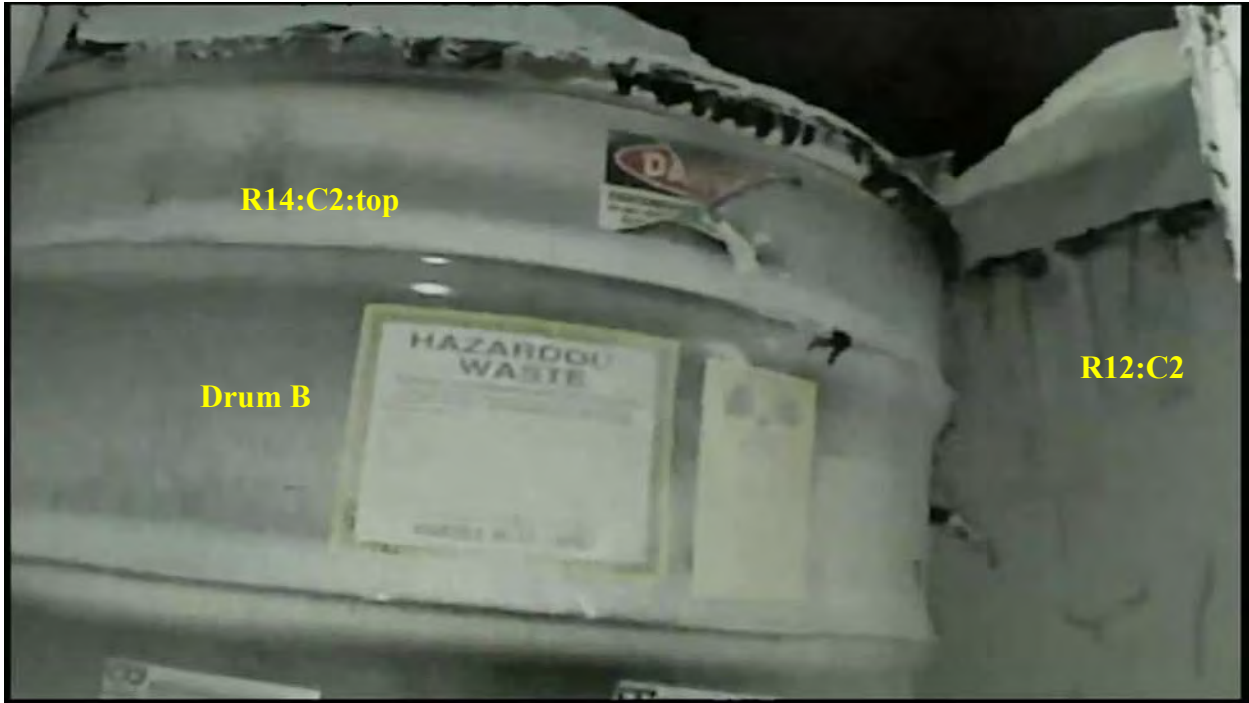
AIB-FST-10924: R12:C2 and R14:C2

AIB-FST-10925: R14:C2 – Drum B and drum C

AIB-FST-10926

AIB-FST-10927

AIB-FST-10928

AIB-FST-10929

AIB-FST-10930: R14:C2 – Drum C
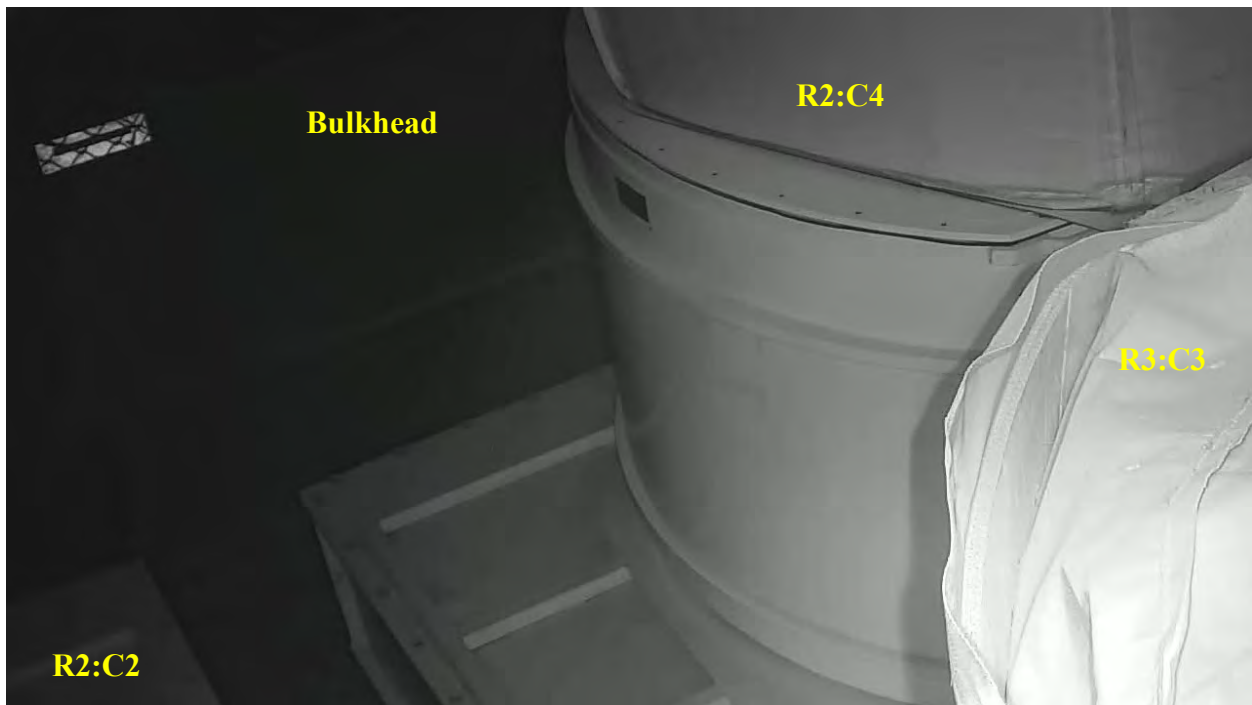
AIB-FST-10931

AIB-FST-10932: R2:C4 and bulkhead

AIB-FST-10933: R2:C4 and bulkhead

AIB-FST-10934: R2:C4 and bulkhead

AIB-FST-10935: R2:C2 and R2:C4

AIB-FST-10936

AIB-FST-10937: R2:C4 - North view – Web-like accumulation

AIB-FST-10938

AIB-FST-10939: R20:C2 – Bulkhead (east) and south views

AIB-FST-10940

AIB-FST-10941

AIB-FST-10942: R20:C2 and north rib

AIB-FST-10943: R20:C2, R20:C2 and north rib

AIB-FST-10945: R14:C4 and R16:C4 – Drum C overhanging TDOP

AIB-FST-10946

AIB-FST-10947: R16:C4 and R18:C4

AIB-FST-10948: R16:C4 – TDOP lid

AIB-FST-10949: R16:C4 - Gap between dunnage drum lid and reinforcing plate

AIB-FST-10950: R16:C4 – Orange material above drum D

AIB-FST-10951: R15:C5 and R16:C4

AIB-FST-10952: R14:C4 and R16:C4

AIB-FST-10953

AIB-FST-10954

AIB-FST-10955: R15:C5 and R16:C4 – Drum E breach – Bulkhead (east) view

AIB-FST-10956: R16:C4 – Drum E breach – Bulkhead (east) view

AIB-FST-10957
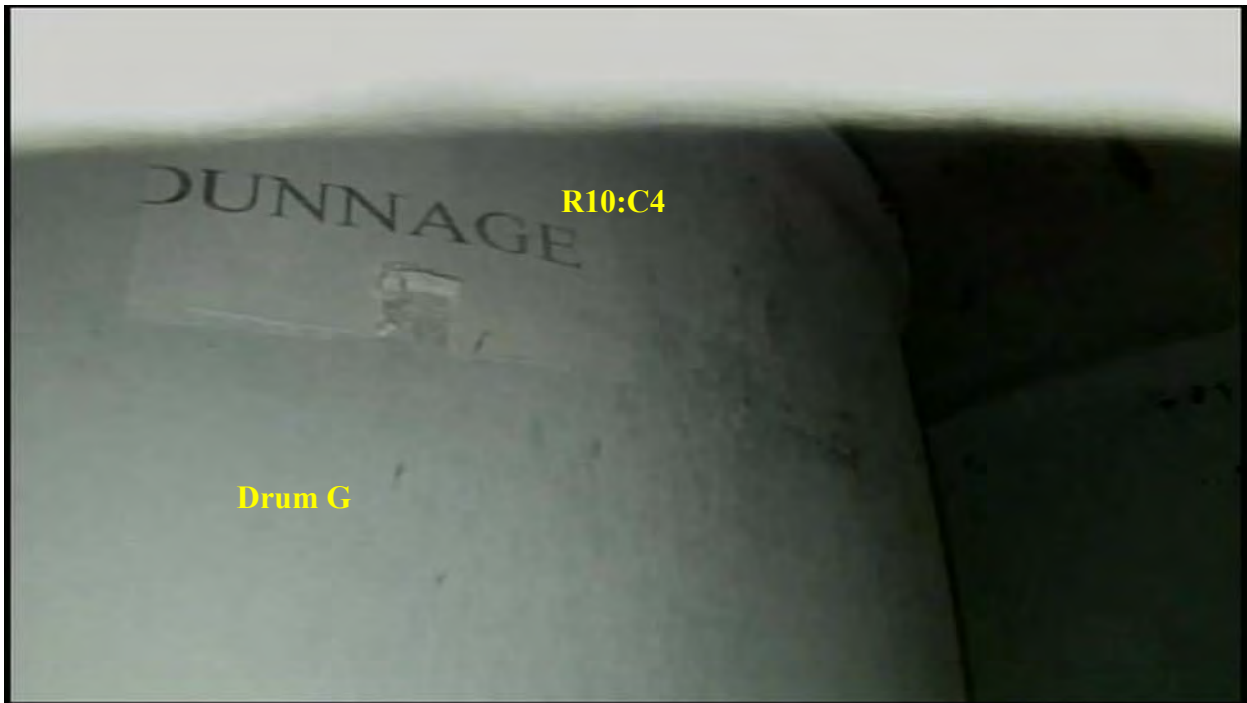
AIB-FST-10958: R10:C4 – Drum G

AIB-FST-10959

AIB-FST-10960

AIB-FST-10961

AIB-FST-10962

AIB-FST-10963

AIB-FST-10964

AIB-FST-10965

AIB-FST-10966

AIB-FST-10967: R5:C1, R07:C1 and north rib

AIB-FST-10968

AIB-FST-10971

AIB-FST-10972

AIB-FST-10973

AIB-FST-10974

AIB-FST-10975

AIB-FST-10976

AIB-FST-10977

AIB-FST-11081: R14:C2 and R15:C1
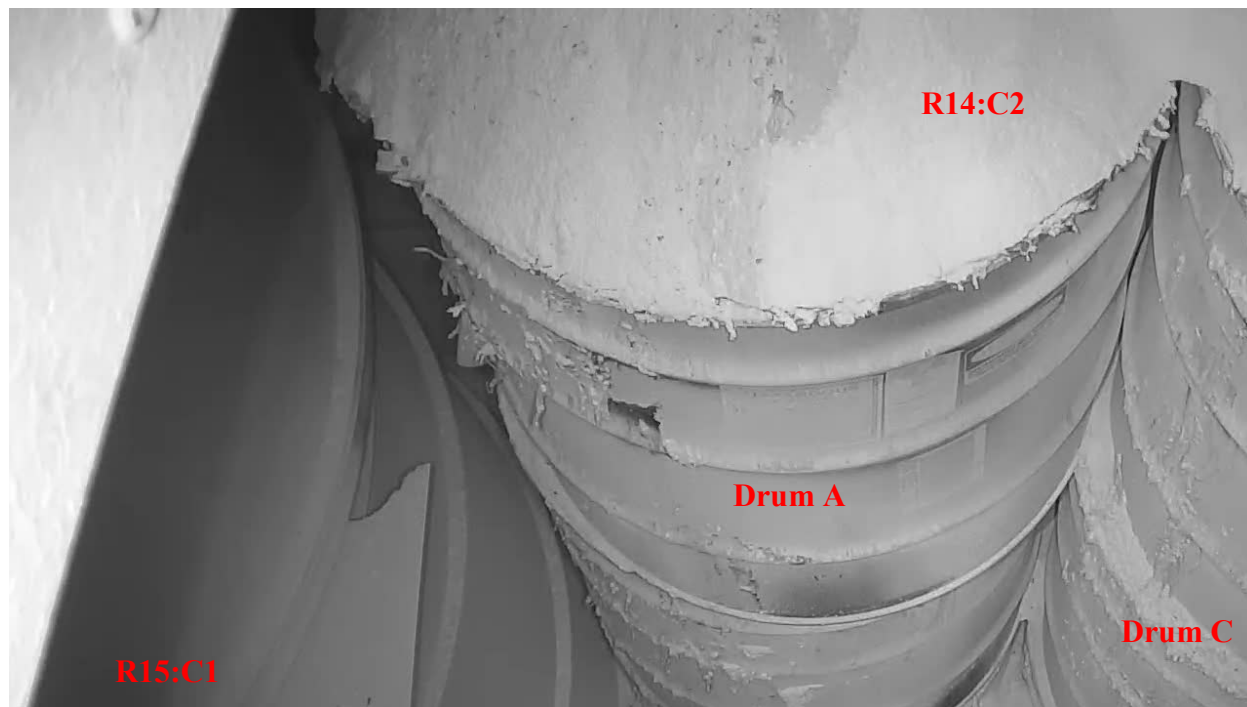
AIB-FST-11082: R14:C2 and R15:C1
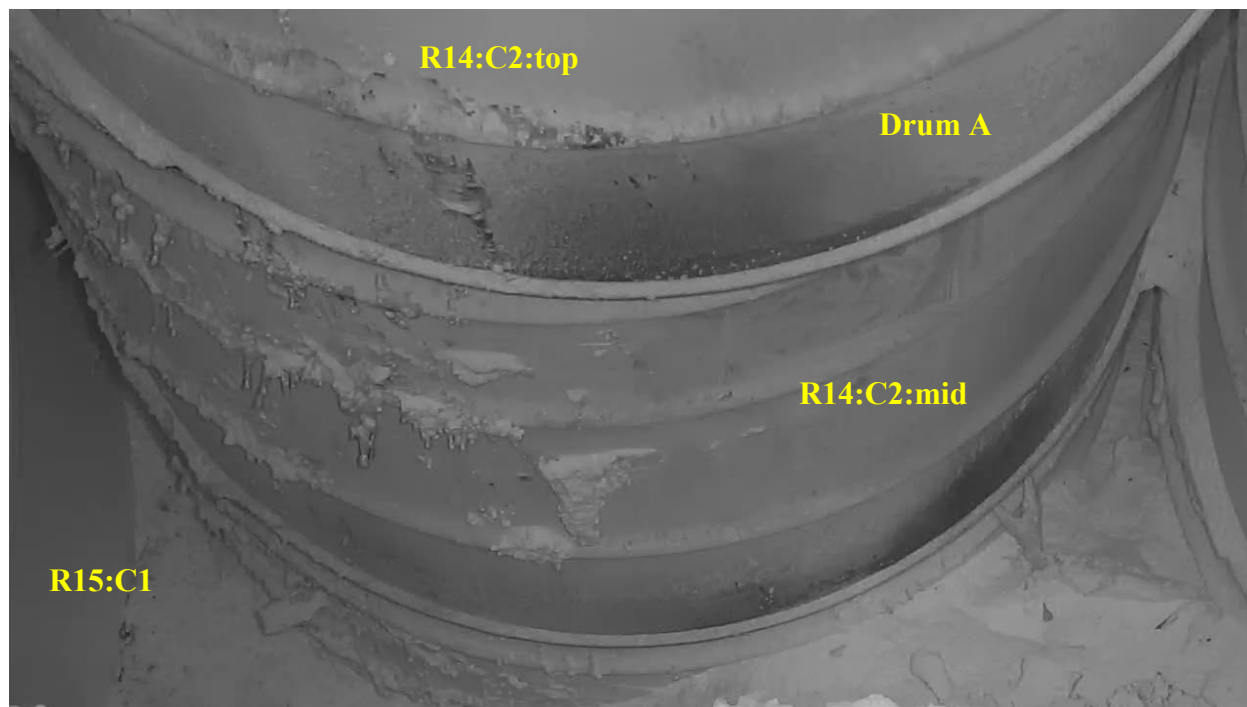
AIB-FST-11083: R14:C2 – Drum A

AIB-FST-11084: R14:C2 – Drum A
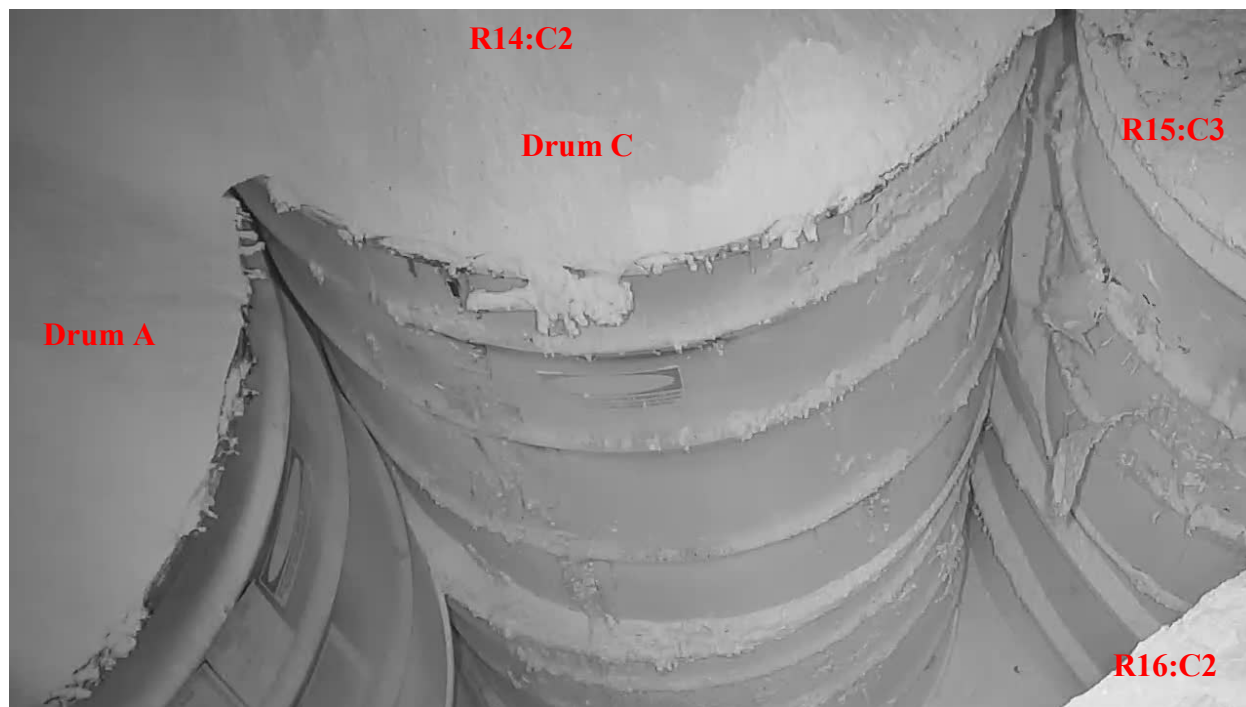
AIB-FST-11085: R14:C2 and R15:C3

AIB-FST-11086: R13:C4 and R14:C2

AIB-FST-11087: R14:C2 and R15:C1

AIB-FST-11089: R14:C2 and R15:C1

AIB-FST-11091: R14:C2 and R15:C1

AIB-FST-11092: R12:C2 and R14:C2

AIB-FST-11093: R14:C2 and R15:C1

AIB-FST-11094: R14:C2 and R15:C1

AIB-FST-11095: R14:C2:top – Drum A
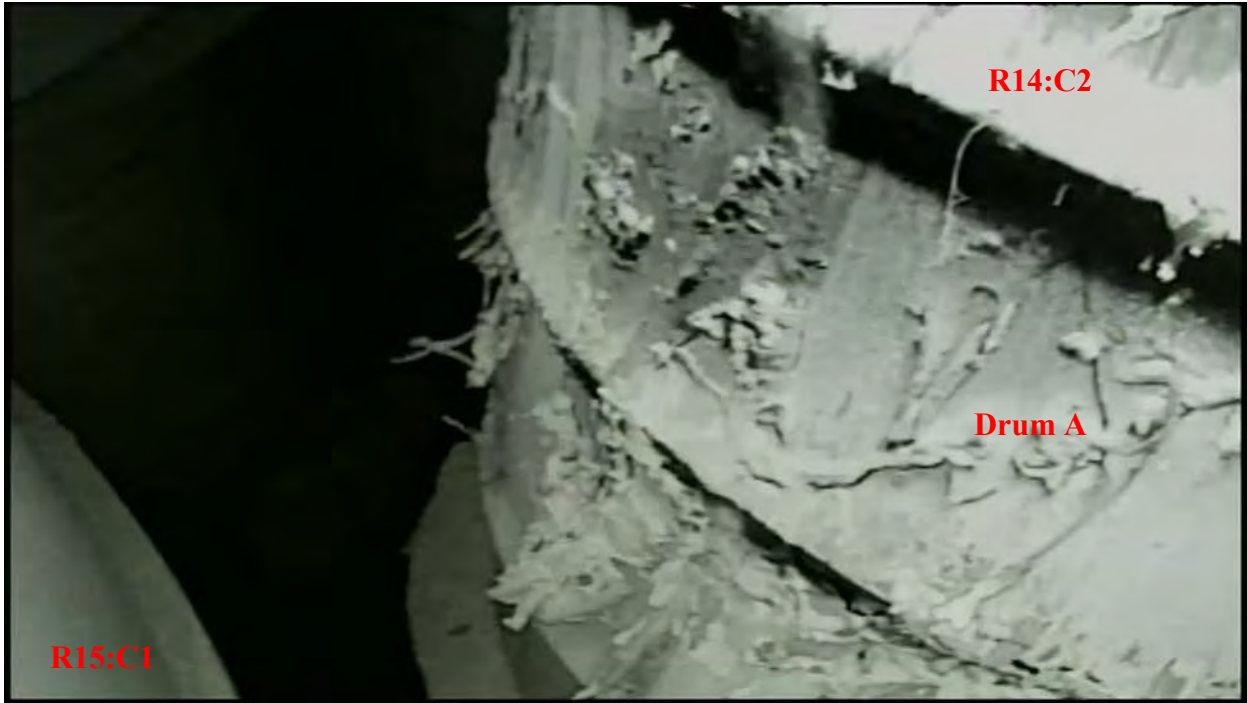
AIB-FST-11096: R14:C2:top – Drum A
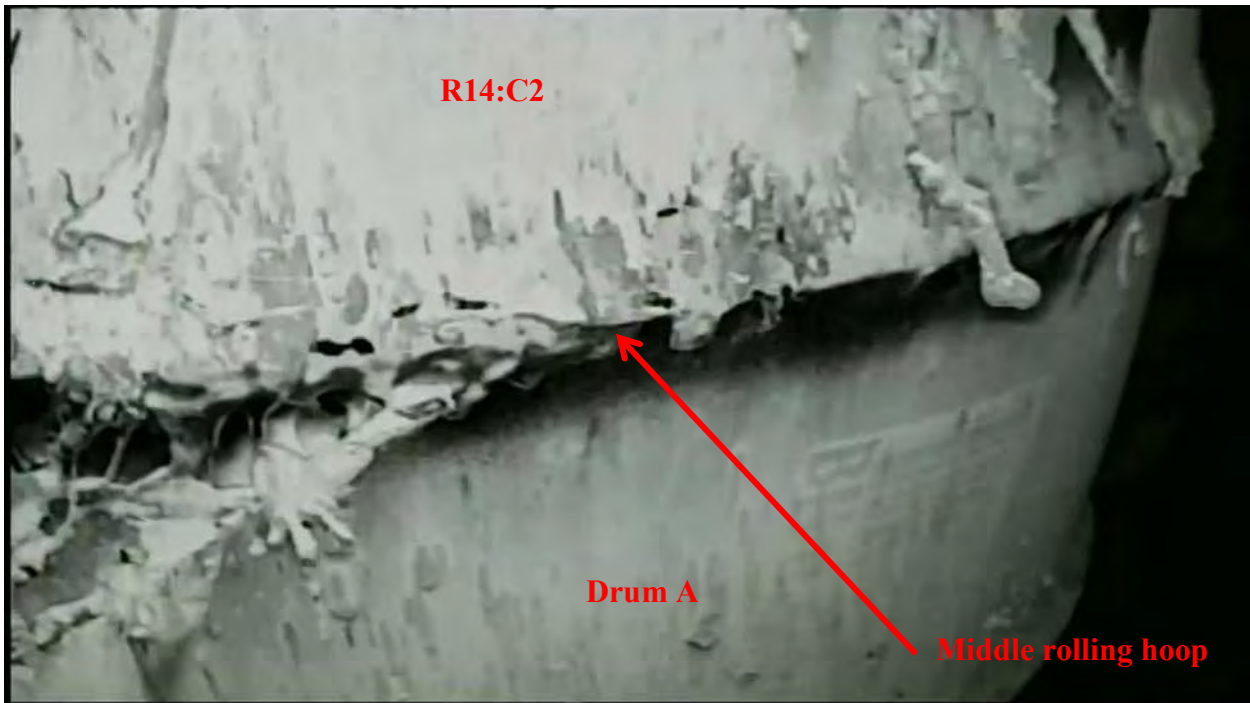
AIB-FST-11097: R14:C2:top – Drum A – North view

AIB-FST-11098: R14:C2 – Drum A

AIB-FST-11100: R14:C2:bot and R16:2:bot

AIB-FST-11101: R14:C2 – Drum C
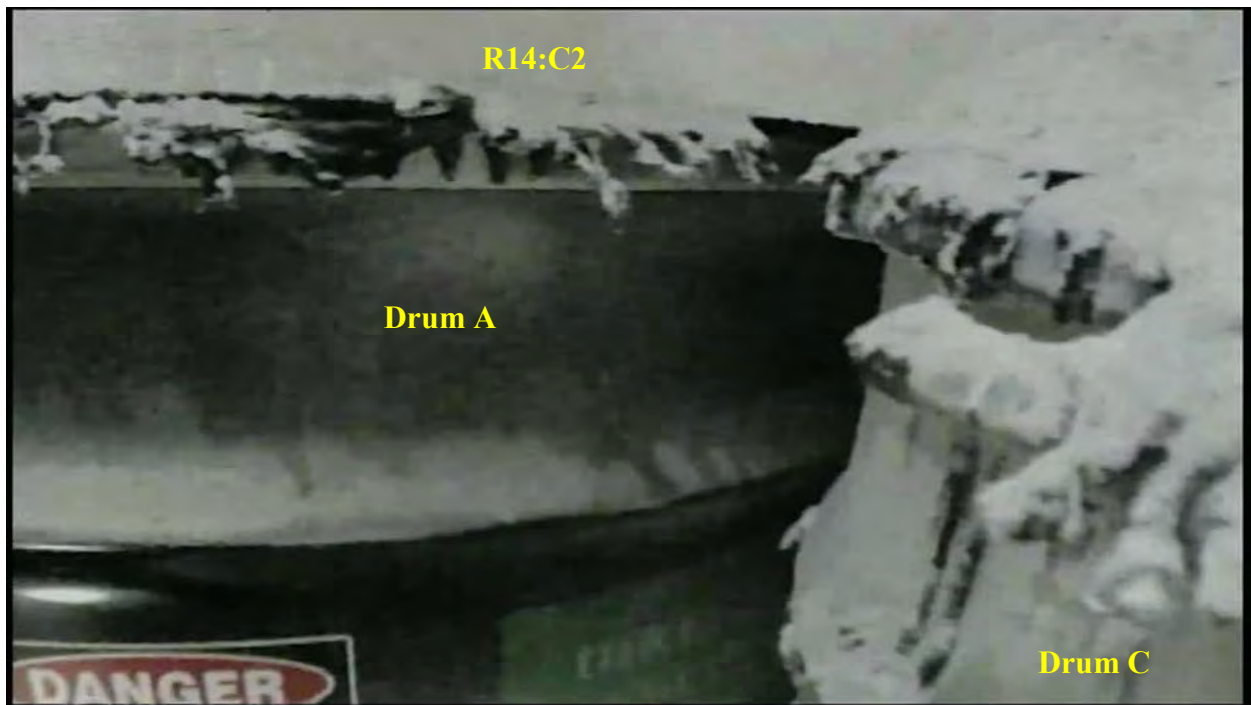
AIB-FST-11102: R14:C2 – Drum A and drum C

AIB-FST-11103: R14:C2 and R15:C1

AIB-FST-11104

AIB-FST-11106: R14:C2 Drum B

AIB-FST-11115: R5:C3 and R7:C3

AIB-FST-11116: R5:C1 – Reinforcement plate

AIB-FST-11117

AIB-FST-11118

AIB-FST-11119

AIB-FST-11120: R12:C2 and R13:C1

AIB-FST-11121

AIB-FST-11122

AIB-FST-11123: R12:C2 – Array face (west) view

AIB-FST-11124

AIB-FST-11125: R12:C2 and R14:C2

AIB-FST-11126

AIB-FST-11127: R12:C2 and R13:C1

AIB-FST-11128: R11:C3 and R12:C2

AIB-FST-11129: R11:C3 and R12:C2
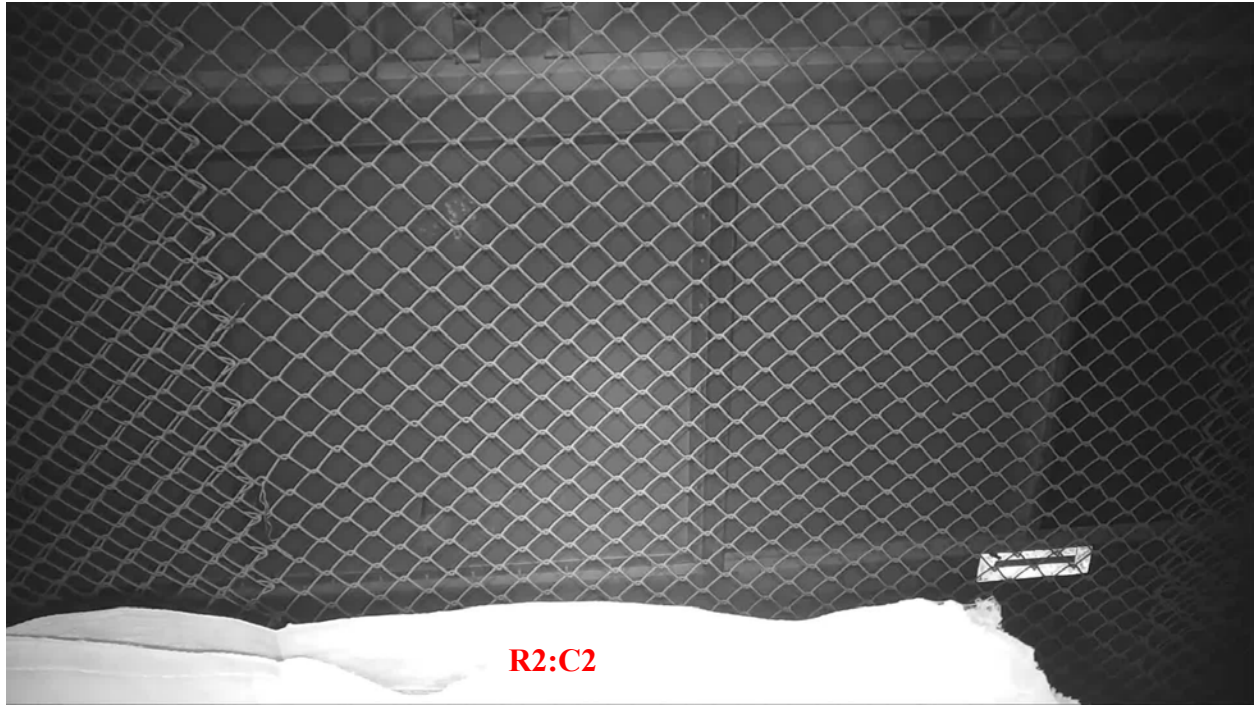
AIB-FST-11130: Room 7, Panel 7 bulkhead near column 2

AIB-FST-11131: Room 7, Panel 7 bulkhead near base of the north rib

AIB-FST-11132: Room 7, Panel 7 bulkhead adjacent to north rib

AIB-FST-11134: Room 7, Panel 7 VOC sample tubing on north rib

AIB-FST-11135: Room 7, Panel 7 bulkhead above column 2

AIB-FST-11136: Room 6, Panel 7, bulkhead (south view)

AIB-FST-11137: Room 7, Panel 7 bulkhead (east view)

AIB-FST-11139

AIB-FST-11140: R3:C1 – Bulkhead (east) view

AIB-FST-11141: R3:C1 – Bulkhead (east) view

AIB-FST-11142: R3:C1, R5:C1 and north rib

AIB-FST-11143: R2:C2 and R3:C1

AIB-FST-11144: R3:C1 and R5:C1

AIB-FST-11145: R5:C1 and R7:C1

AIB-FST-11146: R3:C3 and R4:C2

AIB-FST-11147: R3:C3 and R4:C2

AIB-FST-11149: R23:C1 and R24:C2
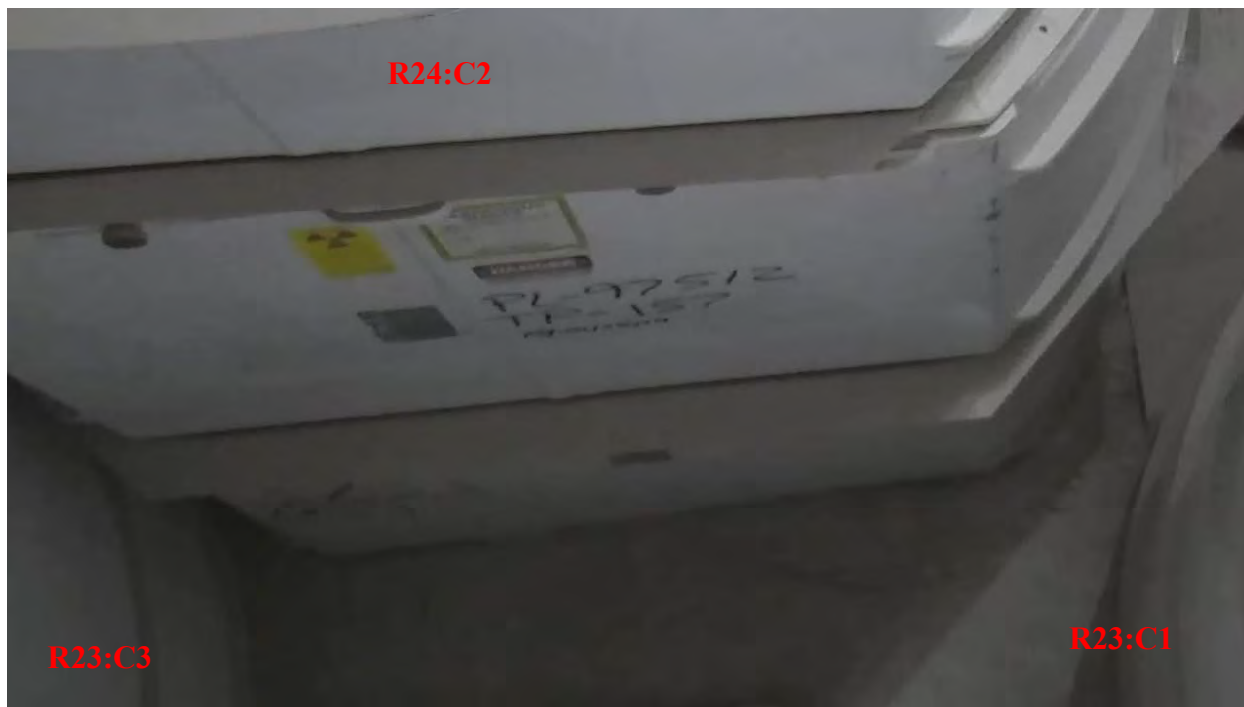
AIB-FST-11150

AIB-FST-11151: R24:C2

AIB-FST-11152: R22:C2 and R24:C2

AIB-FST-11153

AIB-FST-11155

AIB-FST-11156: R21:C1 and R22:C2
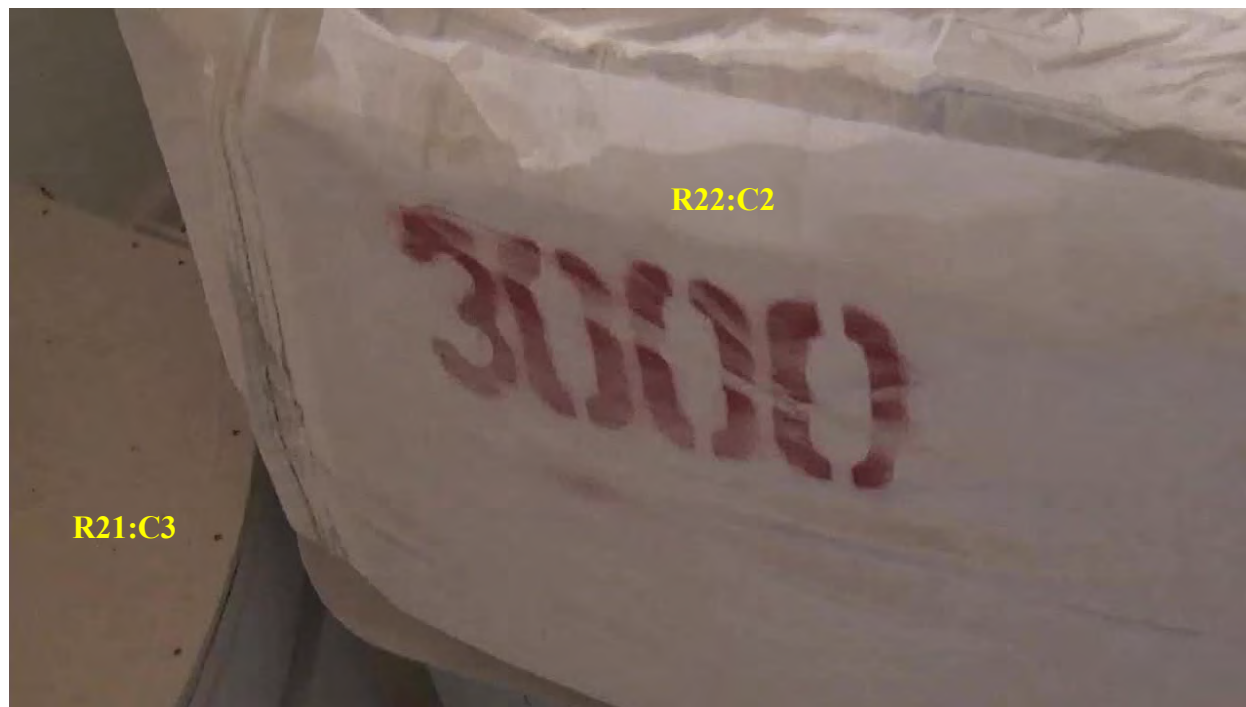
AIB-FST-11157: R21:C3 and R22:C2

AIB-FST-11158

AIB-FST-11159

AIB-FST-11160

AIB-FST-11161

AIB-FST-11162

AIB-FST-11163: R18:C2

AIB-FST-11164: R18:C2 and R19:C3 – Cardboard stiffener bridge

AIB-FST-11165: R18:C2

AIB-FST-11166

AIB-FST-11169

AIB-FST-11170: R17:C3 and R18:C2

AIB-FST-11171

AIB-FST-11172

AIB-FST-11173: R17:C1 and R18:C2

AIB-FST-11174: R18:C2 and R20:C2

AIB-FST-11175
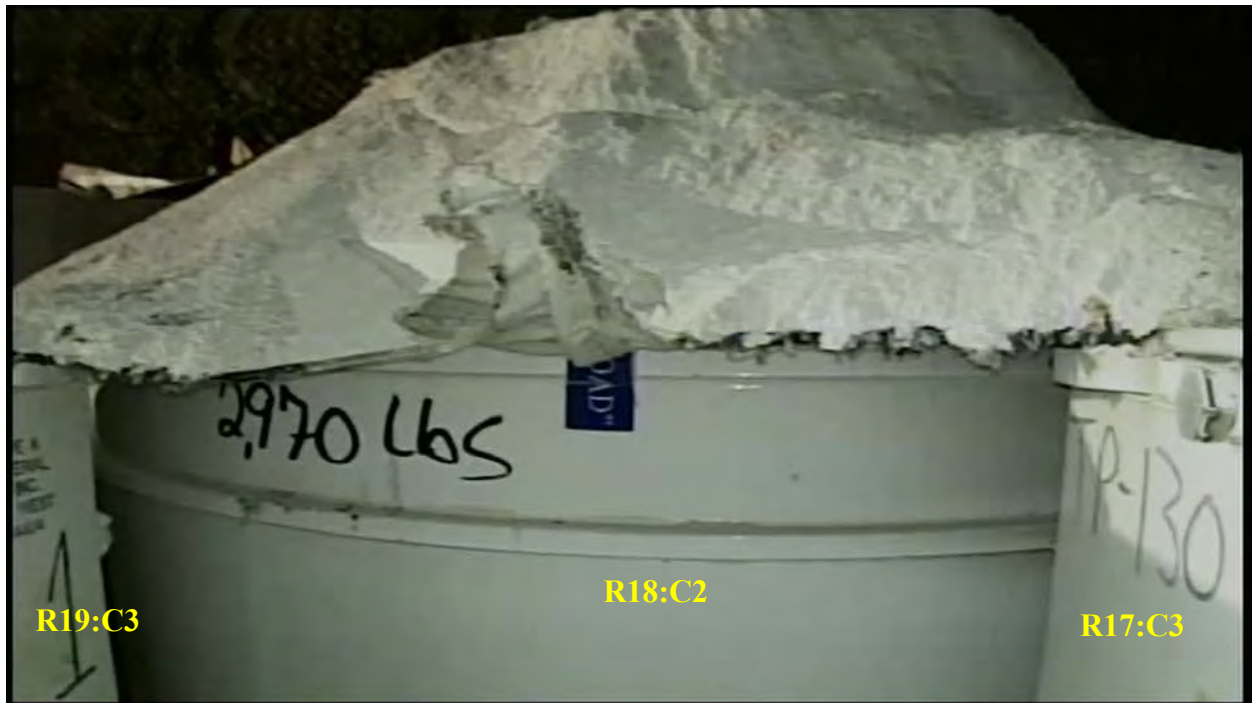
AIB-FST-11177

AIB-FST-11178
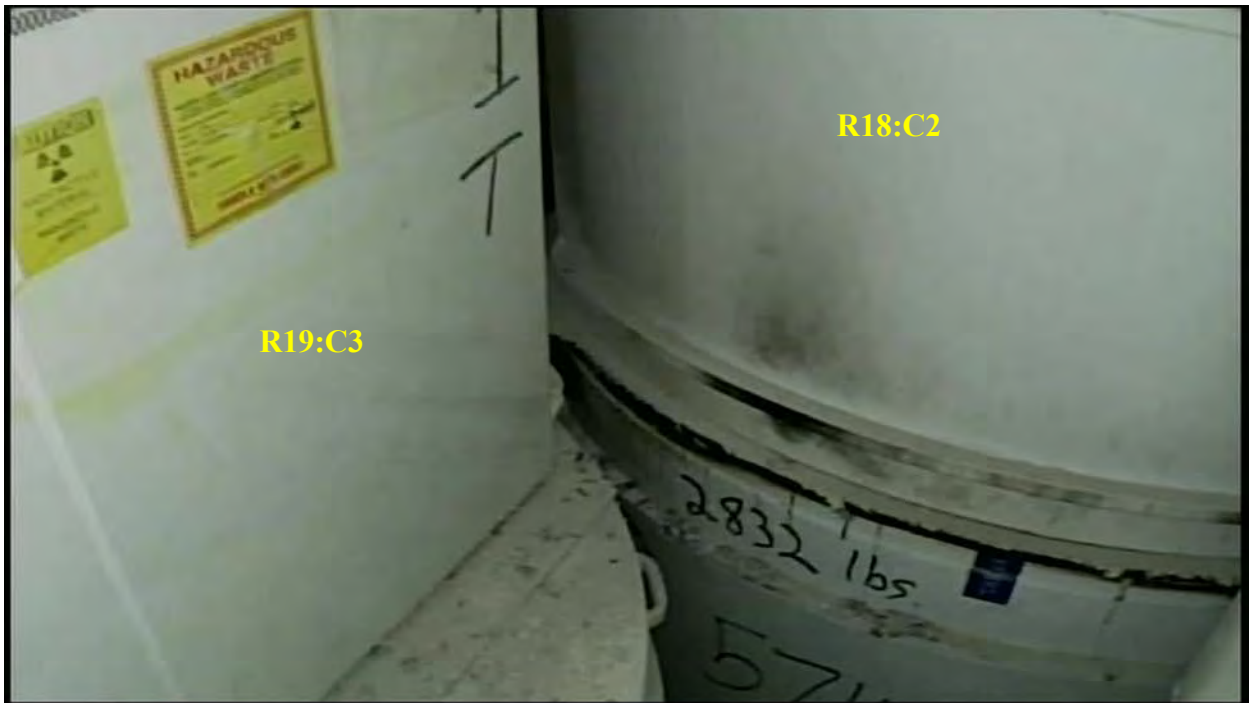
AIB-FST-11179: R18:C2 and R19:C3

AIB-FST-11182

AIB-FST-11183: R17:C1 and R18:C2

AIB-FST-11184: R18:C2 and R20:C2

AIB-FST-11185: R18:C2 and R20:C2

AIB-FST-11186

AIB-FST-11187

AIB-FST-11198

AIB-FST-11199

AIB-FST-11200: R13:C5:top - Bulkhead (east) view

AIB-FST-11201: R12:C4 and R13:C5
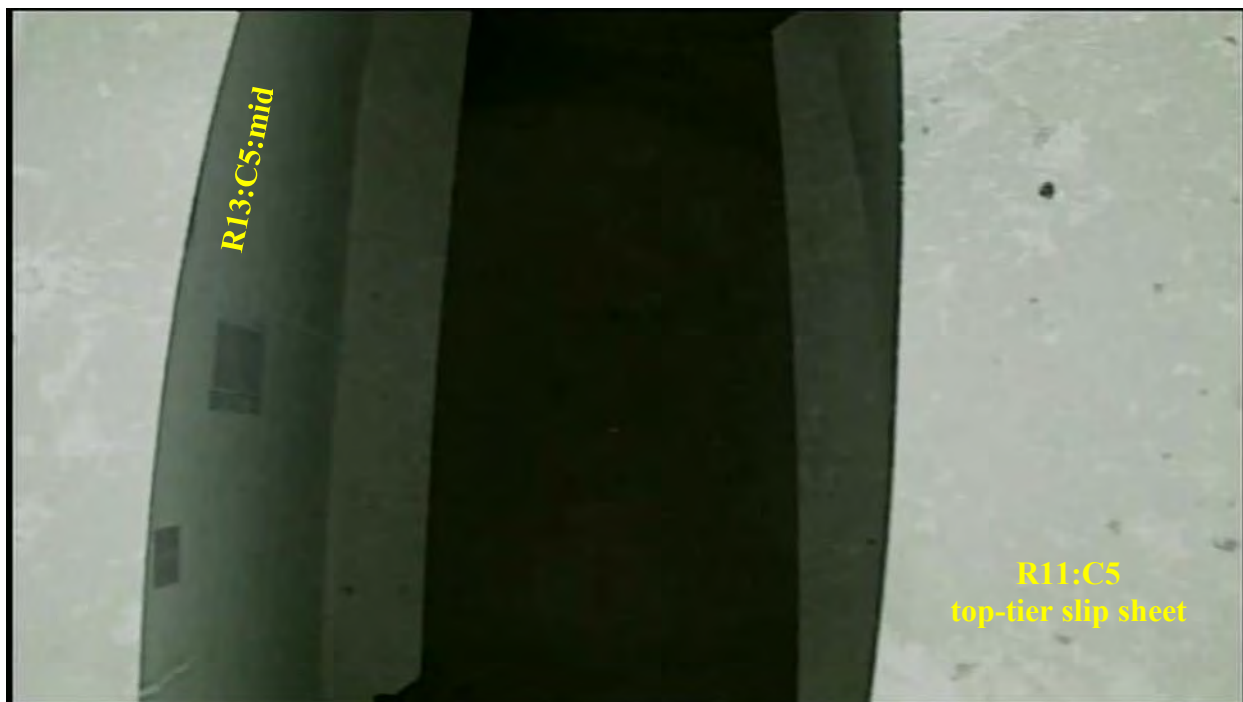
AIB-FST-11202: R11:C5 and R13:C5

AIB-FST-11203: R13:C5 and R11:C5

AIB-FST-11204: R12:C4 and R13:C5

AIB-FST-11205: R12:C4 and R13:C5
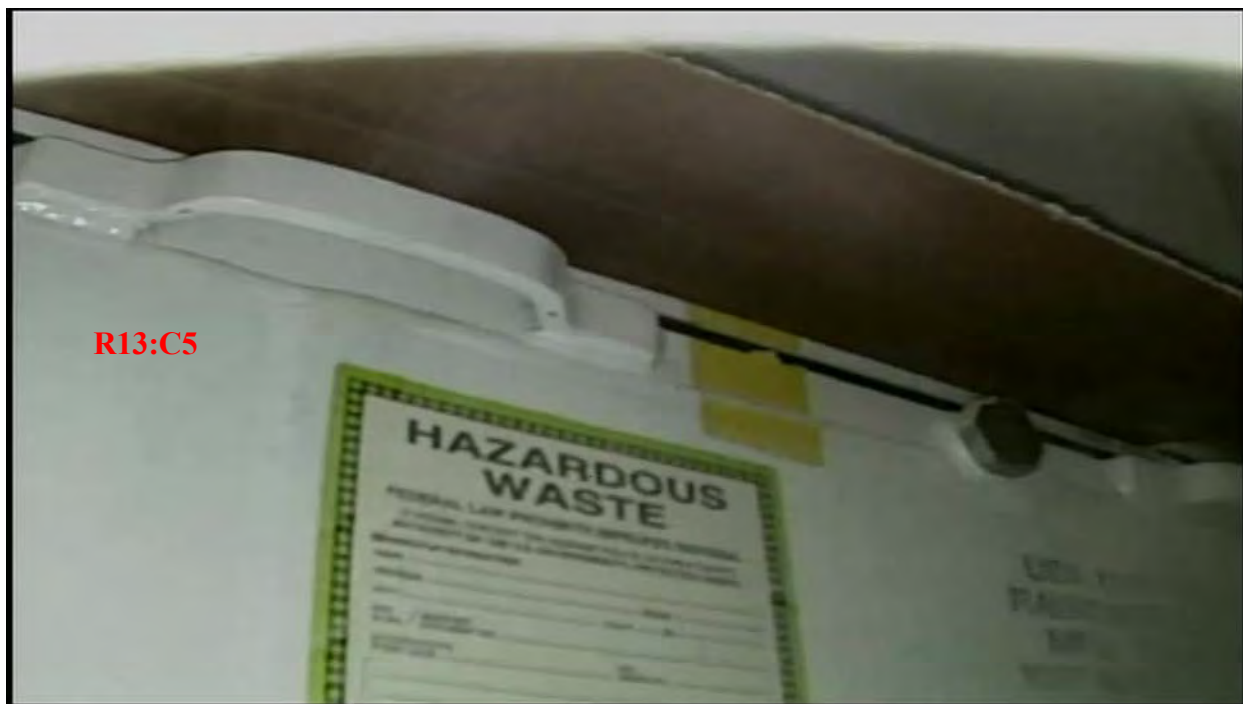
AIB-FST-11206: R13:C5:top - Bulkhead (east) view

AIB-FST-11207: R12:C4 and R13:C5

AIB-FST-11208: R12:C4 and R13:C5

AIB-FST-11209: R12:C6 and R13:C5 – Bottom tier

AIB-FST-11210: R2:C4 and R2:C6

AIB-FST-11211: R2:C4, R2:C6 and bulkhead

AIB-FST-11212: R2:C4, R2:C6 and bulkhead
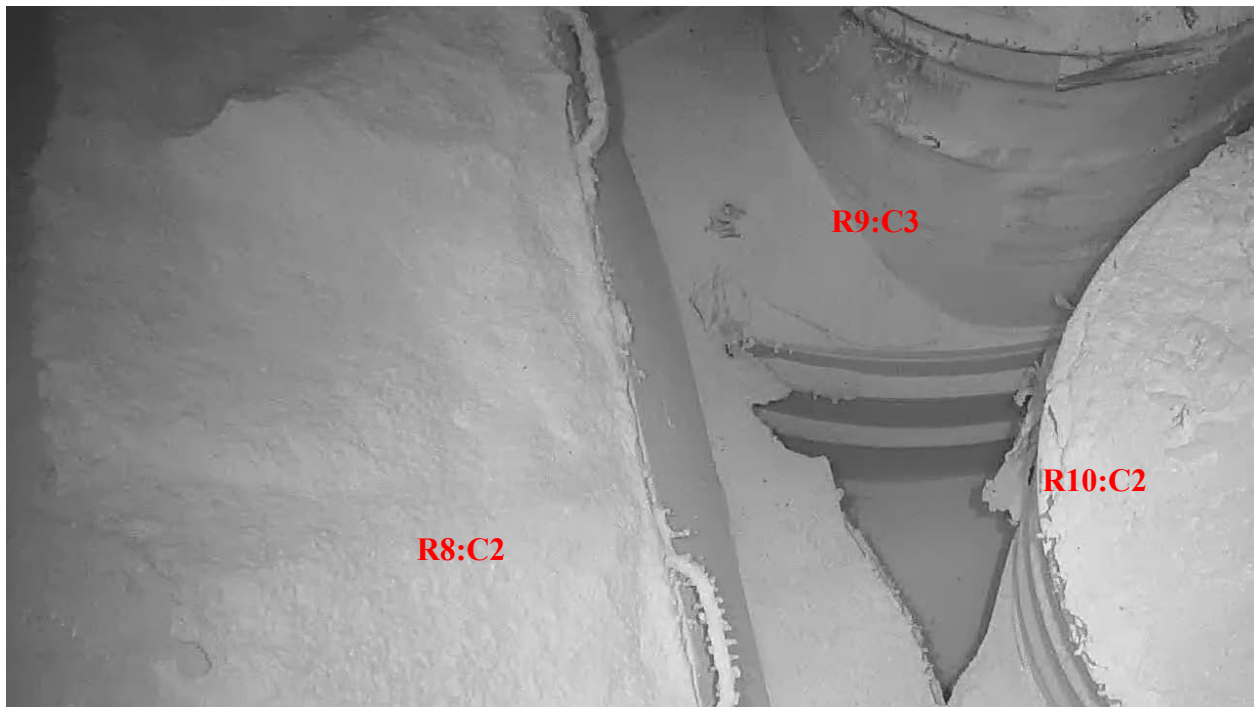
AIB-FST-11213

AIB-FST-11233: R20:C2 and R21:C3

AIB-FST-11234

AIB-FST-11235: R21:C3
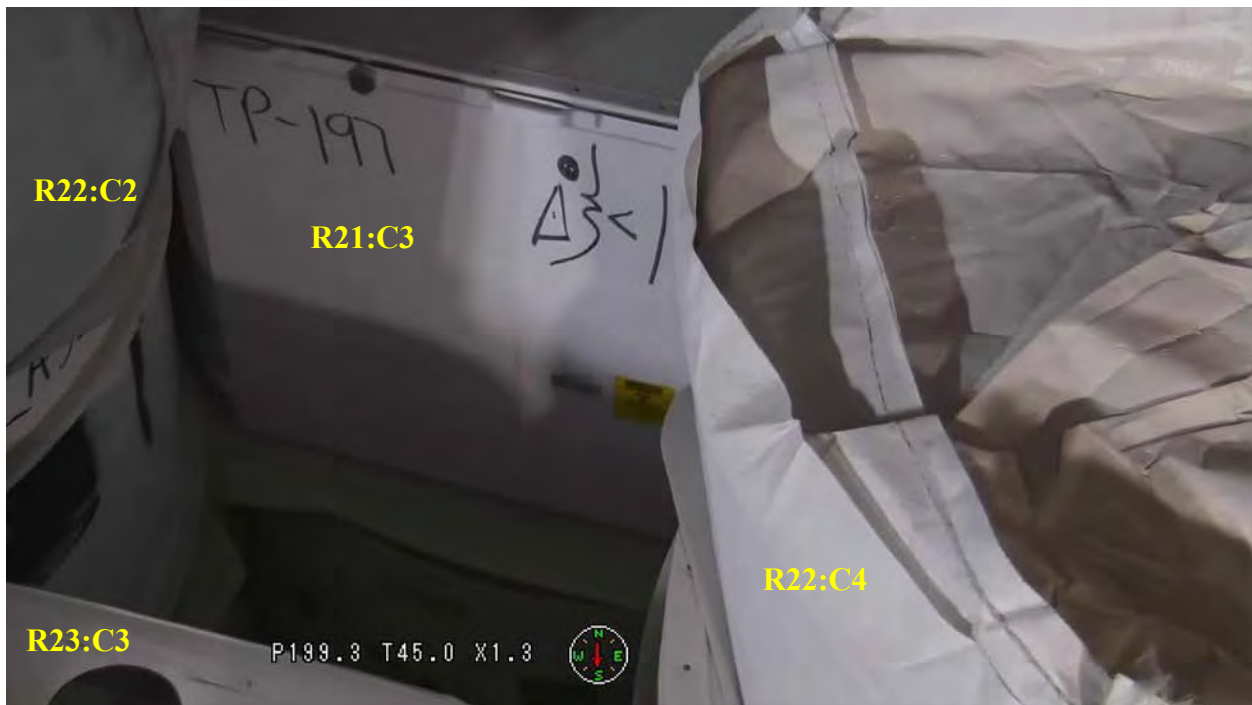
AIB-FST-11236

AIB-FST-11237

AIB-FST-11238

AIB-FST-11239

AIB-FST-11240

AIB-FST-11241

AIB-FST-11242: R21:C3 and R22:C2

AIB-FST-11244: R14:C4 and R15:C3
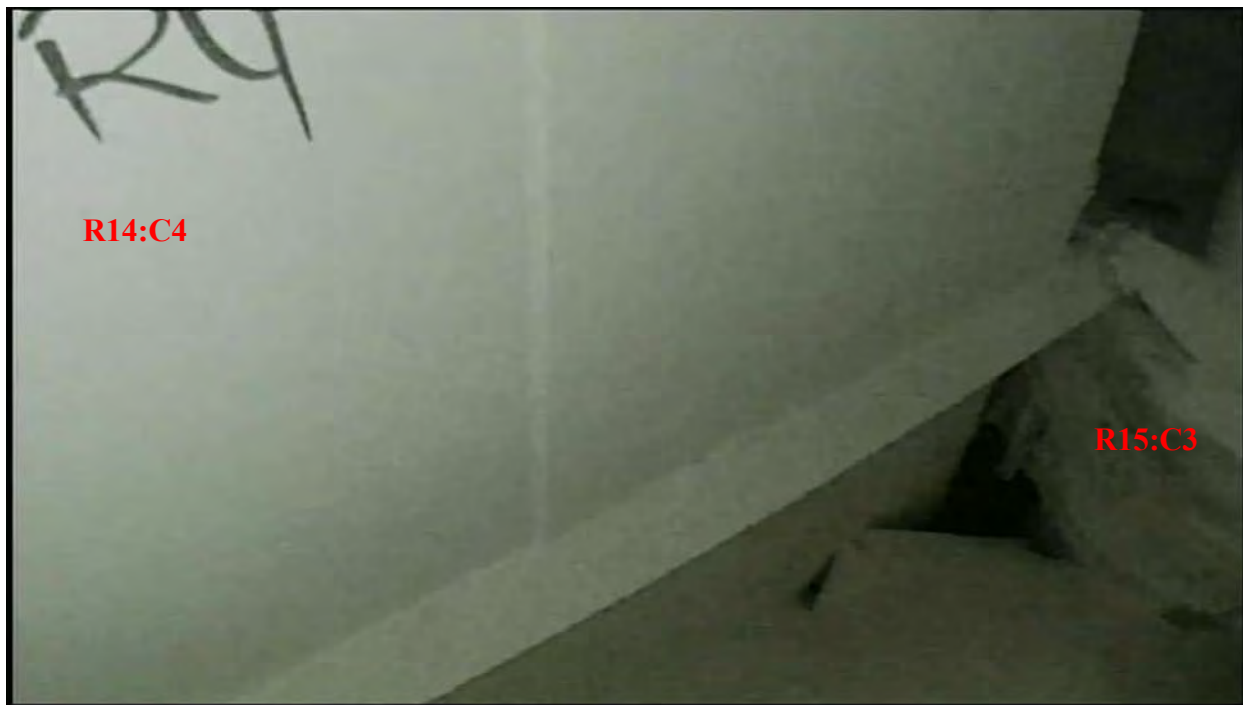
AIB-FST-11245: R14:C4 Bulkhead view – Middle and bottom tier
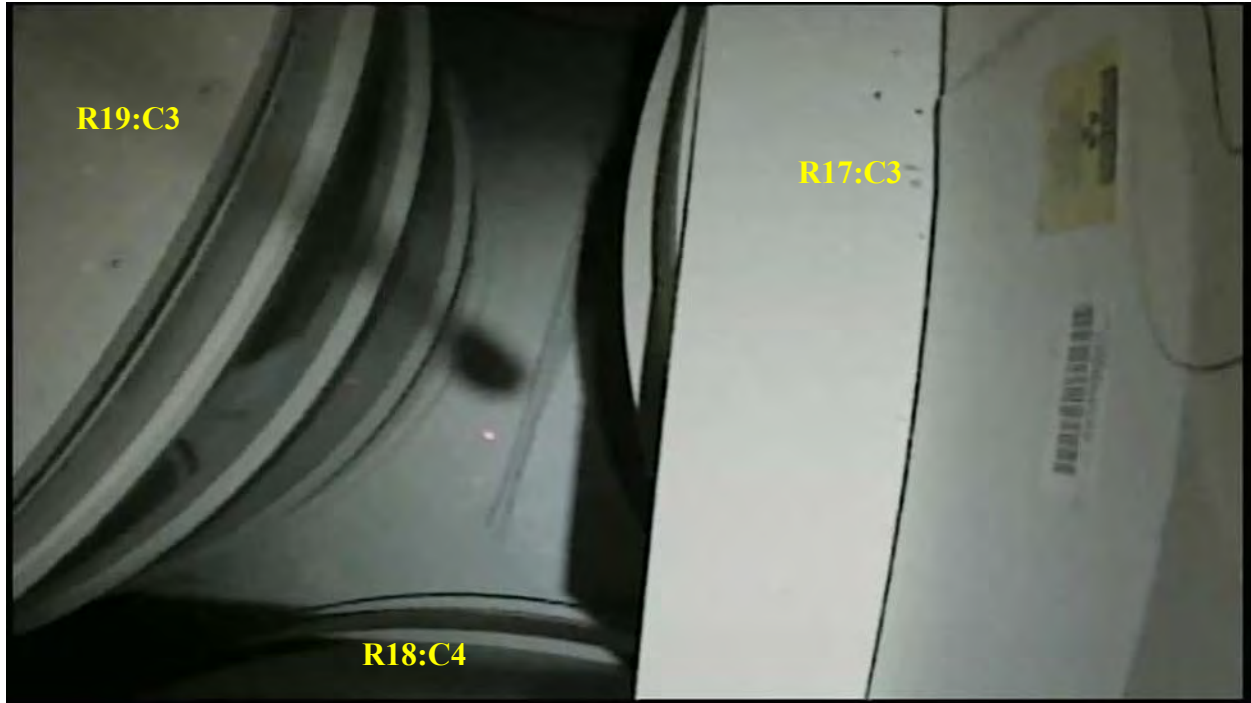
AIB-FST-11315

AIB-FST-11316

AIB-FST-11317

AIB-FST-11322

AIB-FST-11336

AIB-FST-11337

AIB-FST-11338

AIB-FST-11339

AIB-FST-11340
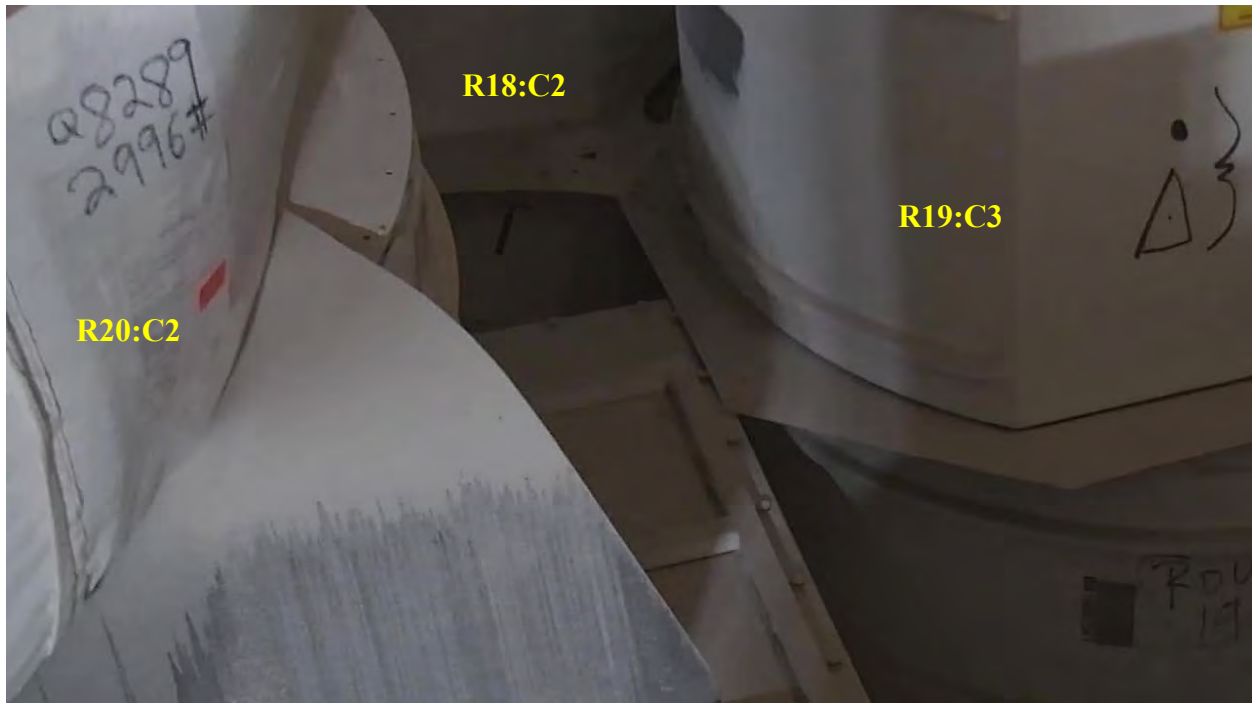
AIB-FST-11341: R19:C3 and R20:C2

AIB-FST-11342: R18:C2 and R19:C3

AIB-FST-11343

AIB-FST-11344: R18:C2 and R19:C3 – Cardboard stiffener bridge

AIB-FST-11345: R18:C2 and R19:C3

AIB-FST-11346: R18:C2 and R19:C3
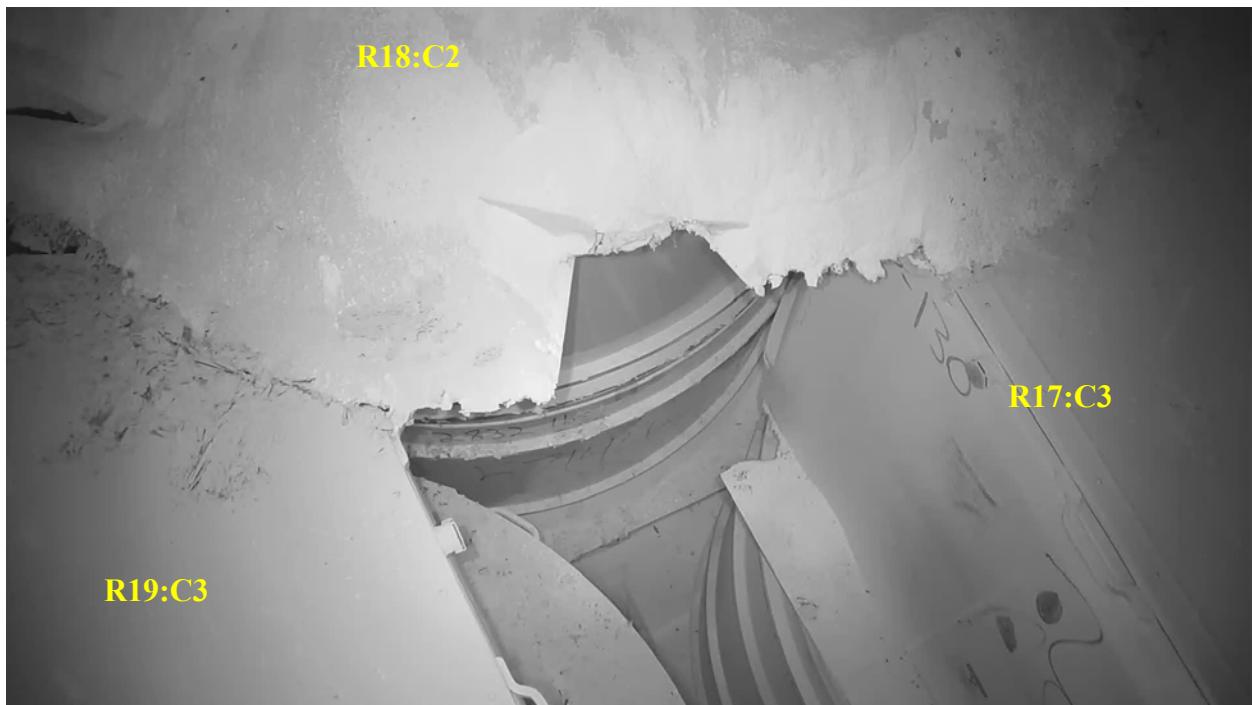
AIB-FST-11347
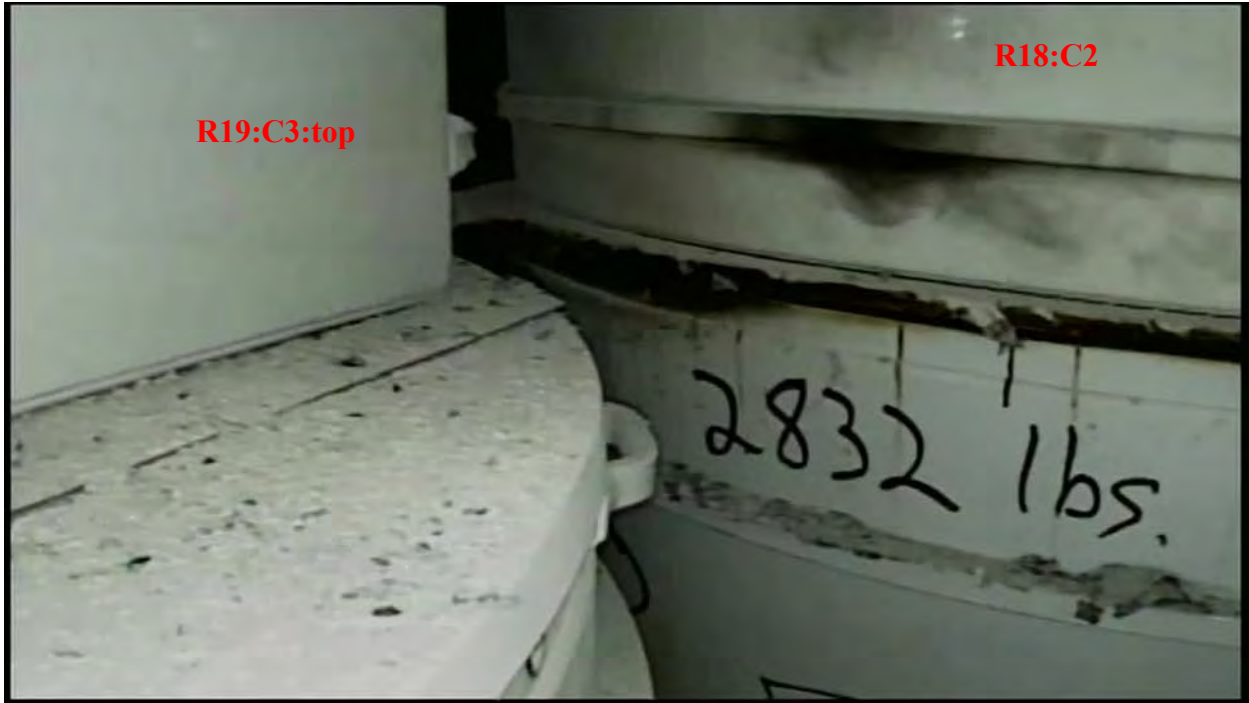
AIB-FST-11348: R18:C2 and R19:C3

AIB-FST-11350: R15:C5 – SWB lid on May 15, 2014

U.S. Department of Energy
Office of Environmental Management
April 2015